NASA TECHNICAL MEMORANDUM

NASA TM X-73307

ASTRONAUTIC STRUCTURES MANUAL
VOLUME III
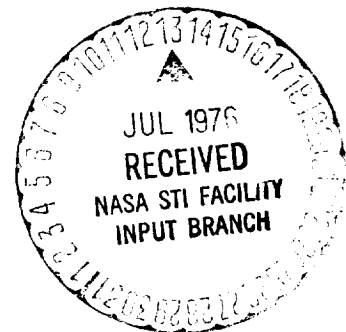
Structures and Propulsion Laboratory

August 1975

NASA

George C. Marshall Space Flight Center

Marshall Space Flight Center, Alabama

1. REPORT NO. NASA TM X-73307	2. GOVERNMENT ACCESSION NO.	3. RECIPIENT'S CATALOG NO.
4. TITLE AND SUBTITLE ASTRONAUTIC STRUCTURES MANUAL VOLUME III		5. REPORT DATE August 1975
		6. PERFORMING ORGANIZATION CODE
7. AUTHOR(S)		8. PERFORMING ORGANIZATION REPORT #
9. PERFORMING ORGANIZATION NAME AND ADDRESS George C. Marshall Space Flight Center Marshall Space Flight Center, Alabama 35812		10. WORK UNIT NO.
		11. CONTRACT OR GRANT NO.
		13. TYPE OF REPORT & PERIOD COVERED
12. SPONSORING AGENCY NAME AND ADDRESS National Aeronautics and Space Administration Washington, D.C. 20546		Technical Memorandum
		14. SPONSORING AGENCY CODE

15. SUPPLEMENTARY NOTES

Prepared by Structures and Propulsion Laboratory, Science and Engineering

16. ABSTRACT

This document (Volumes I, II, and III) presents a compilation of industry-wide methods in aerospace strength analysis that can be carried out by hand, that are general enough in scope to cover most structures encountered, and that are sophisticated enough to give accurate estimates of the actual strength expected. It provides analysis techniques for the elastic and inelastic stress ranges. It serves not only as a catalog of methods not usually available, but also as a reference source for the background of the methods themselves.

An overview of the manual is as follows: Section A is a general introduction of methods used and includes sections on loads, combined stresses, and interaction curves; Section B is devoted to methods of strength analysis; Section C is devoted to the topic of structural stability; Section D is on thermal stresses; Section E is on fatigue and fracture mechanics; Section F is on composites; Section G is on rotating machinery; and Section H is on statistics.

These three volumes supersede Volumes I and II, NASA TM X-60041 and NASA TM X-60042, respectively.

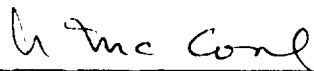| 17. KEY WORDS		18. DISTRIBUTION STATEMENT
ORIGINAL PAGE IS OF POOR QUALITY		Unclassified — Unlimited
19. SECURITY CLASSIF. (of this report) Unclassified	20. SECURITY CLASSIF. (of this page) Unclassified	21. NO. OF PAGES 673 22. PRICE NTIS

MSFC - Form 3292 (Rev December 1972)   For sale by National Technical Information Service, Springfield, Virginia 22151

APPROVAL

ASTRONAUTIC STRUCTURES MANUAL
VOLUME III

The information in this report has been reviewed for security classification. Review of any information concerning Department of Defense or Atomic Energy Commission programs has been made by the MSFC Security Classification Officer. This report, in its entirety, has been determined to be unclassified.

This document has also been reviewed and approved for technical accuracy.

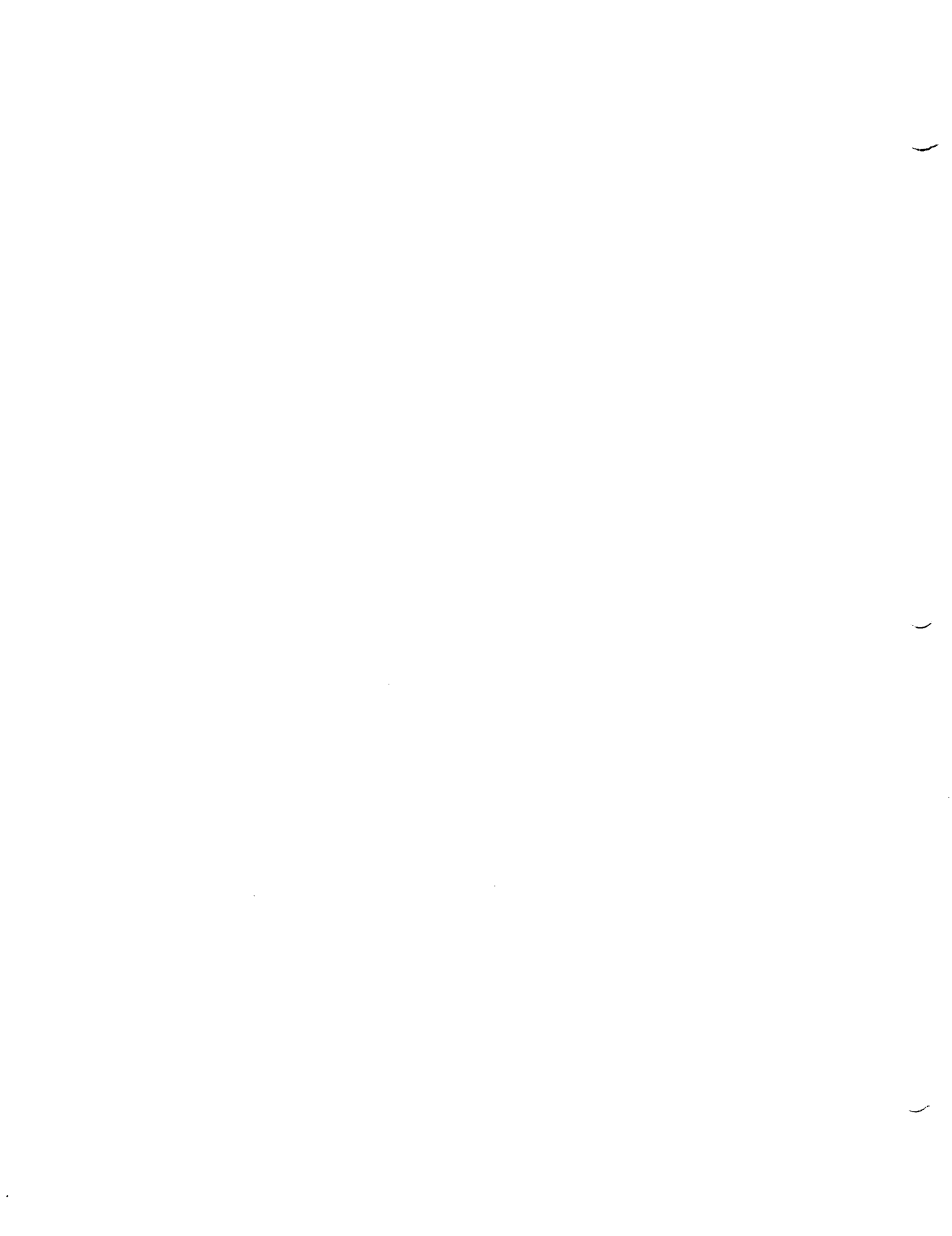_A. A. McCool_

A. A. McCOOL
Director, Structures and Propulsion Laboratory

TABLE OF CONTENTS

TABLE OF CONTENTS (Continued)

TABLE OF CONTENTS (Concluded)

SECTION D
THERMAL STRESSES

DEFINITION OF SYMBOLS

Symbol	Definition
A	Cross-sectional area; area
A_0	Cross-sectional area of beam at $x = 0$
A_{mn}, A_{pq}	Coefficients for the series by which the stresses are expressed, in.
A_1, A_2, A_3, A_4	Constants based on the boundary conditions, equations (95) and (96), dimensionless
A_i', A_1', A_2', A_3'	Constants, psi (Figs. 5.0-8, 5.0-9)
a	Limiting value (lower) for radius; inside radius or radius of middle surface of cylinder
a_0	Maximum value of initial imperfection
a_0'	Constant, °F
a_1'	Constant, °F/in.
B_{mn}, B_{pq}	Coefficients for the series by which the stresses are expressed, in.

NOTES:

1. Bars over any letters denote middle-surface values.

2. The subscript cr denotes critical values for buckling.

3. The superscripts P and C identify quantities associated with the particular and complementary solutions, respectively.

4. The subscript R denotes values required to completely suppress thermal deformations.

DEFINITION OF SYMBOLS (Continued)

Symbol	Definition
B_1, B_2, B_3	Constants, in./(in.)(hr)(Fig. 5.0-10)
b	Breadth (or width) of cross section; limiting value (upper) for radius; outside radius
b_0, b_1, b_2	Constants in polynomial representation of the temperature $T_1(x)$; °F, °F/in., and °F/in.^{2}, respectively
C_p	Specific heat of the material, Btu/(lb)(°F)
C_1, C_2, C_3, C_4	Constants of integration, in.
$C_{-1}, C_0, C_1, \ldots$	Coefficients in polynomial representation of U^P, in.-lb, lb, lb/in., ..., respectively, refer to equation (106)
D	Diameter
D_b	Plate bending stiffness or shell-wall bending stiffness
d_0, d_1, d_2	Constants in polynomial representation of the function $T_2(x)$; °F, °F/in., and °F/in.^{2}, respectively
$d_{-1}, d_0, d_1, \ldots$	Coefficients in polynomial representation of V^P, in., dimensionless, 1/in., ..., respectively; refer to equation (106)
E	Young's modulus of elasticity
E_b	Young's modulus of support-beams, psi
E_p	Young's modulus of plate, psi

Symbol	Definition
E_s	Secant modulus, psi
E_t	Tangent modulus, psi
e	Base for natural logarithms, dimensionless (2.718)
F.E.M.	Fixed-end moment
FF	Fixed-fixed
FS	Fixed-supported
G	Variation in depth of beam along the length
G'	Modulus of rigidity or shear modulus
H	Variation in width of beam along the length
H_A, H_B	Running edge forces acting normal to the axis of revolution at positions A and B, respectively (Figs. 3.0-51 and 3.0-52), lb/in.
I	Moment of inertia
I_b	Support-beam centroidal moment of inertia
I_y, I_z	Area moments of inertia taken about the y and z axes, respectively, in.^{4}
i	Imaginary number, $\sqrt{-1}$
K	Thermal diffusivity of the material, $\text{ft}^2/\text{hr} = k/C_p \rho$
k	An integer (1, 2, 3, 4, 5) exponent

DEFINITION OF SYMBOLS (Continued)

Symbol	Definition
k'	Thermal conductivity of the material, Btu/(hr)(ft)(° F)
L	Length
$L(\ )$	Operator defined by equation (103)
M	Moment
M_A, M_B	Running edge moments acting at positions A and B, respectively (Figs. 3.0-51 and 3.0-52), in.-lb/in.
M_T	Thermal moment
M_b	Thermal bending parameter, in.-lb/in.
$M_r, M_\theta, M_x, M_\phi$	Running bending moments, in.-lb/in.
$M_{r\theta}$	Running twisting moment, in.-lb/in.
M_r', M_θ'	Bending-moment parameters (Table 3.0-5 and Figs. 3.0-15 through 3.0-19)
M_t	Temperature resultant, in.-lb/in.
M_x, M_y	Running bending moments acting on sections of the plate which are perpendicular to the x and y directions, respectively (positive when associated upper-fiber stresses are compressive), in.-lb/in.
M_y	Moment about y axis
M_z	Moment about z axis
M_0	Moment in beam at x = 0

DEFINITION OF SYMBOLS (Continued)

Symbol	Definition
m	Temperature distribution in the z-direction
m_k	Moment coefficients, plotted in Figure 3.0-46, dimensionless
m_ϕ	Surface moment (Fig. 3.0-53) in.-lb/in.^{2}
N	Exponent of thermal variation along the length of the beam; also upper limit for summation indices, dimensionless
N_T	Axial load per unit length on plate edge
$N_r, N_\theta, N_x, N_\phi$	Running membrane loads, lb/in.
$N_{r\theta}$	Running membrane shear load, lb/in.
N_r', N_θ'	Membrane-force parameters (Table 3.0-6), dimensionless
N_t	Temperature resultant, lb/in.
n	Temperature distribution in the y-direction
n_k	Hoop-force coefficients, plotted in Figure 3.0-49, dimensionless
P	Axial force
P_T	Axial force resulting from temperature
P_0	Column load
p	Radial pressure, psi
p, q	Summation indices, dimensionless
Q	Heat input

DEFINITION OF SYMBOLS (Continued)

Symbol	Definition

Q_x — Running transverse shear load, lb/in.

q — Temperature distribution in the x-direction

q_k — Shear coefficients, plotted in Figure 3.0-46, dimensionless

r — Radius

SS — Simply supported

s — Meridional coordinate measured downward from top of the truncated cone (Fig. 3.0-50), in.

s* — Meridional coordinate measured upward from bottom of the truncated cone (Fig. 3.0-50), in.

T — Temperature

$\overline{T}$ — Average value for T, °F

T^* — Weighted average value for T, °F

T_D — Temperature difference between the plate faces, °F

T_{edges} — Temperature at edges of the plate, °F

T_f — Final uniform temperature which the body reaches at sufficiently long times

T_i — Inside temperature; also initial uniform temperature of the body, °F

T_m — Average value for temperature distribution across the wall thickness at any single position, °F

DEFINITION OF SYMBOLS (Continued)

Symbol	Definition
T_s	Temperature of the supports, $^\circ F$
T_{xy}	Temperature at any location in the plate, $^\circ F$
T_0	Outside temperature
T_1, T_2	Temperature functions, $^\circ F$
t	Time (hr) or thickness
t_{cr}	Time to the onset of creep buckling, hr
u	Displacement in the x-direction or r-direction for circular plate
V	Function representing temperature variation in y- and z-directions; also rotations in a meridional plane for a shell
V_P	Component of deflection without thermal effects
V_T	Component of deflection including thermal effects
V_0	Shear at $x = 0$
v	Displacement in the y-direction or θ-direction for circular plate
w	Displacement in the z-direction
w'	Deflection parameter (Table 3.0-5 and Figs. 3.0-15 through 3.0-19), dimensionless

Symbol	Definition
$\overline{w}$	Displacement, in the z-direction, for the case where all edges are simply supported, in.; also radial deflection for shell
w^A	Displacement component, in the z-direction, in. (Note: The superscript A is merely an identification symbol and is not meant to be a generalized exponent.)
w_k	Deflection coefficients, plotted in Figure 3.0-45, dimensionless
x	Coordinate axis
y	Coordinate axis
Z	Upper limit for the summation index k, dimensionless; also surface loads, psi
z	Coordinate axis measured normal to undeformed plate
α	Coefficient of linear thermal expansion, in./(in.)(° F)
$\left(\alpha T_0 b^2/t^2\right)_{cr}$	Critical value of temperature parameter (value at which initial thermal buckling occurs), dimensionless
Γ	Knockdown factor, dimensionless
γ	Knockdown factor (Fig. 4.0-17), dimensionless
γ_{xy}	Shearing strain in planes parallel to and including the x-y plane, in./in.
$\dot{\gamma}_{xy}$	Time rate of change for γ_{xy}, in./(in.)(hr)

DEFINITION OF SYMBOLS (Continued)

Symbol	Definition
δ	Maximum absolute value for deflection measured normal to the x-y plane, in.
∇	Del-operator
ϵ	Unit strain
ϵ_i	Strain intensity defined in equations (1), in./in.
$\dot{\epsilon}_i$	Time rate of change for ϵ_i, in./(in.)(hr)
ϵ_x, ϵ_y	Normal strains acting in the x and y directions, respectively (positive when fibers lengthen), in./in.
$\dot{\epsilon}_x, \dot{\epsilon}_y$	Time rate of change for ϵ_x and ϵ_y, respectively, in./(in.)(hr)
$\zeta(\ )$	Function defined by equations (56) and (76), dimensionless
η	Plasticity reduction factor, dimensionless
θ	Angular coordinate (Fig. 3.0-14), rad
$\theta(\ )$	Function defined by equations (58) and (78), dimensionless
θ_k	Slope coefficients, plotted in Figure 3.0-46, dimensionless
λ	A constant in strain-stress relationship
ν	Poisson's ratio (sometimes written μ, m)
ν_t	$\nu/(1-\nu)$
ρ	Density of the material, lb/ft³

Symbol	Definition
σ_f	Stress induced by restraint
σ_i	Stress intensity defined in equations (1), psi
$(\sigma_i)_{cr}$	Critical value for the stress intensity σ_i, psi
$\left(\sigma_{\overline{P}}\right)_B$	Axial stress due to the artificial force $\overline{P}_B$, psi
$\sigma_r, \sigma_t, \sigma_\theta, \sigma_\phi$	Normal stresses acting in the r, t, θ, and ϕ directions, respectively (positive in tension), psi
$\sigma_{r\theta}$	In-plane shear stress, psi
σ_x, σ_y	Normal stresses acting in the x and y directions, respectively (positive in tension), psi
$(\sigma_x)_{cr}$	Critical axial stress for buckling of the cylinder, psi
σ_{yy}, σ_{zz}	Lateral axial stresses
σ_{yz}	Plane stress
τ_{xy}	Shearing stress acting in planes parallel to and including the x-y plane, psi
ϕ	Stress function [Airy's stress function $I(x,y)$]; also denotes "meridional"; also angular coordinate
$\phi(\ )$	Function defined in equations (76), dimensionless
ϕ_1, ϕ_2, ϕ_3	Parameters tabulated in Tables 6.0-1, 6.0-2, and 6.0-4, respectively, dimensionless

DEFINITION OF SYMBOLS (Concluded)

Symbol	Definition
Ψ_2, Ψ_3	Parameters tabulated in Tables 6.0-3 and 6.0-5, respectively, dimensionless
Ψ_1'	Parameter tabulated in Table 6.0-1, dimensionless
Ψ_2'	Value of Ψ_2 at $r/R = 1$, dimensionless
Ψ_3'	Value of Ψ_3 at $r/R = 1$, dimensionless
$\psi(\ )$	Function defined in equations (78), dimensionless

D.　　　**THERMAL STRESSES.**

1.0　　　INTRODUCTION.

Restrictions imposed on thermal expansion or contraction by continuity of the body or by the conditions at the boundaries induce thermal stresses in the body. In the absence of constraints at boundaries, thermal stresses in a body are self equilibrating.

Except for a few simple cases, the solution of the thermoelasticity problem becomes intractable (see Ref. 1). Therefore, for thermal stress analysis, further approximations leading to the strength of material and finite element methods are used extensively. Depending upon its geometry, a structural element is classified as one of the following: rod, beam, curved beam, plate, or shell. If a structure consists of one of the elements named above, or of some simple combination of them, the method of strength of materials will yield good results. However, if the structure has a complex geometrical shape, the finite element method is easier to use and yields satisfactory results. The method of finite element analysis is suggested for use on an idealized structure which can be represented by a large number of smaller, simpler elements (rods, beams, triangular plates, rectangular plates, etc.) connected at a finite number of points (e.g., only at vertices of triangles or rectangles, or ends of rods, etc.) to provide approximately the configuration of the actual structure.

In a constrained structure, compressive stresses resulting from thermal, or thermal and mechanical, loading may produce instability of the structure. The linear thermoelastic formulation of the problem excludes the question of large deformations. Thus, for buckling, or for problems where loads depend upon deformation, nonlinearity that is due to large deformations must be incorporated in the problem formulation (e.g., beam-column analysis). The extreme difficulties involved in solving the nonlinear thermoelasticity problem have led the researchers to resort to the approximate methods of strength of materials and finite elements.

One of the important problems associated with high temperature is that of creep deformation and relaxation. The phenomenon of the increase in strains with time when the specimen is subject to constant stress and constant high temperature is called creep. The general formulation remains the same as in thermoelasticity or strength of materials, except that the stress-strain relation is expressed by a viscoelastic model. The linear viscoelastic model does not represent many materials; but the complexities multiply if the nonlinear

model is used. Relatively little work has been done towards the solution of
nonlinear viscoelastic theory.

Vibrations that result from thermal shock are quite small in comparison
with those resulting from mechanical load. They are not considered here.

2.0 THERMOELASTICITY.

Three-dimensional equations for equilibrium, displacement, stress, and strain can be found in Ref. 1 in terms of rectangular, cylindrical, or spherical coordinates. Formulas given below are, for the most part, two-dimensional expressions for rectangular coordinates.

2.0.1 Plane Stress Formulation.

For a temperature distribution of the form $\dot{T}(x,y)$ in a long prismatic body, eight quantities, σ_{xx}, σ_{yy}, σ_{xy}, ϵ_{xx}, ϵ_{yy}, ϵ_{xy}, u, and v satisfy, in plane stress concept, the following eight equations.

Equations of equilibrium (no body forces),

$$\frac{\partial \sigma_{xx}}{\partial x} + \frac{\partial \sigma_{xy}}{\partial y} = 0$$

$$\frac{\partial \sigma_{xy}}{\partial x} + \frac{\partial \sigma_{yy}}{\partial y} = 0 \quad ,$$

Stress-Strain Relations,

$$\epsilon_{xx} = \frac{1}{E} (\sigma_{xx} - \nu \sigma_{yy}) + \alpha T$$

$$\epsilon_{yy} = \frac{1}{E} (\sigma_{yy} - \nu \sigma_{xx}) + \alpha T$$

$$\epsilon_{xy} = \frac{1}{2} \gamma_{xy} = \frac{1}{2G} \sigma_{xy} \quad ,$$

Strain-Displacement relations,

$$\epsilon_{xx} = \frac{\partial u}{\partial x} \quad ; \quad \epsilon_{yy} = \frac{\partial v}{\partial y} \quad ; \quad \epsilon_{xy} = \frac{1}{2} \gamma_{xy} = \frac{1}{2} \left(\frac{\partial u}{\partial y} + \frac{\partial v}{\partial x} \right) \quad ,$$

and in the case of plane stress,

$$\sigma_{zz} = \sigma_{xz} = \sigma_{yz} = 0$$

$$\epsilon_{zz} = -\frac{\nu}{E}(\sigma_{xx} + \sigma_{yy}) + \alpha T \quad .$$

2.0.2   Plane Strain Formulation.

In the case of plane strain defined by equations

$$u = u(x, y)$$

$$v = v(x, y)$$

$$w = 0$$

replace E, ν, and α of the stress-strain relations of plane stress formulation by E_1, ν_1, and α_1, respectively, where $E_1 = \dfrac{E}{1 - \nu^2}$; $\nu_1 = \dfrac{\nu}{1 - \nu}$; and $\alpha_1 = \alpha(1 + \nu)$. The equations of equilibrium and strain-displacement relations remain unchanged.

2.0.3   Stress Formulation.

The solution of three partial differential equations satisfying the given boundary condition gives the stress distribution, σ_{xx}, σ_{xy}, and σ_{yy} in the body. The equilibrium equations are

$$\frac{\partial \sigma_{xx}}{\partial x} + \frac{\partial \sigma_{xy}}{\partial y} + X = 0$$

$$\frac{\partial \sigma_{xy}}{\partial x} + \frac{\partial \sigma_{yy}}{\partial y} + Y = 0$$

and the compatibility condition is, for a simply connected body

$$\nabla^2 (\sigma_{xx} + \sigma_{yy} + \alpha ET) + (1 + \nu)\left(\frac{\partial X}{\partial x} + \frac{\partial Y}{\partial y}\right) = 0 \quad .$$

2.0.3.1 Solution of Airy's Stress Function.

I. Plane Stress.

For simply connected regions in the absence of the body forces, X, Y, the solution of this problem is simplified considerably by using Airy's stress function $\Phi(x, y)$. (See Section A1.3.6) Then

$$\sigma_{xx} = \frac{\partial^2 \Phi}{\partial y^2} \quad ; \quad \sigma_{yy} = \frac{\partial^2 \Phi}{\partial x^2} \quad ; \quad \sigma_{xy} = -\frac{\partial^2 \Phi}{\partial x \partial y} \quad .$$

The relations above satisfy the equilibrium equations identically, and substitution of these relations into the stress compatibility equation yields

$$\nabla^4 \Phi + \alpha E \nabla^2 T = 0 \quad ,$$

where

$$\nabla^4 \Phi = \nabla^2(\nabla^2\Phi) = \frac{\partial^2 \Phi}{\partial x^4} + \frac{2 \partial^2 \Phi}{\partial x \partial y} + \frac{\partial^4 \Phi}{\partial y^4} \quad .$$

For this problem the boundary conditions should be expressed in terms of the stress function Φ.

II. Plane Strain.

For plane strain problems the governing equation can be obtained from those above by substituting E_1 and α_1 for E and α respectively, where

$$E_1 = \frac{E}{1 - \gamma^2} \quad ; \quad \alpha_1 = \alpha(1 + \nu) .$$

$$\nabla^4 \Phi + \frac{\alpha E}{1 - \nu^2} \nabla^2 T = 0$$
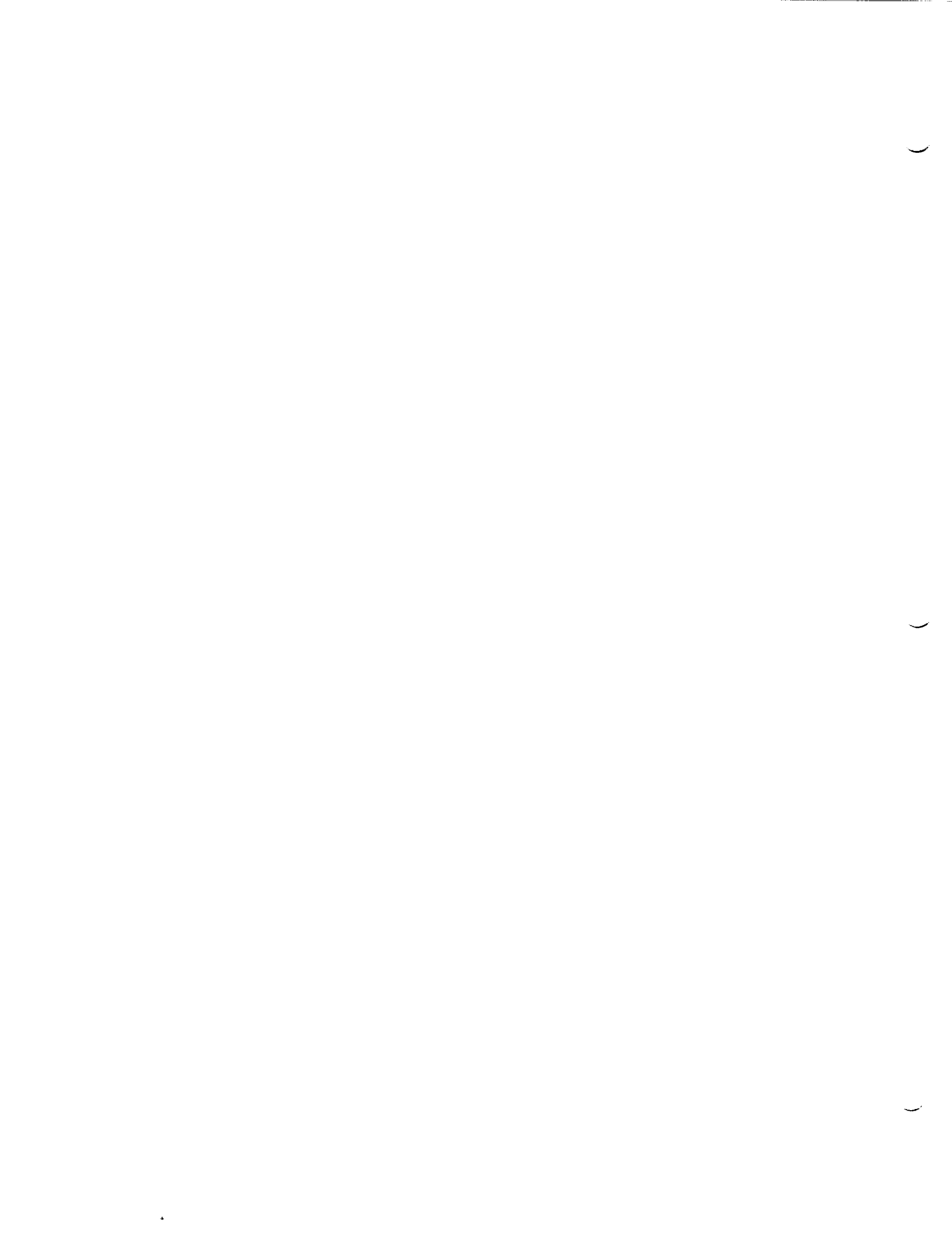
3.0   STRENGTH OF MATERIALS SOLUTIONS.

The assumption that a plane section normal to the reference axis before thermal loading remains normal to the deformed reference axis and plane after thermal loading, along with neglecting the effect on stress distribution of lateral contraction, lays the foundation of the approximate methods of strength of materials. The exact results obtained by the methods of quasistatic thermoelasticity show that the accuracy of the strength of materials solution improves with the reduction of depth-to-span ratio, if the variation of temperature along the length of the beam is smooth. As in the case of mechanical loads, a considerable error results in the vicinity of abrupt changes in the cross sections.

If the temperature is either uniform or linear along the length of the beam, the assumption of a plane section is valid, and the strength of materials method gives the same results as those given by the plane stress thermoelastic method.

Since the effect of lateral contraction is neglected, lateral axial stresses are zero; e.g., $\sigma_{yy} = \sigma_{zz} = 0$ in the case of a beam with x-axis as the reference plane.

3.0.1   Unrestrained Beam — Thermal Loads Only.

3.0.1.1   Axial Stress.

For an unrestrained beam (Fig. 3.0-1) the longitudinal stress (σ_{xx}) is given by

$$\sigma_{xx} = -\alpha ET + \frac{P_T}{A} + \left(\frac{I_y M_{T_z} - I_{yz} M_{T_y}}{I_y I_z - I_{yz}^2}\right) y + \left(\frac{I_z M_{T_y} - I_{yz} M_{T_z}}{I_y I_z - I_{yz}^2}\right) z \tag{1}$$

where

$$T = T(x, y, z)$$

$$P_T = \int_A \alpha ET \, dA \qquad\qquad I_z = \int_A y^2 \, dA$$

$$M_{T_z} = \int_A \alpha E T_y \, dA \qquad\qquad I_y = \int_A z^2 \, dA$$

$$M_{T_y} = \int_A \alpha E T_z \, dA \qquad\qquad I_{yz} = \int_A yz \, dA \quad .$$
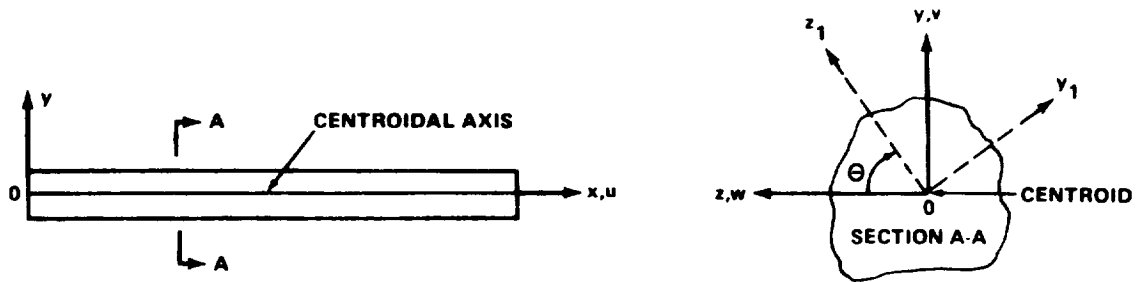
Figure 3.0-1. General unrestrained beam.

CASE a. The y-z axes are principal axes $(I_{yz} = 0)$

$$\sigma_{xx} = -\alpha ET + \frac{P_T}{A} + \frac{M_{T_z}}{I_z} y + \frac{M_{T_y}}{I_y} z \quad .$$ (2)

CASE b. The y-z axes are not principal axes. A new coordinate system y_1, z_1 is chosen which makes an angle θ with y-z axes such that

$$\tan \theta = -\frac{I_y M_{T_y} - I_{yz} M_{T_z}}{I_y M_{T_z} - I_{yz} M_{T_y}} \quad .$$ (3)

In the new coordinate system, which in general does not constitute principal axes, the z axis becomes the neutral axis, and equation (1) in this coordinate system reduces to

$$\sigma_{xx} = -\alpha ET + \frac{P_T}{A} + \frac{M_{T_{z_1}} y_1}{I_{z_1}} \quad ,$$ (4)

where

$$M_{T_{z_1}} = \int_A \alpha ET (x_1 y_1 z_1) y_1 \, dA_1$$

$$I_{z_1} = \int_A y_1^2 \, dA_1 \quad .$$

3.0.1.2 Displacements.

Axial displacement $u(x, y, z)$ with respect to the $u(0, y, z)$ is given by

$$u(x,y,z) = u(0,y,z) + \frac{1}{E} \int_0^x \left[\frac{P_T}{A} + \left(\frac{I_y M_{T_z} - I_{yz} M_{T_y}}{I_y I_z - I_{yz}^2} \right) y + \left(\frac{I_z M_{T_y} - I_{yz} M_{T_z}}{I_y I_z - I_{yz}^2} \right) z \right] dx \quad . \tag{5}$$

The average displacement $u_{av}(x)$ of the cross section at a distance x is

$$u_{av}(x) = u_{av}(0) + \frac{1}{E} \int_0^x \frac{P_T}{A} \, dx \quad . \tag{6}$$

Displacements v and w of the reference axis $[v(x,y,z) = v(x,0,0) ; w(x,y,z) = w(x,0,0)]$ are given by the following differential equations:

$$\frac{d^2 v}{dx^2} = - \frac{1}{E} \left(\frac{I_y M_{T_z} - I_{yz} M_{T_y}}{I_y I_z - I_{yz}^2} \right) \quad ,$$

$$\frac{d^2 w}{dx^2} = - \frac{1}{E} \left(\frac{I_z M_{T_y} - I_{yz} M_{T_z}}{I_y I_z - I_{yz}^2} \right) \quad . \tag{7}$$

If the y-z axes are principal, equations (7) reduce to

$$\frac{d^2 v}{dx^2} = - \frac{M_{T_z}}{EI_z} \quad ,$$

$$\frac{d^2 w}{dx^2} = - \frac{M_{T_y}}{EI_y} \quad . \tag{8}$$

In y_1-z_1 axes, defined by equation (3), equations (7) reduce to

$$\frac{d^2v}{dx^2} = -\frac{M_{T_{z_1}}}{EI_{z_1}}$$

(9)

$$\frac{d^2w_1}{dy^2} = 0 \qquad .$$

3.0.2 Restrained Beam — Thermal Loads Only.

Considered henceforth in this paragraph are cases of beam cross sections having y-z axes for the principal axes.

The values P, M_y, and M_z are the axial force and bending moments at any cross section resulting from the external forces and the reactions to the restraints against thermal expansion; therefore, M_y and M_z depend only on the constraining moments and shears at the restraints.

$$M_z = M_{0_z} + V_{0_z} x \quad ,$$

$$M_y = M_{0_y} + V_{0_y} x \quad ,$$

(10)

where the sign convention on moments and shears and M_0 and V_0 are shown in Fig. 3.0-2.
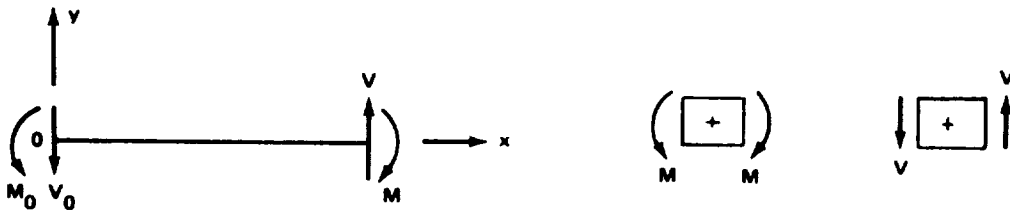
Figure 3.0-2. Sign convention of moments and shears.

The displacements v, w are given by

$$\frac{d^2v}{dx^2} = - \frac{M_{T_z} + M_z}{EI_z} \quad ,$$

$$\frac{d^2w}{dx^2} = - \frac{M_{T_y} + M_y}{EI_y} \quad .$$

(11)

Solutions of equations (11) for the special case described by equation (10) are

$$v(x) = - \int_0^x \int_0^{x_2} \frac{M_{T_z}(y_1)}{EI_z(x_1)} \, dx_1 \, dx_2 + C_{0_z} + C_{1_z} x - M_{0_z} \int_0^x \int_0^{x_2} \frac{dx_1}{EI_z(x_1)} \, dx_2$$

$$- V_{0_z} \int_0^x \int_0^{x_2} \frac{x_1}{EI_z(x_1)} \, dx_1 \, dx_2 \quad ,$$

(12)

$$w(x) = - \int_0^x \int_0^{x_2} \frac{M_{T_y}(x_1)}{EI_y(x_1)} \, dx_1 \, dx_2 + C_{0_y} + C_{1_y} x - M_{0_y} \int_0^x \int_0^{x_2} \frac{dx_1 \, dx_2}{EI_y(x_1)}$$

$$- V_{0_y} \int_0^x \int_0^{x_2} \frac{x_1}{EI_y(x_1)} \, dx_1 \, dx_2 \quad .$$

The bending moment and shear force at any cross section are

$$M_z = - EI_z \frac{d^2v}{dx^2} - M_{T_z} \quad ,$$

$$M_y = - EI_y \frac{d^2w}{dx^2} - M_{T_y} \quad ,$$

(13)

$$V_z = \frac{dM_z}{dx} \quad ; \quad V_y = \frac{dM_y}{dx} \quad .$$

Each of the two equations (12) has four unknowns, C_0, C_1, M_0, V_0, which are calculated from four boundary conditions, two at each end of a beam.

3.0.2.1   Evaluation of Integrals for Varying Cross Sections.

For a general cross section as shown in Fig. 3.0-3 the following notation is chosen:

$$b = b_0 h(x_1) \qquad h(x_1) = 1 + H\left(\frac{x}{L}\right)$$

$$d = d_0 g(x_1) \qquad g(x_1) = 1 + G\left(\frac{x}{L}\right) \quad,$$

where b_0 and d_0 are reference width and depth at $x = 0$; $x_1 = \dfrac{x}{L}$.

$$A = A_0 h(x_1)\, g(x_1)$$

$$I_z = I_{z_0} h(x_1)\, g^3(x_1)$$

$$I_y = I_{y_0} h^3(x_1)\, g(x_1)$$
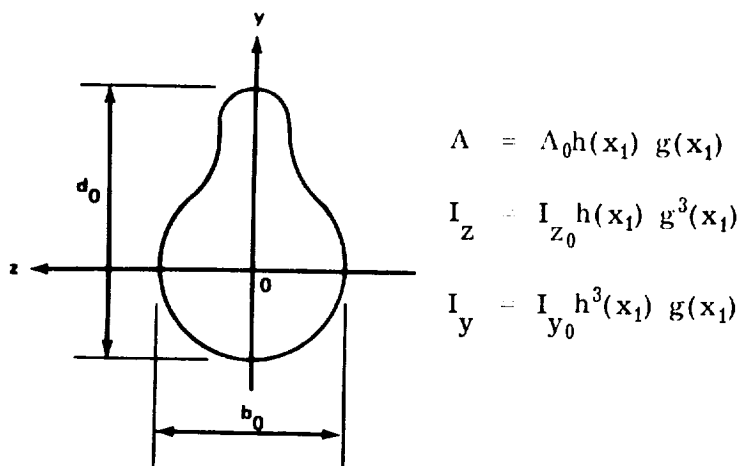
Figure 3.0-3.   General cross section.

Letting the temperature variation be represented by

$$T(x, y, z) = f(x_1)\, V(y, z) \quad,$$

the necessary integrals become:

$$P_T = \int_A \alpha\, ET\, dA = \alpha\, E\, f(x_1)\, g(x_1)\, h(x_1) \int_{A_0} V\, dA_0 \quad,$$

$$M_{T_y} = \int_A \alpha\, ET_z\, dA = \alpha\, E\, f(x_1)\, g(x_1)\, h(x_1) \int_{A_0} V\, z\, dA_0 \quad,$$

$$M_{T_z} = \int_A \alpha\, ET_y\, dA = \alpha\, E\, f(x_1)\, g(x_1)\, h(x_1) \int_{A_0} V\, y\, dA_0 \quad,$$

$$\int_0^x \frac{M_{T_y}}{EI_y}\, dx = \frac{\alpha}{I_{0_y}} \int_{A_0} V\, z\, dA_0 \int_0^{x_1} \frac{f(x_1)}{h^2(x_1)}\, dx_1 \quad,$$

$$\int_0^x \frac{M_{T_z}}{EI_z}\, dx = \frac{\alpha}{I_{z_0}} \int_{A_0} V\, y\, dA_0 \int_0^{x_1} \frac{f(x_1)}{g^2(x_1)}\, dx_1 \quad,$$

$$\int_0^x \frac{x\, dx}{EI_z} = \frac{1}{EI_{z_0}} \int_0^{x_1} \frac{x_1\, dx_1}{h(x_1)\, g^3(x_1)} \quad; \quad \int_0^x \frac{dx}{EI_z} = \frac{1}{EI_{z_0}} \int_0^{x_1} \frac{dx_1}{h(x_1)\, g^3(x_1)} \quad.$$

The integrals necessary to evaluate P_T, M_{T_y}, and M_{T_z} for a particular cross section and temperature distribution can be evaluated as follows:

Let

$$F_0 = \int_{A_0} V\, dA_0 \quad,$$

$$F_{1_y} = \int_{A_0} V\, y\, dA_0 \quad,$$

and

$$F_{1_z} = \int_{A_0} V z \, dA_0 \quad .$$

Then, letting $V(y, z) = V_{mn} y^n z^m$, which is a polynomial representation of the temperature variation in the y- and z-directions, F_0, F_{1_y}, and F_{1_z} can be evaluated for common shapes. Table 3.0-1 gives these evaluations for several common shapes and various values of m and n. Table 3.0-2 gives values of F_0 and F_{1_y} for rectangular, triangular, elliptic, and diamond cross sections when m = 0 and n = 0 - 5. Table 3.0-3 gives values of F_0 and F_{1_y} for several standard shapes for various values of m and n.

3.0.2.2   Restrained Beam Examples.

In the following examples, since deflection, moment and shear equations along the y- and z-directions are similar, only the results of the boundary value problem in the y-direction are given (i.e., m = 0).

I.   Simply Supported Beam.
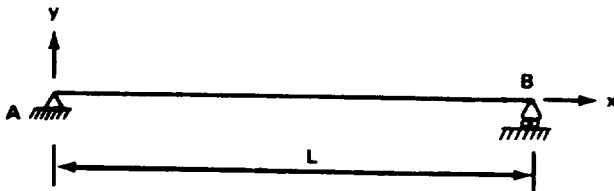
A.   Boundary Conditions:

$$v = 0 \ @ \ x = 0, \ L$$

$$M_z = -EI_z \frac{d^2v}{dx^2} - M_{T_z} = 0 \ @ \ x = 0, \ L$$

$$V_0 = M_0 = 0 \quad .$$

TABLE 3.0-1. EXPRESSIONS FOR F_0, F_{1_y}, AND F_{1_z} FOR COMMON SHAPES.

RECTANGULAR

$$F_0 = \begin{cases} \dfrac{4V_{mn}}{(m+1)(n+1)} \left(\dfrac{b_0}{2}\right)^{m+1} \left(\dfrac{d_0}{2}\right)^{n+1} & m,\ n = 0, 2, 4, 6.. \\[3ex] 0 & m \text{ or } n = 1, 3, 5.. \end{cases}$$

$$F_{1_y} = \begin{cases} \dfrac{4V_{mn}}{(m+1)(n+2)} \left(\dfrac{b_0}{2}\right)^{m+1} \left(\dfrac{d_0}{2}\right)^{n+2} & \begin{array}{l} m=0, 2, 4.. \\ n=1, 3, 5.. \end{array} \\[3ex] 0 & m=1, 3, 5, ..\quad n=0, 2, 4, 6 \end{cases}$$

$$F_{1_z} = \begin{cases} \dfrac{4V_{mn}}{(m+2)(n+1)} \left(\dfrac{b_0}{2}\right)^{m+2} \left(\dfrac{d_0}{2}\right)^{n+1} & \begin{array}{l} n=0, 2, 4.. \\ m=1, 3, 5.. \end{array} \\[3ex] 0 & \begin{array}{l} n=1, 3, 5.. \\ m=0, 2, 4.. \end{array} \end{cases}$$

TABLE 3.0-1. (Continued)

TRIANGULAR
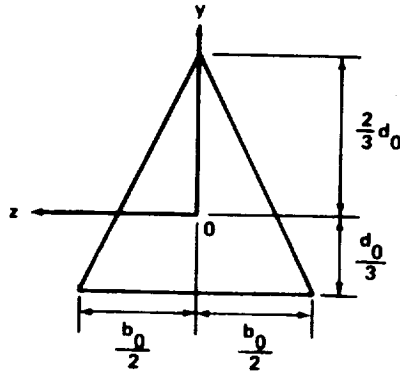
$$F_0 = \begin{cases} \dfrac{2V_{mn}}{(m+1)} \left(\dfrac{b_0}{2}\right)^{m+1} d_0^{\,n+1} \left[-\displaystyle\sum_{i=1}^{m+1} B_i + (-2)^{n+m+2} B_{m+2}\right] & m=0,2,4 \\[2em] 0 & m=1,3,5 \end{cases}$$

where

$$B_i = \frac{(n+1)!}{(m+2-i)!} \cdot \frac{n!}{(n+i)!} \left(-\frac{1}{3}\right)^{n+i}$$

$$F_{1_y} = \begin{cases} \dfrac{2V_{mn}}{(m+1)} \left(\dfrac{b_0}{2}\right)^{m+1} d_0^{\,n+2} \left[-\displaystyle\sum_{i=1}^{m+2} C_i + (-2)^{n+m+3} C_{m+2}\right] & m=0,2,4 \\[2em] 0 & m=1,3,5 \end{cases}$$

where

$$C_i = \frac{(m+1)!}{(m+2-i)!} \cdot \frac{(n+1)!}{(n+1+i)!} \left(-\frac{1}{3}\right)^{n+1+i}$$

$$F_{1_z} = \begin{cases} 0 & m=0,2,4.. \\[2em] \dfrac{2V_{mn}}{m+2} \left(\dfrac{b_0}{2}\right)^{m+2} d_0^{\,n+1} \left[-\displaystyle\sum_{i=1}^{m+3} D_i + (-2)^{n+m+3} D_{m+2}\right] & m=1,3,5.. \end{cases}$$

where

$$D_i = \frac{(m+2)!}{(m+3-i)!} \cdot \frac{n!}{(n+i)!} \left(-\frac{1}{3}\right)^{n+i}$$

TABLE 3.0-1. (Continued)

ELLIPTIC
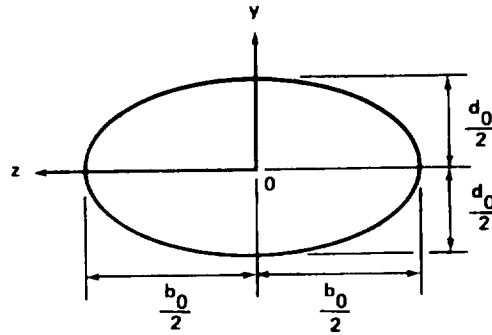
$$F_0 \quad \begin{cases} \dfrac{\pi V_{mn}}{m+1}\left(\dfrac{b_0}{2}\right)^{m+1}\left(\dfrac{d_0}{2}\right)^{n+1}(2)^{\frac{n}{2}}\ \dfrac{n!}{(n+m-1)!}\ \dfrac{(m+n-1)(m+n-3)\ldots(7)(5)(3)(1)}{(m+n+2)(m+n)\ldots(8)(6)(4)} & m,n\ 0,2,4,6 \\[4pt] & \text{and } m+n\ 0 \\[8pt] 0 & m\ \text{or}\ n\ \ 1,3,5\ldots \end{cases}$$

$$F_{t_y} \quad \begin{cases} \dfrac{\pi V_{mn}}{m+1}\left(\dfrac{b_0}{2}\right)^{m+1}\left(\dfrac{d_0}{2}\right)^{n+2}(2)^{\frac{m}{2}}\cdot\dfrac{(n+1)!}{(n+m)!}\cdot\dfrac{(n+m)(n+m-2)\ldots(7)(5)(3)(1)}{(n+m+3)(m+n+1)\ldots(8)(6)(4)} & m\ 0,2,4,6 \\[4pt] & n\ 1,3,5 \\[8pt] 0 & n\ 0,2,4,6\ \text{or}\ m\ 1,3,5\ldots \end{cases}$$

$$F_{t_z} \quad \begin{cases} \dfrac{\pi V_{mn}}{m+2}\left(\dfrac{b_0}{2}\right)^{m+2}\left(\dfrac{d_0}{2}\right)^{n+1}(2)^{\frac{m+1}{2}}\cdot\dfrac{n!}{(n+m)!}\cdot\dfrac{(n+m)(n+m-2)\ldots(7)(5)(3)(1)}{(m+n+3)(m+n+1)\ldots(8)(6)(4)} & m\ 1,3,5 \\[4pt] & n\ 0,2,4 \\[8pt] 0 & n\ 1,3,5\ \text{or}\ m\ 0,2,4,6 \end{cases}$$

TABLE 3.0-1. (Continued)

DIAMOND

$$F_0 = \begin{cases} \dfrac{V_{mn} \, m! \, n!}{(n+m+2)!} \, 4 \left(\dfrac{b_0}{2}\right)^{m+1} \left(\dfrac{d_0}{2}\right)^{n+1} & m, n = 0, 2, 4 \ldots \\[4ex] 0 & m \text{ or } n = 1, 3, 5 \end{cases}$$

$$F_{1_y} = \begin{cases} \dfrac{4 V_{mn} \, m!(n+1)!}{(n+m+3)!} \left(\dfrac{b_0}{2}\right)^{m+1} \left(\dfrac{d_0}{2}\right)^{n+2} & \begin{array}{l} m = 0, 2, 4, 6 \ldots \\ n = 1, 3, 5 \ldots \end{array} \\[4ex] 0 & m = 1, 3, 5 \ldots \text{ or } n = 0, 2, 4 \end{cases}$$

$$F_{1_z} = \begin{cases} \dfrac{4 V_{mn} \, (m+1)! \, n!}{(n+m+3)!} \left(\dfrac{b_0}{2}\right)^{m+2} \left(\dfrac{d_0}{2}\right)^{n+1} & \begin{array}{l} m = 1, 3, 5 \ldots \\ n = 0, 2, 4 \ldots \end{array} \\[4ex] 0 & \begin{array}{l} m = 0, 2, 4 \ldots \\ n = 1, 3, 5 \ldots \end{array} \end{cases}$$

TABLE 3.0-1. (Continued)

T-SECTION
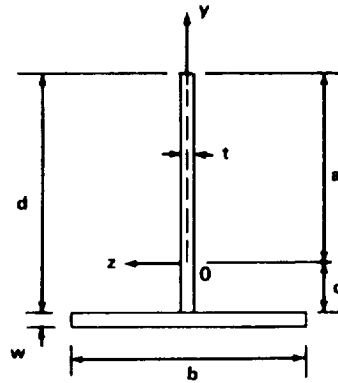
$$F_0 = \begin{cases} \dfrac{2V_{mn}}{(m+1)(n+1)} \left\{ \left(\dfrac{t}{2}\right)^{m+1}\left(a^{n+1} + c^{n+1}\right) + \left(\dfrac{b}{2}\right)^{m+1} \left[(c+w)^{n+1} - c^{n+1}\right] \right\} & \begin{array}{l} m = 0,2,4,6 \\ n = 0,2,4,6 \end{array} \\[3ex] \dfrac{2V_{mn}}{(m+1)(n+1)} \left\{ \left(\dfrac{t}{2}\right)^{m+1}\left(a^{n+1} - c^{n+1}\right) - \left(\dfrac{b}{2}\right)^{m+1} \left[(c+w)^{n+1} - c^{n+1}\right] \right\} & \begin{array}{l} m = 0,2,4,6 \\ n = 1,3,5.. \end{array} \\[3ex] 0 & m = 1,3,5 \quad n = 0,1,2,3 \end{cases}$$

$$F_{1_y} = \begin{cases} \dfrac{2V_{mn}}{(m+1)(n+2)} \left\{ \left(\dfrac{t}{2}\right)^{m+1}\left(a^{n+2} - c^{n+2}\right) + \left(\dfrac{b}{2}\right)^{m+1} \left[c^{n+2} - (c+w)^{n+2}\right] \right\} & \begin{array}{l} m = 0,2,4 \\ n = 0,2,4 \end{array} \\[3ex] \dfrac{2V_{mn}}{(m+1)(n+2)} \left\{ \left(\dfrac{t}{2}\right)^{m+1}\left(a^{n+2} + c^{n+2}\right) + \left(\dfrac{b}{2}\right)^{m+1} \left[(c+w)^{n+2} - c^{n+2}\right] \right\} & \begin{array}{l} m = 0,2,4 \\ n = 1,3,5 \end{array} \\[3ex] 0 & m = 1,3,5 \quad n = 0,1,2,3,4 \end{cases}$$

TABLE 3.0-1. (Continued)

I-SECTION
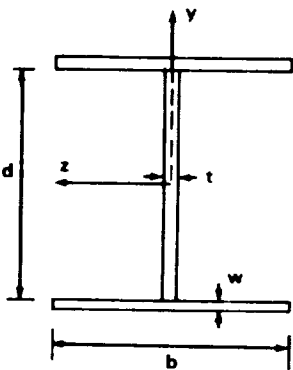
$$F_0 = \begin{cases} \dfrac{4\,V_{mn}\left(\dfrac{d}{2}\right)^{n+1}}{(m+1)\,(n+1)} \left\{\left(\dfrac{t}{2}\right)^{m+1} + \left(\dfrac{b}{2}\right)^{m+1}\left[\left(\dfrac{1}{2} + \dfrac{w}{d}\right)^{n+1} - \left(\dfrac{1}{2}\right)^{n+1}\right]\right\} & m,n = \text{even} \\[4mm] 0 & m \text{ or } n \quad \text{odd} \end{cases}$$

$$F_{1_y} = \begin{cases} \dfrac{4\,V_{mn}\left(\dfrac{d}{2}\right)^{n+2}}{(m+1)\,(n+2)} \left\{\left(\dfrac{t}{2}\right)^{m+1} + \left(\dfrac{b}{2}\right)^{m+1}\left[\left(\dfrac{1}{2} + \dfrac{w}{d}\right)^{n+2} - \left(\dfrac{1}{2}\right)^{n+2}\right]\right\} & \begin{array}{l} m = \text{even} \\ n = \text{odd} \end{array} \\[4mm] 0 & m = \text{odd or } n \quad \text{even} \end{cases}$$

NOTE: z-Section can be approximated by I-Section with respect to its
principal axes. The results above are applicable to this section.

TABLE 3.0-1. (Continued)

HAT-SECTION

$F_0 \quad 0 \qquad\qquad\qquad\qquad\qquad\qquad m \; 1, 3, 5 \ldots$

$$-\frac{2\,V_{mn}}{(n+1)\,(m+1)}\left\{\left[(-c)^{n+1} - (-c-w)^{n+1}\right]\left[\left(\frac{b}{2}+t+\rho\right)^{m+1} - \left(\frac{b}{2}+t\right)^{m+1}\right]\right.$$

$$+\left[a^{n+1} - (-c-w)^{n+1}\right]\left[\left(\frac{b}{2}+t\right)^{m+1} - \left(\frac{b}{2}\right)^{m+1}\right]$$

$$\left.+\left(\frac{b}{2}\right)^{m+1}\left[a^{n+1} - (a-k)^{n+1}\right]\right\} \qquad\qquad m \; 0, 2, 4 \ldots$$
$$n \; 0, 1, 2, 3, 4 \ldots$$

$F_{t_y} = 0 \qquad\qquad\qquad\qquad\qquad\qquad m \; 1, 3, 5 \ldots$

$$\frac{2\,V_{mn}}{(n+2)\,(m+1)}\left\{\left[(-c)^{n+2} - (-c-w)^{n+2}\right]\left[\left(\frac{b}{2}+t+\rho\right)^{m+1} - \left(\frac{b}{2}+t\right)^{m+1}\right]\right.$$

$$+\left[a^{n+2} - (-c-w)^{n+2}\right]\left[\left(\frac{b}{2}+t\right)^{m+1} - \left(\frac{b}{2}\right)^{m+1}\right]$$

$$\left.+\left(\frac{b}{2}\right)^{m+1}\left[a^{n+2} - (a-k)^{n+2}\right]\right\} \qquad\qquad m \; 0, 2, 4 \ldots$$
$$n \; 0, 1, 2, 3, 4 \ldots$$

$F_{t_z} \quad 0 \qquad\qquad\qquad\qquad\qquad\qquad m \; 0, 2, 4 \ldots$

$$-\frac{2\,V_{mn}}{(n+1)\,(m+2)}\left\{\left[(-c)^{n+1} - (-c-w)^{n+1}\right]\left[\left(\frac{b}{2}+t+\rho\right)^{m+2} - \left(\frac{b}{2}+t\right)^{m+2}\right]\right.$$

$$+\left[a^{n+1} - (-c-w)^{n+1}\right]\left[\left(\frac{b}{2}+t\right)^{m+2} - \left(\frac{b}{2}\right)^{m+2}\right]$$

$$\left.+\left(\frac{b}{2}\right)^{m+2}\left[a^{n+1} - (a-k)^{n+1}\right]\right\} \qquad\qquad m \; 1, 3, 5 \ldots$$
$$n \; 0, 1, 2, 3, 4 \ldots$$

TABLE 3.0-1. (Continued)

CHANNEL

$F_0 = 0.0$ $\qquad$ $n = 1, 3, 5 \ldots$

$$= \frac{2\,V_{mn}}{(n+1)(m+1)} \left\{ \left[(c+w)^{m+1} - c^{m+1} \right] \left(\frac{b}{2}\right)^{n+1} + \left[c^{n+1} - (d-c-w)^{m+1} \right] * \right.$$

$$\left. * \left[\left(\frac{b}{2}\right)^{n+1} - \left(\frac{b}{2} - t\right)^{n+1} \right] \right\}$$

$n = 0, 2, 4 \ldots$
$m\ 0, 1, 2, 3, 4, 5 \ldots$

$F_{1_y} = 0.0$ $\qquad$ $n\ 0, 2, 4 \ldots$

$$= \frac{2\,V_{mn}}{(n+2)(m+1)} \left\{ \left[(c+w)^{m+1} - c^{m+1} \right] \left(\frac{b}{2}\right)^{n+2} + \left[c^{m+1} - (d-c-w)^{m+1} \right] * \right.$$

$$\left. * \left[\left(\frac{b}{2}\right)^{n+2} - \left(\frac{b}{2} - t\right)^{n+2} \right] \right\}$$

$m = 0, 1, 2, 3, 4, 5 \ldots$
$n = 1, 3, 5 \ldots$

$F_{1_z} = 0.0$ $\qquad$ $n\ 1, 3, 5 \ldots$

$$= \frac{2\,V_{mn}}{(n+1)(m+2)} \left\{ \left[(c+w)^{m+2} - c^{m+2} \right] \left(\frac{b}{2}\right)^{n+1} + \left[c^{m+2} - (d-c-w)^{m+2} \right] * \right.$$

$$\left. * \left[\left(\frac{b}{2}\right)^{n+1} - \left(\frac{b}{2} - t\right)^{n+1} \right] \right\}$$

$n\ 0, 2, 4 \ldots$
$m = 0, 1, 2, 3, 4, 5 \ldots$

TABLE 3.0-1. (Continued)

RECTANGULAR TUBE
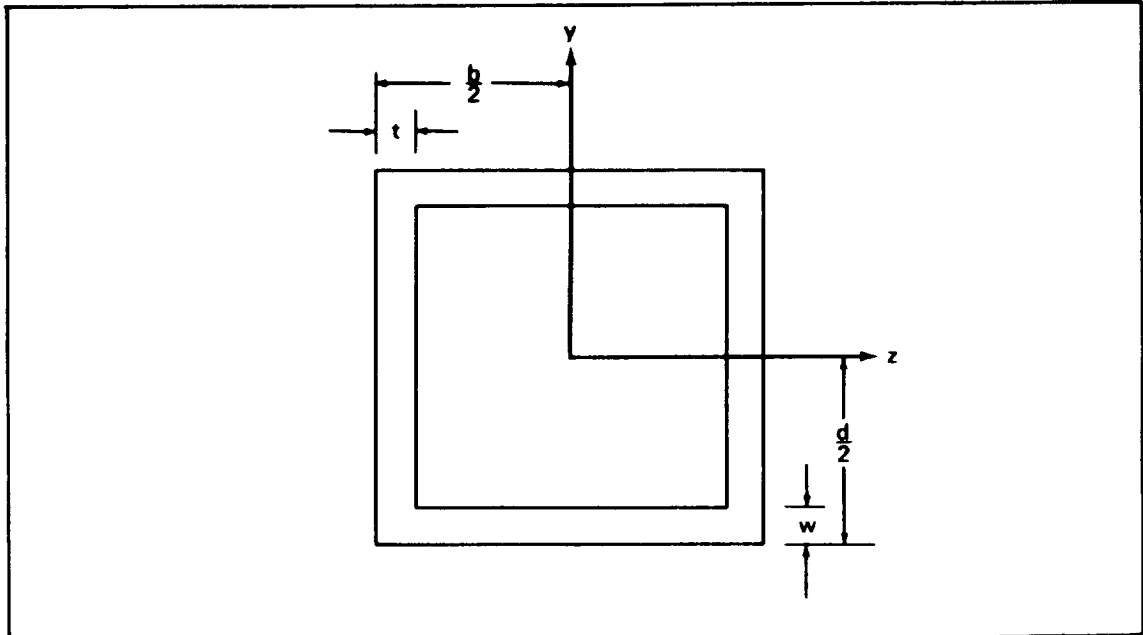
$$F_0 = \begin{cases} 0.0 & n\ 1,3,5\ldots \\ & m\ 1,3,5\ldots \\[1em] 0.0 & \\[1em] \dfrac{4\,V_{mn}}{(n+1)(m+1)}\left\{\left[\left(\dfrac{d}{2}\right)^{n+1}-\left(\dfrac{d}{2}-w\right)^{n+1}\right]\left(\dfrac{b}{2}\right)^{m+1}\right. & \\[1em] \left.+\left(\dfrac{d}{2}-w\right)^{n+1}\left[\left(\dfrac{b}{2}\right)^{m+1}-\left(\dfrac{b}{2}-t\right)^{m+1}\right]\right\} & \begin{array}{l} n\ 0,2,4\ldots \\ m\ 0,2,4\ldots \end{array} \end{cases}$$

$$F_{1_y} = \begin{cases} 0.0 & n\ 0,2,4\ldots \\ & m\ 1,3,5\ldots \\[1em] 0.0 & \\[1em] \dfrac{4\,V_{mn}}{(n+2)(m+1)}\left\{\left[\left(\dfrac{d}{2}\right)^{n+2}-\left(\dfrac{d}{2}-w\right)^{n+2}\right]\left(\dfrac{b}{2}\right)^{m+1}\right. & \\[1em] \left.+\left(\dfrac{d}{2}-w\right)^{n+2}\left[\left(\dfrac{b}{2}\right)^{m+1}-\left(\dfrac{b}{2}-t\right)^{m+1}\right]\right\} & \begin{array}{l} n\ 1,3,5\ldots \\ m\ 0,2,4\ldots \end{array} \end{cases}$$

$$F_{1_z} = \begin{cases} 0.0 & n\ 1,3,5\ldots \\ & m\ 0,2,4\ldots \\[1em] 0.0 & \\[1em] \dfrac{4\,V_{mn}}{(n+1)(m+2)}\left\{\left[\left(\dfrac{d}{2}\right)^{n+1}-\left(\dfrac{d}{2}-w\right)^{n+1}\right]\left(\dfrac{b}{2}\right)^{m+2}\right. & \\[1em] \left.+\left(\dfrac{d}{w}-w\right)^{n+1}\left[\left(\dfrac{b}{2}\right)^{m+2}-\left(\dfrac{b}{2}-t\right)^{m+2}\right]\right\} & \begin{array}{l} n\ 0,2,4\ldots \\ m\ 1,3,5\ldots \end{array} \end{cases}$$

TABLE 3.0-1. (Concluded)

CIRCULAR TUBES
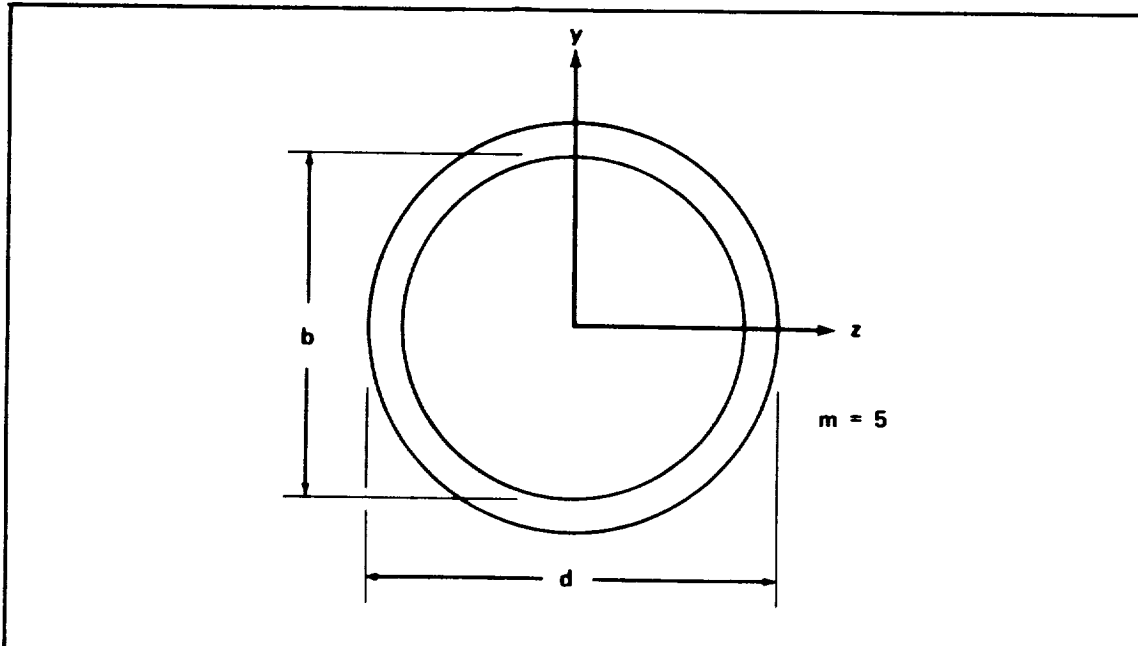
$$F_0 \quad 0.0 \qquad\qquad\qquad\qquad\qquad n\ 1,3,5\ldots$$

$$= 0.0 \qquad\qquad\qquad\qquad\qquad m\ 1,3,5$$

$$-\frac{4V_{mn}}{m+1}\left[\left(\frac{d}{2}\right)^{m+n+2}-\left(\frac{b}{2}\right)^{m+n+2}\right]\left[\frac{1}{n+1}-\frac{m+1}{2(n+3)}+\frac{(m+1)(m-1)}{8(n+5)}\right.$$

$$\left.-\frac{(m+1)(m-1)(m-3)}{48(n+7)}+\frac{(m+1)(m-1)(m-3)(m-5)}{384(n+9)}\right]$$

$$n\ 0,2,4\ldots$$
$$m\ 0,2,4$$

$$F_{t_y}\quad 0.0 \qquad\qquad\qquad\qquad\qquad n\ 0,2,4\ldots$$

$$=0.0 \qquad\qquad\qquad\qquad\qquad m\ 1,3,5$$

$$\frac{4V_{mn}}{m+1}\left[\left(\frac{d}{2}\right)^{m+n+3}-\left(\frac{b}{2}\right)^{m+n+3}\right]\left[\frac{1}{n+2}-\frac{m+1}{2(n+4)}+\frac{(m+1)(m-1)}{8(n+6)}\right.$$

$$\left.-\frac{(m+1)(m-1)(m-3)}{48(n+8)}+\frac{(m+1)(m-1)(m-3)(m-5)}{384(n+10)}\right]$$

$$n\ 1,3,5\ldots$$
$$m\ 0,2,4$$

$$F_{t_z}=0.0 \qquad\qquad\qquad\qquad\qquad n\ 1,3,5\ldots$$

$$0.0 \qquad\qquad\qquad\qquad\qquad m\ 0,2,4$$

$$-\frac{4V_{mn}}{m+2}\left[\left(\frac{d}{2}\right)^{m+n+3}-\left(\frac{b}{2}\right)^{m+n+3}\right]\left[\frac{1}{n+1}-\frac{m+2}{2(n+3)}+\frac{(m+2)m}{8(n+5)}\right.$$

$$\left.-\frac{(m+2)(m)(m-2)}{48(n+7)}+\frac{(m+2)(m)(m-2)(m-4)}{384(n+9)}\right]$$

$$n\ 0,2,4\ldots$$
$$m\ 1,3,5$$

TABLE 3.0-2. VALUES OF F_0 AND F_{1_y} FOR FOUR COMMON SHAPES
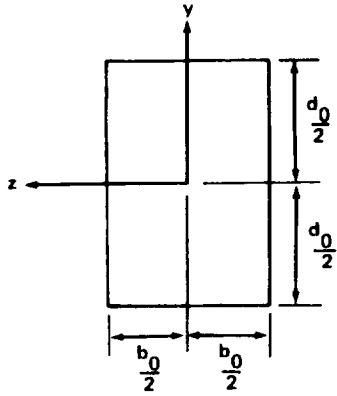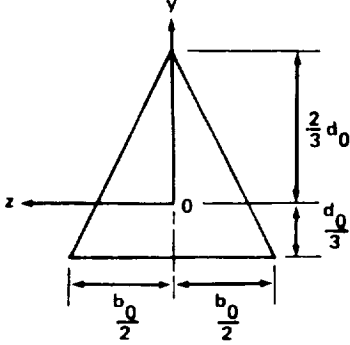
RECTANGULAR	TRIANGULAR

	m=0			m=0	
n	F_0	F_{1_y}	n	F_0	F_{1_y}
0	$b_0 d_0 V_{00}$	0	0	$\frac{1}{2} b_0 d_0 V_{00}$	0
1	0	$\frac{1}{12} b_0 d_0^3 V_{01}$	1	0	$\frac{1}{36} b_0 d_0^3 V_{01}$
2	$\frac{1}{12} b_0 d_0^3 V_{02}$	0	2	$\frac{1}{36} b_0 d_0^3 V_{02}$	$\frac{1}{270} b_0 d_0^4 V_{03}$
3	0	$\frac{1}{80} b_0 d_0^5 V_{03}$	3	$\frac{1}{270} b_0 d_0^4 V_{03}$	$\frac{1}{270} b_0 d_0^5 V_{03}$
4	$\frac{1}{80} b_0 d_0^5 V_{04}$	0	4	$\frac{1}{270} b_0 d_0^5 V_{04}$	$\frac{2}{7(243)} b_0 d_0^6 V_{04}$
5	0	$\frac{1}{448} b_0 d_0^7 V_{05}$	5	$\frac{2}{7(243)} b_0 d_0^6 V_{05}$	$\frac{31}{56(729)} b_0 d_0^7 V_{05}$

TABLE 3.0-2. (Concluded)

ELLIPTIC
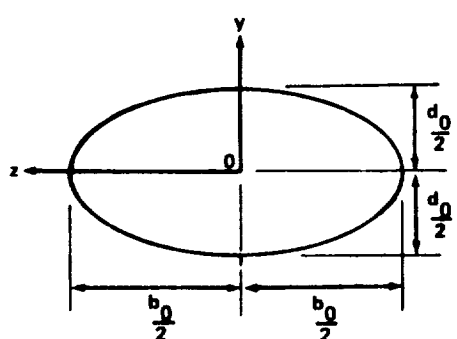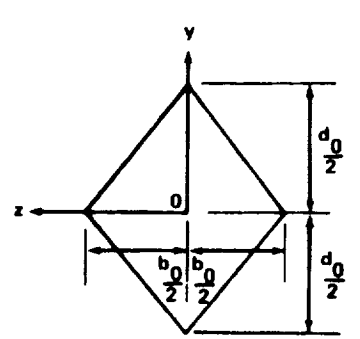
DIAMOND

	m=0			m=0	
n	F_0	F_{1_y}	n	F_0	F_{1_y}
0	$\pi\, b_0 d_0\, V_{00}$	0	0	$\frac{1}{2}\, b_0 d_0\, V_{00}$	0
1	0	$\frac{\pi\, b_0 d_0^3}{32}\, V_{01}$	1	0	$\frac{1}{48}\, b_0 d_0^3\, V_{01}$
2	$\frac{1}{32}\, \pi\, b_0 d_0^3\, V_{02}$	0	2	$\frac{1}{48}\, b_0 d_0^3\, V_{02}$	0
3	6	$\frac{\pi}{128}\, b_0 d_0^5\, V_{03}$	3	0	$\frac{1}{480}\, b_0 d_0^5\, V_{03}$
4	$\frac{\pi}{128}\, b_0 d_0^5\, V_{04}$	0	4	$\frac{1}{480}\, b_0 d_0^5\, V_{04}$	0
5	0	$\frac{15\,\pi}{32(256)}\, b_0 d_0^7\, V_{05}$	5	0	$\frac{1}{28(120)}\, b_0 d_0^7\, V_{05}$

TABLE 3.0-3. VALUES OF F_0 AND F_{1_y} AND F_{1_z} FOR

COMMON SECTIONS.
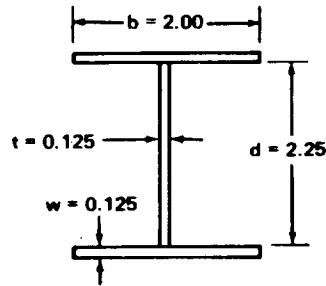
$$F_0 = \frac{1}{V_{mn}} \int V \, dA_0$$

n m	0	2	4	6
0	0.531	0.207	0.121	0.093
2	0.084	0.030	0.011	0.004
4	0.050	0.018	0.006	0.002
6	0.036	0.013	0.004	0.002

$$F_{1_y} = \frac{1}{V_{mn}} \int Vy \, dA_0$$

n m	1	3	5	7
0	0.207	0.121	0.093	0.084
2	0.030	0.011	0.004	0.001
4	0.018	0.006	0.002	0.001
6	0.013	0.004	0.002	0.001
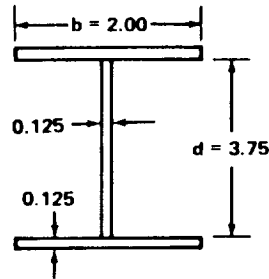
n m	0	2	4	6
0	0.719	0.784	1.379	3.117
2	0.084	0.079	0.075	0.073
4	0.050	0.047	0.044	0.042
6	0.036	0.034	0.032	0.030

n m	1	3	5	7
0	0.784	1.379	3.117	8.152
2	0.079	0.075	0.073	0.076
4	0.047	0.044	0.042	0.039
6	0.034	0.032	0.030	0.028

TABLE 3.0-3. (Continued)
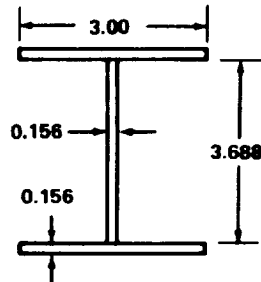
$$F_0 = \frac{1}{V_{mn}} \int V \, dA_0$$

$$F_{1_y} = \frac{1}{V_{mn}} \int V_y \, dA_0$$

n\m	0	2	4	6
0	1.043	1.085	1.731	3.603
2	0.352	0.326	0.303	0.285
4	0.474	0.438	0.405	0.376
6	0.762	0.704	0.652	0.605

n\m	1	3	5	7
0	1.085	1.731	3.603	8.892
2	0.326	0.303	0.285	0.277
4	0.438	0.405	0.376	0.350
6	0.704	0.652	0.605	0.563
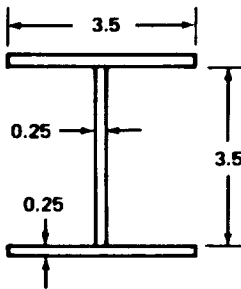
n\m	0	2	4	6
0	1.750	1.663	2.323	4.198
2	0.898	0.791	0.705	0.639
4	1.641	1.445	1.279	1.139
6	3.590	3.160	2.798	2.492

n\m	1	3	5	7
0	1.663	2.323	4.198	9.096
2	0.791	0.705	0.639	0.600
4	1.445	1.279	1.139	1.021
6	3.160	2.798	2.492	2.232

TABLE 3.0-3. (Continued)
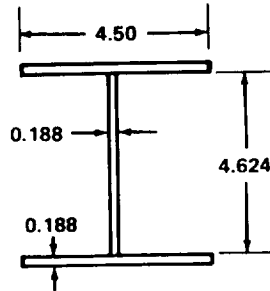
$$F_0 = \frac{1}{V_{mn}} \int V \, dA_0 \qquad\qquad F_{1_y} = \frac{1}{V_{mn}} \int V y \, dA_0$$

n / m	0	2	4	6
0	1.715	2.774	6.745	21.551
2	1.430	2.072	3.014	4.416
4	4.336	6.279	9.110	13.245
6	15.681	22.705	32.942	47.892

n / m	1	3	5	7
0	2.774	6.745	21.551	82.620
2	2.072	3.014	4.416	6.584
4	6.279	9.110	13.245	19.295
6	22.705	32.942	47.892	69.767
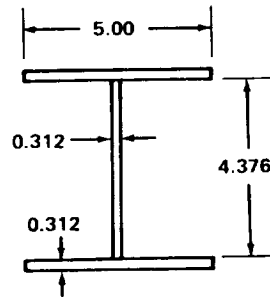
n / m	0	2	4	6
0	2.925	4.325	9.228	25.533
2	3.261	4.488	6.237	8.783
4	12.188	16.766	23.199	32.289
6	54.408	74.845	103.564	144.135

n / m	1	3	5	7
0	4.325	9.228	25.533	85.468
2	4.488	6.237	8.783	12.697
4	16.766	23.199	32.289	45.199
6	74.845	103.564	144.135	201.741

Section D
October 15, 1970
Page 30

TABLE 3.0-3. (Continued)
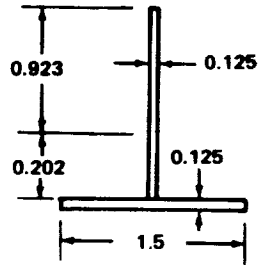
$$F_0 = \frac{1}{V_{mn}} \int V \, dA_0 \qquad\qquad F_1 = \frac{1}{V_{mn}} \int Vy \, dA_0$$

n \ m	0	1	2	3	4
0	0.328	0.001	0.046	0.019	0.018
2	0.035	-0.009	0.003	-0.001	0
4	0.012	-0.003	0.001	0	0
6	0.005	-0.001	0	0	0

n \ m	0	1	2	3	4
0	0.001	0.046	0.019	0.018	0.013
2	-0.009	0.003	-0.001	0	0
4	-0.003	0.001	0	0	0
6	-0.001	0	0	0	0
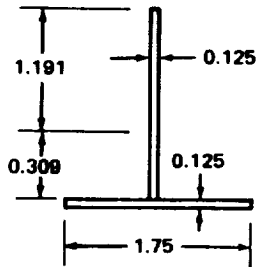
n \ m	0	1	2	3	4
0	0.406	0.001	0.102	0.051	0.064
2	0.056	-0.021	0.008	-0.003	0.001
4	0.026	-0.010	0.004	-0.001	0.001
6	0.014	-0.005	0.002	-0.001	0

n \ m	0	1	2	3	4
0	0.001	0.102	0.051	0.064	0.058
2	-0.021	0.008	-0.003	0.001	0
4	-0.010	0.004	-0.001	0.001	0
6	-0.005	0.002	-0.001	0	0

TABLE 3.0-3. (Continued)
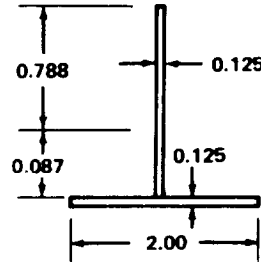
$$F_0 = \frac{1}{V_{mn}} \int V \, dA_0 \qquad\qquad F_1 = \frac{1}{V_{mn}} \int Vy \, dA_0$$

n / m	0	1	2	3	4
0	0.359	0.001	0.026	0.011	0.008
2	0.083	-0.012	0.020	0	0
4	0.050	-0.007	0.001	0	0
6	0.036	-0.005	0.001	0	0

n / m	0	1	2	3	4
0	0.001	0.026	0.011	0.008	0.005
2	-0.012	0.020	0	0	0
4	-0.007	0.001	0	0	0
6	-0.005	0.001	0	0	0
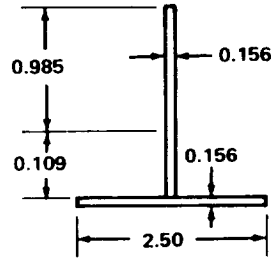
n / m	0	1	2	3	4
0	0.561	0.002	0.064	0.034	0.030
2	0.203	-0.038	0.008	-0.001	0
4	0.190	-0.036	0.007	-0.001	0
6	0.213	-0.040	0.008	-0.002	0

n / m	0	1	2	3	4
0	0.002	0.064	0.034	0.030	0.024
2	-0.038	0.008	-0.001	0	0
4	-0.036	0.007	-0.001	0	0
6	-0.040	0.008	-0.002	0	0

TABLE 3.0-3.   (Continued)
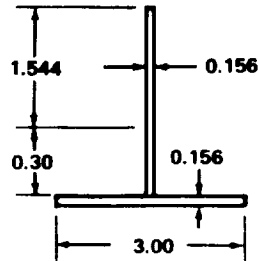
$$F_0 = \frac{1}{V_{mn}} \int V \, dA_0 \qquad\qquad F_1 = \frac{1}{V_{mn}} \int Vy \, dA_0$$

m \ n	0	1	2	3	4
0	0.756	0.002	0.261	0.195	0.284
2	0.352	-0.132	0.051	-0.019	0.008
4	0.474	-0.179	0.069	-0.027	0.011
6	0.762	-0.288	0.110	-0.043	0.017

m \ n	0	1	2	3	4
0	0.002	0.261	0.195	0.284	0.348
2	-0.132	0.051	-0.019	0.008	-0.002
4	-0.179	0.069	-0.027	0.011	-0.004
6	-0.288	0.110	-0.043	0.017	-0.007
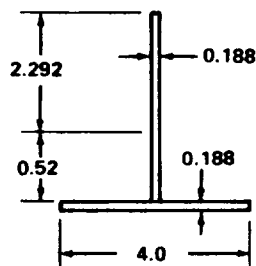
m \ n	0	1	2	3	4
0	1.281	0.007	1.049	1.115	2.492
2	1.004	-0.614	0.383	-0.233	0.156
4	2.406	-1.478	0.914	-0.570	0.358
6	6.875	-4.222	2.612	-1.629	1.023

m \ n	0	1	2	3	4
0	0.007	1.049	1.115	2.492	4.471
2	-0.614	0.383	-0.233	0.156	-0.081
4	-1.478	0.914	-0.570	0.358	-0.226
6	-4.222	2.612	-1.629	1.023	-0.647

TABLE 3.0-3. (Continued)
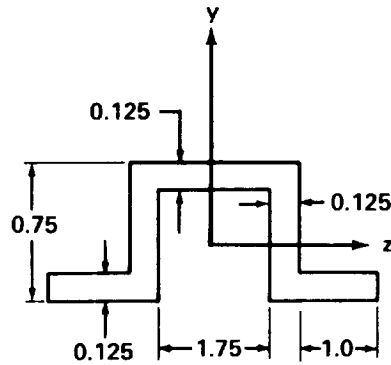
$$F_0 = \frac{1}{V_{mn}} \int V \, dA_0$$

n / m	0	1	2	3	4	5
0	0.656	0.734×10^{-3}	0.55×10^{-1}	0.165×10^{-2}	0.559×10^{-2}	0.34×10^{-3}
1	0.0	0.0	0.0	0.0	0.0	0.0
2	0.804	-0.152	0.659×10^{-1}	-0.135×10^{-1}	0.627×10^{-2}	-0.125×10^{-2}
3	0.0	0.0	0.0	0.0	0.0	0.0
4	0.172×10^{1}	-0.449	0.148	-0.409×10^{-1}	0.14×10^{-1}	-0.393×10^{-2}
5	0.0	0.0	0.0	0.0	0.0	0.0

$$F_{1y} = \frac{1}{V_{mn}} \int V y \, dA_0$$

n / m	0	1	2	3	4	5
0	0.734×10^{-3}	0.55×10^{-1}	0.165×10^{-2}	0.559×10^{-2}	0.34×10^{-3}	0.612×10^{-3}
1	0.0	0.0	0.0	0.0	0.0	0.0
2	-0.152	0.66×10^{-1}	-0.135×10^{-1}	0.627×10^{-1}	-0.125×10^{-2}	0.638×10^{-3}
3	0.0	0.0	0.0	0.0	0.0	0.0
4	-0.449	0.148	-0.409×10^{-1}	0.14×10^{-1}	-0.393×10^{-2}	0.139×10^{-2}
5	0.0	0.0	0.0	0.0	0.0	0.0

$$F_{1z} = \frac{1}{V_{mn}} \int V z \, dA_0$$

n / m	0	1	2	3	4	5
0	0.0	0.0	0.0	0.0	0.0	0.0
1	0.639	-0.155	0.581×10^{-1}	-0.138×10^{-1}	0.561×10^{-2}	-0.13×10^{-2}
2	0.0	0.0	0.0	0.0	0.0	0.0
3	0.158×10^{1}	-0.451	0.141	-0.413×10^{-1}	0.134×10^{-1}	-0.397×10^{-2}
4	0.0	0.0	0.0	0.0	0.0	0.0
5	0.455×10^{1}	-0.134×10^{1}	0.406	-0.123	0.384×10^{-1}	-0.119×10^{-1}

TABLE 3.0-3. (Continued)
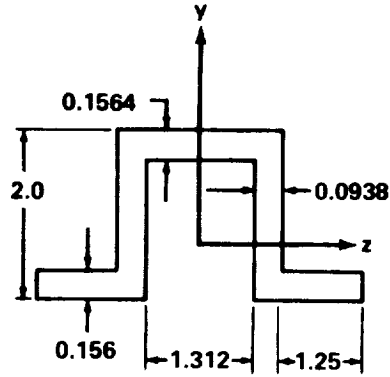
$$F_0 = \frac{1}{V_{mn}} \int V \, dA_0$$

m \ n	0	1	2	3	4	5
0	0.972	-0.901×10^{-2}	0.603	0.161	0.517	0.289
1	0.0	0.0	0.0	0.0	0.0	0.0
2	1.	-0.534	0.554	-0.273	0.352	-0.121
3	0.0	0.0	0.0	0.0	0.0	0.0
4	0.209×10^1	-0.148×10^1	0.118×10^1	-0.838	0.694	-0.476
5	0.0	0.0	0.0	0.0	0.0	0.0

$$F_{1_y} = \frac{1}{V_{mn}} \int V y \, dA_0$$

m \ n	0	1	2	3	4	5
0	-0.901×10^{-2}	0.603	0.161	0.517	0.289	0.514
1	0.0	0.0	0.0	0.0	0.0	0.0
2	-0.534	0.554	-0.273	0.352	-0.121	0.247
3	0.0	0.0	0.0	0.0	0.0	0.0
4	-0.148×10^1	0.118×10^1	-0.838	0.694	-0.476	0.422
5	0.0	0.0	0.0	0.0	0.0	0.0

$$F_{1_z} = \frac{1}{V_{mn}} \int V z \, dA_0$$

m \ n	0	1	2	3	4	5
0	0.0	0.0	0.0	0.0	0.0	0.0
1	0.82	-0.565	0.487	-0.305	0.304	-0.155
2	0.0	0.0	0.0	0.0	0.0	0.0
3	0.2×10^1	-0.149×10^1	0.115×10^1	-0.854	0.67	-0.493
4	0.0	0.0	0.0	0.0	0.0	0.0
5	0.572×10^1	-0.431×10^1	0.327×10^1	-0.248×10^1	0.19×10^1	-0.145×10^1

TABLE 3.0-3. (Continued)
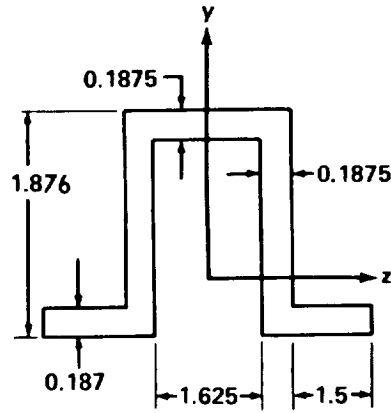
$$F_0 \quad \frac{1}{V_{mn}} \int V \, dA_0$$

m \ n	0	1	2	3	4	5
0	0.157×10^1	0.335×10^{-1}	0.798	0.23	0.584	0.326
1	0.0	0.0	0.0	0.0	0.0	0.0
2	0.248×10^1	-0.109×10^1	0.111×10^1	-0.445	0.602	-0.142
3	0.0	0.0	0.0	0.0	0.0	0.0
4	0.777×10^1	-0.486×10^1	0.36×10^1	-0.227×10^1	0.178×10^1	-0.106×10^1
5	0.0	0.0	0.0	0.0	0.0	0.0

$$F_{1y} \quad \frac{1}{V_{mn}} \int Vy \, dA_0$$

m \ n	0	1	2	3	4	5
0	0.335×10^{-1}	0.798	0.23	0.584	0.326	0.502
1	0.0	0.0	0.0	0.0	0.0	0.0
2	-0.109×10^1	0.111×10^1	-0.445	0.602	-0.142	0.37
3	0.0	0.0	0.0	0.0	0.0	0.0
4	-0.486×10^1	0.36×10^1	-0.227×10^1	0.178×10^1	-0.106×10^1	0.921
5	0.0	0.0	0.0	0.0	0.0	0.0

$$F_{1z} \quad \frac{1}{V_{mn}} \int Vz \, dA_0$$

m \ n	0	1	2	3	4	5
0	0.0	0.0	0.0	0.0	0.0	0.0
1	0.19×10^1	-0.118×10^1	0.93	-0.529	0.485	-0.221
2	0.0	0.0	0.0	0.0	0.0	0.0
3	0.728×10^1	-0.494×10^1	0.345×10^1	-0.234×10^1	0.168×10^1	-0.113×10^1
4	0.0	0.0	0.0	0.0	0.0	0.0
5	0.327×10^2	-0.224×10^2	0.154×10^2	-0.107×10^2	0.745×10^1	-0.52×10^1

TABLE 3.0-3. (Continued)
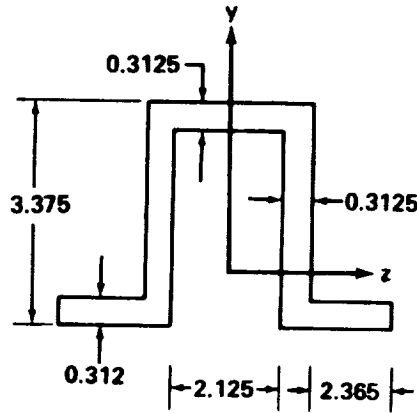
$$F_0 = \frac{1}{V_{mn}} \int V \, dA_0$$

m \ n	0	1	2	3	4	5
0	0.425×10^1	0.604×10^{-1}	0.668×10^1	0.331×10^1	0.157×10^2	0.159×10^2
1	0.0	0.0	0.0	0.0	0.0	0.0
2	0.318×10^2	-0.112×10^2	0.197×10^2	-0.149×10^2	0.337×10^2	-0.159×10^2
3	0.0	0.0	0.0	0.0	0.0	0.0
4	0.959×10^2	-0.109×10^3	0.142×10^3	-0.164×10^3	0.223×10^7	-0.246×10^3
5	0.0	0.0	0.0	0.0	0.0	0.0

$$F_{1_y} = \frac{1}{V_{mn}} \int Vy \, dA_0$$

m \ n	0	1	2	3	4	5
0	0.604×10^{-1}	0.668×10^1	0.331×10^1	0.157×10^2	0.159×10^2	0.440×10^2
1	0.0	0.0	0.0	0.0	0.0	0.0
2	-0.112×10^2	0.197×10^2	-0.149×10^2	0.337×10^2	-0.159×10^2	0.657×10^2
3	0.0	0.0	0.0	0.0	0.0	0.0
4	-0.109×10^3	0.142×10^3	-0.164×10^3	0.223×10^3	-0.246×10^3	0.365×10^3
5	0.0	0.0	0.0	0.0	0.0	0.0

$$F_{1_z} = \frac{1}{V_{mn}} \int Vz \, dA_0$$

m \ n	0	1	2	3	4	5
0	0.0	0.0	0.0	0.0	0.0	0.0
1	0.106×10^2	-0.122×10^2	0.164×10^2	-0.177×10^2	0.269×10^2	-0.246×10^7
2	0.0	0.0	0.0	0.0	0.0	0.0
3	0.911×10^2	-0.111×10^3	0.137×10^3	-0.168×10^3	0.212×10^3	-0.259×10^3
4	0.0	0.0	0.0	0.0	0.0	0.0
5	0.914×10^3	-0.112×10^4	0.138×10^4	-0.17×10^4	0.212×10^4	-0.264×10^4

TABLE 3.0-3. (Continued)
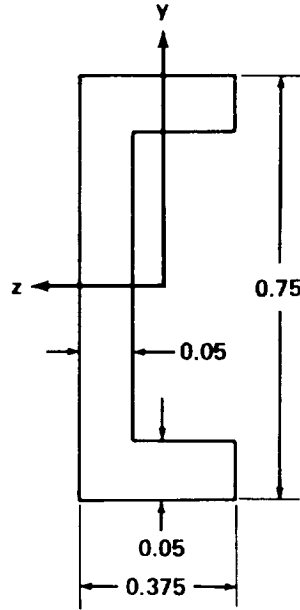
$$F_0 \quad \frac{1}{V_{mn}} \int V\, dA_0$$

n \ m	0	1	2	3	4	5
0	0.174×10^{-1}	0.0	-0.709×10^{-3}	0.0	-0.156×10^{-3}	0.0
1	-0.375×10^{-5}	0.0	-0.248×10^{-3}	0.0	-0.366×10^{-4}	0.0
2	-0.307×10^{-3}	0.0	-0.598×10^{-4}	0.0	-0.792×10^{-5}	0.0
3	-0.925×10^{-4}	0.0	-0.134×10^{-4}	0.0	-0.17×10^{-5}	0.0
4	-0.226×10^{-4}	0.0	-0.297×10^{-5}	0.0	-0.371×10^{-6}	0.0
5	-0.527×10^{-5}	0.0	-0.665×10^{-6}	0.0	-0.826×10^{-7}	0.0

$$F_{1y} \quad \frac{1}{V_{mn}} \int Vy\, dA_0$$

n \ m	0	1	2	3	4	5
0	0.0	-0.709×10^{-3}	0.0	-0.156×10^{-3}	0.0	-0.23×10^{-4}
1	0.0	-0.248×10^{-3}	0.0	-0.366×10^{-4}	0.0	-0.486×10^{-5}
2	0.0	-0.598×10^{-4}	0.0	-0.792×10^{-5}	0.0	-0.101×10^{-5}
3	0.0	-0.134×10^{-4}	0.0	-0.17×10^{-5}	0.0	-0.214×10^{-6}
4	0.0	-0.297×10^{-5}	0.0	-0.371×10^{-6}	0.0	-0.464×10^{-7}
5	0.0	-0.665×10^{-6}	0.0	-0.826×10^{-7}	0.0	-0.103×10^{-7}

$$F_{1z} \quad \frac{1}{V_{mn}} \int Vz\, dA_0$$

n \ m	0	1	2	3	4	5
0	-0.375×10^{-5}	0.0	-0.248×10^{-3}	0.0	-0.366×10^{-4}	0.0
1	-0.307×10^{-3}	0.0	-0.598×10^{-4}	0.0	-0.792×10^{-5}	0.0
2	-0.925×10^{-4}	0.0	-0.134×10^{-4}	0.0	-0.17×10^{-5}	0.0
3	-0.226×10^{-4}	0.0	-0.297×10^{-5}	0.0	-0.371×10^{-6}	0.0
4	-0.527×10^{-5}	0.0	-0.665×10^{-6}	0.0	-0.826×10^{-7}	0.0
5	-0.122×10^{-5}	0.0	-0.151×10^{-6}	0.0	-0.188×10^{-7}	0.0

TABLE 3.0-3. (Continued)
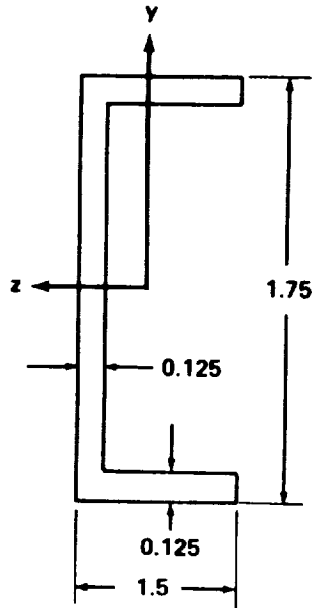
$$F_0 = \frac{1}{V_{mn}} \int V \, dA_0$$

m \ n	0	1	2	3	4	5
0	0.885×10^{-1}	0.0	-0.303×10^{-1}	0.0	-0.318×10^{-1}	0.0
1	0.175×10^{-1}	0.0	-0.319×10^{-1}	0.0	-0.269×10^{-1}	0.0
2	-0.118×10^{-1}	0.0	-0.292×10^{-1}	0.0	-0.223×10^{-1}	0.0
3	-0.223×10^{-1}	0.0	-0.254×10^{-1}	0.0	-0.183×10^{-1}	0.0
4	-0.246×10^{-1}	0.0	-0.215×10^{-1}	0.0	-0.15×10^{-1}	0.0
5	-0.235×10^{-1}	0.0	-0.182×10^{-1}	0.0	-0.125×10^{-1}	0.0

$$F_{i_y} = \frac{1}{V_{mn}} \int Vy \, dA_0$$

m \ n	0	1	2	3	4	5
0	0.0	-0.303×10^{-1}	0.0	-0.318×10^{-1}	0.0	-0.246×10^{-1}
1	0.0	-0.311×10^{-1}	0.0	-0.269×10^{-1}	0.0	-0.197×10^{-1}
2	0.0	-0.292×10^{-1}	0.0	-0.223×10^{-1}	0.0	-0.157×10^{-1}
3	0.0	-0.254×10^{-1}	0.0	-0.183×10^{-1}	0.0	-0.127×10^{-1}
4	0.0	-0.215×10^{-1}	0.0	-0.15×10^{-1}	0.0	-0.103×10^{-1}
5	0.0	-0.182×10^{-1}	0.0	-0.125×10^{-1}	0.0	-0.847×10^{-2}

$$F_{i_z} = \frac{1}{V_{mn}} \int Vz \, dA_0$$

m \ n	0	1	2	3	4	5
0	0.175×10^{-1}	0.0	-0.319×10^{-1}	0.0	-0.269×10^{-1}	0.0
1	-0.118×10^{-1}	0.0	-0.292×10^{-1}	0.0	-0.223×10^{-1}	0.0
2	-0.223×10^{-1}	0.0	-0.254×10^{-1}	0.0	-0.183×10^{-1}	0.0
3	-0.246×10^{-1}	0.0	-0.215×10^{-1}	0.0	-0.15×10^{-1}	0.0
4	-0.215×10^{-1}	0.0	-0.182×10^{-1}	0.0	-0.125×10^{-1}	0.0
5	-0.212×10^{-1}	0.0	-0.154×10^{-1}	0.0	-0.104×10^{-1}	0.0

TABLE 3.0-3. (Continued)
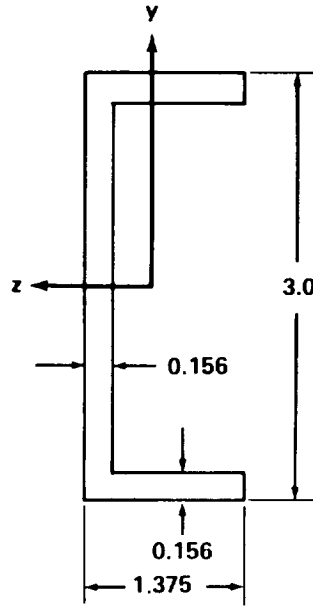
$$F_0 \quad \frac{1}{V_{mn}} \int V \, dA_0$$

n m	0	1	2	3	4	5
0	0.231	0.0	-0.128	0.0	-0.50	0.0
1	-0.19×10^{-3}	0.0	-0.184	0.0	-0.448	0.0
2	-0.54×10^{-1}	0.0	-0.167	0.0	-0.363	0.0
3	-0.598×10^{-1}	0.0	-0.14	0.0	-0.291	0.0
4	-0.542×10^{-1}	0.0	-0.116	0.0	-0.238	0.0
5	-0.471×10^{-1}	0.0	-0.973×10^{-1}	0.0	-0.198	0.0

$$F_{1y} \quad \frac{1}{V_{mn}} \int Vy \, dA_0$$

n m	0	1	2	3	4	5
0	0.0	-0.128	0.0	-0.50	0.0	-0.123×10^{1}
1	0.0	-0.184	0.0	-0.448	0.0	-0.977
2	0.0	-0.167	0.0	-0.363	0.0	-0.76
3	0.0	-0.14	0.0	-0.291	0.0	-0.601
4	0.0	-0.116	0.0	-0.228	0.0	-0.487
5	0.0	-0.073×10^{-1}	0.0	-0.198	0.0	-0.406

$$F_{1z} \quad \frac{1}{V_{mn}} \int Vz \, dA_0$$

n m	0	1	2	3	4	5
0	-0.19×10^{-3}	0.0	-0.184	0.0	-0.448	0.0
1	-0.54×10^{-1}	0.0	-0.167	0.0	-0.363	0.0
2	-0.598×10^{-1}	0.0	-0.14	0.0	-0.291	0.0
3	-0.542×10^{-1}	0.0	-0.116	0.0	-0.238	0.0
4	-0.471×10^{-1}	0.0	-0.473×10^{-1}	0.0	-0.198	0.0
5	-0.407×10^{-1}	0.0	-0.831×10^{-1}	0.0	-0.168	0.0

TABLE 3.0-3. (Continued)
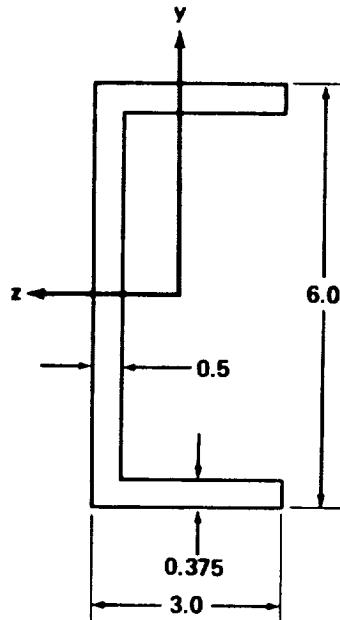
$$F_0 \quad \frac{1}{V_{mn}} \int V\, dA_0$$

n / m	0	1	2	3	4	5
0	0.161×10^1	0.0	-0.197×10^1	0.0	-0.388×10^2	0.0
1	0.375×10^{-3}	0.0	-0.852×10^1	0.0	-0.812×10^2	0.0
2	-0.149×10^1	0.0	-0.171×10^2	0.0	-0.144×10^3	0.0
3	-0.349×10^1	0.0	-0.31×10^2	0.0	-0.253×10^3	0.0
4	-0.681×10^1	0.0	-0.562×10^2	0.0	-0.451×10^3	0.0
5	-0.128×10^2	0.0	-0.103×10^3	0.0	-0.826×10^3	0.0

$$F_{1_y} \quad \frac{1}{V_{mn}} \int Vy\, dA_0$$

n / m	0	1	2	3	4	5
0	0.0	-0.197×10^1	0.0	-0.388×10^2	0.0	-0.388×10^3
1	0.0	-0.852×10^1	0.0	-0.812×10^2	0.0	-0.695×10^3
2	0.0	-0.171×10^2	0.0	-0.144×10^3	0.0	-0.118×10^4
3	0.0	-0.31×10^2	0.0	-0.253×10^3	0.0	-0.204×10^4
4	0.0	-0.562×10^2	0.0	-0.451×10^3	0.0	-0.363×10^4
5	0.0	-0.103×10^3	0.0	-0.826×10^3	0.0	-0.663×10^4

$$F_{1_z} \quad \frac{1}{V_{mn}} \int Vz\, dA_0$$

n / m	0	1	2	3	4	5
0	0.375×10^{-3}	0.0	-0.852×10^1	0.0	-0.812×10^2	0.0
1	-0.149×10^1	0.0	-0.171×10^2	0.0	-0.144×10^3	0.0
2	-0.349×10^1	0.0	-0.31×10^2	0.0	-0.253×10^3	0.0
3	-0.681×10^1	0.0	-0.562×10^2	0.0	-0.451×10^3	0.0
4	-0.128×10^2	0.0	-0.103×10^3	0.0	-0.826×10^3	0.0
5	-0.243×10^3	0.0	-0.193×10^3	0.0	-0.154×10^4	0.0

TABLE 3.0-3. (Continued)
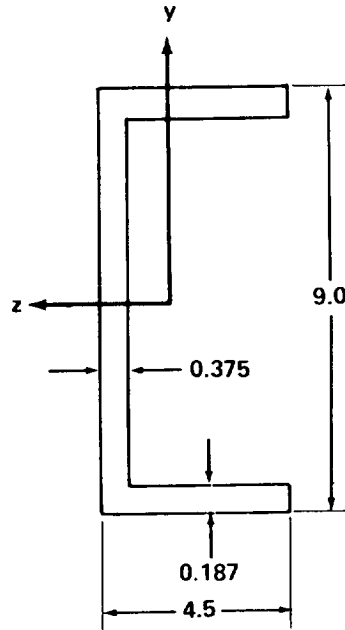
$$F_0 \quad \frac{1}{V_{mn}} \int V\, dA_0$$

n / m	0	1	2	3	4	5
0	0.222×10^1	0.0	0.302	0.0	-0.16×10^3	0.0
1	-0.165×10^{-1}	0.0	-0.304×10^2	0.0	-0.706×10^3	0.0
2	-0.414×10^1	0.0	-0.102×10^3	0.0	-0.207×10^4	0.0
3	-0.146×10^2	0.0	-0.3×10^3	0.0	-0.589×10^4	0.0
4	-0.45×10^2	0.0	-0.884×10^3	0.0	-0.172×10^5	0.0
5	-0.137×10^3	0.0	-0.267×10^4	0.0	-0.52×10^5	0.0

$$F_{1_y} \quad \frac{1}{V_{mn}} \int V y\, dA_0$$

n / m	0	1	2	3	4	5
0	0.0	0.302	0.0	-0.16×10^3	0.0	-0.449×10^4
1	0.0	-0.304×10^2	0.0	-0.706×10^3	0.0	-0.147×10^5
2	0.0	-0.102×10^3	0.0	-0.207×10^4	0.0	-0.409×10^5
3	0.0	-0.3×10^3	0.0	-0.589×10^4	0.0	-0.115×10^6
4	0.0	-0.884×10^3	0.0	-0.172×10^5	0.0	-0.335×10^6
5	0.0	-0.267×10^4	0.0	-0.52×10^5	0.0	-0.101×10^7

$$F_{1_z} \quad \frac{1}{V_{mn}} \int V z\, dA_0$$

n / m	0	1	2	3	4	5
0	-0.165×10^{-1}	0.0	-0.304×10^2	0.0	-0.706×10^3	0.0
1	-0.414×10^1	0.0	-0.102×10^3	0.0	-0.207×10^4	0.0
2	-0.146×10^2	0.0	-0.3×10^3	0.0	-0.589×10^4	0.0
3	-0.45×10^2	0.0	-0.884×10^3	0.0	-0.172×10^5	0.0
4	-0.137×10^3	0.0	-0.267×10^4	0.0	-0.52×10^5	0.0
5	-0.426×10^3	0.0	-0.829×10^4	0.0	-0.161×10^6	0.0

TABLE 3.0-3. (Continued)
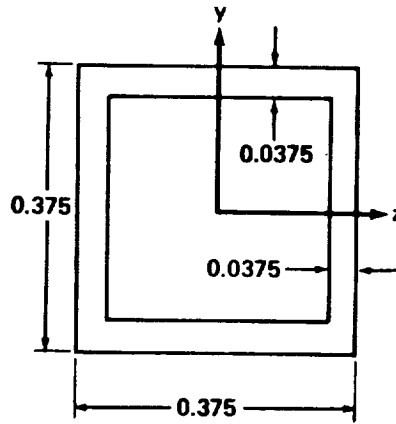
$$F_0 = \frac{1}{V_{mn}} \int V \, dA_0$$

m \ n	0	1	2	3	4	5
0	0.506×10^{-1}	0.0	0.973×10^{-3}	0.0	0.256×10^{-4}	0.0
1	0.0	0.0	0.0	0.0	0.0	0.0
2	0.973×10^{-3}	0.0	0.142×10^{-4}	0.0	0.339×10^{-6}	0.0
3	0.0	0.0	0.0	0.0	0.0	0.0
4	0.256×10^{-4}	0.0	0.339×10^{-6}	0.0	0.767×10^{-8}	0.0
5	0.0	0.0	0.0	0.0	0.0	0.0

$$F_{1y} = \frac{1}{V_{mn}} \int Vy \, dA_0$$

m \ n	0	1	2	3	4	5
0	0.0	0.973×10^{-3}	0.0	0.256×10^{-4}	0.0	0.726×10^{-6}
1	0.0	0.0	0.0	0.0	0.0	0.0
2	0.0	0.142×10^{-4}	0.0	0.339×10^{-6}	0.0	0.913×10^{-8}
3	0.0	0.0	0.0	0.0	0.0	0.0
4	0.0	0.339×10^{-6}	0.0	0.767×10^{-8}	0.0	0.2×10^{-9}
5	0.0	0.0	0.0	0.0	0.0	0.0

$$F_{1z} = \frac{1}{V_{mn}} \int Vz \, dA_0$$

m \ n	0	1	2	3	4	5
0	0.0	0.0	0.0	0.0	0.0	0.0
1	0.973×10^{-3}	0.0	0.142×10^{-4}	0.0	0.339×10^{-6}	0.0
2	0.0	0.0	0.0	0.0	0.0	0.0
3	0.256×10^{-4}	0.0	0.339×10^{-6}	0.0	0.767×10^{-8}	0.0
4	0.0	0.0	0.0	0.0	0.0	0.0
5	0.726×10^{-6}	0.0	0.915×10^{-8}	0.0	0.2×10^{-9}	0.0

TABLE 3.0-3. (Continued)
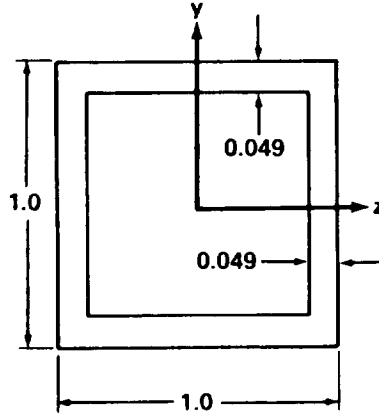
$$F_0 \quad \frac{1}{V_{mn}} \int V \, dA_0$$

m \ n	0	1	2	3	4	5
0	0.186	0.0	0.282×10^{-1}	0.0	0.577×10^{-2}	0.0
1	0.0	0.0	0.0	0.0	0.0	0.0
2	0.282×10^{-1}	0.0	0.32×10^{-2}	0.0	0.585×10^{-3}	0.0
3	0.0	0.0	0.0	0.0	0.0	0.0
4	0.577×10^{-2}	0.0	0.585×10^{-3}	0.0	0.1×10^{-3}	0.0
5	0.0	0.0	0.0	0.0	0.0	0.0

$$F_{1_y} \quad \frac{1}{V_{mn}} \int V y \, dA_0$$

m \ n	0	1	2	3	4	5
0	0.0	0.282×10^{-1}	0.0	0.577×10^{-2}	0.0	0.125×10^{-2}
1	0.0	0.0	0.0	0.0	0.0	0.0
2	0.0	0.32×10^{-2}	0.0	0.585×10^{-3}	0.0	0.12×10^{-3}
3	0.0	0.0	0.0	0.0	0.0	0.0
4	0.0	0.585×10^{-3}	0.0	0.1×10^{-3}	0.0	0.198×10^{-4}
5	0.0	0.0	0.0	0.0	0.0	0.0

$$F_{1_z} \quad \frac{1}{V_{mn}} \int V z \, dA_0$$

m \ n	0	1	2	3	4	5
0	0.0	0.0	0.0	0.0	0.0	0.0
1	0.282×10^{-1}	0.0	0.32×10^{-2}	0.0	0.585×10^{-3}	0.0
2	0.0	0.0	0.0	0.0	0.0	0.0
3	0.577×10^{-2}	0.0	0.585×10^{-3}	0.0	0.1×10^{-3}	0.0
4	0.0	0.0	0.0	0.0	0.0	0.0
5	0.125×10^{-2}	0.0	0.12×10^{-3}	0.0	0.198×10^{-4}	0.0

TABLE 3.0-3. (Continued)
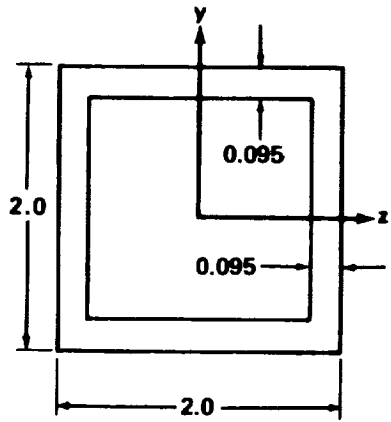
$$F_0 \quad \frac{1}{V_{mn}} \int V \, dA_0$$

n m	0	1	2	3	4	5
0	0.724	0.0	0.439	0.0	0.36	0.0
1	0.0	0.0	0.0	0.0	0.0	0.0
2	0.439	0.0	0.2	0.0	0.147	0.0
3	0.0	0.0	0.0	0.0	0.0	0.0
4	0.36	0.0	0.147	0.0	0.101	0.0
5	0.0	0.0	0.0	0.0	0.0	0.0

$$F_{l_y} \quad \frac{1}{V_{mn}} \int V_y \, dA_0$$

n m	0	1	2	3	4	5
0	0.0	0.439	0.0	0.36	0.0	0.314
1	0.0	0.0	0.0	0.0	0.0	0.0
2	0.0	0.2	0.0	0.147	0.0	0.12
3	0.0	0.0	0.0	0.0	0.0	0.0
4	0.0	0.147	0.0	0.101	0.0	0.798×10^{-1}
5	0.0	0.0	0.0	0.0	0.0	0.0

$$F_{l_z} \quad \frac{1}{V_{mn}} \int V_z \, dA_0$$

n m	0	1	2	3	4	5
0	0.0	0.0	0.0	0.0	0.0	0.0
1	0.439	0.0	0.2	0.0	0.147	0.0
2	0.0	0.0	0.0	0.0	0.0	0.0
3	0.36	0.0	0.147	0.0	0.101	0.0
4	0.0	0.0	0.0	0.0	0.0	0.0
5	0.314	0.0	0.12	0.0	0.798×10^{-1}	0.0

TABLE 3.0-3. (Continued)
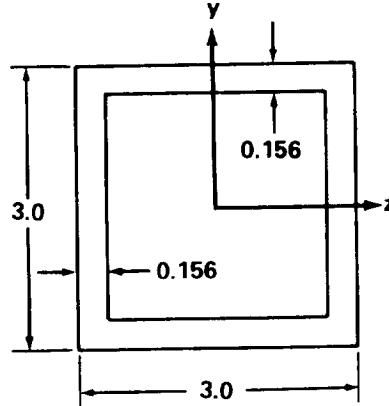
$$F_0 \quad \frac{1}{V_{mn}} \int V \, dA_0$$

m \ n	0	1	2	3	4	5
0	0.177×10^1	0.0	0.24×10^1	0.0	0.44×10^1	0.0
1	0.0	0.0	0.0	0.0	0.0	0.0
2	0.24×10^1	0.0	0.244×10^1	0.0	0.4×10^1	0.0
3	0.0	0.0	0.0	0.0	0.0	0.0
4	0.44×10^1	0.0	0.4×10^1	0.0	0.615×10^1	0.0
5	0.0	0.0	0.0	0.0	0.0	0.0

$$F_{1_y} \quad \frac{1}{V_{mn}} \int Vy \, dA_0$$

m \ n	0	1	2	3	4	5
0	0.0	0.24×10^1	0.0	0.44×10^1	0.0	0.856×10^1
1	0.0	0.0	0.0	0.0	0.0	0.0
2	0.0	0.244×10^1	0.0	0.4×10^1	0.0	0.732×10^1
3	0.0	0.0	0.0	0.0	0.0	0.0
4	0.0	0.4×10^1	0.0	0.615×10^1	0.0	0.109×10^2
5	0.0	0.0	0.0	0.0	0.0	0.0

$$F_{1_z} \quad \frac{1}{V_{mn}} \int Vz \, dA_0$$

m \ n	0	1	2	3	4	5
0	0.0	0.0	0.0	0.0	0.0	0.0
1	0.24×10^1	0.0	0.244×10^1	0.0	0.4×10^1	0.0
2	0.0	0.0	0.0	0.0	0.0	0.0
3	0.44×10^1	0.0	0.4×10^1	0.0	0.615×10^1	0.0
4	0.0	0.0	0.0	0.0	0.0	0.0
5	0.856×10^1	0.0	0.732×10^1	0.0	0.109×10^2	0.0

TABLE 3.0-3. (Continued)
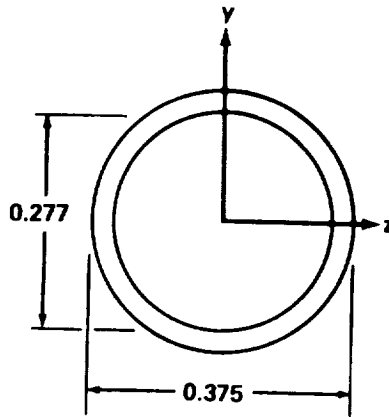
$$F_0 \quad \frac{1}{V_{mn}} \int V \, dA_0$$

n \ m	0	1	2	3	4	5
0	0.508×10^{-1}	0.0	0.712×10^{-3}	0.0	0.154×10^{-4}	0.0
1	0.0	0.0	0.0	0.0	0.0	0.0
2	0.679×10^{-3}	0.0	0.466×10^{-5}	0.0	0.647×10^{-7}	0.0
3	0.0	0.0	0.0	0.0	0.0	0.0
4	0.143×10^{-4}	0.0	0.7×10^{-7}	0.0	0.809×10^{-9}	0.0
5	0.0	0.0	0.0	0.0	0.0	0.0

$$F_{1y} \quad \frac{1}{V_{mn}} \int V_y \, dA_0$$

n \ m	0	1	2	3	4	5
0	0.0	0.712×10^{-3}	0.0	0.154×10^{-4}	0.0	0.382×10^{-6}
1	0.0	0.0	0.0	0.0	0.0	0.0
2	0.0	0.466×10^{-5}	0.0	0.647×10^{-7}	0.0	0.113×10^{-8}
3	0.0	0.0	0.0	0.0	0.0	0.0
4	0.0	0.7×10^{-7}	0.0	0.809×10^{-9}	0.0	0.131×10^{-10}
5	0.0	0.0	0.0	0.0	0.0	0.0

$$F_{1z} \quad \frac{1}{V_{mn}} \int V_z \, dA_0$$

n \ m	0	1	2	3	4	5
0	0.0	0.0	0.0	0.0	0.0	0.0
1	0.679×10^{-3}	0.0	0.466×10^{-5}	0.0	0.647×10^{-7}	0.0
2	0.0	0.0	0.0	0.0	0.0	0.0
3	0.143×10^{-4}	0.0	0.7×10^{-7}	0.0	0.809×10^{-9}	0.0
4	0.0	0.0	0.0	0.0	0.0	0.0
5	0.339×10^{-6}	0.0	0.117×10^{-8}	0.0	0.87×10^{-11}	0.0

TABLE 3.0-3. (Continued)
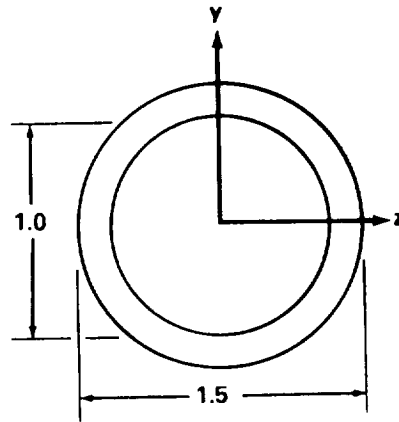
$$F_0 \qquad \frac{1}{V_{mn}} \int V \, dA_0$$

m \ n	0	1	2	3	4	5
0	0.994	0.0	0.208	0.0	0.688×10^{-1}	0.0
1	0.0	0.0	0.0	0.0	0.0	0.0
2	0.199	0.0	0.208×10^{-1}	0.0	0.447×10^{-2}	0.0
3	0.0	0.0	0.0	0.0	0.0	0.0
4	0.64×10^{-1}	0.0	0.484×10^{-2}	0.0	0.876×10^{-3}	0.0
5	0.0	0.0	0.0	0.0	0.0	0.0

$$F_{1y} \qquad \frac{1}{V_{mn}} \int Vy \, dA_0$$

m \ n	0	1	2	3	4	5
0	0.0	0.208	0.0	0.688×10^{-1}	0.0	0.264×10^{-1}
1	0.0	0.0	0.0	0.0	0.0	0.0
2	0.0	0.208×10^{-1}	0.0	0.447×10^{-2}	0.0	0.123×10^{-2}
3	0.0	0.0	0.0	0.0	0.0	0.0
4	0.0	0.484×10^{-2}	0.0	0.876×10^{-3}	0.0	0.224×10^{-3}
5	0.0	0.0	0.0	0.0	0.0	0.0

$$F_{1z} \qquad \frac{1}{V_{mn}} \int Vz \, dA_0$$

m \ n	0	1	2	3	4	5
0	0.0	0.0	0.0	0.0	0.0	0.0
1	0.199	0.0	0.208×10^{-1}	0.0	0.497×10^{-2}	0.0
2	0.0	0.0	0.0	0.0	0.0	0.0
3	0.64×10^{-1}	0.0	0.484×10^{-2}	0.0	0.876×10^{-3}	0.0
4	0.0	0.0	0.0	0.0	0.0	0.0
5	0.234×10^{-1}	0.0	0.127×10^{-2}	0.0	0.149×10^{-3}	0.0

TABLE 3.0-3. (Continued)
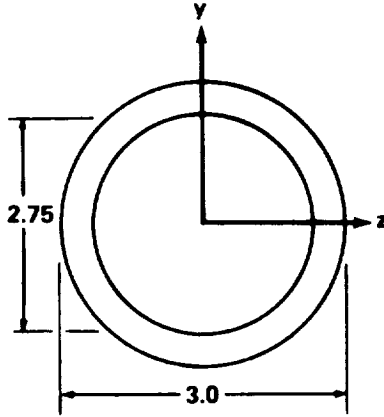
$$F_0 = \frac{1}{V_{mn}} \int V \, dA_0$$

n m	0	1	2	3	4	5
0	0.114×10^1	0.0	0.122×10^1	0.0	0.196×10^1	0.0
1	0.0	0.0	0.0	0.0	0.0	0.0
2	0.116×10^1	0.0	0.593	0.0	0.597	0.0
3	0.0	0.0	0.0	0.0	0.0	0.0
4	0.183×10^1	0.0	0.647	0.0	0.53	0.0
5	0.0	0.0	0.0	0.0	0.0	0.0

$$F_{1y} = \frac{1}{V_{mn}} \int Vy \, dA_0$$

n m	0	1	2	3	4	5
0	0.0	0.122×10^1	0.0	0.196×10^1	0.0	0.352×10^1
1	0.0	0.0	0.0	0.0	0.0	0.0
2	0.0	0.593	0.0	0.597	0.0	0.744
3	0.0	0.0	0.0	0.0	0.0	0.0
4	0.0	0.647	0.0	0.53	0.0	0.598
5	0.0	0.0	0.0	0.0	0.0	0.0

$$F_{1z} = \frac{1}{V_{mn}} \int Vz \, dA_0$$

n m	0	1	2	3	4	5
0	0.0	0.0	0.0	0.0	0.0	0.0
1	0.116×10^1	0.0	0.593	0.0	0.597	0.0
2	0.0	0.0	0.0	0.0	0.0	0.0
3	0.183×10^1	0.0	0.647	0.0	0.53	0.0
4	0.0	0.0	0.0	0.0	0.0	0.0
5	0.313×10^1	0.0	0.769	0.0	0.398	0.0

TABLE 3.0-3. (Continued)
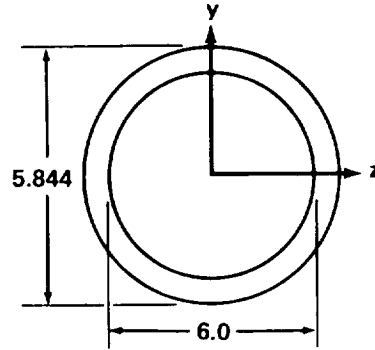
$$F_0 \quad \frac{1}{V_{mn}} \int V \, dA_0$$

m \ n	0	1	2	3	4	5
0	0.147×10^1	0.0	0.664×10^1	0.0	0.452×10^2	0.0
1	0.0	0.0	0.0	0.0	0.0	0.0
2	0.634×10^1	0.0	0.136×10^2	0.0	0.58×10^2	0.0
3	0.0	0.0	0.0	0.0	0.0	0.0
4	0.42×10^2	0.0	0.628×10^2	0.0	0.216×10^3	0.0
5	0.0	0.0	0.0	0.0	0.0	0.0

$$F_{1y} \quad \frac{1}{V_{mn}} \int Vy \, dA_0$$

m \ n	0	1	2	3	4	5
0	0.0	0.664×10^1	0.0	0.452×10^2	0.0	0.342×10^3
1	0.0	0.0	0.0	0.0	0.0	0.0
2	0.0	0.136×10^2	0.0	0.58×10^2	0.0	0.304×10^3
3	0.0	0.0	0.0	0.0	0.0	0.0
4	0.0	0.628×10^2	0.0	0.216×10^3	0.0	0.102×10^4
5	0.0	0.0	0.0	0.0	0.0	0.0

$$F_{1z} \quad \frac{1}{V_{mn}} \int Vz \, dA_0$$

m \ n	0	1	2	3	4	5
0	0.0	0.0	0.0	0.0	0.0	0.0
1	0.634×10^1	0.0	0.136×10^2	0.0	0.58×10^2	0.0
2	0.0	0.0	0.0	0.0	0.0	0.0
3	0.42×10^2	0.0	0.628×10^2	0.0	0.216×10^3	0.0
4	0.0	0.0	0.0	0.0	0.0	0.0
5	0.304×10^3	0.0	0.314×10^3	0.0	0.682×10^3	0.0

TABLE 3.0-3. (Continued)
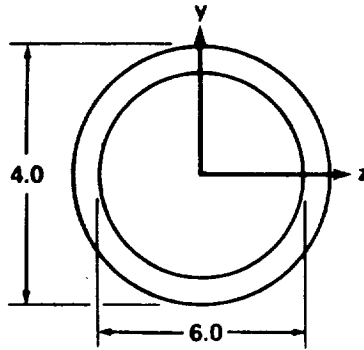
$$F_0 = \frac{1}{V_{mn}} \int V \, dA_0$$

n \ m	0	1	2	3	4	5
0	0.159×10^2	0.0	0.533×10^2	0.0	0.282×10^3	0.0
1	0.0	0.0	0.0	0.0	0.0	0.0
2	0.508×10^2	0.0	0.851×10^2	0.0	0.293×10^3	0.0
3	0.0	0.0	0.0	0.0	0.0	0.0
4	0.262×10^3	0.0	0.317×10^3	0.0	0.918×10^3	0.0
5	0.0	0.0	0.0	0.0	0.0	0.0

$$F_{1_y} = \frac{1}{V_{mn}} \int V y \, dA_0$$

n \ m	0	1	2	3	4	5
0	0.0	0.533×10^2	0.0	0.282×10^3	0.0	0.173×10^4
1	0.0	0.0	0.0	0.0	0.0	0.0
2	0.0	0.851×10^2	0.0	0.293×10^3	0.0	0.129×10^4
3	0.0	0.0	0.0	0.0	0.0	0.0
4	0.0	0.317×10^3	0.0	0.918×10^3	0.0	0.375×10^4
5	0.0	0.0	0.0	0.0	0.0	0.0

$$F_{1_z} = \frac{1}{V_{mn}} \int V z \, dA_0$$

n \ m	0	1	2	3	4	5
0	0.0	0.0	0.0	0.0	0.0	0.0
1	0.508×10^2	0.0	0.851×10^2	0.0	0.293×10^3	0.0
2	0.0	0.0	0.0	0.0	0.0	0.0
3	0.262×10^3	0.0	0.317×10^7	0.0	0.918×10^7	0.0
4	0.0	0.0	0.0	0.0	0.0	0.0
5	0.154×10^4	0.0	0.133×10^4	0.0	0.25×10^4	0.0

TABLE 3.0-3. (Concluded)
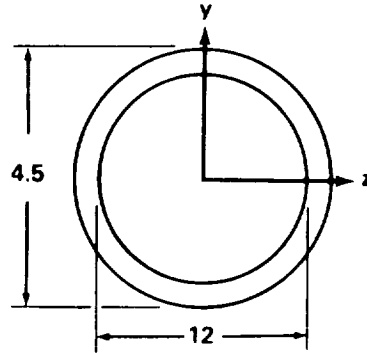
$$F_0 \qquad \frac{1}{V_{mn}} \int V \, dA_0$$

n m	0	1	2	3	4	5
0	0.934×10^1	0.0	0.166×10^3	0.0	0.446×10^4	0.0
1	0.0	0.0	0.0	0.0	0.0	0.0
2	0.159×10^3	0.0	0.135×10^4	0.0	0.225×10^5	0.0
3	0.0	0.0	0.0	0.0	0.0	0.0
4	0.414×10^4	0.0	0.244×10^5	0.0	0.332×10^6	0.0
5	0.0	0.0	0.0	0.0	0.0	0.0

$$F_{1y} \qquad \frac{1}{V_{mn}} \int Vy \, dA_0$$

n m	0	1	2	3	4	5
0	0.0	0.166×10^3	0.0	0.446×10^4	0.0	0.133×10^6
1	0.0	0.0	0.0	0.0	0.0	0.0
2	0.0	0.135×10^4	0.0	0.225×10^5	0.0	0.465×10^6
3	0.0	0.0	0.0	0.0	0.0	0.0
4	0.0	0.244×10^5	0.0	0.332×10^6	0.0	0.619×10^7
5	0.0	0.0	0.0	0.0	0.0	0.0

$$F_{1z} \qquad \frac{1}{V_{mn}} \int Vz \, dA_0$$

n m	0	1	2	3	4	5
0	0.0	0.0	0.0	0.0	0.0	0.0
1	0.159×10^3	0.0	0.135×10^4	0.0	0.225×10^5	0.0
2	0.0	0.0	0.0	0.0	0.0	0.0
3	0.414×10^4	0.0	0.244×10^5	0.0	0.332×10^6	0.0
4	0.0	0.0	0.0	0.0	0.0	0.0
5	0.118×10^6	0.0	0.481×10^6	0.0	0.412×10^7	0.0

B. Results:

$$v(x) = - \int_0^x \int_0^{x_2} \frac{M_{T_z}(x_1)}{EI_z(x_1)} \, dx_1 \, dx_2 + \frac{x}{L} \int_0^L \int_0^{x_2} \frac{M_{T_z}(x_1)}{EI_z(x_1)} \, dx_1 \, dx_2$$

$$v(x) = \frac{\alpha F_1}{I_{0_z}} \left(\frac{x}{L} I_1 - I_{1_x} \right) L^2 \qquad .$$

where

$$I_1 = \int_0^1 \int_0^1 \frac{f(x_1)}{g^2(x_1)} \, dx_1 \, dx_2 \quad \text{and} \quad I_{1_x} = \int_0^x \int_0^{x_2} \frac{f(x_1)}{g^2(x_1)} \, dx_1 \, dx_2$$

$$u_{av}(x) = \frac{1}{E} \int_0^x \frac{1}{A} \int_A \alpha\, ET\, dA\, dx = \frac{\alpha F_0 L}{A_0} \int_0^{x_1} f(x_1) \, dx_1$$

$$M_z(x) = 0$$

$$\sigma_{xx} = - \alpha\, ET + \frac{P_T}{A} + \left(\frac{M_{T_y} + M_y}{I_y} \right) + \left(\frac{M_{T_z}}{I_z} \right) y \qquad .$$

M_y may or may not be zero, depending upon the boundary condition.

If end B is hinged, then

$$u_{av}(x) = 0 \quad ,$$

$$V_0 = M_0 = 0 \quad ,$$

$$v(x) = \text{same as above,}$$

$$\sigma_{xx} = - \alpha\, ET + \left(\frac{M_{T_y} + M_y}{I_y} \right) + \left(\frac{M_{T_z}}{I_z} \right) y \quad ,$$

axial force $P = \int_A \alpha\, ET\, dA \qquad .$

II. Fixed-Fixed Beam.
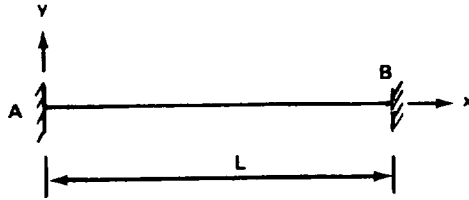
A. Boundary Conditions:

$$v = \frac{dv}{dx} = 0, \quad @ \quad x = 0, L \, ,$$

$$v(x) = - \int_0^x \int_0^{x_2} \left[\frac{M_{T_z}(x_1) + M_{0_z} + x_1 V_{0_z}}{EI_z(x_1)} \right] dx_1 \, dx_2 \qquad ,$$

$$v\left(\frac{x}{L}\right) = - \frac{\alpha F_1}{I_{z_0}} L^2 \left(I_{1x} + F_2 I_{2x} + F_3 I_{3x} \right) \qquad ,$$

where

$$I_{2x} = \int_0^x \int_0^{x_2} \frac{dx}{h(x_1) \, g^3(x_1)} \, dx_2 \quad , \quad I_2 = \int_0^1 \int_0^{x_2} \frac{dx}{h(x_1) \, g^3(x_1)} \, dx_2 \qquad ,$$

$$I_{3x} = \int_0^x \int_0^{x_2} \frac{x \, dx \, dx_2}{h(x_1) \, g^3(x_1)} \quad , \quad I_3 = \int_0^1 \int_0^{x_2} \frac{x \, dx}{h(x_1) \, g^3(x_1)} \, dx_2 \qquad ,$$

$$F_2 = \frac{I_3 \int_0^1 \frac{f(x_1)}{g^2(x_1)} - I_1 \int_0^1 \frac{x_1 \, dx_1}{h(x_1) \, g^3(x_1)}}{I_2 \int_0^1 \frac{x_1 \, dx_1}{h(x_1) \, g^3(x_1)} - I_3 \int_0^1 \frac{dx_1}{h(x_1) \, g^3(x_1)}} \qquad ,$$

$$F_3 = \frac{I_1 \int_0^1 \dfrac{dx_1}{h(x_1)\, g^3(x_1)} - I_2 \int_0^1 \dfrac{f(x_1)}{g^2(x_1)}\, dx_1}{I_2 \int_0^1 \dfrac{x_1\, dx_1}{h(x_1)\, g^3(x_1)} - I_3 \int_0^1 \dfrac{dx_1}{h(x_1)\, g^3(x_1)}}$$

(Table 3.0-4 gives values for F_2 and F_3)

$$M_{0_z} = \alpha\, E\, F_1\, F_2 \qquad ,$$

$$V_{0_z} = \frac{\alpha}{L}\, E\, F_1\, F_3 \qquad ,$$

$$M_z(x) = M_{0_z} + x\, V_{0_z} \qquad ,$$

$$u_{av}(x) = \frac{\alpha\, F_0\, L}{A_0} \int_0^{x_1} f(x_1)\, dx_1 \qquad .$$

If the end B is restrained against longitudinal motion, then

$$u_{av}(x) = 0 \qquad ,$$

$$\sigma_{xx} = -\alpha\, ET + \left(\frac{M_{T_y} + M_y}{I_y} \right) z + \left(\frac{M_{T_z} + M_z}{I_z} \right) y \qquad ,$$

$v(x)$, M_0, V_0 are same as above.

CASE a: $EI_z(x) = $ constant, and $f(x_1) = \left(\dfrac{x}{L} \right)^q$.

$$v\left(\frac{x}{L} \right) = \frac{\alpha\, F_1\, x^2}{I_z\, (q+1)\, (q+2)} \left[\frac{x^q}{L^q} + q\left(1 - \frac{x}{L} \right) - 1 \right] \qquad ,$$

$$M_{0_z} = \frac{2\,\alpha\, E\, F_1(q-1)}{(q+1)\, (q+2)} \qquad ,$$

TABLE 3.0-4. VALUES OF CONSTANTS F_2, F_3, AND F_4

	H = 0				H = 0.5				H = 1.0		
				q = 0 (Uniform Temperature Distribution)							
G	F_2	F_3	F_4	G	F_2	F_3	F_4	G	F_2	F_3	F_4
0	-1.000	0.000	-1.502	0	-1.000	-0.500	-1.675	0	-1.000	-1.000	-1.837
0.1	-1.000	-0.100	-1.514	0.1	-0.993	-0.648	-1.684	0.1	-0.986	-1.191	-1.837
0.2	-1.000	-0.200	-1.525	0.2	-0.986	-0.794	-1.689	0.2	-0.974	-1.384	-1.838
0.3	-1.000	-0.300	-1.535	0.3	-0.981	-0.938	-1.691	0.3	-0.963	-1.571	-1.838
0.4	-1.000	-0.400	-1.544	0.4	-0.975	-1.081	-1.690	0.4	-0.957	-1.755	-1.839
0.5	-1.000	-0.500	-1.553	0.5	-0.970	-1.223	-1.701	0.5	-0.945	-1.937	-1.839
0.6	-1.000	-0.600	-1.561	0.6	-0.966	-1.364	-1.708	0.6	-0.937	-2.116	-1.840
0.7	-1.000	-0.700	-1.569	0.7	-0.962	-1.504	-1.712	0.7	-0.929	-2.294	-1.841
0.8	-1.000	-0.800	-1.575	0.8	-0.958	-1.642	-1.716	0.8	-0.922	-2.470	-1.842
0.9	-1.000	-0.900	-1.584	0.9	-0.956	-1.780	-1.719	0.9	-0.916	-2.643	-1.843
1.0	-1.000	-1.000	-1.590	1.0	-0.952	-1.918	-1.723	1.0	-0.910	-2.815	-1.844

				q = 1 (Linear Temperature Distribution)							
G	F_2	F_3	F_4	G	F_2	F_3	F_4	G	F_2	F_3	F_4
0	0.000	-1.000	-0.502	0	0.072	-1.487	-0.464	0	0.144	-1.954	-0.644
0.1	0.010	-1.098	-0.490	0.1	0.093	-1.614	-0.445	0.1	0.165	-2.109	-0.476
0.2	0.020	-1.194	-0.479	0.2	0.111	-1.739	-0.430	0.2	0.183	-2.298	-0.443
0.3	0.041	-1.284	-0.469	0.3	0.126	-1.864	-0.415	0.3	0.199	-2.480	-0.461
0.4	0.064	-1.373	-0.459	0.4	0.139	-1.985	-0.405	0.4	0.213	-2.657	-0.450
0.5	0.064	-1.460	-0.450	0.5	0.151	-2.108	-0.391	0.5	0.225	-2.801	-0.438
0.6	0.074	-1.544	-0.442	0.6	0.161	-2.186	-0.382	0.6	0.237	-2.208	-0.429
0.7	0.082	-1.626	-0.434	0.7	0.171	-2.290	-0.372	0.7	0.247	-2.457	-0.421
0.8	0.091	-1.705	-0.426	0.8	0.180	-2.391	-0.364	0.8	0.256	-2.641	-0.408
0.9	0.099	-1.785	-0.419	0.9	0.188	-2.490	-0.444	0.9	0.264	-2.862	-0.488
1.0	0.106	-1.862	-0.413	1.0	0.196	-2.588	-0.437	1.0	0.263	-2.982	-0.438

				q = 2 (Quadratic Temperature Distribution)							
G	F_2	F_3	F_4	G	F_2	F_3	F_4	G	F_2	F_3	F_4
0	0.167	-1.000	-0.252	0	0.213	-1.403	-0.281	0	0.319	-1.758	0.308
0.1	0.176	-1.068	-0.251	0.1	0.242	-1.496	-0.268	0.1	0.321	-1.891	0.557
0.2	0.184	-1.133	-0.251	0.2	0.261	-1.573	-0.256	0.2	0.329	-1.959	0.530
0.3	0.191	-1.196	-0.223	0.3	0.267	-1.679	0.246	0.3	0.335	-2.061	0.262
0.4	0.197	-1.254	-0.215	0.4	0.273	-1.753	0.236	0.4	0.341	-2.169	0.256
0.5	0.202	-1.311	-0.207	0.5	0.279	-1.829	0.237	0.5	0.347	-2.254	0.246
0.6	0.206	-1.366	-0.201	0.6	0.284	-1.903	0.249	0.6	0.351	-2.359	0.236
0.7	0.210	-1.419	-0.194	0.7	0.288	-1.970	0.212	0.7	0.354	-2.411	0.226
0.8	0.213	-1.470	-0.189	0.8	0.290	-2.097	0.365	0.8	0.357	-2.484	0.220
0.9	0.217	-1.520	-0.183	0.9	0.293	-2.041	0.199	0.9	0.358	-2.559	0.213
1.0	0.220	-1.569	0.168	1.0	0.296	-2.114	0.195	1.0	0.361	-2.600	0.207

				q = 3 (Cubic Temperature Distribution)							
G	F_2	F_3	F_4	G	F_2	F_3	F_4	G	F_2	F_3	F_4
0	0.200	-0.900	-0.144	0	0.242	-1.258	-0.169	0	0.329	-1.601	-0.185
0.1	0.204	-0.948	-0.144	0.1	0.273	-1.299	-0.157	0.1	0.331	-1.631	-0.161
0.2	0.208	-0.994	-0.135	0.2	0.263	-1.340	-0.150	0.2	0.325	-1.698	-0.163
0.3	0.211	-1.017	-0.129	0.3	0.262	-1.400	-0.145	0.3	0.327	-1.750	-0.161
0.4	0.213	-1.078	-0.123	0.4	0.260	-1.460	-0.149	0.4	0.325	-1.855	-0.147
0.5	0.215	-1.118	0.118	0.5	0.261	-1.509	-0.129	0.5	0.329	-1.873	-0.140
0.6	0.216	-1.156	-0.113	0.6	0.263	-1.560	-0.124	0.6	0.329	-1.933	-0.103
0.7	0.217	-1.192	-0.109	0.7	0.264	-1.609	-0.119	0.7	0.325	-1.986	-0.118
0.8	0.218	-1.227	-0.104	0.8	0.265	-1.643	-0.113	0.8	0.328	-2.036	-0.122
0.9	0.219	-1.261	-0.101	0.9	0.262	-1.685	0.110	0.9	0.337	-2.084	-0.118
1.0	0.219	-1.294	-0.098	1.0	0.265	-1.725	0.106	1.0	0.336	-2.131	-0.113

Notes: $h(x_1) = 1 + H\left(\dfrac{x}{L}\right)$

$g(x_1) = 1 + G\left(\dfrac{x}{L}\right)$

$$V_{0_z} = - \frac{6 \alpha E F_1 q}{(q+1)(q+2)L} \quad ,$$

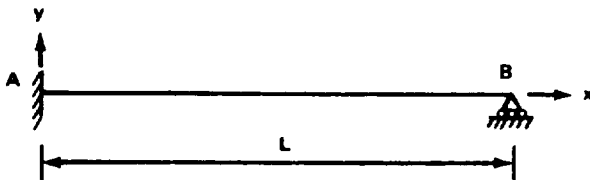$$M_z = \frac{2 \alpha E F_1}{(q+1)(q+2)} \left[\left(1 - 3\frac{x}{L}\right) q - 1 \right] \quad .$$

CASE b:

$$\frac{M_{T_z}(x_1)}{EI_z(x_1)} = \text{constant} \quad ,$$

$$v(x) = 0 \quad ,$$

$$M_{0_z} = -M_{T_z} \quad ,$$

$$V_{0_z} = 0 \qquad M_z = - M_{T_z} = \text{constant}.$$

III. **Fixed-Hinged Beam.**

A. **Boundary Conditions:**

$$v = \frac{dv}{dx} = 0, \quad @ \; x = 0 \quad ,$$

$$v = \frac{d^2 v}{dx^2} + \frac{M_{T_z}}{EI_z} = 0 , \quad @ \; x = L \quad ,$$

$$v\left(\frac{x}{L}\right) = -\frac{\alpha F_1 L^2}{I_{z_0}}\left[I_{x_1} + F_4\left(I_{x_2} - I_{x_3}\right)\right] \qquad ,$$

where

$$F_4 = \frac{I_1}{(I_3 - I_2)} \qquad \text{(refer to Table 3.0-4 for values of } F_4),$$

$$V_{0_z} = -\frac{\alpha E F_1 F_4}{L} \qquad ,$$

$$M_{0_z} = \alpha E F_1 F_4 \qquad ,$$

$$u_{av}(x) = \frac{\alpha F_0 L}{A_0} \int_0^{x_1} f(x_1)\, dx_1 \qquad ,$$

$$\sigma_{xx} = -\alpha E T + \frac{P_T}{A} + \left(\frac{M_{T_z} + M_z}{I_z}\right) y + \left(\frac{M_{T_y} + M_y}{I_y}\right) z \qquad .$$

If the end of B is hinged,

$$u_{av}(x) = 0 \qquad ,$$

$$\sigma_{xx} = -\alpha E T + \left(\frac{M_{T_z} + M_z}{I_z}\right) y + \left(\frac{M_{T_y} + M_y}{I_y}\right) z \qquad .$$

CASE a:

$$EI_z = \text{constant} \qquad ,$$

$$f(x_1) = \left(\frac{x}{L}\right)^q \qquad ,$$

$$v\left(\frac{x}{L}\right) = - \frac{\alpha F_1 L^2}{I_{0_z}} \left\{ \left(\frac{x}{L}\right)^{q+2} - \frac{1}{2}\left[3\left(\frac{x}{L}\right)^2 - \left(\frac{x}{L}\right)^3\right] \right\} \frac{1}{(q+1)(q+2)} \quad ,$$

$$V_{0_z} = \frac{3\alpha E F_1}{(q+1)(q+2) L} \quad ,$$

$$M_{0_z} = - \frac{3\alpha E F_1}{(q+1)(q+2)} \quad ,$$

$$M_z = - \frac{3\alpha E F_1 \left(1 - \frac{x}{L}\right)}{(q+1)(q+2)} \quad .$$

CASE b:

$$\frac{M_{T_z}}{EI_z}(x) = \text{constant} \quad ,$$

$$v(x) = \frac{\alpha F_1}{I_z} \frac{x^2}{4}\left(1 - \frac{x}{L}\right) \quad ,$$

$$V_{0_z} = \frac{3\alpha E F_1}{L} \quad ,$$

$$M_{0_z} = - \frac{3}{2}\alpha E F_1 \quad ,$$

$$M_z = - \frac{3}{2}\left(1 - \frac{x}{L}\right)\alpha E F_1 \quad .$$

IV. <u>Deflection Plots.</u>

From the previous cases the deflection expressions were found to be

A. Simply Supported Beam:

$$v(x) = \frac{F_1 L^2}{I_{0_z}}\left(\frac{x}{L} I_1 - I_{1x}\right)$$

B. Fixed-Fixed Beam:

$$v(x) = -\frac{F_1 L^2}{I_{0_z}} \left(I_{1x} + F_2 I_{2x} + F_3 I_{3x} \right)$$

C. Fixed-Hinged Beam:

$$v(x) = -\frac{F_1 L^2}{I_{0_z}} \left[I_{1x} + F_4 \left(I_{2x} - I_{3x} \right) \right]$$

These expressions have been plotted for parameter variations of beam width, depth, and degree of thermal gradient along the beam length. The plots are made in nondimensional form with the following designation:

$$SS = \left(\frac{x}{L} I_1 - I_{1x} \right) \quad,$$

$$FS = - \left[I_{1x} + F_4 \left(I_{2x} - I_{3x} \right) \right] \quad,$$

and

$$FF = - \left(I_{1x} + F_2 I_{2x} + F_3 I_{3x} \right) .$$

Therefore the deflection, $v(x)$, for any case can be found by multiplying SS,

FS, or FF by $\dfrac{F_1 L^2}{I_{0_z}}$.

Figures 3.0-4 and 3.0-5 show the variation of FF and FS as a function of lengthwise temperature gradient. In the figure, G = H = 0 (constant cross section) and N equals the exponent of the thermal variation along the length of the beam; e.g., N = 0 means constant variation, N 1 means linear variation, etc.

Figures 3.0-6 through 3.0-13 show the three deflection parameters SS, FS, and FF for variation of parameters G, H, and N, where H equals variation in width of beam along the length, G equals variation in depth at x = 0) (refer to Paragraph 3.0.3.1).
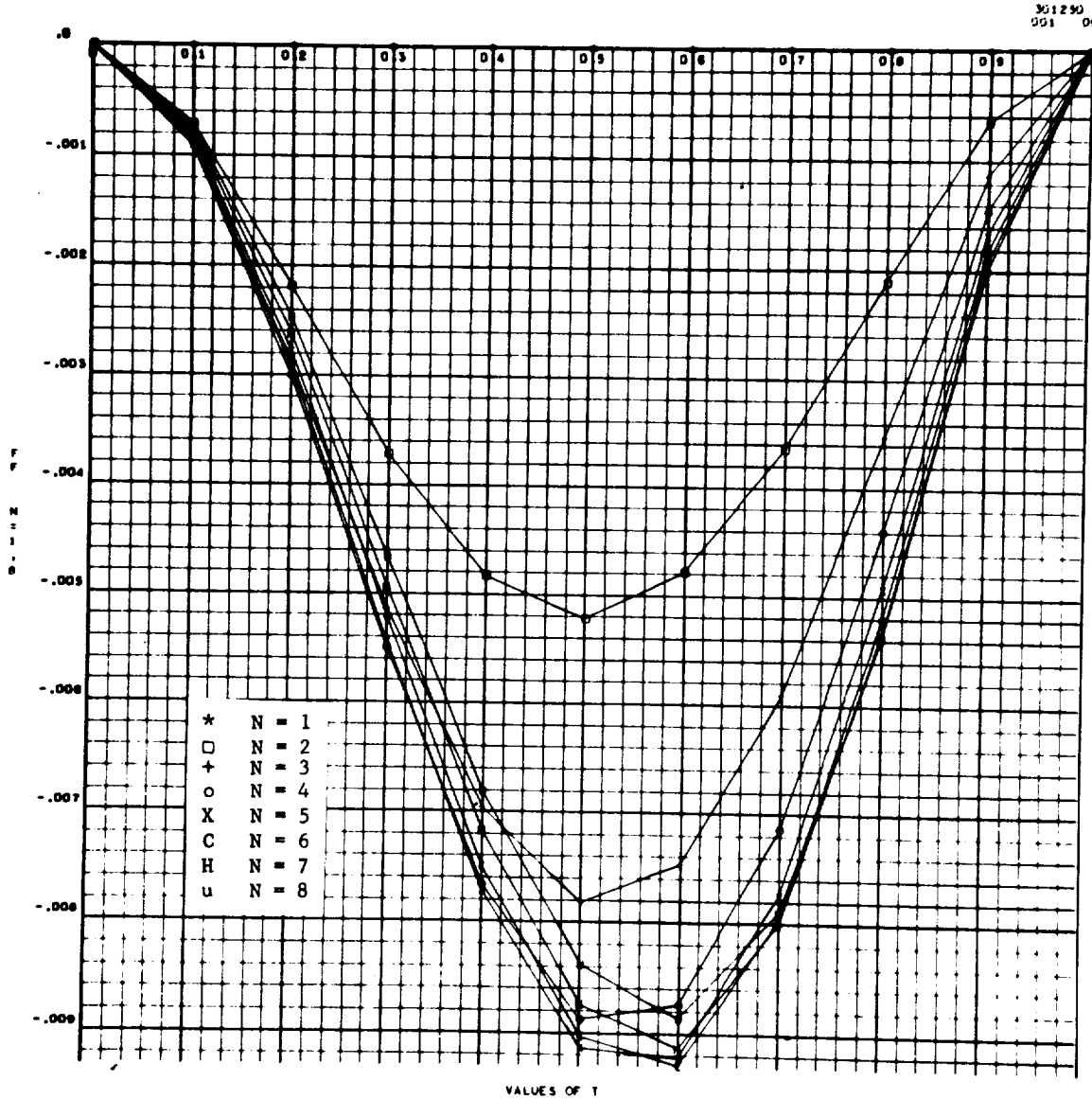
Figure 3.0-4. Deflection parameter FF versus distance along beam for variation of lengthwise temperature gradient.
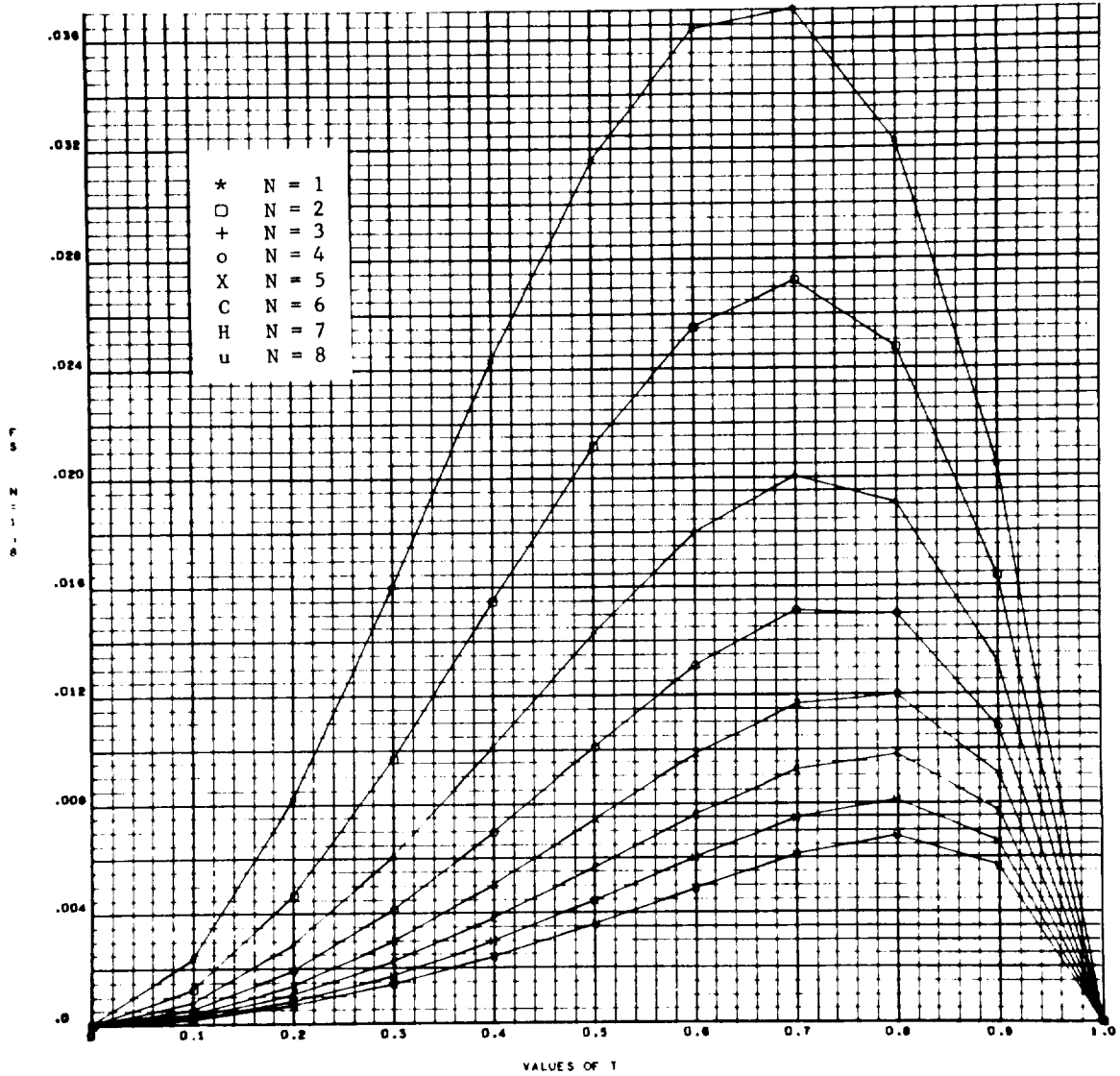
Figure 3. 0-5. Deflection parameter FS versus distance along beam for
variation of lengthwise temperature gradient.
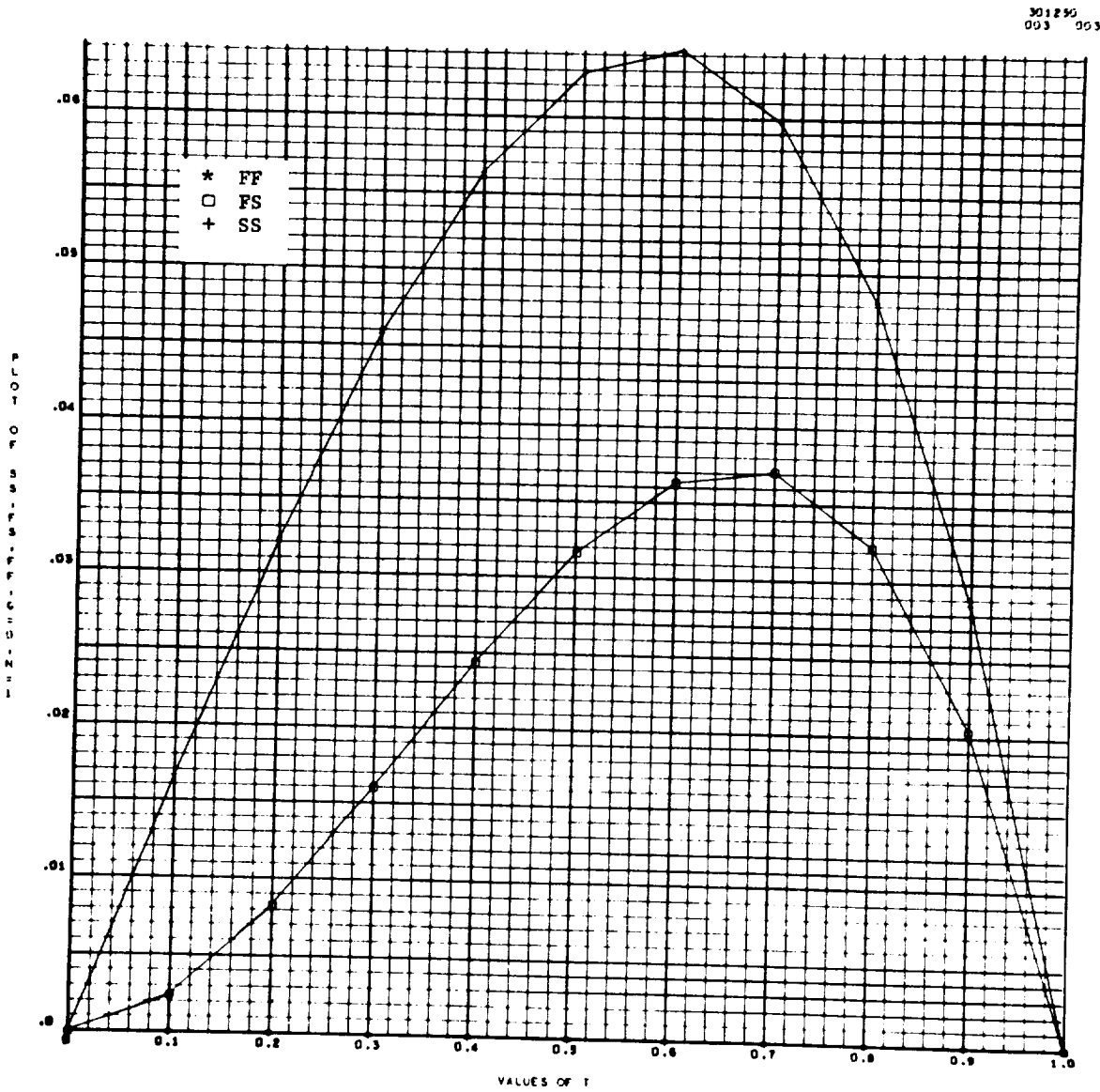
Figure 3.0-6. Values of SS, FS, FF versus values of T(x/L)
for H = 0, G = 0, N = 1.
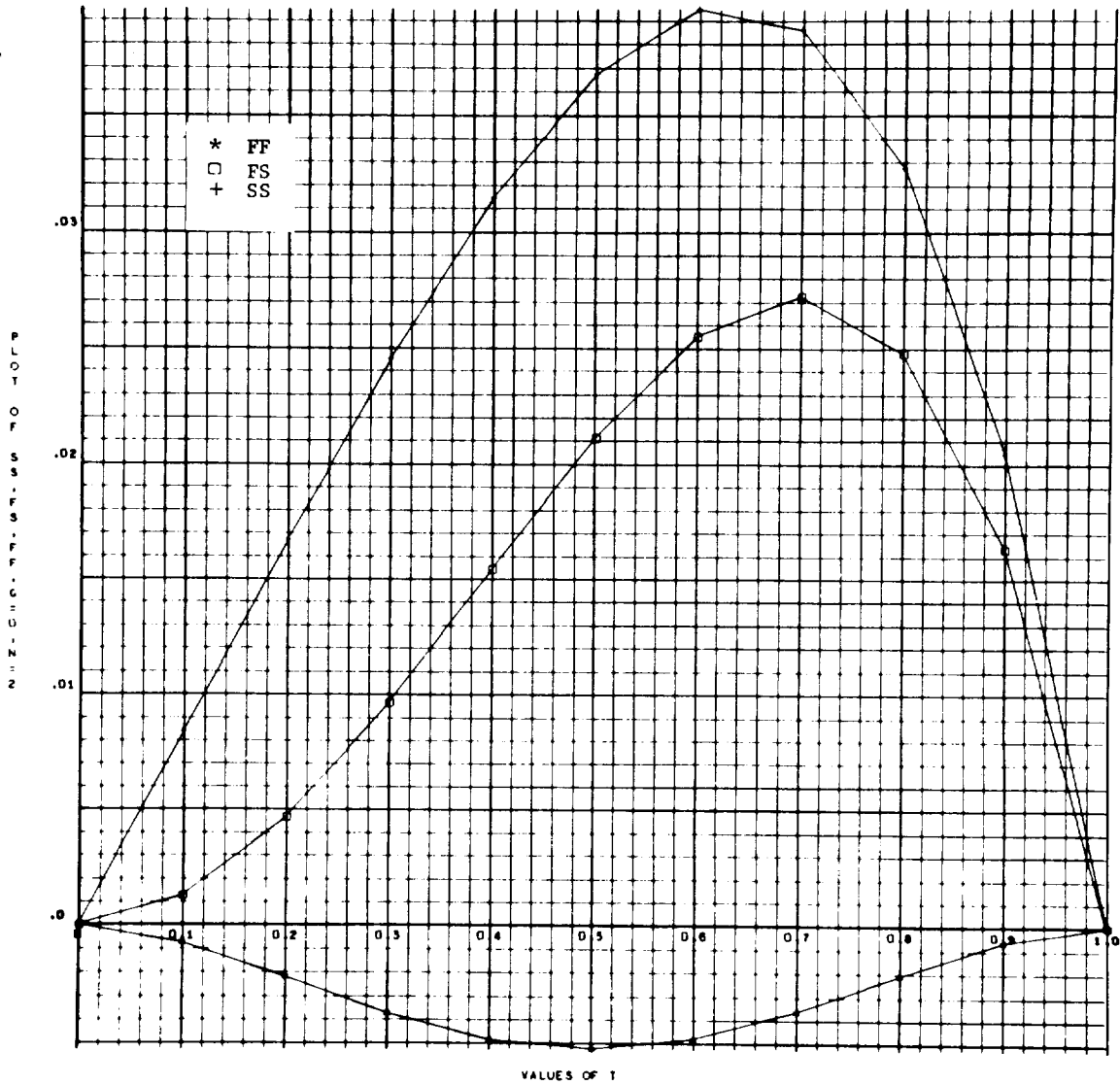
Figure 3.0-7. Values of SS, FS, FF versus values of T
for H = 0, G = 0, N = 2.
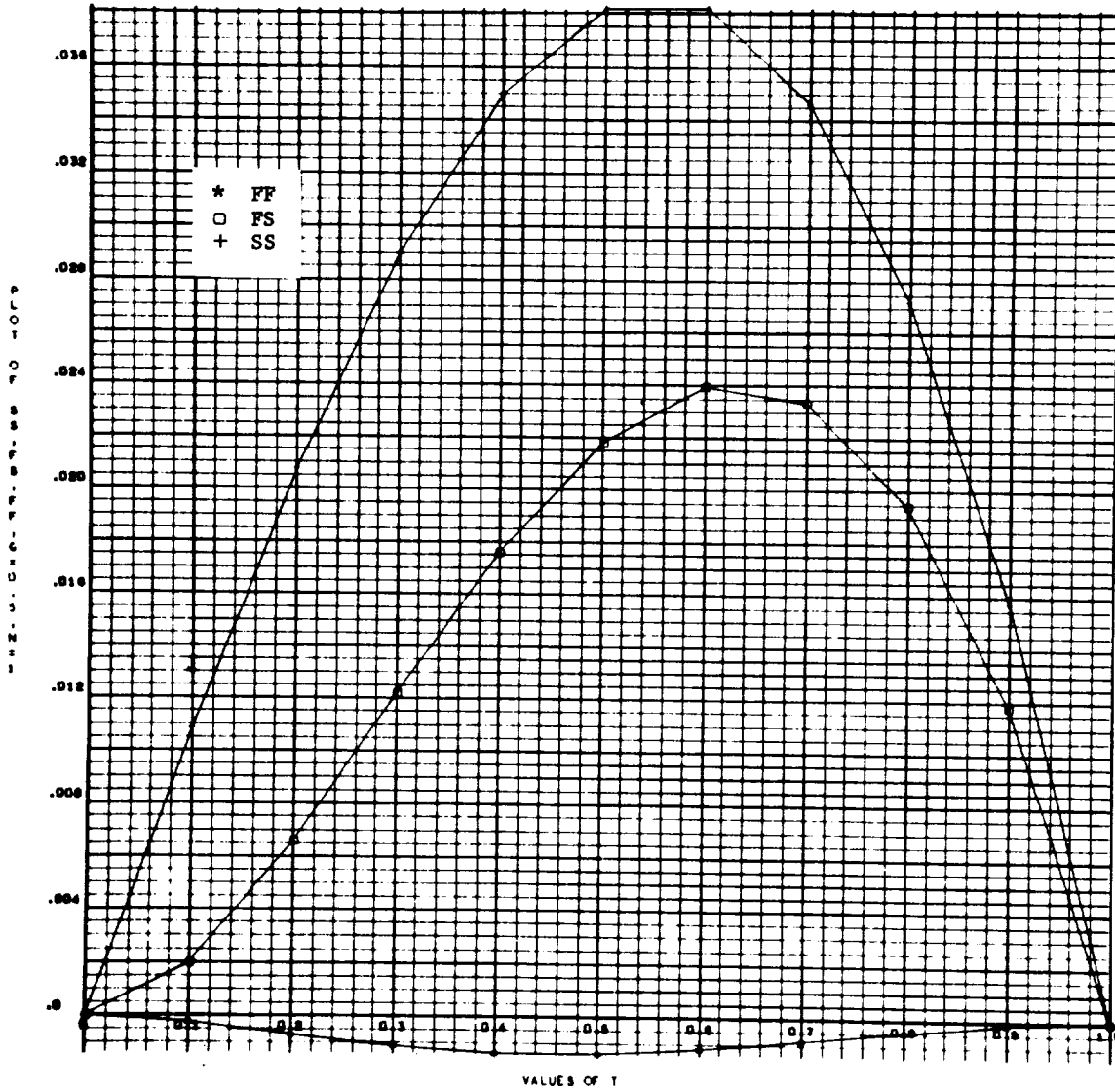
Figure 3.0-8. Values of SS, FS, FF versus values of T
for H = 0, G = 0.5, N = 1.

ORIGINAL PAGE IS
OF POOR QUALITY
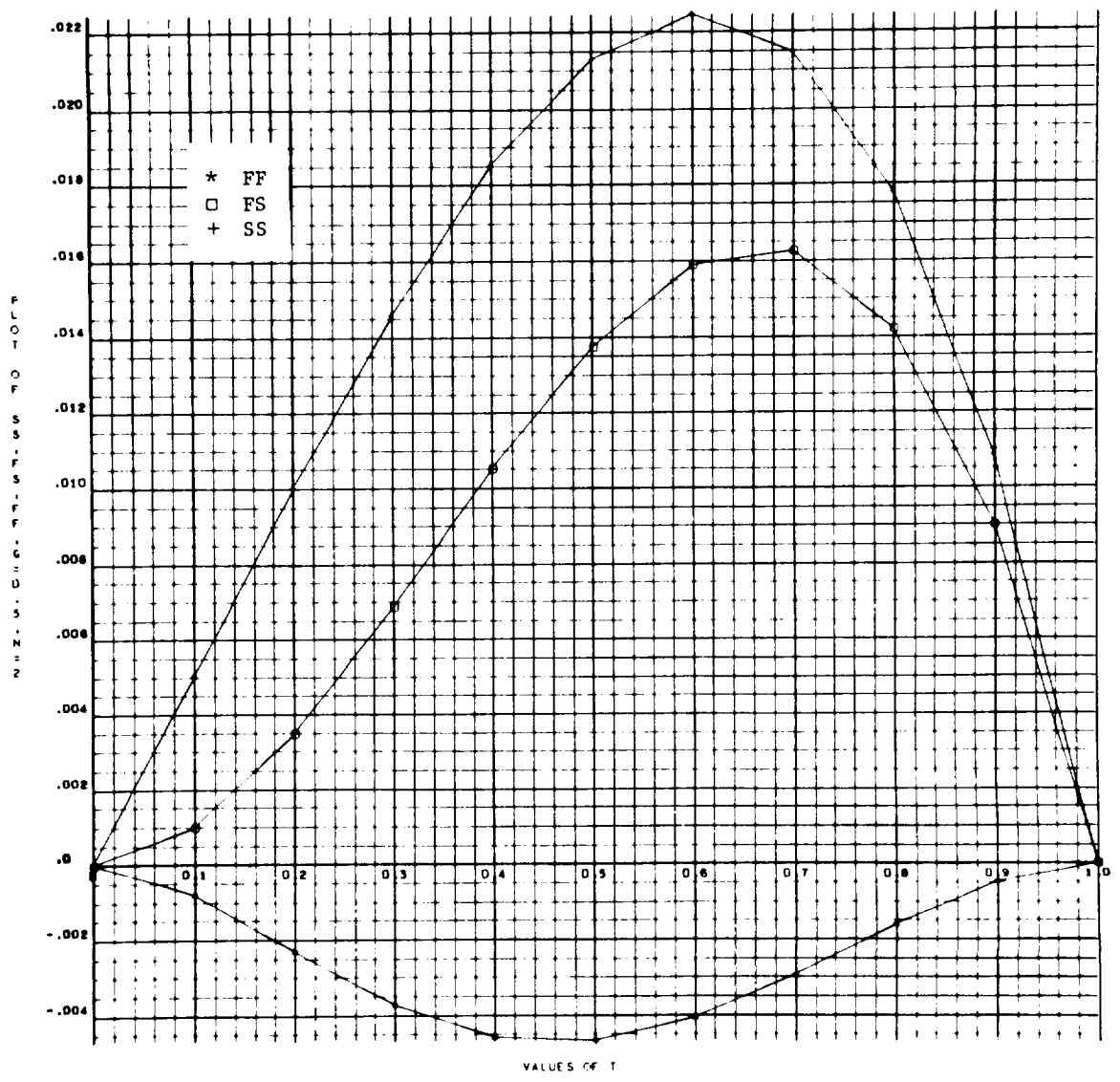
Figure 3.0-9. Values of SS, FS, FF versus values of T
for H = 0, G - 0.5, N = 2.
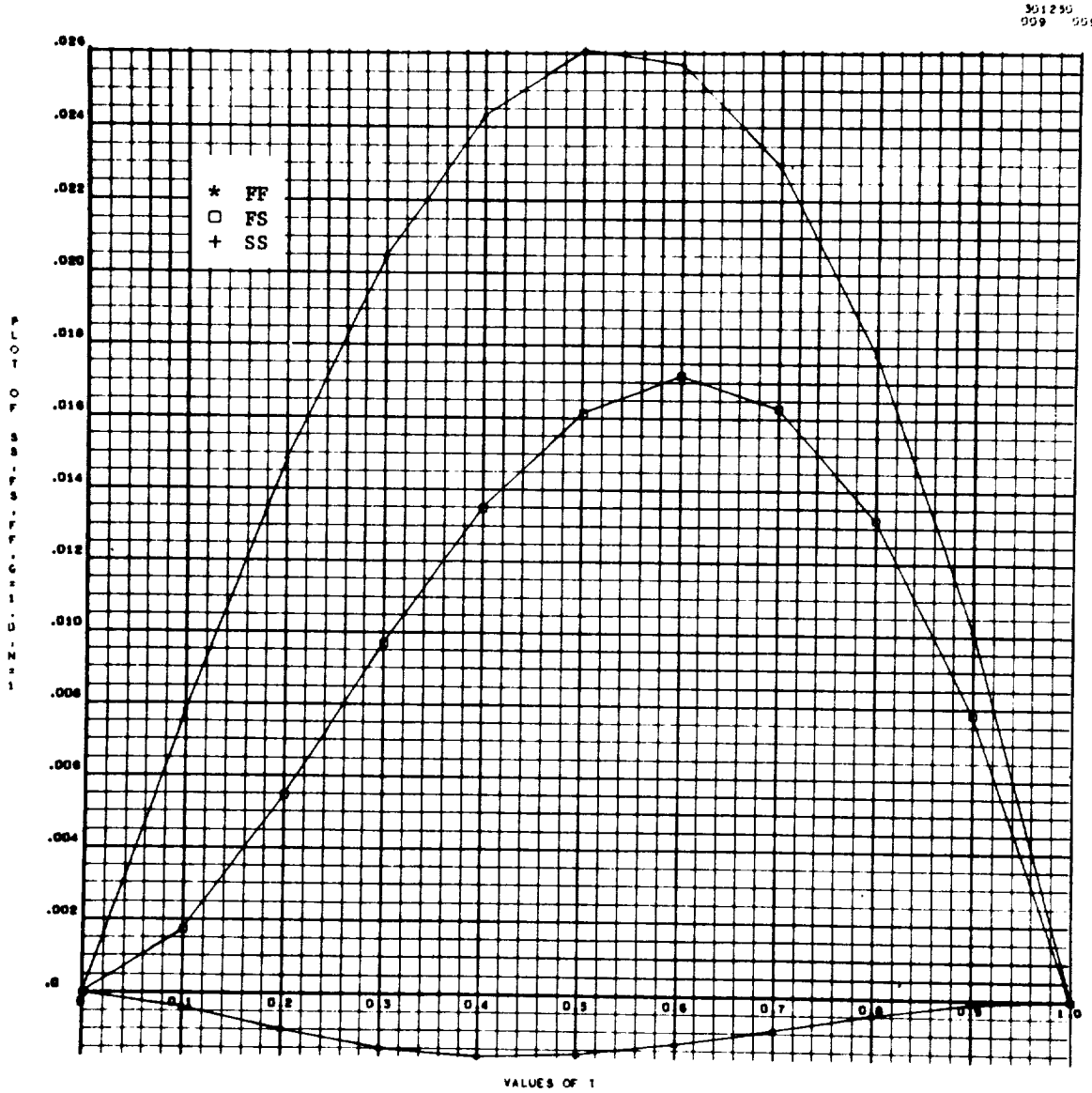
Figure 3.0-10. Values of SS, FS, FF versus values of T
for H = 0, G = 1.0, N = 1.
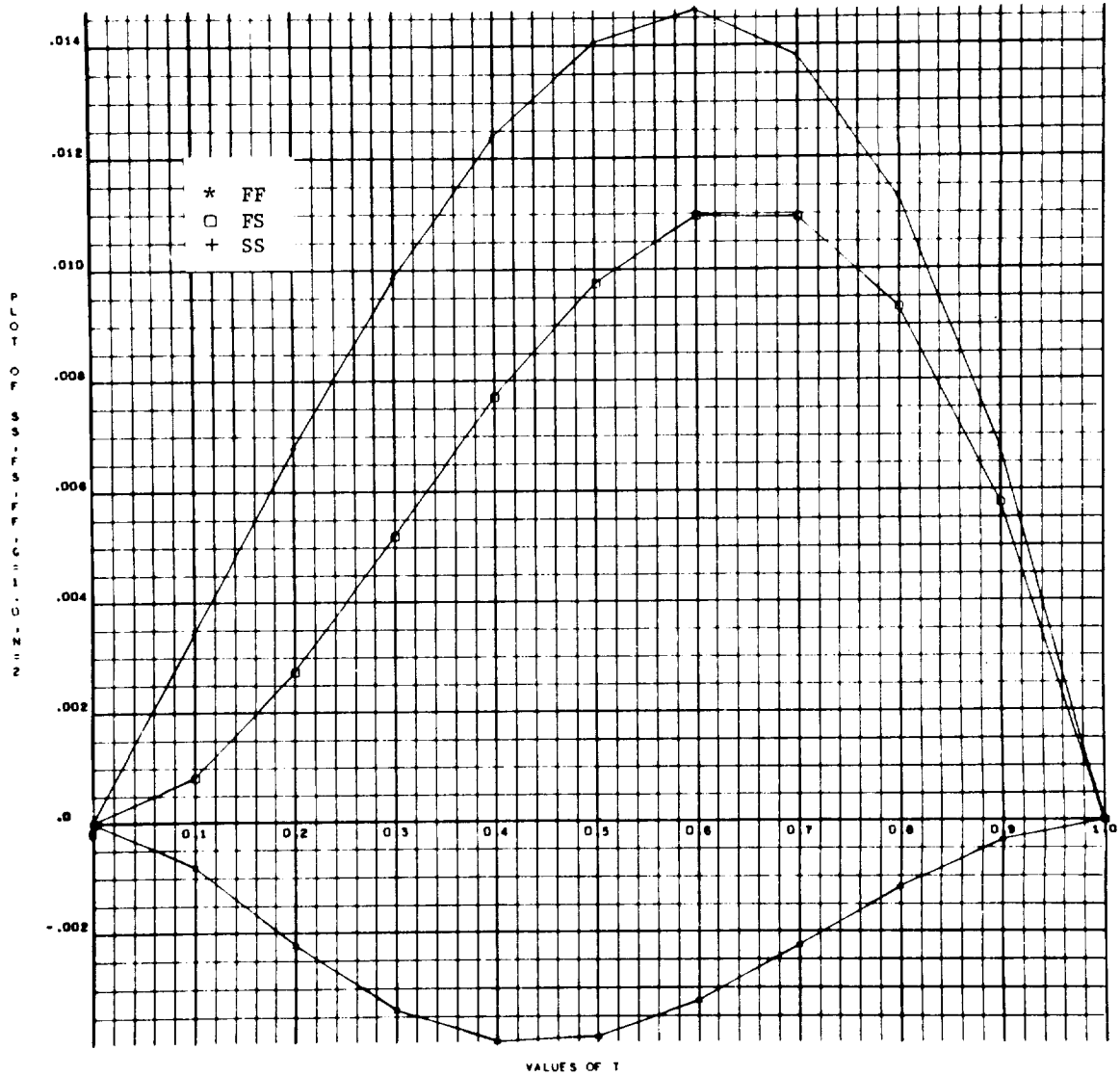
Figure 3.0-11. Values of SS, FS, FF versus values of T
for H = 0, G = 1.0, N = 2.
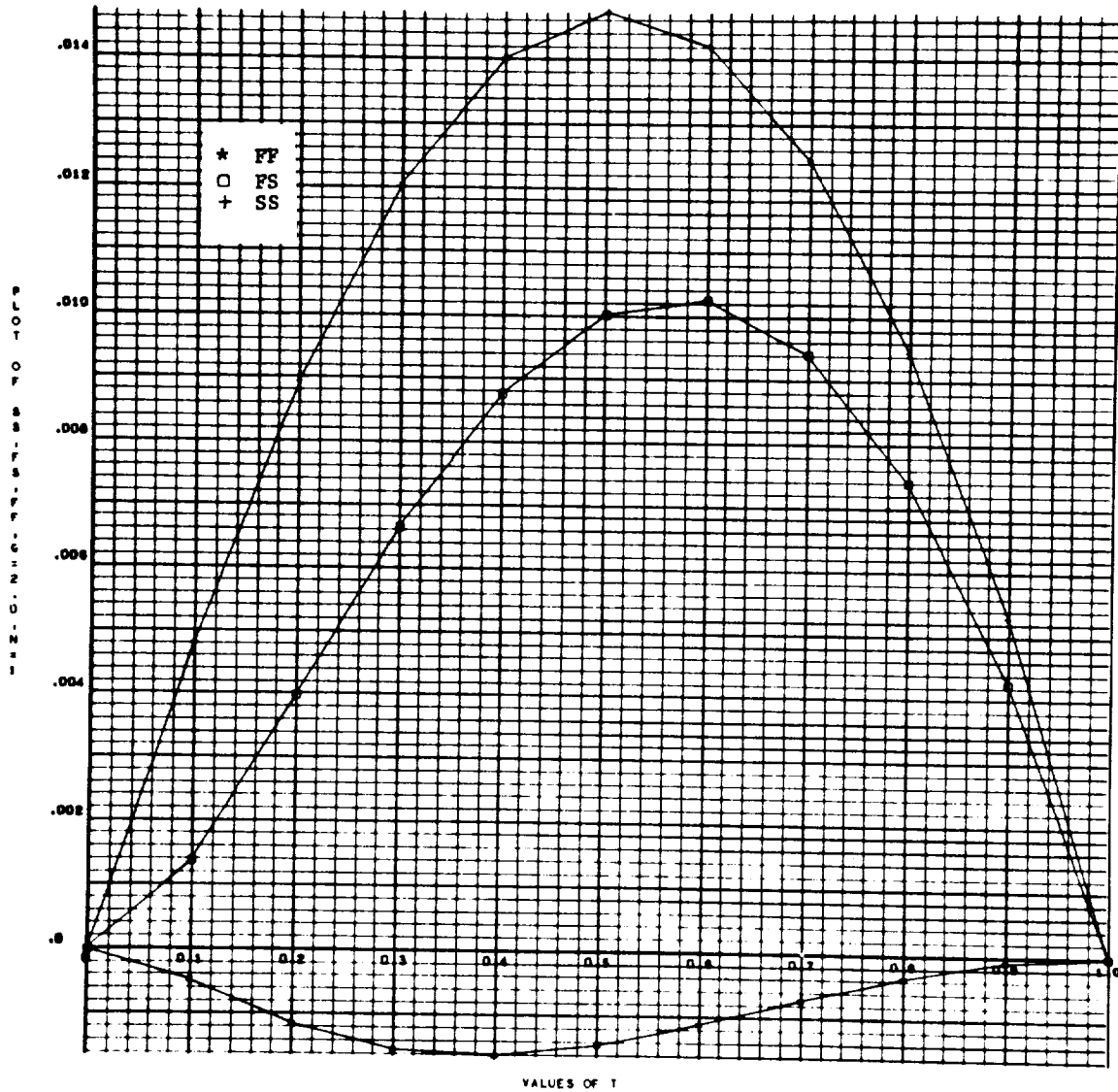
Figure 3.0-12.   Values of SS,   FS,   FF versus values of T
for H = 0,   G = 2.0,   N = 2.
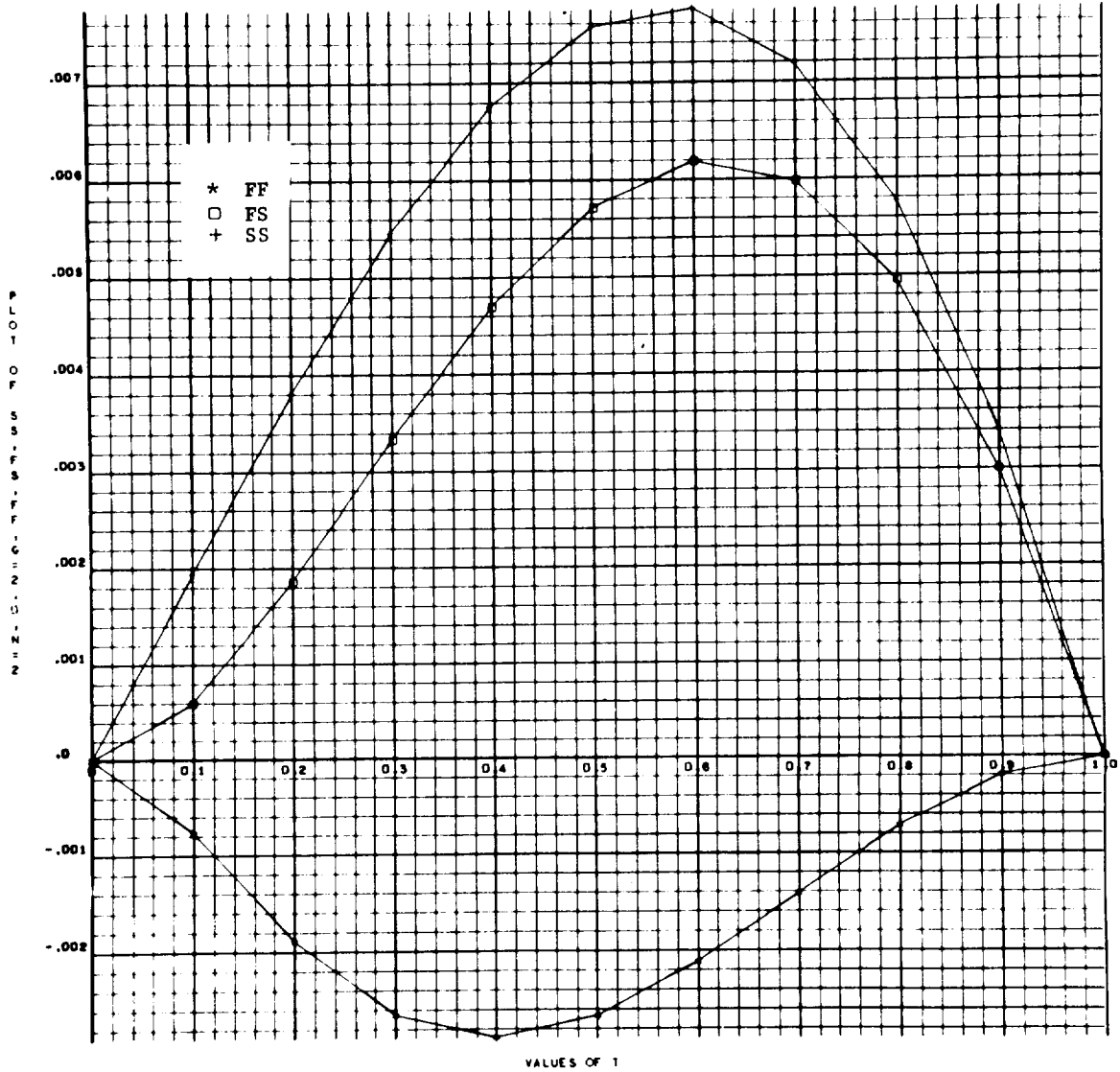
Figure 3.0-13. Values of SS, FS, FF versus values of T
for H = 0, G = 2.0, N = 2.

3.0.2.3 Representation of Temperature Gradient by Polynomial.

A temperature profile obtained analytically or experimentally can be approximated by a polynomial of the form

$$T = \sum_{n=1}^{N} \sum_{m=1}^{M} V_{mn} \, y^n z^m + T_0 \quad .$$

Accuracy of this approximation increases with the increase in the number of terms of the polynomial; but, since the temperature distribution is to be integrated in the process of obtaining the stress distribution, the accuracy of the resulting distribution using a low-order polynomial improves. The total number of grid points required to determine the coefficients V_{mn} uniquely is equal to $(M + N)$.

The coefficients V_{mn} are obtained from the following relations.

$$
\begin{Bmatrix}
V_{11} \\
V_{12} \\
\vdots \\
V_{1N} \\
V_{21} \\
V_{22} \\
\vdots \\
V_{2N} \\
\vdots \\
V_{MN}
\end{Bmatrix}
=
\begin{bmatrix}
a_{1,11} & a_{1,12} & a_{1,13} & \cdots & a_{1,1N} & a_{1,21} & \cdots & a_{1,MN} \\
a_{2,11} & a_{2,12} & a_{2,13} & \cdots & a_{2,1N} & a_{2,21} & \cdots & a_{2,MN} \\
a_{N,11} & a_{N,12} & \cdots & & & & & a_{N,MN} \\
a_{(M+N),11} & a_{(M+N),12} & \cdots & & & & & a_{(M+N),MN}
\end{bmatrix}
\begin{Bmatrix}
T_1 - T_0 \\
T_2 - T_0 \\
\vdots \\
T_N - T_0 \\
\vdots \\
T_{(M+N)} - T_0
\end{Bmatrix}
$$

where $a_{i,mn} = y_i^n z_i^m$. The values (y_i, z_i) = coordinates of the ith grid point at temperature T_i and T_0 = temperature at the centroid of the cross section.

If the temperature difference $(T_i - T_0)$ is continuous and symmetric about the z-axis, then $V_{m1} = V_{m3} = V_{m5} = \ldots = 0$, and if it is continuous and antisymmetric $V_{m2} = V_{m4} = V_{m6} = \ldots 0$. Similarly, for temperature differences that are symmetric about the y-axis, $V_{1n} = V_{3n} = V_{5n} = \ldots 0$, and if it is antisymmetric about the y-axis, $V_{2n} = V_{4n} = V_{6n} = \ldots = 0$.

If the temperature varies only in one direction (e.g., for variation along the y-direction only) along either the y- or z-axis, the polynomial reduces to

$$T - T_0 = \sum_{n=1}^{N} V_n y^n \quad .$$

$$\begin{Bmatrix} V_1 \\ V_2 \\ \cdot \\ \cdot \\ \cdot \\ V_n \end{Bmatrix} = \begin{bmatrix} a_{11} & a_{12} & \cdots & a_{1n} \\ a_{21} & a_{22} & \cdots & a_{2n} \\ & & & \\ & & & \\ & & & \\ a_{n1} & a_{n2} & \cdots & a_{nn} \end{bmatrix} \begin{Bmatrix} T_1 - T_0 \\ T_2 - T_0 \\ \\ \\ T_n - T_0 \end{Bmatrix} \quad .$$

$$a_{1n} = y_i^n$$

As before, if the temperature difference is continuous and symmetric, $V_1 = V_3 = V_5 = \ldots 0$; and for continuous antisymmetric temperature differences $V_2 = V_4 = V_6 = \ldots 0$.

If the grid points are equally spaced on the cross section, say at distance d_1, then the polynomial can be written in nondimensional form as

$$T_1 - T_0 = \sum_{n=1}^{N} V_n d_1^n \left(\frac{y}{d_1}\right)^n \quad .$$

EXAMPLES:

1. Continuous Symmetric Temperature

a. Nine Points:
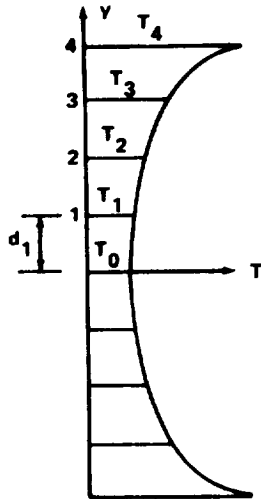
$$T_i - T_0 = \sum_{n=2,4,6} (V_n d_1^n)(i)^n$$

$$
\begin{Bmatrix} V_2 d_1^2 \\ V_4 d_1^4 \\ V_6 d_1^6 \\ V_8 d_1^8 \end{Bmatrix} =
\begin{bmatrix} 1^2 & 1^4 & 1^6 & 1^8 \\ 2^2 & 2^4 & 2^6 & 2^8 \\ 3^2 & 3^4 & 3^6 & 3^8 \\ 4^2 & 4^4 & 4^6 & 4^8 \end{bmatrix}^{-1}
\begin{Bmatrix} T_1 - T_0 \\ T_2 - T_0 \\ T_3 - T_0 \\ T_4 - T_0 \end{Bmatrix}
$$

$$
\begin{Bmatrix} V_2 d_1^2 \\ V_4 d_1^4 \\ V_6 d_1^6 \\ V_8 d_1^8 \end{Bmatrix} =
\begin{bmatrix}
0.16000{+}01 & -0.20000{+}00 & 0.25397{-}01 & -0.17857{-}02 \\
-0.67778{+}00 & 0.23472{+}00 & -0.33333{-}01 & 0.24306{-}02 \\
0.80556{-}01 & -0.36111{-}01 & 0.83333{-}02 & -0.69444{-}03 \\
-0.27778{-}02 & 0.13889{-}02 & -0.39683{-}03 & 0.49603{-}04
\end{bmatrix}
\begin{Bmatrix} T_1{-}T_0 \\ T_2{-}T_0 \\ T_3{-}T_0 \\ T_4{-}T_0 \end{Bmatrix}
$$

b. Seven Points:

$$
\begin{Bmatrix} V_2 d_1^2 \\ V_4 d_1^4 \\ V_6 d_1^6 \end{Bmatrix} =
\begin{bmatrix}
0.15000{+}01 & -0.15000{+}00 & 0.11111{-}01 \\
-0.54167{+}00 & 0.16667{+}00 & -0.13889{-}01 \\
0.41667{-}01 & -0.16667{-}01 & 0.27778{-}02
\end{bmatrix}
\begin{Bmatrix} T_1{-}T_0 \\ T_2{-}T_0 \\ T_3{-}T_0 \end{Bmatrix}
$$

c. Five Points:

$$
\begin{Bmatrix} V_2 d_1^2 \\ V_4 d_1^4 \end{Bmatrix} =
\begin{bmatrix} 1^2 & 1^4 \\ 2^2 & 2^4 \end{bmatrix}^{-1}
\begin{Bmatrix} T_1{-}T_0 \\ T_2{-}T_0 \end{Bmatrix} =
\begin{bmatrix} \dfrac{4}{3} & -\dfrac{1}{3} \\ -\dfrac{1}{12} & \dfrac{1}{12} \end{bmatrix}
\begin{Bmatrix} T_1{-}T_0 \\ T_2{-}T_0 \end{Bmatrix}
$$

2. Continuous Antisymmetric Temperature

a. Nine Points:
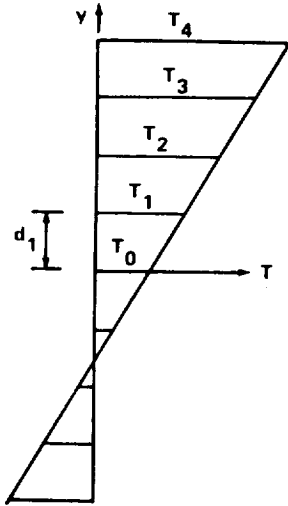
$$
\begin{Bmatrix} V_1\,d_1 \\ V_3\,d_1^3 \\ V_5\,d_1^5 \\ V_7\,d_1^7 \end{Bmatrix} =
\begin{bmatrix} 1 & 1^3 & 1^5 & 1^7 \\ 2 & 2^3 & 2^5 & 2^7 \\ 3 & 3^3 & 3^5 & 3^7 \\ 4 & 4^3 & 4^5 & 4^7 \end{bmatrix}^{-1}
\begin{Bmatrix} T_1 - T_0 \\ T_2 - T_0 \\ T_3 - T_0 \\ T_4 - T_0 \end{Bmatrix}
$$

$$
\begin{Bmatrix} V_1\,d_1 \\ V_3\,d_1^3 \\ V_5\,d_1^5 \\ V_7\,d_1^7 \end{Bmatrix} =
\begin{bmatrix} 0.15003{+}01 & -0.30031{+}00 & 0.33466{-}01 & -0.22126{-}04 \\ -0.54209{+}00 & 0.33375{+}00 & -0.41847{-}01 & 0.30116{-}04 \\ 0.41787{-}01 & -0.33454{-}01 & 0.83850{-}02 & -0.86045{-}05 \\ -0.86045{-}05 & 0.86045{-}05 & -0.36876{-}05 & 0.61461{-}06 \end{bmatrix}
\begin{Bmatrix} T_1 - T_0 \\ T_2 - T_0 \\ T_3 - T_0 \\ T_4 - T_0 \end{Bmatrix}
$$

b. Seven Points:

$$
\begin{Bmatrix} V_1\,d_1 \\ V_3\,d_1^3 \\ V_5\,d_1^5 \end{Bmatrix} =
\begin{bmatrix} 0.15000{+}01 & -0.30000{+}00 & 0.33333{-}01 \\ -0.54167{+}00 & 0.33333{+}00 & -0.41667{-}01 \\ 0.41667{-}01 & -0.33333{-}01 & 0.83333{-}02 \end{bmatrix}
\begin{Bmatrix} T_1 - T_0 \\ T_2 - T_0 \\ T_3 - T_0 \end{Bmatrix}
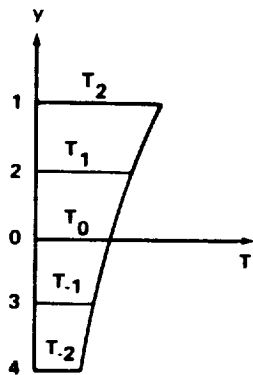$$

c. Five Points:

$$
\begin{Bmatrix} V_1\,d_1 \\ V_3\,d_1^3 \end{Bmatrix} =
\begin{bmatrix} 1 & 1^3 \\ 2 & 2^3 \end{bmatrix}^{-1}
\begin{Bmatrix} T_1 - T_0 \\ T_2 - T_0 \end{Bmatrix} =
\begin{bmatrix} \dfrac{4}{3} & -\dfrac{1}{3} \\ -\dfrac{1}{6} & \dfrac{1}{6} \end{bmatrix}
\begin{Bmatrix} T_1 - T_0 \\ T_2 - T_0 \end{Bmatrix}
$$

d. Three Points:

$$
V_1\,d_1 = T_1 - T_0
$$

3. Arbitrary Temperature Distribution

a. Five Points:

$$\begin{Bmatrix} V_1\,d_1 \\ V_2\,d_1^2 \\ V_3\,d_1^3 \\ V_4\,d_1^4 \end{Bmatrix} = \begin{bmatrix} 2^1 & 2^2 & 2^3 & 2^4 \\ 1^1 & 1^2 & 1^3 & 1^4 \\ (-1)^1 & (-1)^2 & (-1)^3 & (-1)^4 \\ (-2)^1 & (-2)^2 & (-2)^3 & (-2)^4 \end{bmatrix}^{-1} \begin{Bmatrix} T_2 - T_0 \\ T_1 - T_0 \\ T_{-1} - T_0 \\ T_{-2} - T_0 \end{Bmatrix}$$

$$\begin{Bmatrix} V_1\,d_1 \\ V_2\,d_1^2 \\ V_3\,d_1^3 \\ V_4\,d_1^4 \end{Bmatrix} = \begin{bmatrix} -0.83333-01 & 0.66667+00 & -0.66667+00 & 0.83333-01 \\ -0.41667-01 & 0.66667+00 & 0.66667+00 & -0.41667-01 \\ 0.83333-01 & -0.16667+00 & 0.16667+00 & -0.83333-01 \\ 0.41667-01 & -0.16667+00 & -0.16667+00 & 0.41667-01 \end{bmatrix} \begin{Bmatrix} T_2 - T_0 \\ T_1 - T_0 \\ T_{-1} - T_0 \\ T_{-2} - T_0 \end{Bmatrix}$$

b. Three Points:

$$\begin{Bmatrix} V_1\,d_1 \\ V_2\,d_1^2 \end{Bmatrix} = \begin{bmatrix} 1^1 & 1^2 \\ (-1)^1 & (-1)^2 \end{bmatrix}^{-1} \begin{Bmatrix} T_1 - T_0 \\ T_{-1} - T_0 \end{Bmatrix} = \begin{bmatrix} \dfrac{1}{2} & -\dfrac{1}{2} \\ \dfrac{1}{2} & \dfrac{1}{2} \end{bmatrix} \begin{Bmatrix} T_1 - T_0 \\ T_{-1} - T_0 \end{Bmatrix}$$

Once the polynomial coefficients are determined, refer to Table 3.0-2 or 3.0-3 for constant F_1. Refer to Table 3.0-4 for the constants F_2, F_3, and F_4 to be used to find the fixed-end moments, reactions, and deflections of the beam.

I. Example Problem 1.

Given: The beam of rectangular cross section with a temperature distribution constant in the x-direction and varying linearly from 500° F on the top surface to 80° F on the bottom surface.
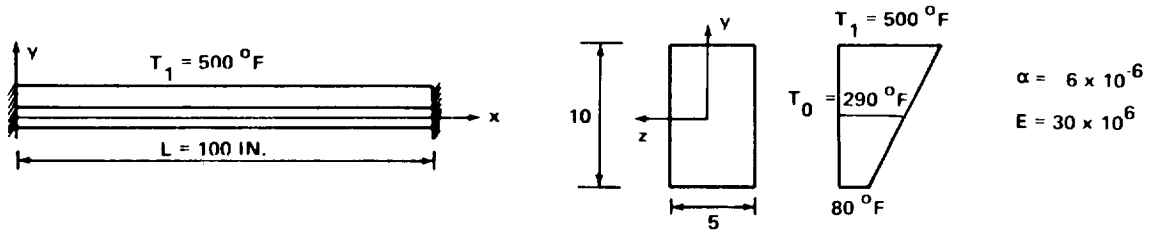
Find: Maximum stresses and maximum deflection v(x) in center of beam.

Solution:

1. Find the polynomial expression representing the given temperature distribution in the y-direction. Refer to Paragraph 3.0.2.3, Continuous Antisymmetric Temperature, Three Points

$$v_1 \, d_1 = T_1 - T_0 \qquad .$$

Therefore

$$v_1(5) = 500 - 290$$

$$v_1 = 42 \qquad .$$

Therefore expression for $T = v_0 + v_1 \, y - 290 + 42y$.

2. Find values of F_0, F_1, F_2, and F_3 for each term of polynomial. Refer to Table 3.0-2.

$$v_0 = 290 \qquad F_0 = 290 \times b_0 d_0 - 290 \times 10(5) = 50 \times 290 \qquad F_1 = 0$$

$$v_1 = 42 \qquad F_0 = 0$$

$$F_1 = \frac{(42)}{12} \, b_0 d_0^3 = \frac{42}{12} (5)(10)^3 = 416.67(42)$$

Refer to Table 3.0-4:

$$(q = 0, \ H = 0, \ G = 0) \qquad f(x) = 500 \left(\frac{x}{L}\right)^q$$

$F_2 = -1.000$ since constant in x-direction
         q = 0

$F_3 = 0$ constant depth G = 0
         constant width H - 0

3. Refer to Paragraph 3.0.2.2 II (Case b)

$$M_{0_Z} = \alpha E F_1 F_2$$

$$M_{0_Z} = 6 \times 10^{-6} \times 30 \times 10^6 \times 416.67 \times 40 \times (-1.00)$$

$$= 3.15 \times 10^6$$

$$\sigma_{xx} = -\alpha ET + \frac{M_{0_Z} y}{I_Z}$$

Top Fiber: $\sigma_{xx} = -6 \times 10^6 \times 30 \times 10^6 \times 500 + \dfrac{(-3.15 \times 10^6) \times 5}{416.67}$
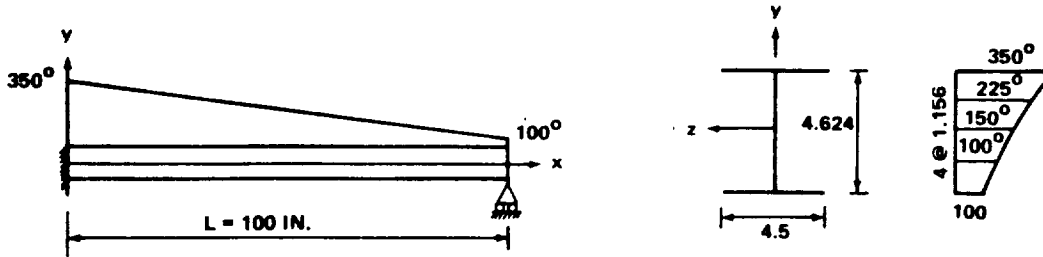
$$\sigma_{xx} = -127\,800 \text{ psi}$$

Deflection: $v(x) = 0$

Therefore the beam remains straight.

II. Example Problem 2.

Given: The I-beam shown below with a linear varying temperature in the x-direction and varying as shown in the y-direction.

Find: Stress σ_{xx} and deflection $v(x)$.

Solution:

1. Find the polynomial expression representing the given temperature distribution in the y-direction. Refer to Paragraph 3.0.2.3, Arbitrary Temperature Distribution, Five Points.

$$
\begin{Bmatrix} V_1\,d_1 \\ V_2\,d_1{}^2 \\ V_3\,d_1{}^3 \\ V_4\,d_1{}^4 \end{Bmatrix} =
\begin{bmatrix}
-0.08333 & 0.6667 & -0.6667 & 0.08333 \\
-0.04167 & 0.6667 & 0.6667 & -0.04167 \\
0.08333 & -0.16667 & 0.16667 & -0.08333 \\
0.04167 & -0.1667 & -0.16667 & 0.04167
\end{bmatrix}
\begin{Bmatrix} 350-150 \\ 225-150 \\ 100-150 \\ 100-150 \end{Bmatrix} =
\begin{Bmatrix} 62.5 \\ 10.42 \\ 0 \\ 2.083 \end{Bmatrix}
$$

$$
T = 150 + \frac{62.5}{1.156}\,y + \frac{10.42}{(1.156)^2}\,y^2 + \frac{2.083}{(1.156)^4}\,y^4
$$

$$
T = 150 + 54.1y + 7.81y^2 + 1.168y^4
$$

2. Refer to Tables 3.0-2 and 3.0-4 for values of F_0, F_1, F_2, F_3, and F_4 for each term of polynomial.

$$n = 0 \quad V_0 = 150 \qquad F_0 = 150(1.715) = 257.3 \qquad F_1 = 0$$

$$n = 1 \quad V_1 = 54.1 \qquad F_0 = 54.1(0) = 0.0 \qquad F_1 = 54.1(2.774) = 150.0$$

$$n = 2 \quad V_2 = 7.81 \qquad F_0 = 7.81(2.774) = 21.6 \qquad F_1 = 0$$

$$n = 4 \quad V_4 = 1.168 \qquad F_0 = 1.168(6.745) = 7.9 \qquad F_1 = 0$$

$$\Sigma\,F_0 = \overline{286.8} \qquad F_1 = \overline{\qquad\qquad 150.0}$$

$$
f\left(\frac{x}{L}\right) = \left(\frac{x}{L}\right)^q = 350 - 250\left(\frac{x}{L}\right)
$$

$$q = 0 \qquad F_2 = -1.000 \qquad F_3 = 0.0 \qquad F_4 = -1.502$$

$$q = 1 \qquad F_2 = 0.0 \qquad F_3 = -1.0 \qquad F_4 = -0.502$$

$$F_2 = \overline{-1.000} \qquad F_3 = \overline{-1.0} \qquad F_4 = \overline{-2.004}$$

3. Refer to Section 3.0.2.2-III (Case b).

$$M_{0_z} = -3/2\,\alpha\,EF_1 = -3/2\,(180)\,(150) = -40,500$$

$$M_z = M_{0_z}(1 - x/L) \qquad\qquad I_z = 10.55 \text{ in}^4.$$

$$\sigma_{xx}\ (@x = 0) = -\alpha ET + \frac{M_{0_z} y}{I_z}$$

$$\sigma_{xx} = -180(350) - \frac{40\ 000(2.312)}{10.55}$$

$$\sigma_{xx} = -71\ 860\ psi$$

Deflection:

$$v(x) = \frac{\alpha F_1}{I_z}\ x^2/4(1 - x/L) = 21.35 \times 10^{-6}\ x^2(1 - x/L)$$

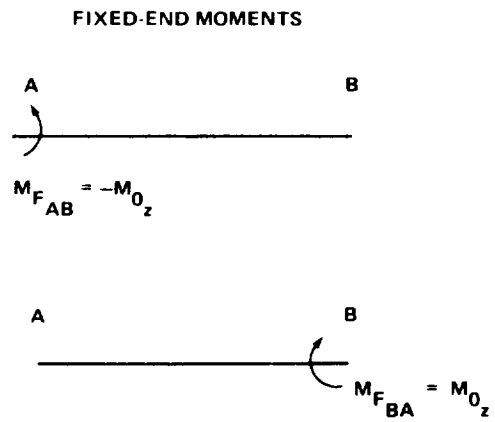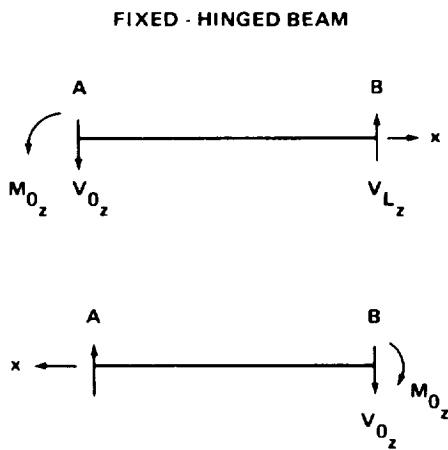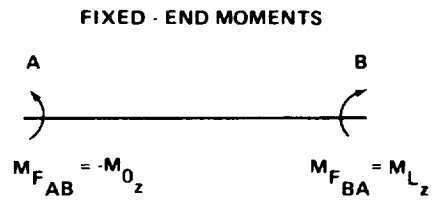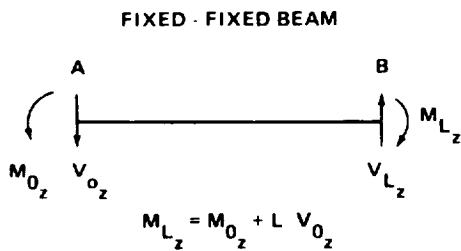| x	v(x)
0	0
10	$90 \times 21.35 \times 10^{-6}$
20	320 × "
40	960 "
50	1250 "
60	1440 "
80	1280 "
90	810 "
100	0

Refer also to Fig. 3.0-6 for the deflection.

3.0.3   Indeterminate Beams and Rigid Frames.

Continuous beams or frames can be analyzed by the method of moment distribution described in Section B5.0, Frames. In this method a continuous beam is fixed against rotation at all the intermediate supports over which the beam is continuous; and, in the case of a frame, all the rigid joints are also fixed against rotation and displacement. For each beam segment the moment required to keep the slope at each of the two supports unchanged is called a fixed-end moment. According to the convention of the method of moment distribution, the fixed-end moment, which is an externally applied moment, is positive if it is clockwise and negative if it is counterclockwise. This convention should not be confused with the convention of strength-of-materials for internal movement (refer to Paragraph 3.0.2). Fixed-end moment is designated by the subscript, F, and is abbreviated F.E.M.
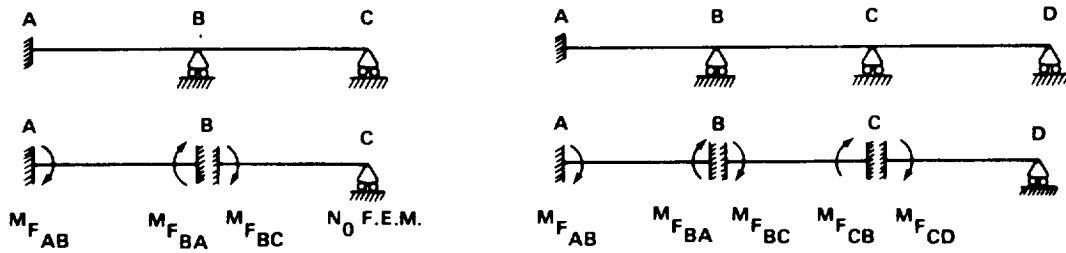
The magnitude of F.E.M. is obtained by analyzing the fixed-fixed beam or the fixed-hinged beam cases of Paragraph 3.0.2. In that paragraph, M_{0_z} is positive when counterclockwise; so, to convert M_{0_z} to F.E.M., one must multiply by -1.

FIXED - FIXED BEAM

FIXED - END MOMENTS

$$M_{L_z} = M_{0_z} + L\, V_{0_z}$$

$$^M F_{AB} = -M_{0_z} \qquad ^M F_{BA} = M_{L_z}$$

FIXED - HINGED BEAM

FIXED-END MOMENTS

$$^M F_{AB} = -M_{0_z}$$

$$^M F_{BA} = M_{0_z}$$

With this information, a normal moment distribution technique can be performed to solve any continuous beam or frame.

3.0.4   Curved Beams.

For a free curved beam of arbitrary, constant cross section, the centerline of which is an arc of a circle lying in one of the centroidal principal planes under a temperature distribution $T(r,\theta)$, the following comments can be made.

1. For a small depth-to-radius ratio, straight-beam theory can be used instead of the curved-beam theory.

2. For linear temperature variation $\left(T = T_1 \dfrac{z}{h}\right)$, the results of curved-beam theory compare well with the solution obtained by exact thermo-elasticity method; e.g., for a rectangular beam where the ratio of outside radius to inside radius is equal to three, the maximum stress obtained by the curved-beam theory differs from the maximum stress obtained by exact solution by only 2.4 percent. Straight-beam theory, however, gives $\sigma_{\theta\theta} = 0$, which is considerably erroneous.

3. For quadratic temperature distribution $T = T_2 \dfrac{z^2}{h^2}$, the difference in maximum stress obtained by curved-beam theory and exact solution is only 4.9 percent for a rectangular section where the ratio of outside to inside radius is equal to 3.0.

For solutions other than those mentioned above, see Ref. 1.

3.0.5   Rings.

A ring may be regarded as a closed, thin, curved beam, and can therefore be studied by the methods given in 3.0.4 and in Ref. 1.

3.0.6   Trusses.

3.0.6.1   Statically Determinate.

Every member of a pin-jointed determinate truss is not constrained to elongate because of thermal loading. As a result, the net axial force in each member is zero. Therefore, members of a pin-jointed determinate truss are regarded as simply supported beams under thermal loading and should be analyzed accordingly.

Deflections of joints of a truss can be obtained by the conventional "dummy-load" method described in Section B4.2.2.

3.0.6.2   Statically Indeterminate.

The forces in the bars of a statically indeterminate pin-jointed truss are not zero, but are easily determined from the results of the previous paragraph.

3.0.7   Plates.

The analysis of plates presented in this section is based on the following classical theory of plates assumptions:

1.   The material is isotropic, homogeneous, and linearly elastic.

2.   The constant thickness of the plate is small when compared with its other dimensions.

3.   Plane sections, which before bending are normal to the median plane of the plate, remain plane and normal to the median plane after bending.

4.   The deflections of the plate are of the order of magnitude of the plate thickness.

Solutions are given herein for circular and rectangular plates with various boundary conditions and temperature distributions.

Analysis techniques for plates made of composite materials are given in Section F.

3.0.7.1   Circular Plates.

I.   Temperature Gradient Through the Thickness.

A.   Configuration.

The design curves and equations presented here apply only to flat, circular plates having central circular holes (Fig. 3.0-14). The plates must

C-2

be of constant thickness, be made of an isotropic material, and obey Hooke's

law. Curves are given which deal with bending phenomena for a/b ratios of

0.2, 0.4, 0.6, and 0.8 and are based on the assumption that $\nu = 0.30$. These

plots cover only a portion of the boundary conditions considered in connection

with bending behavior. The remainder of these conditions, as well as all the

membrane solutions, are given as closed-form algebraic equations which are

valid for arbitrary values of Poisson's ratio and the inner and outer radii of

the plate. When the ratio a/b approaches unity, the member is more properly

identified as a ring.

POSITIVE DIRECTIONS OF THE
STRESS RESULTANTS

MIDDLE SURFACE

NOTE: r, θ, z, u, v, and w
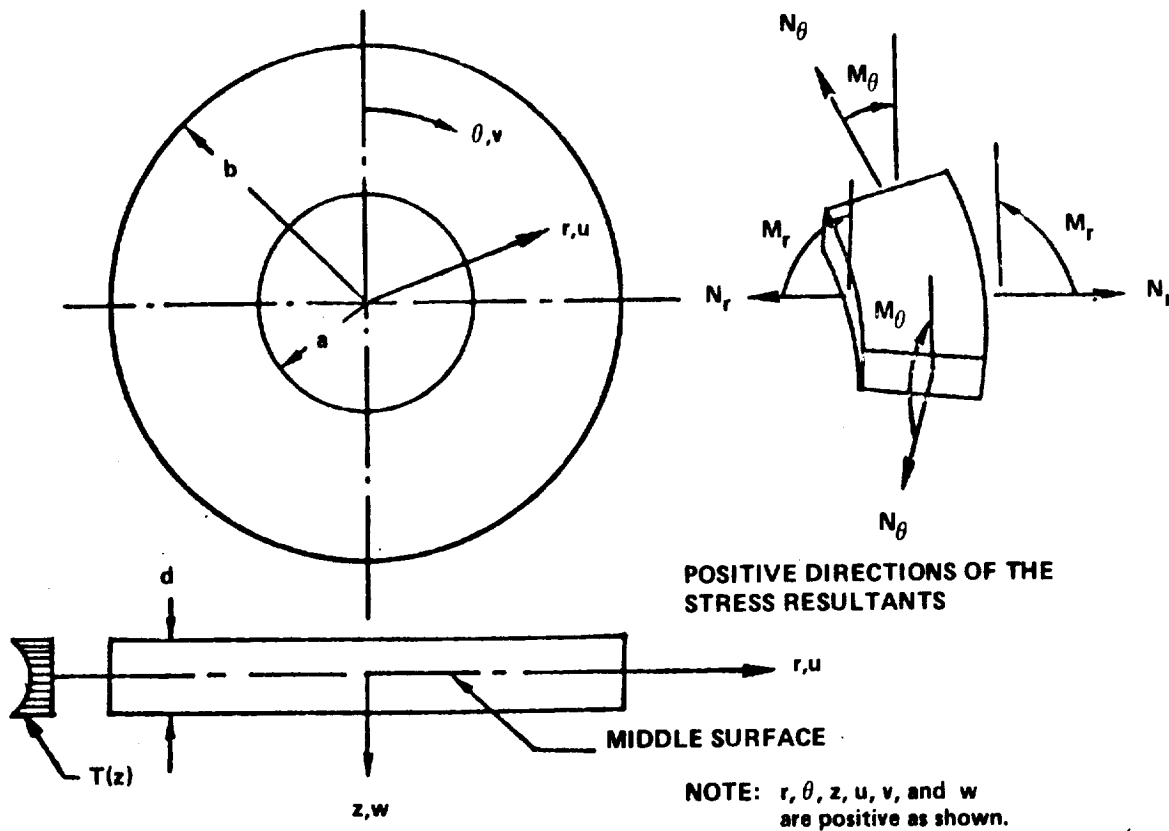are positive as shown.

Figure 3.0-14. Circular flat plate.

B.   Boundary Conditions.

Solutions are given for various combinations of the following boundary conditions for bending and membrane behavior, respectively.

Bending Phenomena.

1.   Clamped, that is,

$$w = \frac{\partial w}{\partial r} = 0 \quad \text{at} \quad r = b \quad \text{and/or} \quad r = a \; ;$$

2.   Simply supported, that is,

$$w = M_r = 0 \quad \text{at} \quad r = b \quad \text{and/or} \quad r = a \; ;$$

3.   Free, that is,

$$\left. \begin{aligned} M_r &= 0 \\[2em] \frac{\partial M_r}{\partial r} - 2\frac{\partial M_{r\theta}}{\partial \theta} &= 0 \end{aligned} \right\} \quad \text{at} \quad r = b \quad \text{and/or} \quad r = a \; .$$

Membrane Phenomena.

1.   Radially fixed, that is,

$$\bar{u} = \bar{v} = 0 \quad \text{at} \quad r = b \quad \text{and/or} \quad r = a \; ;$$

2.   Radially free, that is,

$$N_r = N_{r\theta} = 0 \quad \text{at} \quad r = b \quad \text{and/or} \quad r = a \; .$$

C. Temperature Distribution.

Arbitrary temperature variations may be present through the plate thickness. However, it is required that there be no gradients over the surface. Hence, the permissible distributions can be expressed in the form

$$T = T(z) \quad .$$

D. Design Curves and Equations.

In Ref. 2, Newman and Forray present the simple method given here to determine the thermal stresses and deflections for stable plates that satisfy the foregoing requirements. This technique is based on classical small-deflection theory and is an extension of the procedures published in Refs. 3 through 5 by the same authors. To perform the analysis, use is made of a number of equations and design curves. These are provided in the summary which follows.

It is assumed that Young's modulus and Poisson's ratio are unaffected by temperature variations. On the other hand, the temperature-dependence of the thermal-expansion coefficient can be accounted for by recognizing that it is the product αT which governs; that is, the actual temperature distribution can be suitably modified to compensate for variations in α .

E. Summary of Equations and Curves.

$$w = - \frac{w' a^2 M_T}{D_b (1 - \nu^2)} \quad ,$$

$$\sigma_r = \frac{1}{t}\left[N_r + \frac{N_T}{(1-\nu)}\right] + \frac{12z}{t^3}\left[M_r + \frac{M_T}{(1-\nu)}\right] - \frac{E\alpha T}{(1-\nu)} \quad,$$

and

$$\sigma_\theta = \frac{1}{t}\left[N_\theta + \frac{N_T}{(1-\nu)}\right] + \frac{12z}{t^3}\left[M_\theta + \frac{M_T}{(1-\nu)}\right] - \frac{E\alpha T}{(1-\nu)}$$

where

$$D_b = \frac{Et^3}{12\,(1-\nu^2)}$$

$$M_T = E\alpha \int_{-t/2}^{t/2} Tz\ dz \quad,$$

$$N_T = E\alpha \int_{-t/2}^{t/2} T\ dz \quad,$$

$$M_r = -12\ M_T M_r{}' \quad,$$

$$M_\theta = -12\ M_T M_\theta{}' \quad,$$

$$N_r = N_T N_r{}' \quad,$$

and

$$N_\theta = N_T N_\theta{}' \quad.$$

The values for w', M_r', and M_θ' are obtained either from Table 3.0-5 or Figures 3.0-15 through 3.0-19. When the figures are used, Poisson's ratio must be taken to be 0.3 throughout the analysis of bending phenomena. When Table 3.0-5 is employed, there are no restrictions on ν. Also note that, in most of the plots, the parameters include multiplication factors. The values for N_r' and N' are obtained from Table 3.0-6 and are also valid for any value of Poisson's ratio.

F.   Linear Gradient.

For the special case of a linear temperature gradient through the thickness for a solid plate represented by

$$T(z) = \frac{T_0 + T_1}{2} + \frac{T_0 - T_1}{2} z$$

the following solutions apply.

__Unrestrained Solid Circular Plate.__

$$\sigma_r = \sigma_\theta = 0 \quad .$$

The plate becomes curved and fits a sphere of radius inversely proportional to the difference in surface temperatures and directly proportional to the thickness.

__Clamped Plate.__

$$w = 0$$

TABLE 3.0-5. NONDIMENSIONAL PARAMETERS FOR BENDING PHENOMENA

Boundary Conditions		w'	M_r'	M_θ'
Outer Edge	Inner Edge			
Free	Free	$\frac{1}{2}\left(\frac{r^2}{a^2}-1\right)$ (Relative to Inner Boundary)	0	0
Clamped	Clamped	0	$\frac{1}{12(1-\nu)}$	$\frac{1}{12(1-\nu)}$
Simply Supported	Free	$\frac{1}{2}\left(\frac{r^2}{a^2}-\frac{b^2}{a^2}\right)$	0	0
Free	Simply Supported	$\frac{1}{2}\left(\frac{r^2}{a^2}-1\right)$	0	0

TABLE 3.0-6. NONDIMENSIONAL PARAMETERS FOR MEMBRANE PHENOMENA

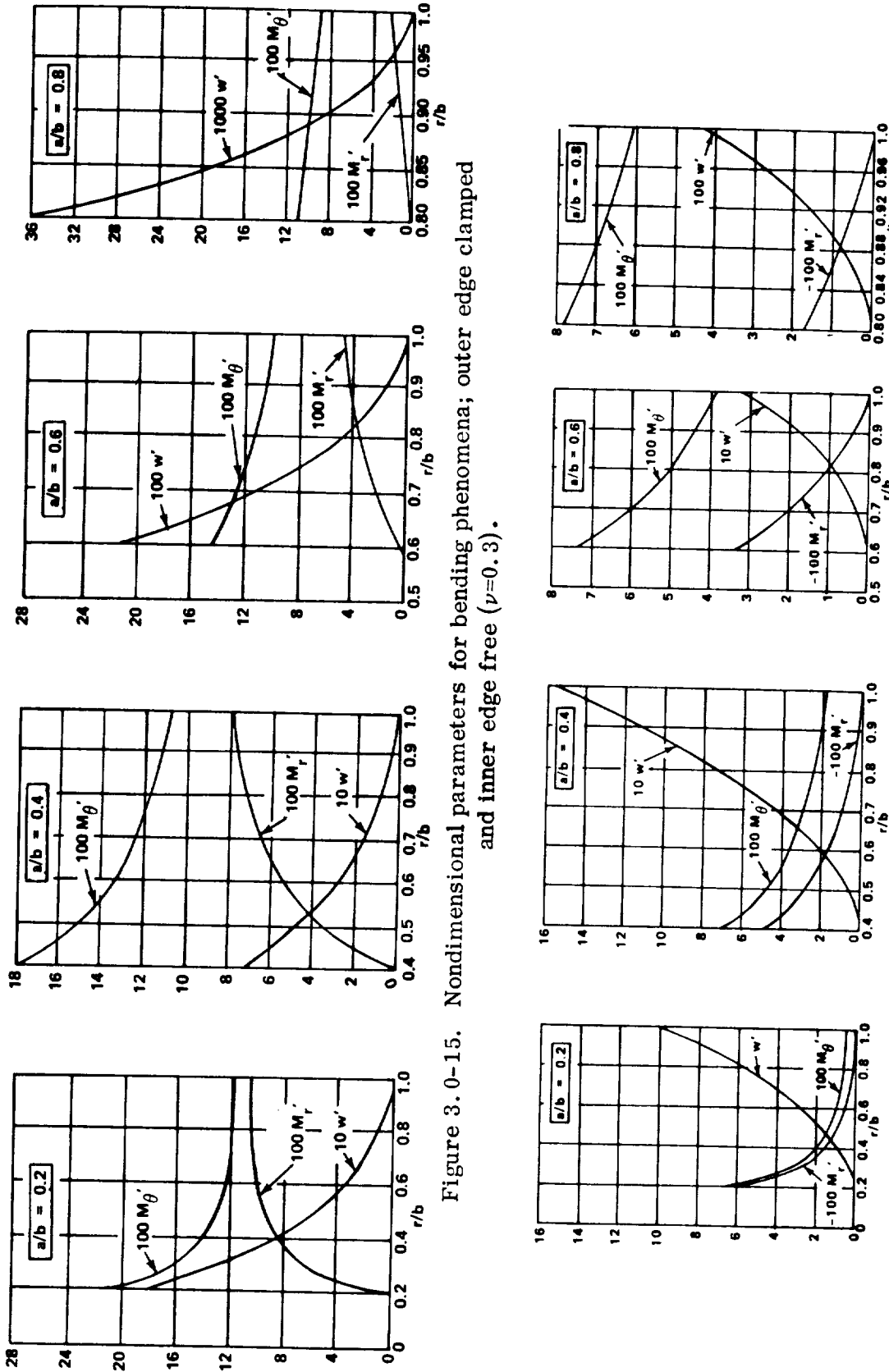| Boundary Conditions		N_r'	N_θ'
Outer Edge	Inner Edge		
Radially Free	Radially Free	0	0
Radially Fixed	Radially Free	$\dfrac{\left[\left(\frac{a}{r}\right)^2-1\right]}{\left[(1+\nu)\left(\frac{a}{b}\right)^2+(1-\nu)\right]}$	$\dfrac{-\left[\left(\frac{a}{r}\right)^2+1\right]}{\left[(1+\nu)\left(\frac{a}{b}\right)^2+(1-\nu)\right]}$
Radially Free	Radially Fixed	$\dfrac{\left[\left(\frac{b}{r}\right)^2-1\right]}{\left[(1+\nu)\left(\frac{b}{a}\right)^2+(1-\nu)\right]}$	$\dfrac{-\left[\left(\frac{a}{r}\right)^2+1\right]}{\left[(1+\nu)\left(\frac{b}{a}\right)^2+(1-\nu)\right]}$
Radially Fixed	Radially Fixed	$-\dfrac{1}{(1-\nu)}$	$-\dfrac{1}{(1-\nu)}$

Figure 3.0-15. Nondimensional parameters for bending phenomena; outer edge clamped and inner edge free ($\nu=0.3$).

Figure 3.0-16. Nondimensional parameters for bending phenomena; outer edge free and inner edge clamped ($\nu=0.3$).

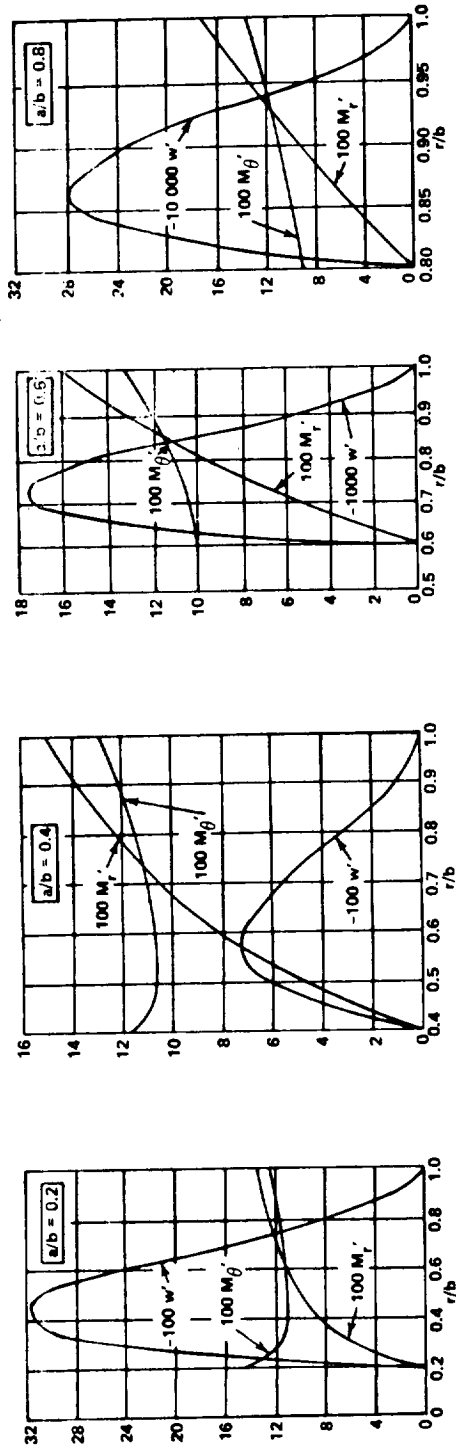Figure 3.0-17. Nondimensional parameters for bending phenomena; outer edge clamped and inner edge simply supported ($\nu = 0.3$).
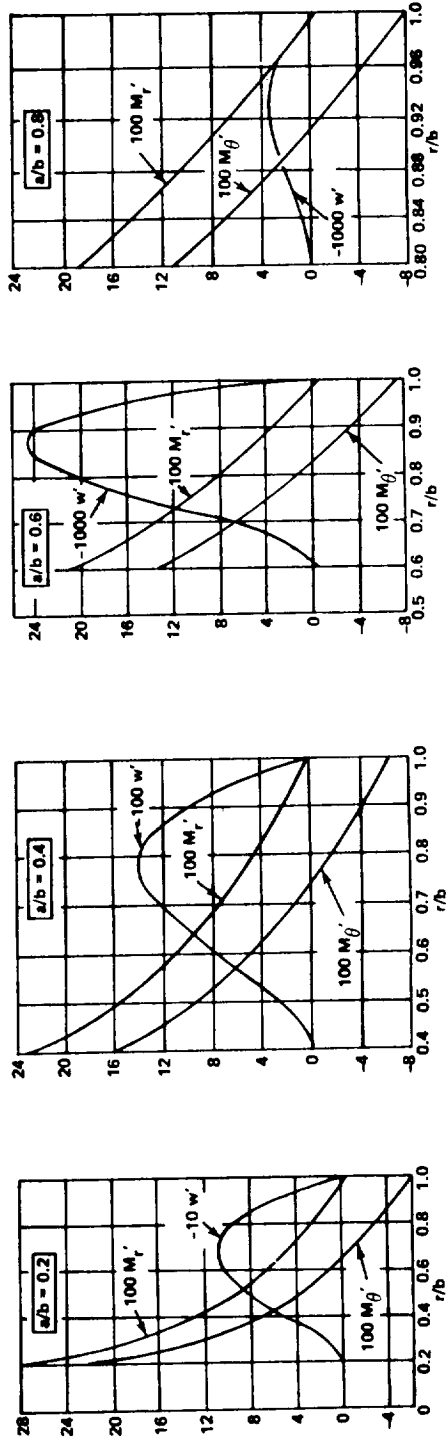
Figure 3.0-18. Nondimensional parameters for bending phenomena; outer edge simply supported and inner edge clamped ($\nu = 0.3$).
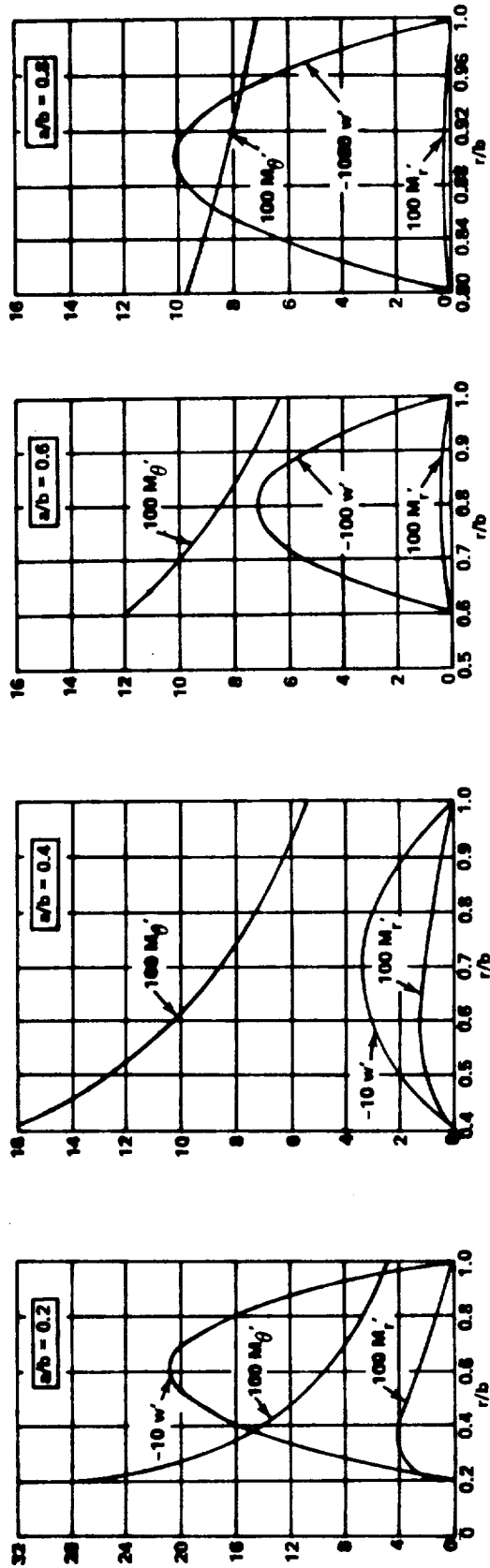
Figure 3.0-19. Nondimensional parameters for bending phenomena; outer edge simply supported and inner edge simply supported (ν=0.3).

and

$$\sigma_r\big|_{max} = \sigma_\theta\big|_{max} = \frac{\alpha E(T_1 - T_0)}{2(1 - \nu)} \quad .$$

Simply Supported Plate.

$$\sigma_r = \sigma_\theta = 0$$

and

$$w = \frac{-\alpha(T_1 - T_0)}{2t}(a^2 - r^2) \quad .$$

II. <u>Temperature Difference as a Function of the Radial Coordinates</u>.

A. Clamped Plate.

For the variation of temperature, assumed to be linear through the thickness, and the variation with r given by the monomial,

$$T = -\frac{z}{h}A_\kappa r^\kappa + c$$

where A_κ and c are constants.

$$T_D = A_\kappa r^\kappa \quad ,$$

$$T_D(a) = A_\kappa a^\kappa \quad ,$$

$$w = \frac{(1 + \nu)a^2\alpha T_D(a)}{(\kappa + 2)^2} \left[\left(\frac{r}{a}\right)^{\kappa+2} - \left(\frac{\kappa}{2} + 1\right)\left(\frac{r}{a}\right)^2 + \frac{\kappa}{2} \right] ,$$

$$M_r = \frac{Eh^2\alpha T_D(a)}{12(\kappa + 2)} \left[\left(\frac{r}{a}\right)^\kappa + \frac{1 + \nu}{1 - \nu} \right]$$

and

$$M_\theta = \frac{Eh^2\alpha T_D(a)}{12(\kappa + 2)} \left[(\kappa + 1)\left(\frac{r}{a}\right)^\kappa + \frac{1 + \nu}{1 - \nu} \right] ,$$

where T_D is the temperature difference between the surfaces.

Curves of nondimensional deflection and moments are presented in Figures 3.0-20 through 3.0-22 for $\kappa = 1, 2, \ldots 5$. Superposition may then be used for T_D given by polynomials in r . The determination of a polynomial describing the radial variation of T_D can be obtained in the same manner as shown in Paragraph 3.0.2.3.

B. Radially Fixed or Radially Free Plate.

Configuration.

The design equations provided here apply only to flat, circular plates which may or may not have a central circular hole. The plate must be of constant thickness, be made of an isotropic material, and obey Hooke's law. Formulas are given which cover the range

$$0 \le \frac{a}{b} < 1 .$$
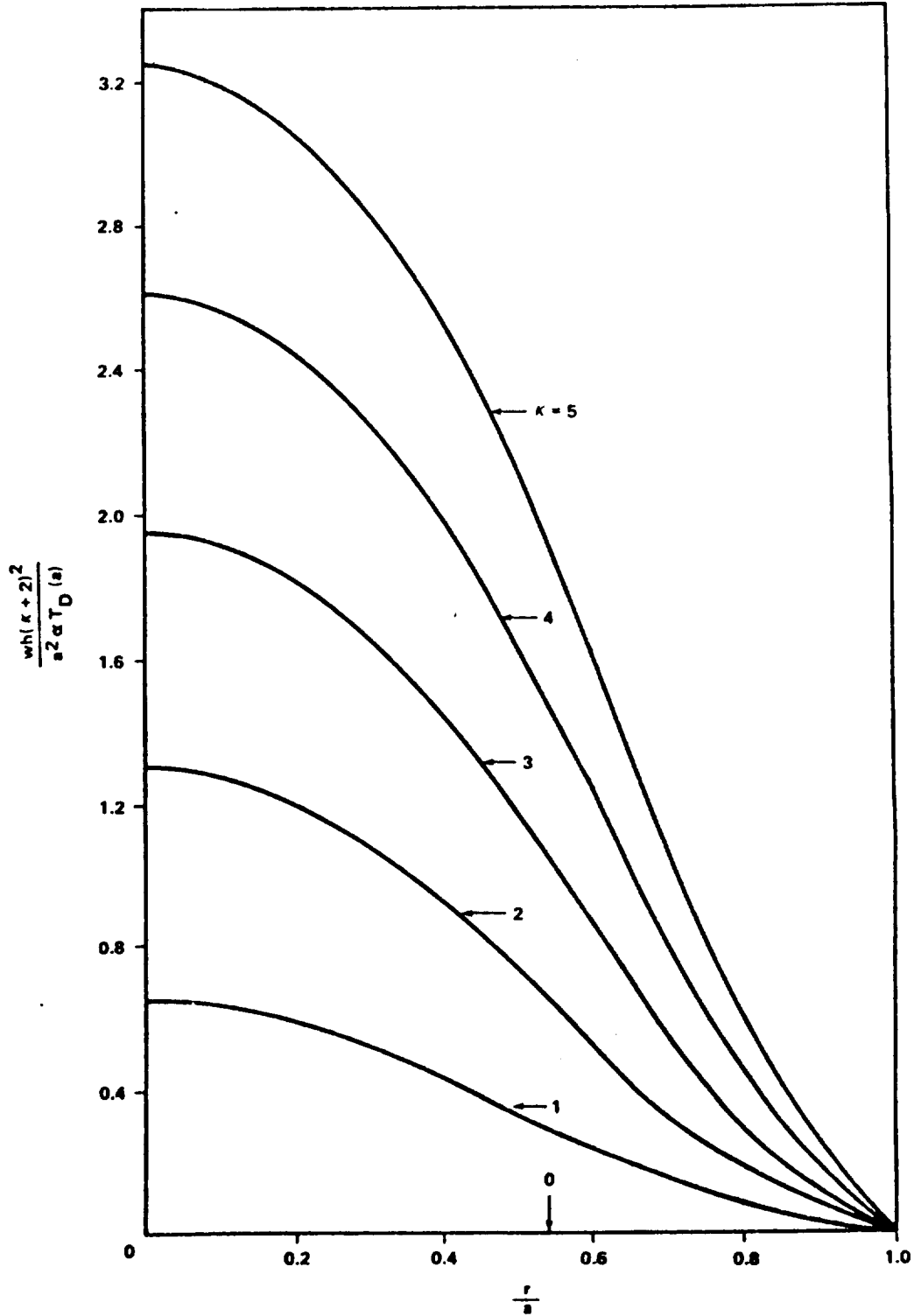
Figure 3.0-20. Nondimensional deflection.
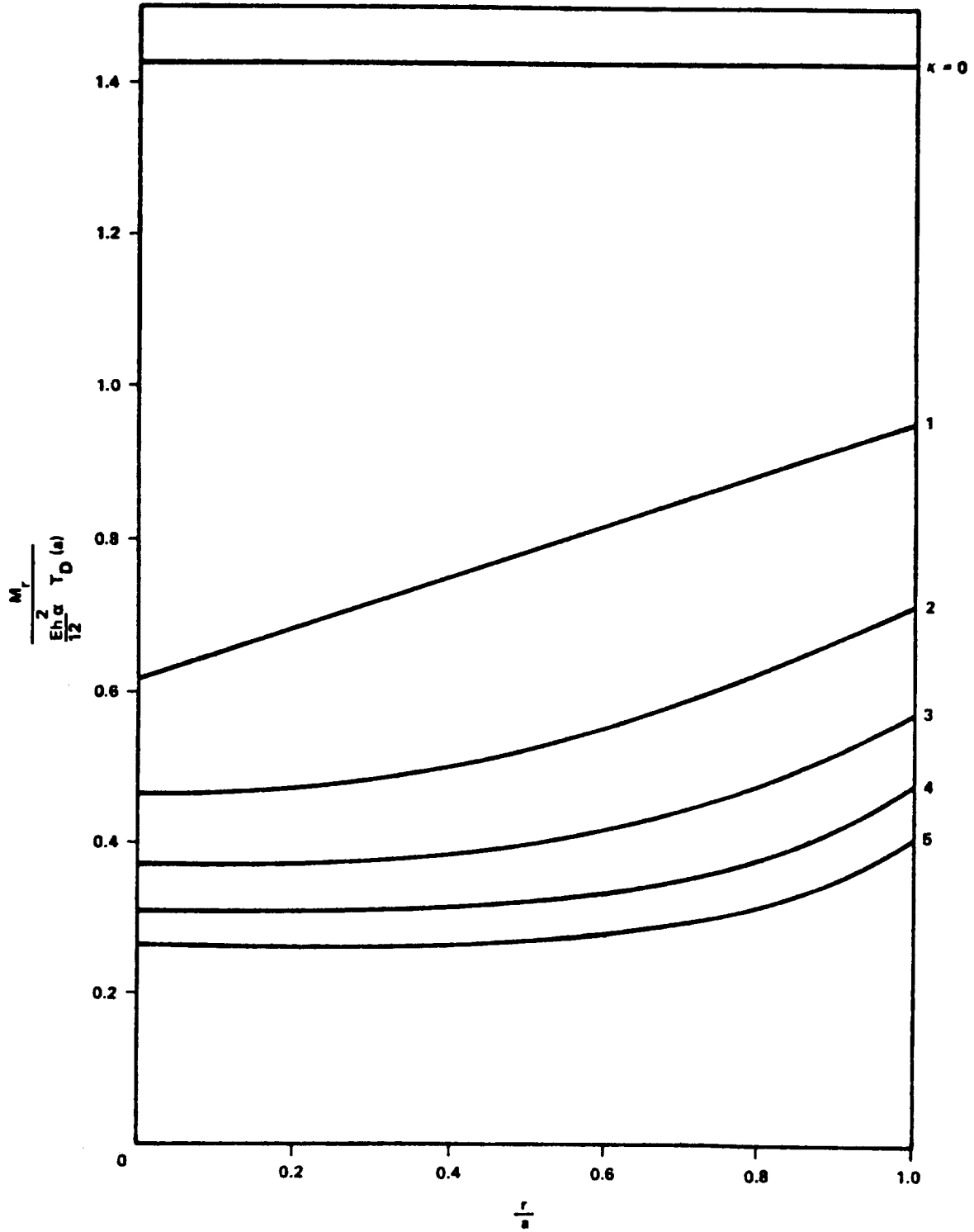
Figure 3.0-21. Nondimensional radial moment.
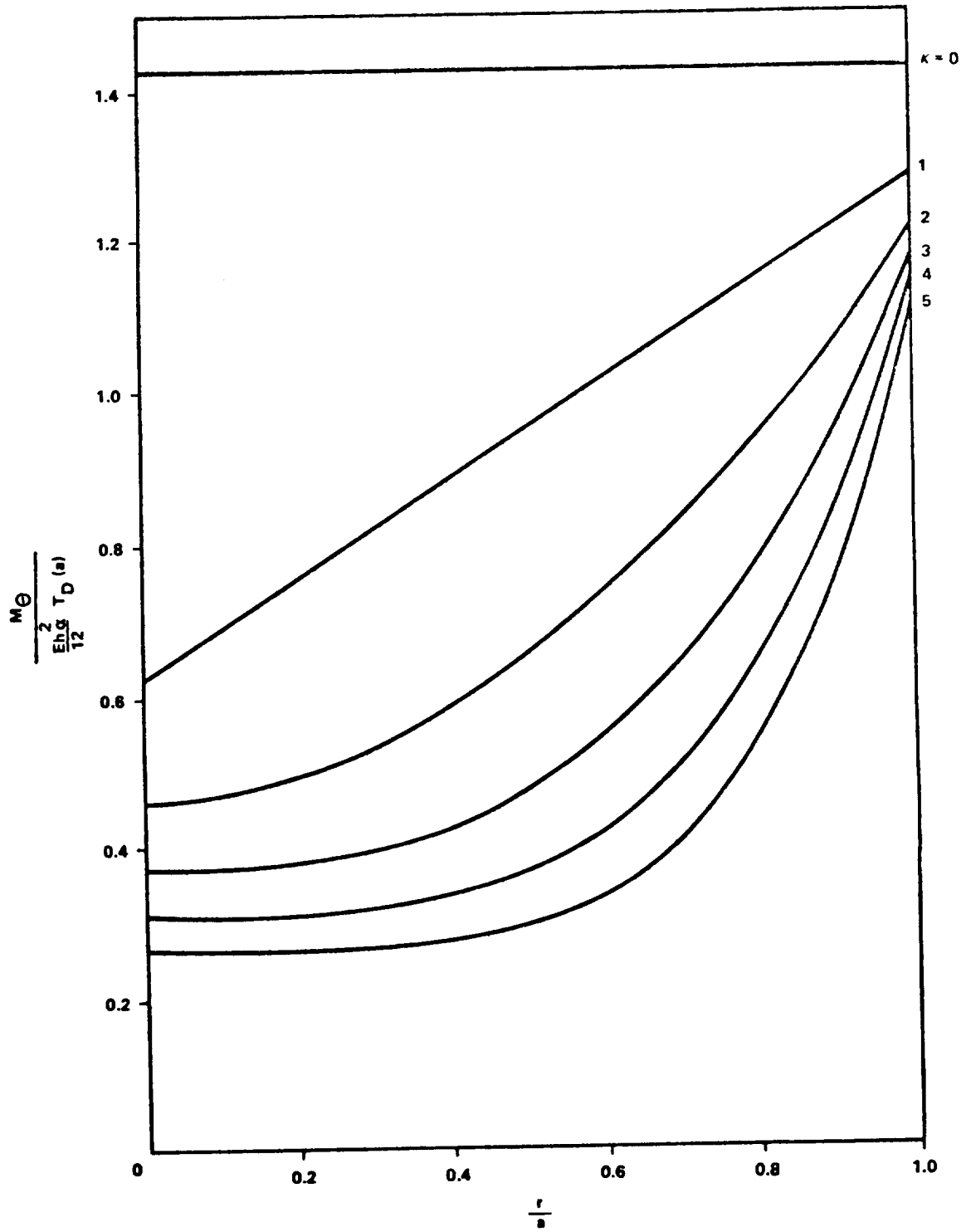
Figure 3.0-22.   Nondimensional tangential moment.

As this ratio approaches unity, the member is more properly identified as a ring.

Boundary Conditions.

Solutions are given for each of the following types of boundary conditions.

1. Radially free; that is,

$$\sigma_r = \sigma_{r\theta} = 0 \quad \text{at} \quad r = b$$

and

$$\sigma_r = \sigma_{r\theta} = 0 \quad \text{at} \quad r = a$$

if hole is present.

2. Outer boundary radially fixed (if hole is present, the inner boundary is radially free); that is,

$$u = v = 0 \quad \text{at} \quad r = b$$

and

$$\sigma_r = \sigma_{r\theta} = 0 \quad \text{at} \quad r = a$$

if hole is present.

Temperature Distribution.

The supposition is made that the temperature is uniform through the thickness. However, the plate may be subjected to a surface distribution

which has an arbitrary radial gradient but no circumferential variations.

Hence, the permissible distributions can be expressed in the form

$$T = T(r) \quad .$$

Design Equations.

In this section, it is assumed that Young's modulus and Poisson's

ratio are unaffected by temperature changes. Therefore, the user must select

single effective values for each of these properties by using some type of

averaging technique. The same approach may be taken with regard to the

coefficient of thermal expansion. On the other hand, the temperature-

dependence of this property can be accounted for by recognizing that it is the

product αT which governs; that is, the actual temperature distribution can

be suitably modified to compensate for variations in α .

The design equations are given in the summary which follows and are

based on classical small-deflection theory. The expressions for the radially

free plates were taken directly from Ref. 1. The equations for plates with

radially fixed outer boundaries were derived by superposition of the free-plate

formulas and the relationships given in Ref. 6 for cylinders subjected solely

to external radial pressure. Depending upon the complexity of the temperature

distribution, the required integrations may be performed either analytically

or by numerical procedures.

Summary of Equations.

Solid Plates (No Central Hole).

1. Radially free boundary:

$$\sigma_r = \alpha E \left(\frac{1}{b^2} \int_0^b Tr \, dr - \frac{1}{r^2} \int_0^r Tr \, dr \right) \, ,$$

$$\sigma_\theta = \alpha E \left(-T + \frac{1}{b^2} \int_0^b Tr \, dr + \frac{1}{r^2} \int_0^r Tr \, dr \right) \, ,$$

and

$$u = \frac{\alpha}{r} \left[(1 + \nu) \int_0^r Tr \, dr + (1 - \nu)\left(\frac{r}{b}\right)^2 \int_0^b Tr \, dr \right] \, .$$

These three equations are indeterminate at $r = 0$. However, by the application of l'Hospital's rule, it is found that [1]

$$(\sigma_r)_{r=0} = (\sigma_\theta)_{r=0} = \alpha E \left[\frac{1}{b^2} \int_0^b Tr \, dr - \frac{1}{2}(T)_{r=0} \right]$$

and

$$u_{r=0} = 0 \, .$$

2.   Radially fixed boundary:

$$\sigma_r = \alpha E \left[\frac{1}{b^2} \int_0^b Tr \, dr - \frac{1}{r^2} \int_0^r Tr \, dr - \frac{2}{b^2(1-\nu)} \int_0^b Tr \, dr \right] \quad ,$$

$$\sigma_\theta = \alpha E \left[-T + \frac{1}{b^2} \int_0^b Tr \, dr + \frac{1}{r^2} \int_0^r Tr \, dr - \frac{2}{b^2(1-\nu)} \int_0^b Tr \, dr \right] \quad ,$$

and

$$u = \frac{\alpha}{r} \left[(1 + \nu) \int_0^r Tr \, dr - (1 + \nu) \left(\frac{r}{b}\right)^2 \int_0^b Tr \, dr \right] \quad .$$

These three equations are indeterminate at $r = 0$. However, by the application of l' Hospital's rule, it is found that

$$\left(\sigma_r\right)_{r=0} = \left(\sigma_\theta\right)_{r=0} = \alpha E \left[\frac{1}{b^2} \int_0^b Tr \, dr - \frac{2}{b^2(1-\nu)} \int_0^b Tr \, dr - \frac{1}{2} T_{r=0} \right]$$

and

$$u_{r=0} = 0 \quad .$$

Plates with Central Hole.

1.   Both boundaries radially free:

$$\sigma_r = \frac{\alpha E}{r^2} \left(\frac{r^2 - a^2}{b^2 - a^2} \int_a^b Tr \, dr - \int_a^r Tr \, dr \right) \quad ,$$

$$\sigma_\theta = \frac{\alpha E}{r^2} \left(\frac{r^2 + a^2}{b^2 - a^2} \int\limits_a^b Tr \, dr + \int\limits_a^r Tr \, dr - Tr^2 \right) ,$$

and

$$u = \frac{\alpha}{r} \left[(1 + \nu) \int\limits_a^r Tr \, dr + \frac{(1 - \nu) r^2 + (1 + \nu) a^2}{b^2 - a^2} \int\limits_a^b Tr \, dr \right] .$$

2. Inner boundary radially free and outer boundary radially fixed:

$$\sigma_r = \frac{\alpha E}{r^2} \left[\frac{r^2 - a^2}{b^2 - a^2} \int\limits_a^b Tr \, dr - \int\limits_a^r Tr \, dr \right] + (\sigma_r)_{r=b} \left[\frac{b^2}{b^2 - a^2} \left(1 - \frac{a^2}{r^2} \right) \right] ,$$

$$\sigma_\theta = \frac{\alpha E}{r^2} \left[\frac{r^2 + a^2}{b^2 - a^2} \int\limits_a^b Tr \, dr + \int\limits_a^r Tr \, dr - Tr^2 \right]$$

$$+ (\sigma_r)_{r=b} \left[\frac{b^2}{b^2 - a^2} \left(1 + \frac{a^2}{r^2} \right) \right] ,$$

$$u = \frac{\alpha}{r} \left[(1 + \nu) \int\limits_a^r Tr \, dr + \frac{(1 - \nu) r^2 + (1 + \nu) a^2}{(b^2 - a^2)} \int\limits_a^b Tr \, dr \right]$$

$$+ (\sigma_r)_{r=b} \left\{ \frac{b^2}{E(b^2 - a^2)} \left[(1 - \nu) r + \frac{(1 + \nu)}{r} a^2 \right] \right\} ,$$

where

$$(\sigma_r)_{r=b} = - \frac{\alpha E}{b^2} \frac{1}{\left(\frac{b^2 + a^2}{b^2 - a^2} - \nu \right)} \left[(1 + \nu) \int\limits_a^b Tr \, dr \right.$$

$$+ \frac{(1-\nu)\, b^2 + (1+\nu)\, a^2}{(b^2 - a^2)} \int_a^b Tr\, dr \Bigg] \quad .$$

III.   Disk With Central Shaft.

Boundary conditions for this plane-stress problem are $u\big|_{r=a} = 0$

and $\sigma_{rr}\big|_{r=a} = 0$.

$$T = T_b \left(\frac{r-a}{b-a} \right)^n \quad ,$$

$$\frac{\sigma_{rr}}{\alpha E T_b} = \frac{1}{2} \left[\frac{T_b^*}{T_b} \left(1 - \frac{a^2}{b^2} \right) \frac{\left(\frac{1+\nu}{1-\nu} + \frac{a^2}{r^2} \right)}{\left(\frac{1+\nu}{1-\nu} + \frac{a^2}{r^2} \right)} - \frac{T^*}{T_b} \left(1 - \frac{a^2}{r^2} \right) \right] \quad ,$$

$$\frac{\sigma_{\theta\theta}}{\alpha E T_b} = \frac{1}{2} \left[\frac{T_b^*}{T_b} \left(1 - \frac{a^2}{r^2} \right) \frac{\left(\frac{1+\nu}{1-\nu} + \frac{a^2}{r^2} \right)}{\left(\frac{1+\nu}{1-\nu} + \frac{a^2}{r^2} \right)} + \frac{T^*}{T_b} \left(1 - \frac{a^2}{r^2} \right) - \frac{2T}{T_b} \right] \quad ,$$

$$\frac{\sigma_{rr}}{\alpha E T_b} \bigg|_{r=a} = \left\{ \frac{T_b^*}{T_b} \left(1 - \frac{a^2}{b^2} \right) \left[\frac{1}{(1+\nu) + \frac{a^2}{b^2}(1-\nu)} \right] \right\} \quad ,$$

$$\frac{\sigma_{\theta\theta}}{\alpha E T_b} \bigg|_{r=a} = \left\{ \frac{T_b^*}{T_b} \left(1 - \frac{a^2}{b^2} \right) \left[\frac{\nu}{(1+\nu) + \frac{a^2}{b^2}(1-\nu)} \right] \right\} \quad ,$$

$$\frac{\sigma_{\theta\theta}}{\alpha E T_b} \bigg|_{r=b} = \left\{ \frac{T_b^*}{T_b} \left(1 - \frac{a^2}{b^2} \right) \left[\frac{1}{1 + \left(\frac{1-\nu}{1+\nu} \right) \frac{a^2}{b^2}} \right] - 1 \right\} \quad ,$$

and

$$T^* = \frac{2}{r^2 - a^2} \int_a^r Tr\, dr = \frac{2T_b}{r+a} \left(\frac{r-a}{b-a} \right)^n \frac{[(n+1)\, r + a]}{(n+1)(n+2)}$$

where

$$T_b^* = \frac{2}{r^2 - a^2} \int_a^b Tr \, dr = \frac{2T_b}{a + b} \frac{[(n+1)\,b + a]}{(n+1)(n+2)} \quad .$$

Curves showing the variations of $\left.\dfrac{\sigma_{rr}}{\alpha ET_b}\right|_{r=a}$ and $\left.\dfrac{\sigma_{\theta\theta}}{\alpha ET_b}\right|_{r=b}$ with n

and a/b are given in Figures 3.0-23 through 3.0-25.
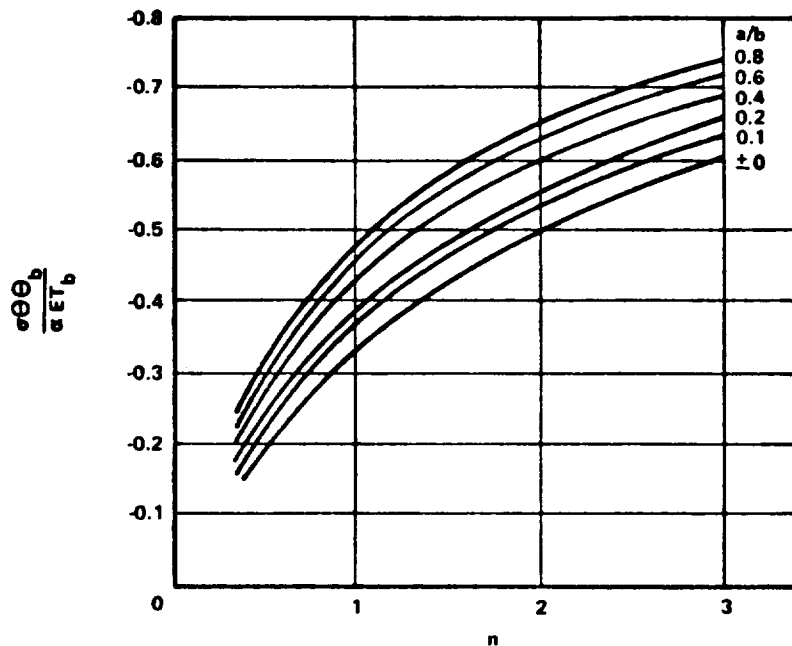
Figure 3.0-23.   Variation of tangential stress at outer boundary with n
and a/b for a disk on a shaft.

Additional cases that may be obtained from Refs. 7 and 8 are as follows:

1. Circular plate with asymmetrical temperature distribution

2. Circular disk with concentric hole subjected to asymmetrical

temperature distribution

3. Circular plate with a central hot spot.
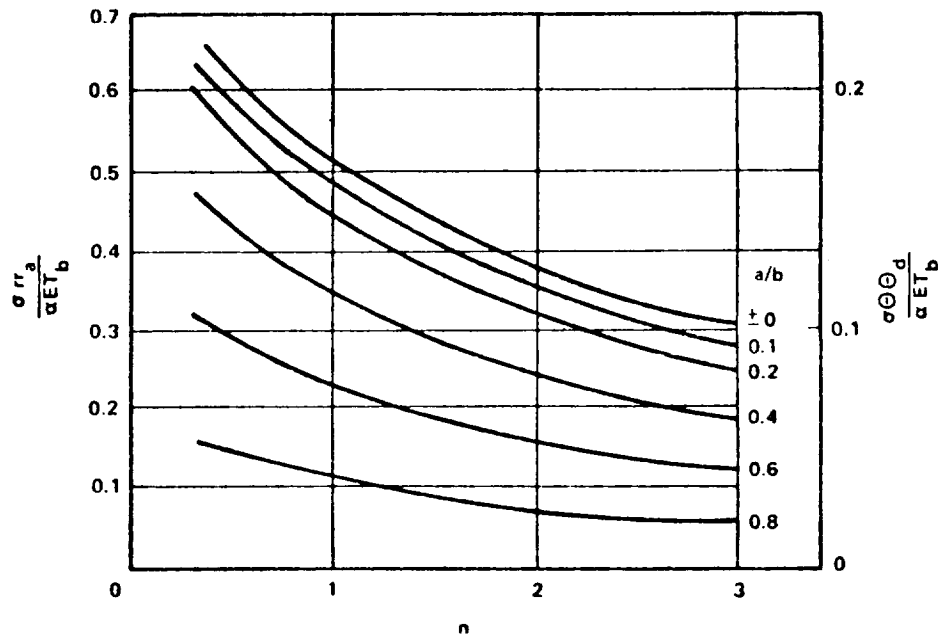
Figure 3.0-24. Variation of radial and tangential stress at inner
boundary of disk with n and a/b for a disk on a shaft.
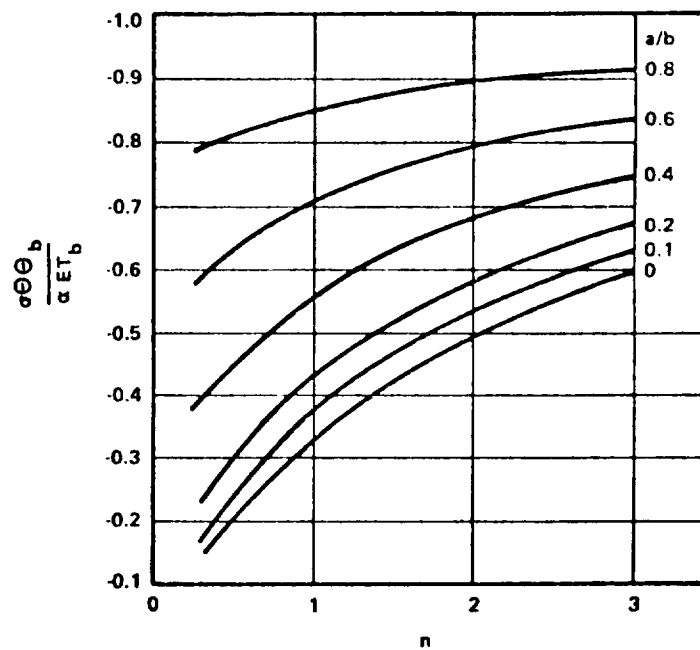
Figure 3.0-25. Variation of tangential stress at outer boundary
of disk with n and a/b for a disk on a shaft.

3.0.7.2   Rectangular Plates.

    I.   <u>Temperature Gradient Through the Thickness</u>.

        A. Configuration.

The design curves and equations provided here apply only to flat, rectangular plates which are of constant thickness and are made of isotropic material. The two long edges of the plate are supported by flexible beams. It is assumed that both the plate and the support beams are free of holes and that no stresses exceed the elastic limit in either of these members. The design curves cover aspect ratios b/a of 1.0, 1.5, and 3.0.

        B. Boundary Conditions.

The edges $x = 0$ and $x = a$ are elastically supported by beams having equal flexural stiffnesses $E_b I_b$. Both beams are simply supported at their ends (Fig. 3.0-26) and are free to undergo axial expansions or contractions. These members offer no constraint to each of the following plate deformations:

    1. Edge-Rotation

    2. In-Place Edge-Displacements u and v.

The beams resist only transverse deflections w. The edges $y = 0$ and $y = b$ are simply supported; that is,

$$w = M_y = 0$$

along these two boundaries.

**ARBITRARY
ONE-DIMENSIONAL
TEMPERATURE
DISTRIBUTION**
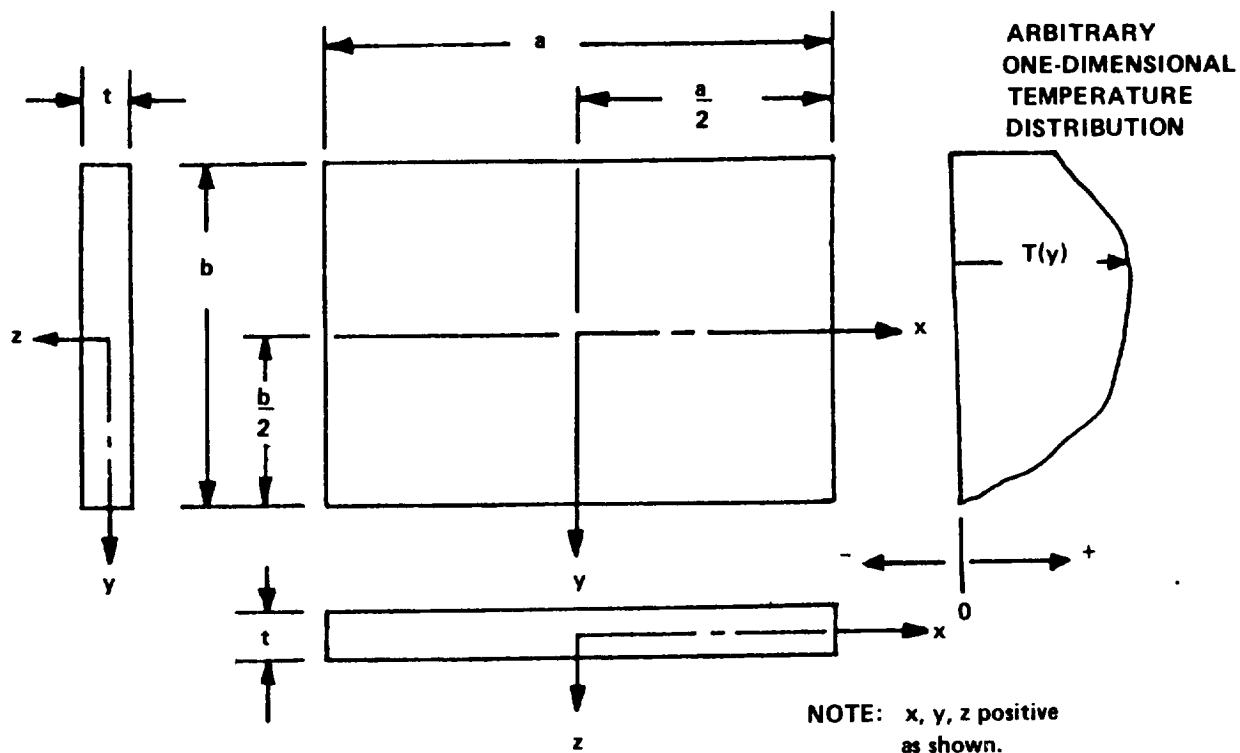
Figure 3.0-26. Rectangular flat plate with one-dimensional
temperature distribution over surface.

C. Temperature Distribution.

Separate coverage is provided for each of the following temperature

distributions through the thickness:

1. Linear gradient $T = a_0' + a_1'z$

2. Arbitrary gradient $T = f(z)$.

It is assumed that there are no temperature variations in directions parallel

to the middle surface of the plate.

D. Design Curves and Equations.

In Ref. 9, Forray, et al., present the simple methods given here to

compute thermal stresses and deflections at virtually any point in flat,

rectangular plates which comply with the foregoing specifications. These techniques consist of a variety of equations and curves, all of which are based on the conventional small-deflection theory of plates. It is assumed that Young's modulus and Poisson's ratio are unaffected by temperature variations. Hence, the user must select single effective values for each of these properties by employing some type of averaging technique. The same approach may be taken with regard to the coefficient of thermal expansion. On the other hand, the temperature-dependence of this property can be accounted for by recognizing that it is the product T which governs; that is, the actual temperature distribution can be suitably modified to compensate for variations in α. When this approach is taken, the user must adopt the viewpoint that any mention of a linear temperature distribution is actually referring to a straight-line variation of the product αT.

Linear Temperature Gradient.

For a linear temperature gradient expressed by

$$T = a'_0 + a'_1 z$$

and with

$$T_D = T_{(z=-t/2)} - T_{(z=t/2)} \quad ,$$

$$D_b = \frac{E_p t^3}{12(1 - \nu^2)}$$

and

$$M = \frac{4D_b \alpha\, T_D (1 - \nu^2)}{t} \quad .$$

The transverse deflections are expressed by

$$w = \overline{w}(x,y) + w^A(x,y) + w^A(a - x,y)$$

where

$$\overline{w}(x,y) = \frac{(1+\nu)\alpha\, T_D\, a^2}{2t}\left[\frac{x}{a}\left(1 - \frac{x}{a}\right) - \frac{8}{\pi^3}\sum_{n=1,3,\ldots}^{\infty}{}' \frac{\sin\frac{n\pi x}{a}\left[\cosh\frac{n\pi}{a}\left(y - \frac{b}{2}\right)\right]}{n^3\cosh\frac{n\pi b}{2a}}\right] \quad ,$$

$$w^A(x,y) = \sum_{m=1,3,\ldots}^{\infty} G_m^*\left[\frac{m\pi x}{b}\cosh\frac{m\pi x}{b} - \left(\frac{2}{1-\nu} + \frac{m\pi a}{b}\coth\frac{m\pi a}{b}\right)\sinh\frac{m\pi x}{b}\right]\sin\frac{m\pi y}{b}$$

and

$$G_m^* = \frac{-\frac{4M}{m\pi a}\left[\sum_{k=1,3,\ldots}^{2N-1}\frac{1}{1 + \left(\frac{k\,b}{m\,a}\right)^2}\right]\sinh\frac{m\pi a}{b}}{D_b\left(\frac{m\pi}{b}\right)^3\left\{\left(\cosh\frac{m\pi a}{b} - 1\right)\left[(3+\nu)\sinh\frac{m\pi a}{b} - (1-\nu)\frac{m\pi a}{b}\right] + \frac{2}{1-\nu}\left(\frac{E_b I_b}{D_b b}\right)m\pi\sinh^2\left(\frac{m\pi a}{b}\right)\right\}}$$

The component $\overline{w}(x,y)$ is the deflection where all edges are simply supported.

The bending moments M_x and M_y can be obtained by substituting the final deflection relation into the following equations:

$$M_x = -D_b \left[\frac{\partial^2 w}{\partial x^2} + \nu \frac{\partial^2 w}{\partial y^2} + \frac{\alpha T_D}{t}(1 + \nu) \right]$$

and

$$M_y = -D_b \left[\frac{\partial^2 w}{\partial y^2} + \nu \frac{\partial^2 w}{\partial x^2} + \frac{\alpha T_D}{t}(1 + \nu) \right] \quad .$$

Forray et al. [9] used these deflection and moment expressions to generate the design curves of Figures 3.0-27 through 3.0-35, where it is assumed that $\nu = 0.30$. Some of the curves are discontinued near the corners of the plate $x/a = 0$, $y/b = 0$ since the conventional theory breaks down at these locations. Certain of these results also appear in Ref. 10, where a different plotting format was used. In addition, the latter reference includes supplementary curves for the case where $E_b I_b / D_b b \rightarrow \infty$. This corresponds to the condition of simple support on all four edges.

Because of symmetry about the centerlines $(x = a/2 , y = b/2)$, it was necessary to show only one quadrant of the plate in Figures 3.0-27 through 3.0-35. The assortment of curves covers a wide range of values in the variables and should accommodate most practical problems of this particular class. For any situations where the plots prove to be inadequate, the equations can be used to obtain solutions. However, a considerable amount of rather routine mathematics would be required in making the necessary substitutions to obtain bending-moment equations in series form. Once these were available, it might
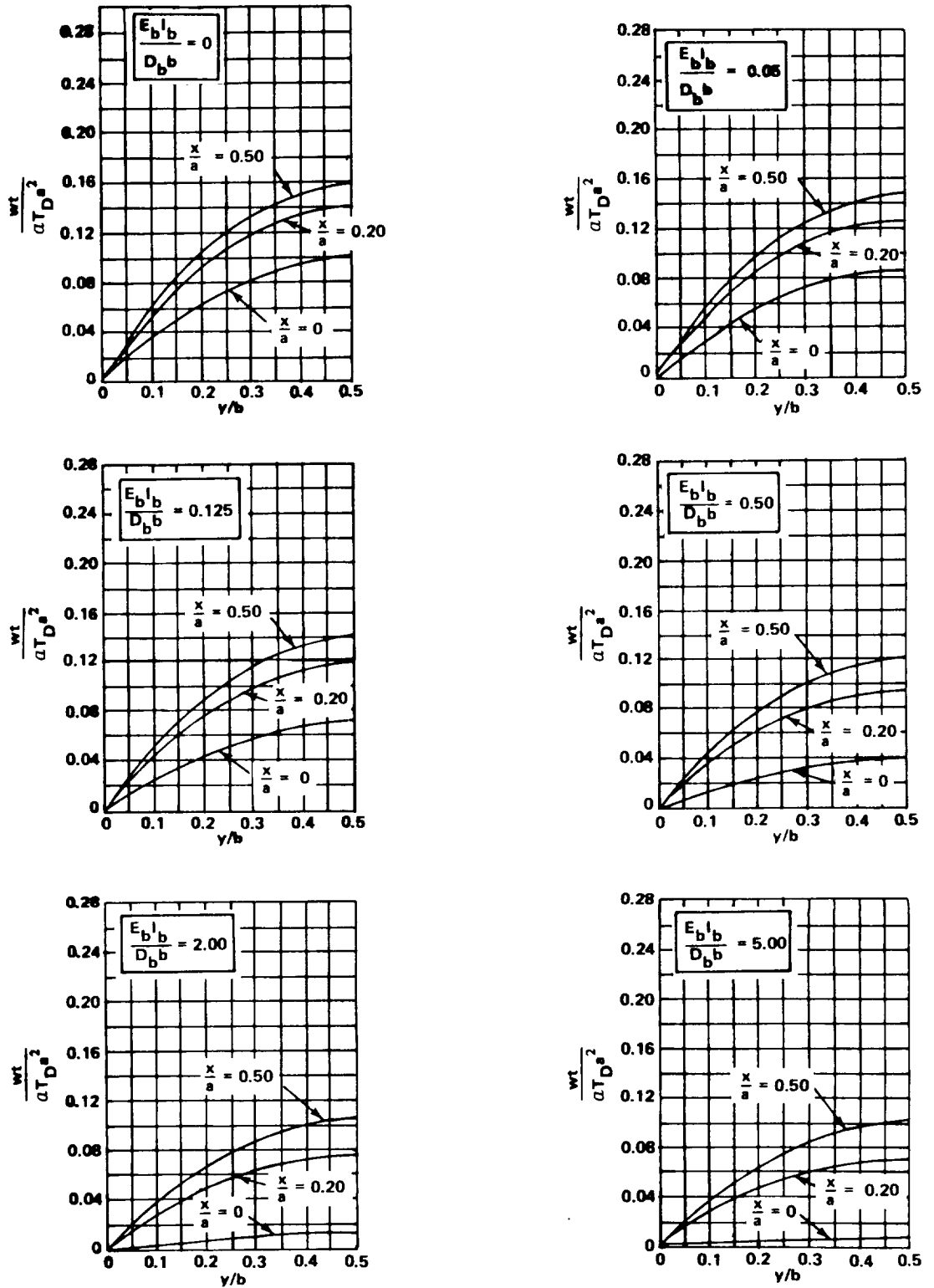
Figure 3.0-27. Nondimensional deflections for a plate with two
opposite edges elastically supported and the other
two edges simply supported; $b/a = 1.0$, $\nu = 0.30$.
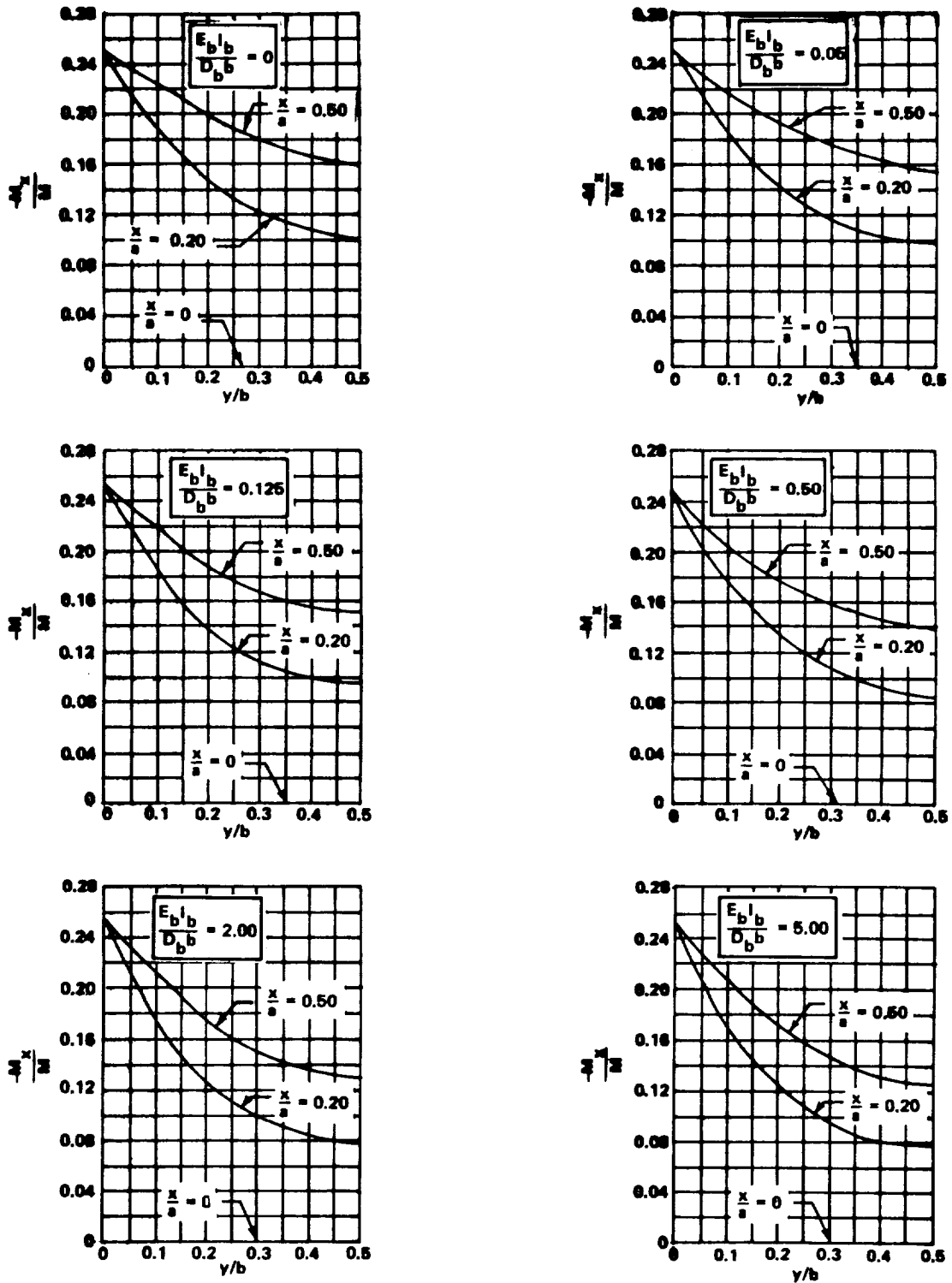
Figure 3.0-28. Nondimensional bending moments M_x/M for a plate
with two opposite edges elastically supported and the other
two edges simply supported; $b/a = 1.0$, $\nu = 0.30$.
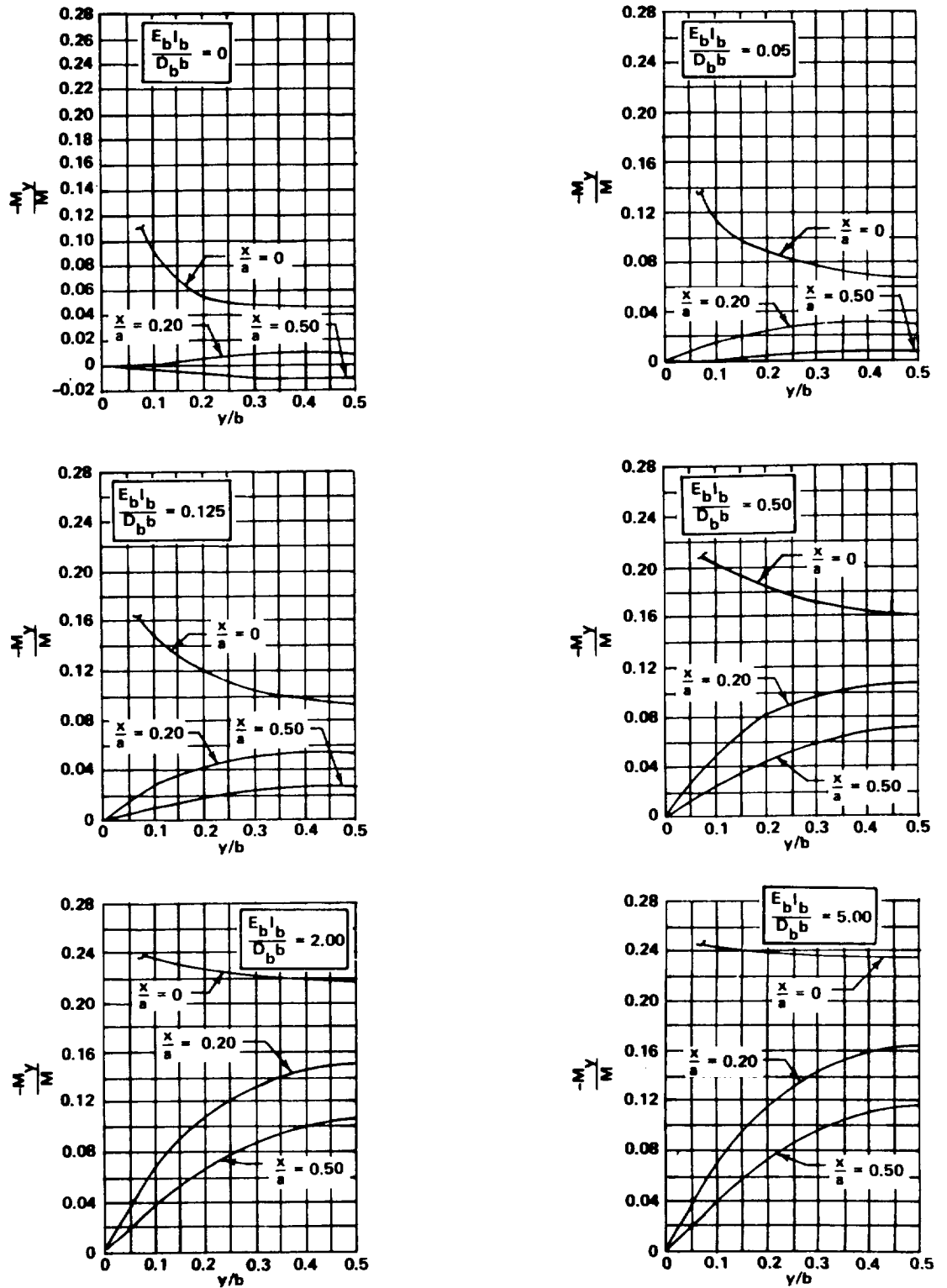
Figure 3.0-29. Nondimensional bending moments M_y/M for a plate
with two opposite edges elastically supported and the other
two edges simply supported; $b/a = 1.0$, $\nu = 0.30$.
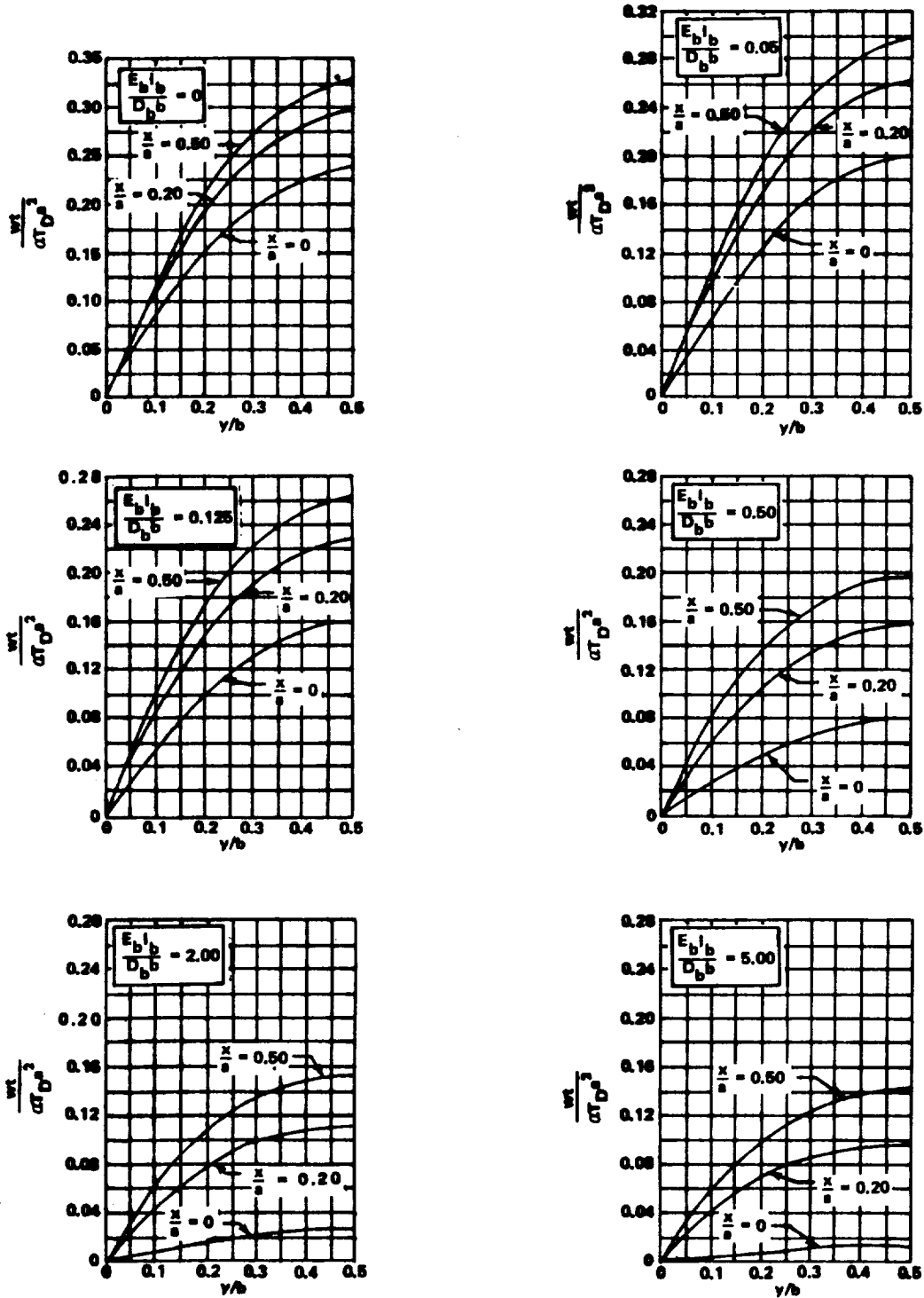
Figure 3. 0-30. Nondimensional deflections for a plate with both
long edges elastically supported and the short edges
simply supported; b/a = 1.5, ν = 0.30 .
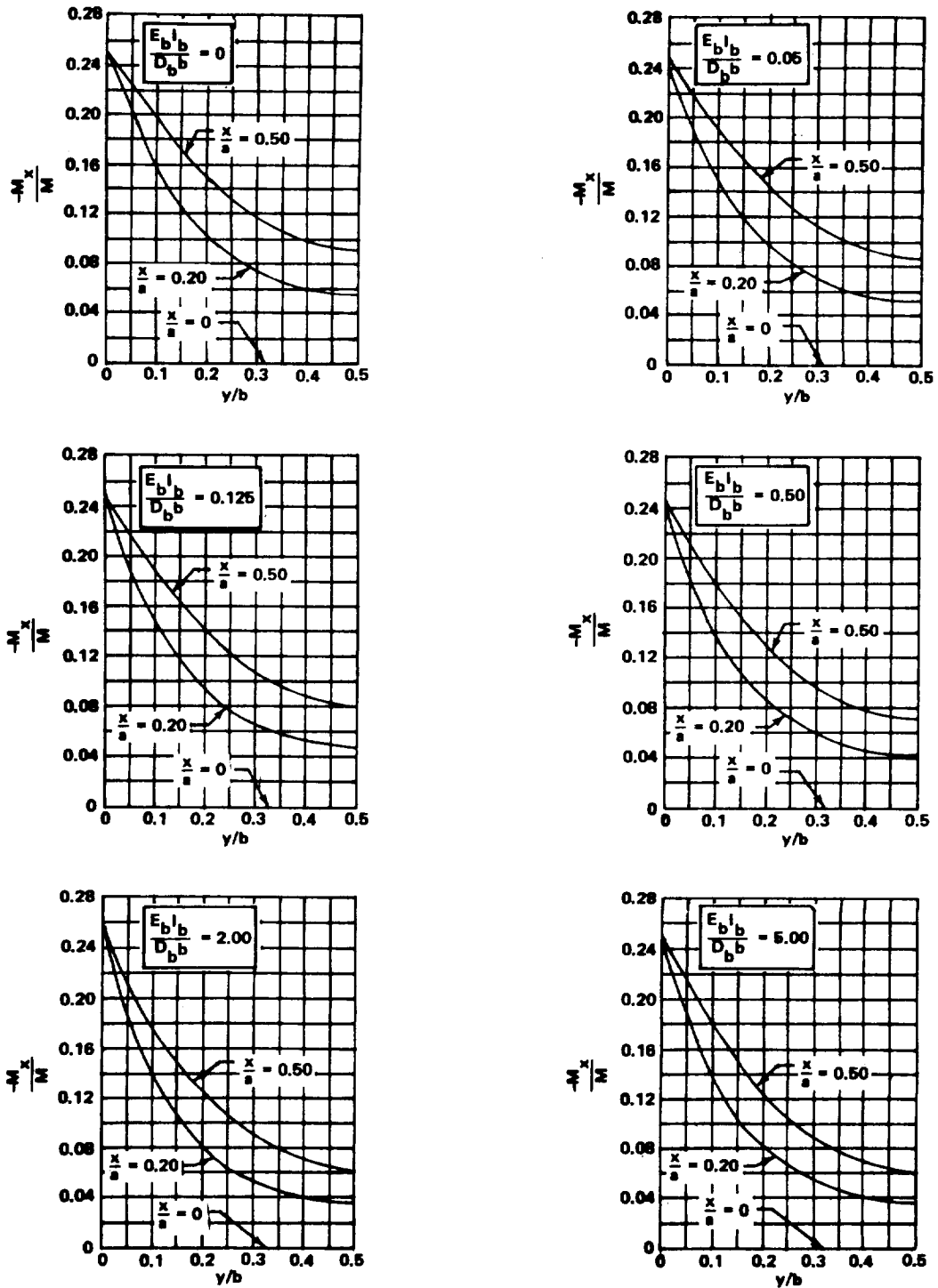
Figure 3. 0-31. Nondimensional bending moments M_x/M for a plate
with both long edges elastically supported and the short
edges simply supported; b/a = 1. 5, ν = 0.30.
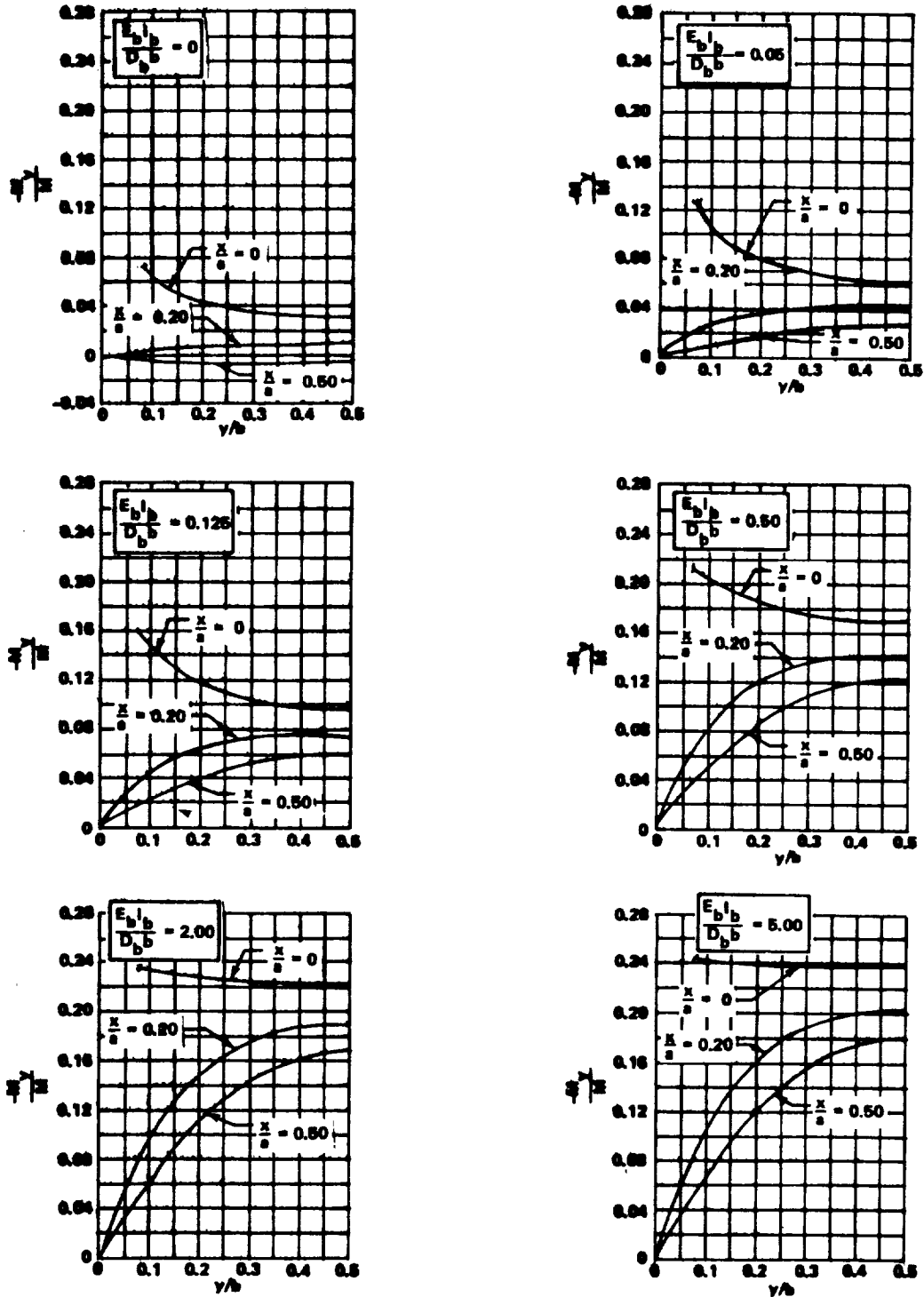
Figure 3.0-32. Nondimensional bending moments M_y/M for a plate with both long edges elastically supported and the short edges simply supported; b/a = 1.5, ν = 0.30.
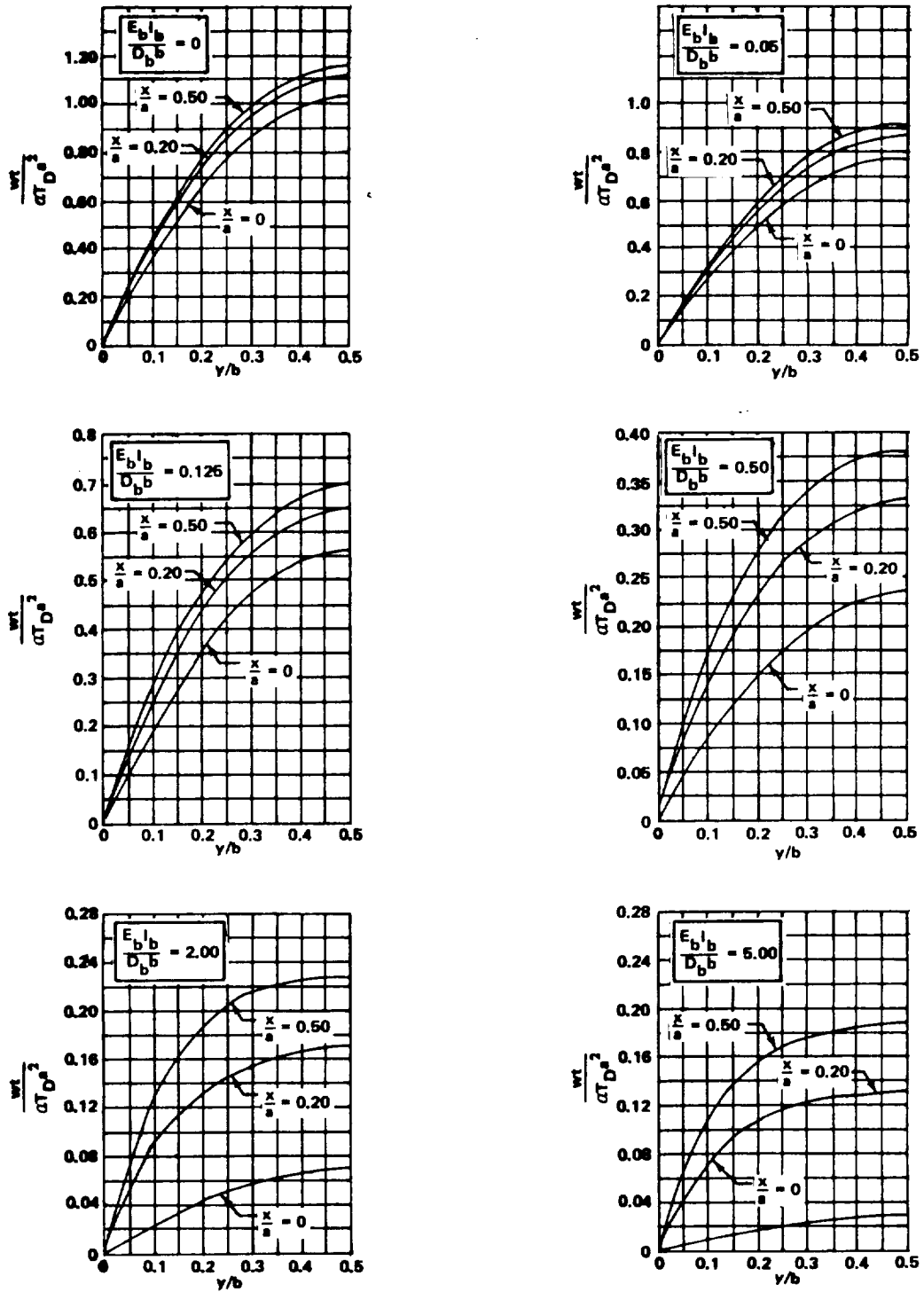
Figure 3.0-33. Nondimensional deflections for a plate with both
long edges elastically supported and the short edges
simply supported; b/a = 3.0, ν = 0.30.
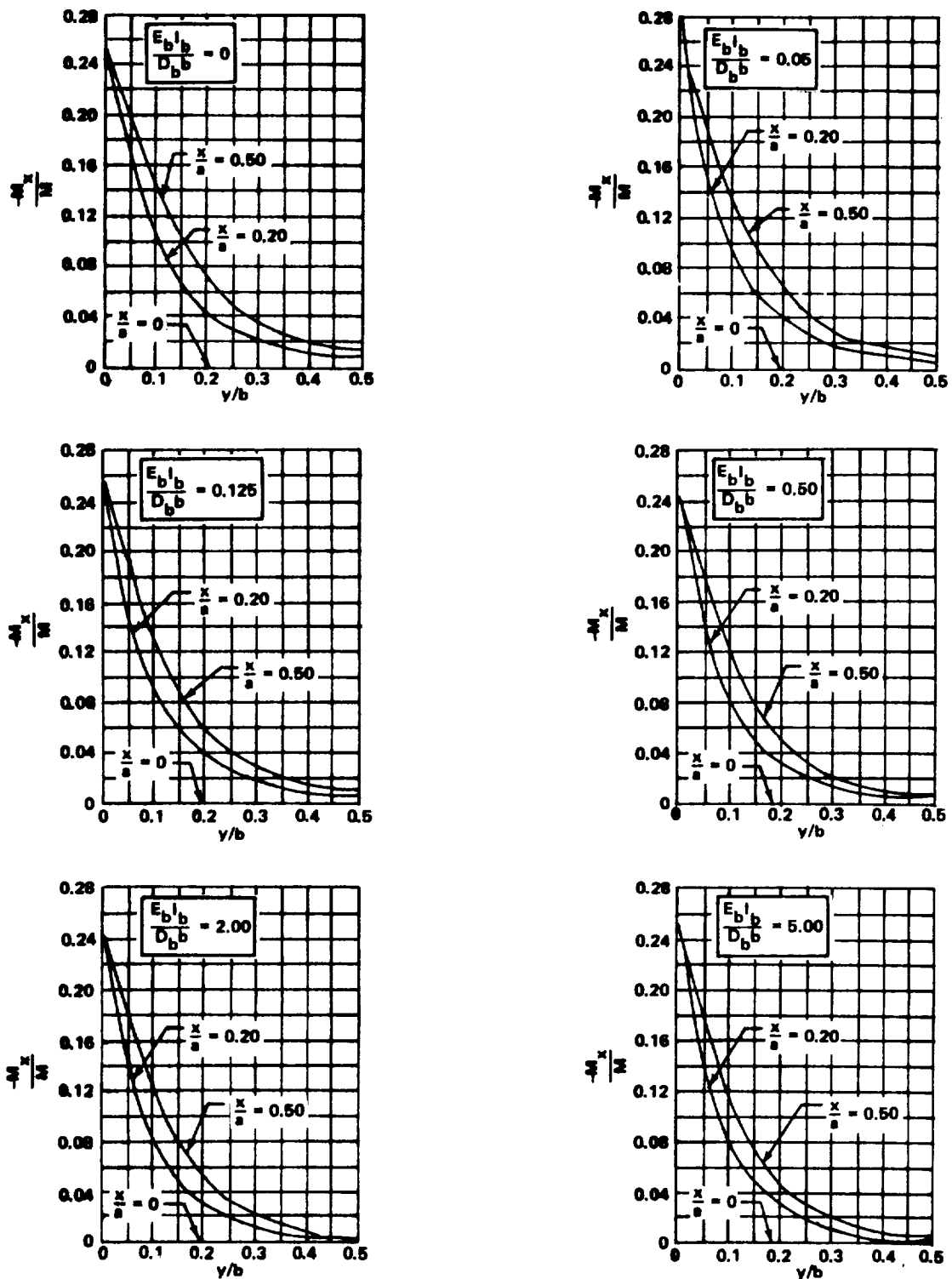
Figure 3.0-34. Nondimensional bending moments M_x/M for a plate with both long edges elastically supported and the short edges simply supported; $b/a = 3.0$, $\nu = 0.30$.
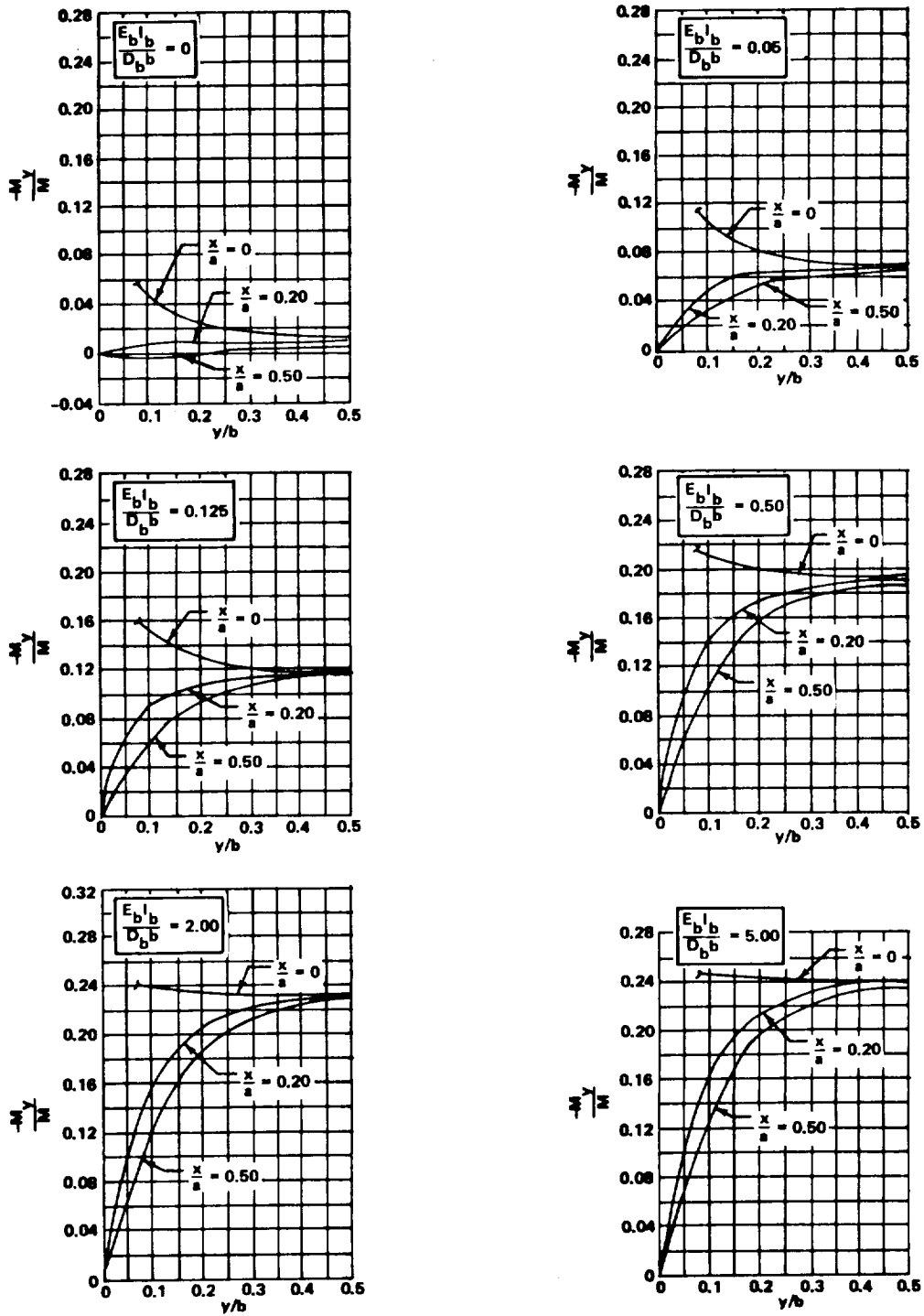
Figure 3. 0-35. Nondimensional bending moments M_y/M for a plate

with both long edges elastically supported and the short edges
simply supported; b/a = 3. 0, ν = 0. 30.

prove profitable to develop a simple digital computer program to perform the summations embodied both in the deflection and moment expressions.

It is important to note that the peak moments always occur at the simply supported boundaries and are oriented so that the corresponding peak values for the stresses σ_x and σ_y act parallel to the edges. The maximum moments can be computed from the following [11]:

$$M_{x(max)} = -\frac{\alpha T_D (1 - \nu^2) D_b}{t} - - E_p t^2 \frac{\alpha T_D}{12} \quad .$$

These moments result from the boundary condition, which demands that $w = 0$ along the simply supported edges. This imposes a straightness constraint that completely suppresses the thermally induced tendency to develop curvatures in vertical planes which pass through these edges.

Arbitrary Temperature Gradient [T = f(z)].

The following procedures may be used for the analysis of plates having arbitrary temperature distributions through the thickness $T = f(z)$:

1. The deflections w and bending moments M_x and M_y may be obtained from the equations and figures given for the linear temperature gradient, provided that T_D is replaced by T^*, which may be computed from the following:

$$T^* = \frac{12}{t^2} \int_{-t/2}^{t/2} Tz \, dz \quad .$$

2. The normal stresses x and y may then be established from the relationships

$$\sigma_x = M_x \left(\frac{12z}{t^3} \right) + \frac{E_p \alpha}{(1 - \nu)} \left(\overline{T} + \frac{T^*z}{t} - T \right)$$

and

$$\sigma_y = M_y \left(\frac{12z}{t^3} \right) + \frac{E_p \alpha}{(1 - \nu)} \left(\overline{T} + \frac{T^*z}{t} - T \right)$$

where

$$\overline{T} = \frac{1}{d} \int_{-d/z}^{d/z} T \, dz \quad .$$

II.   Temperature Variation Over the Surface.

A.   Edges Free or Constrained Against In-Plane Bending.

Configuration.

The design equations provided here apply only to flat, rectangular plates which are of constant thickness and are made of isotropic material. It is assumed that the plate is free of holes and that no stresses exceed the elastic limit. The equations are applicable only for large values of the aspect ratio a/b .

<u>Boundary Conditions</u>.

Consideration is given to each of the following two types of boundary

conditions:

1. All edges are free.

2. Plate is fully constrained against in-plane bending but is otherwise

completely free.

<u>Temperature Distribution</u>.

The supposition is made that no thermal gradients exist through the

plate thickness but a one-dimensional, arbitrary variation occurs over the

surface; that is, the temperature is a function only of either x or y .

<u>Design Equations</u>.

It is assumed here that Young's modulus is unaffected by temperature

changes. Therefore, in applying the contents of this section, a single effective

value must be selected for this property by using some type of averaging

technique. On the other hand, the results are presented in a form such that

the user may fully account for temperature-dependence of the coefficient of

thermal expansion α .

The appropriate stress formulation is developed as follows for the

problem which was illustrated in Figure 3.0-26, which shows a rectangular

plate with a temperature distribution $T(y)$ and free of any external constraints.

The results may be obtained by first imposing a fictitious stress distribution

σ_A on the edges $x = \pm a/2$ such that all thermal deformations are entirely suppressed. It follows that

$$\sigma_A = -\alpha ET(y) \quad .$$

These stresses may be integrated over the width b and the thickness t to arrive at the force

$$P_A = -Et \int_{-b/2}^{b/2} \alpha T(y) \, dy$$

and the moment about the z axis

$$M_A = -Et \int_{-b/2}^{b/2} \alpha T(y) \, y \, dy \quad .$$

Since, at this point in the derivation, it is assumed that no constraints are present, the actual plate must be free of forces and moments on all edges. To restore the plate to such a state, it is necessary to superimpose both a force P_B equal and opposite to P_A and a moment M_B which is equal and opposite to M_A. Hence,

$$P_B = -P_A$$

and

$$M_B = -M_A \quad .$$

The stress corresponding to P_B is easily found to be

$$\sigma_{P_B} = \frac{P_B}{A} = \frac{P_B}{bd} = \frac{E}{b} \int_{-b/2}^{b/2} \alpha T(y) \, dy \quad .$$

The stress corresponding to M_B is

$$\sigma_{M_B} = \frac{M_B y}{I_z} = \frac{12 M_B y}{tb^3} = \frac{12y}{b^3} E \int_{-b/2}^{b/2} \alpha T(y) \, y \, dy \quad .$$

It should be noted that the procedure being used constitutes an application of Saint-Venant's principle. Hence, the stresses σ_{P_B} and σ_{M_B} will be accurate representations only at sufficient distances from the edges $x = \pm a/2$. Subject to this limitation, the actual thermal stresses at various points in the plate may be computed from the relationship

$$\sigma = \sigma_A + \sigma_{P_B} + \sigma_{M_B}$$

or

$$\sigma_x = -\alpha E T(y) + \frac{E}{b} \int_{-b/2}^{b/2} \alpha T(y) \, dy + \frac{12y}{b^3} E \int_{-b/2}^{b/2} \alpha T(y) y \, dy \quad .$$

The foregoing discussion has been restricted to those cases where the temperature varies only in the y direction. However, the same method

can be used to arrive at the following expression when T is a function only of x :

$$\sigma_y = -\alpha ET(x) + \frac{E}{a} \int_{-a/2}^{a/2} \alpha T(x)\, dx + \frac{12x}{a^3} E \int_{-a/2}^{a/2} \alpha T(x)\, x\, dx \quad .$$

Complex one-dimensional temperature distributions may often be encountered which make it difficult to perform the integrations required by the preceding equations. In such instances, numerical techniques can be used whereby the integral signs are replaced by summation symbols.

The equations were derived for rectangular plates having no edge restraints. However, these relationships can easily be modified to apply when the plate is fully constrained against in-plane bending but is otherwise completely free. This is achieved simply by deleting the final terms from each equation.

Summary of Equations.

    1. All Edges Free.

$$T = T(y) \quad ,$$

$$\sigma_x = -\alpha ET(y) + \frac{E}{b} \int_{-b/2}^{b/2} \alpha T(y)\, dy + \frac{12y}{b^3} E \int_{-b/2}^{b/2} \alpha T(y)\, y\, dy \quad ,$$

$$T = T(x) \quad ,$$

and

$$\sigma_y = -\alpha ET(x) + \frac{E}{a} \int_{-a/2}^{a/2} \alpha T(x)\, dx + \frac{12x}{a^3} E \int_{-a/2}^{a/2} \alpha T(x)\, x\, dx \quad .$$

2. Plate Fully Constrained Against In-Plane Bending But Otherwise Completely Free.

$$T = T(y) \quad ,$$

$$\sigma_x = -\alpha ET(y) + \frac{E}{b} \int_{-b/2}^{b/2} \alpha T(y)\, dy \quad ,$$

$$T = T(x) \quad ,$$

and

$$\sigma_y = -\alpha ET(x) + \frac{E}{a} \int_{-a/2}^{a/2} \alpha T(x)\, dx \quad .$$

B. Edges Fixed.

<u>Configuration.</u>

The equations and sample solution provided here apply only to flat, rectangular plates which are of constant thickness and are made of isotropic material (Fig. 3.0-36). It is assumed that the plate is free of holes and that no stresses exceed the elastic limit. The equations are applicable to any aspect ratio a/b .
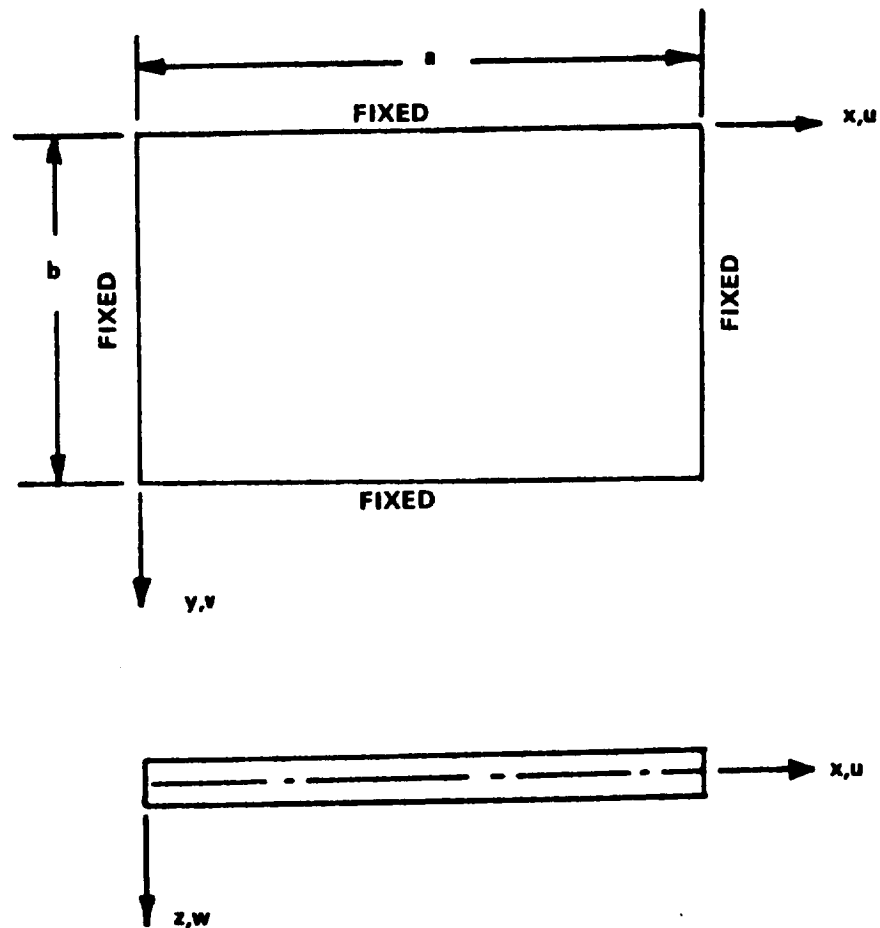
Figure 3.0-36. Rectangular flat plate: all sides fully constrained
against in-plane displacements.

Boundary Conditions.

Consideration is given only to plates having all sides completely

restrained against in-plane displacements (fixed) ; that is, both of the

following conditions must be satisfied by each edge:

$$u = 0$$

and

$$v = 0 \ .$$

Temperature Distribution.

The supposition is made that no thermal gradients exist through the plate thickness. However, temperature variations over the surface may be arbitrary.

Design Equations.

As noted previously, a so-called body-force analogy exists between certain isothermal problems and thermal stress problems for flat plates which experience no transverse displacements w. This method is derived in a number of different references [12, 13, 14] and is frequently referred to as Duhamel's analogy. In Ref. 15, this approach is used to solve the problem being treated here. Assuming that buckling does not occur, solutions in series form were obtained for the in-plane stresses σ_x, σ_y and τ_{xy}. The series coefficients can be obtained by solving the following simultaneous equations:

$$A_{mn} \frac{\pi^2 ab}{4} \left[\left(\frac{m}{a}\right)^2 + \frac{1-\nu}{2} \left(\frac{n}{b}\right)^2 \right] + 2(1+\nu) \sum_{p=1}^{\infty} \sum_{q=1}^{\infty} B_{pq} \frac{mn\,pq}{(p^2-m^2)(n^2-q^2)}$$

$$= -\alpha(1+\nu) \int_0^b \int_0^b \frac{\partial T}{\partial x} \sin \frac{m\pi x}{a} \sin \frac{n\pi y}{b} \, dx \, dy$$

and

$$B_{mn} \frac{\pi^2 ab}{4} \left[\left(\frac{n}{b}\right)^2 + \frac{1-\nu}{2} \left(\frac{m}{a}\right)^2 \right] + 2(1+\nu) \sum_{p=1}^{\infty} \sum_{q=1}^{\infty} A_{pq} \frac{mn\,pq}{(p^2-m^2)(n^2-q^2)}$$

$$= -\alpha(1+\nu) \int_0^b \int_0^a \frac{\partial T}{\partial y} \sin \frac{m\pi x}{a} \sin \frac{n\pi y}{b} \, dx \, dy \quad ,$$

where the indices m, n, p, and q each take on the values 1, 2, 3, ...

subject to the restriction that those values of p and q must be deleted for

which (m ± p) and (n ± q) are even numbers.

For any given temperature distribution, the right-hand side of the

preceding equations must be integrated. In many cases it will be desirable to

perform these operations by numerical procedures. The integers m, n, p,

and q may be assumed to vary from unity to any value N . This will result

in $2N^2$ equations involving N^2 coefficients A_{mn} and N^2 coefficients B_{mn}.

This set of equations can be solved simultaneously to determine appropriate

values for the coefficients. Once this has been accomplished, the stresses

at any point may be computed from

$$\sigma_x = \frac{E}{1-\nu^2} \left(\sum_{m=1}^{N} \sum_{n=1}^{N} \frac{m\pi}{a} A_{mn} \cos \frac{m\pi x}{a} \sin \frac{n\pi y}{b} \right.$$

$$\left. + \nu \sum_{m=1}^{N} \sum_{n=1}^{N} \frac{n\pi}{b} B_{mn} \sin \frac{m\pi x}{a} \cos \frac{n\pi y}{b} \right) - \frac{E\alpha}{1-\nu} T(x,y) \quad ,$$

$$\sigma_y = \frac{E}{1 - \nu^2} \left(\sum_{m=1}^{N} \sum_{n=1}^{N} \frac{n\pi}{b} B_{mn} \sin \frac{m\pi x}{a} \cos \frac{n\pi y}{b} \right.$$

$$\left. + \nu \sum_{m=1}^{N} \sum_{n=1}^{N} \frac{m\pi}{a} A_{mn} \cos \frac{m\pi x}{a} \sin \frac{n\pi y}{b} \right) - \frac{E\alpha}{1 - \nu} T(x,y) \quad ,$$

and

$$\tau_{xy} = G' \sum_{m=1}^{N} \sum_{n=1}^{N} \left(A_{mn} \frac{n\pi}{b} \sin \frac{m\pi x}{a} \cos \frac{n\pi y}{b} \right.$$

$$\left. + B_{mn} \frac{m\pi}{a} \cos \frac{m\pi x}{a} \sin \frac{n\pi y}{b} \right) \quad .$$

Then the strains at any point can be determined from

$$\epsilon_x = \frac{1}{E} \left(\sigma_x - \nu \sigma_y \right) \quad ,$$

$$\epsilon_y = \frac{1}{E} \left(\sigma_y - \nu \sigma_x \right) \quad ,$$

and

$$\gamma_{xy} = \frac{\tau_{xy}}{G'} \quad .$$

Example.

Let a rectangular plate having all four edges fixed (refer to Fig. 3.0-36) be subjected to a temperature gradient

$$T(x,y) = T_0 \left(1 - \frac{x}{a} \right) .$$

Then

$$\frac{\partial T}{\partial x} = - \frac{T_0}{a} \text{ and } \frac{\partial T}{\partial y} = 0 .$$

Substituting these expressions into the right-hand side of the design equation, the following is obtained after integration:

$$A_{mn} \frac{\pi^2 ab}{4} \left[\left(\frac{m}{a}\right)^2 + \frac{1-\nu}{2} \left(\frac{n}{b}\right)^2 \right] + 2(1+\nu) \sum_{p=1}^{N} \sum_{q=1}^{N} B_{pq} \frac{mn \ pq}{(p^2-m^2)(n^2-q^2)}$$

$$= \begin{cases} \dfrac{4(1+\nu) \ b\alpha T_0}{mn \ \pi^2} & \text{if } m \text{ and } n \text{ are odd numbers} \\ \\ 0 & \text{if } m \text{ and } n \text{ are even numbers} \end{cases} ,$$

and

$$B_{mn} \frac{\pi^2 ab}{4} \left[\left(\frac{n}{b}\right)^2 + \frac{1-\nu}{2} \left(\frac{m}{a}\right)^2 \right]$$

$$+ 2(1+\nu) \sum_{p=1}^{N} \sum_{q=1}^{N} A_{pq} \frac{mn \ pq}{(p^2-m^2)(n^2-q^2)} = 0 .$$

Let $N = 2$. Then the preceding equation becomes

$$\frac{\pi^2 ab}{4} A_{11} \left[\left(\frac{1}{a}\right)^2 + \frac{1-\nu}{2} \left(\frac{1}{b}\right)^2 \right] + 2(1+\nu) B_{22} \frac{2 \times 2}{(2^2-1)(1-2^2)} = 4 \frac{(1+\nu) b\alpha T_0}{\pi^2} ,$$

$$\frac{\pi^2 ab}{4} A_{12} \left[\left(\frac{1}{a}\right)^2 + \frac{1-\nu}{2}\left(\frac{2}{b}\right)^2 \right] + 2(1+\nu) \, B_{21} \frac{2 \times 2}{(2^2-1)(2^2-1)} = 0 \quad,$$

$$\frac{\pi^2 ab}{4} A_{21} \left[\left(\frac{2}{a}\right)^2 + \frac{1-\nu}{2}\left(\frac{1}{b}\right)^2 \right] + 2(1+\nu) \, B_{12} \frac{2 \times 2}{(1-2^2)(1-2^2)} = 0 \quad,$$

$$\frac{\pi^2 ab}{4} A_{22} \left[\left(\frac{2}{a}\right)^2 + \frac{1-\nu}{2}\left(\frac{2}{b}\right)^2 \right] + 2(1+\nu) \, B_{11} \frac{2 \times 2}{(1-2^2)(2^2-1)} = 0 \quad,$$

and

$$\frac{\pi^2 ab}{4} B_{11} \left[\left(\frac{1}{b}\right)^2 + \frac{1-\nu}{2}\left(\frac{1}{a}\right)^2 \right] + 2(1+\nu) \, A_{22} \frac{2 \times 2}{(2^2-1)(1-2^2)} = 0 \quad,$$

$$\frac{\pi^2 ab}{4} B_{12} \left[\left(\frac{2}{b}\right)^2 + \frac{1-\nu}{2}\left(\frac{1}{a}\right)^2 \right] + 2(1+\nu) \, A_{21} \frac{2 \times 2}{(2^2-1)(2^2-1)} = 0 \quad,$$

$$\frac{\pi^2 ab}{4} B_{21} \left[\left(\frac{1}{b}\right)^2 + \frac{1-\nu}{2}\left(\frac{2}{a}\right)^2 \right] + 2(1+\nu) \, A_{12} \frac{2 \times 2}{(1-2^2)(1-2^2)} = 0 \quad,$$

$$\frac{\pi^2 ab}{4} B_{22} \left[\left(\frac{2}{b}\right)^2 + \frac{1-\nu}{2}\left(\frac{2}{a}\right)^2 \right] + 2(1+\nu) \, A_{11} \frac{2 \times 2}{(1-2^2)(2^2-1)} = 0$$

Solving these equations gives the results,

$$A_{12} = A_{21} = A_{22} = B_{11} = B_{21} = B_{12} = 0 \quad,$$

while A_{11} and B_{22} can be obtained from the following relationships:

$$A_{11} \frac{\pi^2 ab}{4} \left(\frac{1}{a^2} + \frac{1-\nu}{2}\right) - \frac{8}{9} B_{22} = \frac{4(1+\nu) b \alpha T_0}{\pi^2}$$

and

$$\frac{8}{9}(1+\nu)\,A_{11} - \pi^2 ab\,B_{22}\left(\frac{1}{b^2} + \frac{1-\nu}{2a^2}\right) = 0 \quad .$$

For any plate dimensions and material properties, the stresses may then be determined by using the appropriate design equations. This gives

$$\sigma_x = \frac{E}{1-\nu^2}\left(A_{11}\frac{\pi}{a}\cos\frac{\pi x}{a}\sin\frac{\pi y}{b} + \nu\frac{2\pi}{b}B_{22}\sin\frac{2\pi x}{a}\cos\frac{2\pi y}{b}\right)$$

$$- \frac{E\alpha}{1-\nu}T_0\left(1-\frac{x}{a}\right) \quad ,$$

$$\sigma_y = \frac{E}{1-\nu^2}\left(\frac{2\pi}{b}B_{22}\sin\frac{2\pi x}{a}\cos\frac{2\pi y}{b} + \nu\frac{\pi}{a}A_{11}\cos\frac{\pi x}{a}\sin\frac{\pi y}{b}\right)$$

$$- \frac{E\alpha}{(1-\nu)}T_0\left(1-\frac{x}{a}\right) \quad ,$$

and

$$\tau_{xy} = G'\left(A_{11}\frac{\pi}{b}\sin\frac{\pi x}{a}\cos\frac{\pi y}{b} + B_{22}\frac{2\pi}{a}\cos\frac{2\pi x}{a}\sin\frac{2\pi y}{a}\right) \quad .$$

It can be seen that, for more complicated temperature distributions and higher values of N , efficiency considerations would dictate the use of a relatively simple digital computer program in applying this method of analysis.

3.0.8   Shells.

The analysis of shells subjected to temperature variations has, for the most part, taken the approach of treating thermal loadings as equivalent

mechanical loadings and hence solving the stresses and displacements by

techniques such as in Section B7.3. These approaches are discussed in

Refs. 7 and 8. Some of the more common temperature distributions in shells

will be discussed in the following section.

3.0.8.1 Isotropic Circular Cylindrical Shells.

This section covers the thermostructural analysis of thin-walled,

right circular, isotropic cylindrical shells. The middle-surface curvilinear

coordinate axes (x and y) are always taken parallel to the axis of revolution

and the circumferential direction, respectively.

The organization of this section is somewhat different from that of

the sections which cover isotropic flat plates. This is due to certain funda-

mental differences between the physical behavior of flat plates and shells.

Flat-plate deformations are of such a nature that it is helpful to group the

solutions for stable constructions into the following categories:

1. Temperature gradients through the thickness

2. Uniform temperatures through the thickness.

Except for the special case of self-equilibrating gradients through the thick-

ness $\left(N_T = 0, M_T = 0\right)$, the first of these two cases involves out-of-plane

bending which is, of course, accompanied by displacements normal to the

middle surface of the undeformed plate. In case 1, the plate remains flat;

that is, the only displacements occur in directions parallel to the original

middle surface and no out-of-plane bending occurs. The governing differential

equations in these two instances are quite different and the indicated separation

of the cases is a logical format for the sections dealing with flat plates.

However, the situation is not the same for circular cylindrical shell structures.

For these components, a single governing differential equation includes the

phenomena related to both cases 1 and 2 and there is no need to isolate

these two types of thermal conditions. This is because either type of

temperature distribution, in conjunction with clamped or simply supported

boundaries, will lead to both membrane loading and bending about the shell-

wall middle surface. Consequently, for stable constructions which comply

with either case 1 or 2, the solutions are given in a single grouping as follows.

I.   Analogies with Isothermal Problems.

A.   Configuration.

This discussion is restricted to thin-walled, right circular cylinders

which are of constant thickness and are made of isotropic material. It is

assumed that the shell wall is free of holes and that it obeys Hooke's law.

Figure 3.0-37 depicts the isotropic cylindrical shell configuration.

Figure 3.0-38 shows the sign convention for forces, moments, and pressure.

B.   Boundary Conditions.

The following three types of boundary conditions are discussed:

1. Clamped edge; that is,

$$w = \frac{dw}{dx} = 0 \qquad \text{at } x = 0 \text{ and/or } x = L \tag{1}$$
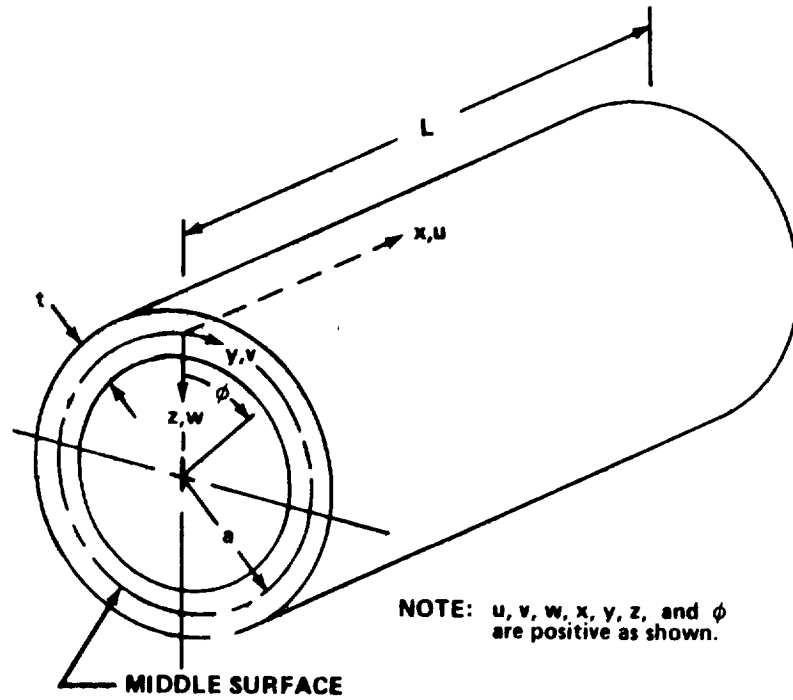
Figure 3. 0-37. Isotropic cylindrical shell configuration for analogies with isothermal problems.
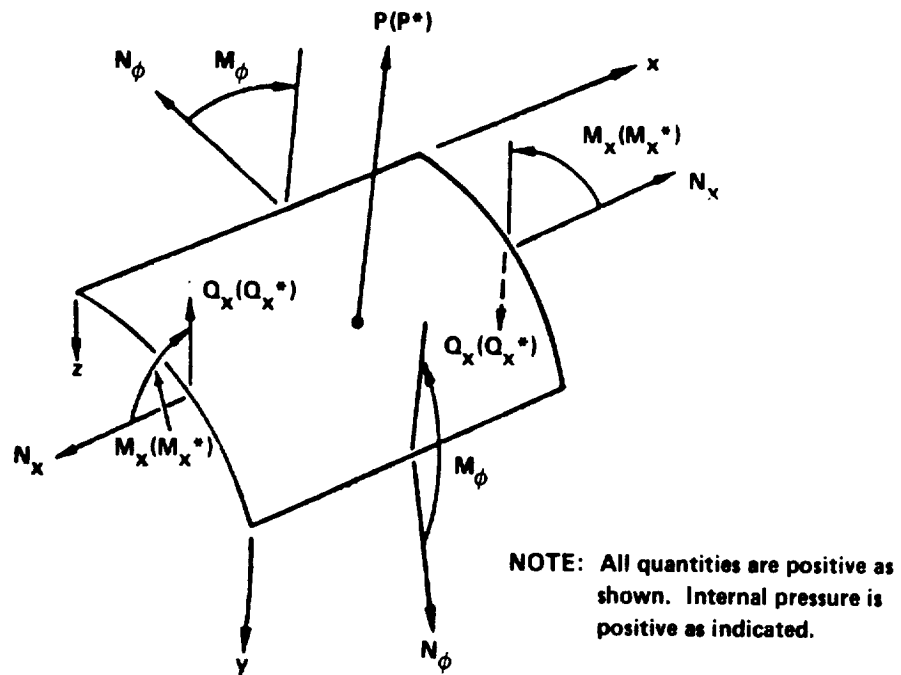
Figure 3. 0-38. Sign convention for forces, moments, and pressure for analogies with isothermal problems.

2. Simply supported edge; that is,

$$w = M_x = 0 \qquad \text{at } x = 0 \text{ and/or } x = L \tag{2}$$

3. Free edge; that is,

$$M_x = Q_x = 0 \qquad \text{at } x = 0 \text{ and/or } x = L \; . \tag{3}$$

All possible combinations of these boundary conditions are permitted. Hence, it is not required that those at $x = 0$ be the same as those at $x = L$. In every case, it is assumed that the cylinder is unrestrained in the axial direction $(N_x = 0)$.

C. Temperature Distribution.

The temperature distribution must be axisymmetric but arbitrary gradients may be present both through the wall thickness and in the axial direction. The permissible distributions can therefore be expressed in the form

$$T = T(x, z) \; . \tag{4}$$

Any of the special cases for this equation are acceptable, including that where the entire shell is at constant temperature.

D. Analogies.

It is helpful for the user to recognize that, for circular cylinders, analogies exist between problems involving axisymmetric temperature

distributions and certain problems where mechanical loading is present but thermal effects are entirely absent (isothermal problems). The various types of correspondence are discussed herein where it is assumed that Young's modulus and Poisson's ratio are unaffected by temperature changes. On the other hand, one can account for temperature dependence of the thermal-expansion coefficient α by observing that it is the product αT which governs; that is, the actual temperature distribution can be suitably modified to compensate for variations in α. When this approach is taken, the user must recognize that any reference to linear temperature distribution is actually a reference to a straight-line variation of the product αT.

It is also helpful for the user to recognize that, regardless of the complexity of a thermal gradient through the thickness, at any location (x,y) the distribution can be resolved into

    1. A self-equilibrating component, and/or

    2. A uniform component, and/or

    3. A nonuniform linear component passing through $T = 0$ at the middle surface.

A self-equilibrating temperature component is one for which

$$\int_{-t/2}^{t/2} T \, dz = 0$$

and

$$\int_{-t/2}^{t/2} T z \, dz = 0 \quad . \tag{5}$$

An example of such a distribution is illustrated in Figure 3.0-39.
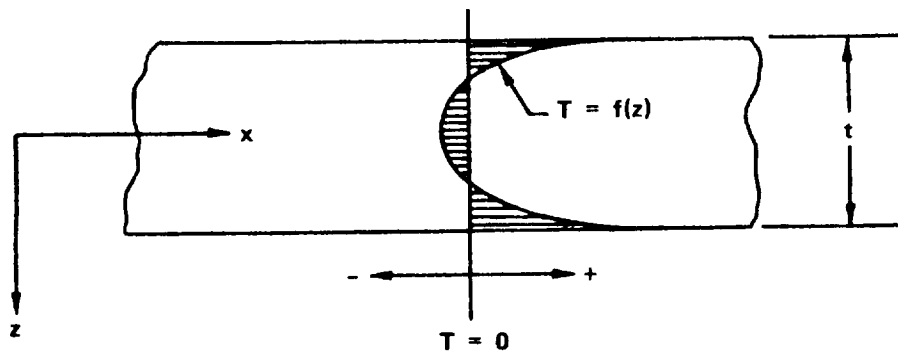
Figure 3.0-39. Sample self-equilibrating temperature distribution.

From a practical viewpoint, it may be assumed that gradients of this type will

not cause any deformation of the cylinder. Their only influence will be on

the stresses σ_x and σ_ϕ . If, for example, a solution is available for any

arbitrary temperature distribution $T = T(x, z)$, the effects can be easily

superimposed from a component $T_1(x, z)$ which satisfies equations (5). It

is necessary only to algebraically add the stresses

$$\sigma_x = \sigma_\phi = - \frac{E \alpha T_1}{(1 - \nu)} \tag{6}$$

to the previously determined values for the appropriate locations (x, z) .

In this section, the following two categories are treated separately:

1. Uniform temperatures through the thickness with or without axisymmetric, longitudinal gradients; that is,

$$T = T(x) \quad . \tag{7}$$

2. Nonuniform linear temperature gradients through the thickness, passing through $T = 0$ at the middle surface with or without axisymmetric longitudinal variations and possibly including self-equilibrating components; that is,

$$T = T_1(x,z) + T_2(x) \frac{z}{t} \tag{8}$$

where T_1 satisfies equations (5).

Uniform Temperatures Through the Thickness $[T = T(x)]$.

In Ref. 16, Tsui presents the small-deflection governing differential equation for the subject shell. After conversion to the notation and sign convention used here, this expression becomes

$$\frac{d^4w}{dx^4} + 4\beta^4 w = -\frac{p}{D_b} - \frac{N_T}{D_b a} - \frac{1}{D_b(1-\nu)} \frac{d^2 M_T}{dx^2} \tag{9}$$

where

$$\beta = \sqrt[4]{\frac{Et}{4D_b a^2}} = \sqrt[4]{\frac{3(1-\nu^2)}{a^2 t^2}} \quad ,$$

$$N_T = E\alpha \int_{-t/2}^{t/2} T \, dz \quad,$$

$$M_T = E\alpha \int_{-t/2}^{t/2} Tz \, dz \quad,$$

(10)

and

$$D_b = \frac{Et^3}{12(1 - \nu^2)} \quad .$$

An inspection of equation (9) reveals the key to an analogy which applies to the problem under discussion. Note that, for the isothermal problem, this equation reduces to

$$\frac{d^4w}{dx^4} + 4\beta^4 w = -\frac{p}{D_b} \quad .$$

(11)

For thermostructural problems where pressure differentials are absent and the temperature is uniform through the wall thickness $(M_T = 0)$, one obtains

$$\frac{d^4w}{dx^4} + 4\beta^4 w = \frac{N_T}{D_b a} \quad .$$

(12)

A comparison of equations (11) and (12) suggests that the latter problem may be treated by means of an isothermal model that is loaded by a pressure differential, $p = p^*$, where

$$p^*(x) = \frac{N_T}{a} = \frac{E\alpha Tt}{a} \quad . \tag{13}$$

With regard to the edges, it should be noted that, since $M_T = 0$, the boundary

conditions for the actual cylinder can be expressed as follows [16]:

1. Clamped edge:

$$w = \frac{dw}{dx} = 0 \qquad \text{at } x = 0 \text{ and/or } x = L \quad . \tag{14}$$

2. Simply supported edge:

$$w = \frac{d^2w}{dx^2} = 0 \qquad \text{at } x = 0 \text{ and/or } x = L \quad . \tag{15}$$

3. Free edge:

$$\frac{d^2w}{dx^2} = \frac{d^3w}{dx^3} = 0 \qquad \text{at } x = 0 \text{ and/or } x = L \quad . \tag{16}$$

These relationships do not contain any temperature terms and are therefore

identical to those for the corresponding isothermal cases. Therefore, the

major equivalence between the subject temperature distribution $[T = T(x)]$

and the isothermal model is bound up in the governing differential equation (9).

Hence, the desired analogy is achieved by simply substituting p^* for p in

equation (11). When this pressure is positive, it acts radially outward. It

is important to note, however, that the analogy is complete only insofar as

the radial deflections and the axial stresses are concerned; that is, the thermal

deflections w and the thermal stresses σ_x will be identical to those due solely to a pressure p^* acting on a cylinder having the same geometry and boundary conditions as the actual structure. On the other hand, to determine the thermal stress σ_ϕ, the quantity $(-E\alpha T)$ must be added to the corresponding value obtained from the pressure solution. This accounts for the fact that strains ϵ_ϕ in the amount αT are associated with stress-free thermal growths or shrinkages.

To facilitate the application of this analogy, the user should refer to Section 2.40 of Ref. 17, which includes solutions for numerous cases of pressure-loaded cylindrical shells (a wide variety of pressure distributions and boundary conditions are treated).

Temperature Gradients Through the Thickness [T = T(x,z)].

This subsection discusses factors associated with cylindrical shells having nonuniform linear temperature gradients through the thickness, passing through $T = 0$ at the middle surface, with or without axisymmetric longitudinal variations, and possibly including self-equilibrating components; that is,

$$T = T_1(x,z) + T_2(x)\frac{z}{t} \tag{17}$$

where

$$\int_{-t/2}^{t/2} T_1 \, dz = 0$$

and

$$\int_{-t/2}^{t/2} T_1 z \, dz = 0 \quad . \tag{18}$$

Here again, it is helpful for the user to study the following small-deflection governing differential equation which was obtained by converting the corresponding formulation of Ref. 16 to the notation and sign convention of this section:

$$\frac{d^4 w}{dx^4} + 4 \beta^4 w = -\frac{p}{D_b} \frac{N_T}{D_b a} - \frac{1}{D_b (1 - \nu)} \frac{d^2 M_T}{dx^2} \tag{19}$$

where

$$\beta = \sqrt[4]{\frac{Et}{4 D_b a^2}} = \sqrt[4]{\frac{3(1 - \nu^2)}{a^2 t^2}} \quad ,$$

$$N_T = E\alpha \int_{-t/2}^{t/2} T \, dz \quad , \tag{20}$$

$$M_T = E\alpha \int_{-t/2}^{t/2} Tz \, dz \quad ,$$

and

$$D_b = \frac{Et^3}{12(1 - \nu^2)} \quad .$$

For the isothermal problem, this equation reduces to

$$\frac{d^4w}{dx^4} + 4\beta^4 w = -\frac{p}{D_b} \qquad (21)$$

while, for the subject thermostructural problem,

$$N_T = 0 \qquad (22)$$

and equation (19) becomes

$$\frac{d^4w}{dx^4} + 4\beta^4 w = -\frac{1}{D_b(1-\nu)}\frac{d^2 M_T}{dx^2} \quad . \qquad (23)$$

A comparison of equations (21) and (23) suggests that the latter problem may be treated by means of an isothermal model that is loaded by a pressure differential, $p = p^*$, where

$$p^*(x) = \frac{1}{(1-\nu)}\frac{d^2 M_T}{dx^2} \quad . \qquad (24)$$

This does not, however, provide a complete basis for the desired analogy since the boundary conditions which are likewise part of the problem formulation must be considered. From a study of conventional types of boundaries, it is clear that the simplest form of the subject analogy is that associated with a cylinder having both ends clamped. In this case, both the radial deflection and the related slope must vanish at the boundaries; that is,

$$
\left.
\begin{array}{l}
w = 0 \\[2ex]
\dfrac{dw}{dx} = 0
\end{array}
\right\}
\quad \text{at } x = 0 \text{ and } x = L \ .
\tag{25}
$$

The simplicity of the analogy for this situation comes about because these relationships do not contain any temperature terms and are therefore identical to those for the corresponding isothermal problem. As a result, the major equivalence between the subject temperature distribution and the pressure loading is bound up in the governing differential equation (19). Hence for cylinders clamped at both ends, the analogy is achieved by simply substituting p^* for p in equation (21). When this pressure is positive, it acts radially outward. It is important to note, however, that the analogy is complete only insofar as the radial deflections are concerned. That is, the thermal deflections w will be identical to those due solely to a pressure p^* acting on a cylinder having the same geometry and boundary conditions as the actual structure. On the other hand, to determine the thermal stresses σ_x and σ_ϕ, the quantity $[-E\alpha T/(1 - \nu)]$ must be added to each of the corresponding values obtained from the pressure solution. This accounts for the possible presence of a self-equilibrating temperature component and for the fact that strains ϵ_x and ϵ_ϕ, in the amount αT, are due dolely to stress-free thermal growths or shrinkages.

Although the analogy under discussion takes on its simplest form where both boundaries are clamped, this general method need not be ruled out for a

simply supported shell. In the latter case, the analogy with respect to
equation (19) still holds true. The added complexity is introduced only through
the boundary-condition formulations. In this connection, the bending moment
M_x may be expressed as follows [16]:

$$M_x = -D_b \frac{d^2w}{dx^2} - \frac{M_T}{(1 - \nu)} \quad . \tag{26}$$

This relationship is applicable anywhere in the shell, including positions
around the boundaries. Only the latter locations need be considered here. It
should be recalled that the condition of simple support includes the requirement
that

$$M_x = 0 \qquad \text{at } x = 0 \text{ and/or } x = L \quad . \tag{27}$$

Suppose a uniformly distributed external bending moment M_x^* is applied
around such a boundary, as defined by the equation

$$M_x^* = \frac{M_T}{(1 - \nu)} \quad . \tag{28}$$

The user must remember that the sign convention being used specifies that
a positive bending moment causes compressive stresses on the outer surface
of the shell wall (refer to Fig. 3.0-38). By superimposing moments M_x^*
around a simply supported end, the related expressions for the boundary
conditions become

$$M_x = -D_b \frac{d^2w}{dx^2} - \frac{M_T}{(1 - \nu)} + \frac{M_T}{(1 - \nu)} = 0 \qquad \text{at } x = 0 \text{ and/or } x = L$$

(29)

or

$$M_x = -D_b \frac{d^2w}{dx^2} = 0 \qquad \text{at } x = 0 \text{ and/or } x = L \quad .$$

(30)

Equation (30) is the same as that for a simply supported boundary of a cylinder which does not experience any thermal influences. Hence, for a circular, cylindrical shell having both ends simply supported and subjected to the temperature distribution defined by equations (17) and (18), thermal deflections w can be obtained by superposition of the following:

1. The radial deflections of a simply supported cylinder which is identical to the actual structure but is free of any thermal influences and is subjected to a pressure p* where

$$p^*(x) = \frac{1}{(1 - \nu)} \frac{d^2 M_T}{dx^2}$$

(31)

and bursting pressures are positive.

2. The radial deflections of a cylinder which is free of thermal influences,. is identical to the actual structure, and whose boundaries conform with the condition of simple-support except for the application of uniformly distributed moments M_x^* at each end, where

$$M_x{}^* = \frac{M_T}{(1 - \nu)} \; .$$ (32)

The thermal stresses σ_x and σ_ϕ are found by adding the quantity

$[-E \alpha T/(1 - \nu)]$ to the algebraic sum of these stresses associated with steps

1 and 2. To facilitate the application of this analogy, the user should refer

to Section 2.40 of Ref. 17, which includes numerous solutions that will often

be useful in performing step 1 . In addition, Refs. 17, 11, and 18 provide

simple methods by which step 2 may be accomplished.

A situation similar to the foregoing arises when both boundaries of

the shell are free. As before, the analogy with respect to equation (19)

remains valid but still greater complexity is introduced through the applicable

boundary-condition formulations. In this case, when the cylinder is subjected

to the temperature distribution defined by equations (17) and (18), thermal

deflections w can be obtained by superposition of the following:

1. The radial deflections of a cylinder which has both ends free and is

identical to the actual structure but is free of any thermal influences and is

subjected to a pressure p^* where

$$p^*(x) = \frac{1}{(1 - \nu)} \frac{d^2 M_T}{dx^2}$$ (33)

and bursting pressures are positive.

2. The radial deflection of a cylinder which is free of thermal influences, is identical to the actual structure, and has the prescribed boundary conditions except for the application of uniformly distributed moments M_x^* at each end, where

$$M_x^* = \frac{M_T}{(1 - \nu)} \ .$$

(34)

3. The radial deflection of a cylinder which is free of thermal influences, is identical to the actual structure, and has the prescribed boundary conditions except for the application of uniformly distributed shear forces Q_x^* at each end, where

$$Q_x^* = \frac{1}{(1 - \nu)} \frac{dM_T}{dx} \ .$$

(35)

The thermal stresses σ_x and σ_ϕ are found by adding the quantity $[-E\alpha T/(1 - \nu)]$ to the algebraic sum of these stresses associated with items 1 and 2. To facilitate the application of this analogy, the user should refer to Section 2.40 of Ref. 17, which includes numerous solutions that will often be useful in the accomplishment of step 1 . In addition, Refs. 17, 11, and 18 provide simple methods by which steps 2 and 3 may be accomplished.

Analogies of the types presented in this section perform a two-fold function in that they can help the user to develop some physical insight into thermostructural behavior and also enable him to solve thermal stress

problems by using existing solutions for members subjected solely to
mechanical loading. Although the emphasis has been on cases where both
ends of the cylinder have the same boundary conditions, the user should find
it relatively easy to apply the same basic concepts when the two boundaries
are not identical (for example, one end clamped while the other is simply
supported).

II.   Thermal Stresses and Deflections — Linear Radial Gradient,

Axisymmetric Axial Gradient.

A. Configuration.

The design equations provided here apply only to long $(L \geq 2\pi/\beta)$,
thin-walled, right circular cylinders which are of constant thickness and are
made of isotropic material. It is assumed that the shell wall is free of holes
and that it obeys Hooke's law. Figure 3.0-37 depicts the isotropic cylindrical
shell configuration. Figure 3.0-38 shows the sign convention used for the
stress resultants of interest.

B. Boundary Conditions.

The following types of boundary conditions are discussed:

1. Free edges

2. Simply supported edges

3. Clamped edges.

All possible combinations of these boundary conditions are permitted; that is,
it is not required that those at $x = 0$ be the same as those at $x = L$. However,

In every case, it is assumed that the cylinder is unrestrained in the axial direction $(N_x = 0)$.

C. Temperature Distribution.

The following types of temperature distributions may be present:

1. A radial gradient which is linear through the wall thickness and need not vanish at the middle surface

2. Axisymmetric axial gradients.

The permissible distributions can therefore be expressed in the form

$$T = T_1(x) + T_2(y) \frac{z}{t} \quad . \tag{36}$$

Certain restrictions must sometimes be imposed on the complexities of the functions $T_1(x)$ and $T_2(x)$, depending upon the method of analysis employed. These conditions are explained in a subsequent paragraph. Any of the special cases for equation (36) are acceptable; that is, either or both of $T_1(x)$ and $T_2(x)$ can be finite constants and either can be equal to zero.

D. Design Equations.

Throughout this section, it is assumed that Young's modulus and Poisson's ratio are unaffected by temperature changes. Hence, the user must select single effective values for each of these properties by employing some type of averaging technique. The same approach may be taken with regard to the coefficient of thermal expansion. On the other hand,

the temperature-dependence of this property can be accounted for by recognizing that it is the product of αT which governs; that is, the actual temperature distribution can be suitably modified to compensate for variations in α. When this approach is taken, the user must recognize that any reference to a linear temperature distribution is actually a reference to a straight-line variation of the product αT.

In addition, the several types of solutions cited here are based on classical small-deflection theory. Therefore, it is important for the user to be aware of this when applying the given methods to pressurized cylinders by superimposing the thermal stresses and deflections upon the corresponding values due solely to pressure; that is, because of their dependence upon classical theory, the methods presented here cannot account for nonlinear coupling between thermal deflections and the pressure-related meridional loads.

The small-deflection governing differential equation for the subject cylindrical shell (refer to Fig. 3.0-37) can be written as follows [19]:

$$\frac{d^4w}{dx^4} + 4\beta^4 w = -\frac{N_T}{D_b a} - \frac{1}{D_b(1-\nu)} \frac{d^2 M_T}{dx^2} \tag{37}$$

where

$$\beta = \sqrt[4]{\frac{Et}{4D_b a^2}} = \sqrt[4]{\frac{3(1 - \nu^2)}{a^2 t^2}} \quad ,$$

$$N_T = E\alpha \int_{-t/2}^{t/2} T \, dz \quad ,$$

$$M_T = E\alpha \int_{-t/2}^{t/2} Tz \, dz \quad ,$$

(38)

and

$$D_b = \frac{Et^3}{12(1 - \nu^2)} \quad .$$

If $L \geq 2\pi/\beta$, then overlapping effects from boundary conditions at the two ends of the cylinder can be neglected and the following approximate solutions to equation (37) apply to each half of the structure:

<u>CASE I $(0 \leq x \leq L/2)$</u>:

$$w = e^{-\beta x} (C_1 \cos \beta x + C_2 \sin \beta x) - \frac{aN_T}{Et} - \frac{a^2}{Et(1 - \nu)} \frac{d^2M_T}{dx^2} \quad . \quad (39)$$

<u>CASE II $(L/2 \leq x \leq L)$</u>:

$$w = e^{-\beta(L-x)} [C_3 \cos \beta(L - x) + C_4 \sin \beta(L - x)]$$

$$- \frac{aN_T}{Et} - \frac{a^2}{Et(1 - \nu)} \frac{d^2M_T}{dx^2} \quad . \quad (40)$$

The terms $e^{-\beta x}(C_1 \cos \beta x + C_2 \sin \beta x)$ and $e^{-\beta(L-x)}[C_3 \cos \beta(L-x)$

$+ C_4 \sin \beta(L-x)]$ comprise the respective complementary solutions to

equation (37). All of the boundary-condition influences are embodied in these

terms. The remaining portions of equations (39) and (40) are the so-called

particular solutions and those given here are somewhat inexact. They were

obtained by Przemieniecki [20] as first-order approximations from an

asymptotic integration process and will give exact results only if the functions

$T_1(x)$ and $T_2(x)$ are truly polynomials of second degree or lower; for example,

$T_1(x) = b_0 + b_1 x + b_2 x^2$ and $T_2(x) = d_0 + d_1 x + d_2 x^2$.

When the temperature distribution is such that polynomial expansions

of T_1 and/or T_2 require terms higher than the second degree, approximate

solutions can be obtained by using either of the following two procedures:

1. Truncate the series by eliminating terms having exponents greater

than two and perform the analysis as though the resulting series were exact

representations of $T_1(x)$ and $T_2(x)$.

2. Ignore the stated restriction on the polynomial expansions and use

the actual higher-degree formulations.

Either of these two possibilities will introduce inaccuracies and, at present,

no studies have been performed to determine the orders of magnitudes for

the errors associated with various ranges of the parameters involved. For

those cases where accurate results are required but equations (39) and (40)

are inexact, the user can always resort to an alternative procedure whereby

these expressions are suitably modified. This can be accomplished by

retaining the foregoing complementary solutions but introducing more

appropriate particular solutions. The latter can be established by standard

mathematical operations such as variation of parameters or the method of

undetermined coefficients [21, 22].

For any case, the constants C_1 through C_4 in the deflection relation-

ships must be evaluated from the boundary conditions. It therefore becomes

necessary to express the various physical possibilities by means of the

following formulas:

1. Free edge:

$$Q_x = M_x = 0 .$$

2. Simply supported edge:

$$w = M_x = 0 . \tag{41}$$

3. Clamped edge:

$$w = \frac{dw}{dx} = 0 .$$

where

$$Q_x = \frac{dM_x}{dx}$$

and (42)

$$M_x = -D_b \frac{d^2w}{dx^2} - \frac{M_T}{(1 - \nu)} \quad .$$

The method to be used will be illustrated by using the example of a cylinder

having a simply supported edge at $x = 0$ and a clamped edge at $x = L$. For

the portion of the cylinder where $0 \leq x \leq L/2$, the values $x = 0$, $w = 0$

would be inserted into equation (39) to obtain a relationship which may be

identified as equation (39a). Following this, equation (39) must be substituted

into

$$D_b \frac{d^2w}{dx^2} + \frac{M_T}{(1 - \nu)} = 0 \tag{43}$$

and x must then be set equal to zero in the resulting formulation to obtain an

equation which may be identified as (39b). The constants of integration C_1

and C_2 can then be determined by the simultaneous solution of equations (39a)

and (39b). For the portion of the cylinder where $L/2 \leq x \leq L$, the values

$x = L$, $w = 0$ would be inserted into equation (40) to obtain a relationship

which may be identified as (40a). Following this, equation (40) must be

substituted into

$$\frac{dw}{dx} = 0 \tag{44}$$

and x must then be set equal to L in the resulting formulation to obtain an equation which may be identified as (40b). The constants of integration C_3 and C_4 can then be determined by the simultaneous solution of equations (40a) and (40b).

Once the deflection equations have been found for both halves of the cylinder, the bending moments M_x and M_ϕ at any point can be established from

$$M_x = -D_b \frac{d^2w}{dx^2} - \frac{M_T}{(1 - \nu)}$$

and $\tag{45}$

$$M_\phi = -\nu D_b \frac{d^2w}{dx^2} - \frac{M_T}{(1 - \nu)} \quad .$$

Then the stresses at any location are given by the following:

$$\sigma_x = \frac{12z}{t^3} M_x$$

and $\tag{46}$

$$\sigma_\phi = \frac{N_\phi}{t} + \frac{12z}{t^3} M_\phi$$

where

$$N_\phi = -N_T - \frac{w}{a} Et \quad .$$ (47)

Example No. 1.

A thin-walled, right circular cylinder of length $L(> 2\pi/\beta)$ has both ends simply supported and is subjected to the temperature distribution

$$T = d_0 \frac{z}{t}$$ (48)

where d_0 is a constant. It is desired that the deflections and extreme-fiber stresses be found, assuming that $L = 40$ in. and $\beta = 0.2$.

For the given temperature distribution, equations (38) yield

$$N_T = 0$$

(49)

and

$$M_T = \frac{E\alpha t^2 d_0}{12} \quad .$$

Then, for $0 \leq x \leq L/2$, equation (39) becomes

$$w = e^{-\beta x}(C_1 \cos \beta x + C_2 \sin \beta x) \quad .$$

At $x = 0$, the boundary condition of simple support requires that

$$w = M_x = 0 \tag{51}$$

where

$$M_x = -D_b \frac{d^2w}{dx^2} - \frac{M_T}{(1 - \nu)} \quad . \tag{52}$$

From equations (50), (51), and (52), the constants C_1 and C_2 are found to be

$$C_1 = 0$$

and $\tag{53}$

$$C_2 = \frac{\alpha t a^2 \beta^2}{6(1 - \nu)} d_0 \quad .$$

Hence, equation (50) may now be rewritten as follows:

$$w = \frac{\alpha t a^2 \beta^2}{6(1 - \nu)} d_0 e^{-\beta x} \sin \beta x \quad . \tag{54}$$

The function $\zeta(\beta x)$, tabulated by Timoshenko and Woinowsky-Krieger [11] may now be introduced to obtain

$$w = \frac{\alpha t a^2 \beta^2}{6(1 - \nu)} d_0 \zeta(\beta x) \tag{55}$$

where

$$\zeta(\beta x) = e^{-\beta x} \sin \beta x \quad . \tag{56}$$

By substituting equation (55) into (45), the bending moments can be expressed

as

$$M_x = \frac{E \alpha t^2 d_0}{12(1 - \nu)} [\theta(\beta x) - 1]$$

and   (57)

$$M_\phi = \frac{E \alpha t^2 d_0}{12(1 - \nu)} [\nu \theta(\beta x) - 1]$$

where the function $\theta(\beta x)$ is tabulated by Timoshenko and Woinowsky-Krieger

[11] and is defined as follows:

$$\theta(\beta x) = e^{-\beta x} \cos \beta x \quad .$$ (58)

The extreme-fiber stresses can then be determined from

$$\sigma_x = \mp \frac{6M_x}{t^2}$$

and   (59)

$$\sigma_\phi = \frac{N_\phi}{t} \mp \frac{6M_\phi}{t^2}$$

where the upper signs correspond to the outermost fibers. By substituting

equation (55) and the first of equations (49) into (47), the following expression

is obtained for N_ϕ :

$$N_\phi = -\frac{E\alpha t^2 a \beta^2}{6(1-\nu)}\, d_0\, \zeta(\beta x) \quad . \tag{60}$$

For the other half of the cylinder $(L/2 \cdot x \le L)$, equation (40) must be used, which, in view of equations (49), becomes

$$w = e^{-\beta(L-x)}[C_3 \cos \beta(L-x) + C_4 \sin \beta(L-x)] \quad . \tag{61}$$

At $x = L$, the boundary condition of simple support requires that

$$w = M_x = 0 \tag{62}$$

where

$$M_x = -D_b \frac{d^2 w}{dx^2} - \frac{M_T}{(1-\nu)} \quad . \tag{63}$$

From equations (61), (62), and (63), the constants C_3 and C_4 are found to be

$$C_3 = 0$$

and $\tag{64}$

$$C_4 = \frac{\alpha t a^2 \beta^2}{6(1-\nu)}\, d_0 \quad .$$

Then, proceeding in the same manner as for the other half of the cylinder, the following expressions are found for the deflections, moments, and extreme-fiber stresses:

$$w = \frac{\alpha t \, a^2 \beta^2}{6(1-\nu)} \, d_0 \, \zeta[\beta(L-x)] \quad , \tag{65}$$

$$M_x = \frac{E \alpha t^2 d_0}{12(1-\nu)} \{\theta[\beta(L-x)] - 1\} \quad , \tag{66}$$

$$M_\phi = \frac{E \alpha t^2 d_0}{12(1-\nu)} \{\nu\theta[\beta(L-x)] - 1\} \quad , $$

$$\sigma_x = \mp \frac{6 M_x}{t^2} \quad , $$

and $\tag{67}$

$$\sigma_\phi = \frac{N_\phi}{t} \mp \frac{6 M_\phi}{t^2}$$

where

$$N_\phi = -\frac{E \alpha t^2 \, a\beta^2}{6(1-\nu)} \, d_0 \, \zeta[\beta(L-x)] \quad . \tag{68}$$

Here again, the upper signs in the stress formulas correspond to the outermost fibers.

The foregoing relationships for the two halves of the cylinder were used to obtain the nondimensional solution listed in Table 3.0-7. These results are plotted in Figure 3.0-40.

Example No. 2.

A thin-walled, right circular cylinder of length $L(> 2\pi/\beta)$ has both ends clamped and is subjected to the temperature distribution

$$T = b_0 + b_1 x \tag{69}$$

TABLE 3.0-7. NONDIMENSIONAL TABULAR SOLUTION FOR w AND M_x (EXAMPLE NO. 1)[a,b,c]

	0 ≤ x ≤ L/2							L/2 ≤ x ≤ L		
x	βx	$\zeta(\beta x)$	$\theta(\beta x)$	$\theta(\beta x)-1$	x	(L-x)	$\beta(L-x)$	$\zeta[\beta(L-x)]$	$\theta[\beta(L-x)]$	$\theta[\beta(L-x)]-1$
0	0	0	1.000	0	20.0	20.0	4.0	-0.0139	-0.0120	-1.0120
0.5	0.1	0.0903	0.9003	-0.0997	25.0	15.0	3.0	0.0071	-0.0493	-1.0493
1.0	0.2	0.1627	0.8024	-0.1976	30.0	10.0	2.0	0.1230	-0.0563	-1.0563
2.0	0.4	0.2610	0.6174	-0.3826	35.0	5.0	1.0	0.3096	0.1988	-0.8012
3.0	0.6	0.3099	0.4530	-0.5470	37.0	3.0	0.6	0.3099	0.4530	-0.5470
5.0	1.0	0.3096	0.1988	-0.8012	38.0	2.0	0.4	0.2610	0.6174	-0.3826
10.0	2.0	0.1230	-0.0563	-1.0563	39.0	1.0	0.2	0.1627	0.8024	-0.1976
15.0	3.0	0.0071	-0.0493	-1.0493	39.5	0.5	0.1	0.0903	0.9003	-0.0997
20.0	4.0	-0.0130	-0.0120	-1.0120	40.0	0	0	0	1.000	0

a. $\beta = 0.20$.

b. $\zeta(\beta x) = w/[(\alpha t a^2 \beta^2 d_0)/6(1-\nu)] = \zeta[\beta(L-x)]$.

c. $\theta(\beta x) - 1 = M_x/[(E\alpha t^2 d_0)/12(1-\nu)] = \theta[\beta(L-x)] = \theta[\beta(L-x)] - 1$.

where b_0 and b_1 are constants. It is desired that the deflections and extreme-fiber stresses be found, assuming that $L = 40$ in., $\beta = 0.2$, and $b_1/b_0 = 2$.

For the given temperature distribution, equations (38) yield

$$N_T = E\alpha t \left(b_0 + b_1 x\right)$$

and (70)

$$M_T = 0 \quad .$$
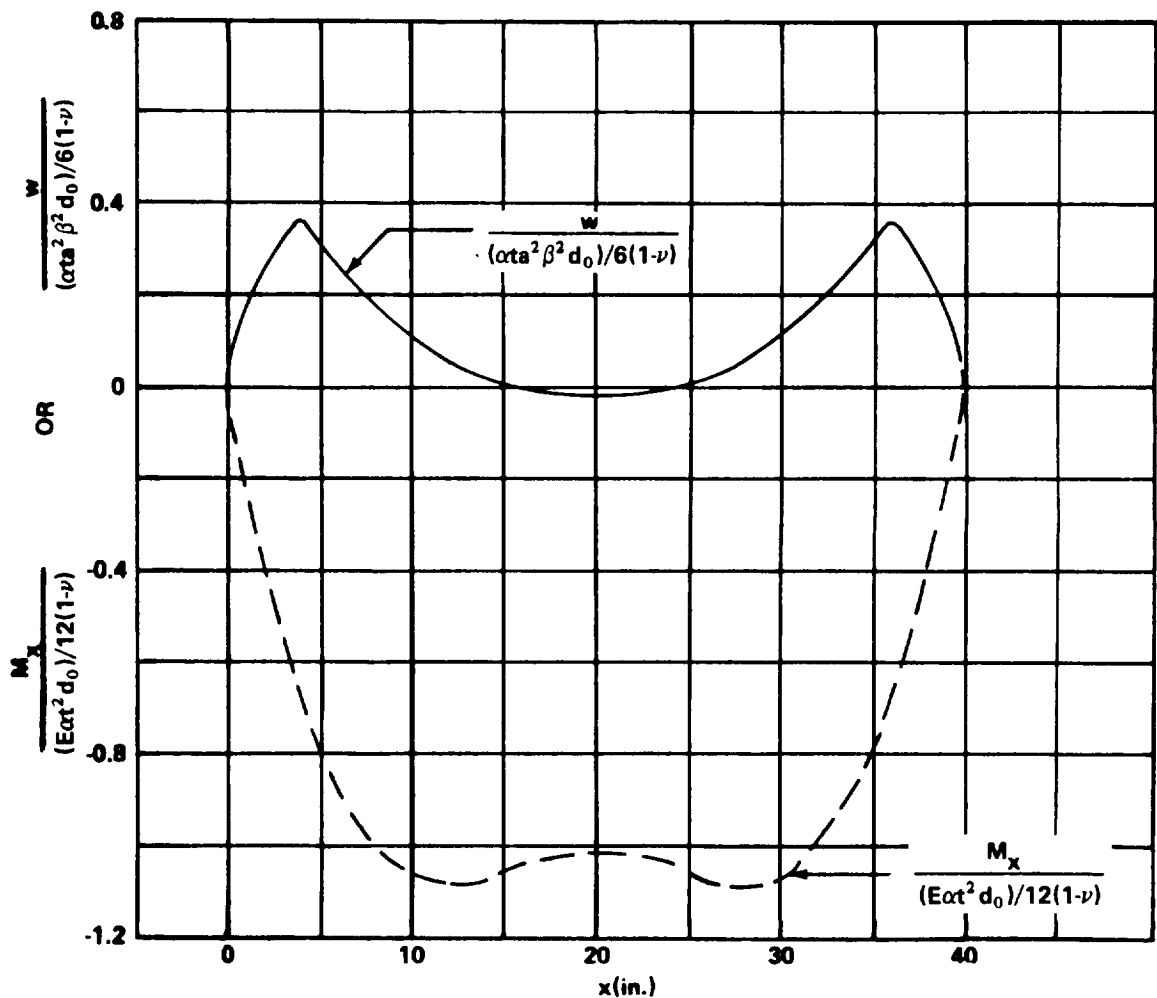
Figure 3.0-40. Nondimensional deflections and axial bending moments for example problem No. 1.

Then for $0 \leq x \leq L/2$, equation (4) becomes

$$w = e^{-\beta x}(C_1 \cos \beta x + C_2 \sin \beta x) - a\alpha (b_0 + b_1 x) \quad . \tag{71}$$

At $x = 0$, the clamped condition requires that

$$w = \frac{dw}{dx} = 0 \quad . \tag{72}$$

From equations (71) and (72) , the constants C_1 and C_2 are found to be

$$C_1 = \alpha ab_0$$

and $\tag{73}$

$$C_2 = \alpha ab_0 + \frac{\alpha ab_1}{\beta} \quad .$$

Hence, equation (71) may now be rewritten as follows:

$$w = e^{-\beta x}\left[\alpha ab_0(\cos \beta x + \sin \beta x) + \frac{\alpha ab_1}{\beta} \sin \beta x \right] - \alpha a(b_0 + b_1 x) \quad . \tag{74}$$

The functions $\phi(\beta x)$ and $\zeta(\beta x)$, tabulated by Timoshénko and Woinowsky-Krieger [11] , may now be introduced to obtain

$$w = \alpha ab_0\phi(\beta x) + \frac{\alpha ab_1}{\beta} \zeta(\beta x) - \alpha a(b_0 + b_1 x) \tag{75}$$

where

$$\phi(\beta x) = e^{-\beta x}(\cos \beta x + \sin \beta x) \tag{76}$$

and

$$\zeta(\beta x) = e^{-\beta x} \sin \beta x \quad .$$

(76)
(Con.)

By substituting equation (75) into (45), the bending moments can be expressed as

$$M_x = 2 \, cab_0 \, D_b \beta^2 \left[\psi(\beta x) + \frac{b_1}{b_0 \beta} \theta(\beta x) \right]$$

and   (77)

$$M_\phi = \nu M_x$$

where the functions $\psi(\beta x)$ and $\theta(\beta x)$ are tabulated by Timoshenko and Woinowsky-Krieger [11] and are defined as follows:

$$\psi(\beta x) = e^{-\beta x} (\cos \beta x - \sin \beta x)$$

and   (78)

$$\theta(\beta x) = e^{-\beta x} \cos \beta x \quad .$$

The extreme-fiber stresses can then be determined from

$$\sigma_x = \mp \frac{6M_x}{t^2} .$$

(79)

and

$$\sigma_\phi = \frac{N_\phi}{t} \mp \frac{6M_\phi}{t^2}$$

(79)
(Con.)

where the upper signs correspond to the outermost fibers. By substituting equations (75) and (70) into (47), the following expression is obtained for N_ϕ :

$$N_\phi = -E\alpha b_0 t \phi(\beta x) - \frac{E\alpha b_1 t}{\beta} \zeta(\beta x) \quad .$$

(80)

For the other half of the cylinder $(L/2 \leq x \leq L)$, equation (40) must be used, which, in view of equations (70), becomes

$$w = e^{-\beta(L-x)} [C_3 \cos \beta(L - x) + C_4 \sin \beta(L - x)] - \alpha a(b_0 + b_1 x) \quad .$$

(81)

At $x = L$, the clamped condition requires that

$$w = \frac{dw}{dx} = 0 \quad .$$

(82)

From equations (81) and (82), the constants C_3 and C_4 are found to be

$$C_3 = \alpha a(b_0 + b_1 L)$$

and

(83)

$$C_4 = -\frac{\alpha a b_1}{\beta} + \alpha a(b_0 + b_1 L) \quad .$$

Then proceeding in the same manner as for the other half of the cylinder, the following expressions are found for the deflections, moments, and extreme-fiber stresses:

$$w = \alpha a b_0 \left(1 + \frac{b_1}{b_0} L\right) \phi[\beta(L - x)] - \frac{\alpha a b_1}{\beta} \zeta[\beta(L - x)] - \alpha a b_0 \left(1 + \frac{b_1}{b_0} x\right) ,$$
(84)

$$M_x = 2 a \alpha \beta^2 b_0 D_0 \left\{\left(1 + \frac{b_1}{b_0} L\right) \psi[\beta(L - x)] - \frac{b_1}{b_0 \beta} \theta[\beta(L - x)]\right\} ,$$
(85)

$$M_\phi = \nu M_x ,$$

$$\sigma_x = \mp \frac{6 M_x}{t^2} ,$$

and
(86)

$$\sigma_\phi = \frac{N_\phi}{t} \mp \frac{6 M_\phi}{t^2}$$

where

$$N_\phi = -E \alpha b_0 t \left(1 + \frac{b_1}{b_0} L\right) \phi[\beta(L - x)] + \frac{E \alpha b_1 t}{\beta} \zeta[\beta(L - x)] .$$
(87)

Here again, the upper signs in the stress formulas correspond to the outer-most fibers.

The foregoing relationships for the two halves of the cylinder were used to obtain the nondimensional solution shown in Table 3.0-8. These results are plotted in Figure 3.0-41.

TABLE 3.0-8. NONDIMENSIONAL TABULAR SOLUTION FOR w AND M_x (EXAMPLE NO. 2)

1	2	3	4	5	6	7	8	9
x	βx	$\phi(\beta x)$	$\frac{b_1}{\beta b_0}\zeta(\beta x)$	$-\left(1+\frac{b_1}{b_0}x\right)$	$A_1{}^a$	$\psi(\beta x)$	$\frac{b_1}{b_0\beta}\theta(\beta x)$	$A_2{}^b$
0	0	1.000	0	-1	0	1.0	10.0	11.0
0.5	0.1	0.9907	0.903	-2	-0.1063	0.81	9.003	9.813
1.0	0.2	0.9651	1.627	-3	-0.4079	0.6398	8.024	8.6638
2.0	0.4	0.8784	2.610	-5	-1.5116	0.3564	6.174	6.5304
3.0	0.6	0.7628	3.099	-7	-3.1382	0.1431	4.530	4.6731
5.0	1.0	0.5083	3.096	-11	-7.3957	-0.1108	1.988	1.8772
10.0	2.0	0.0667	1.230	-21	-19.7033	-0.1794	-0.563	-0.7424
15.0	3.0	-0.0423	0.071	-31	-30.9713	-0.0563	-0.493	-0.5493
20.0	4.0	-0.0258	-0.117	-41	-41.1428	0.0019	-0.120	-0.1181

a. $A_1 = (w/\alpha ab_0) = (3)+(4)+(5)$.

b. $A_2 = (M_x/2\alpha ab_0 D_b\beta^2) = (7)+(8)$.

x	(L-x)	$\beta(L-x)$	$\left(1+\frac{b_1}{b_0}L\right)\times\phi[\beta(L-x)]$	$-\frac{b_1}{b_0\beta}\times\zeta[\beta(L-x)]$	$-\left(1+\frac{b_1}{b_0}x\right)$	$\frac{w}{\alpha ab_0}$ = (4)+(5)+(6)	$\left(1+\frac{b_1}{b_0}L\right)\times\psi[\beta(L-x)]$	$\frac{b_1}{b_0\beta}\times\theta[\beta(L-x)]$	$\frac{M_x}{2\alpha ab_0 D_b\beta^2}$ = (8)-(9)
1	2	3	4	5	6	7	8	9	10
20	20	4	-2.0898	0.117	-41	-42.9728	0.1539	-0.120	0.2739
25	15	3	-3.4263	-0.071	-51	-54.4973	-4.5603	-0.493	-4.0673
30	10	2	5.4027	-1.230	-61	-56.8273	-14.5314	-0.563	-13.9684
35	5	1.0	41.1723	-3.096	-71	-32.9237	-8.9748	1.988	-10.9628
37	3	0.6	61.7869	-3.099	-75	-16.3121	11.5911	4.530	7.0611
38	2	0.4	71.1504	-2.610	-77	-8.4596	28.8684	6.174	22.6944
39	1.0	0.2	78.1731	-1.627	-79	-2.4539	51.8238	8.024	43.7998
39.5	0.5	0.1	80.2467	-0.903	-80	-0.6563	65.610	9.003	56.607
40	0	0	81.00	0	-81	0	81.0	10.00	71.00
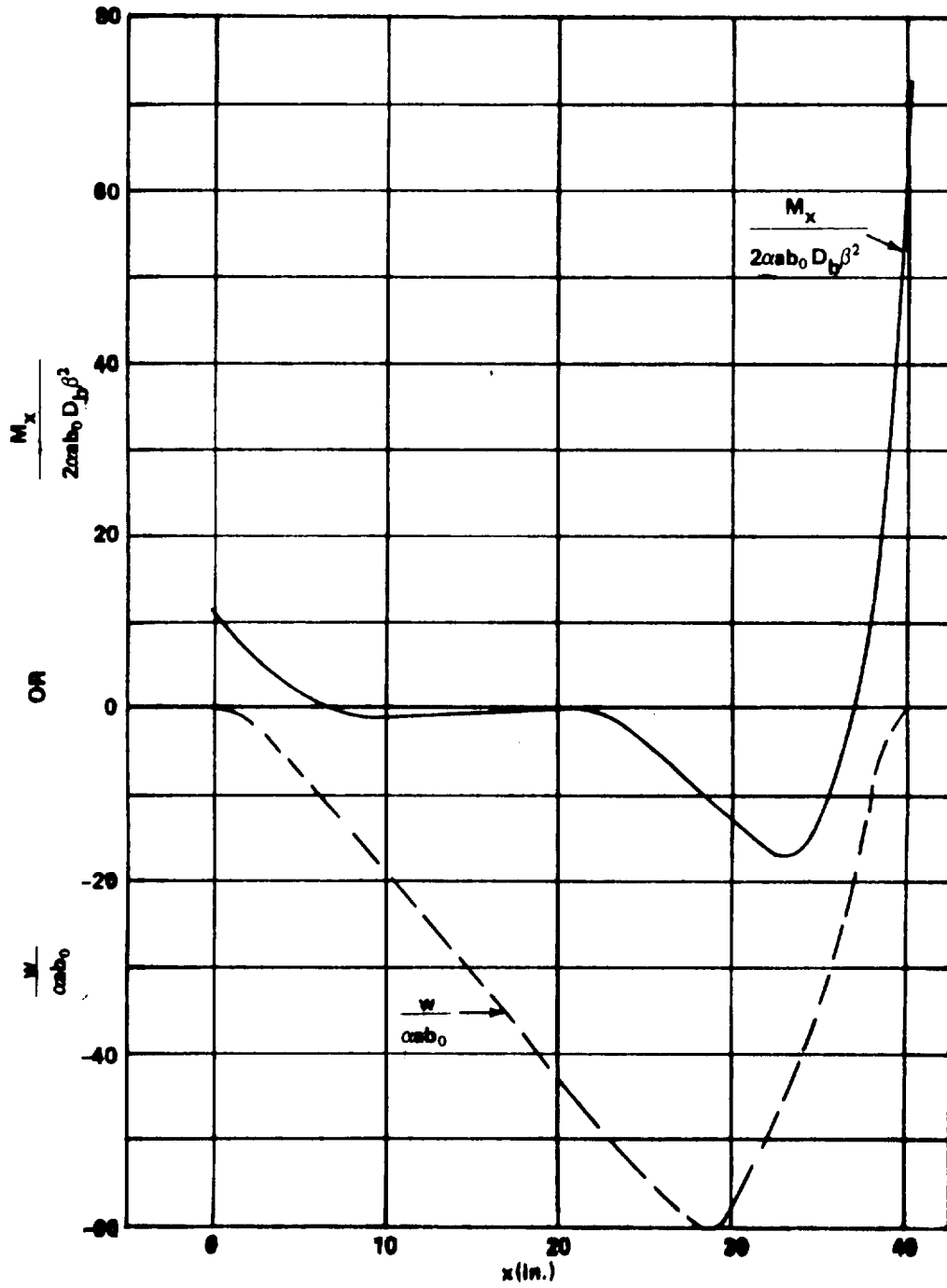
Figure 3. 0-41.   Nondimensional deflections and axial bending
moments for example problem No. 2.

III. <u>Thermal Stresses and Deflections - Constant Radial Gradient,</u>

<u>Axisymmetric Axial Gradient.</u>

A. Configuration.

The design curves and equations presented here apply only to thin-walled, right circular cylinders which are of constant thickness and are made of isotropic material. It is assumed that the shell wall is free of holes and that it obeys Hooke's law. The method is valid only when $\lambda \geq \pi$. Figure 3.0-42 depicts the isotropic cylinder shell configuration. Figure 3.0-43 shows the sign convention for forces, moments, and pressures.

B. Boundary Conditions.

The following types of boundary conditions are discussed:

1. Free edge; that is,

$$Q_x = M_x = 0 \quad . \tag{88}$$

2. Simply supported edge; that is,

$$w = M_x = 0 \quad . \tag{89}$$

3. Clamped edge; that is,

$$w = \frac{dw}{dx} = 0 \quad . \tag{90}$$

All possible combinations of these boundary conditions are permitted. Hence, it is not required that those at $x = 0$ be the same as those at $x = L$. However,
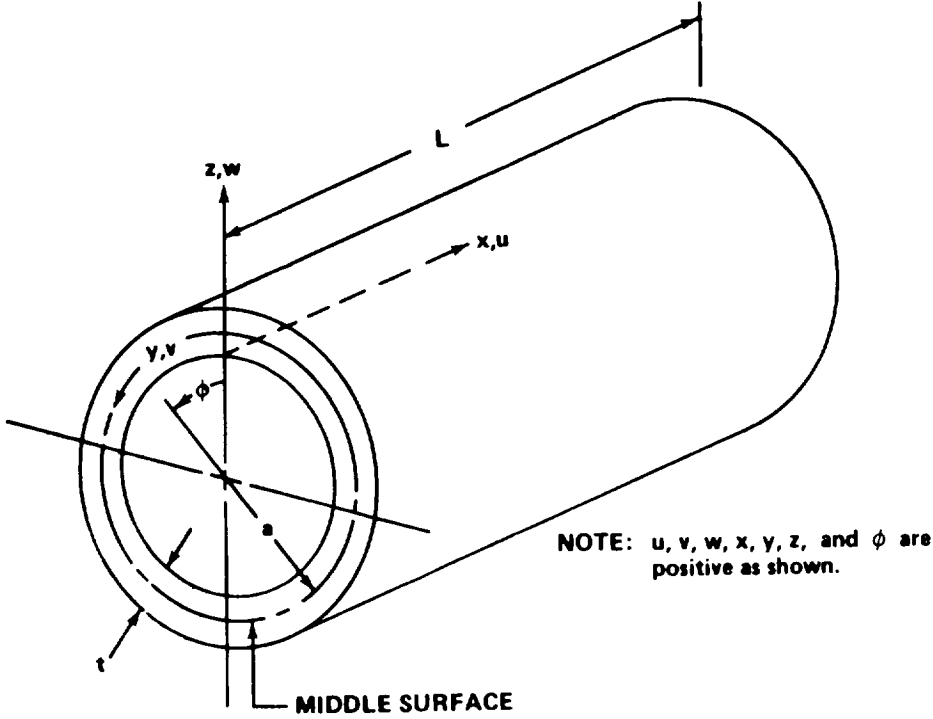
Figure 3.0-42. Isotropic cylindrical shell configuration for thermal stresses and deflections.
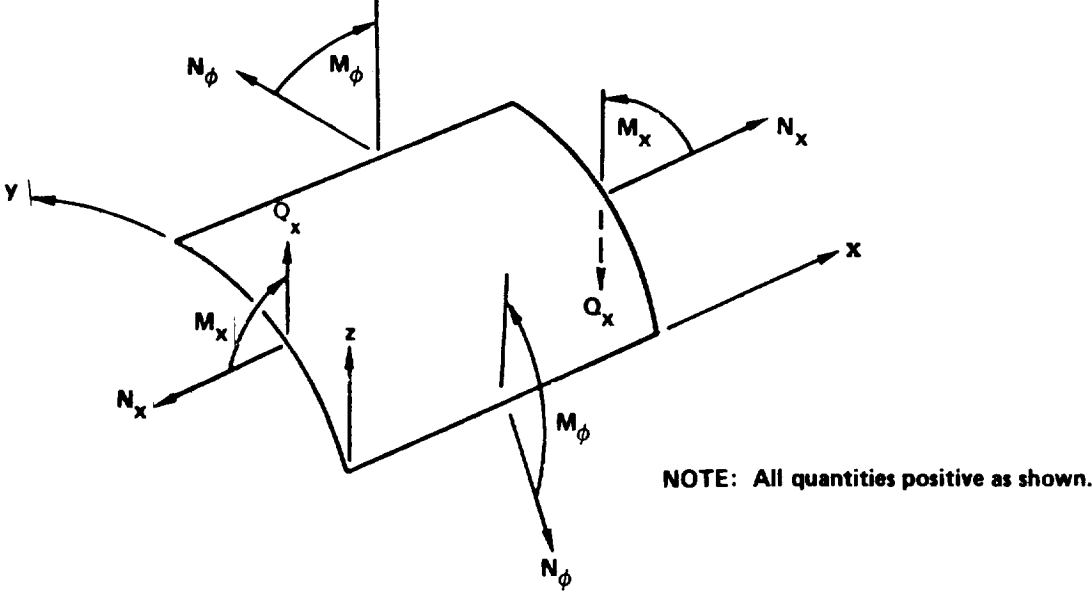
Figure 3.0-43. Sign convention for forces, moments, and pressures for thermal stresses and deflections.

in every case, it is assumed that the cylinder is unrestrained in the axial

direction $(N_x \quad 0)$.

C. Temperature Distribution.

The supposition is made that no temperature variations occur through

the wall thickness. However, the cylinder may have any axisymmetric surface

gradient for which the product αT can be adequately represented by a fifth-

degree (or lower) polynomial. Therefore, subject to that restriction, the

permissible distributions are of the form

$$\alpha T = \alpha(x) T(x) \quad . \tag{91}$$

D. Design Curves and Equations.

In Ref. 23, Newman and Forray present the practical method given

below to compute the thermal stresses, deflections, and rotations in circular

cylindrical shells which comply with the foregoing specifications. The primary

relationships are expressed in series form and the necessary term-by-term

coefficients can be obtained from Figures 3.0-44 through 3.0-49. As indicated

by equation (91), the product αT will be a function of x and, in order to

apply this method, this function must first be approximated by the polynomial

$$\alpha T = d_0 + d_1 \xi + d_2 \xi^2 + \dots d_z \xi^z = \sum_{k=0}^{z} d_k \xi^k \tag{92}$$

where ξ is a dimensionless axial coordinate defined by the relationship

$$\xi = \frac{x}{L} \quad . \tag{93}$$
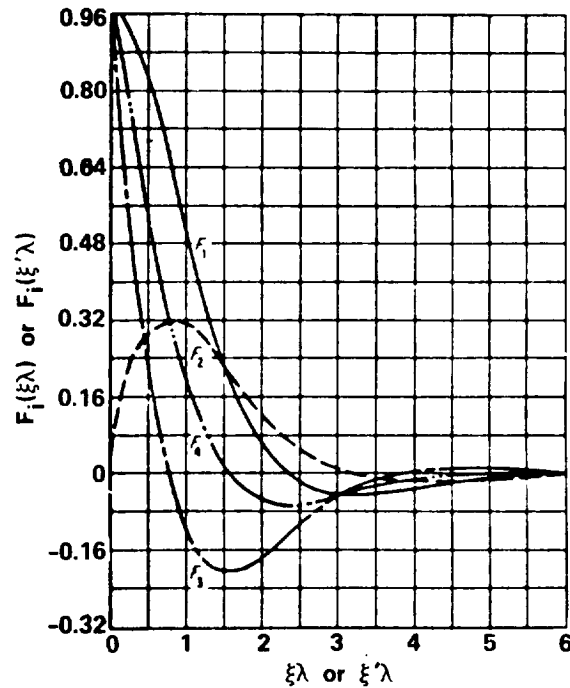
Figure 3.0-44. Functions F_i .

For the purposes of the technique given here, the following inequality must be satisfied:

$$Z \leq 5 \quad . \tag{94}$$

After the coefficients d_k have been established, the thermal stresses and distortions can be determined by using equations (96) through (98) in conjunction with the design curves. The constants A_1 and A_2 are based on the boundary conditions at $x = 0$ ($\xi = 0$) while A_3 and A_4 depend on the boundary conditions at $x = L$ ($\xi = 1$) . The formulas for these four values are listed in Table 3.0-9.
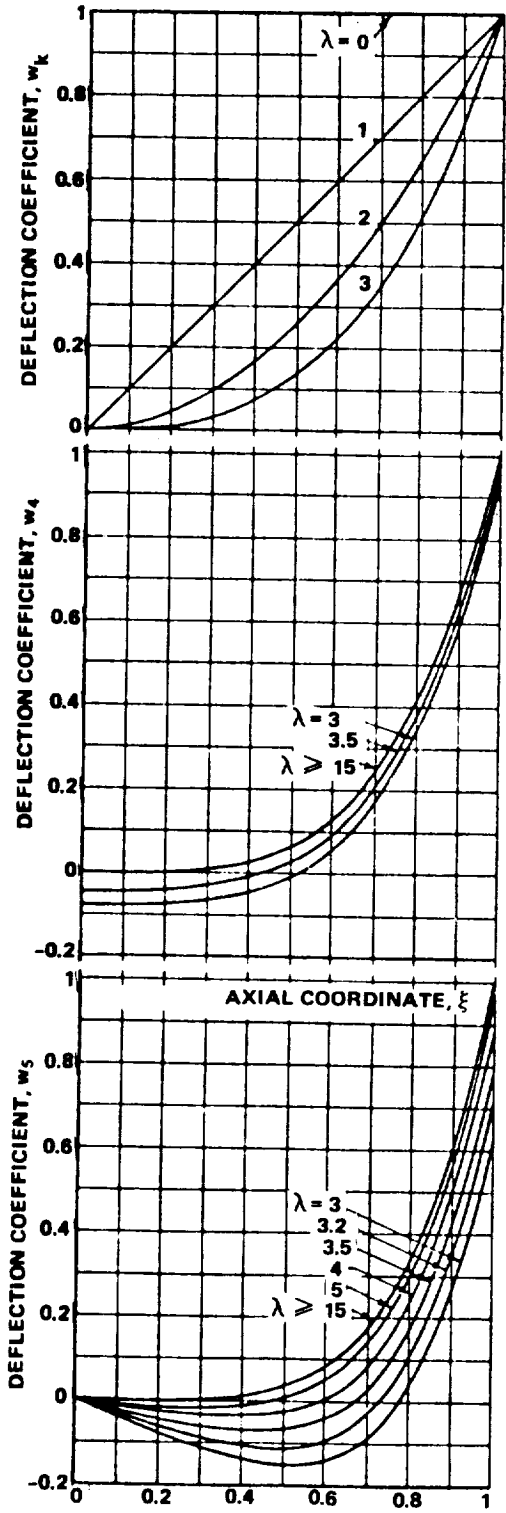
Figure 3.0-45. Deflection
coefficients and k = 5 , the
coefficient depends on λ .
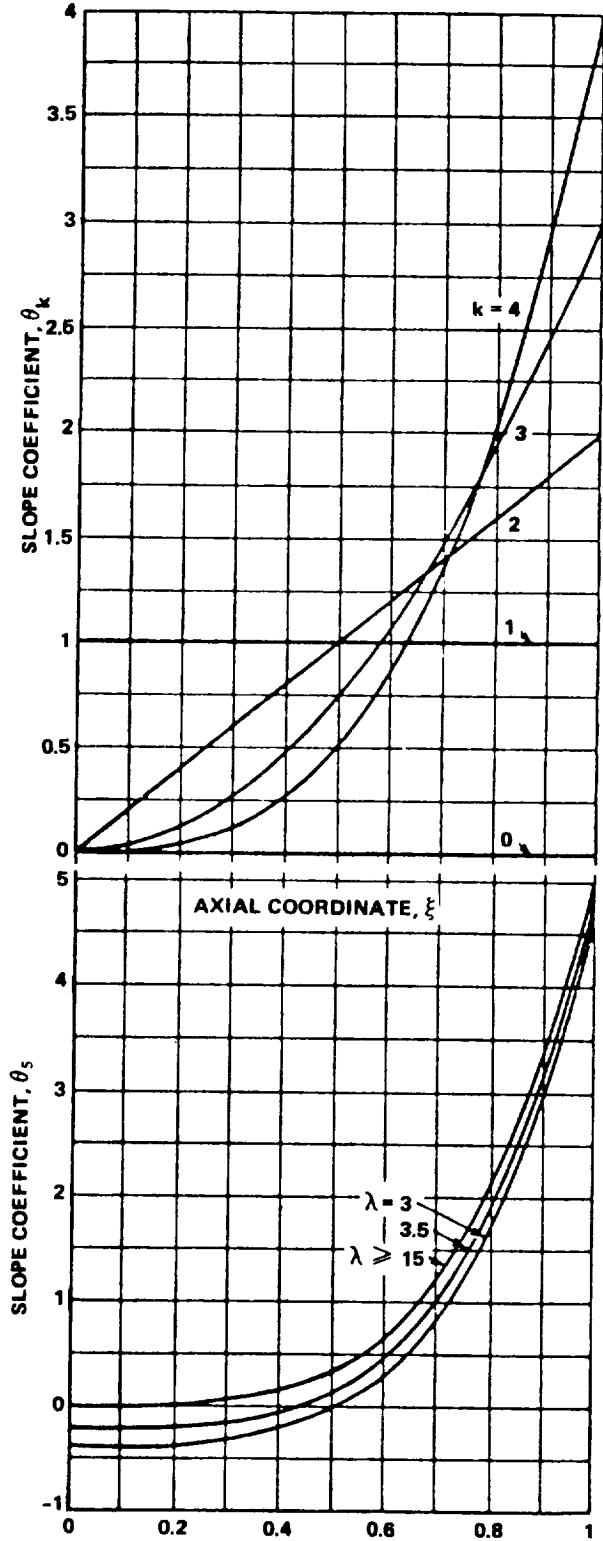
Figure 3.0-46. Slope coefficients
(for k = 5 , the coefficient
depends on λ) .
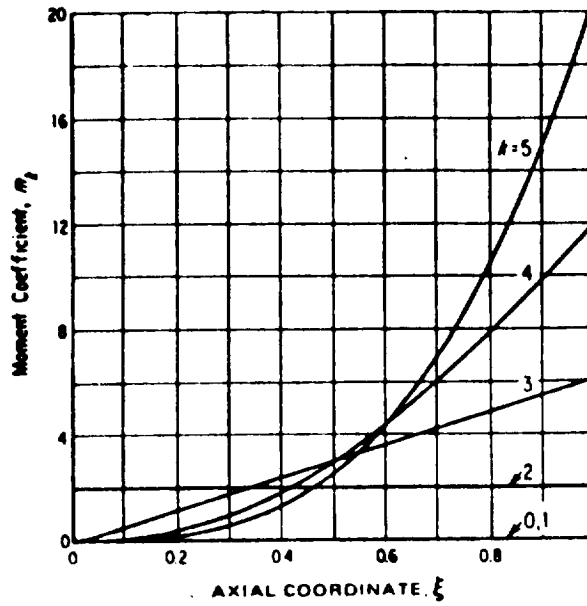
Figure 3.0-47.   Moment coefficients.
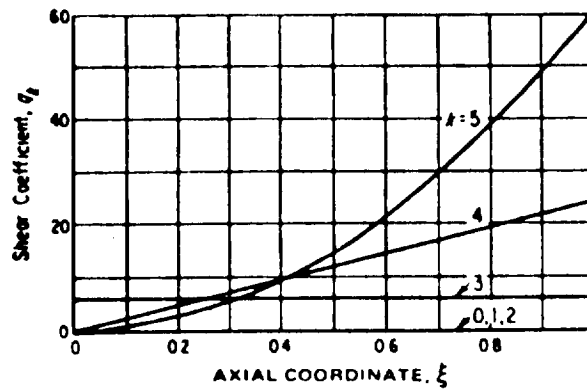
Figure 3.0-48.   Shear coefficients.
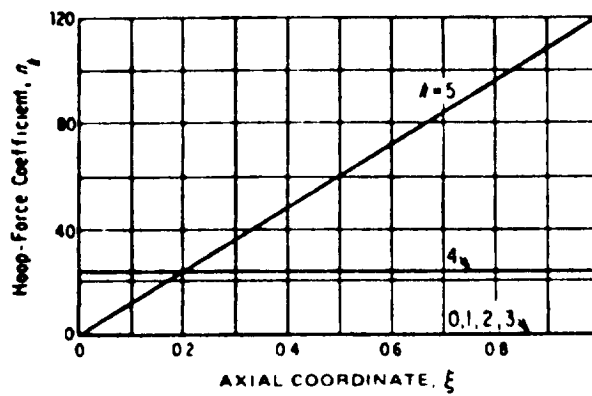
Figure 3.0-49.   Hoop-force coefficients.

TABLE 3.0-9.   FORMULAS FOR THE CONSTANTS A_1 THROUGH A_4

Cylinder End	Boundary Condition	Constants A_1
$\xi = 0$ $(x = 0)$	Free	$A_1 \quad \dfrac{1}{2\lambda^2} \displaystyle\sum_{k=0}^{Z} d_k m_k(0)$ $A_2 \quad -\dfrac{1}{2\lambda^2} \displaystyle\sum_{k=0}^{Z} d_k \left[m_k(0) + \dfrac{1}{\lambda} q_k(0) \right]$
$\xi = 0$ $(x = 0)$	Simple support	$A_1 \quad \dfrac{1}{2\lambda^2} \displaystyle\sum_{k=0}^{Z} d_k m_k(0)$ $A_2 \quad - \displaystyle\sum_{k=0}^{Z} d_k w_k(0)$
$\xi = 0$ $(x = 0)$	Clamped	$A_1 = - \displaystyle\sum_{k=0}^{Z} d_k \left[w_k(0) + \dfrac{1}{\lambda} \theta_k(0) \right]$ $A_2 \quad - \displaystyle\sum_{k=0}^{Z} d_k w_k(0)$
$\xi = 1$ $(x = L)$	Free	$A_3 \quad \dfrac{1}{2\lambda^2} \displaystyle\sum_{k=0}^{Z} d_k m_k(1)$ $A_4 = \dfrac{1}{2\lambda^2} \displaystyle\sum_{k=0}^{Z} d_k \left[\dfrac{1}{\lambda} q_k(1) - m_k(1) \right]$
$\xi = 1$ $(x = L)$	Simple support	$A_3 = \dfrac{1}{2\lambda^2} \displaystyle\sum_{k=0}^{Z} d_k m_k(1)$ $A_4 = - \displaystyle\sum_{k=0}^{Z} d_k w_k(1)$
$\xi = 1$ $(x = L)$	Clamped	$A_3 = \displaystyle\sum_{k=0}^{Z} d_k \left[\dfrac{1}{\lambda} \theta_k(1) - w_k(1) \right]$ $A_4 - - \displaystyle\sum_{k=0}^{Z} d_k w_k(1)$

The solutions are based on classical small-deflection shell theory.
Therefore, it is important for the user to be aware of this when the method is
applied to pressurized cylinders by superimposing the thermal stresses and
deformations upon the corresponding values due solely to pressure; that is,
because of the dependence upon classical theory, the method presented here
cannot account for nonlinear coupling between thermal deflections and the
pressure-related meridional loads.

In addition, it is assumed that Young's modulus and Poisson's ratio
are unaffected by temperature changes. Hence, the user must select single
effective values for each of these properties by employing some type of
averaging technique.

E. Summary of Equations and Nondimensional Coefficients.

$$\alpha T = d_0 + d_1\xi + d_2\xi^2 + \ldots d_z\xi^z = \sum_{k=0}^{z} d_k\xi^k \quad , \tag{95}$$

$$\frac{w}{a} = A_1 F_2(\xi\lambda) + A_2 F_4(\xi\lambda) + A_3 F_2(\xi'\lambda) + A_4 F_4(\xi'\lambda) + \sum_{k=0}^{z} d_k w_k \quad ,$$

$$\frac{L}{a}\theta = \lambda[A_1 F_3(\xi\lambda) - A_2 F_1(\xi\lambda) - A_3 F_3(\xi'\lambda) + A_4 F_1(\xi'\lambda)] + \sum_{k=0}^{z} d_k \theta_k \quad ,$$

$$\frac{L^2 M_x}{a D_b} = 2\lambda^2[-A_1 F_4(\xi\lambda) + A_2 F_2(\xi\lambda) - A_3 F_4(\xi'\lambda) + A_4 F_2(\xi'\lambda)] + \sum_{k=0}^{z} d_k m_k \quad ,$$

$$M_\phi = \nu M_x \quad , \tag{96}$$

$$\frac{L^3 Q_x}{a D_b} = 2\lambda^3 [A_1 F_1(\xi\lambda) + A_2 F_3(\xi\lambda) - A_3 F_1(\xi'\lambda) - A_4 F_3(\xi'\lambda)] + \sum_{k=0}^{Z} d_k q_k \quad ,$$

and

$$\frac{L^4 N_\phi}{a^2 D_b} = 4\lambda^4 [A_1 F_2(\xi\lambda) + A_2 F_4(\xi\lambda) + A_3 F_2(\xi'\lambda) + A_4 F_4(\xi'\lambda)] - \sum_{k=0}^{Z} d_k n_k \quad ,$$

where

$$\lambda = L \frac{4\sqrt{3(1 - \nu^2)}}{(at)^{1/2}} \quad ,$$

$$D_b = \frac{Et^3}{12(1 - \nu^2)} \quad , \tag{97}$$

$$\xi = \frac{x}{L} \quad ,$$

and

$$\xi' = 1 - \xi \quad .$$

The stresses at any location are given by the following:

$$\sigma_x = -\frac{12z}{t^3} M_x \tag{98}$$

C-3

and

$$\sigma_\phi = \frac{N_\phi}{t} - \frac{12z}{t^3} M_\phi \quad .$$

(98)
(Con.)

3.0.8.2 Isotropic Conical Shells.

This section concerns the thermostructural analysis of thin-walled,

right circular, isotropic conical shells. The organization here is somewhat

different from that of previous sections which cover isotropic flat plates.

This is due to certain fundamental differences between the physical behavior

of flat plates and shells. Flat-plate deformations are of such a nature that

it is helpful to group the solutions for stable constructions into the following

categories:

1. Temperature gradients through the thickness

2. Uniform temperatures through the thickness.

Except for the special case of self-equilibrating gradients through the

thickness $(N_T = M_T = 0)$, the first of these two cases involves out-of-plane

bending which is, of course, accompanied by displacements normal to the

middle surface of the undeformed plate. In case 2, the plate remains flat;

that is, the only displacements occur in directions parallel to the original

middle surface and no out-of-plane bending occurs. The indicated separation

of cases is therefore a logical format for the sections dealing with flat plates.

However, the situation is not the same for shell structures. For these com-

ponents, there is no need to isolate the foregoing types of thermal conditions.

This is because either type of temperature distribution, in conjunction with clamped or simply supported boundaries, will lead to both membrane loading and bending about the shell-wall middle surface. Consequently, for stable shell constructions which comply with either case 1 or 2, the analysis methods are given as follows as a single grouping.

Configuration.

The design equations provided here apply only to long $(L \geq 2\pi/\lambda B)$, thin-walled, truncated, right circular cones which are of constant thickness, are made of isotropic material, and satisfy the inequality

$$x_A > 3t \cot \phi \quad . \tag{99}$$

It is assumed that the shell wall is free of holes and obeys Hooke's law. Figure 3.0-50 depicts the subject configuration, as well as most of the notation and sign conventions of interest.

Boundary Conditions.

The method presented here can be applied where any of the following boundary conditions are present:

1. Free edges

2. Simply supported edges

3. Clamped edges.

All possible combinations of these boundaries are permitted; that is, it is not required that those at x_A be the same as those at x_B. However, in every case, it is assumed that the cone is unrestrained in the axial direction.

NOTE: 1. s* = L-s
2. H_A, H_B, M_A, M_B,
V, and $\overline{W}$ are axisymmetric.
3. All coordinates, forces,
moments, and deformations are
positive as shown.
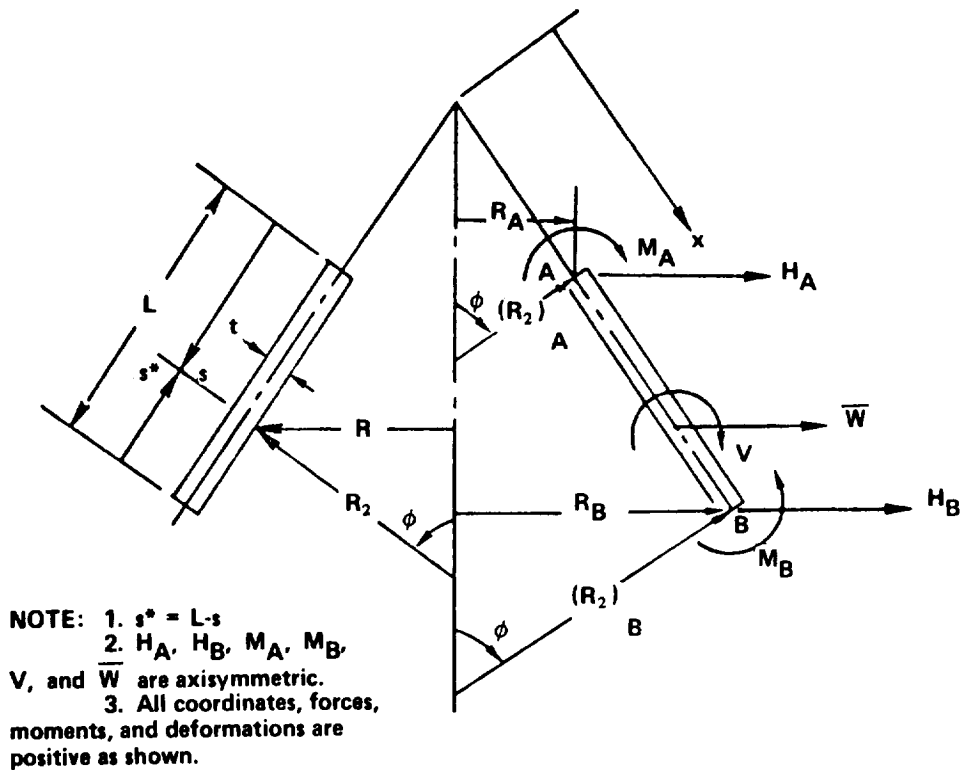
a. Overall truncated cone.
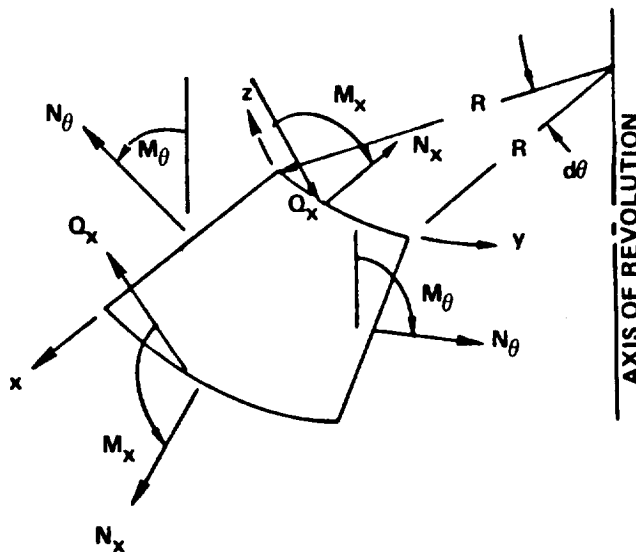
b. Positive directions for the stress resultants and coordinates.

Figure 3.0-50. Configuration, notation, and sign convention for conical shell.

Temperature Distribution.

The following types of temperature distributions may be present:

1. A linear gradient through the wall thickness subject to the provision that the temperature change T need not vanish at the middle surface.

2. Axisymmetric meridional gradients.

The permissible distributions can therefore be expressed in the form

$$T = T_1(s) + T_2(s) \frac{z}{t} \ . \tag{100}$$

Naturally, any of the special cases for this equation are applicable; that is, either or both of $T_1(s)$ and $T_2(s)$ can be finite constants and either may be equal to zero.

Design Equations.

A number of methods for solving the subject problem have been published, including those of Refs. 24 through 27. In the approach presented here, particular solutions to the governing differential equations are found in the manner suggested by Tsui [16]. As in Refs. 25 and 28, the complementary solutions are obtained by an equivalent-cylinder approximation. When greater accuracy is desired, the exact complementary solutions published by Johns and Orange [29] may be used.

Throughout this section it is assumed that Young's modulus and Poisson's ratio are unaffected by temperature changes. Hence, the user must select single effective values for each of these properties by employing some type of averaging technique. The same approach may be taken with regard to

the coefficient of thermal expansion. On the other hand, the temperature-dependence of this property may be accounted for by recognizing that it is the product αT which governs; that is, the actual temperature distribution can be suitably modified to compensate for variations in α. When this approach is taken, any mention of a linear temperature distribution is actually making reference to a straight-line variation of the product αT.

In addition, the method outlined here is based on classical small-deflection theory. It is important to keep this in mind when applying to pressurized cones by superimposing the thermal stresses and deformations upon the corresponding values due solely to pressure; that is, because of the dependence upon classical theory, the method of this manual cannot account for nonlinear coupling between thermal deflections and pressure-related meridional loads.

The governing differential equations for the subject cone are given by Tsui [16] as follows:

$$L'(U) - VEt \tan \phi = -x \frac{dN_T}{dx}$$

and

(101)

$$L'(V) + U \frac{1}{D_b} \cot \phi = -\frac{1}{D_b} \frac{\cot \phi}{(1 - \nu)} \frac{dM_T}{dx}$$

where

$$D_b = \frac{Et^3}{12(1 - \nu^2)} \quad ,$$

$$M_T = E\alpha \int_{-t/2}^{t/2} Tz \, dz \quad ,$$

$$N_T = E\alpha \int_{-t/2}^{t/2} T \, dz \quad ,$$

(102)

and

$$U = x\,Q_x$$

and L' is the operator,

$$L'(\,) = \cot\phi \left[x\frac{d^2(\,)}{dx^2} + \frac{d(\,)}{dx} - \frac{(\,)}{x} \right] \quad .$$

(103)

To obtain the desired solution, a three-step procedure is employed as out-lined below:

Step 1. Find a particular solution to equations (101).

Step 2. Find a solution to the homogeneous equations,

$$L'(U) - VEt \tan\phi = 0$$

and

(104)

$$L'(V) + U\frac{1}{D_b} \cot\phi = 0 \quad ,$$

such that superposition of these results upon those of Step 1 satisfies the

boundary conditions which can be expressed as follows:

Free edge: $\qquad Q_x = M_x = 0$.

Simply supported edge: $\qquad \overline{W} = M_x = 0$. $\qquad\qquad$ (105)

Clamped edge: $\qquad \overline{W} = V = 0$.

The results from this step are referred to as the complementary solution.

Note that equations (104) are obtained by setting the right-hand sides of

equations (101) equal to zero.

$\qquad$ Step 3. Superimpose the particular and complementary solutions.

To accomplish the first of these steps, the functions N_T and M_T are first

approximated as polynomials. It is then assumed that the particular solutions

U^P and V^P can be expressed in the form

$$U^P = C_{-1}x^{-1} + C_0 + C_1 x + C_2 x^2 + C_3 x^3 + \ldots + C_n x^n$$

and $\qquad\qquad\qquad\qquad\qquad\qquad\qquad\qquad\qquad\qquad\qquad\qquad$ (106)

$$V^P = d_{-1}x^{-1} + d_0 + d_1 x + d_2 x^2 + d_3 x^3 + \ldots + d_n x^n$$

where n is an integer whose value is a function of the polynomial degree

required for a sufficiently accurate representation of N_T and M_T . If these

formulations for N_T , M_T , U^P , and V^P are substituted into equations (101)

and like powers of x are equated, a system of simultaneous equations is obtained where the unknowns are the various polynomial coefficients. These equations can be solved for $C_{(\ )}$ and $d_{(\ )}$ and hence U^P and V^P. The associated radial deflection and stress resultants of interest can then be determined from

$$\overline{W}^P = \frac{\cos^2 \phi}{Et \sin \phi} \left(x \frac{dU^P}{dx} - \nu U^P \right) + \alpha R T_m \quad ,$$

$$Q_x^P = \frac{U^P}{x} \quad ,$$

$$N_x^P = Q_x \cot \phi \quad , \tag{107}$$

$$N_\theta^P = \frac{d}{dx} (R_2 Q_x) = \cot \phi \frac{dU^P}{dx} \quad ,$$

$$M_x^P = D_b \left(\frac{dV^P}{dx} + \frac{\nu}{R_2} V^P \cot \phi \right) - \frac{M_T}{(1-\nu)} \quad ,$$

and

$$M_\theta^P = D_b \left(\frac{1}{R_2} V^P \cot \phi + \nu \frac{dV^P}{dx} \right) - \frac{M_T}{(1-\nu)}$$

where

$$T_m = \frac{1}{t} \int_{-t/2}^{t/2} T \, dz \quad . \tag{108}$$

The complementary solutions corresponding to the edge-loaded cone of

Figure 3.0-51 are given as equations (109) and (110). Those corresponding

to the edge-loaded cone of Figure 3.0-52 are given as equations (111) and (112).
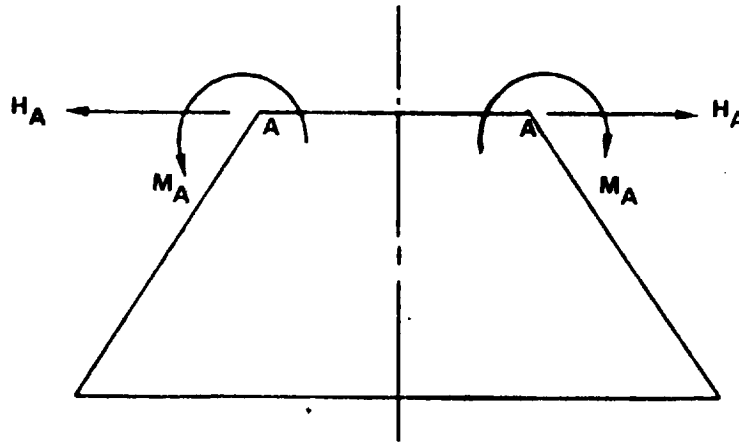
Figure 3.0-51. Truncated cone edge-loaded at top.

$$\overline{W}_A^C = \frac{\sin \phi}{2\lambda_A^3 D_b} (\lambda_A M_A + H_A \sin \phi) \quad ,$$

$$V_A^C = \frac{1}{2\lambda_A^2 D_b} (2\lambda_A M_A + H_A \sin \phi) \quad ,$$

$$\overline{W}^C = \frac{\sin \phi}{2\lambda_A^3 D_b} [\lambda_A M_A \overline{\psi}(\lambda_A s) + H_A (\sin \phi) \overline{\theta} (\lambda_A s)] \quad ,$$

$$(109)$$

$$V^C = \frac{1}{2\lambda_A^2 D_b} [2\lambda_A M_A \overline{\theta}(\lambda_A s) + H_A (\sin \phi) \overline{\phi} (\lambda_A s)] \quad ,$$

$$Q_x^C = [2\lambda_A M_A \overline{\zeta} (\lambda_A s) - H_A (\sin \phi) \overline{\psi} (\lambda_A s)] \quad ,$$

$$N_x{}^C = Q_x \cot \phi \quad ,$$

$$N_\theta{}^C = \frac{\overline{W} Et}{R} + \nu N_x \quad ,$$

<div align="right">(109)
(Con.)</div>

$$M_x{}^C = -\frac{1}{2\lambda_A} \left[2\lambda_A M_A \, \overline{\phi} \, (\lambda_A s) + 2 H_A \, (\sin \phi) \, \overline{\zeta} \, (\lambda_A s) \right] \quad ,$$

and

$$M_\theta{}^C = \nu M_x$$

where

$$\lambda_A = \sqrt[4]{\frac{3 \left(1 - \nu^2\right)}{\left(R_2\right)^2_A \, t^2}} \quad ,$$

$$\left(R_2\right)_A = \frac{R_A}{\sin \phi} \quad ,$$

<div align="right">(110)</div>

and

$$D_b = \frac{Et^3}{12 \left(1 - \nu^2\right)}$$

and $\overline{\phi}$, $\overline{\psi}$, $\overline{\theta}$, and $\overline{\zeta}$ are the functions ϕ, ψ, θ, and ζ, respectively, which are tabulated on pages 472–473 of Ref. 11.
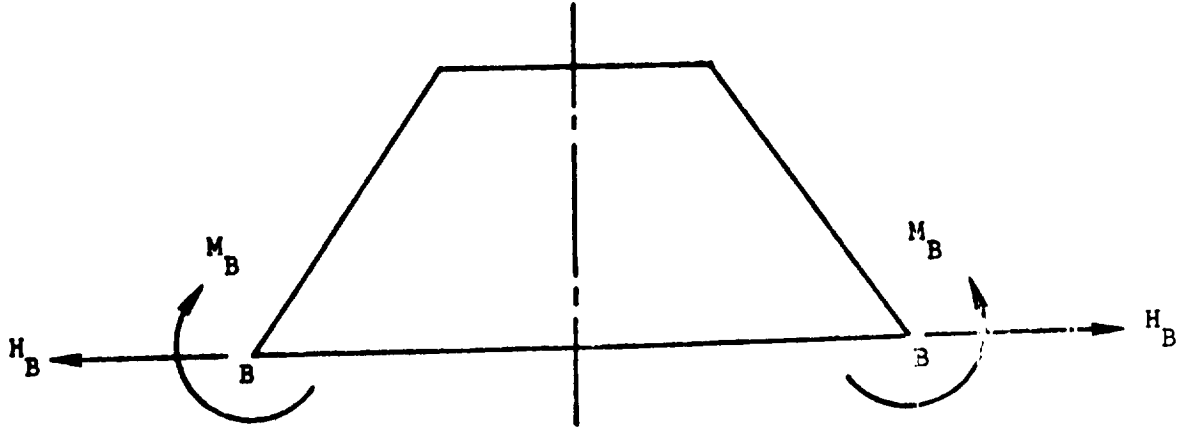
Figure 3.0-52. Truncated cone edge-loaded at bottom.

$$\overline{W}_B^C = \frac{\sin\phi}{2\lambda_B^3 D_b}\left(\lambda_B M_B + H_B \sin\phi\right) \quad ,$$

$$V_B^C = -\frac{1}{2\lambda_B^2 D_b}\left(2\lambda_B M_B + H_B \sin\phi\right) \quad ,$$

$$\overline{W}^C = \frac{\sin\phi}{2\lambda_B^3 D_b}\left[\lambda_B M_B \overline{\psi}(\lambda_B s^*) + H_B (\sin\phi)\,\overline{\theta}(\lambda_B s^*)\right] \quad ,$$

$$v^C = -\frac{1}{2\lambda_B^2 D_b}\left[2\lambda_B M_B \overline{\theta}(\lambda_B s^*) + H_B (\sin\phi)\,\overline{\psi}(\lambda_B s^*)\right] \quad ,$$

$$Q_x^C = -\left[2\lambda_B M_B \overline{\zeta}(\lambda_B s^*) - H_B(\sin\phi)\,\overline{\psi}(\lambda_B s^*)\right] \quad ,$$

$$N_x^C = Q_x \cot\phi \quad ,$$

$$N_\theta^C = \frac{\overline{W}Et}{R} + \nu N_x \quad ,$$

(111)

$$M_x^C = -\frac{1}{2\lambda_B} \left[2\lambda_B M_B \, \overline{\phi} \, (\lambda_B s^*) + 2 \, H_B \, (\sin \phi) \, \overline{\zeta} \, (\lambda_B s^*) \right] \quad ,$$

and

$$M_\theta^C = \nu M_x \qquad\qquad\qquad (111)$$
$$(\text{Con.})$$

where

$$\lambda_B = \sqrt[4]{\frac{3(1 - \nu^2)}{(R_2)_B^2 t^2}} \quad ,$$

$$(R_2)_B = \frac{R_B}{\sin \phi} \quad , \qquad\qquad\qquad (112)$$

and

$$D_b = \frac{Et^3}{12(1 - \nu^2)}$$

and $\overline{\phi}$, $\overline{\psi}$, $\overline{\theta}$, and $\overline{\zeta}$ are the functions ϕ, ψ, θ, and ζ, respectively, which are tabulated on pages 472-473 of Ref. 11.

After the particular and complementary solutions have been super-imposed, the final thermal stresses can be computed from the following formulas:

$$\sigma_x = \frac{12z}{t^3} M_x + \frac{N_x}{t} \qquad \text{and} \qquad \sigma_\theta = \frac{12z}{t^3} M_\theta + \frac{N_\theta}{t} \quad . \qquad (113)$$

3.0.8.3   Isotropic Shells of Revolution of Arbitrary Shape.

The discussion presented here is concerned with approximate small-deflection solutions for thin-walled shells of revolution having otherwise arbitrary shapes and made of isotropic material. A typical configuration, along with pertinent notation and sign conventions, is shown in Figure 3.0-53. It is assumed that the shell wall is free of holes and obeys Hooke's law. The temperature distribution must be axisymmetric but arbitrary gradients may be present both through the wall thickness and in the meridional direction. To determine the thermal stresses and deformations for the structures under discussion, the following sets of equations are available:

1. Equilibrium equations

2. Strain-displacement relationships

3. Stress-strain relationships.

In principle, together with prescribed boundary conditions, these formulations should provide a sufficient basis for the development of closed-form, small-deflection solutions to the subject problems. However, it will often be extremely difficult, if not impossible, to achieve such solutions. Therefore, numerical integration procedures in conjunction with a digital computer program are frequently used to achieve the desired solution. On the other hand, still another approach may be taken by using approximations such as those cited by Fitzgerald in Ref. 30 or Christensen in Ref. 31. Since these approximations avoid the need for sophisticated mathematical and/or numerical
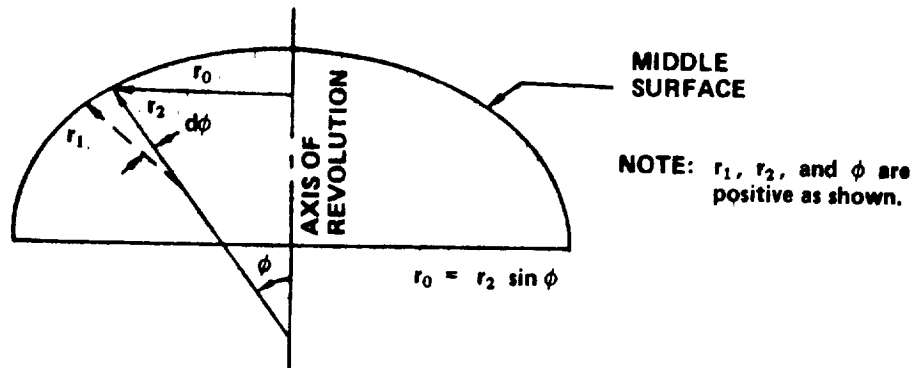
a. Overall shell of revolution.
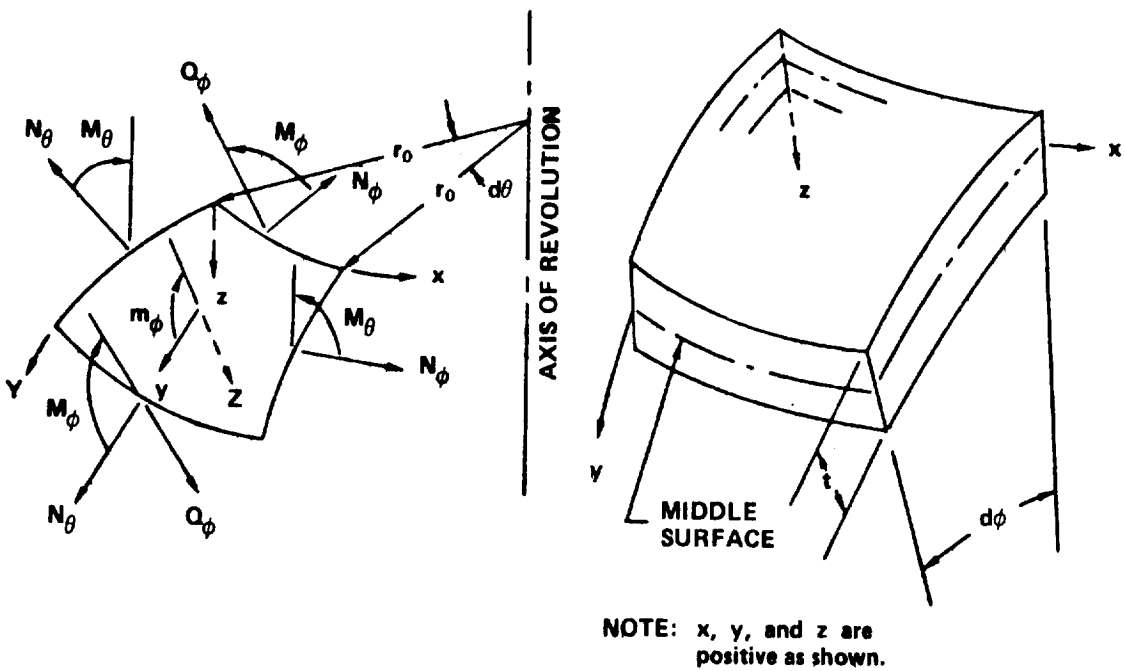
b. Positive directions for forces, moments, pressures, and coordinates.

c. Element of shell wall.

Figure 3.0-53. Configuration, notation, and sign convention for arbitrary shell of revolution.

operations, they are well suited to a manual of this type. It would therefore be desirable to prepare a section which outlines detailed procedures along these lines. However, from a brief study of Refs. 30 and 31, it was concluded that they should be thoroughly explored before specific recommendations are made. Consequently, in the following paragraphs only the related broad concepts are presented.

The method of Ref. 30 relies heavily on the following set of equilibrium equations, which, except for the term involving m_ϕ , are derived in Ref. 11:

$$\frac{d}{d\phi} (N_\phi r_0) - N_\theta r_1 \cos \phi - r_0 Q_\phi + r_0 r_1 Y = 0 \quad ,$$

$$N_\phi r_0 + N_\theta r_1 \sin \phi + \frac{d}{d\phi} (Q_\phi r_0) + Z r_1 r_0 = 0 \quad , \tag{114}$$

and

$$\frac{d}{d\phi} (M_\phi r_0) - M_\theta r_1 \cos \phi - Q_\phi r_1 r_0 + m_\phi r_1 r_0 = 0 \quad .$$

These expressions are used in the following manner:

1. First the assumption is made that membrane forces

$$N_\theta = N_\phi = N_R \tag{115}$$

and bending moments

$$M_\theta = M_\phi = M_R \tag{116}$$

are present which completely arrest all thermal displacements.

These forces and moments simply furnish a starting point for the computations and do not represent the actual values which will be determined later in the procedure.

It follows that

$$N_R = -\frac{E}{(1-\nu)} \int_{-t/2}^{t/2} \alpha T \, dz \tag{117}$$

and

$$M_R = -\frac{E}{(1-\nu)} \int_{-t/2}^{t/2} \alpha Tz \, dz \quad . \tag{118}$$

2. In general, the above type of force and moment distribution will not be in equilibrium unless one or more of the following is applied:

$$Q_\phi = (Q_\phi)_R \quad ,$$

$$Y = Y_R \quad , \tag{119}$$

$$Z = Z_R \quad ,$$

and

$$m_\phi = m_r \quad .$$

At this point, in order to achieve an approximate solution, Fitzgerald [30]

makes the assumption that

$$Q_\phi = (Q_\phi)_R = 0 \tag{120}$$

and justifies this practice by performing an order-of-magnitude study of the

error introduced. Then, proceeding with the analysis, equations (120) and

(115) through (118) are substituted into the equilibrium relationships (114) to

arrive at simple formulas for Y_R, Z_R, and m_R.

3. Recognizing that the actual shell is free of any of the above types of

loading, it is necessary to restore the structure to this state by application

of the following:

$$-Y_R; \ -Z_R; \ -m_R \quad .$$

This is done in a two-step procedure as outlined below.

4. The expressions

$$Y = -Y_R$$

and $\hspace{8cm}$ (121)

$$Z = -Z_R$$

are inserted into the first two of the equilibrium equations (114) while the

assumption that

$$Q_\phi = 0 \tag{122}$$

is retained. The resulting equations are then solved for N_θ and N_ϕ. From the stress-strain relationships, the corresponding strains can be determined. After this, the strain-displacement formulations may be used to express the related rotations and deflections of the shell wall in terms of N_θ and N_ϕ. The bending moments M_θ and M_ϕ can then be established from the equations

$$M_\theta = - D_b \left(\chi_\theta + \nu \chi_\phi \right)$$

and $\tag{123}$

$$M_\phi = - D_b \left(\chi_\phi + \nu \chi_\theta \right)$$

where

$$D_b = \frac{Et^3}{12(1 - \nu^2)} , \tag{124}$$

while χ_θ and χ_ϕ are the curvature changes of the hoop and meridional fibers, respectively.

5. One may now proceed to substitute

$$m_\phi = - m_R \tag{125}$$

into the third of the equilibrium equations (114), along with the assumption that

$$M_\theta = M_\phi = 0 . \tag{126}$$

Simple transformation then yields a formula for Q_ϕ which, together with equations (126) and the first two of (114), leads to simple expressions for N_θ and N_ϕ in terms of M_R. The use of equations (126) in this phase of the development is justified by Fitzgerald [30] on the basis of an error-magnitude study. Using the stress-strain and strain-displacement relationships, practical formulations can be derived for the rotations and displacements associated with the membrane loads N_θ and N_ϕ obtained in this step.

6. The final approximate values for the membrane loads, bending moments, rotations, and displacements are found by superposition of appropriate values from steps 1, 4, and 5. The stresses due to these membrane loads and bending moments must be augmented by those stresses associated with any self-equilibrating temperature distributions which exist through the thickness.

To focus attention on the general concepts involved in Fitzgerald's [30] approach, no mention is made in the foregoing steps of the need to satisfy prescribed boundary conditions in the problem solution. Therefore, it might now be helpful to note that, for this method, it is probably best first to obtain results under the assumption that no external constraints are present. Following this, edge forces and/or moments may be superimposed which enforce the required conditions at the boundaries.

The general philosophy behind the approach of Christensen [31] is very similar to that of Fitzgerald, although the details are quite different.

Christensen also relies heavily upon the equilibrium equations (114) but, for pure thermostructural problems, he makes no use of the loadings Y, Z, and m_ϕ. Hence, these quantities are taken equal to zero throughout the entire analysis, which is performed in the following manner:

1. First the assumption is made that

$$M_\theta = M_\phi = M_R \tag{127}$$

where

$$M_R = -\frac{E}{(1 - \nu)} \int_{-t/2}^{t/2} \alpha T z \, dz \ . \tag{128}$$

Here again, these moments simply furnish a starting point for the computations and do not represent the actual values which will be determined later in the procedure. These moments are inserted into the equilibrium equations (114). The third of these equations is then combined with the other two and two equations in the unknowns N_θ and N_ϕ are obtained.

2. By using the stress-strain and strain-displacement relationships, the two equations from step 1 are rewritten in terms of the temperature distribution and the middle-surface displacements v and w, where v is measured in the meridional direction and w is taken normal to the middle surface.

3. The two equations from step 2 are combined to arrive at a single formulation in terms of v and the temperature distribution.

4. The equation from step 3 is then solved subject to the boundary conditions at the shell apex. This is accomplished by assuming that v can be expressed as a polynomial and then calling upon the method of undetermined coefficients. The resulting expression for v must then be substituted into the appropriate equation from step 2 to obtain a solution for the displacement w .

5. From Timoshenko [11], the bending moments M_θ and M_ϕ which are associated with the displacements v and w can be determined. Christensen [31] refers to these as corrective moments and, if they are not small with respect to M_R , an iterative process must be used whereby the initially assumed moments are successively revised. However, the study reported in Ref. 31 seems to indicate that the first cycle will often be sufficiently accurate for most engineering applications.

6. From the stress-strain and strain-displacement relationships, the membrane loads N_θ and N_ϕ due to v and w can now be found.

7. The final approximate values for the bending moments, membrane loads, and displacements are found as follows:

    a. Final $M_\theta = M_R$ + corrective M_θ .

    b. Final $M_\phi = M_R$ + corrective M_ϕ .

    c. Final N_θ and N_ϕ = obtained from step 6.

    d. Final v and w = obtained from step 4.

(129)

The total approximate values for the stresses are obtained by superimposing those associated with the final bending moments, final membrane loads, and any self-equilibrating temperature distributions through the wall thickness.

To focus attention on the general concepts proposed by Christensen [33], no mention is made in the foregoing steps of the need to satisfy prescribed boundary conditions at locations removed from the apex. Therefore, it might now be helpful to note that, for this method, it is probably best first to obtain results under the assumption that no external constraints are present at such positions. Following this, edge forces and/or moments may be superimposed which enforce the required conditions at the boundaries.

The foregoing approaches are only two of a number of possibilities for the subject problem and can be used to obtain approximate values without the need for sophisticated mathematical and/or numerical operations. However, solutions can also be obtained by the use of existing digital computer programs, many c which use either discrete-element or finite-difference methods. Such programs are probably the best approach for obtaining rapid, accurate solutions. However, to retain a physical feel for the problem, it would be helpful to convert temperature distributions into equivalent mechanical loadings, such as was done for isotropic circular cylinders. It is recommended that future efforts include work along these lines to arrive at the equivalent pressures for shells of revolution having arbitrary shapes.

I.   Sphere Under Radial Temperature Variation.

   A.   Hollow Sphere.

Inside radius = a .

Outside radius = b .

$$\sigma_{rr} = \frac{2\alpha E}{1-\nu}\left[\frac{r^3-a^3}{(b^3-a^3)\,r^3}\int_a^b Tr^2\,dr - \frac{1}{r^3}\int_a^r Tr^2\,dr\right] \quad ,$$

$$\sigma_{\theta\theta} = \sigma_{\phi\phi} = \frac{\alpha E}{1-\nu}\left[\frac{a^3+2r^3}{(b^3-a^3)\,r^3}\int_a^b Tr^2\,dr + \frac{1}{r^3}\int_a^{r_1} Tr^2\,dr - T\right] \quad ,$$

$$u = \alpha\left(\frac{1+\nu}{1-\nu}\right)\frac{1}{b^3-a^3}\left[\frac{a^3}{r^2}\int_r^b Tr^2\,dr + \frac{b^3}{r^2}\int_a^r Tr^2\,dr\right.$$

$$\left. + \frac{2(1-2\nu)\,r}{(1+\nu)}\int_a^b Tr^2\,dr\right] \quad ,$$

$$T(r) = t_0 = \text{constant},$$

$$\sigma_{rr} = \sigma_{00} = \sigma_{\phi\phi} = 0 \quad ,$$

and

$$u = \alpha T_0 r \quad .$$

B. Solid Sphere.

$$\sigma_{rr} = \frac{2\alpha E}{1-\nu}\left(\frac{1}{b^3}\int_0^b Tr^2\,dr - \frac{1}{r^3}\int_0^r Tr^2\,dr\right)\ ,$$

$$\sigma_{\theta\theta} = \sigma_{\phi\phi} = \frac{\alpha E}{1-\nu}\left(\frac{2}{b^3}\int_0^b Tr^2\,dr + \frac{1}{r^3}\int_0^r Tr^2\,dr - T\right)\ ,$$

$$u = \alpha\left(\frac{1+\nu}{1-\nu}\right)\left[\frac{1}{r^2}\int_a^r Tr^2\,dr + \frac{2(1-\nu)}{(1+\nu)}\left(\frac{r}{b^3}\right)\int_0^b Tr^2\,dr\right]\ ,$$

$$\sigma_{rr}(\theta) = \sigma_{\theta\theta}(0) = \sigma_{\phi\phi}(0) = \frac{2\alpha E}{1-\nu}\left[\frac{1}{b^3}\int_0^b Tr^2\,dr - \frac{T(0)}{3}\right]\ ,$$

$$T(r) = T_0 = \text{constant}\ ,$$

$$\sigma_{rr} = \sigma_{\theta\theta} = \sigma_{\phi\phi} = 0\ ,$$

and

$$u = \alpha T_0 r\ .$$

4.0   THERMOELASTIC STABILITY.

The thermoelastic problems considered in the previous paragraphs have followed formulations of the linear theory of thermoelasticity; they have thus excluded questions of buckling, problems in which the effect of the loading depends on the deformations (as in the case of beam-columns), large deflections, and other similar effects. It is the purpose of this paragraph to discuss some of the principal problems of this type. It should be remembered that the solutions are approximate from the viewpoint of an exact thermoelastic formulation. The nature of these approximations was treated in the previous subsections.

4.0.1   Heated Beam Columns.

If a beam-column is subjected to the action of heat, the influence of temperature must, in general, be taken into account. The analysis in the cases in which the ends of the beam are restrained in the axial direction is slightly different from that used when the ends are free to displace in that direction. The latter case will be considered in paragraph 4.0.1.1 while the former is considered in paragraph 4.0.1.2.

4.0.1.1   Ends Axially Unrestrained.

The buckling behavior of beams (and therefore also their behavior as beam-columns under any combination of transverse and axial loads) depends on the shape of the cross section: For example, a beam whose cross section possesses no axes of symmetry can buckle only by a combination of twisting

and bending, whereas in other cases some of the uncoupled modes are also possible. The general formulation and solution of this problem are discussed in Ref. 1, but for simplicity, the following analysis is restricted to doubly symmetrical beams, with least principal moment of inertia under a transverse distributed load $p = p(x)$ acting in the xy plane, and subjected to a temperature distribution such that $M_{T_y} = 0$. The beam will thus bend in the xy plane without twisting and with $w = 0$. The governing differential equation is

$$\frac{d^2}{dx^2}\left(EI_z \frac{d^2v}{dx^2}\right) + P \frac{d^2v}{dx^2} = p - \frac{d^2M_{T_z}}{dx^2} \qquad . \qquad (1)$$

It is convenient to obtain the solution in two parts, by separating the effects of temperature and of transverse load. For this purpose v_T is the deflection the beam would undergo if only temperature and the axial load P were present (transverse loads absent); it therefore satisfies the differential equation

$$\frac{d^2}{dx^2}\left(EI_z \frac{d^2v_T}{dx^2}\right) + P \frac{d^2v_T}{dx^2} = -\frac{d^2M_{T_z}}{dx^2} \qquad . \qquad (2)$$

The quantity v_P is the deflection the beam would undergo if only transverse loads and the axial load P were present (temperature effects omitted); it therefore satisfies the differential equation

$$\frac{d^2}{dx^2}\left(EI_z \frac{d^2v_P}{dx^2}\right) + P \frac{d^2v_P}{dx^2} = p \qquad . \qquad (3)$$

With the definitions, the solutions of the combined problem in which all loads are acting is

$$v = v_T + v_P \quad .$$

The component deflection v_P represents the solution of the ordinary isothermal beam-column problem and can often be found in the literature (see Section B4.4). The determination of v_T must, in general, be carried out anew for each new problem. However, in the special case of uniform beam under a temperature distribution of the form of a polynomial of a degree not higher than the third in the spanwise direction, that is, when

$$M_{T_z} = a_0 + a_1 x + a_2 x^2 + a_3 x^3 \quad ,$$

then

$$v_T = - \frac{M_{T_z}}{P} + c_0 + c_1 x + c_2 \sin kx + c_3 \cos kx \quad ,$$

where $k = \sqrt{\dfrac{P}{EI_z}}$ and the constants c_0, c_1, c_2, and c_3 are determined from the boundary conditions. Solutions for v_T for three important special examples for which

$$M_{T_z} = a_0 + a_1 x$$

are given as follows.

I. <u>Both Ends Fixed.</u>
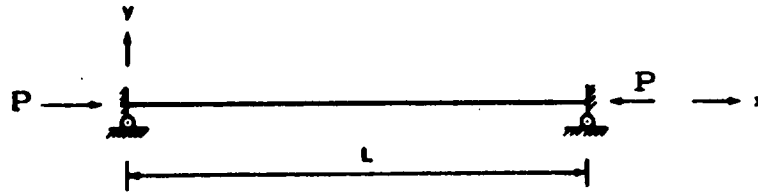
$$v_T = 0 \text{ for } P < P_{cr} = \frac{4\pi^2 EI_z}{L^2} \quad .$$

II. <u>Both Ends Simply Supported.</u>
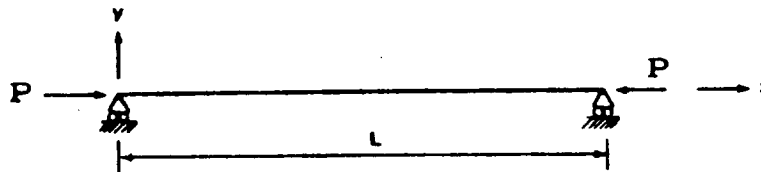
$$v_T = -\frac{a_0}{P}\left(\frac{\cos kL - 1}{\sin kL}\sin kx + 1 - \cos kx\right) - \frac{a_1}{P}\left(x - L\,\frac{\sin kx}{\sin kL}\right)$$

and

$$P_{cr} = \frac{\pi^2 EI_z}{L^2} \quad .$$

III. <u>Cantilever.</u>
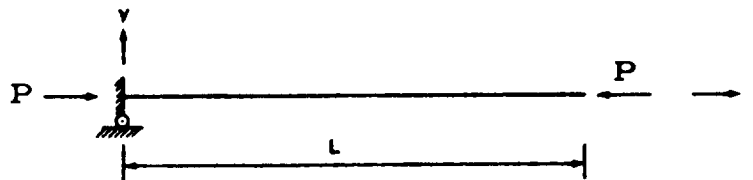
$$v_T = -\frac{a_0}{P}\frac{1 - \cos kx}{\cos kL} - \frac{a_1}{Pk}\left[\left(\frac{kL - \sin kL}{\cos kL}\right)(1 - \cos kx) + kx - \sin kx\right]$$

and

$$P_{cr} = \frac{\pi^2 EI_z}{4L^2} \qquad .$$

The axial stress is given by

$$\sigma_{xx} = -\alpha ET + \frac{P_T - P}{A} + \frac{y}{I_z} \left(M_{T_z} + M_z + P_v \right) \qquad .$$

In these analyses, the beam-column has been assumed to carry a compressive axial load. If the load is tensile, the appropriate results may be obtained by replacing the quantity P by (-P) in the corresponding expressions valid for a compressive load: accordingly, the quantity (k) must be replaced by (ik), (k^2) by $(-k^2)$, (sin kx) by (i sinh kx), (cos kx) by (cosh kx), (tan kx) by (i tanh kx), etc. Here $i = \sqrt{-1}$ and the symbol k denotes

$$k = \sqrt{\frac{|P|}{EI_z}} \qquad .$$

4.0.1.2 Ends Axially Restrained.

In this case, the basic equation to be solved is still equation (1) of 4.0.1.1, but the magnitude of the load P is unknown and must be determined from an additional condition concerning the axial displacements of the ends. If both ends are rigidly fixed in the axial direction, these conditions shall be stipulated: The axial distance between the ends of the bar must remain unchanged and temperatures must remain constant along the span. Expressed mathematically,

$$(P - P_T) \frac{L}{AE} + \Delta = 0 \tag{4}$$

where

$$\Delta = \frac{1}{2} \int_0^L \left(\frac{dv}{dx}\right)^2 dx \ . \tag{5}$$

The analogous condition appropriate to the case in which the ends of the bar are elastically restrained in the axial direction is easily derived. If, for example, the ends are attached to linear springs with modulus K, equation (4) takes the form

$$\left[P \left(1 + \frac{AE}{KL}\right) - P_T \right] \frac{L}{AE} + \Delta = 0 \ . \tag{6}$$

The transverse deflection v appearing in the quantity Δ must be calculated by the equations given in the preceding paragraph (4.0.1.1); as a consequence, the analysis of beam-columns which have ends fixed in the axial direction is quite cumbersome, since the unknown P and v must be determined by the simultaneous solution of equations (1) and (6). However, if the temperature is expressed as a polynomial, the calculations are greatly facilitated by the use of a series of graphs in conjunction with a rapidly convergent iteration procedure. This technique and its results are available in Ref. 7 within the following limits:

1. Distributed transverse loads are uniform over the span, whereas concentrated loads are at the midspan.

2. The temperature varies linearly through the depth and is constant in a spanwise direction.

3. The beam is assumed to be simply supported at its ends for bending and elastically restrained axially.

Tables of numerical results in nondimensional form are presented for the cases of zero and full axial end restraint in rectangular beams. These tables may be used to determine maximum deflections and bending moments.

4.0.2 Thermal Buckling of Plates.

4.0.2.1 Circular Plates.

General.

This section contains curves and data based on nonlinear, elastic behavior and involving the use of large-deflection theory. This is because plate stresses and deflections in the post-buckled state represent the major considerations. The basis for this is the well-known fact that certain compression structures can support some increment of additional loading before complete collapse and, in the process of so doing, accept increased stresses and deflections. This can be readily seen by an inspection of the plate buckling stress and allowable compression stress for specific materials, taken as a function of the crippling parameter $(a/t\sqrt{k})$. Particular considerations and background, as developed by Newman and Forray in Refs. 32 and 33, are given in the following paragraphs, along with the solution of an example problem for demonstration of the methods involved.

Configuration.

The design curves and equations provided here apply only to flat,

circular plates which are of constant thickness and are made of an isotropic

material. It is assumed that the plate is free of holes, obeys Hooke's law,

and that Poisson's ratio is equal to 0.3.

Boundary Conditions.

The solution is valid only where both of the following conditions are

satisfied:

1. The boundary is simple supported; that is,

$$w = M_r = 0 \text{ at } r = b \quad . \tag{7}$$

2. The middle surface of the plate is radially fixed; that is,

$$\bar{u} = \bar{v} = 0 \quad \text{at} \quad r = b \quad . \tag{8}$$

Temperature Distribution.

The plate may have a thermal gradient through the thickness, provided

that the distribution is symmetrical about the middle surface. However, it is

required that the temperature be uniform over the surface. Therefore, the

permissible distributions can be expressed in the form

$$T = T(z) \tag{9}$$

subject to the restriction that

$$T(+z) = T(-z) \quad . \tag{10}$$

Obviously, the special case of a plate at uniform temperature complies with

these specifications.

Design Curves and Equations.

If a heated plate is constrained against free, in-plane expansion, compressive stresses are developed in the plate. Initial out-of-plane buckling occurs at very low temperature increments in the case of thin plates constrained in this manner. However, in many structural situations, the usefulness of the plate is not completely lost as a result of this initial buckling since it is able to carry some additional load after it has reached the buckled state. In view of this, cases may arise in which a knowledge of the magnitudes of the post-buckled stresses and deflections would be most helpful. To determine the stresses and deflections of a plate after initial buckling has occurred, large deflection theory must be used in the analysis since the actual deflection at that stage may be several times the thickness of the plate.

In Ref. 33 Newman and Forray present a large-deflection analysis of a circular plate under mechanical and thermal loading. Since a closed-form solution of the basic differential equations was not possible, they used a finite-difference procedure to set up the governing differential equations for digital computer solution. Numerical results were then obtained for a wide range of temperature resultants, N_T'. These results are presented in curve form in Figures 4.0-1 through 4.0-5 for deflections, radial and tangential forces, and moments for various temperature gradients, as defined in equations (9), (10), and (16).
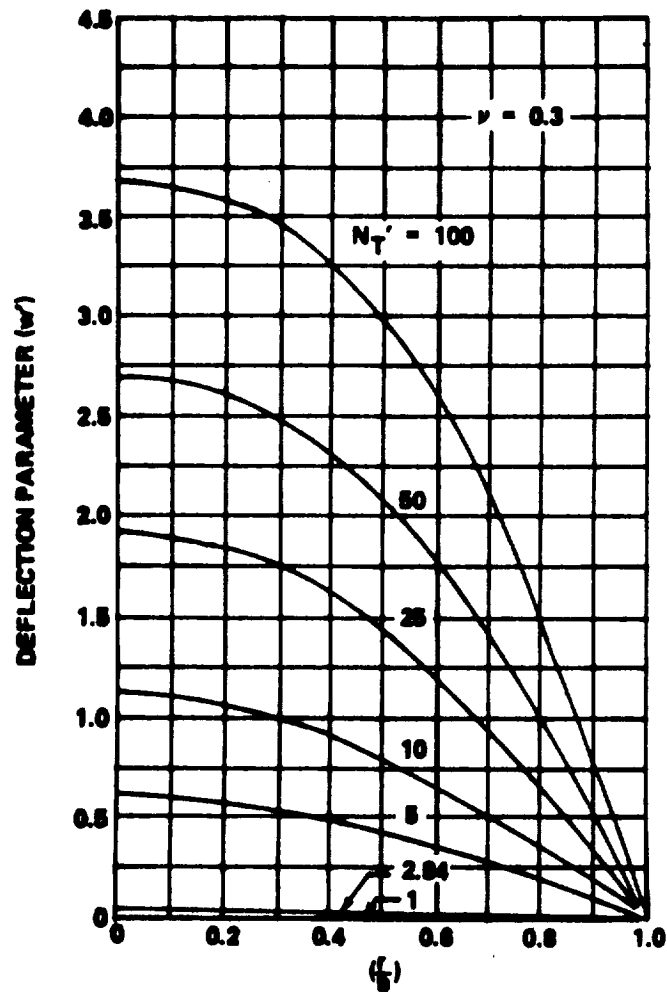
Figure 4.0-1. Nondimensional deflection parameter.

Even though nonlinear analysis methods are used to find the post-buckling deflections and stresses, these solutions hold since it has been shown in Ref. 34 that initial buckling can occur when the edge compressive stress exceeds the lowest eigenvalue of the small deflection buckling problem. Timoshenko [35] shows that this critical compressive stress for a circular plate with $\nu = 0.3$ is given by

Figure 4.0-3. Nondimensional tangential membrane-force parameter.

Figure 4.0-2. Nondimensional radial membrane-force parameter.
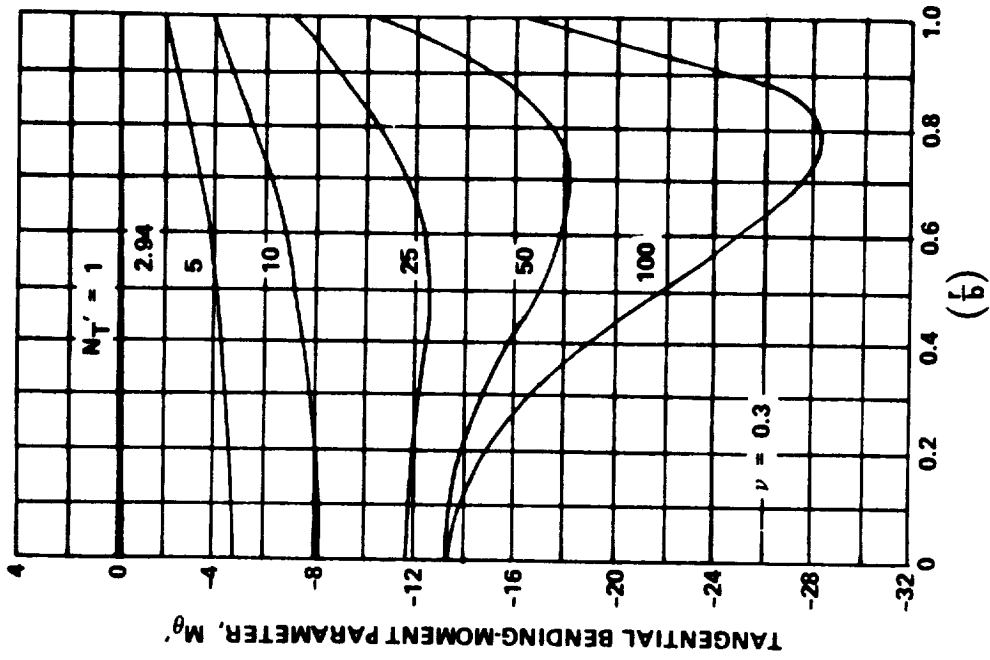
Figure 4.0-5. Nondimensional tangential bending-moment parameter.
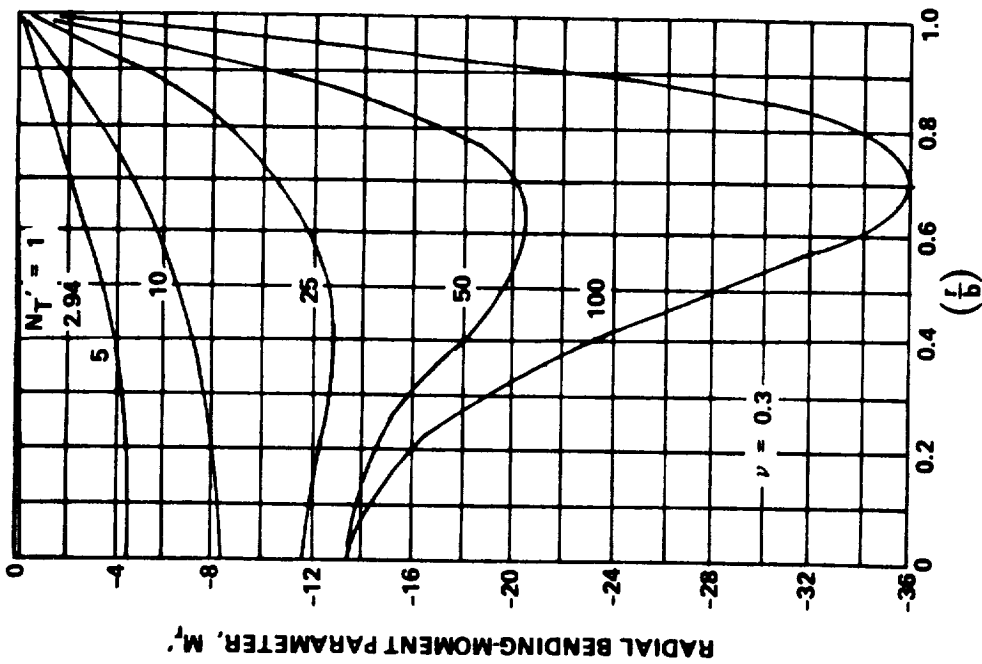
Figure 4.0-4. Nondimensional radial bending-moment parameter.

$$\left(\sigma_r\right)_{cr} = (2.05)^2 \frac{D_b}{b^2 t} \quad . \tag{11}$$

For the thermal problem, the compressive stress just before buckling is

given by

$$\sigma_r = \frac{-N_T}{t(1-\nu)} \tag{12}$$

where

$$N_T = E\alpha \int_{-t/2}^{t/2} T \, dz \quad . \tag{13}$$

From equations (11) and (12), the critical nondimensional value for N_T at

buckling is given by

$$\left(N_T{'}\right)_{cr} = \left(N_T\right)_{cr} \frac{b^2}{D_b} = 2.94 \quad . \tag{14}$$

Equation (14) shows that initial buckling of the plate will occur when

$N_T{'} = 2.94$, provided that $\nu = 0.3$. Hence, when $N_T{'} < 2.94$, the plate will

remain flat and the deflection w, as well as the bending moments M_r and M_θ,

must equal zero. An inspection of equations (17) and (18) together with

Figures 4.0-4 and 4.0-5 reveals that this requirement is essentially satisfied

by the given method.

The deflection pattern of the buckled plate will consist of an axisym-

metric bulge which can occur in either the upward or downward direction.

In actual practice, the direction will be determined by the type of initial

imperfections present in the plate, the nature of external disturbances, etc. The formulas and design curves associated with the deflections and the bending moments are based on the assumption that the plate deflects downward. On the other hand, the sense of the membrane forces (compressive versus tensile) at any point will be independent of the bulge direction. Hence, the expressions for N_r and N_θ, taken in conjunction with Figures 4.0-2 and 4.0-3, are valid for both types of deformation.

It is assumed that Young's modulus and Poisson's ratio are unaffected by temperature variations. On the other hand, the temperature-dependence of the thermal-expansion coefficient can be accounted for by recognizing that it is the product αT which governs; that is, the actual temperature distribution can be suitably modified to compensate for variations in α.

It should be noted that there is a typographical error in equation (5) of Ref. 32 where the quantity $(1 - \nu)^2$ should be changed to $(1 - \nu^2)$. The contents of this section have been corrected accordingly.

Example Problems.

For the first example problem, consider a circular steel plate which is 0.10 in. in thickness and has an outer radius a of 10.0 in. The outer edges are fully restrained against in-plane expansion; however, they are simply supported otherwise. The plate is heated such that the temperature gradient is given by

$$T = 3.0 + 6.0 \left(z/t \right)^2 \quad .$$

Using $\alpha = 6.0 \times 10^{-6}$ in./(in.) ($^\bullet$F), $\nu = 0.30$, and $E = 30.0 \times 10^6$ psi, determine whether buckling has occurred and find the stresses and deflections.

From equations (16)

$$N_T' = \frac{12(1-\nu^2) \, b^2}{Et^3} \, E\alpha \int_{-t/2}^{t/2} [3.0 + 6.0 \, (z/t)^2] \, dz \quad ,$$

$$N_T' = \frac{12(1.0-0.09)(10.0)^2}{(30.0 \times 10^6)(0.10^3)} \, (30.0 \times 10^6)(6.0 \times 10^{-6})$$

$$\left[3.0(z) + \frac{6.0(z^3)}{(t^2) \, 3} \right]_{-t/2}^{t/2} \quad ,$$

$$N_T' = 6.55 \left[3.0 \left(\frac{t}{2} + \frac{t}{2} \right) + \frac{2.0}{(t^2)} \left(\frac{t^3}{8} + \frac{t^3}{8} \right) \right] = 6.55(3.5)(t) \quad ,$$

and

$$N_T' = 2.29 \quad .$$

Since this is less than the critical buckling value given by equation (14), the plate has not buckled and thus the deflection, as well as the bending moments M_r and M_θ, are equal to zero.

However, from an inspection of equations (17) for the stresses and knowing that, for $N_T' = 2.29$, $M_r' = M_\theta' = 0$ and the values of N_r' and N_θ' can be obtained from Figures 4.0-2 and 4.0-3 as a function of (r/b), the stresses may be easily calculated by inserting the appropriate values in the equations.

For a second example use the same plate as for the first; however, apply a temperature gradient to the plate as follows:

$$T = 33.0 + 66.0(z/t)^2 \quad .$$

For this thermal loading

$$N_T' = 6.55 \, [33.0(t) + 5.5(t)] = 6.55(38.5)(0.10) = 25.2 \quad .$$

Since this is greater than the critical buckling value of 2.94, as given in equation (15), the plate has buckled. Then, using Figures 4.0-1 through 4.0-5 the deflections, stress resultants and moments may be obtained for the calculated value of N_T'. These values may then be substituted into equations (17) to obtain the stresses and deflections. For this problem assume that the stresses and deflections are needed for values of $(r/b) = 0.3$ and $= 0.6$. Then, on the basis of $N_T' = 25.2$, the following table gives values for the terms needed in the stress and deflection calculations.

r/b	w' (Fig. 4.0-1)	N_r' (Fig. 4.0-2)	N_θ' (Fig. 4.0-3)	M_r' (Fig. 4.0-4)	M_θ' (Fig. 4.0-5)
0.30	1.75	1.40	-1.20	-12.70	-12.30
0.60	1.20	-1.70	-10.00	-12.00	-12.40

Setting up equations (17) for calculation of the stresses and deflections for this problem,

$$w = w'(t) = 0.10(w')$$

and

$$\sigma_r = \left[\frac{-12z \, (M_r')}{t\sqrt{6(1-\nu^2)}} + \frac{(N_T')}{(1-\nu)} - 12(1+\nu) \, \left(\frac{b^2}{t^2}\right)\alpha \, T + (N_r') \right] \frac{D_b}{b^2 t} \quad .$$

Letting $z = t/2; \; T = [33.0 + 66.0(0.5)^2] = 49.5$,

$$\frac{D_b}{b^4 t} = \frac{30.0 \times 10^6 \times (0.10)^3}{12(1.0 - 0.09)(10.0)^2(0.10)} = 2750.0 \quad .$$

Then,

$$\sigma_r = 2750.0 \left[\frac{-12(0.5t)(M_r')}{t\sqrt{6(1.0 - 0.09)}} + \frac{25.2}{(1.0 - 0.3)} \right.$$

$$\left. - 12(1.0 + 0.3)\left(\frac{10.0}{0.10}\right)^2 (6.0 \times 10^{-6}(49.5) + (N_r')) \right],$$

$$\sigma_r = [-7060(M_r') + 99\,000 - 127\,320 + 2750(N_r')] \quad , \qquad \rceil$$

and

$$\sigma_r = [-7060(M_r') + 2750(N_r') - 28\,320] \quad .$$

Also,

$$\sigma_\theta = [-7060(M_\theta') + 2750(N_\theta') - 28\,320] \qquad .$$

Then, for $(r/b) = 0.30$,

$$w = 0.10(w') = 0.10(1.75) = 0.175 \text{ in.}$$

and

$$\sigma_r = -7060(-12.70) + 2750(1.40) - 28\,320$$

$$= +80\,660 + 3850 - 28\,320 = +65\,190 \text{ psi} \qquad .$$

Similarly,

$$\sigma_\theta = +55\,220 \text{ psi} \quad \text{(Note that these are tension stresses.)}$$

for $(r/b) = 0.60$.

As before,

$$w = 0.120 \text{ in.},$$

$$\sigma_r = +51\ 720 \text{ psi},$$

and

$$\sigma_\theta = +31\ 720 \text{ psi} \quad .$$

The previously calculated stresses represent the critical tension values.

Critical compression stresses are found by letting $z = -t/2$ in the first stress

term. Then

$$\sigma_r = [\ 7060\ (M_r') + 2750\ (N_r') - 28\ 320]$$

and

$$\sigma_\theta = [\ 7060\ (M_\theta') + 2750\ (N_\theta') - 28\ 320] \quad .$$

The following table gives the critical tensile and compressive stresses and

deflections at the plate stations.

(r/b)	w (in.)	Tensile Stress (psi)		Compressive Stress (psi)	
		σ_r	σ_θ	σ_r	σ_θ
0.30	0.175	+65 190	+55 220	-114 130	-118 460
0.60	0.125	+51 720	+31 720	-117 720	-143 360

Summary of Equations and Curves.

Critical Condition for Buckling.

$$(N_T')_{cr} = (2.94)_{\nu = 0.3} \tag{15}$$

where

$$N_T' = \frac{N_T b^2}{D_b} \qquad E\alpha \left(\int_{-t/2}^{t/2} T \, dz \right) \frac{b^2 12(1 - \nu^2)}{Et^3} \quad ,$$

$$D_b = \frac{Et^3}{12(1 - \nu^2)} \quad , \tag{16}$$

and

$$N_T = E\alpha \int_{-t/2}^{t/2} T \, dz.$$

Postbuckling Deflections and Stresses.

$$w = w' \, t$$

$$\sigma_r = \left[- \frac{12zM_r'}{t\sqrt{6(1 - \nu^2)}} + \frac{N_T'}{(1 - \nu)} - 12(1 + \nu) \frac{b^2}{t^2} \alpha T + N_r' \right] \frac{D_b}{b^2 t} \tag{17}$$

and

$$\sigma_\theta = \left[- \frac{12zM_\theta'}{t\sqrt{6(1 - \nu^2)}} + \frac{N_T'}{(1 - \nu)} - 12(1 + \nu) \frac{b_2}{t^2} \alpha T + N_\theta' \right] \frac{D_b}{b^2 t}$$

where

$$M_r' = - \frac{M_r b^2}{D_b t} \sqrt{6(1 - \nu^2)} \quad ,$$

$$M_\theta' = - \frac{M_\theta b^2}{D_b t} \sqrt{6(1 - \nu^2)} \quad , \tag{18}$$

$$N_r' = \frac{N_r b^2}{D_b} \quad ,$$

and

$$N_\theta' = \frac{N_\theta b^2}{D_b} \qquad .$$

The values for w', M_r', M_θ', N_r', and N_θ' are obtained from Figures

4.0-1 through 4.0-5 for the case of $\nu = 0.3$.

For values of ν other than 0.3, the values of M_r' and M_θ' may be

found by using equations (18) as shown:

$$\left(M_r'\right)_\nu = \left[\left(M_r'\right)_{\nu\,=\,0.3}\right] \sqrt{\frac{(1 - \nu^2)}{(1.0 - 0.3^2)}} = 1.049 \ \sqrt{(1 - \nu^2)}\left(M_r'\right)_{\nu\,=\,0.3} .$$

Similarly,

$$\left(M_\theta'\right)_\nu = 1.049 \ \sqrt{(1 - \nu^2)} \ \left(M_\theta'\right)_{\nu\,=\,0.3} \ .$$

N_r' and N_θ' are independent of ν .

4.0.2.2   Rectangular Plates

I.   <u>Heated Plates Loaded in Plane — Edges Unrestrained in the Plane.</u>

Consider the plate strip, shown on the following page, loaded at the

ends by a uniformly distributed stress σ_0 , subjected to a uniformly distributed

heat input Q, and reinforced along the edges (y = 0, y = b) by longitudinals.

The temperature in the plate will be higher in the center of the panel than near

the edges because of the heat sink provided by the longitudinals.   For the

present purposes the temperature will be taken to be uniform across the

thickness and of the form

$$T = T_0 - T_1 \cos \ \left(\frac{2\,\pi\,y}{b}\right) \tag{19}$$

in the plane of the plate, where T_0 and T_1 are constants to be adjusted to fit the available data.
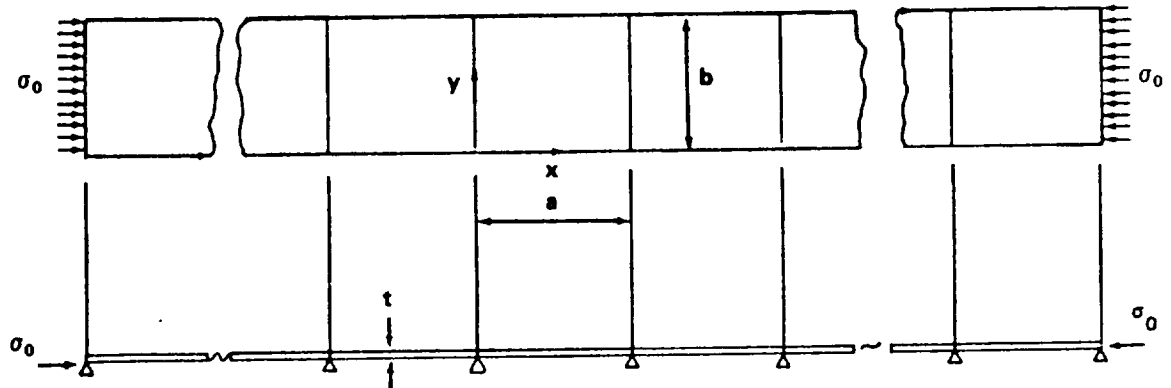
The following solution pertains to a single panel of the strip, extending from $x = 0$ to $x = a$. This panel is assumed to be at a sufficient distance from the ends of the strip, so that the stresses may be taken to be independent of x. Transverse displacements are prevented at $x = 0$, a.

From the solution in Ref. 1 the critical combination of σ_0 and T_1 (note: T_0 has no effect on buckling) is found by obtaining the determinant of simultaneous equations. It was shown that the symmetric case corresponds to the lower buckling load and that the problem can be solved approximately by the interaction of two special cases. These cases are (1) $T_1 = 0$ and σ_0 is acting alone and (2) $\sigma_0 = 0$ and T is acting alone.

The solution to (1) is the standard plate buckling expression found in Ref. 1; that is, when $T_1 = 0$,

$$\sigma_{cr_0} = - \frac{k \pi^2 E}{12(1 - \nu^2)} \left(\frac{t}{b} \right)^2 \tag{20}$$

where

$$k = 4 \text{ for } \frac{a}{b} \geq 1$$

and

$$k = \left(\frac{b}{a} + \frac{a}{b} \right)^2 \quad \text{for } \frac{a}{b} \leq 1 \quad .$$

The solution to (2) when $\sigma_0 = 0$ is as follows. The critical value of $T_1 (= T_{cr_0})$.

$$\frac{\alpha E T_{cr_0}}{2} = \frac{k_1 \pi^2 E}{12(1 - \nu^2)} \left(\frac{t}{b} \right)^2 \tag{21}$$

where k_1 is determined from Figure 4.0-6.
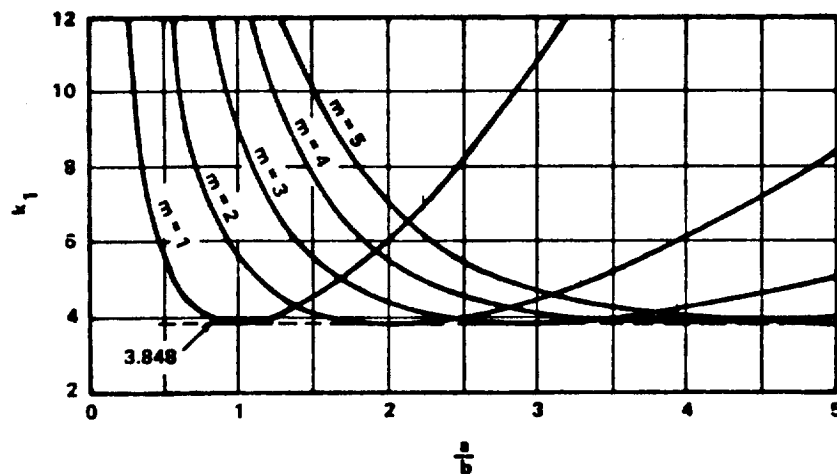
Figure 4.0-6. Values of the coefficient k_1.

Then, for the general case in which both heat and edge stresses are acting, the following interaction curve is used:

$$\frac{T_{cr}}{T_{cr_0}} + \frac{\sigma_{cr}}{\sigma_{cr_0}} = 1 \qquad . \tag{22}$$

II. Heated Plates Loaded in Plane — Edges Restrained in the Plane.

A. Configuration.

The design curves presented here apply only to flat, rectangular plates which are of constant thickness and are made of isotropic material. It is assumed that the plste is free of holes and that no stresses exceed the elastic limit. The edge support members must have the same coefficient of thermal expansion as the plate proper. The design curves cover aspect ratios a/b from 1 through 4. However, since these plots become quite flat at a/b = 4, they must be used to obtain approximate results for aspect ratios greater than 4.

B. Boundary Conditions.

Solutions are given for each of the following two types of boundary conditions:

1. Type I — The boundaries satisfy both the following conditions:

   a. All edges of the plate are simply supported.

   b. The edge supports fully restrain in-plane plate displacements such that these displacements are equal to the free thermal expansions (or contractions) of the supports.

2. Type II — The boundaries satisfy both of the following conditions:

   a. All edges of the plate are clamped.

b.   The supports fully restrain in-plane edge displacements of the plate such that these displacements are equal to the free thermal expansions (or contractions) of the supports.

C.   Temperature Distribution.

It is assumed that no thermal gradients exist through the plate thickness. The following three types of temperature distributions over the surface are considered and are illustrated in Figure 4.0-7:

1.   Sinusoidal distributions which can be expressed mathematically as

$$T = T_o + T_1 \sin\frac{\pi x}{a} \sin \frac{\pi y}{b} \quad . \tag{23}$$

2.   Parabolic distributions which can be expressed mathematically as

$$T = T_o + T_1 \left[1 - \left(\frac{2x}{a} - 1\right)^2\right]\left[1 - \left(\frac{2y}{b} - 1\right)^2\right] \quad . \tag{24}$$

3.   Tent-like distributions which can be expressed mathematically as

$$T = T_o + T_1 \left[1 - \left(\frac{2x}{a} - 1\right)\right]\left[1 - \left(\frac{2y}{b} - 1\right)\right] \quad . \tag{25}$$
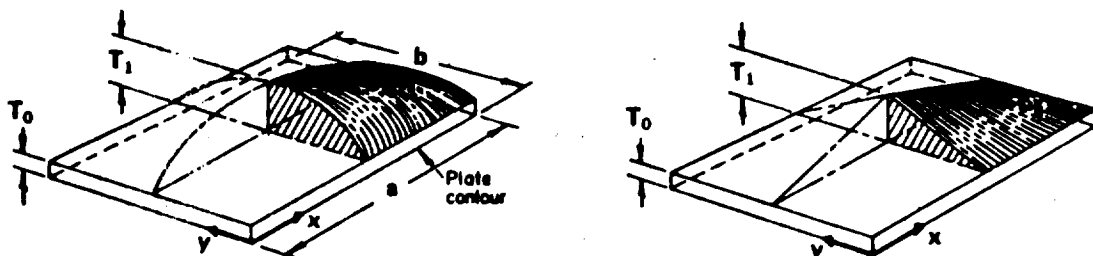
a.   Sinusoidal or parabolic distribution.

b.   Tent-like distribution.

Figure 4.0-7.   Selected temperature distributions over the surface of a rectangular plate.

D. Design Curves.

In Ref. 36 Forray and Newman present the simple means given here to compute the critical temperature values for the initial thermal buckling of flat, rectangular plates. Curves are given for the combinations of boundary conditions and temperature distributions tabulated in Table 4.0-1. The temperature variations were chosen to be representative of what would be expected if the panel were subjected to rapid heating. This condition is conducive to thermal buckling since it will usually cause the plate to be much hotter than the supports. The results of Forray and Newman are plotted in Figure 4.0-8 for plates having $\nu = 0.3$. The curves do not account for nonuniformities in the material properties such as those variations that arise because of temperature-dependence of the material behavior. Hence, the user must select a single effective value for α by employing some type of averaging technique.

TABLE 4.0-1. COMBINATIONS OF BOUNDARY CONDITIONS AND TEMPERATURE DISTRIBUTIONS

Boundary Conditions	Type I	Type II
Temperature Distributions Over the Surface	Sinusoidal	--
	Parabolic	Parabolic
	Tent-Like	--

A nondimensional plot of the deflection at the center of rectangular plates of various aspect ratios against temperature level is presented in Figure 4.0-9 where
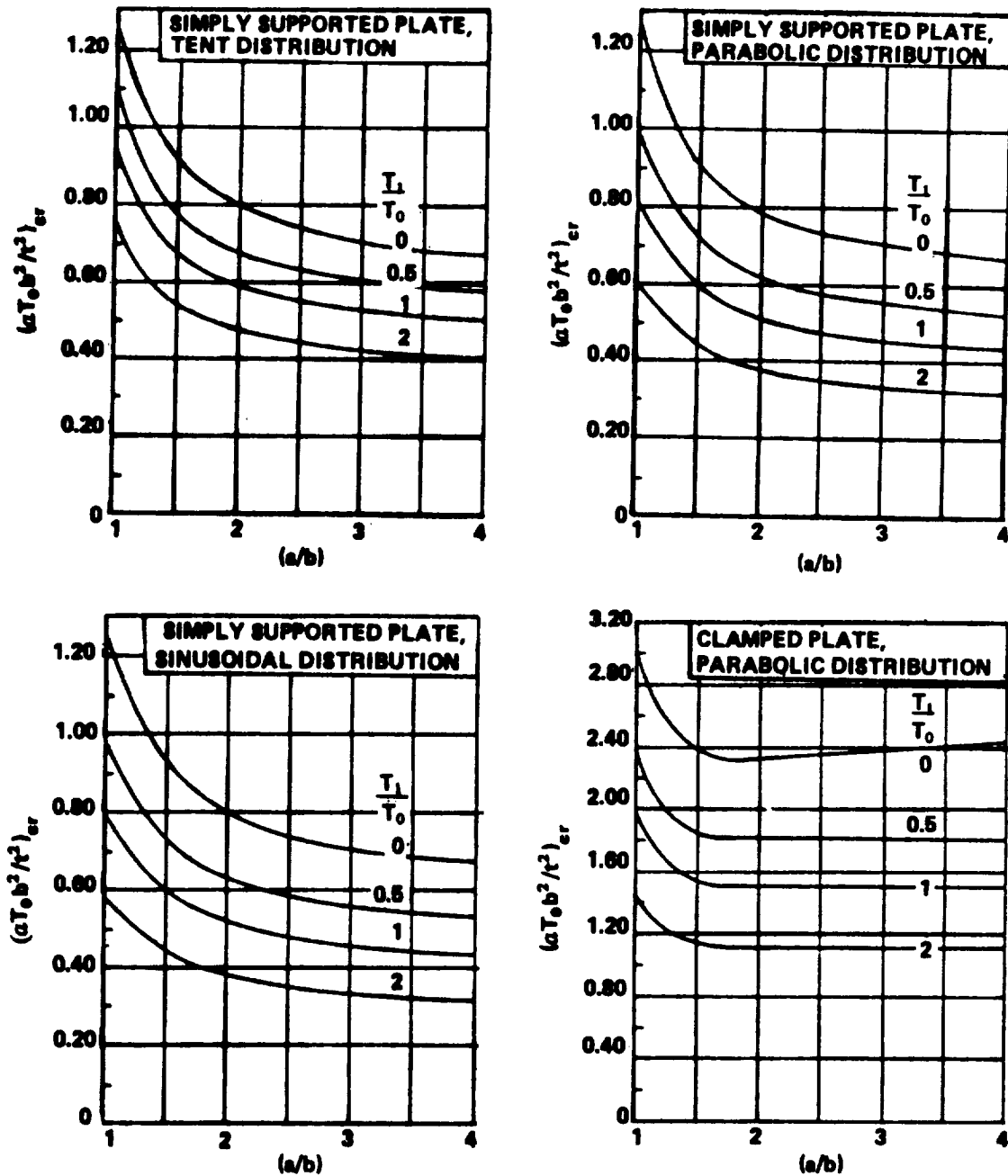
Figure 4.0-8. Critical temperature parameter for rectangular plates.
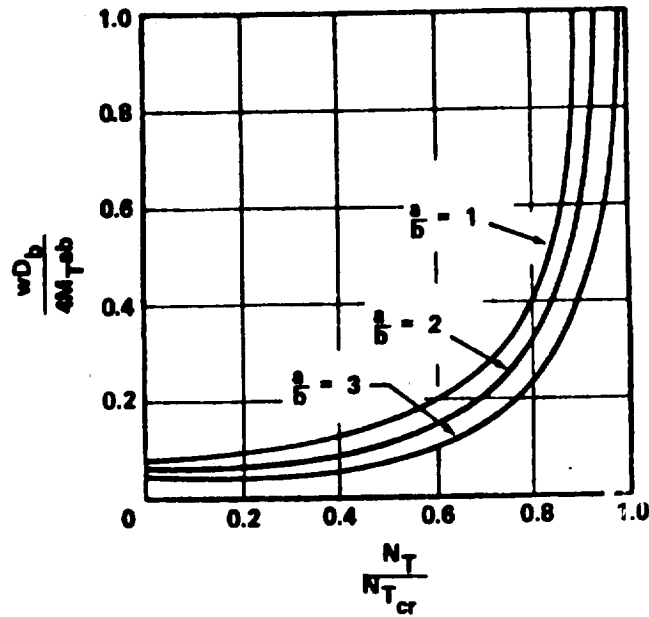
Figure 4.0-9. Deflection w at the center of a rectangular plate for loads in plane of plate $\left(\text{Poisson's ratio } \nu = \dfrac{1}{4} \right)$.

$$N_T = \alpha \; E \int_{-t/2}^{t/2} T \; dz, \qquad (26)$$

$$M_T = \alpha \; E \int_{-t/2}^{t/2} Tz \; dz, \qquad (27)$$

and

$$D_b = \frac{Et^3}{12(1 - \nu^2)} \qquad .$$

In this figure, the nondimensional parametric indicating the temperature level is $\left(N_T / N_{T_{cr}} \right)$, where $N_{T_{cr}}$, the value of N_T at which buckling occurs, is

$$N_{T_{cr}} = (1 - \nu) \left(1 + \frac{a^2}{b^2}\right) \frac{\pi^2 D}{a^2} b \quad . \tag{28}$$

Plots showing in nondimensional form the variation of M_x in one quadrant of a square plate and presented in Figures 4.0-10 and 4.0-11 for two different temperature levels. Because of the double symmetry of the plate, such a plot is sufficient to determine the distribution of both M_x and M_y throughout the entire plate. These plots indicate that the maximum bending moment occurs, for the cases considered, in the center of the plate. Curves showing the variation of center moment with temperature level for various aspect ratios are shown in Figure 4.0-12.

It should be noted that the preceding results were obtained on the assumption that nonlinear terms in the strain-displacement relations could be neglected. Therefore, as is usual in problems of this type, the results are valid only for values of N_T sufficiently small relative to $N_{T_{cr}}$.

III. Post-Buckling Deflections With All Edges Simply Supported.

A. Configuration.

The design curves presented here apply only to flat, rectangular plates which are of constant thickness and are made of isotropic material. It is assumed that the plate is free of holes and that no stresses exceed the elastic limit. The edge support members must have the same coefficient of thermal expansion as the plate proper. The design curves cover aspect ratios a/b of 1, 2, 3, and a/b $\geq$ 5.
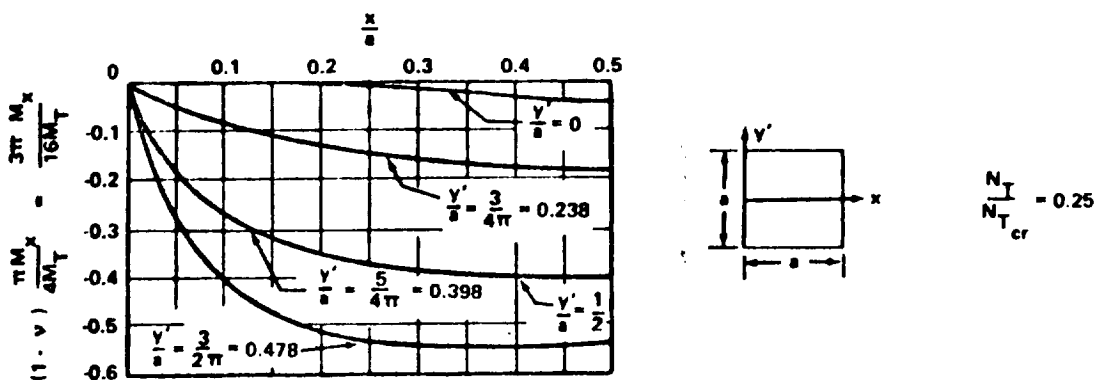
Figure 4.0-10. Distribution of the bending moment M_x in a square plate for

$$\frac{N_T}{N_{T_{cr}}} = 0.25 \quad \left(\text{Poisson's ratio } \nu = \frac{1}{4} \right) \quad .$$

B. Boundary Conditions.

The solution applies only to cases where both the following boundary conditions are satisfied:

1. All edges are simply supported.

2. Supports fully restrain in-plane edge displacement of the plate such that these displacements are equal to the free thermal expansions (or contractions) of the supports.

C. Temperature Distribution.

It is assumed that no thermal gradients exist through the plate thickness. Temperature distribution over the surface is taken to be parabolic (Fig. 4.0-13) and can be expressed mathematically as

$$T = T_0 + T_1 \left[1 - \left(\frac{2x}{a} - 1 \right)^2 \right] \left[1 - \left(\frac{2y'}{b} - 1 \right)^2 \right] \quad . \tag{29}$$
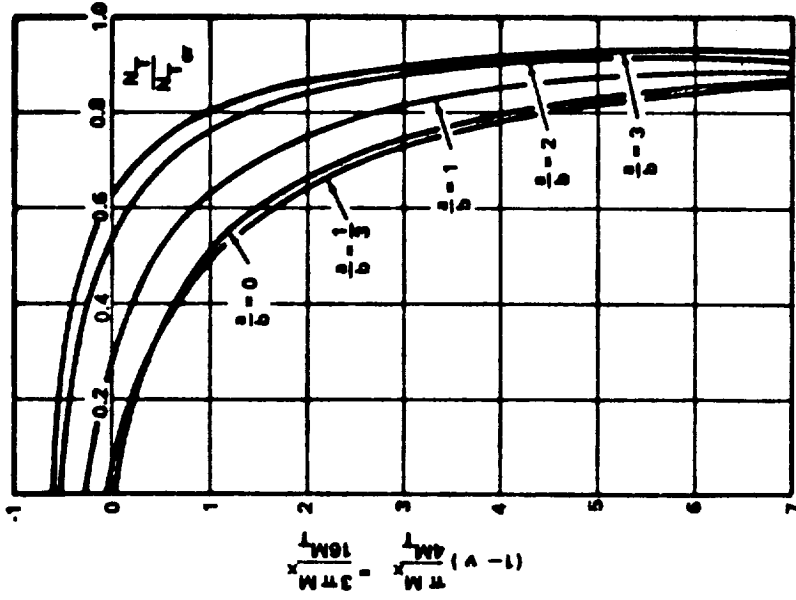
Figure 4.0-12. Bending moment M_x at the center of a rectangular plate.
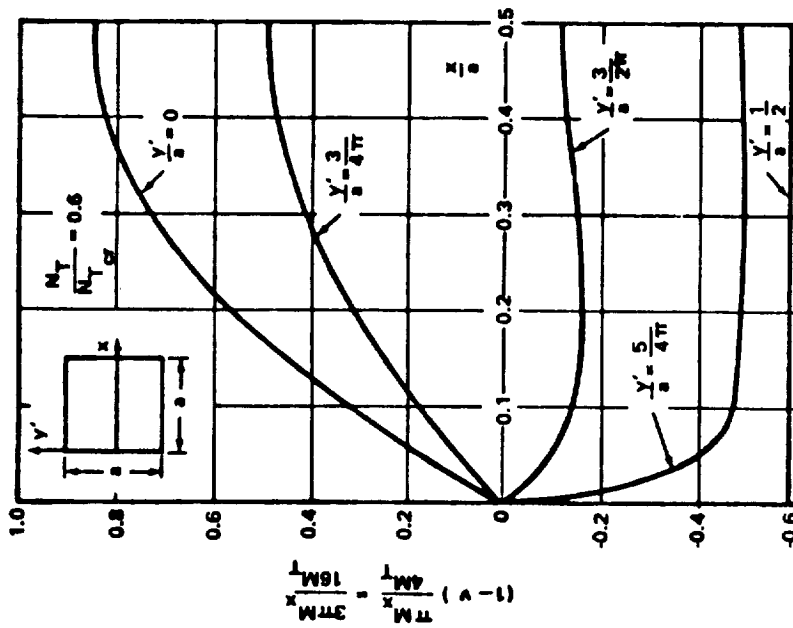
Figure 4.0-11. Distribution of the bending moment M_x in a square plate for $\dfrac{N_T}{N_{T_{cr}}} = 0.6$

$\left(\text{Poisson's ratio } \nu = \dfrac{1}{4}\right)$.

D. Design Curves.

In many aerospace applications, thermal buckling of flat, rectangular

plates can be tolerated if the post-buckling deflections do not cause excessive

losses of aerodynamic efficiency, do not produce destructive aerodynamic

disturbances, etc. In Ref. 37, Newman and Forray present the simple means

given as follows to compute absolute values of the maximum post-buckling

deflections for such plates. The temperature variation was chosen to be

representative of what would be expected when the panel is subjected to rapid

heating. This condition is conducive to thermal buckling since it will usually

cause the plate to be much hotter than the supports.
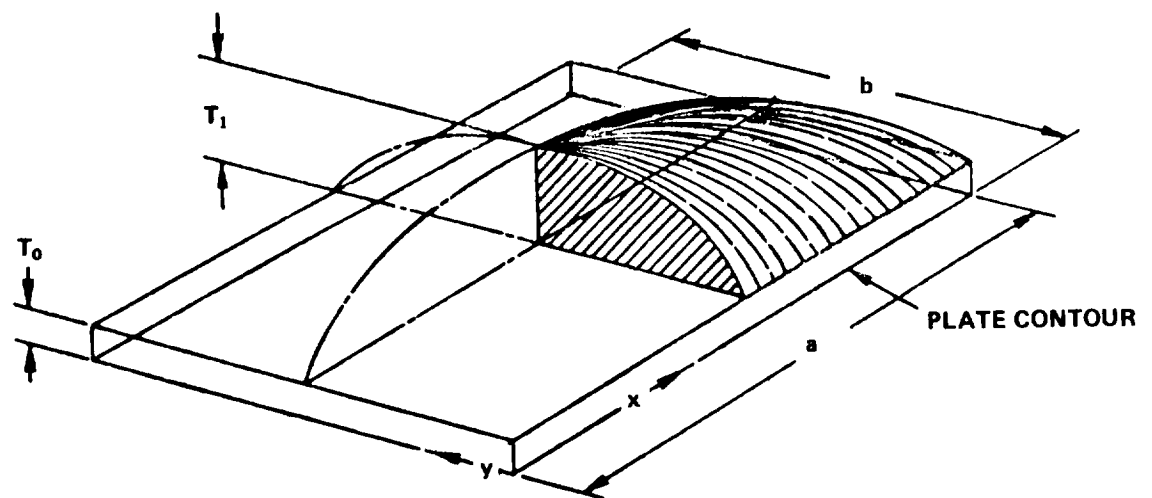
Figure 4.0-13. Parabolic temperature distribution over
the surface of a rectangular plate.

The maximum post-buckling deflection occurs at the center of the plate and

can be calculated from the relationship

$$\frac{T_1}{\beta} = \frac{\pi^2}{24} \left[\frac{K^2 + \frac{3}{4} \left[(3 - \nu^2) \left(1 + \frac{b^4}{a^4} \right) + 4 \nu \left(\frac{b^2}{a^2} \right) \right] \frac{\delta^2}{t^2}}{\left(\frac{2}{1 - \nu} \right) (K) \left(\frac{T_0}{T_1} + \frac{4}{9} \right) + \left(\frac{8}{3\pi^2} \right) (K)} \right] \quad (30)$$

where

$$K = 1 + \frac{b^2}{a^2} \quad (31)$$

and

$$\beta = \frac{1}{\alpha (1 - \nu^2)} \left(\frac{t}{b} \right)^2 . \quad (32)$$

Solutions to equation (30) are plotted in Figures 4.0-14 and 4.0-15 for plates

having $\nu = 0.30$. It is useful to note that, for given values of T_0/T_1, initial

thermal buckling occurs at T_1/β values corresponding to $\delta/t = 0$. The

curves do not account for nonuniformities in the material properties such as

those variations that arise because of temperature-dependence of the material

behavior. Hence, the user must select a single effective value for α by

employing some type of averaging technique.

4.0.3   Thermal Buckling of Cylinders.

Configuration.

The design curves and equations provided here apply only to thin-

walled, right circular cylinders which satisfy the relationship

$$L/R \geq \frac{3.2}{\left(\frac{R}{t} \right)^{1/2}} \quad (33)$$
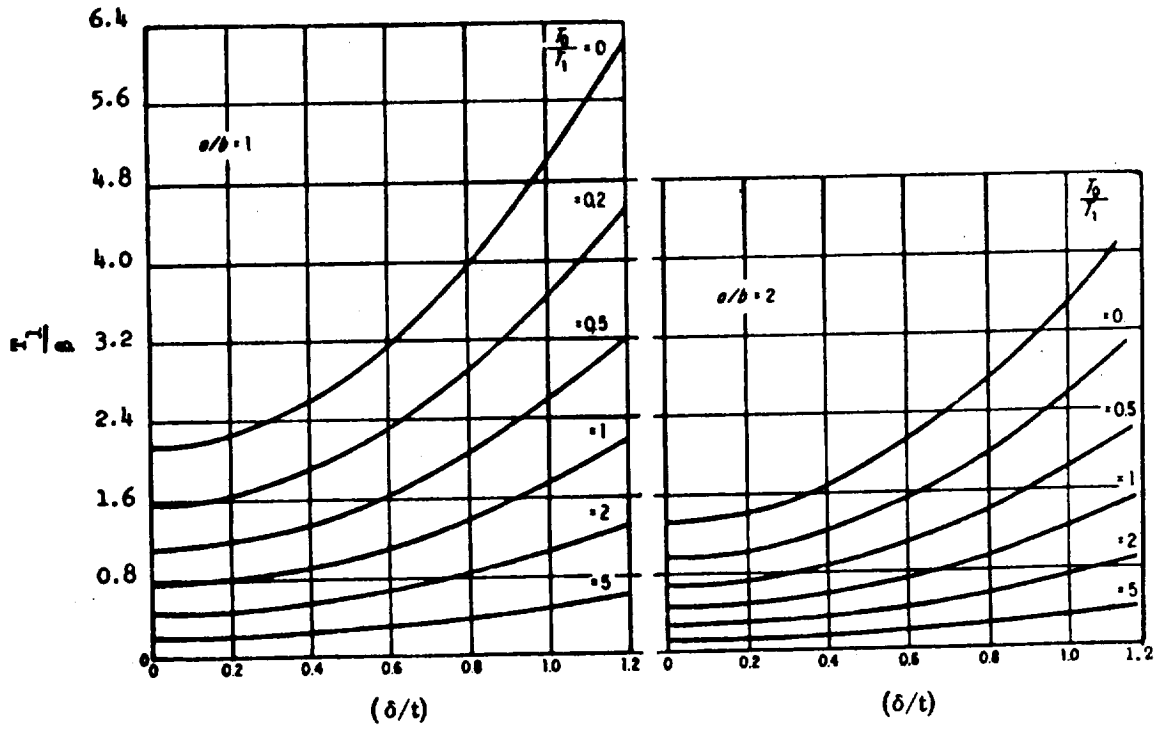
Figure 4.0-14. Post-buckling parameters for heated rectangular plates.
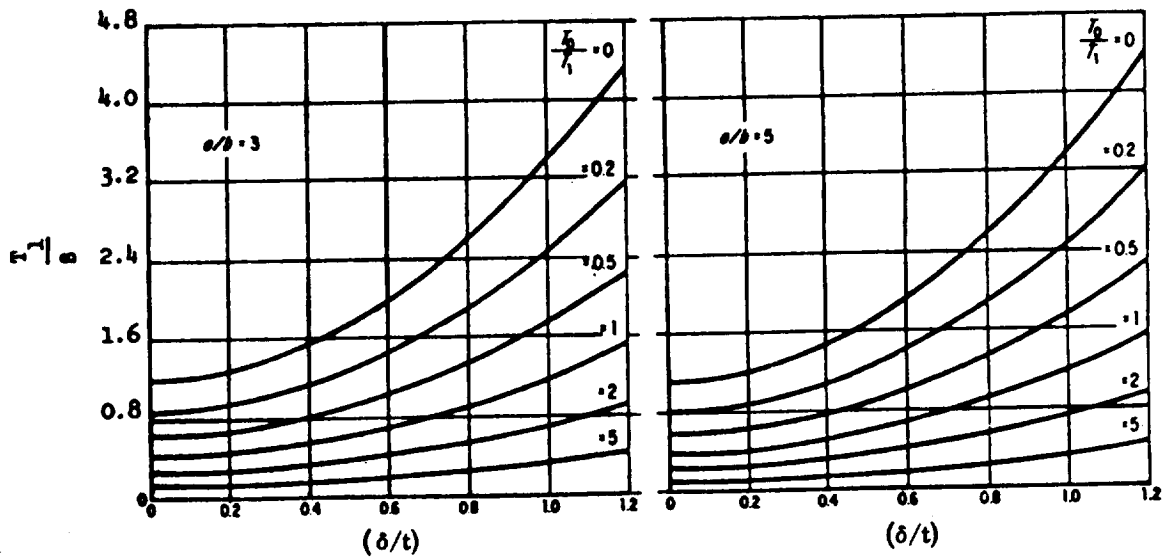
Figure 4.0-15. Post-buckling parameters for heated rectangular plates.

and are made of isotropic material. It is assumed that the shell wall is free

of holes, obeys Hooke's law, and is of constant thickness. Figure 4.0-16

depicts the isotropic cylindrical shell configuration. Figure 4.0-17 shows the

sign convention for forces, moments, and pressures.

Boundary Conditions.

The following types of boundary conditions are covered:

1. Simply supported edge; that is,

$$w = M_x = 0 \text{ at } x = 0 \text{ and/or } x = L. \tag{34}$$

2. Clamped edge; that is,

$$w = \frac{\partial w}{\partial x} = 0 \text{ at } x = 0 \text{ and/or } x = L . \tag{35}$$

It is not required that the conditions at the two ends be the same. In every

case, it is assumed that the cylinder (including any end rings) is not subjected

to external axial constraints at any location around the boundaries at $x = 0$ and

$x = L$.

Temperature Distribution.

The supposition is made that no thermal gradients exist through the

wall thickness and in the axial direction. However, arbitrary circumferential

variations may be present. The permissible distributions can therefore be

expressed in the form

$$T = T (\phi) . \tag{36}$$
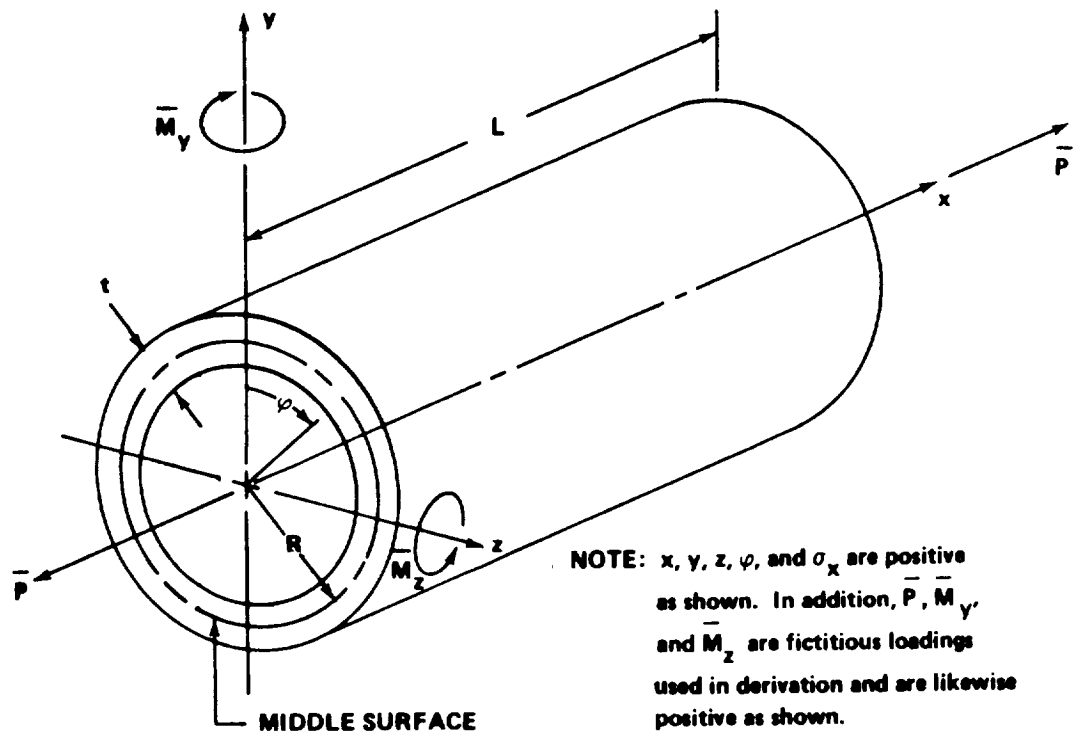
Figure 4.0-16. Isotropic cylindrical shell configuration for thermal buckling.
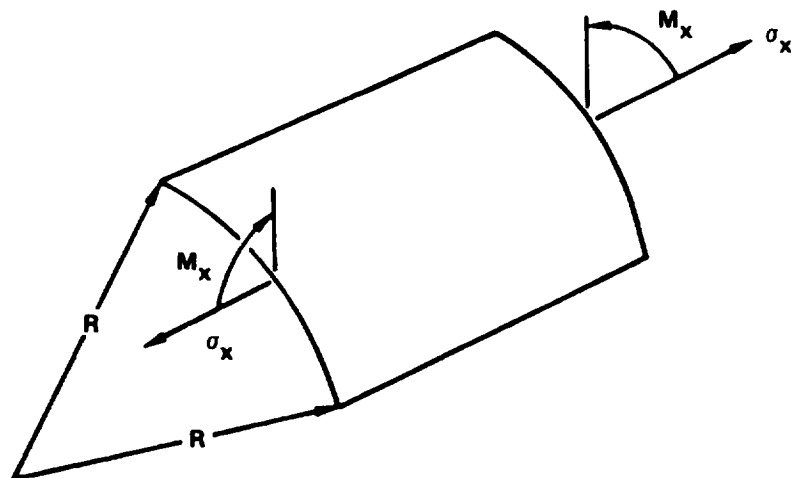
Figure 4.0-17. Sign convention for forces, moments, and pressure for thermal buckling.

Hoop membrane compression may develop in regions adjacent to the two ends because of external radial constraint. However, the buckling mode associated with this condition is not considered. Because of this and the lack of external axial constraints, the special case of a uniform temperature is of no interest here.

Design Curves and Equations.

It is assumed that Young's modulus and Poisson's ratio are unaffected by temperature changes. Hence, in using the contents of this manual, the user must select effective values for each of these properties by applying engineering judgement. It will sometimes be desirable to employ different effective moduli in each of the following operations:

1. Computation of the stresses σ_x present in the cylinder

2. Computation of the critical buckling stress $(\sigma_x)_{cr}$.

On the other hand, the results are presented in a form which enables the user to fully account for temperature-dependence of the thermal-expansion coefficient α.

The appropriate formulation for σ_x can be obtained by first imposing a fictitious stress distribution σ_A around the boundaries at $x = 0$ and $x = L$ such that all axial thermal deformations are entirely suppressed. It follows that

$$\sigma_A = -\alpha \, ET \, (\phi) \quad . \tag{37}$$

These stresses may be integrated around the circumference and through the

wall thickness to arrive at the force

$$\overline{P}_A = - EtR \int_0^{2\pi} \alpha T(\phi) \, d\phi \tag{38}$$

and the moments

$$(\overline{M}_y)_A = - ER^2t \int_0^{2\pi} \alpha T(\phi) \sin \phi \, d\phi$$

and $\hspace{8cm}$ (39)

$$(\overline{M}_z)_A = - ER^2t \int_0^{2\pi} \alpha T(\phi) \cos \phi \, d\phi \quad .$$

Since it is assumed that the shell is free of external axial constraints, the

conditions

$$\overline{P} = \overline{M}_y = \overline{M}_z = 0 \tag{40}$$

must be satisfied at $x = 0$ and $x = L$. To restore the shell to such a state,

it is necessary to superimpose a force $\overline{P}_B$ equal and opposite to $\overline{P}_A$ as well

as moments $(\overline{M}_y)_B$ and $(\overline{M}_z)_B$, which are equal and opposite to $(\overline{M}_y)_A$ and

$(\overline{M}_z)_A$, respectively. Hence,

$$\overline{P}_B = - \overline{P}_A ,$$

$$(\overline{M}_y)_B = - (\overline{M}_y)_A , \tag{41}$$

and

$$\left(\overline{M}_z\right)_B = - \left(\overline{M}_z\right)_A \quad .$$

The stress corresponding to $\overline{P}_B$ is easily found to be

$$\left(\sigma_{\overline{P}}\right)_B = \frac{\overline{P}_B}{A} = \frac{\overline{P}_B}{2\pi R t} = \frac{E}{2\pi} \int_0^{2\pi} \alpha \, T(\phi) \, d\phi \quad . \tag{42}$$

The stresses due to $\left(\overline{M}_y\right)_B$ are

$$\left(\sigma_{\overline{M}_y}\right)_B = \frac{\left(\overline{M}_y\right)_B z}{I_y} = \frac{\left(\overline{M}_y\right)_B z}{\pi R^3 t} = \frac{E \sin \phi}{\pi} \int_0^{2\pi} \alpha \, T(\phi) \, \sin \phi \, d\phi \tag{43}$$

and those due to $\left(\overline{M}_z\right)_B$ are

$$\left(\sigma_{\overline{M}_z}\right)_B = \frac{\left(\overline{M}_z\right)_B y}{I_z} = \frac{\left(\overline{M}_z\right)_B y}{\pi R^3 t} = \frac{E \cos \phi}{\pi} \int_0^{2\pi} \alpha \, T(\phi) \, \cos \phi \, d\phi \quad . \tag{44}$$

The procedure being used constitutes an application of Saint-Venant's principle. Hence, the stresses from equations (42) through (44) will be accurate representations only at sufficient distances from the ends x = 0 and x = L. If end rings are present, the greater their resistance to out-of-plane bending, the shorter will be this distance. Subject to these conditions, the actual longitudinal thermal stresses at various points in the shell may be computed from the relationship

$$\sigma_x = \sigma_A + \left(\sigma_{\overline{P}}\right)_B + \left(\sigma_{\overline{M}_y}\right)_B + \left(\sigma_{\overline{M}_z}\right)_B \tag{45}$$

or

$$\sigma_x = - \alpha \, ET(\phi) + \frac{E}{2\pi} \int_0^{2\pi} \alpha \, T(\phi) \, d\phi$$

$$+ \frac{E \sin \phi}{\pi} \int_0^{2\pi} \alpha \, T(\phi) \sin \phi \, d\phi$$

$$+ \frac{E \cos \phi}{\pi} \int_0^{2\pi} \alpha \, T(\phi) \cos \phi \, d\phi \quad . \tag{46}$$

Complex distributions may be encountered which make it difficult to perform the required integrations. In such instances, use can be made of numerical techniques whereby the integral signs are replaced by summation symbols.

To investigate the stability of a particular shell, the maximum longitudinal stress $(\sigma_x)_{max}$ must be compared against the critical value which can be obtained from the formula

$$(\sigma_x)_{cr} = \gamma \, \frac{Et}{R \sqrt{3(1 - \nu^2)}} \quad . \tag{47}$$

For the design to be satisfactory, it is required that

$$(\sigma_x)_{max} < (\sigma_x)_{cr} \quad . \tag{48}$$

The quantity γ appearing in equation (47) is a so-called knockdown factor, which mainly accounts for the detrimental effects from initial imperfections. Note that equation (47) is identical to that used for uniformly compressed circular, cylindrical shells. Its application to the present problem is justified on the basis of small-deflection studies reported in Refs. 38 and 39. From the results given in these references, it can be concluded that, regardless of the nature of the circumferential stress distribution, classical theoretical instability is reached when the peak axial compressive stress satisfies the expression

$$(\sigma_x)_{max} \approx \frac{Et}{R\sqrt{3(1 - \nu^2)}} \quad . \tag{49}$$

In view of this, the values used here for γ were determined from the 99 percent probability (confidence = 0.95) data for uniformly compressed cylinders, as reported in Ref. 40. The resulting γ values are plotted in Figure 4.0-18 for L/R ratios of 0.25, 1.0, and 4.0.

<u>Summary of Equations and Curves.</u>

$$\sigma_x = -\alpha \, ET(\phi) + \frac{E}{2\pi} \int_0^{2\pi} \alpha \, T(\phi) \, d\phi$$

$$+ \frac{E \sin \phi}{\pi} \int_0^{2\pi} \alpha \, T(\phi) \sin \phi \, d\phi$$

$$+ \frac{E \cos \phi}{\pi} \int_0^{2\pi} \alpha \, T(\phi) \cos \phi \, d\phi \tag{50}$$

and

$$(\sigma_x)_{cr} = \gamma \, \frac{Et}{R\sqrt{3(1 - \nu^2)}} \quad . \tag{51}$$

When $\nu = 0.3$ this gives

$$(\sigma_x)_{cr} = - 0.606 \, \gamma \, \frac{Et}{R} \quad . \tag{52}$$

The knockdown factor γ is obtained from Figure 4.0-18.
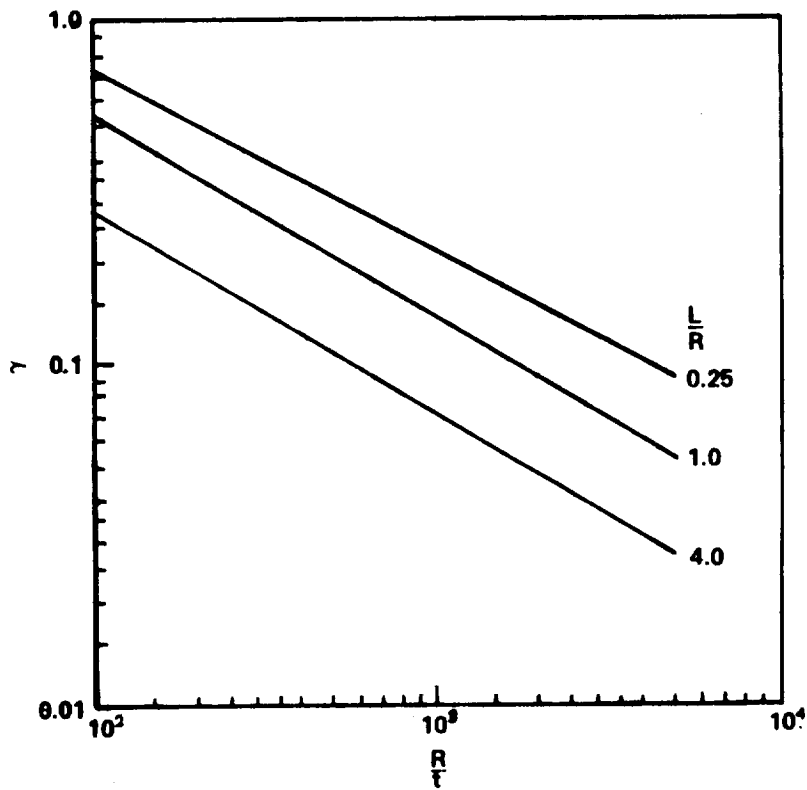
Figure 4.0-18. Knockdown factor.
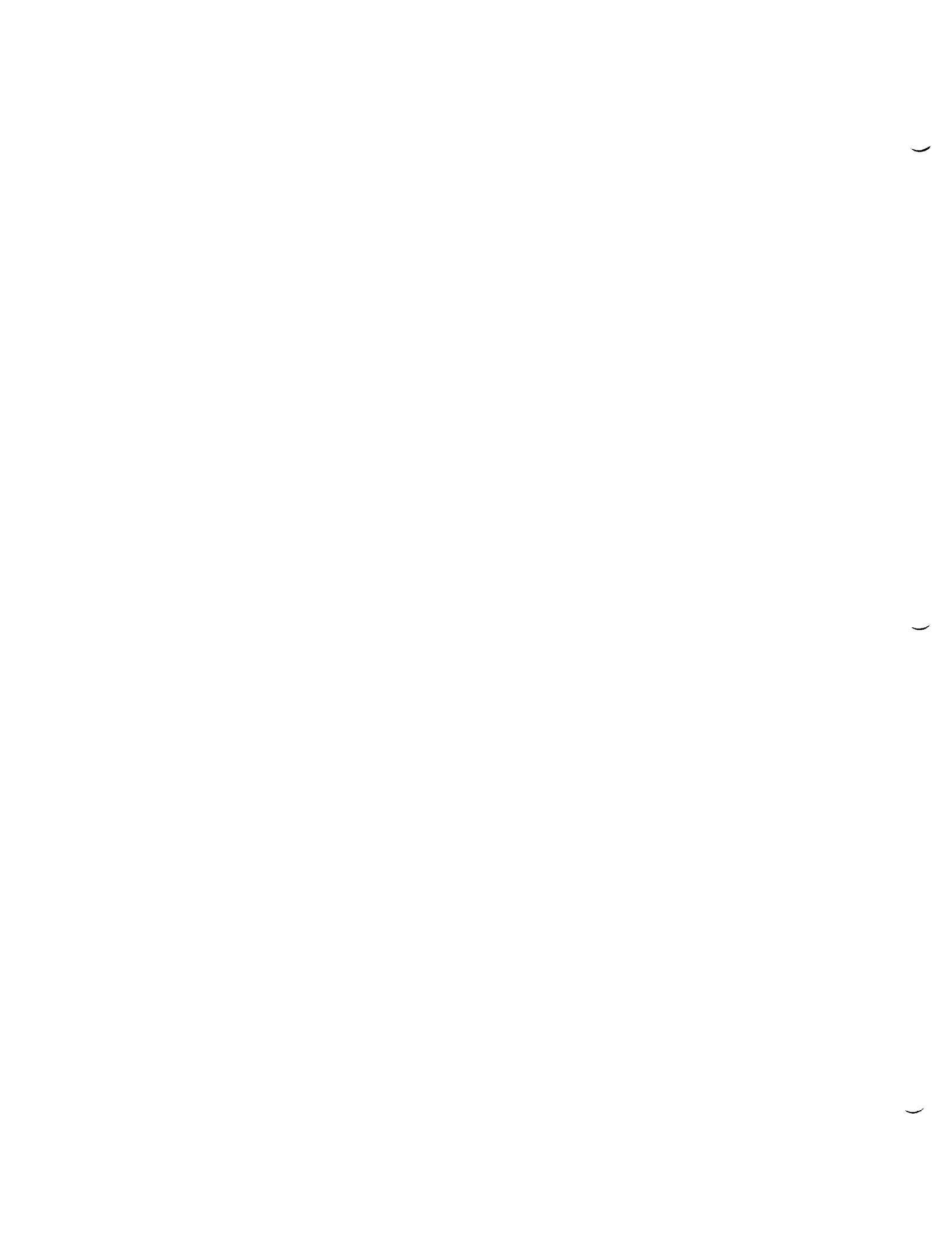
5.0   INELASTIC EFFECTS.

In the preceding paragraphs, elastic behavior was assumed. This

assumption is sufficiently accurate for large classes of materials at relatively

low temperature and stress levels.

At higher temperature and for higher stress levels, however, the

divergence between the behavior of real solids and that of the ideal elastic

solid increases and the elastic idealization becomes inadequate; the behavior

of the real solid is then said to be inelastic. To predict the inelastic behavior

of a solid under given thermal and loading conditions, it is necessary to

generalize the stress-strain relationship. There are three types of approaches

to this generalization, although the borderlines between them are not well

defined.

1.   The most basic studies of this problem make use of the concepts

and methods of solid-state physics. In this approach, the microstructure of

the material is taken into consideration and it is attempted to predict the

mechanical behavior of materials from this information.

2.   It is also possible to disregard the microstructure of the material

and to regard it as a continuum; the general principles of mechanics and

thermodynamics as applied to continua are then used to determine the forms

of stress-strain relations which are compatible with these principles.

3.   The most direct procedure is to postulate simple inelastic stress-

strain relations; these define various ideal inelastic bodies which, though not

representing any actual materials, nevertheless incorporate in simple combinations some of the different types of inelastic phenomena, such as creep, relaxation, plastic flow, or work-hardening.

Although considerable progress has been made in methods 1 and 2, thus far only the third approach has yielded information of direct utility to the stress analyst. In this paragraph, inelastic stress-strain relations are discussed from the third of these viewpoints.

5.0.1   <u>Creep.</u>

Creep is the time-dependent deformation that occurs under stress. Creep is normally observed by placing a constant load on a specimen and measuring its deformation with time at a constant elevated temperature. The curve showing the deformation as a function of time is known as a creep curve. Creep curves obtained for various materials, temperatures, and stresses have certain common features, which are illustrated in Figure 5.0-1. These are:

1.   From A to B, the specimen undergoes an initial, almost instantaneous, extension on loading.

2.   From B to C, the specimen creeps at a rate that decreases with time (primary stage or transient creep).

3.   From C to D, the specimen creeps at a rate that is nearly constant (secondary stage or viscous creep).

4.   From D to E, the specimen creeps at a rate that increases with time (tertiary stage or accelerating creep).

5.   At E, the specimen fractures.
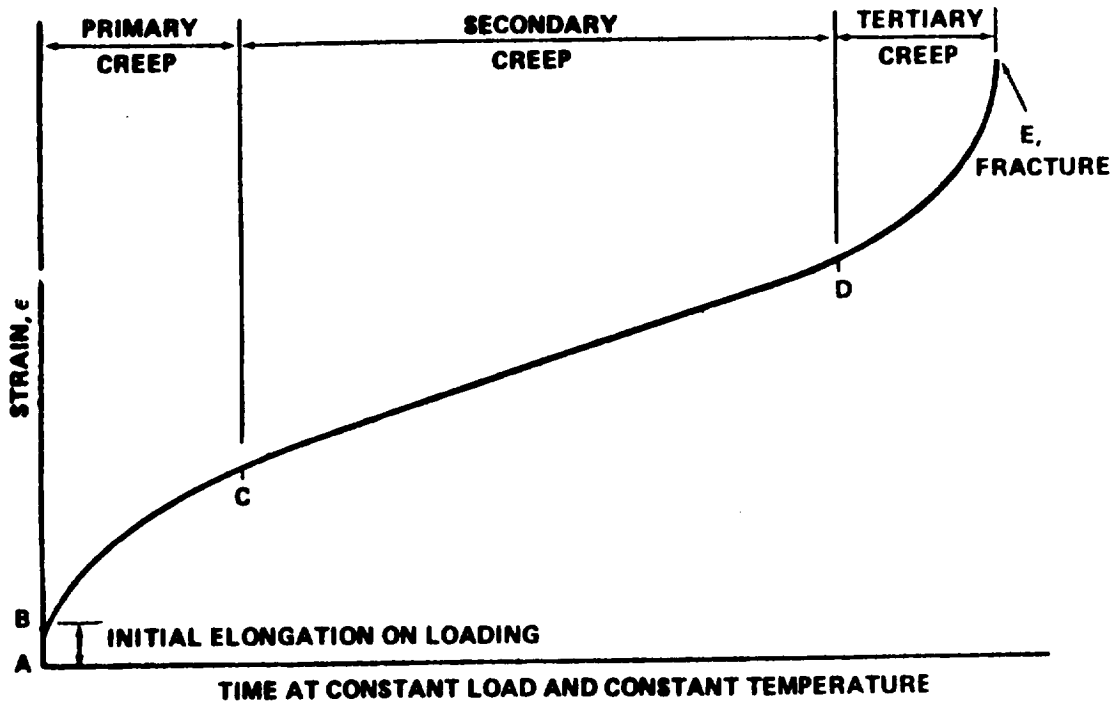
Figure 5.0-1. The idealized creep curve.

The rate of creep changes in the manner shown in Figure 5.0-2.

During the secondary stage, the rate of creep drops to a minimum value that

is approximately constant, as shown by the essentially straight line of the

curve (refer to Fig. 5.0-1).

The primary stage of creep is a work- or strain-hardening stage,

during which the resistance of the material to further creep is being built up

by virture of its own deformation. For this reason, the rate of creep continual-

ly decreases. The secondary stage of creep (C-D) represents a balance be-

tween strengthening by work-hardening and weakening by thermal softening.
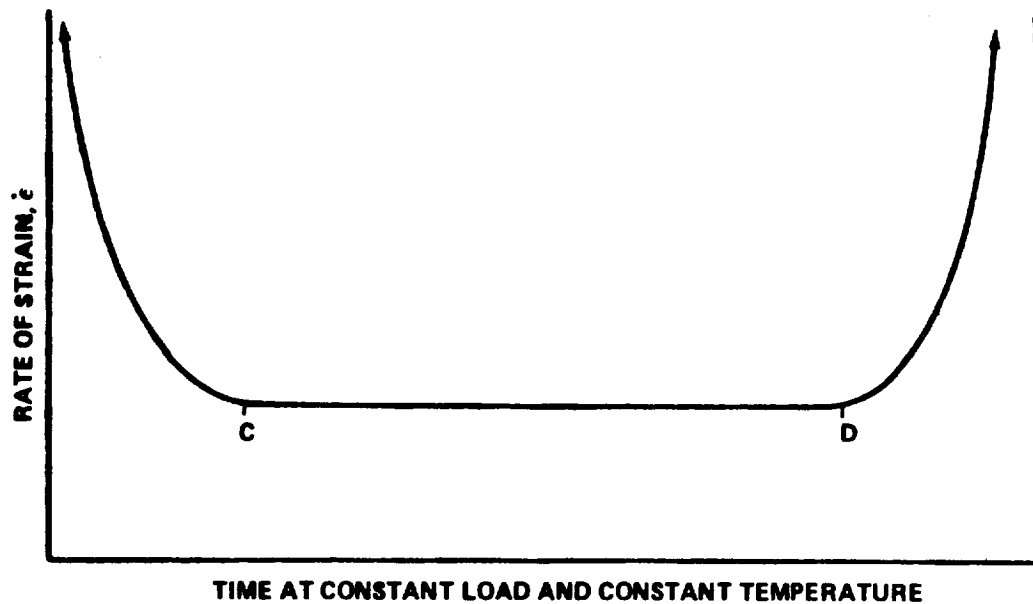
Figure 5.0-2. Variation in rate of creep with time.

The tertiary stage, or accelerating rate of creep immediately before fracture, is often caused by an increase in stress that accompanies the decrease in cross-sectional area of the specimen during creep under a constant load. This decrease in the load-carrying area may be due either to the decrease of the diameter of the specimen as it elongates or to the formation of intercrystalline cracks. These cracks can also act as stress-raisers. In other cases, the accelerating creep rate is due to a change in the metallurgical structure, such as recrystallization.

5.0.1.1 Design Curves.

For engineering purposes, the results of tests at various stresses and temperatures are summarized in more convenient form. Figure 5.0-3 shows

a plot that is most useful when the temperature and the lifetime of a part are fixed by the conditions of operation, and an allowable stress must be determined so that the part will not fracture or deform more than a certain amount during service. Having a set of these curves at the proper temperature, the designer can set off the lifetime along the abscissa and project it upwards; the intersection of this vertical line with the proper curve then determines the maximum allowable stress, and the design stress will be this quantity less a suitable factor of safety. Time and stress are usually plotted on logarithmic scales, where stress is the load divided by the original cross-sectional area. Frequently the data points on the rupture curves are identified with a number that gives the percent elongation, or reduction in area, at fracture; thus, some measurement of the ductility of the material is provided.

When the requirements are simply that a part must not fracture in service, and there are no limits on the amount of tolerable deformation, only the rupture curve in Figure 5.0-3 is needed. In such cases, the rupture curves for a number of temperatures can be collected on a single diagram, as in Figure 5.0-4. which is usually known as a "stress-rupture diagram." These curves show the variation in the time to fracture as a function of stress at several constant temperatures, and they are used in the same manner as the curves in Figure 5.0-3.

There are various ways of cross-plotting the previous figures. Plots of the stress versus temperature for lines of constant rupture life or constant
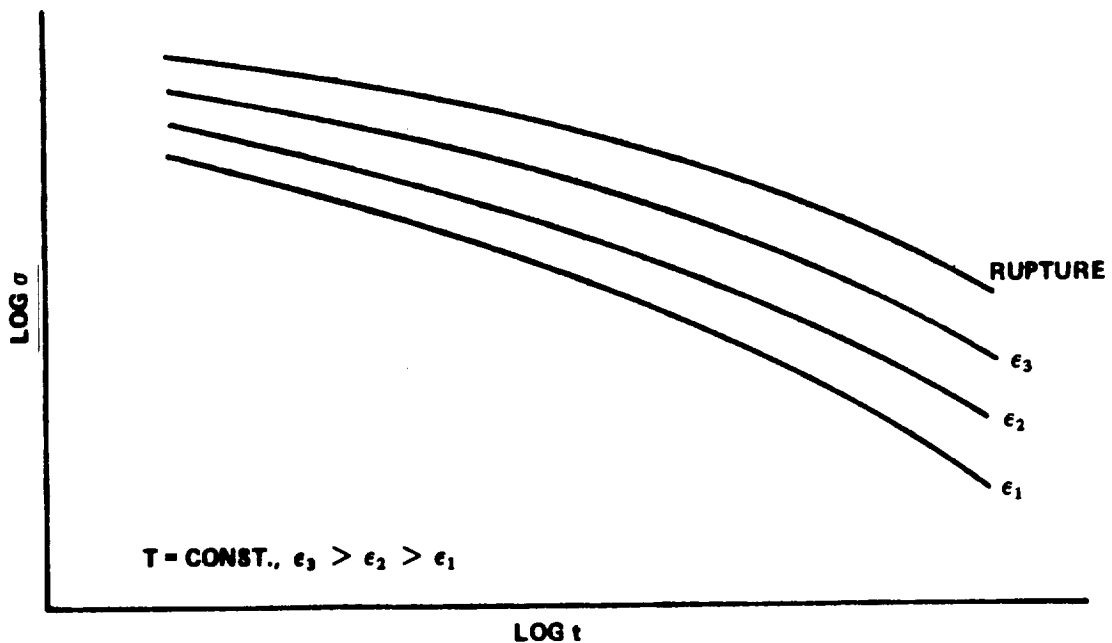
Figure 5.0-3. Schematic presentation of creep-rupture data showing effect of stress at constant temperature on the time to rupture or specific amounts of strain.

minimum creep rate are common. These curves are sometimes plotted on the same diagram with curves showing results from short-time tensile tests, as in Figure 5.0-5. Such diagrams give complete descriptions of the mechanical behavior over wide temperature ranges. At low temperatures, where creep is unimportant, designs are based on the results of short-time tensile tests; at higher temperatures, where the creep-rupture strength curves are below the tensile test curves, designs must be based on the creep-rupture behavior.

Curves of this type are readily available for most common metals in MIL-HDBK-5 [41].
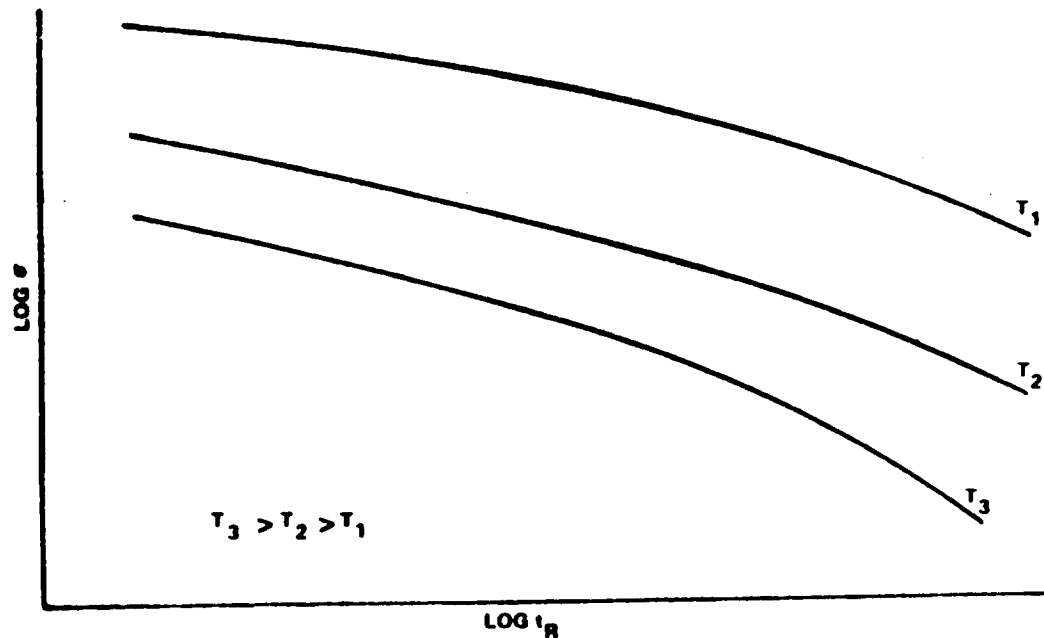
Figure 5.0-4. Schematic presentation of creep-rupture data showing effect of stress on the time to rupture at various temperatures.

5.0.1.2 Stress Relaxation.

Creep assumes a constant force; if, on the other hand, a bar is subjected to a constant elongation and the temperature is raised to a high level, with the elongation being maintained constant, the force required to produce this elongation will be observed to decrease continuously with time (Fig. 5.0-6). This mode of inelastic behavior is known as stress relaxation.

An important characteristic of both creep and stress relaxation is that time is required for their action. Thus, it may be expected that effects of this type will be unimportant for processes of relatively short duration.
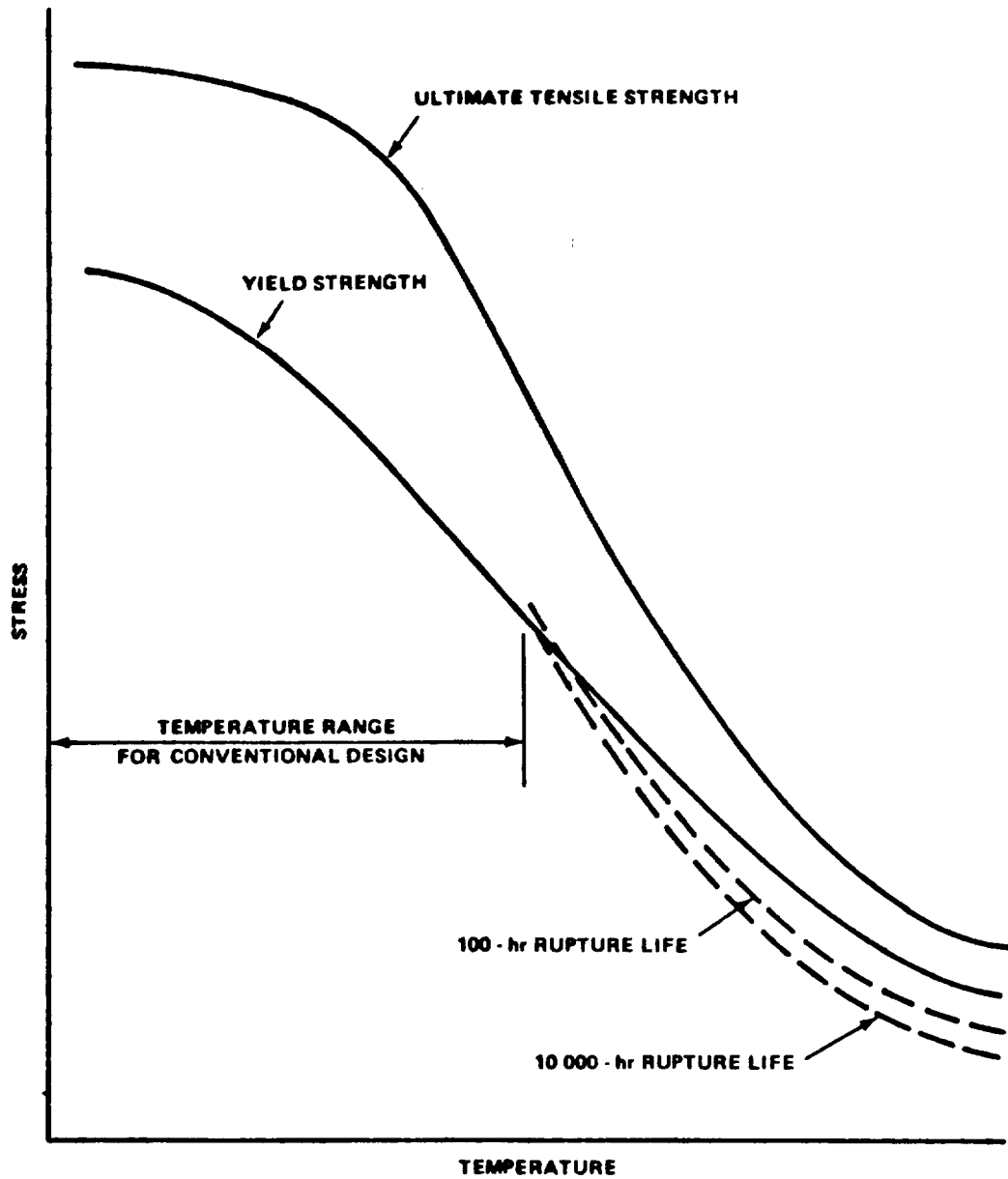
Figure 5.0-5. Schematic presentation of tensile and creep-rupture properties.
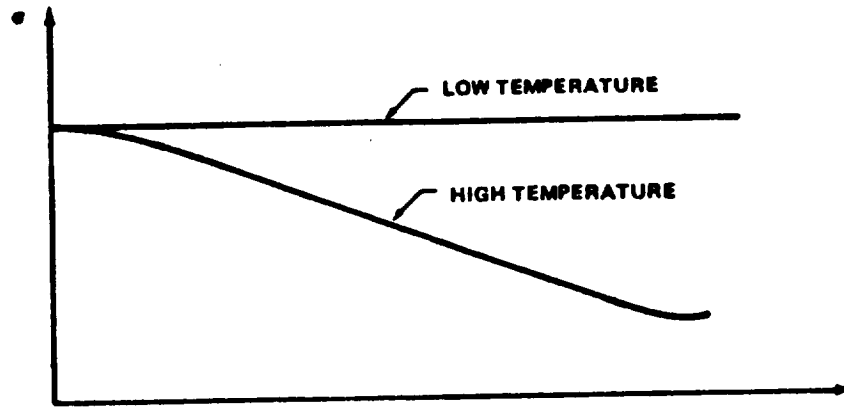
Figure 5.0-6. Stress relaxation under constant deformation.

5.0.2 Viscoelasticity.

Often, idealized bodies are defined which exhibit the characteristics of creep and stress relaxation. These idealized bodies take the form of simple mechanical models composed of springs and dashpots, whose deformation defines the stress-strain relationship for the given material. This approach is called viscoelasticity.

To represent the creep behavior of a material, many various mechanical models can be formulated composed of different combinations of springs and dashpots. Some of the more common ones can be found in Refs. 1 and 42.

5.0.3 Creep Buckling.

Consider a column under a constant axial compressive load; if the column is not perfectly straight initially (as is always the case because of unavoidable manufacturing inaccuracies), then some bending will occur. The

bending stresses are accompanied by a certain strain rate, which implies increasing deflections; these in turn cause higher stresses so that a self-excited or unstable situation arises. This process leads to collapse at a finite critical time and is known as creep buckling.

The following observations apply to creep buckling (Ref. 1):

1.   The phenomenon of creep buckling is, both physically and mathematically, quite different from the usual type of buckling phenomenon. The usual buckling load represents a "point of bifurcation" on a load versus deflection plot, a point beyond which more than one equilibrium configuration is possible; creep buckling is characterized by deflections increasing beyond all bounds.

2.   Mathematically, creep buckling can occur at a finite time only if the material follows a nonlinear creep law.

3.   The column will undergo creep buckling at any value of the compressive axial load, no matter how small.

4.   Creep buckling will occur whenever the column has initial imperfections, and only then.

5.   The value of t_{cr} depends on the initial deflection and on the magnitude of the load; it has been found to be not too strongly affected by changes in the former but very sensitive to changes in the latter.

6.   The small-deflection analysis is, of course, not valid in the immediate neighborhood of the critical time because the deflections are then

large. However, calculations based on a small-deflection theory are valid up to times very close to the critical; they thus cover, in effect, the entire range of practical interest.

5.0.3.1 Column of Idealized H-Cross Section.

The critical time for creep buckling to occur for a simply supported column of idealized H-cross section [two concentrated flanges, of area (A/2) each, at a distance h apart] is given by:

$$t_{cr} = k \log \left[1 + \left(\frac{4}{a_0^2} \right) \right]$$

where

$$k = \frac{1}{24} \left(\frac{\pi h}{L} \right)^2 \left(\frac{\lambda A}{P_0} \right)^3 \qquad ,$$

L = length of column ,

P_0 = column load,

a_0 = maximum value of initial imperfection,

and

λ = constant in the strain-stress relationship.

$$\frac{d\epsilon}{dt} = \left(\frac{\sigma}{\lambda} \right)^n \qquad .$$

5.0.3.2 Rectangular Column.

Analysis of the critical buckling time for rectangular columns is very difficult. A way of circumventing this difficulty has been established, whereby

upper and lower bounds for the critical time are obtained (t^*_{cr}) and are so designated by the use of an asterisk.

For a column with a rectangular cross section of height h and width b, subjected to an average stress $\sigma_0 = P_0/bh$ and obeying a stress-strain law of

$$\dot{E} = (\dot{\sigma}/E) = (\sigma/\lambda)^n ,$$

upper and lower bounds for the nondimensional critical time t^*_{cr} are plotted in Figure 5.0-7 against the ratio (z_0/h) of the initial center-deflection to the height of the bar. For small values of this ratio (say $z_0/h < 0.015$) these bounds may be determined from the asymptotic expression

$$t^*_{cr} = \log \frac{h}{z_0} - c$$

with the values of the coefficient c listed in Table 5.0-1.

The spread between the bounds may be seen from Figure 5.0-7 to vary with the ratio z_0/h. However, from Ref. 1, if $\sigma_0/\sigma_E > 0.8$, then the lower bound will be a good approximation for t^*_{cr}, whereas if $\sigma_0/\sigma_E < 0.2$, the upper bound on t^*_{cr} will be a good approximation to the actual value of the critical time. $\left(\sigma_E = \text{Euler buckling stress} = \dfrac{\pi^2 E h^2}{12 L^2} \right)$.

5.0.3.3   Flat Plates and Shells of Revolution.

The method presented here may be used to predict critical conditions for the creep buckling of flat plates and shells of revolution which satisfy the following requirements:

TABLE 5.0-1.   VALUES OF C

n	For Lower Bound	For Upper Bound
3	0.987	0.26
4	1.57	0.56
5	1.95	0.81
6	2.26	1.02
7	2.45	1.16
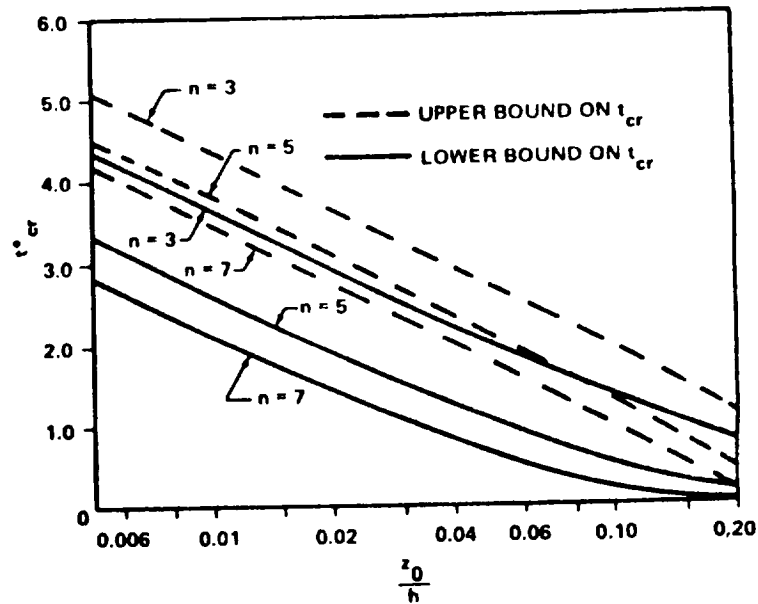
Figure 5.0-7.   Upper and lower bounds for the critical time t^*_{cr} for creep buckling of a rectangular column.

1.   The member is made of an isotropic material.

2.   The stress intensity σ_i [see equations (1)] is uniform throughout the structure.

3.   The configuration, boundary conditions, and type of loading are such that appropriate formulas are available for room-temperature values of both the critical stress intensity σ_i [see equations (1)] and the plasticity reduction factor.

Temperature Distribution.

It is assumed that the member is at a uniform elevated temperature.

Method.

The method presented here is essentially that which was published by Gerard in Ref. 43 and constitutes a classical stability approach based on the concepts set forth by Rabotnov and Shesterikov [44]. In Ref. 45, Jahsman and Field show comparisons of various theoretical predictions with column test data. The theory attributed there to Gerard is that of Ref. 46, which was published before Ref. 43 and has a different basis. On the other hand, the curves which Jahsman and Field [45] identify with the Rabotnov-Shesterikov label were developed from the method given in this paragraph. The aforementioned comparisons seem to indicate that this technique will give conservative predictions. However, this conclusion could possibly be because:

1.   The test data were corrected to eliminate the effects of initial imperfections.

2.   The analysis is concerned with the onset of instability, whereas the experimental data are for final collapse.

The presentation by Jahsman and Field includes plots obtained from each of three different theoretical approaches [43, 46, 47]. Of these, the approach of Ref. 43 gave the most conservative predictions. This is a desirable situation in view of the uncertainties associated with classical stability approaches to creep buckling problems. For one thing, this general theoretical concept ignores the detrimental effects from initial imperfections. However, to properly account for this influence, much more complicated methods would be required and these would not fall within the intended scope of this handbook. Therefore, in the procedure recommended below, an attempt is made at least to partially account for the imperfection effects in shells of revolution. This is done by the introduction of available room-temperature knockdown factors.

Recommended Procedure.

Obtain from the literature, or a suitable test program, a family of creep curves for specimens made of the desired material and subjected to unaxial loading while at the appropriate service temperature. These curves should be of the type shown in Figure 5.0-8 where σ_i and ϵ_i are the stress intensity and strain intensity, respectively, and are defined as follows for plane-stress conditions:

$$\sigma_i = \left(\sigma_x^2 + \sigma_y^2 - \sigma_x \sigma_y + 3\tau_{xy}^2 \right)^{1/2}$$

and

$$\epsilon_i = \frac{2}{\sqrt{3}} \left(\epsilon_x^2 + \epsilon_y^2 + \epsilon_x \epsilon_y + \frac{\gamma_{xy}^2}{4} \right)^{1/2}$$

(1)

Using data obtained from these plots, create a family of curves similar to those of Figure 5.0-9 where $\dot{\epsilon}_i$ is the strain-rate intensity defined as follows for a state of plane stress:

$$\dot{\epsilon}_i = \frac{2}{\sqrt{3}} \left(\dot{\epsilon}_x^2 + \dot{\epsilon}_y^2 + \dot{\epsilon}_x \dot{\epsilon}_y + \frac{\dot{\gamma}_{xy}^2}{4} \right)^{1/2} . \tag{2}$$

The dots indicate differentiation with respect to time; for example,

$$\dot{\epsilon}_x^2 = \left(\frac{\partial \epsilon_x}{\partial t} \right)^2 . \tag{3}$$

The results embodied in Figure 5.0-9 are then used to develop still another family, which is illustrated in Figure 5.0-10. Following this, select appropriate formulations for conventional room-temperature values of both the critical stress intensity $(\sigma_i)_{cr}$ and the plasticity reduction factor η. For example, in the case of an axially compressed, moderate-length, circular cylinder, one obtains

$$\left(\sigma_i \right)_{cr} = \eta \, \Gamma \, \frac{Eh}{R\sqrt{3(1 - \nu_e^2)}} \tag{4}$$

and

$$\eta = \left(\frac{1 - \nu_e^2}{1 - \nu^2} \right)^{1/2} \frac{\sqrt{E_t E_s}}{E} \tag{5}$$

where Γ is the room-temperature knockdown factor and

$$\nu = 0.50 - \frac{E_s}{E} (0.50 - \nu_e) . \tag{6}$$
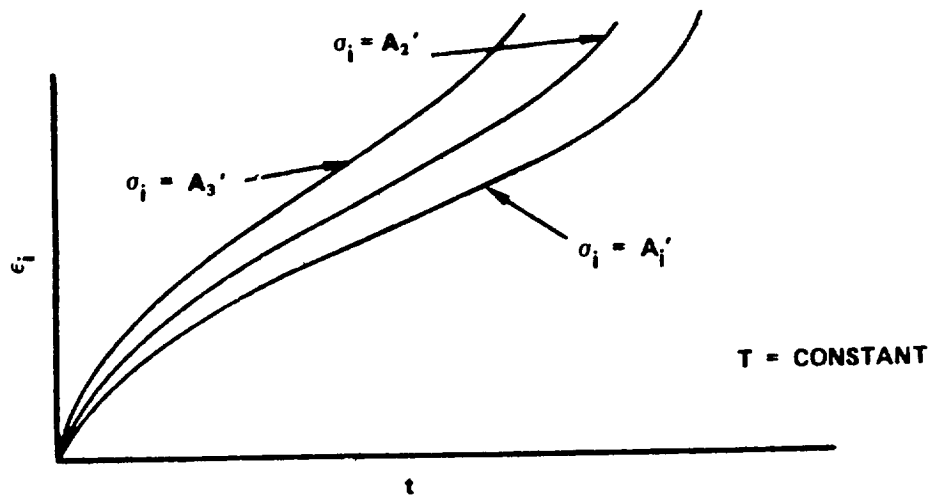
Figure 5.0-8. Constant-load creep curves.
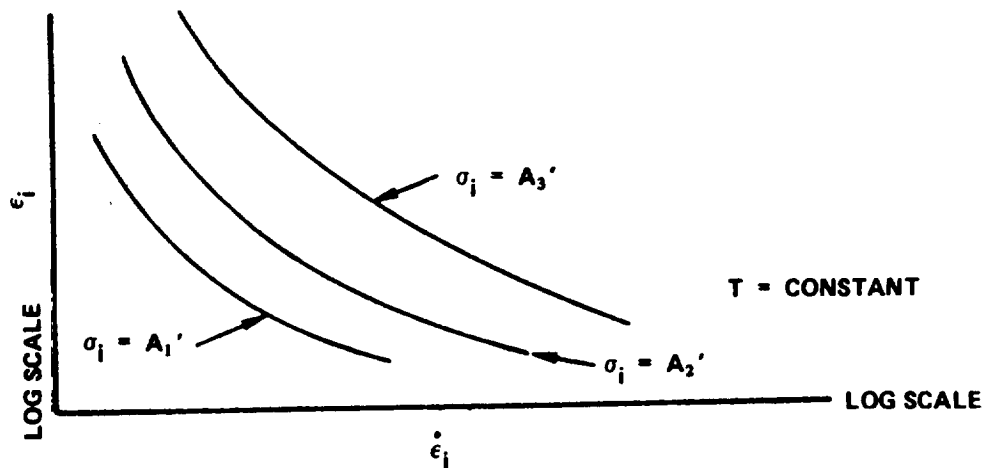
Figure 5.0-9. Curves derived from Figure 5.0-8.

Values for Γ may be obtained from Ref. 48 or other suitable sources.

In addition, use the short-time elevated-temperature values for E and ν_e.

On the other hand, the tangent and scant moduli (E_t and E_s, respectively) are

those associated with the curves illustrated in Figure 5.0-10. Therefore,
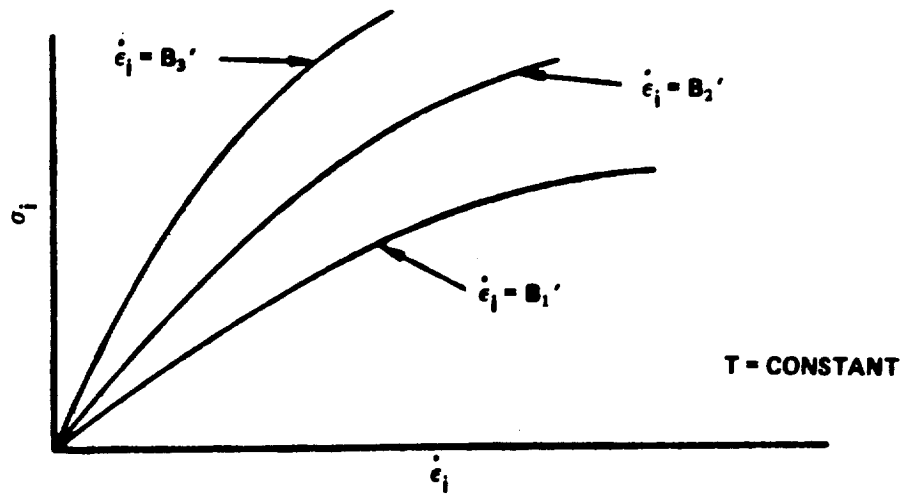
Figure 5.0-10. Curves derived from Figure 5.0-9.

working with this figure, proceed from left to right along the σ_i line corresponding to the applied load and use a trial-and-error procedure to determine the strain intensity ϵ_i at which

$$\text{applied } \sigma_i = \eta \ \Gamma \ \frac{Eh}{R\sqrt{3(1 - \nu_e^2)}} \ . \tag{7}$$

Following this, return to Figure 5.0-8 and establish the time t associated with this combination of σ_i and ϵ_i. This is the predicted time to the onset of creep buckling and can be denoted as t_{cr}.

Although the preceding presentation has dealt with the specific case of an axially compressed circular cylinder, it should be obvious that this method constitutes a general approach which can be used for the analysis of creep buckling in various types of plates and shells subjected to an assortment of loading conditions. It should be noted, however, that $\Gamma = 1.0$ for flat plates (and columns).

6.0   THERMAL SHOCK.

6.0.1   General.

Thermal shock refers to the phenomenon whereby a body undergoes sudden changes in temperature, usually caused by a rapid change in the external environment. It is the presence of severe transients that distinguishes thermal shock from the more common conditions of steady-state and slowly varying temperatures. Severe transients are experienced by reentry aerospace structures, such as those of the space-shuttle variety. The selection and comparison of candidate materials for structures of this type should be accomplished by means of a screening process that considers thermal-shock resistance, which may be evaluated by both analytical and experimental methods. The analytical method may include comparisons of thermal-shock indices, as well as the theoretical analysis of simple models such as a flat slab which is suddenly immersed in a hot medium. The experimental investigation may be of similar scope. In the theoretical treatment of such models as well as the actual complex configurations, it is usually unnecessary to perform a true shock-type analysis which involves mass inertia effects. Generally, it is sufficiently accurate to compute the pertinent thermal stresses by the same methods as are used for steady-state problems, except that one must determine the temperature and stress distributions at a number of time increments during the transient behavior. As a rule, however, it will be necessary to consider the material strain-rate-sensitivity when allowable stresses are established.

6.0.2   Stresses and Deformations.

Configuration.

The equations and tables provided here cover each of the following, as illustrated in Figure 6.0-1:

1.   Flat slabs, of infinite extent, which are of uniform thickness and are free of holes

2.   Solid cylinders of infinite length

3.   Solid spheres.

In all cases, it is assumed that Hooke's law applies.

Boundary Conditions.

All bodies are free of any external constraint.

Temperature Distribution.

The supposition is made that the subject bodies experience a sudden change in surface temperature. The upper and lower surfaces of the flat slab are always subjected to identical temperatures.

Equations and Tables.

This section is based on the assumption that Young's modulus, Poisson's ratio, the thermal diffusivity, and the coefficient of thermal expansion are unaffected by temperature changes. Hence, the user must select single effective values for each of these properties by employing some type of averaging technique.

The method presented here was published by Adams and Waxler in Ref. 49. It can be used to determine the temperature and stress distributions during the subject transient phenomena. To accomplish this, several simple formulas must be used in conjunction with appropriate tabulated values. All of these are given in the summary which follows. In applying this method, care should be taken to ensure that the units specified under NOTATION are used.

The method makes use of a temperature function, ϕ_j, which may be called the fractional temperature excess and is defined as follows:

$$\phi_j = \frac{T - T_f}{T_i - T_f} \quad , \quad j = 1, 2, 3 \quad . \tag{1}$$

The subscripts 1, 2, and 3 denote that the ϕ value is for an infinite solid slab, an infinite-length solid cylinder, or a solid sphere, respectively. The tabulations of ϕ_j published by Adams and Waxler and appearing in the summary of this section were developed from a study of the heat transfer phenomena associated with the subject configurations. The tables also include values for the temperature parameters Ψ_1', Ψ_2', and Ψ_3, which are defined as follows:

Infinite Solid Slab.

$$\Psi_1' = \int_0^1 \phi_1 \, d\left(\frac{x}{a}\right) \quad .$$

Infinite-Length Solid Cylinder.

$$\psi_2' = \frac{1}{\left(\frac{r}{R}\right)^2} \int_0^{\frac{r}{R}} \frac{r}{R} \, \phi_2 \, d\left(\frac{r}{R}\right) \qquad . \tag{2}$$

Solid Sphere.

$$\psi_3 = \frac{1}{\left(\frac{r}{R}\right)^3} \int_0^{\frac{r}{R}} \left(\frac{r}{R}\right)^2 \phi_3 \, d\left(\frac{r}{R}\right) \qquad .$$
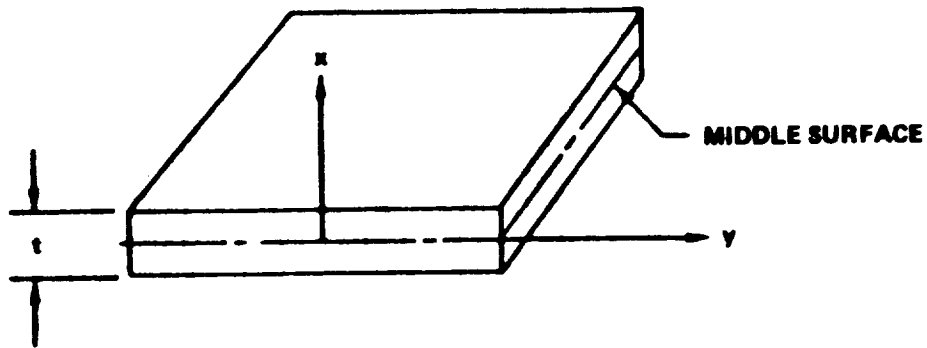
a. Segment of infinite solid slab.
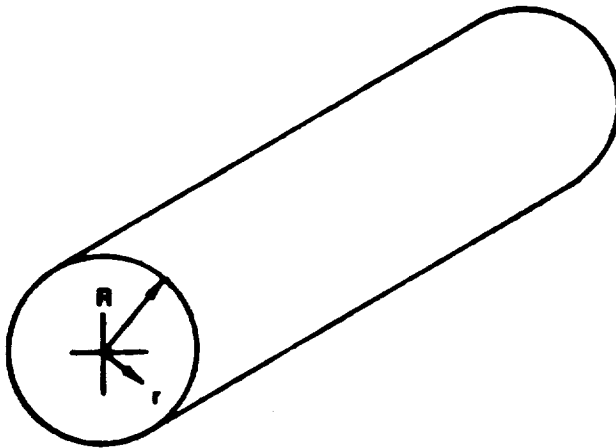
b. Segment of infinite-length
solid cylinder.
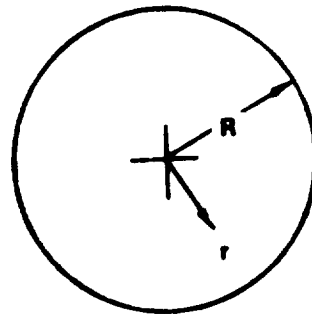
d. Solid sphere.

Figure 6.0-1. Configurations.

Summary of Equations and Tables.

The parameters q and β, which appear in the tables, are defined as follows:

$$q = \frac{t}{\sqrt{Kt}} \qquad (3)$$

and

$$\beta = \frac{r}{R} \qquad$$

where

$$K = \frac{k'}{C_p \rho} \qquad . \qquad (4)$$

Infinite Solid Slab.

$$T = \phi_1 (T_i - T_f) + T_f \qquad (5)$$

and

$$\sigma_x = \sigma_y = \frac{E\alpha (T_i - T_f)}{(1 - \nu)} (\Psi_1' - \phi_1) \qquad . \qquad (6)$$

The values for ϕ_1 and Ψ_1' are obtained from Table 6.0-1.

Infinite-Length Solid Cylinder.

$$T = \phi_2 (T_i - T_f) + T_f \qquad , \qquad (7)$$

$$\sigma_r = \frac{E\alpha (T_i - T_f)}{(1 - \nu)} (\Psi_2' - \Psi_2) \qquad , \qquad (8)$$

and

$$\sigma_t = \frac{E\alpha (T_i - T_f)}{(1 - \nu)} (\Psi_2' + \Psi_2 - \phi_2) \qquad (9)$$

where Ψ_2' is the value of Ψ_2 at $r/R = 1$. The values for ϕ_2 and Ψ_2 are obtained from Tables 6.0-2 and 6.0-3, respectively.

Solid Sphere.

$$T = \phi_3 \left(T_i - T_f\right) + T_f \quad , \tag{10}$$

$$\sigma_r = \frac{2E\alpha \left(T_i - T_f\right)}{(1 - \nu)} \quad \left(\Psi_3' - \Psi_3\right) \quad , \tag{11}$$

and

$$\sigma_t = \frac{E\alpha \left(T_i - T_f\right)}{(1 - \nu)} \quad \left(2\Psi_3' + \Psi_3 - \phi_3\right) \tag{12}$$

where Ψ_3' is the value of Ψ_3 at $r/R = 1$. The values for ϕ_3 and Ψ_3 are obtained from Tables 6.0-4 and 6.0-5, respectively.

TABLE 6.0-1. SLAB-PARAMETERS ϕ_1 AND ψ_1'

q / x/a	0.3000	0.3200	0.3400	0.3600	0.3800	0.4000	0.4200	0.4400	0.4600	0.4800
0.	0.0013	0.0031	0.0061	0.0109	0.0174	0.0270	0.0386	0.0526	0.0690	0.0875
0.10	0.0013	0.0030	0.0061	0.0108	0.0176	0.0266	0.0381	0.0520	0.0682	0.0865
0.20	0.0013	0.0029	0.0058	0.0104	0.0169	0.0256	0.0367	0.0500	0.0656	0.0832
0.30	0.0012	0.0027	0.0055	0.0097	0.0158	0.0240	0.0344	0.0469	0.0615	0.0780
0.40	0.0011	0.0025	0.0050	0.0088	0.0144	0.0218	0.0312	0.0426	0.0558	0.0708
0.50	0.0010	0.0022	0.0043	0.0077	0.0126	0.0191	0.0273	0.0372	0.0488	0.0619
0.60	0.0008	0.0018	0.0036	0.0064	0.0104	0.0158	0.0227	0.0309	0.0406	0.0515
0.70	0.0006	0.0014	0.0028	0.0050	0.0081	0.0122	0.0175	0.0239	0.0313	0.0397
0.80	0.0004	0.0010	0.0019	0.0034	0.0055	0.0083	0.0119	0.0163	0.0213	0.0270
0.90	0.0002	0.0005	0.0010	0.0017	0.0028	0.0042	0.0060	0.0082	0.0108	0.0137
1.00	0.0000	0.0000	0.0000	0.0000	0.0000	0.0000	0.0000	0.0000	0.0000	0.0000
ψ_1'	0.0009	0.0020	0.0039	0.0069	0.0113	0.0172	0.0246	0.0335	0.0439	0.0557

q / x/a	0.5000	0.5200	0.5400	0.5600	0.5800	0.6000	0.6200	0.6400	0.6600	0.6800
0.	0.1080	0.1301	0.1535	0.1781	0.2035	0.2295	0.2559	0.2824	0.3090	0.3354
0.10	0.1066	0.1285	0.1516	0.1759	0.2010	0.2267	0.2527	0.2789	0.3052	0.3313
0.20	0.1027	0.1237	0.1460	0.1694	0.1935	0.2183	0.2433	0.2686	0.2938	0.3190
0.30	0.0962	0.1159	0.1368	0.1587	0.1812	0.2045	0.2280	0.2516	0.2753	0.2988
0.40	0.0874	0.1052	0.1242	0.1441	0.1646	0.1857	0.2070	0.2285	0.2500	0.2713
0.50	0.0764	0.0920	0.1086	0.1259	0.1439	0.1623	0.1809	0.1997	0.2185	0.2372
0.60	0.0635	0.0765	0.0902	0.1047	0.1196	0.1349	0.1504	0.1660	0.1816	0.1971
0.70	0.0490	0.0591	0.0697	0.0809	0.0924	0.1042	0.1162	0.1282	0.1403	0.1523
0.80	0.0334	0.0402	0.0474	0.0550	0.0629	0.0709	0.0791	0.0873	0.0955	0.1036
0.90	0.0169	0.0203	0.0240	0.0279	0.0318	0.0359	0.0400	0.0442	0.0483	0.0525
1.00	0.0000	0.0000	0.0000	0.0000	0.0000	0.0000	0.0000	0.0000	0.0000	0.0000
ψ_1'	0.0687	0.0828	0.0977	0.1134	0.1295	0.1461	0.1629	0.1798	0.1967	0.2135

q / x/a	0.7000	0.7200	0.7400	0.7600	0.7800	0.8000	0.8200	0.8400	0.8600	0.8800
0.	0.3616	0.3874	0.4127	0.4376	0.4619	0.4858	0.5086	0.5310	0.5527	0.5738
0.10	0.3571	0.3826	0.4077	0.4322	0.4562	0.4796	0.5024	0.5245	0.5459	0.5667
0.20	0.3439	0.3684	0.3925	0.4162	0.4393	0.4618	0.4838	0.5051	0.5258	0.5458
0.30	0.3222	0.3452	0.3678	0.3899	0.4116	0.4327	0.4533	0.4733	0.4927	0.5115
0.40	0.2925	0.3134	0.3339	0.3541	0.3737	0.3929	0.4116	0.4298	0.4474	0.4645
0.50	0.2557	0.2739	0.2919	0.3095	0.3267	0.3435	0.3598	0.3757	0.3912	0.4062
0.60	0.2125	0.2277	0.2426	0.2573	0.2716	0.2855	0.2991	0.3124	0.3252	0.3377
0.70	0.1642	0.1759	0.1874	0.1987	0.2098	0.2206	0.2311	0.2413	0.2513	0.2609
0.80	0.1117	0.1197	0.1276	0.1353	0.1428	0.1501	0.1572	0.1643	0.1711	0.1777
0.90	0.0566	0.0606	0.0646	0.0685	0.0723	0.0760	0.0796	0.0832	0.0866	0.0900
1.00	0.0000	0.0000	0.0000	0.0000	0.0000	0.0000	0.0000	0.0000	0.0000	0.0000
ψ_1'	0.2302	0.2466	0.2628	0.2786	0.2941	0.3092	0.3239	0.3382	0.3521	0.3655

q / x/a	0.9000	0.9200	0.9400	0.9600	0.9800	1.0000	1.0200	1.0400	1.0600	1.0800
0.	0.5941	0.6137	0.6327	0.6509	0.6685	0.6854	0.7017	0.7173	0.7323	0.7467
0.10	0.5868	0.6062	0.6250	0.6430	0.6604	0.6772	0.6933	0.7087	0.7236	0.7378
0.20	0.5652	0.5839	0.6020	0.6195	0.6363	0.6525	0.6681	0.6831	0.6976	0.7114
0.30	0.5297	0.5473	0.5643	0.5807	0.5966	0.6119	0.6267	0.6410	0.6547	0.6680
0.40	0.4811	0.4972	0.5127	0.5278	0.5423	0.5564	0.5700	0.5831	0.5958	0.6081
0.50	0.4207	0.4348	0.4485	0.4617	0.4746	0.4870	0.4991	0.5108	0.5221	0.5331
0.60	0.3499	0.3617	0.3731	0.3842	0.3950	0.4054	0.4156	0.4255	0.4351	0.4445
0.70	0.2704	0.2795	0.2884	0.2970	0.3054	0.3136	0.3215	0.3293	0.3368	0.3442
0.80	0.1841	0.1903	0.1964	0.2023	0.2081	0.2137	0.2191	0.2245	0.2297	0.2348
0.90	0.0932	0.0964	0.0995	0.1025	0.1054	0.1082	0.1110	0.1137	0.1164	0.1190
1.00	0.0000	0.0000	0.0000	0.0000	0.0000	0.0000	0.0000	0.0000	0.0000	0.0000
ψ_1'	0.3786	0.3912	0.4034	0.4153	0.4267	0.4378	0.4485	0.4588	0.4688	0.4784

TABLE 6.0-1. (CONTINUED)

x/a \ q	1.1000	1.1200	1.1400	1.1600	1.1800	1.2000	1.2200	1.2400	1.2600	1.2800
0.	0.7604	0.7736	0.7862	0.7982	0.8097	0.8206	0.8311	0.8410	0.8505	0.8595
0.10	0.7515	0.7645	0.7771	0.7890	0.8005	0.8114	0.8218	0.8318	0.8412	0.8503
0.20	0.7248	0.7376	0.7498	0.7616	0.7729	0.7837	0.7941	0.8040	0.8135	0.8226
0.30	0.6807	0.6930	0.7048	0.7162	0.7272	0.7378	0.7480	0.7578	0.7672	0.7763
0.40	0.6200	0.6315	0.6426	0.6534	0.6638	0.6739	0.6837	0.6932	0.7024	0.7113
0.50	0.5438	0.5542	0.5643	0.5741	0.5837	0.5930	0.6020	0.6109	0.6195	0.6280
0.60	0.4536	0.4625	0.4712	0.4797	0.4880	0.4962	0.5042	0.5120	0.5197	0.5272
0.70	0.3514	0.3585	0.3655	0.3723	0.3789	0.3855	0.3920	0.3984	0.4046	0.4109
0.80	0.2398	0.2447	0.2496	0.2543	0.2590	0.2636	0.2682	0.2727	0.2772	0.2816
0.90	0.1216	0.1241	0.1266	0.1291	0.1315	0.1339	0.1362	0.1386	0.1409	0.1432
1.00	0.0000	0.0000	0.0000	0.0000	0.0000	0.0000	0.0000	0.0000	0.0000	0.0000
ψ_1'	0.4878	0.4968	0.5055	0.5140	0.5221	0.5301	0.5377	0.5451	0.5523	0.5593

x/a \ q	1.3000	1.3200	1.3400	1.3600	1.3800	1.4000	1.4200	1.4400	1.4600	1.4800
0.	0.8680	0.8761	0.8838	0.8911	0.8980	0.9046	0.9108	0.9166	0.9221	0.9273
0.10	0.8589	0.8670	0.8748	0.8822	0.8892	0.8958	0.9021	0.9081	0.9137	0.9191
0.20	0.8313	0.8396	0.8475	0.8551	0.8624	0.8693	0.8759	0.8822	0.8882	0.8939
0.30	0.7850	0.7935	0.8016	0.8094	0.8169	0.8242	0.8312	0.8379	0.8444	0.8506
0.40	0.7200	0.7283	0.7365	0.7444	0.7521	0.7596	0.7668	0.7739	0.7808	0.7874
0.50	0.6362	0.6443	0.6522	0.6599	0.6674	0.6748	0.6821	0.6892	0.6962	0.7030
0.60	0.5346	0.5419	0.5491	0.5562	0.5632	0.5701	0.5769	0.5836	0.5902	0.5967
0.70	0.4170	0.4231	0.4291	0.4350	0.4409	0.4467	0.4525	0.4582	0.4639	0.4696
0.80	0.2860	0.2904	0.2947	0.2990	0.3033	0.3075	0.3118	0.3160	0.3202	0.3243
0.90	0.1455	0.1478	0.1501	0.1523	0.1546	0.1568	0.1590	0.1613	0.1635	0.1657
1.00	0.0000	0.0000	0.0000	0.0000	0.0000	0.0000	0.0000	0.0000	0.0000	0.0000
ψ_1'	0.5661	0.5726	0.5790	0.5852	0.5912	0.5970	0.6027	0.6082	0.6136	0.6188

x/a \ q	1.5000	1.5200	1.5400	1.5600	1.5800	1.6000	1.6200	1.6400	1.6600	1.6800
0.	0.9322	0.9368	0.9412	0.9453	0.9491	0.9527	0.9561	0.9592	0.9622	0.9650
0.10	0.9241	0.9289	0.9334	0.9377	0.9417	0.9455	0.9491	0.9524	0.9556	0.9585
0.20	0.8994	0.9046	0.9096	0.9143	0.9188	0.9231	0.9272	0.9311	0.9348	0.9383
0.30	0.8566	0.8624	0.8680	0.8734	0.8785	0.8835	0.8883	0.8930	0.8974	0.9017
0.40	0.7939	0.8002	0.8064	0.8124	0.8182	0.8239	0.8294	0.8348	0.8400	0.8451
0.50	0.7097	0.7163	0.7227	0.7291	0.7353	0.7414	0.7474	0.7533	0.7591	0.7648
0.60	0.6032	0.6095	0.6158	0.6221	0.6282	0.6343	0.6403	0.6462	0.6521	0.6579
0.70	0.4752	0.4807	0.4863	0.4918	0.4972	0.5026	0.5080	0.5133	0.5187	0.5240
0.80	0.3285	0.3326	0.3368	0.3409	0.3450	0.3491	0.3532	0.3572	0.3613	0.3653
0.90	0.1679	0.1702	0.1724	0.1746	0.1768	0.1790	0.1812	0.1834	0.1856	0.1878
1.00	0.0000	0.0000	0.0000	0.0000	0.0000	0.0000	0.0000	0.0000	0.0000	0.0000
ψ_1'	0.6239	0.6288	0.6336	0.6383	0.6429	0.6474	0.6517	0.6560	0.6601	0.6642

x/a \ q	1.7000	1.7200	1.7400	1.7600	1.7800	1.8000	1.8200	1.8400	1.8600	1.8800
0.	0.9676	0.9700	0.9723	0.9744	0.9763	0.9782	0.9799	0.9815	0.9829	0.9843
0.10	0.9613	0.9640	0.9664	0.9687	0.9709	0.9729	0.9748	0.9766	0.9783	0.9798
0.20	0.9416	0.9448	0.9479	0.9507	0.9535	0.9560	0.9585	0.9608	0.9631	0.9652
0.30	0.9058	0.9098	0.9136	0.9173	0.9209	0.9243	0.9276	0.9308	0.9338	0.9367
0.40	0.8501	0.8549	0.8596	0.8642	0.8686	0.8730	0.8772	0.8813	0.8853	0.8891
0.50	0.7704	0.7758	0.7812	0.7865	0.7917	0.7968	0.8018	0.8067	0.8115	0.8162
0.60	0.6637	0.6693	0.6749	0.6805	0.6860	0.6914	0.6967	0.7020	0.7073	0.7124
0.70	0.5292	0.5344	0.5396	0.5447	0.5498	0.5549	0.5600	0.5650	0.5700	0.5749
0.80	0.3693	0.3734	0.3774	0.3814	0.3854	0.3893	0.3933	0.3972	0.4012	0.4051
0.90	0.1900	0.1922	0.1944	0.1966	0.1987	0.2009	0.2031	0.2053	0.2075	0.2097
1.00	0.0000	0.0000	0.0000	0.0000	0.0000	0.0000	0.0000	0.0000	0.0000	0.0000
ψ_1'	0.6681	0.6720	0.6758	0.6794	0.6830	0.6866	0.6900	0.6934	0.6967	0.6999

TABLE 6.0-1. (CONTINUED)

x/a \ q	1.9000	1.9200	1.9400	1.9600	1.9800	2.0000	2.0200	2.0400	2.0600	2.0800
0.	0.9856	0.9868	0.9878	0.9889	0.9898	0.9906	0.9914	0.9922	0.9928	0.9935
0.10	0.9813	0.9826	0.9839	0.9851	0.9862	0.9872	0.9882	0.9891	0.9899	0.9907
0.20	0.9672	0.9690	0.9708	0.9725	0.9741	0.9757	0.9771	0.9785	0.9798	0.9810
0.30	0.9395	0.9422	0.9448	0.9473	0.9497	0.9520	0.9543	0.9564	0.9584	0.9604
0.40	0.8929	0.8966	0.9001	0.9036	0.9070	0.9102	0.9134	0.9165	0.9195	0.9224
0.50	0.8208	0.8254	0.8298	0.8342	0.8385	0.8427	0.8468	0.8508	0.8548	0.8586
0.60	0.7175	0.7226	0.7275	0.7324	0.7373	0.7421	0.7468	0.7515	0.7561	0.7607
0.70	0.5798	0.5847	0.5895	0.5943	0.5991	0.6039	0.6086	0.6132	0.6179	0.6225
0.80	0.4090	0.4129	0.4168	0.4207	0.4245	0.4284	0.4322	0.4361	0.4399	0.4437
0.90	0.2118	0.2140	0.2162	0.2184	0.2205	0.2227	0.2249	0.2270	0.2292	0.2314
1.00	0.0000	0.0000	0.0000	0.0000	0.0000	0.0000	0.0000	0.0000	0.0000	0.0000
Ψ_1'	0.7031	0.7062	0.7092	0.7121	0.7151	0.7179	0.7207	0.7234	0.7261	0.7288

x/a \ q	2.1000	2.1200	2.1400	2.1600	2.1800	2.2000	2.2200	2.2400	2.2600	2.2800
0.	0.9940	0.9946	0.9951	0.9955	0.9959	0.9963	0.9966	0.9969	0.9972	0.9975
0.10	0.9914	0.9921	0.9927	0.9932	0.9938	0.9943	0.9947	0.9951	0.9955	0.9959
0.20	0.9821	0.9832	0.9842	0.9852	0.9861	0.9870	0.9878	0.9886	0.9893	0.9900
0.30	0.9623	0.9641	0.9658	0.9674	0.9690	0.9705	0.9720	0.9734	0.9747	0.9760
0.40	0.9252	0.9279	0.9306	0.9332	0.9356	0.9381	0.9404	0.9428	0.9448	0.9470
0.50	0.8624	0.8661	0.8698	0.8733	0.8768	0.8802	0.8835	0.8868	0.8900	0.8931
0.60	0.7651	0.7696	0.7739	0.7782	0.7825	0.7867	0.7908	0.7949	0.7989	0.8029
0.70	0.6270	0.6316	0.6361	0.6405	0.6450	0.6494	0.6537	0.6581	0.6624	0.6666
0.80	0.4475	0.4512	0.4550	0.4588	0.4625	0.4662	0.4699	0.4736	0.4773	0.4810
0.90	0.2335	0.2357	0.2378	0.2400	0.2421	0.2443	0.2464	0.2486	0.2507	0.2529
1.00	0.0000	0.0000	0.0000	0.0000	0.0000	0.0000	0.0000	0.0000	0.0000	0.0000
Ψ_1'	0.7313	0.7339	0.7364	0.7388	0.7412	0.7436	0.7459	0.7481	0.7504	0.7525

x/a \ q	2.3000	2.3200	2.3500	2.3600	2.3800	2.4000	2.4200	2.4400	2.4600	2.4800
0.	0.9977	0.9979	0.9981	0.9983	0.9985	0.9986	0.9988	0.9989	0.9990	0.9991
0.10	0.9962	0.9965	0.9968	0.9971	0.9973	0.9976	0.9978	0.9980	0.9981	0.9983
0.20	0.9906	0.9912	0.9918	0.9924	0.9929	0.9933	0.9938	0.9942	0.9946	0.9950
0.30	0.9772	0.9783	0.9795	0.9805	0.9815	0.9825	0.9834	0.9843	0.9851	0.9859
0.40	0.9490	0.9510	0.9529	0.9548	0.9566	0.9583	0.9600	0.9616	0.9631	0.9647
0.50	0.8961	0.8991	0.9020	0.9048	0.9076	0.9103	0.9130	0.9155	0.9180	0.9205
0.60	0.8068	0.8106	0.8144	0.8181	0.8218	0.8254	0.8290	0.8325	0.8360	0.8394
0.70	0.6708	0.6750	0.6792	0.6833	0.6874	0.6914	0.6954	0.6994	0.7034	0.7073
0.80	0.4847	0.4883	0.4919	0.4956	0.4992	0.5027	0.5063	0.5099	0.5134	0.5170
0.90	0.2550	0.2572	0.2593	0.2614	0.2636	0.2657	0.2678	0.2700	0.2721	0.2742
1.00	0.0000	0.0000	0.0000	0.0000	0.0000	0.0000	0.0000	0.0000	0.0000	0.0000
Ψ_1'	0.7547	0.7568	0.7589	0.7609	0.7629	0.7649	0.7669	0.7688	0.7707	0.7725

x/a \ q	2.5000	2.5200	2.5400	2.5600	2.5800	2.6000	2.6200	2.6400	2.6600	2.6800
0.	0.9992	0.9993	0.9993	0.9994	0.9995	0.9995	0.9996	0.9996	0.9997	0.9997
0.10	0.9984	0.9986	0.9987	0.9988	0.9989	0.9990	0.9991	0.9992	0.9993	0.9993
0.20	0.9953	0.9956	0.9959	0.9962	0.9965	0.9967	0.9970	0.9972	0.9974	0.9976
0.30	0.9867	0.9874	0.9881	0.9887	0.9894	0.9899	0.9905	0.9910	0.9915	0.9920
0.40	0.9661	0.9675	0.9689	0.9702	0.9714	0.9726	0.9738	0.9749	0.9760	0.9770
0.50	0.9229	0.9252	0.9275	0.9297	0.9319	0.9340	0.9361	0.9381	0.9400	0.9419
0.60	0.8427	0.8460	0.8492	0.8524	0.8556	0.8586	0.8617	0.8647	0.8676	0.8705
0.70	0.7112	0.7150	0.7188	0.7226	0.7263	0.7300	0.7337	0.7373	0.7409	0.7445
0.80	0.5205	0.5240	0.5275	0.5310	0.5344	0.5379	0.5413	0.5448	0.5482	0.5516
0.90	0.2763	0.2784	0.2806	0.2827	0.2848	0.2869	0.2890	0.2911	0.2932	0.2953
1.00	0.0000	0.0000	0.0000	0.0000	0.0000	0.0000	0.0000	0.0000	0.0000	0.0000
Ψ_1'	0.7743	0.7761	0.7779	0.7796	0.7813	0.7830	0.7847	0.7863	0.7879	0.7895

TABLE 6.0-1. (CONTINUED)

x/a \ q	2.7000	2.7200	2.7400	2.7600	2.7800	2.8000	2.8200	2.8400	2.8600	2.8800
0.	0.9997	0.9998	0.9998	0.9998	0.9998	0.9998	0.9999	0.9999	0.9999	0.9999
0.10	0.9994	0.9994	0.9995	0.9995	0.9996	0.9996	0.9997	0.9997	0.9997	0.9997
0.20	0.9977	0.9979	0.9981	0.9982	0.9983	0.9985	0.9986	0.9987	0.9988	0.9989
0.30	0.9925	0.9929	0.9933	0.9937	0.9941	0.9944	0.9948	0.9951	0.9954	0.9956
0.40	0.9780	0.9790	0.9799	0.9808	0.9817	0.9825	0.9833	0.9840	0.9848	0.9855
0.50	0.9438	0.9456	0.9473	0.9490	0.9507	0.9523	0.9539	0.9554	0.9569	0.9583
0.60	0.8733	0.8761	0.8789	0.8815	0.8842	0.8868	0.8893	0.8918	0.8943	0.8967
0.70	0.7480	0.7515	0.7550	0.7584	0.7618	0.7651	0.7685	0.7718	0.7750	0.7782
0.80	0.5549	0.5583	0.5617	0.5650	0.5683	0.5716	0.5749	0.5782	0.5814	0.5847
0.90	0.2974	0.2995	0.3016	0.3037	0.3058	0.3079	0.3100	0.3120	0.3141	0.3162
1.00	0.0000	0.0000	0.0000	0.0000	0.0000	0.0000	0.0000	0.0000	0.0000	0.0000
Ψ_1'	0.7910	0.7926	0.7941	0.7956	0.7971	0.7985	0.7999	0.8013	0.8027	0.8041

x/a \ q	2.9000	2.9200	2.9400	2.9600	2.9800	3.0000	3.0200	3.0400	3.0600	3.0800
0.	0.9999	0.9999	0.9999	0.9999	0.9999	1.0000	1.0000	1.0000	1.0000	1.0000
0.10	0.9998	0.9998	0.9998	0.9998	0.9998	0.9999	0.9999	0.9999	0.9999	0.9999
0.20	0.9990	0.9990	0.9991	0.9992	0.9993	0.9993	0.9994	0.9994	0.9995	0.9995
0.30	0.9959	0.9962	0.9964	0.9966	0.9968	0.9970	0.9972	0.9974	0.9975	0.9977
0.40	0.9861	0.9868	0.9874	0.9880	0.9885	0.9891	0.9896	0.9901	0.9906	0.9910
0.50	0.9597	0.9611	0.9624	0.9637	0.9649	0.9661	0.9673	0.9684	0.9695	0.9706
0.60	0.8991	0.9014	0.9037	0.9060	0.9082	0.9103	0.9124	0.9145	0.9165	0.9185
0.70	0.7814	0.7846	0.7877	0.7908	0.7939	0.7969	0.7999	0.8029	0.8058	0.8087
0.80	0.5879	0.5911	0.5943	0.5975	0.6007	0.6039	0.6070	0.6101	0.6132	0.6163
0.90	0.3183	0.3204	0.3224	0.3245	0.3266	0.3286	0.3307	0.3327	0.3348	0.3369
1.00	0.0000	0.0000	0.0000	0.0000	0.0000	0.0000	0.0000	0.0000	0.0000	0.0000
Ψ_1'	0.8055	0.8068	0.8081	0.8094	0.8107	0.8119	0.8132	0.8144	0.8156	0.8168

x/a \ q	3.1000	3.2000	3.3000	3.4000	3.5000	3.6000	3.7000	3.8000	3.9000	4.0000
0.	1.0000	1.0000	1.0000	1.0000	1.0000	1.0000	1.0000	1.0000	1.0000	1.0000
0.10	0.9999	1.0000	1.0000	1.0000	1.0000	1.0000	1.0000	1.0000	1.0000	1.0000
0.20	0.9995	0.9997	0.9998	0.9999	0.9999	1.0000	1.0000	1.0000	1.0000	1.0000
0.30	0.9979	0.9985	0.9989	0.9992	0.9995	0.9996	0.9998	0.9998	0.9999	0.9999
0.40	0.9915	0.9934	0.9949	0.9961	0.9970	0.9977	0.9983	0.9987	0.9991	0.9993
0.50	0.9716	0.9763	0.9804	0.9838	0.9867	0.9891	0.9911	0.9928	0.9942	0.9953
0.60	0.9205	0.9297	0.9381	0.9456	0.9523	0.9583	0.9637	0.9684	0.9726	0.9763
0.70	0.8116	0.8254	0.8385	0.8508	0.8624	0.8733	0.8835	0.8931	0.9020	0.9103
0.80	0.6194	0.6346	0.6494	0.6638	0.6778	0.6914	0.7047	0.7175	0.7300	0.7421
0.90	0.3389	0.3491	0.3593	0.3694	0.3794	0.3893	0.3992	0.4090	0.4187	0.4284
1.00	0.0000	0.0000	0.0000	0.0000	0.0000	0.0000	0.0000	0.0000	0.0000	0.0000
Ψ_1'	0.8180	0.8237	0.8290	0.8341	0.8388	0.8433	0.8475	0.8515	0.8553	0.8590

x/a \ q	4.1000	4.2000	4.3000	4.4000	4.5000	4.6000	4.7000	4.8000	4.9000	5.0000
0.	1.0000	1.0000	1.0000	1.0000	1.0000	1.0000	1.0000	1.0000	1.0000	1.0000
0.10	1.0000	1.0000	1.0000	1.0000	1.0000	1.0000	1.0000	1.0000	1.0000	1.0000
0.20	1.0000	1.0000	1.0000	1.0000	1.0000	1.0000	1.0000	1.0000	1.0000	1.0000
0.30	1.0000	1.0000	1.0000	1.0000	1.0000	1.0000	1.0000	1.0000	1.0000	1.0000
0.40	0.9995	0.9996	0.9997	0.9998	0.9999	0.9999	0.9999	1.0000	1.0000	1.0000
0.50	0.9963	0.9970	0.9976	0.9981	0.9985	0.9989	0.9991	0.9993	0.9995	0.9996
0.60	0.9796	0.9825	0.9850	0.9872	0.9891	0.9907	0.9922	0.9934	0.9944	0.9953
0.70	0.9181	0.9252	0.9319	0.9381	0.9438	0.9490	0.9539	0.9583	0.9624	0.9661
0.80	0.7538	0.7651	0.7761	0.7867	0.7969	0.8068	0.8163	0.8254	0.8342	0.8427
0.90	0.4380	0.4475	0.4569	0.4662	0.4755	0.4847	0.4937	0.5028	0.5117	0.5205
1.00	0.0000	0.0000	0.0000	0.0000	0.0000	0.0000	0.0000	0.0000	0.0000	0.0000
Ψ_1'	0.8624	0.8657	0.8688	0.8718	0.8746	0.8774	0.8800	0.8825	0.8849	0.8872

TABLE 6.0-1. (CONTINUED)

x/a \ q	5.1000	5.2000	5.3000	5.4000	5.5000	5.6000	5.7000	5.8000	5.9000	6.0000
0.	1.0000	1.0000	1.0000	1.0000	1.0000	1.0000	1.0000	1.0000	1.0000	1.0000
0.10	1.0000	1.0000	1.0000	1.0000	1.0000	1.0000	1.0000	1.0000	1.0000	1.0000
0.20	1.0000	1.0000	1.0000	1.0000	1.0000	1.0000	1.0000	1.0000	1.0000	1.0000
0.30	1.0000	1.0000	1.0000	1.0000	1.0000	1.0000	1.0000	1.0000	1.0000	1.0000
0.40	1.0000	1.0000	1.0000	1.0000	1.0000	1.0000	1.0000	1.0000	1.0000	1.0000
0.50	0.9997	0.9998	0.9998	0.9999	0.9999	0.9999	0.9999	1.0000	1.0000	1.0000
0.60	0.9961	0.9967	0.9973	0.9977	0.9981	0.9985	0.9987	0.9990	0.9992	0.9993
0.70	0.9695	0.9726	0.9755	0.9780	0.9804	0.9825	0.9844	0.9861	0.9877	0.9891
0.80	0.8508	0.8587	0.8661	0.8733	0.8802	0.8868	0.8931	0.8991	0.9048	0.9103
0.90	0.5292	0.5379	0.5465	0.5549	0.5633	0.5716	0.5798	0.5879	0.5959	0.6039
1.00	0.0000	0.0000	0.0000	0.0000	0.0000	0.0000	0.0000	0.0000	0.0000	0.0000
Ψ_1'	0.8894	0.8915	0.8935	0.8955	0.8974	0.8993	0.9010	0.9027	0.9044	0.9060

x/a \ q	6.1000	6.2000	6.3000	6.4000	6.5000	6.6000	6.7000	6.8000	6.9000	7.0000
0.	1.0000	1.0000	1.0000	1.0000	1.0000	1.0000	1.0000	1.0000	1.0000	1.0000
0.10	1.0000	1.0000	1.0000	1.0000	1.0000	1.0000	1.0000	1.0000	1.0000	1.0000
0.20	1.0000	1.0000	1.0000	1.0000	1.0000	1.0000	1.0000	1.0000	1.0000	1.0000
0.30	1.0000	1.0000	1.0000	1.0000	1.0000	1.0000	1.0000	1.0000	1.0000	1.0000
0.40	1.0000	1.0000	1.0000	1.0000	1.0000	1.0000	1.0000	1.0000	1.0000	1.0000
0.50	1.0000	1.0000	1.0000	1.0000	1.0000	1.0000	1.0000	1.0000	1.0000	1.0000
0.60	0.9994	0.9995	0.9996	0.9997	0.9998	0.9998	0.9998	0.9999	0.9999	0.9999
0.70	0.9903	0.9915	0.9925	0.9934	0.9942	0.9949	0.9955	0.9961	0.9966	0.9970
0.80	0.9155	0.9205	0.9252	0.9297	0.9340	0.9381	0.9419	0.9456	0.9490	0.9523
0.90	0.6117	0.6194	0.6270	0.6346	0.6420	0.6494	0.6566	0.6638	0.6708	0.6778
1.00	0.0000	0.0000	0.0000	0.0000	0.0000	0.0000	0.0000	0.0000	0.0000	0.0000
Ψ_1'	0.9075	0.9090	0.9104	0.9118	0.9132	0.9145	0.9158	0.9170	0.9182	0.9194

x/a \ q	7.1000	7.2000	7.3000	7.4000	7.5000	7.6000	7.7000	7.8000	7.9000	8.0000
0.	1.0000	1.0000	1.0000	1.0000	1.0000	1.0000	1.0000	1.0000	1.0000	1.0000
0.10	1.0000	1.0000	1.0000	1.0000	1.0000	1.0000	1.0000	1.0000	1.0000	1.0000
0.20	1.0000	1.0000	1.0000	1.0000	1.0000	1.0000	1.0000	1.0000	1.0000	1.0000
0.30	1.0000	1.0000	1.0000	1.0000	1.0000	1.0000	1.0000	1.0000	1.0000	1.0000
0.40	1.0000	1.0000	1.0000	1.0000	1.0000	1.0000	1.0000	1.0000	1.0000	1.0000
0.50	1.0000	1.0000	1.0000	1.0000	1.0000	1.0000	1.0000	1.0000	1.0000	1.0000
0.60	0.9999	1.0000	1.0000	1.0000	1.0000	1.0000	1.0000	1.0000	1.0000	1.0000
0.70	0.9974	0.9977	0.9980	0.9983	0.9985	0.9987	0.9989	0.9991	0.9992	0.9993
0.80	0.9554	0.9583	0.9611	0.9637	0.9661	0.9684	0.9706	0.9726	0.9745	0.9763
0.90	0.6847	0.6914	0.6981	0.7047	0.7112	0.7175	0.7238	0.7300	0.7361	0.7421
1.00	0.0000	0.0000	0.0000	0.0000	0.0000	0.0000	0.0000	0.0000	0.0000	0.0000
Ψ_1'	0.9205	0.9216	0.9227	0.9238	0.9248	0.9258	0.9267	0.9277	0.9286	0.9295

x/a \ q	8.1000	8.2000	8.3000	8.4000	8.5000	8.6000	8.7000	8.8000	8.9000	9.0000
0.	1.0000	1.0000	1.0000	1.0000	1.0000	1.0000	1.0000	1.0000	1.0000	1.0000
0.10	1.0000	1.0000	1.0000	1.0000	1.0000	1.0000	1.0000	1.0000	1.0000	1.0000
0.20	1.0000	1.0000	1.0000	1.0000	1.0000	1.0000	1.0000	1.0000	1.0000	1.0000
0.30	1.0000	1.0000	1.0000	1.0000	1.0000	1.0000	1.0000	1.0000	1.0000	1.0000
0.40	1.0000	1.0000	1.0000	1.0000	1.0000	1.0000	1.0000	1.0000	1.0000	1.0000
0.50	1.0000	1.0000	1.0000	1.0000	1.0000	1.0000	1.0000	1.0000	1.0000	1.0000
0.60	1.0000	1.0000	1.0000	1.0000	1.0000	1.0000	1.0000	1.0000	1.0000	1.0000
0.70	0.9994	0.9995	0.9996	0.9996	0.9997	0.9997	0.9998	0.9998	0.9998	0.9999
0.80	0.9780	0.9796	0.9811	0.9825	0.9838	0.9850	0.9861	0.9872	0.9882	0.9891
0.90	0.7480	0.7538	0.7595	0.7651	0.7707	0.7761	0.7814	0.7867	0.7918	0.7969
1.00	0.0000	0.0000	0.0000	0.0000	0.0000	0.0000	0.0000	0.0000	0.0000	0.0000
Ψ_1'	0.9303	0.9312	0.9320	0.9328	0.9336	0.9344	0.9351	0.9359	0.9366	0.9373

TABLE 6.0-1. (CONCLUDED)

q x/a	9.1000	9.2000	9.3000	9.4000	9.5000	9.6000	9.7000	9.8000	9.9000	10.0000
0.	1.0000	1.0000	1.0000	1.0000	1.0000	1.0000	1.0000	1.0000	1.0000	1.0000
0.10	1.0000	1.0000	1.0000	1.0000	1.0000	1.0000	1.0000	1.0000	1.0000	1.0000
0.20	1.0000	1.0000	1.0000	1.0000	1.0000	1.0000	1.0000	1.0000	1.0000	1.0000
0.30	1.0000	1.0000	1.0000	1.0000	1.0000	1.0000	1.0000	1.0000	1.0000	1.0000
0.40	1.0000	1.0000	1.0000	1.0000	1.0000	1.0000	1.0000	1.0000	1.0000	1.0000
0.50	1.0000	1.0000	1.0000	1.0000	1.0000	1.0000	1.0000	1.0000	1.0000	1.0000
0.60	1.0000	1.0000	1.0000	1.0000	1.0000	1.0000	1.0000	1.0000	1.0000	1.0000
0.70	0.9999	0.9999	0.9999	0.9999	0.9999	1.0000	1.0000	1.0000	1.0000	1.0000
0.80	0.9899	0.9907	0.9915	0.9922	0.9928	0.9934	0.9939	0.9944	0.9949	0.9953
0.90	0.8019	0.8068	0.8116	0.8163	0.8209	0.8254	0.8299	0.8342	0.8385	0.8427
1.00	0.0000	0.0000	0.0000	0.0000	0.0000	0.0000	0.0000	0.0000	0.0000	0.0000
¥1	0.9380	0.9387	0.9393	0.9400	0.9406	0.9412	0.9418	0.9424	0.9430	0.9436

q x/a	10.1000	10.2000	10.3000	10.4000	10.5000	10.6000	10.7000	10.8000	10.9000	11.0000
0.	1.0000	1.0000	1.0000	1.0000	1.0000	1.0000	1.0000	1.0000	1.0000	1.0000
0.10	1.0000	1.0000	1.0000	1.0000	1.0000	1.0000	1.0000	1.0000	1.0000	1.0000
0.20	1.0000	1.0000	1.0000	1.0000	1.0000	1.0000	1.0000	1.0000	1.0000	1.0000
0.30	1.0000	1.0000	1.0000	1.0000	1.0000	1.0000	1.0000	1.0000	1.0000	1.0000
0.40	1.0000	1.0000	1.0000	1.0000	1.0000	1.0000	1.0000	1.0000	1.0000	1.0000
0.50	1.0000	1.0000	1.0000	1.0000	1.0000	1.0000	1.0000	1.0000	1.0000	1.0000
0.60	1.0000	1.0000	1.0000	1.0000	1.0000	1.0000	1.0000	1.0000	1.0000	1.0000
0.70	1.0000	1.0000	1.0000	1.0000	1.0000	1.0000	1.0000	1.0000	1.0000	1.0000
0.80	0.9957	0.9961	0.9964	0.9967	0.9970	0.9973	0.9975	0.9977	0.9979	0.9981
0.90	0.8468	0.8508	0.8548	0.8586	0.8624	0.8661	0.8698	0.8733	0.8768	0.8802
1.00	0.0000	0.0000	0.0000	0.0000	0.0000	0.0000	0.0000	0.0000	0.0000	0.0000
¥1	0.9441	0.9447	0.9452	0.9457	0.9463	0.9468	0.9473	0.9478	0.9482	0.9487

TABLE 6.0-2. CYLINDER-PARAMETER ϕ_2

β \ q	0.4000	0.4200	0.4400	0.4600	0.4800	0.5000	0.5200	0.5400	0.5600	0.5800
0.	0.0002	0.0004	0.0009	0.0017	0.0030	0.0049	0.0076	0.0113	0.0159	0.0218
0.10	0.0002	0.0004	0.0009	0.0017	0.0030	0.0049	0.0075	0.0111	0.0157	0.0215
0.20	0.0002	0.0004	0.0009	0.0016	0.0028	0.0047	0.0072	0.0106	0.0150	0.0205
0.30	0.0002	0.0004	0.0008	0.0015	0.0026	0.0043	0.0067	0.0098	0.0139	0.0190
0.40	0.0001	0.0003	0.0007	0.0013	0.0024	0.0039	0.0060	0.0088	0.0125	0.0170
0.50	0.0001	0.0003	0.0006	0.0012	0.0020	0.0033	0.0051	0.0075	0.0107	0.0146
0.60	0.0001	0.0002	0.0005	0.0009	0.0016	0.0027	0.0041	0.0061	0.0087	0.0118
0.70	0.0001	0.0002	0.0004	0.0007	0.0012	0.0020	0.0031	0.0046	0.0065	0.0089
0.80	0.0001	0.0001	0.0002	0.0005	0.0008	0.0013	0.0020	0.0030	0.0043	0.0058
0.90	0.0000	0.0001	0.0001	0.0002	0.0004	0.0006	0.0010	0.0015	0.0021	0.0028
1.00	0.0000	0.0000	0.0000	0.0000	0.0000	0.0000	0.0000	0.0000	0.0000	0.0000

β \ q	0.6000	0.6200	0.6400	0.6600	0.6800	0.7000	0.7200	0.7400	0.7600	0.7800
0.	0.0289	0.0373	0.0470	0.0580	0.0703	0.0838	0.0985	0.1143	0.1311	0.1488
0.10	0.0285	0.0367	0.0463	0.0571	0.0693	0.0826	0.0971	0.1126	0.1292	0.1467
0.20	0.0272	0.0351	0.0443	0.0547	0.0663	0.0790	0.0929	0.1078	0.1236	0.1403
0.30	0.0252	0.0326	0.0410	0.0507	0.0614	0.0732	0.0861	0.0999	0.1148	0.1301
0.40	0.0226	0.0291	0.0367	0.0453	0.0549	0.0655	0.0770	0.0893	0.1025	0.1163
0.50	0.0193	0.0250	0.0315	0.0388	0.0471	0.0561	0.0660	0.0766	0.0878	0.0997
0.60	0.0157	0.0202	0.0255	0.0315	0.0382	0.0455	0.0535	0.0621	0.0712	0.0809
0.70	0.0118	0.0152	0.0191	0.0236	0.0286	0.0342	0.0401	0.0466	0.0534	0.0606
0.80	0.0077	0.0100	0.0126	0.0155	0.0188	0.0225	0.0264	0.0306	0.0351	0.0399
0.90	0.0038	0.0049	0.0061	0.0076	0.0092	0.0109	0.0128	0.0149	0.0171	0.0194
1.00	0.0000	0.0000	0.0000	0.0000	0.0000	0.0000	0.0000	0.0000	0.0000	0.0000

β \ q	0.8000	0.8200	0.8400	0.8600	0.8800	0.9000	0.9200	0.9400	0.9600	0.9800
0.	0.1673	0.1866	0.2064	0.2268	0.2476	0.2687	0.2901	0.3117	0.3334	0.3551
0.10	0.1649	0.1839	0.2034	0.2235	0.2440	0.2649	0.2860	0.3072	0.3286	0.3500
0.20	0.1578	0.1759	0.1947	0.2139	0.2335	0.2534	0.2736	0.2940	0.3145	0.3350
0.30	0.1463	0.1631	0.1804	0.1983	0.2164	0.2349	0.2537	0.2725	0.2915	0.3106
0.40	0.1308	0.1458	0.1614	0.1773	0.1936	0.2101	0.2269	0.2438	0.2608	0.2779
0.50	0.1121	0.1250	0.1383	0.1520	0.1659	0.1801	0.1945	0.2090	0.2236	0.2382
0.60	0.0909	0.1014	0.1122	0.1233	0.1346	0.1461	0.1578	0.1696	0.1814	0.1933
0.70	0.0682	0.0760	0.0841	0.0924	0.1010	0.1096	0.1184	0.1272	0.1361	0.1451
0.80	0.0448	0.0500	0.0553	0.0608	0.0664	0.0721	0.0778	0.0836	0.0895	0.0954
0.90	0.0218	0.0243	0.0269	0.0295	0.0323	0.0350	0.0378	0.0407	0.0435	0.0464
1.00	0.0000	0.0000	0.0000	0.0000	0.0000	0.0000	0.0000	0.0000	0.0000	0.0000

β \ q	1.0000	1.0200	1.0400	1.0600	1.0800	1.1000	1.1200	1.1400	1.1600	1.1800
0.	0.3768	0.3984	0.4199	0.4412	0.4622	0.4830	0.5035	0.5236	0.5433	0.5627
0.10	0.3714	0.3927	0.4139	0.4349	0.4557	0.4762	0.4964	0.5162	0.5357	0.5548
0.20	0.3555	0.3759	0.3962	0.4163	0.4362	0.4559	0.4753	0.4944	0.5132	0.5316
0.30	0.3296	0.3486	0.3674	0.3862	0.4047	0.4231	0.4412	0.4590	0.4766	0.4938
0.40	0.2949	0.3119	0.3289	0.3457	0.3624	0.3789	0.3952	0.4114	0.4272	0.4429
0.50	0.2529	0.2675	0.2821	0.2966	0.3110	0.3252	0.3394	0.3533	0.3671	0.3807
0.60	0.2053	0.2172	0.2290	0.2408	0.2526	0.2642	0.2758	0.2872	0.2986	0.3098
0.70	0.1540	0.1630	0.1719	0.1808	0.1897	0.1985	0.2072	0.2159	0.2245	0.2330
0.80	0.1013	0.1072	0.1131	0.1190	0.1248	0.1306	0.1364	0.1421	0.1478	0.1535
0.90	0.0493	0.0521	0.0550	0.0579	0.0607	0.0636	0.0664	0.0692	0.0720	0.0747
1.00	0.0000	0.0000	0.0000	0.0000	0.0000	0.0000	0.0000	0.0000	0.0000	0.0000

TABLE 6.0-2. (CONTINUED)

β \ q	1.2000	1.2200	1.2400	1.2600	1.2800	1.300	1.3200	1.3400	1.3600	1.3800
0.	0.5816	0.6001	0.6181	0.6356	0.6527	0.6692	0.6853	0.7008	0.7158	0.7303
0.10	0.5735	0.5918	0.6096	0.6270	0.6439	0.6603	0.6762	0.6916	0.7066	0.7210
0.20	0.5497	0.5673	0.5845	0.6014	0.6178	0.6337	0.6492	0.6643	0.6789	0.6931
0.30	0.5108	0.5274	0.5436	0.5595	0.5751	0.5902	0.6050	0.6194	0.6335	0.6471
0.40	0.4583	0.4734	0.4882	0.5028	0.5171	0.5311	0.5448	0.5582	0.5713	0.5841
0.50	0.3941	0.4073	0.4204	0.4332	0.4458	0.4582	0.4703	0.4823	0.4941	0.5056
0.60	0.3208	0.3318	0.3426	0.3532	0.3638	0.3741	0.3844	0.3945	0.4044	0.4142
0.70	0.2414	0.2497	0.2580	0.2662	0.2743	0.2823	0.2902	0.2980	0.3058	0.3135
0.80	0.1591	0.1647	0.1702	0.1756	0.1811	0.1864	0.1918	0.1971	0.2023	0.2075
0.90	0.0775	0.0802	0.0829	0.0856	0.0883	0.0909	0.0935	0.0962	0.0988	0.1013
1.00	0.0000	0.0000	0.0000	0.0000	0.0000	0.0000	0.0000	0.0000	0.0000	0.0000

β \ q	1.4000	1.4200	1.4400	1.4600	1.4800	1.500	1.5200	1.5400	1.5600	1.5800
0.	0.7443	0.7578	0.7708	0.7833	0.7952	0.8067	0.8177	0.8282	0.8382	0.84700
0.10	0.7349	0.7484	0.7613	0.7738	0.7857	0.7972	0.8082	0.8188	0.8289	0.83868
0.20	0.7068	0.7201	0.7329	0.7453	0.7572	0.7687	0.7798	0.7905	0.8007	0.8106
0.30	0.6604	0.6733	0.6858	0.6980	0.7097	0.7212	0.7322	0.7429	0.7533	0.7633
0.40	0.5966	0.6088	0.6207	0.6323	0.6437	0.6547	0.6655	0.6760	0.6863	0.6962
0.50	0.5169	0.5280	0.5389	0.5496	0.5601	0.5704	0.5805	0.5905	0.6002	0.6097
0.60	0.4239	0.4335	0.4429	0.4522	0.4613	0.4704	0.4793	0.4881	0.4967	0.5053
0.70	0.3210	0.3286	0.3360	0.3434	0.3507	0.3579	0.3651	0.3722	0.3793	0.3862
0.80	0.2127	0.2178	C.2229	0.2280	0.2330	0.2380	0.2430	0.2480	0.2529	0.2578
0.90	0.1039	0.1065	0.1090	0.1116	0.1141	0.1166	0.1191	0.1216	0.1240	0.1265
1.00	0.0000	0.0000	0.0000	0.0000	0.0000	0.0000	0.0000	0.0000	0.0000	0.0000

β \ q	1.6000	1.6200	1.6400	1.6600	1.6800	1.700	1.7200	1.7400	1.7600	1.7800
0.	0.8570	0.8657	0.8740	0.8818	0.8893	0.8964	0.9031	0.9095	0.9155	0.9212
0.10	0.8478	0.8566	0.8650	0.8730	0.8806	0.8879	0.8947	0.9013	0.9075	0.9133
0.20	0.8200	0.8291	0.8378	0.8461	0.8541	0.8617	0.8690	0.8760	0.8827	0.8890
0.30	0.7730	0.7823	0.7914	0.8001	0.8085	0.8166	0.8244	0.8320	0.8393	0.8463
0.40	0.7060	0.7154	0.7248	0.7336	0.7423	0.7508	0.7590	0.7670	0.7748	0.7824
0.50	0.6191	0.6282	0.6372	0.6460	0.6547	0.6631	0.6714	0.6796	0.6876	0.6954
0.60	0.5137	0.5220	0.5302	0.5383	0.5463	0.5542	0.5620	0.5697	0.5772	0.5847
0.70	0.3931	0.4000	0.4068	0.4135	0.4202	0.4268	0.4334	0.4399	0.4464	0.4528
0.80	0.2626	0.2674	0.2723	0.2770	0.2818	0.2865	0.2913	0.2960	0.3006	0.3053
0.90	0.1290	0.1314	0.1339	0.1363	0.1387	0.1412	0.1436	0.1460	0.1484	0.1508
1.00	0.0000	0.0000	0.0000	0.0000	0.0000	0.0000	0.0000	0.0000	0.0000	0.0000

β \ q	1.8000	1.8200	1.8400	1.8600	1.8800	1.9000	1.9200	1.9400	1.9600	1.9800
0.	0.9265	0.9316	0.9363	0.9408	0.9450	0.9489	0.9527	0.9561	0.9594	0.9624
0.10	0.9189	0.9241	0.9291	0.9337	0.9381	0.9423	0.9462	0.9499	0.9534	0.9566
0.20	0.8951	0.9008	0.9063	0.9116	0.9166	0.9213	0.9258	0.9301	0.9341	0.9380
0.30	0.8530	0.8595	0.8657	0.8717	0.8775	0.8830	0.8884	0.8935	0.8984	0.9031
0.40	0.7898	0.7969	0.8039	0.8106	0.8172	0.8236	0.8297	0.8357	0.8416	0.8472
0.50	0.7030	0.7105	0.7179	0.7251	0.7322	0.7391	0.7458	0.7525	0.7590	0.7653
0.60	0.5921	0.5994	0.6066	0.6136	0.6206	0.6275	0.6343	0.6410	0.6476	0.6542
0.70	0.4592	0.4655	0.4717	0.4779	0.4841	0.4902	0.4963	0.5023	0.5082	0.5141
0.80	0.3099	0.3145	0.3191	0.3237	0.3282	0.3328	0.3373	0.3418	0.3463	0.3507
0.90	0.1532	0.1556	0.1580	0.1604	0.1628	0.1651	0.1675	0.1699	0.1722	0.1746
1.00	0.0000	0.0000	0.0000	0.0000	0.0000	0.0000	0.0000	0.0000	0.0000	0.0000

C-4

TABLE 6.0-2. (CONTINUED)

q / β	2.0000	2.0200	2.0400	2.0600	2.0800	2.1000	2.1200	2.1400	2.1600	2.1800
0.	0.9653	0.9679	0.9704	0.9727	0.9748	0.9768	0.9787	0.9804	0.9820	0.9835
0.10	0.9597	0.9625	0.9652	0.9677	0.9701	0.9723	0.9743	0.9762	0.9780	0.9797
0.20	0.9416	0.9451	0.9484	0.9515	0.9544	0.9572	0.9598	0.9623	0.9646	0.9669
0.30	0.9077	0.9120	0.9162	0.9202	0.9240	0.9276	0.9311	0.9345	0.9377	0.9408
0.40	0.8527	0.8580	0.8632	0.8682	0.8730	0.8777	0.8822	0.8866	0.8909	0.8950
0.50	0.7716	0.7776	0.7836	0.7894	0.7951	0.8007	0.8062	0.8115	0.8167	0.8218
0.60	0.6606	0.6669	0.6732	0.6794	0.6854	0.6914	0.6973	0.7032	0.7089	0.7146
0.70	0.5200	0.5258	0.5316	0.5373	0.5430	0.5486	0.5542	0.5597	0.5652	0.5707
0.80	0.3552	0.3596	0.3640	0.3684	0.3728	0.3771	0.3815	0.3858	0.3901	0.3944
0.90	0.1769	0.1793	0.1816	0.1840	0.1863	0.1887	0.1910	0.1933	0.1956	0.1980
1.00	0.0000	0.0000	0.0000	0.0000	0.0000	0.0000	0.0000	0.0000	0.0000	0.0000

q / β	2.2000	2.2200	2.2400	2.2600	2.2800	2.3000	2.3200	2.3400	2.3600	2.3800
0.	0.9849	0.9861	0.9873	0.9884	0.9894	0.9903	0.9912	0.9920	0.9927	0.9933
0.10	0.9812	0.9827	0.9840	0.9853	0.9864	0.9875	0.9885	0.9894	0.9903	0.9911
0.20	0.9690	0.9709	0.9728	0.9745	0.9762	0.9777	0.9792	0.9805	0.9818	0.9830
0.30	0.9437	0.9466	0.9492	0.9518	0.9543	0.9566	0.9588	0.9610	0.9630	0.9650
0.40	0.8990	0.9029	0.9066	0.9102	0.9137	0.9171	0.9204	0.9235	0.9266	0.9295
0.50	0.8268	0.8317	0.8365	0.8411	0.8457	0.8501	0.8544	0.8587	0.8628	0.8669
0.60	0.7202	0.7256	0.7311	0.7364	0.7416	0.7468	0.7519	0.7569	0.7619	0.7667
0.70	0.5760	0.5814	0.5867	0.5920	0.5972	0.6023	0.6075	0.6125	0.6176	0.6226
0.80	0.3986	0.4029	0.4071	0.4113	0.4155	0.4197	0.4239	0.4280	0.4321	0.4362
0.90	0.2003	0.2026	0.2049	0.2072	0.2095	0.2118	0.2141	0.2164	0.2187	0.2210
1.00	0.0000	0.0000	0.0000	0.0000	0.0000	0.0000	0.0000	0.0000	0.0000	0.0000

q / β	2.4000	2.4200	2.4400	2.4600	2.4800	2.5000	2.5200	2.5400	2.5600	2.5800
0.	0.9939	0.9945	0.9950	0.9955	0.9959	0.9963	0.9966	0.9970	0.9972	0.9975
0.10	0.9918	0.9925	0.9931	0.9937	0.9942	0.9947	0.9952	0.9956	0.9960	0.9963
0.20	0.9842	0.9853	0.9863	0.9872	0.9881	0.9889	0.9897	0.9904	0.9911	0.9917
0.30	0.9668	0.9686	0.9703	0.9718	0.9734	0.9748	0.9762	0.9775	0.9787	0.9799
0.40	0.9324	0.9351	0.9377	0.9403	0.9428	0.9451	0.9474	0.9496	0.9517	0.9538
0.50	0.8708	0.8746	0.8784	0.8820	0.8856	0.8891	0.8925	0.8958	0.8990	0.9021
0.60	0.7715	0.7762	0.7809	0.7854	0.7899	0.7943	0.7987	0.8029	0.8072	0.8113
0.70	0.6275	0.6324	0.6373	0.6421	0.6468	0.6515	0.6562	0.6608	0.6654	0.6700
0.80	0.4403	0.4444	0.4485	0.4525	0.4565	0.4605	0.4645	0.4685	0.4724	0.4764
0.90	0.2233	0.2256	0.2279	0.2301	0.2324	0.2347	0.2370	0.2392	0.2415	0.2437
1.00	0.0000	0.0000	0.0000	0.0000	0.0000	0.0000	0.0000	0.0000	0.0000	0.0000

q / β	2.6000	2.6200	2.6400	2.6600	2.6800	2.7000	2.7200	2.7400	2.7600	2.7800
0.	0.9978	0.9980	0.9982	0.9984	0.9985	0.9987	0.9988	0.9989	0.9991	0.9992
0.10	0.9967	0.9970	0.9972	0.9975	0.9977	0.9979	0.9981	0.9983	0.9984	0.9986
0.20	0.9923	0.9928	0.9934	0.9938	0.9943	0.9947	0.9951	0.9955	0.9958	0.9961
0.30	0.9810	0.9821	0.9831	0.9841	0.9850	0.9859	0.9867	0.9875	0.9882	0.9889
0.40	0.9558	0.9577	0.9595	0.9613	0.9629	0.9646	0.9661	0.9676	0.9691	0.9705
0.50	0.9052	0.9082	0.9111	0.9139	0.9166	0.9193	0.9219	0.9244	0.9269	0.9293
0.60	0.8154	0.8193	0.8233	0.8271	0.8309	0.8346	0.8383	0.8419	0.8454	0.8489
0.70	0.6745	0.6789	0.6833	0.6877	0.6920	0.6963	0.7006	0.7048	0.7089	0.7131
0.80	0.4803	0.4842	0.4881	0.4919	0.4958	0.4996	0.5034	0.5072	0.5110	0.5148
0.90	0.2460	0.2483	0.2505	0.2528	0.2550	0.2572	0.2595	0.2617	0.2639	0.2662
1.00	0.0000	0.0000	0.0000	0.0000	0.0000	0.0000	0.0000	0.0000	0.0000	0.0000

TABLE 6.0-2. (CONTINUED)

q β	2.8000	2.8200	2.8400	2.8600	2.8800	2.9000	2.9200	2.9400	2.9600	2.9800
0.	0.9993	0.9993	0.9994	0.9995	0.9995	0.9996	0.9996	0.9997	0.9997	0.9997
0.10	0.9987	0.9988	0.9990	0.9991	0.9991	0.9992	0.9993	0.9994	0.9994	0.9995
0.20	0.9964	0.9967	0.9969	0.9972	0.9974	0.9976	0.9978	0.9979	0.9981	0.9983
0.30	0.9895	0.9902	0.9908	0.9913	0.9918	0.9923	0.9928	0.9932	0.9937	0.9941
0.40	0.9718	0.9731	0.9743	0.9755	0.9766	0.9777	0.9787	0.9797	0.9807	0.9816
0.50	0.9316	0.9338	0.9360	0.9382	0.9402	0.9423	0.9442	0.9461	0.9480	0.9497
0.60	0.8523	0.8557	0.8589	0.8622	0.8653	0.8684	0.8715	0.8745	0.8774	0.8803
0.70	0.7171	0.7212	0.7251	0.7291	0.7330	0.7369	0.7407	0.7445	0.7482	0.7519
0.80	0.5185	0.5223	0.5260	0.5297	0.5333	0.5370	0.5406	0.5442	0.5478	0.5514
0.90	0.2684	0.2706	0.2728	0.2751	0.2773	0.2795	0.2817	0.2839	0.2861	0.2883
1.00	0.0000	0.0000	0.0000	0.0000	0.0000	0.0000	0.0000	0.0000	0.0000	0.0000

q β	3.0000	3.1000	3.2000	3.3000	3.4000	3.5000	3.6000	3.7000	3.8000	3.9000
0.	0.9998	0.9999	0.9999	0.9999	1.0000	1.0000	1.0000	1.0000	1.0000	1.0000
0.10	0.9995	0.9997	0.9998	0.9999	0.9999	1.0000	1.0000	1.0000	1.0000	1.0000
0.20	0.9984	0.9990	0.9993	0.9996	0.9997	0.9998	0.9999	0.9999	1.0000	1.0000
0.30	0.9944	0.9960	0.9971	0.9980	0.9986	0.9990	0.9993	0.9995	0.9997	0.9998
0.40	0.9825	0.9863	0.9894	0.9918	0.9937	0.9952	0.9964	0.9973	0.9980	0.9985
0.50	0.9515	0.9594	0.9662	0.9720	0.9769	0.9810	0.9844	0.9873	0.9897	0.9917
0.60	0.8831	0.8965	0.9085	0.9194	0.9292	0.9380	0.9458	0.9528	0.9590	0.9645
0.70	0.7556	0.7733	0.7901	0.8058	0.8207	0.8347	0.8478	0.8601	0.8716	0.8823
0.80	0.5550	0.5726	0.5897	0.6064	0.6226	0.6384	0.6538	0.6687	0.6832	0.6972
0.90	0.2905	0.3015	0.3123	0.3231	0.3338	0.3445	0.3550	0.3655	0.3759	0.3862
1.00	0.0000	0.0000	0.0000	0.0000	0.0000	0.0000	0.0000	0.0000	0.0000	0.0000

q β	4.0000	4.1000	4.2000	4.3000	4.4000	4.5000	4.6000	4.7000	4.8000	4.9000
0.	1.0000	1.0000	1.0000	1.0000	1.0000	1.0000	1.0000	1.0000	1.0000	1.0000
0.10	1.0000	1.0000	1.0000	1.0000	1.0000	1.0000	1.0000	1.0000	1.0000	1.0000
0.20	1.0000	1.0000	1.0000	1.0000	1.0000	1.0000	1.0000	1.0000	1.0000	1.0000
0.30	0.9999	0.9999	0.9999	1.0000	1.0000	1.0000	1.0000	1.0000	1.0000	1.0000
0.40	0.9989	0.9992	0.9994	0.9996	0.9997	0.9998	0.9999	0.9999	0.9999	1.0000
0.50	0.9933	0.9947	0.9958	0.9967	0.9973	0.9979	0.9984	0.9987	0.9990	0.9992
0.60	0.9693	0.9736	0.9773	0.9806	0.9834	0.9859	0.9880	0.9899	0.9914	0.9928
0.70	0.8923	0.9016	0.9103	0.9183	0.9257	0.9325	0.9388	0.9446	0.9500	0.9549
0.80	0.7108	0.7240	0.7367	0.7490	0.7609	0.7724	0.7834	0.7941	0.8044	0.8143
0.90	0.3964	0.4066	0.4166	0.4266	0.4365	0.4463	0.4560	0.4656	0.4751	0.4846
1.00	0.0000	0.0000	0.0000	0.0000	0.0000	0.0000	0.0000	0.0000	0.0000	0.0000

q β	5.0000	5.1000	5.2000	5.3000	5.4000	5.5000	5.6000	5.7000	5.8000	5.9000
0.	1.0000	1.0000	1.0000	1.0000	1.0000	1.0000	1.0000	1.0000	1.0000	1.0000
0.10	1.0000	1.0000	1.0000	1.0000	1.0000	1.0000	1.0000	1.0000	1.0000	1.0000
0.20	1.0000	1.0000	1.0000	1.0000	1.0000	1.0000	1.0000	1.0000	1.0000	1.0000
0.30	1.0000	1.0000	1.0000	1.0000	1.0000	1.0000	1.0000	1.0000	1.0000	1.0000
0.40	1.0000	1.0000	1.0000	1.0000	1.0000	1.0000	1.0000	1.0000	1.0000	1.0000
0.50	0.9994	0.9996	0.9997	0.9997	0.9998	0.9998	0.9999	0.9999	1.0000	1.0000
0.60	0.9939	0.9949	0.9958	0.9965	0.9971	0.9976	0.9980	0.9984	0.9986	0.9989
0.70	0.9594	0.9635	0.9672	0.9706	0.9737	0.9765	0.9790	0.9813	0.9834	0.9853
0.80	0.8238	0.8329	0.8416	0.8501	0.8581	0.8658	0.8732	0.8803	0.8870	0.8934
0.90	0.4939	0.5032	0.5123	0.5214	0.5303	0.5392	0.5480	0.5566	0.5652	0.5737
1.00	0.0000	0.0000	0.0000	0.0000	0.0000	0.0000	0.0000	0.0000	0.0000	0.0000

TABLE 6.0-2. (CONTINUED)

β \ q	6.0000	6.1000	6.2000	6.3000	6.4000	6.5000	6.6000	6.7000	6.8000	6.9000
0.	1.0000	1.0000	1.0000	1.0000	1.0000	1.0000	1.0000	1.0000	1.0000	1.0000
0.10	1.0000	1.0000	1.0000	1.0000	1.0000	1.0000	1.0000	1.0000	1.0000	1.0000
0.20	1.0000	1.0000	1.0000	1.0000	1.0000	1.0000	1.0000	1.0000	1.0000	1.0000
0.30	1.0000	1.0000	1.0000	1.0000	1.0000	1.0000	1.0000	1.0000	1.0000	1.0000
0.40	1.0000	1.0000	1.0000	1.0000	1.0000	1.0000	1.0000	1.0000	1.0000	1.0000
0.50	1.0000	1.0000	1.0000	1.0000	1.0000	1.0000	1.0000	1.0000	0.9999	0.9999
0.60	0.9991	0.9993	0.9994	0.9995	0.9996	0.9997	0.9998	0.9998	0.9999	0.9999
0.70	0.9870	0.9884	0.9898	0.9910	0.9921	0.9930	0.9939	0.9946	0.9953	0.9959
0.80	0.8996	0.9054	0.9110	0.9163	0.9213	0.9261	0.9307	0.9350	0.9390	0.9429
0.90	0.5820	0.5903	0.5985	0.6065	0.6145	0.6224	0.6301	0.6378	0.6453	0.6528
1.00	0.0000	0.0000	0.0000	0.0000	0.0000	0.0000	0.0000	0.0000	0.0000	0.0000

β \ q	7.0000	7.1000	7.2000	7.3000	7.4000	7.5000	7.6000	7.7000	7.8000	7.9000
0.	1.0000	1.0000	1.0000	1.0000	1.0000	1.0000	1.0000	1.0000	1.0000	1.0000
0.10	1.0000	1.0000	1.0000	1.0000	1.0000	1.0000	1.0000	1.0000	1.0000	1.0000
0.20	1.0000	1.0000	1.0000	1.0000	1.0000	1.0000	1.0000	1.0000	1.0000	1.0000
0.30	1.0000	1.0000	1.0000	1.0000	1.0000	1.0000	1.0000	1.0000	1.0000	1.0000
0.40	1.0000	1.0000	1.0000	1.0000	1.0000	1.0000	1.0000	1.0000	1.0000	1.0000
0.50	1.0000	1.0000	1.0000	1.0000	1.0000	1.0000	1.0000	1.0000	1.0000	1.0000
0.60	0.9999	0.9999	1.0000	1.0000	1.0000	1.0000	1.0000	1.0000	1.0000	1.0000
0.70	0.9964	0.9969	0.9973	0.9977	0.9980	0.9982	0.9985	0.9987	0.9989	0.9990
0.80	0.9484	0.9500	0.9533	0.9564	0.9593	0.9621	0.9646	0.9671	0.9693	0.9715
0.90	0.6601	0.6674	0.6745	0.6816	0.6885	0.6953	0.7021	0.7087	0.7152	0.7217
1.00	0.0000	0.0000	0.0000	0.0000	0.0000	0.0000	0.0000	0.0000	0.0000	0.0000

β \ q	8.0000	8.1000	8.2000	8.3000	8.4000	8.5000	8.6000	8.7000	8.8000	8.9000
0.	1.0000	1.0000	1.0000	1.0000	1.0000	1.0000	1.0000	1.0000	1.0000	1.0000
0.10	1.0000	1.0000	1.0000	1.0000	1.0000	1.0000	1.0000	1.0000	1.0000	1.0000
0.20	1.0000	1.0000	1.0000	1.0000	1.0000	1.0000	1.0000	1.0000	1.0000	1.0000
0.30	1.0000	1.0000	1.0000	1.0000	1.0000	1.0000	1.0000	1.0000	1.0000	1.0000
0.40	1.0000	1.0000	1.0000	1.0000	1.0000	1.0000	1.0000	1.0000	1.0000	1.0000
0.50	1.0000	1.0000	1.0000	1.0000	1.0000	1.0000	1.0000	1.0000	1.0000	1.0000
0.60	1.0000	1.0000	1.0000	1.0000	1.0000	1.0000	1.0000	1.0000	1.0000	1.0000
0.70	0.9991	0.9993	0.9994	0.9995	0.9996	0.9996	0.9997	0.9997	0.9998	0.9998
0.80	0.9735	0.9754	0.9772	0.9789	0.9804	0.9819	0.9832	0.9845	0.9857	0.9868
0.90	0.7290	0.7342	0.7404	0.7464	0.7523	0.7581	0.7639	0.7695	0.7750	0.7805
1.00	0.0000	0.0000	0.0000	0.0000	0.0000	0.0000	0.0000	0.0000	0.0000	0.0000

β \ q	9.0000	9.1000	9.2000	9.3000	9.4000	9.5000	9.6000	9.7000	9.8000	9.9000
0.	1.0000	1.0000	1.0000	1.0000	1.0000	1.0000	1.0000	1.0000	1.0000	1.0000
0.10	1.0000	1.0000	1.0000	1.0000	1.0000	1.0000	1.0000	1.0000	1.0000	1.0000
0.20	1.0000	1.0000	1.0000	1.0000	1.0000	1.0000	1.0000	1.0000	1.0000	1.0000
0.30	1.0000	1.0000	1.0000	1.0000	1.0000	1.0000	1.0000	1.0000	1.0000	1.0000
0.40	1.0000	1.0000	1.0000	1.0000	1.0000	1.0000	1.0000	1.0000	1.0000	1.0000
0.50	1.0000	1.0000	1.0000	1.0000	1.0000	1.0000	1.0000	1.0000	1.0000	1.0000
0.60	1.0000	1.0000	1.0000	1.0000	1.0000	1.0000	1.0000	1.0000	1.0000	1.0000
0.70	0.9998	0.9999	0.9999	0.9999	0.9999	0.9999	1.0000	1.0000	1.0000	1.0000
0.80	0.9875	0.9886	0.9897	0.9905	0.9913	0.9920	0.9926	0.9932	0.9938	0.9943
0.90	0.7856	0.7911	0.7962	0.8013	0.8063	0.8111	0.8159	0.8206	0.8252	0.8297
1.00	0.0000	0.0000	0.0000	0.0000	0.0000	0.0000	0.0000	0.0000	0.0000	0.0000

TABLE 6.0-2. (CONCLUDED)

β \ q	10.0000	10.1000	10.2000	10.3000	10.4000	10.5000	10.6000	10.7000	10.8000	10.9000
0.	1.0000	1.0000	1.0000	1.0000	1.0000	1.0000	1.0000	1.0000	1.0000	1.0000
0.10	1.0000	1.0000	1.0000	1.0000	1.0000	1.0000	1.0000	1.0000	1.0000	1.0000
0.20	1.0000	1.0000	1.0000	1.0000	1.0000	1.0000	1.0000	1.0000	1.0000	1.0000
0.30	1.0000	1.0000	1.0000	1.0000	1.0000	1.0000	1.0000	1.0000	1.0000	1.0000
0.40	1.0000	1.0000	1.0000	1.0000	1.0000	1.0000	1.0000	1.0000	1.0000	1.0000
0.50	1.0000	1.0000	1.0000	1.0000	1.0000	1.0000	1.0000	1.0000	1.0000	1.0000
0.60	1.0000	1.0000	1.0000	1.0000	1.0000	1.0000	1.0000	1.0000	1.0000	1.0000
0.70	1.0000	1.0000	1.0000	1.0000	1.0000	1.0000	1.0000	1.0000	1.0000	1.0000
0.80	0.9948	0.9952	0.9956	0.9960	0.9964	0.9967	0.9970	1.0000	1.0000	1.0000
0.90	0.8341	0.8385	0.8427	0.8469	0.8510	0.8549	0.8588	0.9972	0.9975	0.9977
1.00	0.0000	0.0000	0.0000	0.0000	0.0000	0.0000	0.0000	0.8627	0.8664	0.8701
								0.0000	0.0000	0.0000

TABLE 6.0-3. CYLINDER-PARAMETER ψ_2

β \ q	0.4000	0.4200	0.4400	0.4600	0.4800	0.5000	0.5200	0.5400	0.5600	0.5800
0.	0.0001	0.0002	0.0005	0.0009	0.0015	0.0025	0.0038	0.0056	0.0080	0.0109
0.10	0.0001	0.0002	0.0005	0.0009	0.0015	0.0024	0.0038	0.0056	0.0079	0.0108
0.20	0.0001	0.0002	0.0004	0.0008	0.0015	0.0024	0.0037	0.0055	0.0077	0.0106
0.30	0.0001	0.0002	0.0004	0.0008	0.0014	0.0023	0.0036	0.0053	0.0075	0.0102
0.40	0.0001	0.0002	0.0004	0.0008	0.0013	0.0022	0.0034	0.0050	0.0071	0.0097
0.50	0.0001	0.0002	0.0004	0.0007	0.0013	0.0020	0.0032	0.0047	0.0066	0.0090
0.60	0.0001	0.0002	0.0003	0.0007	0.0011	0.0019	0.0029	0.0043	0.0061	0.0083
0.70	0.0001	0.0002	0.0003	0.0006	0.0010	0.0017	0.0026	0.0039	0.0055	0.0075
0.80	0.0001	0.0001	0.0003	0.0005	0.0009	0.0015	0.0023	0.0034	0.0048	0.0066
0.90	0.0000	0.0001	0.0002	0.0004	0.0008	0.0013	0.0020	0.0029	0.0041	0.0056
1.00	0.0000	0.0001	0.0002	0.0004	0.0007	0.0011	0.0016	0.0024	0.0034	0.0047

β \ q	0.6000	0.6200	0.6400	0.6600	0.6800	0.7000	0.7200	0.7400	0.7600	0.7800
0.	0.0144	0.0186	0.0235	0.0290	0.0351	0.0419	0.0492	0.0571	0.0655	0.0744
0.10	0.0143	0.0185	0.0233	0.0288	0.0349	0.0416	0.0489	0.0567	0.0651	0.0739
0.20	0.0140	0.0181	0.0228	0.0282	0.0341	0.0407	0.0478	0.0555	0.0637	0.0723
0.30	0.0135	0.0174	0.0220	0.0271	0.0329	0.0392	0.0461	0.0535	0.0614	0.0697
0.40	0.0128	0.0166	0.0209	0.0258	0.0312	0.0372	0.0438	0.0508	0.0582	0.0661
0.50	0.0120	0.0155	0.0195	0.0211	0.0292	0.0348	0.0409	0.0474	0.0544	0.0617
0.60	0.0110	0.0142	0.0179	0.0221	0.0267	0.0319	0.0375	0.0435	0.0499	0.0566
0.70	0.0099	0.0128	0.0161	0.0199	0.0241	0.0287	0.0337	0.0392	0.0449	0.0510
0.80	0.0087	0.0112	0.0142	0.0175	0.0212	0.0253	0.0297	0.0345	0.0396	0.0449
0.90	0.0075	0.0097	0.0122	0.0150	0.0182	0.0217	0.0255	0.0296	0.0340	0.0386
1.00	0.0062	0.0080	0.0101	0.0125	0.0152	0.0181	0.0213	0.0247	0.0283	0.0321

β \ q	0.8000	0.8200	0.8400	0.8600	0.8800	0.9000	0.9200	0.9400	0.9600	0.9800
0.	0.0837	0.0933	0.1032	0.1134	0.1238	0.1344	0.1451	0.1559	0.1667	0.1776
0.10	0.0831	0.0926	0.1025	0.1126	0.1229	0.1334	0.1440	0.1547	0.1655	0.1763
0.20	0.0813	0.0906	0.1002	0.1101	0.1203	0.1305	0.1409	0.1514	0.1619	0.1725
0.30	0.0783	0.0873	0.0966	0.1062	0.1159	0.1258	0.1359	0.1460	0.1561	0.1663
0.40	0.0743	0.0829	0.0917	0.1008	0.1100	0.1194	0.1290	0.1386	0.1482	0.1579
0.50	0.0694	0.0774	0.0856	0.0941	0.1027	0.1115	0.1204	0.1294	0.1384	0.1475
0.60	0.0637	0.0710	0.0786	0.0863	0.0943	0.1023	0.1105	0.1187	0.1270	0.1353
0.70	0.0573	0.0639	0.0707	0.0777	0.0848	0.0921	0.0995	0.1069	0.1143	0.1218
0.80	0.0505	0.0563	0.0623	0.0684	0.0747	0.0811	0.0876	0.0941	0.1007	0.1073
0.90	0.0434	0.0483	0.0535	0.0588	0.0642	0.0697	0.0752	0.0808	0.0865	0.0921
1.00	0.0361	0.0403	0.0446	0.0490	0.0535	0.0580	0.0627	0.0673	0.0721	0.0768

β \ q	1.0000	1.0200	1.0400	1.0600	1.0800	1.1000	1.1200	1.1400	1.1600	1.1800
0.	0.1884	0.1992	0.2100	0.2206	0.2311	0.2415	0.2517	0.2618	0.2717	0.2813
0.10	0.1871	0.1978	0.2085	0.2190	0.2295	0.2398	0.2500	0.2600	0.2698	0.2794
0.20	0.1831	0.1936	0.2040	0.2144	0.2246	0.2347	0.2447	0.2545	0.2548	0.2735
0.30	0.1765	0.1866	0.1967	0.2067	0.2166	0.2264	0.2360	0.2455	0.2548	0.2640
0.40	0.1675	0.1772	0.1868	0.1963	0.2057	0.2150	0.2242	0.2332	0.2422	0.2509
0.50	0.156	0.1655	0.1745	0.1834	0.1922	0.2009	0.2095	0.2180	0.2080	0.2346
0.60	0.143	0.1519	0.1602	0.1683	0.1516	0.1845	0.1924	0.1733	0.1874	0.1943
0.70	0.139	0.1368	0.1442	0.1516	0.1589	0.1662	0.1733	0.1804	0.1874	0.1943
0.80	0.1139	0.1205	0.1270	0.1335	0.1400	0.1464	0.1528	0.1590	0.1652	0.1713
0.90	0.0978	0.1035	0.1091	0.1147	0.1203	0.1258	0.1313	0.1367	0.1420	0.1472
1.00	0.0815	0.0862	0.0909	0.0956	0.1002	0.1048	0.1094	0.1139	0.1183	0.1277

TABLE 6.0-3. (CONTINUED)

β \ q	1.2000	1.2200	1.2400	1.2600	1.2800	1.3000	1.3200	1.3400	1.3600	1.3800
0.	0.2908	0.3000	0.3090	0.3178	0.3263	0.3346	0.3426	0.3504	0.3579	0.3652
0.10	0.2888	0.2980	0.3069	0.3157	0.3241	0.3324	0.3404	0.3481	0.3556	0.3628
0.20	0.2828	0.2918	0.3006	0.3092	0.3176	0.3257	0.3336	0.3412	0.3487	0.3558
0.30	0.2729	0.2817	0.2903	0.2986	0.3068	0.3147	0.3224	0.3299	0.3372	0.3443
0.40	0.2595	0.2679	0.2761	0.2841	0.2920	0.2996	0.3071	0.3144	0.3214	0.3283
0.50	0.2427	0.2507	0.2584	0.2660	0.2735	0.2807	0.2878	0.2948	0.3015	0.3081
0.60	0.2231	0.2305	0.2377	0.2447	0.2517	0.2585	0.2651	0.2716	0.2780	0.2842
0.70	0.2011	0.2078	0.2144	0.2208	0.2271	0.2333	0.2394	0.2454	0.2512	0.2570
0.80	0.1774	0.1833	0.1891	0.1948	0.2005	0.2060	0.2114	0.2168	0.2220	0.2271
0.90	0.1524	0.1576	0.1626	0.1675	0.1724	0.1772	0.1819	0.1865	0.1911	0.1955
1.00	0.1270	0.1318	0.1355	0.1397	0.1437	0.1477	0.1517	0.1555	0.1593	0.1631

β \ q	1.4000	1.4200	1.4400	1.4600	1.4800	1.5000	1.5200	1.5400	1.5600	1.5800
0.	0.3722	0.3789	0.3854	0.3916	0.3976	0.4033	0.4088	0.4141	0.4191	0.4239
0.10	0.3698	0.3765	0.3830	0.3893	0.3952	0.4010	0.4065	0.4117	0.4168	0.4216
0.20	0.3628	0.3695	0.3759	0.3821	0.3881	0.3939	0.3994	0.4047	0.4098	0.4146
0.30	0.3511	0.3577	0.3641	0.3703	0.3762	0.3820	0.3875	0.3928	0.3980	0.4029
0.40	0.3349	0.3414	0.3477	0.3538	0.3596	0.3653	0.3708	0.3762	0.3813	0.3863
0.50	0.3145	0.3208	0.3268	0.3328	0.3385	0.3441	0.3495	0.3547	0.3598	0.3648
0.60	0.2902	0.2961	0.3019	0.3076	0.3130	0.3184	0.3236	0.3287	0.3336	0.3384
0.70	0.2626	0.2680	0.2734	0.2786	0.2838	0.2888	0.2937	0.2985	0.3032	0.3077
0.80	0.2322	0.2371	0.2420	0.2467	0.2513	0.2559	0.2604	0.2647	0.2690	0.2732
0.90	0.1999	0.2042	0.2085	0.2126	0.2167	0.2207	0.2246	0.2284	0.2322	0.2359
1.00	0.1667	0.1703	0.1739	0.1773	0.1808	0.1841	0.1874	0.1906	0.1938	0.1969

β \ q	1.6000	1.6200	1.6400	1.6600	1.6800	1.7000	1.7200	1.7400	1.7600	1.7800
0.	0.4285	0.4328	0.4370	0.4409	0.4446	0.4482	0.4516	0.4547	0.4577	0.4606
0.10	0.4262	0.4306	0.4347	0.4387	0.4425	0.4461	0.4495	0.4527	0.4557	0.4586
0.20	0.4193	0.4237	0.4280	0.4320	0.4359	0.4396	0.4431	0.4464	0.4496	0.4526
0.30	0.4076	0.4122	0.4165	0.4207	0.4247	0.4285	0.4322	0.4357	0.4390	0.4422
0.40	0.3911	0.3957	0.4001	0.4044	0.4085	0.4125	0.4164	0.4200	0.4236	0.4270
0.50	0.3695	0.3742	0.3787	0.3830	0.3872	0.3913	0.3953	0.3991	0.4028	0.4063
0.60	0.3431	0.3477	0.3521	0.3564	0.3606	0.3647	0.3687	0.3726	0.3763	0.3800
0.70	0.3122	0.3165	0.3208	0.3250	0.3290	0.3330	0.3369	0.3407	0.3444	0.3480
0.80	0.2773	0.2814	0.2853	0.2892	0.2930	0.2967	0.3003	0.3039	0.3074	0.3108
0.90	0.2395	0.2431	0.2466	0.2500	0.2534	0.2567	0.2599	0.2631	0.2663	0.2693
1.00	0.2000	0.2030	0.2059	0.2088	0.2117	0.2144	0.2172	0.2199	0.2225	0.2251

β \ q	1.8000	1.8200	1.8400	1.8600	1.8800	1.9000	1.9200	1.9400	1.9600	1.9800
0.	0.4633	0.4658	0.4682	0.4704	0.4725	0.4745	0.4763	0.4781	0.4797	0.4812
0.10	0.4613	0.4639	0.4663	0.4686	0.4708	0.4728	0.4747	0.4765	0.4782	0.4798
0.20	0.4555	0.4582	0.4608	0.4632	0.4655	0.4677	0.4697	0.4717	0.4735	0.4752
0.30	0.4453	0.4482	0.4510	0.4536	0.4561	0.4585	0.4608	0.4630	0.4651	0.4670
0.40	0.4302	0.4334	0.4364	0.4393	0.4421	0.4447	0.4473	0.4497	0.4520	0.4543
0.50	0.4098	0.4131	0.4163	0.4195	0.4225	0.4254	0.4282	0.4309	0.4335	0.4360
0.60	0.3835	0.3870	0.3904	0.3936	0.3968	0.3999	0.4029	0.4058	0.4086	0.4113
0.70	0.3515	0.3550	0.3583	0.3616	0.3648	0.3679	0.3710	0.3740	0.3769	0.3798
0.80	0.3141	0.3174	0.3206	0.3238	0.3269	0.3299	0.3328	0.3358	0.3386	0.3414
0.90	0.2723	0.2753	0.2782	0.2811	0.2839	0.2866	0.2893	0.2920	0.2946	0.2972
1.00	0.2277	0.2302	0.2327	0.2351	0.2375	0.2398	0.2421	0.2444	0.2466	0.2488

TABLE 6.0-3. (CONTINUED)

β \ q	2.0000	2.0200	2.0400	2.0600	2.0800	2.1000	2.1200	2.1400	2.1600	2.1800
0.	0.4826	0.4840	0.4852	0.4864	0.4874	0.4884	0.4894	0.4902	0.4910	0.4918
0.10	0.4812	0.4826	0.4839	0.4851	0.4862	0.4873	0.4883	0.4892	0.4900	0.4908
0.20	0.4769	0.4784	0.4798	0.4812	0.4825	0.4837	0.4848	0.4858	0.4868	0.4877
0.30	0.4689	0.4707	0.4723	0.4739	0.4754	0.4769	0.4782	0.4795	0.4807	0.4819
0.40	0.4564	0.4585	0.4605	0.4623	0.4641	0.4659	0.4675	0.4691	0.4706	0.4720
0.50	0.4385	0.4408	0.4431	0.4453	0.4474	0.4494	0.4514	0.4533	0.4551	0.4568
0.60	0.4140	0.4166	0.4191	0.4216	0.4239	0.4263	0.4285	0.4307	0.4328	0.4348
0.70	0.3825	0.3853	0.3879	0.3905	0.3931	0.3955	0.3979	0.4003	0.4026	0.4049
0.80	0.3441	0.3468	0.3495	0.3521	0.3546	0.3571	0.3595	0.3619	0.3643	0.3666
0.90	0.2997	0.3022	0.3046	0.3070	0.3094	0.3117	0.3140	0.3162	0.3184	0.3206
1.00	0.2510	0.2531	0.2552	0.2572	0.2592	0.2612	0.2632	0.2651	0.2670	0.2689

β \ q	2.2000	2.2200	2.2400	2.2600	2.2800	2.3000	2.3200	2.3400	2.3600	2.3800
0.	0.4924	0.4931	0.4937	0.4942	0.4947	0.4952	0.4956	0.4960	0.4963	0.4967
0.10	0.4915	0.4922	0.4928	0.4934	0.4940	0.4945	0.4949	0.4954	0.4957	0.4961
0.20	0.4886	0.4894	0.4902	0.4909	0.4915	0.4922	0.4927	0.4933	0.4938	0.4942
0.30	0.4829	0.4840	0.4849	0.4859	0.4867	0.4875	0.4883	0.4890	0.4897	0.4904
0.40	0.4734	0.4747	0.4760	0.4772	0.4783	0.4794	0.4804	0.4814	0.4824	0.4833
0.50	0.4585	0.4602	0.4617	0.4633	0.4647	0.4661	0.4675	0.4688	0.4700	0.4712
0.60	0.4368	0.4388	0.4406	0.4425	0.4442	0.4459	0.4476	0.4492	0.4508	0.4523
0.70	0.4071	0.4092	0.4113	0.4134	0.4154	0.4173	0.4192	0.4211	0.4229	0.4247
0.80	0.3688	0.3710	0.3732	0.3753	0.3774	0.3795	0.3815	0.3835	0.3854	0.3873
0.90	0.3227	0.3248	0.3269	0.3289	0.3309	0.3329	0.3348	0.3368	0.3386	0.3405
1.00	0.2707	0.2725	0.2743	0.2760	0.2778	0.2795	0.2812	0.2828	0.2844	0.2860

β \ q	2.4000	2.4200	2.4400	2.4600	2.4800	2.5000	2.5200	2.5400	2.5600	2.5800
0.	0.4970	0.4972	0.4975	0.4977	0.4979	0.4981	0.4983	0.4985	0.4986	0.4988
0.10	0.4964	0.4967	0.4970	0.4973	0.4975	0.4978	0.4980	0.4981	0.4983	0.4985
0.20	0.4947	0.4951	0.4954	0.4958	0.4961	0.4964	0.4967	0.4970	0.4972	0.4974
0.30	0.4910	0.4915	0.4921	0.4926	0.4931	0.4935	0.4939	0.4943	0.4947	0.4950
0.40	0.4841	0.4849	0.4857	0.4864	0.4871	0.4878	0.4884	0.4891	0.4896	0.4902
0.50	0.4724	0.4735	0.4746	0.4756	0.4766	0.4776	0.4785	0.4794	0.4802	0.4811
0.60	0.4538	0.4553	0.4566	0.4580	0.4593	0.4606	0.4618	0.4630	0.4642	0.4653
0.70	0.4265	0.4282	0.4298	0.4315	0.4331	0.4346	0.4361	0.4376	0.4391	0.4405
0.80	0.3892	0.3911	0.3929	0.3946	0.3964	0.3981	0.3998	0.4014	0.4030	0.4046
0.90	0.3423	0.3441	0.3459	0.3476	0.3493	0.3510	0.3527	0.3543	0.3559	0.3575
1.00	0.2876	0.2892	0.2907	0.2922	0.2937	0.2952	0.2967	0.2981	0.2995	0.3009

β \ q	2.6000	2.6200	2.6400	2.6600	2.6800	2.7000	2.7200	2.7400	2.7600	2.7800
0.	0.4989	0.4990	0.4991	0.4992	0.4993	0.4993	0.4994	0.4995	0.4995	0.4996
0.10	0.4986	0.4987	0.4989	0.4990	0.4991	0.4992	0.4992	0.4993	0.4994	0.4994
0.20	0.4976	0.4978	0.4980	0.4982	0.4983	0.4984	0.4986	0.4987	0.4988	0.4989
0.30	0.4954	0.4957	0.4960	0.4962	0.4965	0.4967	0.4970	0.4972	0.4973	0.4975
0.40	0.4907	0.4912	0.4917	0.4921	0.4925	0.4930	0.4933	0.4937	0.4940	0.4944
0.50	0.4818	0.4826	0.4833	0.4840	0.4847	0.4853	0.4860	0.4866	0.4871	0.4877
0.60	0.4664	0.4675	0.4685	0.4695	0.4705	0.4714	0.4723	0.4732	0.4741	0.4749
0.70	0.4419	0.4432	0.4445	0.4458	0.4471	0.4483	0.4495	0.4507	0.4519	0.4530
0.80	0.4062	0.4077	0.4092	0.4107	0.4122	0.4136	0.4150	0.4164	0.4178	0.4191
0.90	0.3591	0.3606	0.3621	0.3636	0.3651	0.3666	0.3680	0.3694	0.3708	0.3722
1.00	0.3023	0.3036	0.3050	0.3063	0.3076	0.3089	0.3101	0.3114	0.3126	0.3138

TABLE 6.0-3. (CONTINUED)

β \ q	2.8000	2.8200	2.8400	2.8600	2.8800	2.9000	2.9200	2.9400	2.9600	2.9800
0.	0.4996	0.4997	0.4997	0.4997	0.4998	0.4998	0.4998	0.4998	0.4998	0.4999
0.10	0.4995	0.4995	0.4996	0.4996	0.4997	0.4997	0.4997	0.4998	0.4998	0.4998
0.20	0.4990	0.4991	0.4992	0.4992	0.4993	0.4994	0.4994	0.4995	0.4995	0.4996
0.30	0.4977	0.4979	0.4980	0.4981	0.4983	0.4984	0.4985	0.4986	0.4987	0.4988
0.40	0.4947	0.4950	0.4952	0.4955	0.4958	0.4960	0.4962	0.4964	0.4966	0.4968
0.50	0.4882	0.4887	0.4892	0.4897	0.4901	0.4905	0.4909	0.4913	0.4917	0.4921
0.60	0.4757	0.4765	0.4773	0.4780	0.4787	0.4794	0.4801	0.4807	0.4814	0.4820
0.70	0.4541	0.4552	0.4562	0.4572	0.4582	0.4592	0.4602	0.4611	0.4620	0.4629
0.80	0.4204	0.4217	0.4230	0.4242	0.4254	0.4266	0.4278	0.4290	0.4301	0.4312
0.90	0.3735	0.3749	0.3762	0.3775	0.3788	0.3800	0.3813	0.3825	0.3837	0.3849
1.00	0.3151	0.3162	0.3174	0.3186	0.3197	0.3209	0.3220	0.3231	0.3242	0.3252

β \ q	3.0000	3.1000	3.2000	3.3000	3.4000	3.5000	3.6000	3.7000	3.8000	3.9000
0.	0.4999	0.4999	0.5000	0.5000	0.5000	0.5000	0.5000	0.5000	0.5000	0.5000
0.10	0.4998	0.4999	0.4999	0.5000	0.5000	0.5000	0.5000	0.5000	0.5000	0.5000
0.20	0.4996	0.4997	0.4998	0.4999	0.4999	0.5000	0.5000	0.5000	0.5000	0.5000
0.30	0.4989	0.4992	0.4995	0.4997	0.4998	0.4998	0.4999	0.4999	0.5000	0.5000
0.40	0.4970	0.4976	0.4984	0.4988	0.4991	0.4994	0.4995	0.4997	0.4998	0.4998
0.50	0.4924	0.4940	0.4953	0.4962	0.4970	0.4977	0.4982	0.4986	0.4989	0.4991
0.60	0.4826	0.4853	0.4876	0.4896	0.4912	0.4926	0.4938	0.4948	0.4957	0.4964
0.70	0.4638	0.4679	0.4715	0.4747	0.4776	0.4802	0.4825	0.4845	0.4863	0.4879
0.80	0.4323	0.4376	0.4424	0.4469	0.4510	0.4547	0.4582	0.4614	0.4644	0.4671
0.90	0.3861	0.3918	0.3971	0.4022	0.4069	0.4113	0.4154	0.4194	0.4231	0.4266
1.00	0.3263	0.3315	0.3363	0.3409	0.3452	0.3493	0.3532	0.3569	0.3604	0.3638

β \ q	4.0000	4.1000	4.2000	4.3000	4.4000	4.5000	4.6000	4.7000	4.8000	4.9000
0.	0.5000	0.5000	0.5000	0.5000	0.5000	0.5000	0.5000	0.5000	0.5000	0.5000
0.10	0.5000	0.5000	0.5000	0.5000	0.5000	0.5000	0.5000	0.5000	0.5000	0.5000
0.20	0.5000	0.5000	0.5000	0.5000	0.5000	0.5000	0.5000	0.5000	0.5000	0.5000
0.30	0.5000	0.5000	0.5000	0.5000	0.5000	0.5000	0.5000	0.5000	0.5000	0.5000
0.40	0.4999	0.4999	0.4999	0.5000	0.5000	0.5000	0.5000	0.5000	0.5000	0.5000
0.50	0.4993	0.4995	0.4996	0.4997	0.4998	0.4998	0.4999	0.4999	0.4999	0.4999
0.60	0.4970	0.4975	0.4980	0.4983	0.4986	0.4989	0.4991	0.4992	0.4994	0.4995
0.70	0.4894	0.4906	0.4917	0.4927	0.4936	0.4944	0.4951	0.4957	0.4963	0.4967
0.80	0.4696	0.4720	0.4741	0.4761	0.4780	0.4797	0.4812	0.4827	0.4840	0.4853
0.90	0.4299	0.4331	0.4361	0.4389	0.4416	0.4441	0.4465	0.4488	0.4510	0.4531
1.00	0.3670	0.3700	0.3729	0.3757	0.3784	0.3809	0.3834	0.3857	0.3880	0.3902

β \ q	5.0000	5.1000	5.2000	5.3000	5.4000	5.5000	5.6000	5.7000	5.8000	5.9000
0.	0.5000	0.5000	0.5000	0.5000	0.5000	0.5000	0.5000	0.5000	0.5000	0.5000
0.10	0.5000	0.5000	0.5000	0.5000	0.5000	0.5000	0.5000	0.5000	0.5000	0.5000
0.20	0.5000	0.5000	0.5000	0.5000	0.5000	0.5000	0.5000	0.5000	0.5000	0.5000
0.30	0.5000	0.5000	0.5000	0.5000	0.5000	0.5000	0.5000	0.5000	0.5000	0.5000
0.40	0.5000	0.5000	0.5000	0.5000	0.5000	0.5000	0.5000	0.5000	0.5000	0.5000
0.50	0.5000	0.5000	0.5000	0.5000	0.5000	0.5000	0.5000	0.5000	0.5000	0.5000
0.60	0.4996	0.4997	0.4997	0.4998	0.4998	0.4999	0.4999	0.4999	0.4999	0.4999
0.70	0.4971	0.4975	0.4978	0.4981	0.4984	0.4986	0.4988	0.4989	0.4991	0.4992
0.80	0.4864	0.4875	0.4885	0.4894	0.4902	0.4910	0.4917	0.4924	0.4930	0.4936
0.90	0.4550	0.4569	0.4587	0.4605	0.4621	0.4637	0.4652	0.4666	0.4680	0.4693
1.000	0.3923	0.3943	0.3962	0.3981	0.3999	0.4016	0.4033	0.4049	0.4066	0.4080

TABLE 6.0-3. (CONTINUED)

β \ q	6.0000	6.1000	6.2000	6.3000	6.4000	6.5000	6.6000	6.7000	6.8000	6.9000
0.	0.5000	0.5000	0.5000	0.5000	0.5000	0.5000	0.5000	0.5000	0.5000	0.5000
0.10	0.5000	0.5000	0.5000	0.5000	0.5000	0.5000	0.5000	0.5000	0.5000	0.5000
0.20	0.5000	0.5000	0.5000	0.5000	0.5000	0.5000	0.5000	0.5000	0.5000	0.5000
0.30	0.5000	0.5000	0.5000	0.5000	0.5000	0.5000	0.5000	0.5000	0.5000	0.5000
0.40	0.5000	0.5000	0.5000	0.5000	0.5000	0.5000	0.5000	0.5000	0.5000	0.5000
0.50	0.5000	0.5000	0.5000	0.5000	0.5000	0.5000	0.5000	0.5000	0.5000	0.5000
0.60	0.4999	0.5000	0.5000	0.5000	0.5000	0.5000	0.5000	0.5000	0.5000	0.5000
0.70	0.4993	0.4994	0.4995	0.4996	0.4997	0.4997	0.4997	0.4998	0.4998	0.4998
0.80	0.4941	0.4946	0.4950	0.4954	0.4958	0.4962	0.4965	0.4968	0.4970	0.4973
0.90	0.4705	0.4717	0.4728	0.4739	0.4750	0.4760	0.4769	0.4779	0.4788	0.4796
1.00	0.4095	0.4109	0.4123	0.4136	0.4149	0.4162	0.4174	0.4186	0.4198	0.4209

β \ q	7.0000	7.1000	7.2000	7.3000	7.4000	7.5000	7.6000	7.7000	7.8000	7.9000
0.	0.5000	0.5000	0.5000	0.5000	0.5000	0.5000	0.5000	0.5000	0.5000	0.5000
0.10	0.5000	0.5000	0.5000	0.5000	0.5000	0.5000	0.5000	0.5000	0.5000	0.5000
0.20	0.5000	0.5000	0.5000	0.5000	0.5000	0.5000	0.5000	0.5000	0.5000	0.5000
0.30	0.5000	0.5000	0.5000	0.5000	0.5000	0.5000	0.5000	0.5000	0.5000	0.5000
0.40	0.5000	0.5000	0.5000	0.5000	0.5000	0.5000	0.5000	0.5000	0.5000	0.5000
0.50	0.5000	0.5000	0.5000	0.5000	0.5000	0.5000	0.5000	0.5000	0.5000	0.5000
0.60	0.5000	0.5000	0.5000	0.5000	0.5000	0.5000	0.5000	0.5000	0.5000	0.5000
0.70	0.4999	0.4999	0.4999	0.4999	0.4999	0.4999	0.4999	0.5000	0.5000	0.5000
0.80	0.4975	0.4977	0.4979	0.4981	0.4983	0.4984	0.4985	0.4987	0.4988	0.4989
0.90	0.4804	0.4812	0.4819	0.4827	0.4834	0.4840	0.4847	0.4853	0.4859	0.4864
1.00	0.4220	0.4230	0.4241	0.4251	0.4261	0.4270	0.4279	0.4288	0.4297	0.4306

β \ q	8.0000	8.1000	8.2000	8.3000	8.4000	8.5000	8.6000	8.7000	8.8000	8.9000
0.	0.5000	0.5000	0.5000	0.5000	0.5000	0.5000	0.5000	0.5000	0.5000	0.5000
0.10	0.5000	0.5000	0.5000	0.5000	0.5000	0.5000	0.5000	0.5000	0.5000	0.5000
0.20	0.5000	0.5000	0.5000	0.5000	0.5000	0.5000	0.5000	0.5000	0.5000	0.5000
0.30	0.5000	0.5000	0.5000	0.5000	0.5000	0.5000	0.5000	0.5000	0.5000	0.5000
0.40	0.5000	0.5000	0.5000	0.5000	0.5000	0.5000	0.5000	0.5000	0.5000	0.5000
0.50	0.5000	0.5000	0.5000	0.5000	0.5000	0.5000	0.5000	0.5000	0.5000	0.5000
0.60	0.5000	0.5000	0.5000	0.5000	0.5000	0.5000	0.5000	0.5000	0.5000	0.5000
0.70	0.5000	0.5000	0.5000	0.5000	0.5000	0.5000	0.5000	0.5000	0.5000	0.5000
0.80	0.4990	0.4991	0.4992	0.4993	0.4993	0.4994	0.4994	0.4995	0.4995	0.4996
0.90	0.4869	0.4875	0.4880	0.4884	0.4889	0.4893	0.4898	0.4902	0.4906	0.4909
1.00	0.4315	0.4323	0.4331	0.4339	0.4346	0.4354	0.4361	0.4368	0.4375	0.4382

β \ q	9.0000	9.1000	9.2000	9.3000	9.4000	9.5000	9.6000	9.7000	9.8000	9.9000
0.	0.5000	0.5000	0.5000	0.5000	0.5000	0.5000	0.5000	0.5000	0.5000	0.5000
0.10	0.5000	0.5000	0.5000	0.5000	0.5000	0.5000	0.5000	0.5000	0.5000	0.5000
0.20	0.5000	0.5000	0.5000	0.5000	0.5000	0.5000	0.5000	0.5000	0.5000	0.5000
0.30	0.5000	0.5000	0.5000	0.5000	0.5000	0.5000	0.5000	0.5000	0.5000	0.5000
0.40	0.5000	0.5000	0.5000	0.5000	0.5000	0.5000	0.5000	0.5000	0.5000	0.5000
0.50	0.5000	0.5000	0.5000	0.5000	0.5000	0.5000	0.5000	0.5000	0.5000	0.5000
0.60	0.5000	0.5000	0.5000	0.5000	0.5000	0.5000	0.5000	0.5000	0.5000	0.5000
0.70	0.5000	0.5000	0.5000	0.5000	0.4998	0.4998	0.4998	0.4998	0.4999	0.4999
0.80	0.4996	0.4997	0.4997	0.4997	0.4998	0.4998	0.4998	0.4998	0.4999	0.4999
0.90	0.4913	0.4916	0.4920	0.4923	0.4926	0.4929	0.4932	0.4935	0.4937	0.4940
1.00	0.4389	0.4395	0.4401	0.4408	0.4414	0.4420	0.4426	0.4431	0.4437	0.4443

TABLE 6.0-3. (CONCLUDED)

β＼q	10.0000	10.1000	10.2000	10.3000	10.4000	10.5000	10.6000	10.7000	10.8000	10.9000
0.	0.5000	0.5000	0.5000	0.5000	0.5000	0.5000	0.5000	0.5000	0.5000	0.5000
0.10	0.5000	0.5000	0.5000	0.5000	0.5000	0.5000	0.5000	0.5000	0.5000	0.5000
0.20	0.5000	0.5000	0.5000	0.5000	0.5000	0.5000	0.5000	0.5000	0.5000	0.5000
0.30	0.5000	0.5000	0.5000	0.5000	0.5000	0.5000	0.5000	0.5000	0.5000	0.5000
0.40	0.5000	0.5000	0.5000	0.5000	0.5000	0.5000	0.5000	0.5000	0.5000	0.5000
0.50	0.5000	0.5000	0.5000	0.5000	0.5000	0.5000	0.5000	0.5000	0.5000	0.5000
0.60	0.5000	0.5000	0.5000	0.5000	0.5000	0.5000	0.5000	0.5000	0.5000	0.5000
0.70	0.5000	0.5000	0.5000	0.5000	0.5000	0.5000	0.5000	0.5000	0.5000	0.5000
0.80	0.4999	0.4999	0.4999	0.4999	0.4999	0.5000	0.5000	0.5000	0.5000	0.5000
0.90	0.4942	0.4945	0.4947	0.4949	0.4951	0.4953	0.4955	0.4957	0.4958	0.4960
1.00	0.4448	0.4454	0.4459	0.4464	0.4469	0.4474	0.4479	0.4484	0.4488	0.4493

TABLE 6.0-4. SPHERE-PARAMETER ϕ_3

β＼q	0.5000	0.5200	0.5400	0.5600	0.5800	0.6000	0.6200	0.6400	0.6600	0.6800
0.	0.0001	0.0002	0.0004	0.0008	0.0013	0.0021	0.0033	0.0048	0.0069	0.0096
0.10	0.0001	0.0002	0.0004	0.0008	0.0013	0.0021	0.0032	0.0048	0.0068	0.0095
0.20	0.0001	0.0002	0.0004	0.0007	0.0012	0.0020	0.0031	0.0045	0.0065	0.0090
0.30	0.0001	0.0002	0.0004	0.0007	0.0011	0.0018	0.0028	0.0042	0.0060	0.0083
0.40	0.0001	0.0002	0.0003	0.0006	0.0010	0.0016	0.0025	0.0037	0.0052	0.0073
0.50	0.0001	0.0001	0.0003	0.0005	0.0008	0.0013	0.0021	0.0031	0.0044	0.0061
0.60	0.0001	0.0001	0.0002	0.0004	0.0007	0.0011	0.0016	0.0024	0.0035	0.0049
0.70	0.0000	0.0001	0.0002	0.0003	0.0005	0.0008	0.0012	0.0018	0.0026	0.0035
0.80	0.0000	0.0001	0.0001	0.0002	0.0003	0.0005	0.0008	0.0011	0.0016	0.0023
0.90	0.0000	0.0000	0.0000	0.0001	0.0001	0.0002	0.0004	0.0005	0.0008	0.0011
1.00	0.0000	0.0000	0.0000	0.0000	0.0000	0.0000	0.0000	0.0000	0.0000	0.0000

β＼q	0.7000	0.7200	0.7400	0.7600	0.7800	0.8000	0.8200	0.8400	0.8600	0.8800
0.	0.0130	0.0171	0.0221	0.0279	0.0347	0.0423	0.0510	0.0606	0.0711	0.0827
0.10	0.0128	0.0169	0.0217	0.0275	0.0341	0.0416	0.0501	0.0596	0.0700	0.0813
0.20	0.0122	0.0160	0.0207	0.0261	0.0324	0.0396	0.0477	0.0567	0.0666	0.0773
0.30	0.0112	0.0147	0.0190	0.0240	0.0297	0.0363	0.0438	0.0520	0.0611	0.0709
0.40	0.0098	0.0130	0.0167	0.0211	0.0262	0.0320	0.0386	0.0459	0.0538	0.0626
0.50	0.0083	0.0109	0.0141	0.0178	0.0221	0.0270	0.0325	0.0386	0.0453	0.0526
0.60	0.0066	0.0086	0.0111	0.0141	0.0175	0.0214	0.0257	0.0306	0.0359	0.0417
0.70	0.0048	0.0063	0.0081	0.0103	0.0127	0.0156	0.0188	0.0223	0.0262	0.0304
0.80	0.0030	0.0040	0.0052	0.0065	0.0081	0.0099	0.0119	0.0142	0.0166	0.0193
0.90	0.0014	0.0019	0.0024	0.0031	0.0038	0.0046	0.0056	0.0066	0.0078	0.0090
1.00	0.0000	0.0000	0.0000	0.0000	0.0000	0.0000	0.0000	0.0000	0.0000	0.0000

β＼q	0.9000	0.9200	0.9400	0.9600	0.9800	1.0000	1.0200	1.0400	1.0600	1.0800
0.	0.0951	0.1084	0.1225	0.1375	0.1531	0.1695	0.1865	0.2041	0.2222	0.2407
0.10	0.0935	0.1066	0.1205	0.1352	0.1506	0.1667	0.1835	0.2008	0.2186	0.2368
0.20	0.0889	0.1014	0.1146	0.1286	0.1433	0.1586	0.1745	0.1910	0.2079	0.2253
0.30	0.0816	0.0930	0.1052	0.1180	0.1315	0.1455	0.1602	0.1753	0.1908	0.2068
0.40	0.0720	0.0820	0.0927	0.1041	0.1159	0.1283	0.1412	0.1546	0.1683	0.1824
0.50	0.0605	0.0690	0.0780	0.0875	0.0975	0.1080	0.1188	0.1301	0.1416	0.1535
0.60	0.0480	0.0547	0.0618	0.0694	0.0773	0.0856	0.0942	0.1031	0.1123	0.1217
0.70	0.0350	0.0399	0.0451	0.0506	0.0564	0.0624	0.0687	0.0752	0.0819	0.0888
0.80	0.0222	0.0254	0.0287	0.0322	0.0358	0.0397	0.0437	0.0478	0.0521	0.0565
0.90	0.0104	0.0118	0.0134	0.0150	0.0168	0.0185	0.0204	0.0224	0.0243	0.0264
1.00	0.0000	0.0000	0.0000	0.0000	0.0000	0.0000	0.0000	0.0000	0.0000	0.0000

β＼q	1.1000	1.1200	1.1400	1.1600	1.1800	1.2000	1.2200	1.2400	1.2600	1.2800
0.	0.2597	0.2790	0.2986	0.3183	0.3383	0.3584	0.3785	0.3986	0.4187	0.4388
0.10	0.2555	0.2745	0.2937	0.3132	0.3328	0.3526	0.3724	0.3923	0.4121	0.4318
0.20	0.2430	0.2611	0.2795	0.2980	0.3168	0.3356	0.3545	0.3735	0.3924	0.4113
0.30	0.2231	0.2398	0.2566	0.2737	0.2910	0.3084	0.3260	0.3433	0.3609	0.3783
0.40	0.1968	0.2115	0.2265	0.2416	0.2569	0.2723	0.2875	0.3034	0.3190	0.3346
0.50	0.1657	0.1781	0.1907	0.2035	0.2164	0.2295	0.2426	0.2559	0.2691	0.2824
0.60	0.1314	0.1413	0.1513	0.1615	0.1718	0.1822	0.1927	0.2033	0.2139	0.2246
0.70	0.0959	0.1031	0.1104	0.1179	0.1254	0.1331	0.1408	0.1486	0.1564	0.1642
0.80	0.0610	0.0656	0.0702	0.0750	0.0798	0.0847	0.0896	0.0946	0.0996	0.1047
0.90	0.0285	0.0307	0.0328	0.0351	0.0373	0.0396	0.0419	0.0443	0.0466	0.0490
1.00	0.0000	0.0000	0.0000	0.0000	0.0000	0.0000	0.0000	0.0000	0.0000	0.0000

TABLE 6.0-4. (CONTINUED)

β＼q	1.3000	1.3200	1.3400	1.3600	1.3800	1.4000	1.4200	1.4400	1.4600	1.4800
0.	0.4587	0.4784	0.4979	0.5172	0.5362	0.5550	0.5734	0.5914	0.6091	0.6263
0.10	0.4514	0.4709	0.4902	0.5092	0.5280	0.5465	0.5647	0.5825	0.6000	0.6171
0.20	0.4301	0.4488	0.4673	0.4856	0.5036	0.5215	0.5390	0.5563	0.5732	0.5899
0.30	0.3958	0.4131	0.4303	0.4474	0.4643	0.4810	0.4974	0.5137	0.5297	0.5454
0.40	0.3502	0.3657	0.3811	0.3965	0.4117	0.4268	0.4417	0.4565	0.4711	0.4855
0.50	0.2957	0.3090	0.3222	0.3354	0.3485	0.3616	0.3745	0.3874	0.4001	0.4128
0.60	0.2353	0.2460	0.2566	0.2673	0.2780	0.2886	0.2992	0.3097	0.3202	0.3306
0.70	0.1721	0.1800	0.1880	0.1959	0.2038	0.2117	0.2197	0.2276	0.2354	0.2433
0.80	0.1097	0.1148	0.1199	0.1250	0.1302	0.1353	0.1404	0.1456	0.1507	0.1558
0.90	0.0514	0.0538	0.0562	0.0586	0.0610	0.0634	0.0659	0.0683	0.0707	0.0732
1.00	0.0000	0.0000	0.0000	0.0000	0.0000	0.0000	0.0000	0.0000	0.0000	0.0000

β＼q	1.5000	1.5200	1.5400	1.5600	1.5800	1.6000	1.6200	1.6400	1.6600	1.6800
0.	0.6432	0.6595	0.6756	0.6912	0.7063	0.7209	0.7350	0.7487	0.7618	0.7746
0.10	0.6339	0.6502	0.6661	0.6815	0.6965	0.7111	0.7252	0.7388	0.7520	0.7647
0.20	0.6061	0.6220	0.6375	0.6527	0.6674	0.6818	0.6957	0.7093	0.7224	0.7351
0.30	0.5608	0.5760	0.5908	0.6054	0.6196	0.6335	0.6471	0.6603	0.6732	0.6857
0.40	0.4997	0.5137	0.5275	0.5410	0.5543	0.5674	0.5802	0.5928	0.6051	0.6172
0.50	0.4252	0.4376	0.4498	0.4619	0.4738	0.4856	0.4972	0.5086	0.5199	0.5310
0.60	0.3409	0.3512	0.3614	0.3715	0.3815	0.3915	0.4013	0.4111	0.4208	0.4304
0.70	0.2511	0.2589	0.2667	0.2744	0.2821	0.2898	0.2974	0.3050	0.3126	0.3201
0.80	0.1609	0.1661	0.1712	0.1763	0.1814	0.1865	0.1915	0.1966	0.2017	0.2067
0.90	0.0756	0.0780	0.0805	0.0829	0.0854	0.0878	0.0902	0.0927	0.0951	0.0976
1.00	0.0000	0.0000	0.0000	0.0000	0.0000	0.0000	0.0000	0.0000	0.0000	0.0000

β＼q	1.7000	1.7200	1.7400	1.7600	1.7800	1.8000	1.8200	1.8400	1.8600	1.8800
0.	0.7868	0.7985	0.8098	0.8206	0.8310	0.8409	0.8504	0.8594	0.8680	0.8762
0.10	0.7770	0.7888	0.8001	0.8110	0.8214	0.8315	0.8410	0.8502	0.8590	0.8673
0.20	0.7474	0.7593	0.7707	0.7818	0.7925	0.8027	0.8126	0.8221	0.8312	0.8400
0.30	0.6979	0.7098	0.7213	0.7325	0.7434	0.7539	0.7641	0.7740	0.7835	0.7927
0.40	0.6290	0.6406	0.6519	0.6629	0.6737	0.6842	0.6945	0.7045	0.7143	0.7238
0.50	0.5420	0.5527	0.5633	0.5738	0.5840	0.5941	0.6040	0.6137	0.6233	0.6327
0.60	0.4398	0.4492	0.4585	0.4677	0.4768	0.4868	0.4947	0.5035	0.5122	0.5208
0.70	0.3276	0.3350	0.3424	0.3497	0.3570	0.3642	0.3714	0.3786	0.3857	0.3927
0.80	0.2117	0.2167	0.2217	0.2267	0.2317	0.2367	0.2416	0.2465	0.2515	0.2564
0.90	0.1000	0.1024	0.1049	0.1073	0.1097	0.1122	0.1146	0.1170	0.1194	0.1218
1.00	0.0000	0.0000	0.0000	0.0000	0.0000	0.0000	0.0000	0.0000	0.0000	0.0000

β＼q	1.9000	1.9200	1.9400	1.9600	1.9800	2.0000	2.0200	2.0400	2.0600	2.0800
0.	0.8840	0.8914	0.8984	0.9051	0.9114	0.9173	0.9230	0.9283	0.9333	0.9380
0.10	0.8753	0.8828	0.8900	0.8969	0.9034	0.9095	0.9154	0.9209	0.9261	0.9310
0.20	0.8484	0.8564	0.8641	0.8715	0.8785	0.8852	0.8916	0.8977	0.9035	0.9090
0.30	0.8016	0.8102	0.8186	0.8266	0.8343	0.8417	0.8489	0.8558	0.8624	0.8688
0.40	0.7331	0.7422	0.7510	0.7595	0.7679	0.7760	0.7838	0.7915	0.7989	0.8062
0.50	0.6419	0.6509	0.6598	0.6685	0.6771	0.6854	0.6937	0.7017	0.7096	0.7173
0.60	0.5293	0.5376	0.5459	0.5541	0.5622	0.5702	0.5781	0.5858	0.5935	0.6011
0.70	0.3997	0.4067	0.4136	0.4205	0.4273	0.4341	0.4408	0.4475	0.4541	0.4607
0.80	0.2613	0.2661	0.2710	0.2758	0.2807	0.2855	0.2903	0.2951	0.2998	0.3046
0.90	0.1243	0.1267	0.1291	0.1315	0.1339	0.1363	0.1387	0.1412	0.1436	0.1460
1.00	0.0000	0.0000	0.0000	0.0000	0.0000	0.0000	0.0000	0.0000	0.0000	0.0000

TABLE 6.0-4. (CONTINUED)

β \ q	2.1000	2.1200	2.1400	2.1600	2.1800	2.2000	2.2200	2.2400	2.2600	2.2800
0.	0.9424	0.9466	0.9505	0.9541	0.9575	0.9607	0.9637	0.9665	0.9691	0.9716
0.10	0.9357	0.9400	0.9442	0.9481	0.9517	0.9551	0.9583	0.9613	0.9642	0.9668
0.20	0.9143	0.9193	0.9240	0.9286	0.9328	0.9369	0.9407	0.9444	0.9478	0.9511
0.30	0.8750	0.8808	0.8865	0.8919	0.8971	0.9021	0.9069	0.9115	0.9159	0.9201
0.40	0.8132	0.8200	0.8266	0.8330	0.8392	0.8452	0.8510	0.8567	0.8621	0.8674
0.50	0.7249	0.7323	0.7396	0.7467	0.7536	0.7604	0.7671	0.7736	0.7799	0.7862
0.60	0.6086	0.6160	0.6232	0.6304	0.6375	0.6445	0.6514	0.6582	0.6648	0.6714
0.70	0.4672	0.4737	0.4801	0.4865	0.4928	0.4991	0.5053	0.5115	0.5177	0.5237
0.80	0.3093	0.3141	0.3188	0.3235	0.3281	0.3328	0.3374	0.3420	0.3467	0.3512
0.90	0.1484	0.1508	0.1532	0.1555	0.1579	0.1603	0.1627	0.1651	0.1675	0.1699
1.00	0.0000	0.0000	0.0000	0.0000	0.0000	0.0000	0.0000	0.0000	0.0000	0.0000

β \ q	2.3000	2.3200	2.3400	2.3600	2.3800	2.4000	2.4200	2.4400	2.4600	2.4800
0.	0.9738	0.9759	0.9779	0.9797	0.9814	0.9829	0.9844	0.9857	0.9869	0.9881
0.10	0.9693	0.9716	0.9737	0.9757	0.9776	0.9794	0.9810	0.9825	0.9839	0.9852
0.20	0.9542	0.9571	0.9598	0.9624	0.9648	0.9671	0.9693	0.9713	0.9732	0.9750
0.30	0.9241	0.9279	0.9316	0.9351	0.9385	0.9417	0.9447	0.9477	0.9504	0.9531
0.40	0.8726	0.8775	0.8823	0.8869	0.8914	0.8957	0.8999	0.9040	0.9079	0.9116
0.50	0.7922	0.7982	0.8040	0.8097	0.8152	0.8206	0.8259	0.8311	0.8361	0.8410
0.60	0.6779	0.6844	0.6907	0.6969	0.7030	0.7090	0.7150	0.7208	0.7266	0.7323
0.70	0.5298	0.5358	0.5417	0.5476	0.5534	0.5592	0.5649	0.5706	0.5763	0.5818
0.80	0.3558	0.3604	0.3649	0.3694	0.3739	0.3784	0.3829	0.3874	0.3918	0.3962
0.90	0.1722	0.1746	0.1770	0.1794	0.1817	0.1841	0.1865	0.1888	0.1912	0.1936
1.00	0.0000	0.0000	0.0000	0.0000	0.0000	0.0000	0.0000	0.0000	0.0000	0.0000

β \ q	2.5000	2.5200	2.5400	2.5600	2.5800	2.6000	2.6200	2.6400	2.6600	2.6800
0.	0.9891	0.9901	0.9910	0.9918	0.9925	0.9932	0.9938	0.9944	0.9949	0.9954
0.10	0.9864	0.9875	0.9885	0.9895	0.9904	0.9912	0.9919	0.9926	0.9932	0.9938
0.20	0.9767	0.9783	0.9798	0.9812	0.9825	0.9837	0.9849	0.9859	0.9869	0.9879
0.30	0.9556	0.9580	0.9603	0.9624	0.9645	0.9665	0.9684	0.9701	0.9718	0.9734
0.40	0.9153	0.9188	0.9221	0.9254	0.9285	0.9316	0.9345	0.9373	0.9400	0.9426
0.50	0.8458	0.8505	0.8550	0.8595	0.8638	0.8680	0.8721	0.8761	0.8800	0.8838
0.60	0.7378	0.7433	0.7487	0.7540	0.7593	0.7644	0.7695	0.7744	0.7793	0.7841
0.70	0.5874	0.5929	0.5983	0.6037	0.6090	0.6143	0.6195	0.6247	0.6299	0.6350
0.80	0.4006	0.4050	0.4094	0.4137	0.4181	0.4224	0.4267	0.4309	0.4352	0.4395
0.90	0.1959	0.1983	0.2006	0.2030	0.2053	0.2077	0.2100	0.2123	0.2147	0.2170
1.00	0.0000	0.0000	0.0000	0.0000	0.0000	0.0000	0.0000	0.0000	0.0000	0.0000

β \ q	2.7000	2.7200	2.7400	2.7600	2.7800	2.8000	2.8200	2.8400	2.8600	2.8800
0.	0.9958	0.9962	0.9966	0.9969	0.9972	0.9975	0.9978	0.9980	0.9982	0.9984
0.10	0.9944	0.9949	0.9953	0.9957	0.9961	0.9965	0.9968	0.9971	0.9974	0.9976
0.20	0.9888	0.9896	0.9903	0.9910	0.9917	0.9923	0.9929	0.9934	0.9939	0.9944
0.30	0.9749	0.9764	0.9777	0.9790	0.9803	0.9814	0.9825	0.9836	0.9845	0.9855
0.40	0.9451	0.9475	0.9498	0.9520	0.9542	0.9562	0.9582	0.9601	0.9619	0.9637
0.50	0.8875	0.8911	0.8946	0.8980	0.9013	0.9046	0.9077	0.9108	0.9137	0.9166
0.60	0.7889	0.7935	0.7981	0.8026	0.8070	0.8113	0.8156	0.8197	0.8238	0.8279
0.70	0.6400	0.6450	0.6499	0.6548	0.6597	0.6645	0.6692	0.6739	0.6786	0.6832
0.80	0.4437	0.4479	0.4521	0.4562	0.4604	0.4645	0.4686	0.4727	0.4768	0.4809
0.90	0.2194	0.2217	0.2240	0.2263	0.2287	0.2310	0.2333	0.2356	0.2379	0.2402

TABLE 6.0-4. (CONTINUED)

β \ q	2.9000	2.9200	2.9400	2.9600	2.9800	3.0000	3.0200	3.0400	3.0600	3.0800
0.	0.9985	0.9987	0.9988	0.9990	0.9991	0.9992	0.9993	0.9993	0.9994	0.9995
0.10	0.9978	0.9980	0.9982	0.9984	0.9985	0.9987	0.9988	0.9989	0.9990	0.9991
0.20	0.9948	0.9952	0.9956	0.9959	0.9963	0.9965	0.9968	0.9971	0.9973	0.9975
0.30	0.9864	0.9872	0.9880	0.9887	0.9894	0.9901	0.9907	0.9913	0.9918	0.9923
0.40	0.9653	0.9669	0.9685	0.9700	0.9714	0.9727	0.9740	0.9753	0.9765	0.9776
0.50	0.9194	0.9221	0.9247	0.9273	0.9298	0.9322	0.9346	0.9368	0.9390	0.9412
0.60	0.8318	0.8357	0.8395	0.8432	0.8469	0.8505	0.8540	0.8575	0.8609	0.8642
0.70	0.6878	0.6923	0.6968	0.7012	0.7055	0.7099	0.7141	0.7184	0.7226	0.7267
0.80	0.4849	0.4889	0.4929	0.4969	0.5009	0.5048	0.5088	0.5127	0.5165	0.5204
0.90	0.2425	0.2448	0.2471	0.2494	0.2517	0.2540	0.2563	0.2586	0.2609	0.2632
1.00	0.0000	0.0000	0.0000	0.0000	0.0000	0.0000	0.0000	0.0000	0.0000	0.0000

β \ q	3.0000	3.1000	3.2000	3.3000	3.4000	3.5000	3.6000	3.7000	3.8000	3.9000
0.	0.9992	0.9995	0.9997	0.9999	0.9999	1.0000	1.0000	1.0000	1.0000	1.0000
0.10	0.9987	0.9992	0.9995	0.9997	0.9999	0.9999	1.0000	1.0000	1.0000	1.0000
0.20	0.9965	0.9977	0.9985	0.9991	0.9994	0.9996	0.9998	0.9999	0.9999	0.9999
0.30	0.9901	0.9928	0.9949	0.9964	0.9975	0.9982	0.9988	0.9992	0.9994	0.9996
0.40	0.9727	0.9787	0.9834	0.9872	0.9902	0.9925	0.9944	0.9957	0.9968	0.9977
0.50	0.9322	0.9432	0.9527	0.9608	0.9676	0.9734	0.9782	0.9822	0.9856	0.9884
0.60	0.8505	0.8675	0.8829	0.8968	0.9093	0.9205	0.9305	0.9394	0.9474	0.9544
0.70	0.7099	0.7308	0.7506	0.7693	0.7869	0.8035	0.8190	0.8336	0.8472	0.8600
0.80	0.5048	0.5243	0.5432	0.5617	0.5797	0.5973	0.6143	0.6309	0.6469	0.6625
0.90	0.2540	0.2655	0.2768	0.2881	0.2993	0.3104	0.3215	0.3324	0.3433	0.3542
1.00	0.0000	0.0000	0.0000	0.0000	0.0000	0.0000	0.0000	0.0000	0.0000	0.0000

β \ q	4.0000	4.1000	4.2000	4.3000	4.4000	4.5000	4.6000	4.7000	4.8000	4.9000
0.	1.0000	1.0000	1.0000	1.0000	1.0000	1.0000	1.0000	1.0000	1.0000	1.0000
0.10	1.0000	1.0000	1.0000	1.0000	1.0000	1.0000	1.0000	1.0000	1.0000	1.0000
0.20	1.0000	1.0000	1.0000	1.0000	1.0000	1.0000	1.0000	1.0000	1.0000	1.0000
0.30	0.9997	0.9998	0.9999	0.9999	0.9999	1.0000	1.0000	1.0000	1.0000	1.0000
0.40	0.9983	0.9987	0.9991	0.9993	0.9995	0.9997	0.9998	0.9999	0.9999	0.9999
0.50	0.9906	0.9925	0.9940	0.9953	0.9963	0.9971	0.9977	0.9982	0.9986	0.9989
0.60	0.9606	0.9660	0.9708	0.9750	0.9787	0.9818	0.9846	0.9869	0.9890	0.9907
0.70	0.8719	0.8829	0.8932	0.9027	0.9115	0.9197	0.9272	0.9341	0.9404	0.9462
0.80	0.6776	0.6923	0.7064	0.7201	0.7334	0.7461	0.7585	0.7703	0.7818	0.7928
0.90	0.3649	0.3755	0.3861	0.3965	0.4069	0.4172	0.4274	0.4375	0.4475	0.4574
1.00	0.0000	0.0000	0.0000	0.0000	0.0000	0.0000	0.0000	0.0000	0.0000	0.0000

β \ q	5.0000	5.1000	5.2000	5.3000	5.4000	5.5000	5.6000	5.7000	5.8000	5.9000
0.	1.0000	1.0000	1.0000	1.0000	1.0000	1.0000	1.0000	1.0000	1.0000	1.0000
0.10	1.0000	1.0000	1.0000	1.0000	1.0000	1.0000	1.0000	1.0000	1.0000	1.0000
0.20	1.0000	1.0000	1.0000	1.0000	1.0000	1.0000	1.0000	1.0000	1.0000	1.0000
0.30	1.0000	1.0000	1.0000	1.0000	1.0000	1.0000	1.0000	1.0000	1.0000	1.0000
0.40	0.9999	1.0000	1.0000	1.0000	1.0000	1.0000	1.0000	1.0000	1.0000	1.0000
0.50	0.9992	0.9994	0.9995	0.9996	0.9997	0.9998	0.9999	0.9999	0.9999	0.9999
0.60	0.9922	0.9935	0.9946	0.9955	0.9962	0.9969	0.9974	0.9979	0.9983	0.9986
0.70	0.9516	0.9565	0.9609	0.9649	0.9686	0.9720	0.9750	0.9777	0.9802	0.9824
0.80	0.8034	0.8135	0.8233	0.8327	0.8417	0.8503	0.8585	0.8663	0.8739	0.8810
0.90	0.4672	0.4769	0.4866	0.4961	0.5055	0.5148	0.5240	0.5331	0.5421	0.5510
1.00	0.0000	0.0000	0.0000	0.0000	0.0000	0.0000	0.0000	0.0000	0.0000	0.0000

TABLE 6.0-4. (CONTINUED)

β \ q	6.0000	6.1000	6.2000	6.3000	6.4000	6.5000	6.6000	6.7000	6.8000	6.9000
0.	1.0000	1.0000	1.0000	1.0000	1.0000	1.0000	1.0000	1.0000	1.0000	1.0000
0.10	1.0000	1.0000	1.0000	1.0000	1.0000	1.0000	1.0000	1.0000	1.0000	1.0000
0.20	1.0000	1.0000	1.0000	1.0000	1.0000	1.0000	1.0000	1.0000	1.0000	1.0000
0.30	1.0000	1.0000	1.0000	1.0000	1.0000	1.0000	1.0000	1.0000	1.0000	1.0000
0.40	1.0000	1.0000	1.0000	1.0000	1.0000	1.0000	1.0000	1.0000	1.0000	1.0000
0.50	1.0000	1.0000	1.0000	1.0000	1.0000	1.0000	1.0000	1.0000	1.0000	1.0000
0.60	0.9989	0.9991	0.9992	0.9994	0.9995	0.9996	0.9997	0.9998	0.9998	0.9999
0.70	0.9844	0.9862	0.9878	0.9893	0.9905	0.9917	0.9927	0.9936	0.9944	0.9951
0.80	0.8879	0.8944	0.9006	0.9065	0.9122	0.9175	0.9226	0.9274	0.9319	0.9363
0.90	0.5598	0.5685	0.5771	0.5856	0.5940	0.6023	0.6104	0.6185	0.6264	0.6343
1.00	0.0000	0.0000	0.0000	0.0000	0.0000	0.0000	0.0000	0.0000	0.0000	0.0000

β \ q	7.0000	7.1000	7.2000	7.3000	7.4000	7.5000	7.6000	7.7000	7.8000	7.9000
0.	1.0000	1.0000	1.0000	1.0000	1.0000	1.0000	1.0000	1.0000	1.0000	1.0000
0.10	1.0000	1.0000	1.0000	1.0000	1.0000	1.0000	1.0000	1.0000	1.0000	1.0000
0.20	1.0000	1.0000	1.0000	1.0000	1.0000	1.0000	1.0000	1.0000	1.0000	1.0000
0.30	1.0000	1.0000	1.0000	1.0000	1.0000	1.0000	1.0000	1.0000	1.0000	1.0000
0.40	1.0000	1.0000	1.0000	1.0000	1.0000	1.0000	1.0000	1.0000	1.0000	1.0000
0.50	1.0000	1.0000	1.0000	1.0000	1.0000	1.0000	1.0000	1.0000	1.0000	1.0000
0.60	0.9999	0.9999	0.9999	1.0000	1.0000	1.0000	1.0000	1.0000	1.0000	1.0000
0.70	0.9957	0.9963	0.9968	0.9972	0.9976	0.9979	0.9982	0.9984	0.9987	0.9988
0.80	0.9403	0.9442	0.9478	0.9513	0.9546	0.9576	0.9605	0.9632	0.9658	0.9682
0.90	0.6420	0.6496	0.6572	0.6646	0.6719	0.6791	0.6862	0.6931	0.7000	0.7068
1.00	0.0000	0.0000	0.0000	0.0000	0.0000	0.0000	0.0000	0.0000	0.0000	0.0000

β \ q	8.0000	8.1000	8.2000	8.3000	8.4000	8.5000	8.6000	8.7000	8.8000	8.9000
0.	1.0000	1.0000	1.0000	1.0000	1.0000	1.0000	1.0000	1.0000	1.0000	1.0000
0.10	1.0000	1.0000	1.0000	1.0000	1.0000	1.0000	1.0000	1.0000	1.0000	1.0000
0.20	1.0000	1.0000	1.0000	1.0000	1.0000	1.0000	1.0000	1.0000	1.0000	1.0000
0.30	1.0000	1.0000	1.0000	1.0000	1.0000	1.0000	1.0000	1.0000	1.0000	1.0000
0.40	1.0000	1.0000	1.0000	1.0000	1.0000	1.0000	1.0000	1.0000	1.0000	1.0000
0.50	1.0000	1.0000	1.0000	1.0000	1.0000	1.0000	1.0000	1.0000	1.0000	1.0000
0.60	1.0000	1.0000	1.0000	1.0000	1.0000	1.0000	1.0000	1.0000	1.0000	1.0000
0.70	0.9990	0.9991	0.9993	0.9994	0.9995	0.9996	0.9996	0.9997	0.9997	0.9998
0.80	0.9704	0.9726	0.9745	0.9764	0.9781	0.9797	0.9813	0.9827	0.9840	0.9852
0.90	0.7135	0.7200	0.7265	0.7328	0.7391	0.7452	0.7512	0.7572	0.7630	0.7687
1.00	0.0000	0.0000	0.0000	0.0000	0.0000	0.0000	0.0000	0.0000	0.0000	0.0000

β \ q	9.0000	9.1000	9.2000	9.3000	9.4000	9.5000	9.6000	9.7000	9.8000	9.9000
0.	1.0000	1.0000	1.0000	1.0000	1.0000	1.0000	1.0000	1.0000	1.0000	1.0000
0.10	1.0000	1.0000	1.0000	1.0000	1.0000	1.0000	1.0000	1.0000	1.0000	1.0000
0.20	1.0000	1.0000	1.0000	1.0000	1.0000	1.0000	1.0000	1.0000	1.0000	1.0000
0.30	1.0000	1.0000	1.0000	1.0000	1.0000	1.0000	1.0000	1.0000	1.0000	1.0000
0.40	1.0000	1.0000	1.0000	1.0000	1.0000	1.0000	1.0000	1.0000	1.0000	1.0000
0.50	1.0000	1.0000	1.0000	1.0000	1.0000	1.0000	1.0000	1.0000	1.0000	1.0000
0.60	1.0000	1.0000	1.0000	1.0000	1.0000	1.0000	1.0000	1.0000	1.0000	1.0000
0.70	0.9998	0.9998	0.9999	0.9999	0.9999	0.9999	1.0000	1.0000	1.0000	1.0000
0.80	0.9864	0.9875	0.9885	0.9894	0.9902	0.9910	0.9918	0.9924	0.9930	0.9936
0.90	0.7743	0.7799	0.7853	0.7906	0.7959	0.8010	0.8060	0.8110	0.8158	0.8206
1.00	0.0000	0.0000	0.0000	0.0000	0.0000	0.0000	0.0000	0.0000	0.0000	0.0000

TABLE 6.0-4. (CONCLUDED)

q / β	10.0000	10.1000	10.2000	10.3000	10.4000	10.5000	10.6000	10.7000	10.8000	10.9000
0.	1.0000	1.0000	1.0000	1.0000	1.0000	1.0000	1.0000	1.0000	1.0000	1.0000
0.10	1.0000	1.0000	1.0000	1.0000	1.0000	1.0000	1.0000	1.0000	1.0000	1.0000
0.20	1.0000	1.0000	1.0000	1.0000	1.0000	1.0000	1.0000	1.0000	1.0000	1.0000
0.30	1.0000	1.0000	1.0000	1.0000	1.0000	1.0000	1.0000	1.0000	1.0000	1.0000
0.40	1.0000	1.0000	1.0000	1.0000	1.0000	1.0000	1.0000	1.0000	1.0000	1.0000
0.50	1.0000	1.0000	1.0000	1.0000	1.0000	1.0000	1.0000	1.0000	1.0000	1.0000
0.60	1.0000	1.0000	1.0000	1.0000	1.0000	1.0000	1.0000	1.0000	1.0000	1.0000
0.70	1.0000	1.0000	1.0000	1.0000	1.0000	1.0000	1.0000	1.0000	1.0000	1.0000
0.80	0.9942	0.9947	0.9951	0.9955	0.9959	0.9963	0.9966	0.9969	0.9972	0.9974
0.90	0.8252	0.8298	0.8343	0.8387	0.8429	0.8472	0.8513	0.8553	0.8593	0.8631
1.00	0.0000	0.0000	0.0000	0.0000	0.0000	0.0000	0.0000	0.0000	0.0000	0.0000

TABLE 6.0-5. SPHERE-PARAMETER ψ_3

β \ q	0.5000	0.5200	0.5400	0.5600	0.5800	0.6000	0.6200	0.6400	0.6600	0.6800
0.	0.0000	0.0001	0.0001	0.0003	0.0004	0.0007	0.0011	0.0016	0.0023	0.0032
0.10	0.0000	0.0001	0.0001	0.0003	0.0004	0.0007	0.0011	0.0016	0.0022	0.0031
0.20	0.0000	0.0001	0.0001	0.0002	0.0004	0.0007	0.0010	0.0015	0.0021	0.0029
0.30	0.0000	0.0001	0.0001	0.0002	0.0004	0.0006	0.0009	0.0014	0.0020	0.0027
0.40	0.0000	0.0001	0.0001	0.0002	0.0004	0.0006	0.0008	0.0012	0.0018	0.0025
0.50	0.0000	0.0001	0.0001	0.0002	0.0003	0.0005	0.0007	0.0011	0.0016	0.0022
0.60	0.0000	0.0000	0.0001	0.0002	0.0003	0.0005	0.0006	0.0010	0.0014	0.0019
0.70	0.0000	0.0000	0.0001	0.0002	0.0003	0.0004	0.0006	0.0008	0.0011	0.0016
0.80	0.0000	0.0000	0.0001	0.0001	0.0002	0.0003	0.0005	0.0008	0.0011	0.0016
0.90	0.0000	0.0000	0.0001	0.0001	0.0002	0.0003	0.0004	0.0006	0.0009	0.0013
1.00	0.0000	0.0000	0.0000	0.0001	0.0001	0.0002	0.0003	0.0005	0.0007	0.0010

β \ q	0.7000	0.7200	0.7400	0.7600	0.7800	0.8000	0.8200	0.8400	0.8600	0.8800
0.	0.0043	0.0057	0.0074	0.0093	0.0116	0.0141	0.0170	0.0202	0.0237	0.0276
0.10	0.0043	0.0057	0.0073	0.0092	0.0114	0.0140	0.0168	0.0200	0.0235	0.0273
0.20	0.0042	0.0055	0.0071	0.0089	0.0111	0.0136	0.0163	0.0194	0.0228	0.0265
0.30	0.0040	0.0052	0.0067	0.0085	0.0106	0.0129	0.0155	0.0185	0.0217	0.0252
0.40	0.0037	0.0049	0.0063	0.0079	0.0098	0.0120	0.0145	0.0172	0.0202	0.0234
0.50	0.0034	0.0044	0.0057	0.0072	0.0089	0.0109	0.0132	0.0156	0.0184	0.0213
0.60	0.0030	0.0039	0.0051	0.0064	0.0079	0.0097	0.0117	0.0139	0.0163	0.0189
0.70	0.0026	0.0034	0.0044	0.0055	0.0068	0.0084	0.0101	0.0120	0.0141	0.0163
0.80	0.0021	0.0028	0.0036	0.0046	0.0057	0.0070	0.0084	0.0100	0.0117	0.0136
0.90	0.0017	0.0023	0.0029	0.0037	0.0046	0.0056	0.0068	0.0080	0.0094	0.0110
1.00	0.0013	0.0017	0.0022	0.0028	0.0035	0.0043	0.0052	0.0061	0.0072	0.0084

β \ q	0.9000	0.9200	0.9400	0.9600	0.9800	1.0000	1.0200	1.0400	1.0600	1.0800
0.	0.0317	0.0361	0.0408	0.0458	0.0510	0.0565	0.0622	0.0680	0.0741	0.0802
0.10	0.0314	0.0358	0.0404	0.0454	0.0505	0.0559	0.0616	0.0674	0.0733	0.0795
0.20	0.0305	0.0347	0.0392	0.0440	0.0491	0.0543	0.0598	0.0654	0.0712	0.0771
0.30	0.0290	0.0330	0.0373	0.0419	0.0467	0.0516	0.0568	0.0622	0.0677	0.0734
0.40	0.0270	0.0307	0.0347	0.0390	0.0434	0.0481	0.0529	0.0579	0.0630	0.0683
0.50	0.0245	0.0280	0.0316	0.0355	0.0395	0.0438	0.0481	0.0527	0.0574	0.0622
0.60	0.0218	0.0240	0.0281	0.0315	0.0351	0.0388	0.0427	0.0468	0.0509	0.0552
0.70	0.0188	0.0214	0.0242	0.0272	0.0303	0.0335	0.0369	0.0404	0.0440	0.0477
0.80	0.0157	0.0179	0.0202	0.0227	0.0253	0.0280	0.0308	0.0337	0.0367	0.0398
0.90	0.0126	0.0144	0.0163	0.0182	0.0203	0.0225	0.0248	0.0271	0.0295	0.0320
1.00	0.0096	0.0110	0.0124	0.0139	0.0155	0.0172	0.0189	0.0207	0.0226	0.0244

β \ q	1.1000	1.1200	1.1400	1.1600	1.1800	1.2000	1.2200	1.2400	1.2600	1.2800
0.	0.0866	0.0930	0.0995	0.1061	0.1128	0.1195	0.1262	0.1329	0.1396	0.1463
0.10	0.0857	0.0921	0.0985	0.1051	0.1117	0.1183	0.1249	0.1316	0.1382	0.1449
0.20	0.0832	0.0894	0.0957	0.1020	0.1084	0.1149	0.1214	0.1278	0.1343	0.1407
0.30	0.0792	0.0851	0.0910	0.0971	0.1032	0.1093	0.1155	0.1217	0.1279	0.1340
0.40	0.0737	0.0792	0.0848	0.0904	0.0961	0.1019	0.1076	0.1134	0.1192	0.1250
0.50	0.0671	0.0721	0.0772	0.0823	0.0875	0.0928	0.0981	0.1034	0.1087	0.1140
0.60	0.0596	0.0640	0.0685	0.0731	0.0778	0.0824	0.0871	0.0919	0.0966	0.1014
0.70	0.0514	0.0553	0.0592	0.0632	0.0672	0.0712	0.0753	0.0794	0.0835	0.0876
0.80	0.0430	0.0462	0.0495	0.0528	0.0562	0.0596	0.0630	0.0664	0.0699	0.0733
0.90	0.0345	0.0371	0.0398	0.0424	0.0451	0.0479	0.0506	0.0534	0.0562	0.0590
1.00	0.0264	0.0284	0.0304	0.0324	0.0345	0.0366	0.0387	0.0408	0.0429	0.0451

TABLE 6.0-5. (CONTINUED)

β \ q	1.3000	1.3200	1.3400	1.3600	1.3800	1.4000	1.4200	1.4400	1.4600	1.4800
0.	0.1529	0.1595	0.1660	0.1724	0.1787	0.1850	0.1911	0.1971	0.2030	0.2088
0.10	0.1514	0.1580	0.1644	0.1708	0.1771	0.1833	0.1894	0.1953	0.2012	0.2069
0.20	0.1471	0.1535	0.1598	0.1660	0.1722	0.1783	0.1842	0.1901	0.1958	0.2014
0.30	0.1402	0.1463	0.1523	0.1583	0.1642	0.1700	0.1758	0.1815	0.1870	0.1925
0.40	0.1308	0.1365	0.1422	0.1478	0.1534	0.1589	0.1644	0.1697	0.1750	0.1802
0.50	0.1193	0.1245	0.1298	0.1350	0.1401	0.1452	0.1503	0.1553	0.1602	0.1650
0.60	0.1061	0.1108	0.1155	0.1202	0.1248	0.1294	0.1340	0.1385	0.1430	0.1474
0.70	0.0918	0.0959	0.1000	0.1041	0.1081	0.1122	0.1162	0.1202	0.1241	0.1280
0.80	0.0768	0.0803	0.0837	0.0872	0.0906	0.0940	0.0974	0.1008	0.1042	0.1075
0.90	0.0618	0.0646	0.0674	0.0702	0.0729	0.0757	0.0785	0.0812	0.0839	0.0866
1.00	0.0472	0.0493	0.0515	0.0536	0.0558	0.0579	0.0600	0.0621	0.0642	0.0663

β \ q	1.5000	1.5200	1.5400	1.5600	1.5800	1.6000	1.6200	1.6400	1.6600	1.6800
0.	0.2144	0.2199	0.2252	0.2304	0.2354	0.2403	0.2450	0.2496	0.2539	0.2582
0.10	0.2125	0.2180	0.2233	0.2285	0.2335	0.2383	0.2430	0.2476	0.2520	0.2562
0.20	0.2070	0.2123	0.2176	0.2227	0.2276	0.2325	0.2371	0.2417	0.2461	0.2503
0.30	0.1978	0.2030	0.2082	0.2132	0.2180	0.2228	0.2274	0.2318	0.2362	0.2404
0.40	0.1853	0.1903	0.1952	0.2000	0.2047	0.2093	0.2138	0.2182	0.2225	0.2266
0.50	0.1698	0.1745	0.1792	0.1837	0.1882	0.1925	0.1968	0.2010	0.2051	0.2091
0.60	0.1518	0.1561	0.1604	0.1646	0.1687	0.1727	0.1767	0.1806	0.1845	0.1882
0.70	0.1319	0.1357	0.1395	0.1432	0.1469	0.1505	0.1541	0.1577	0.1612	0.1646
0.80	0.1108	0.1140	0.1173	0.1205	0.1237	0.1268	0.1299	0.1329	0.1360	0.1390
0.90	0.0893	0.0920	0.0946	0.0972	0.0998	0.1024	0.1049	0.1074	0.1099	0.1124
1.00	0.0683	0.0704	0.0724	0.0744	0.0764	0.0784	0.0803	0.0823	0.0842	0.0861

β \ q	1.7000	1.7200	1.7400	1.7600	1.7800	1.8000	1.8200	1.8400	1.8600	1.8800
0.	0.2623	0.2662	0.2699	0.2735	0.2770	0.2803	0.2835	0.2865	0.2893	0.2921
0.10	0.2603	0.2642	0.2680	0.2716	0.2751	0.2784	0.2816	0.2846	0.2875	0.2903
0.20	0.2544	0.2583	0.2621	0.2658	0.2693	0.2727	0.2759	0.2790	0.2820	0.2849
0.30	0.2445	0.2485	0.2523	0.2560	0.2596	0.2630	0.2663	0.2695	0.2726	0.2756
0.40	0.2307	0.2346	0.2384	0.2421	0.2457	0.2492	0.2526	0.2559	0.2591	0.2621
0.50	0.2131	0.2169	0.2206	0.2243	0.2279	0.2313	0.2347	0.2380	0.2412	0.2443
0.60	0.1920	0.1956	0.1991	0.2026	0.2061	0.2094	0.2127	0.2159	0.2190	0.2221
0.70	0.1680	0.1713	0.1746	0.1778	0.1809	0.1840	0.1871	0.1901	0.1931	0.1960
0.80	0.1419	0.1448	0.1477	0.1505	0.1533	0.1561	0.1588	0.1615	0.1641	0.1667
0.90	0.1148	0.1172	0.1196	0.1220	0.1243	0.1266	0.1289	0.1311	0.1333	0.1355
1.00	0.0880	0.0898	0.0916	0.0935	0.0953	0.0971	0.0988	0.1006	0.1023	0.1040

β \ q	1.9000	1.9200	1.9400	1.9600	1.9800	2.000	2.0200	2.0400	2.0600	2.0800
0.	0.2947	0.2971	0.2995	0.3017	0.3038	0.3058	0.3077	0.3094	0.3111	0.3127
0.10	0.2929	0.2954	0.2978	0.3001	0.3022	0.3042	0.3061	0.3079	0.3097	0.3113
0.20	0.2876	0.2902	0.2927	0.2950	0.2973	0.2994	0.3015	0.3034	0.3052	0.3070
0.30	0.2784	0.2811	0.2836	0.2863	0.2887	0.2910	0.2932	0.2953	0.2973	0.2992
0.40	0.2651	0.2679	0.2707	0.2734	0.2759	0.2784	0.2808	0.2831	0.2853	0.2875
0.50	0.2473	0.2503	0.2531	0.2559	0.2586	0.2612	0.2638	0.2662	0.2686	0.2709
0.60	0.2251	0.2280	0.2309	0.2337	0.2364	0.2391	0.2417	0.2443	0.2468	0.2492
0.70	0.1988	0.2016	0.2044	0.2071	0.2097	0.2123	0.2149	0.2174	0.2198	0.2222
0.80	0.1693	0.1718	0.1743	0.1767	0.1791	0.1815	0.1839	0.1862	0.1884	0.1907
0.90	0.1377	0.1398	0.1419	0.1440	0.1460	0.1481	0.1501	0.1520	0.1540	0.1559
1.00	0.1056	0.1073	0.1089	0.1106	0.1122	0.1137	0.1153	0.1168	0.1184	0.1199

TABLE 6.0-5. (CONTINUED)

β \ q	2.1000	2.1200	2.1400	2.1600	2.1800	2.2000	2.2200	2.2400	2.2600	2.2800
0.	0.3141	0.3155	0.3168	0.3180	0.3192	0.3202	0.3212	0.3222	0.3230	0.3239
0.10	0.3128	0.3142	0.3156	0.3168	0.3180	0.3191	0.3202	0.3211	0.3221	0.3229
0.20	0.3086	0.3102	0.3116	0.3130	0.3143	0.3156	0.3168	0.3179	0.3189	0.3199
0.30	0.3011	0.3028	0.3045	0.3061	0.3076	0.3090	0.3104	0.3117	0.3129	0.3141
0.40	0.2895	0.2915	0.2934	0.2952	0.2969	0.2986	0.3002	0.3018	0.3033	0.3047
0.50	0.2732	0.2753	0.2775	0.2795	0.2815	0.2834	0.2852	0.2870	0.2888	0.2904
0.60	0.2515	0.2539	0.2561	0.2583	0.2604	0.2625	0.2645	0.2665	0.2685	0.2703
0.70	0.2246	0.2269	0.2292	0.2314	0.2336	0.2357	0.2378	0.2399	0.2419	0.2438
0.80	0.1929	0.1950	0.1972	0.1993	0.2014	0.2034	0.2054	0.2074	0.2093	0.2112
0.90	0.1578	0.1597	0.1615	0.1634	0.1652	0.1670	0.1687	0.1704	0.1722	0.1738
1.00	0.1214	0.1228	0.1243	0.1257	0.1271	0.1285	0.1299	0.1313	0.1326	0.1340

β \ q	2.3000	2.3200	2.3400	2.3600	2.3800	2.4000	2.4200	2.4400	2.4600	2.4800
0.	0.3246	0.3253	0.3260	0.3266	0.3271	0.3276	0.3281	0.3286	0.3290	0.3294
0.10	0.3237	0.3244	0.3251	0.3258	0.3264	0.3269	0.3274	0.3279	0.3284	0.3288
0.20	0.3208	0.3216	0.3225	0.3232	0.3239	0.3246	0.3252	0.3258	0.3263	0.3269
0.30	0.3152	0.3163	0.3173	0.3182	0.3191	0.3200	0.3208	0.3216	0.3223	0.3229
0.40	0.3060	0.3073	0.3086	0.3098	0.3109	0.3120	0.3131	0.3141	0.3150	0.3159
0.50	0.2920	0.2936	0.2951	0.2966	0.2980	0.2994	0.3007	0.3019	0.3032	0.3043
0.60	0.2722	0.2739	0.2757	0.2774	0.2790	0.2806	0.2822	0.2837	0.2852	0.2866
0.70	0.2458	0.2477	0.2495	0.2514	0.2531	0.2549	0.2566	0.2583	0.2599	0.2615
0.80	0.2131	0.2150	0.2168	0.2186	0.2204	0.2221	0.2238	0.2255	0.2272	0.2288
0.90	0.1755	0.1772	0.1788	0.1804	0.1820	0.1835	0.1851	0.1866	0.1881	0.1896
1.00	0.1353	0.1366	0.1379	0.1392	0.1404	0.1417	0.1429	0.1441	0.1453	0.1465

β \ q	2.5000	2.5200	2.5400	2.5600	2.5800	2.6000	2.6200	2.6400	2.6600	2.6800
0.	0.3297	0.3300	0.3303	0.3306	0.3308	0.3311	0.3313	0.3315	0.3316	0.3318
0.10	0.3292	0.3295	0.3298	0.3301	0.3304	0.3307	0.3309	0.3311	0.3313	0.3315
0.20	0.3273	0.3278	0.3282	0.3286	0.3289	0.3293	0.3296	0.3299	0.3301	0.3304
0.30	0.3236	0.3242	0.3248	0.3253	0.3258	0.3263	0.3267	0.3272	0.3276	0.3279
0.40	0.3168	0.3176	0.3184	0.3192	0.3199	0.3206	0.3212	0.3219	0.3225	0.3230
0.50	0.3055	0.3066	0.3076	0.3087	0.3096	0.3106	0.3115	0.3124	0.3132	0.3141
0.60	0.2880	0.2894	0.2907	0.2920	0.2932	0.2944	0.2956	0.2968	0.2979	0.2990
0.70	0.2631	0.2646	0.2662	0.2676	0.2691	0.2705	0.2719	0.2733	0.2746	0.2759
0.80	0.2304	0.2320	0.2336	0.2351	0.2366	0.2381	0.2396	0.2410	0.2424	0.2438
0.90	0.1911	0.1925	0.1940	0.1954	0.1968	0.1981	0.1995	0.2008	0.2022	0.2035
1.00	0.1477	0.1488	0.1500	0.1511	0.1522	0.1533	0.1544	0.1555	0.1566	0.1576

β \ q	2.7000	2.7200	2.7400	2.7600	2.7800	2.8000	2.8200	2.8400	2.8600	2.8800
0.	0.3319	0.3321	0.3322	0.3323	0.3324	0.3325	0.3326	0.3327	0.3327	0.3328
0.10	0.3317	0.3318	0.3320	0.3321	0.3322	0.3323	0.3324	0.3325	0.3326	0.3326
0.20	0.3306	0.3308	0.3310	0.3312	0.3314	0.3315	0.3317	0.3318	0.3320	0.3321
0.30	0.3283	0.3286	0.3289	0.3292	0.3295	0.3398	0.3300	0.3302	0.3304	0.3306
0.40	0.3236	0.3241	0.3246	0.3250	0.3255	0.3259	0.3263	0.3267	0.3270	0.3274
0.50	0.3148	0.3156	0.3163	0.3170	0.3177	0.3184	0.3190	0.3196	0.3202	0.3207
0.60	0.3000	0.3011	0.3021	0.3030	0.3040	0.3049	0.3058	0.3066	0.3075	0.3083
0.70	0.2772	0.2784	0.2797	0.2809	0.2820	0.2832	0.2843	0.2854	0.2865	0.2876
0.80	0.2452	0.2466	0.2479	0.2492	0.2505	0.2518	0.2530	0.2543	0.2555	0.2567
0.90	0.2048	0.2061	0.2073	0.2086	0.2098	0.2110	0.2122	0.2134	0.2146	0.2157
1.00	0.1587	0.1597	0.1607	0.1617	0.1627	0.1637	0.1647	0.1657	0.1666	0.1676

TABLE 6.0-5. (CONTINUED)

q / β	2.9000	2.9200	2.9400	2.9600	2.9800	3.0000	3.0200	3.0400	3.0600	3.0800
0.	0.3328	0.3329	0.3329	0.3330	0.3330	0.3331	0.3331	0.3331	0.3331	0.3332
0.10	0.3327	0.3328	0.3328	0.3329	0.3329	0.3330	0.3330	0.3330	0.3331	0.3331
0.20	0.3322	0.3323	0.3324	0.3324	0.3325	0.3326	0.3327	0.3327	0.3328	0.3328
0.30	0.3308	0.3310	0.3312	0.3313	0.3315	0.3316	0.3317	0.3318	0.3319	0.3320
0.40	0.3277	0.3280	0.3283	0.3286	0.3289	0.3291	0.3293	0.3296	0.3298	0.3300
0.50	0.3212	0.3218	0.3223	0.3227	0.3232	0.3236	0.3240	0.3244	0.3248	0.3252
0.60	0.3091	0.3098	0.3106	0.3113	0.3120	0.3127	0.3134	0.3140	0.3146	0.3152
0.70	0.2886	0.2896	0.2906	0.2916	0.2925	0.2934	0.2944	0.2952	0.2961	0.2970
0.80	0.2578	0.2590	0.2602	0.2613	0.2624	0.2635	0.2645	0.2656	0.2666	0.2677
0.90	0.2169	0.2180	0.2191	0.2203	0.2213	0.2224	0.2235	0.2245	0.2256	0.2266
1.00	0.1685	0.1694	0.1703	0.1713	0.1722	0.1730	0.1739	0.1748	0.1756	0.1765

q / β	3.0000	3.1000	3.2000	3.3000	3.4000	3.5000	3.6000	3.7000	3.8000	3.9000
0.	0.3331	0.3332	0.3332	0.3333	0.3333	0.3333	0.3333	0.3333	0.3333	0.3333
0.10	0.3330	0.3331	0.3332	0.3333	0.3333	0.3333	0.3333	0.3333	0.3333	0.3333
0.20	0.3326	0.3329	0.3330	0.3332	0.3332	0.3333	0.3333	0.3333	0.3333	0.3333
0.30	0.3316	0.3321	0.3325	0.3328	0.3330	0.3331	0.3332	0.3332	0.3333	0.3333
0.40	0.3291	0.3302	0.3310	0.3316	0.3321	0.3324	0.3327	0.3328	0.3330	0.3331
0.50	0.3236	0.3256	0.3271	0.3284	0.3294	0.3303	0.3309	0.3314	0.3319	0.3322
0.60	0.3127	0.3158	0.3185	0.3208	0.3228	0.3244	0.3259	0.3271	0.3281	0.3290
0.70	0.2934	0.2978	0.3017	0.3052	0.3083	0.3112	0.3137	0.3159	0.3179	0.3197
0.80	0.2635	0.2687	0.2735	0.2779	0.2820	0.2859	0.2894	0.2927	0.2957	0.2985
0.90	0.2224	0.2276	0.2326	0.2372	0.2416	0.2457	0.2497	0.2534	0.2569	0.2603
1.00	0.1730	0.1773	0.1814	0.1853	0.1890	0.1925	0.1959	0.1991	0.2022	0.2051

q / β	4.0000	4.1000	4.2000	4.3000	4.4000	4.5000	4.6000	4.7000	4.8000	4.9000
0.	0.3333	0.3333	0.3333	0.3333	0.3333	0.3333	0.3333	0.3333	0.3333	0.3333
0.10	0.3333	0.3333	0.3333	0.3333	0.3333	0.3333	0.3333	0.3333	0.3333	0.3333
0.20	0.3333	0.3333	0.3333	0.3333	0.3333	0.3333	0.3333	0.3333	0.3333	0.3333
0.30	0.3333	0.3333	0.3333	0.3333	0.3333	0.3333	0.3333	0.3333	0.3333	0.3333
0.40	0.3331	0.3332	0.3332	0.3333	0.3333	0.3333	0.3333	0.3333	0.3333	0.3333
0.50	0.3325	0.3327	0.3328	0.3329	0.3330	0.3331	0.3332	0.3332	0.3332	0.3333
0.60	0.3297	0.3303	0.3308	0.3313	0.3316	0.3319	0.3322	0.3324	0.3326	0.3327
0.70	0.3213	0.3227	0.3239	0.3251	0.3261	0.3270	0.3277	0.3284	0.3290	0.3296
0.80	0.3011	0.3036	0.3058	0.3079	0.3098	0.3116	0.3133	0.3148	0.3162	0.3175
0.90	0.2634	0.2665	0.2693	0.2721	0.2747	0.2771	0.2795	0.2818	0.2839	0.2859
1.00	0.2079	0.2106	0.2132	0.2156	0.2180	0.2203	0.2225	0.2246	0.2266	0.2286

q / β	5.0000	5.1000	5.2000	5.3000	5.4000	5.5000	5.6000	5.7000	5.8000	5.9000
0.	0.3333	0.3333	0.3333	0.3333	0.3333	0.3333	0.3333	0.3333	0.3333	0.3333
0.10	0.3333	0.3333	0.3333	0.3333	0.3333	0.3333	0.3333	0.3333	0.3333	0.3333
0.20	0.3333	0.3333	0.3333	0.3333	0.3333	0.3333	0.3333	0.3333	0.3333	0.3333
0.30	0.3333	0.3333	0.3333	0.3333	0.3333	0.3333	0.3333	0.3333	0.3333	0.3333
0.40	0.3333	0.3333	0.3333	0.3333	0.3333	0.3333	0.3333	0.3333	0.3333	0.3333
0.50	0.3333	0.3333	0.3333	0.3333	0.3333	0.3333	0.3333	0.3333	0.3333	0.3333
0.60	0.3328	0.3329	0.3330	0.3331	0.3331	0.3332	0.3332	0.3332	0.3332	0.3333
0.70	0.3300	0.3305	0.3308	0.3312	0.3314	0.3317	0.3319	0.3321	0.3323	0.3324
0.80	0.3188	0.3199	0.3209	0.3219	0.3228	0.3236	0.3244	0.3251	0.3257	0.3263
0.90	0.2879	0.2897	0.2915	0.2932	0.2949	0.2964	0.2979	0.2993	0.3007	0.3020
1.00	0.2305	0.2323	0.2341	0.2358	0.2374	0.2390	0.2406	0.2420	0.2435	0.2449

TABLE 6.0-5. (CONTINUED)

β \ q	6.0000	6.1000	6.2000	6.3000	6.4000	6.5000	6.6000	6.7000	6.8000	6.9000
0.	0.3333	0.3333	0.3333	0.3333	0.3333	0.3333	0.3333	0.3333	0.3333	0.3333
0.10	0.3333	0.3333	0.3333	0.3333	0.3333	0.3333	0.3333	0.3333	0.3333	0.3333
0.20	0.3333	0.3333	0.3333	0.3333	0.3333	0.3333	0.3333	0.3333	0.3333	0.3333
0.30	0.3333	0.3333	0.3333	0.3333	0.3333	0.3333	0.3333	0.3333	0.3333	0.3333
0.40	0.3333	0.3333	0.3333	0.3333	0.3333	0.3333	0.3333	0.3333	0.3333	0.3333
0.50	0.3333	0.3333	0.3333	0.3333	0.3333	0.3333	0.3333	0.3333	0.3333	0.3333
0.60	0.3333	0.3333	0.3333	0.3333	0.3333	0.3333	0.3333	0.3333	0.3333	0.3333
0.70	0.3326	0.3327	0.3328	0.3329	0.3329	0.3330	0.3330	0.3331	0.3331	0.3331
0.80	0.3269	0.3274	0.3279	0.3283	0.3288	0.3291	0.3295	0.3298	0.3301	0.3304
0.90	0.3033	0.3045	0.3056	0.3067	0.3077	0.3088	0.3097	0.3107	0.3116	0.3124
1.00	0.2462	0.2475	0.2488	0.2501	0.2513	0.2525	0.2536	0.2547	0.2558	0.2568

β \ q	7.0000	7.1000	7.2000	7.3000	7.4000	7.5000	7.6000	7.7000	7.8000	7.9000
0.	0.3333	0.3333	0.3333	0.3333	0.3333	0.3333	0.3333	0.3333	0.3333	0.3333
0.10	0.3333	0.3333	0.3333	0.3333	0.3333	0.3333	0.3333	0.3333	0.3333	0.3333
0.20	0.3333	0.3333	0.3333	0.3333	0.3333	0.3333	0.3333	0.3333	0.3333	0.3333
0.30	0.3333	0.3333	0.3333	0.3333	0.3333	0.3333	0.3333	0.3333	0.3333	0.3333
0.40	0.3333	0.3333	0.3333	0.3333	0.3333	0.3333	0.3333	0.3333	0.3333	0.3333
0.50	0.3333	0.3333	0.3333	0.3333	0.3333	0.3333	0.3333	0.3333	0.3333	0.3333
0.60	0.3333	0.3333	0.3333	0.3333	0.3333	0.3333	0.3333	0.3333	0.3333	0.3333
0.70	0.3332	0.3332	0.3332	0.3332	0.3333	0.3333	0.3333	0.3333	0.3333	0.3333
0.80	0.3306	0.3309	0.3311	0.3313	0.3314	0.3316	0.3317	0.3319	0.3320	0.3321
0.90	0.3132	0.3140	0.3148	0.3155	0.3162	0.3169	0.3175	0.3182	0.3188	0.3193
1.00	0.2578	0.2588	0.2598	0.2607	0.2616	0.2625	0.2634	0.2643	0.2651	0.2659

β \ q	8.0000	8.1000	8.2000	8.3000	8.4000	8.5000	8.6000	8.7000	8.8000	8.9000
0.	0.3333	0.3333	0.3333	0.3333	0.3333	0.3333	0.3333	0.3333	0.3333	0.3333
0.10	0.3333	0.3333	0.3333	0.3333	0.3333	0.3333	0.3333	0.3333	0.3333	0.3333
0.20	0.3333	0.3333	0.3333	0.3333	0.3333	0.3333	0.3333	0.3333	0.3333	0.3333
0.30	0.3333	0.3333	0.3333	0.3333	0.3333	0.3333	0.3333	0.3333	0.3333	0.3333
0.40	0.3333	0.3333	0.3333	0.3333	0.3333	0.3333	0.3333	0.3333	0.3333	0.3333
0.50	0.3333	0.3333	0.3333	0.3333	0.3333	0.3333	0.3333	0.3333	0.3333	0.3333
0.60	0.3333	0.3333	0.3333	0.3333	0.3333	0.3333	0.3333	0.3333	0.3333	0.3333
0.70	0.3333	0.3333	0.3333	0.3333	0.3333	0.3333	0.3333	0.3333	0.3333	0.3333
0.80	0.3322	0.3323	0.3324	0.3325	0.3326	0.3327	0.3327	0.3328	0.3328	0.3329
0.90	0.3199	0.3204	0.3209	0.3214	0.3219	0.3223	0.3227	0.3232	0.3236	0.3240
1.00	0.2667	0.2675	0.2682	0.2690	0.2697	0.2704	0.2711	0.2718	0.2724	0.2731

β \ q	9.0000	9.1000	9.2000	9.3000	9.4000	9.5000	9.6000	9.7000	9.8000	9.9000
0.	0.3333	0.3333	0.3333	0.3333	0.3333	0.3333	0.3333	0.3333	0.3333	0.3333
0.10	0.3333	0.3333	0.3333	0.3333	0.3333	0.3333	0.3333	0.3333	0.3333	0.3333
0.20	0.3333	0.3333	0.3333	0.3333	0.3333	0.3333	0.3333	0.3333	0.3333	0.3333
0.30	0.3333	0.3333	0.3333	0.3333	0.3333	0.3333	0.3333	0.3333	0.3333	0.3333
0.40	0.3333	0.3333	0.3333	0.3333	0.3333	0.3333	0.3333	0.3333	0.3333	0.3333
0.50	0.3333	0.3333	0.3333	0.3333	0.3333	0.3333	0.3333	0.3333	0.3333	0.3333
0.60	0.3333	0.3333	0.3333	0.3333	0.3333	0.3333	0.3333	0.3333	0.3333	0.3333
0.70	0.3333	0.3333	0.3333	0.3333	0.3333	0.3333	0.3333	0.3333	0.3333	0.3333
0.80	0.3329	0.3330	0.3330	0.3330	0.3331	0.3331	0.3331	0.3331	0.3332	0.3332
0.90	0.3243	0.3247	0.3250	0.3254	0.3257	0.3260	0.3263	0.3266	0.3268	0.3271
1.00	0.2737	0.2743	0.2749	0.2755	0.2761	0.2767	0.2773	0.2778	0.2783	0.2789

TABLE 6.0-5. (CONCLUDED)

q β	10.0000	10.1000	10.2000	10.3000	10.4000	10.5000	10.6000	10.7000	10.8000	10.9000
0.	0.3333	0.3333	0.3333	0.3333	0.3333	0.3333	0.3333	0.3333	0.3333	0.3333
0.10	0.3333	0.3333	0.3333	0.3333	0.3333	0.3333	0.3333	0.3333	0.3333	0.3333
0.20	0.3333	0.3333	0.3333	0.3333	0.3333	0.3333	0.3333	0.3333	0.3333	0.3333
0.30	0.3333	0.3333	0.3333	0.3333	0.3333	0.3333	0.3333	0.3333	0.3333	0.3333
0.40	0.3333	0.3333	0.3333	0.3333	0.3333	0.3333	0.3333	0.3333	0.3333	0.3333
0.50	0.3333	0.3333	0.3333	0.3333	0.3333	0.3333	0.3333	0.3333	0.3333	0.3333
0.60	0.3333	0.3333	0.3333	0.3333	0.3333	0.3333	0.3333	0.3333	0.3333	0.3333
0.70	0.3333	0.3333	0.3333	0.3333	0.3333	0.3333	0.3333	0.3333	0.3333	0.3333
0.80	0.3332	0.3332	0.3332	0.3333	0.3333	0.3333	0.3333	0.3333	0.3333	0.3333
0.90	0.3273	0.3276	0.3278	0.3290	0.3283	0.3284	0.3286	0.3288	0.3290	0.3292
1.00	0.2794	0.2799	0.2804	0.2809	0.2814	0.2819	0.2823	0.2826	0.2832	0.2837

REFERENCES

1. Boley, B. A.; and Weiner, J. H.: Theory of Thermal Stresses. John Wiley and Sons, Inc., New York, 1962.

2. Newman, M. and Forray, M.: Thermal Stresses in Circular Rings. Machine Design, Nov. 8, 1962.

3. Newman, M. and Forray, M.: Bending Stresses Due to Temperature in Hollow Circular Plates, Part I. Journal of the Aerospace Sciences, October 1960.

4. Forray, M. and Newman, M.: Bending Stresses Due to Temperature in Hollow Circular Plates, Part II. Journal of the Aerospace Sciences, November 1960.

5. Newman, M. and Forray, M.: Bending Stresses Due to Temperature in Hollow Circular Plates, Part III. Journal of the Aerospace Sciences, December 1960.

6. Timoshenko, S.: Strength of Materials. Part II, Advanced Theory and Problems. Third ed., D. Van Nostrand Co., Inc., New York, 1956.

7. Thermo-Structural Analysis Manual. Technical Report No. WADD-TR-60-517, vol. I, August 1962.

8. Thermo-Structural Analysis Manual. Technical Report No. WADD-TR-60-517, Vol. II, October 1962.

REFERENCES (Continued)

9. Forray, M. J.; Newman, M.; and Kossar, J.: Thermal Stresses and Deflections in Rectangular Plates. Part 1, The Analysis and Test of Rectangular Panels with Temperature Gradients Through the Thickness. Technical Report No. ASD-TR-61-537 Part 1, Flight Dynamics Laboratory, Aeronautical Systems Division, Air Force Systems Command, Wright-Patterson Air Force Base, Ohio, December 1962.

10. Forray, M.; and Newman, M.: Stress and Deflection in Heated Plates on Beam Supports. Machine Design, Feb. 15, 1962.

11. Timoshenko, S.; and Woinowsky-Krieger, S.: Theory of Plates and Shells. McGraw-Hill Book Co., New York, 1959.

12. Timoshenko, S.; and Goodier, J.N.: Theory of Elasticity. McGraw-Hill Book Co., Inc., New York, 1951.

13. Gatewood, B.E.: Thermal Stresses. McGraw-Hill Book Co., Inc., New York, 1957.

14. Morgan, A. J. A.: A Proof of Duhamel's Analogy for Thermal Stresses. Journal of the Aerospace Sciences, July 1958.

15. Dharmarajan, S.: In-Plane Thermal Stress Analysis. General Dynamics, Convair Division, Memo No. SA-70-13, July 17, 1970.

16. Tsui, Y. W.: Stresses in Shells of Revolution. Pacific Coast Publishers, Menlo Park, Calif., 1968.

REFERENCES (Continued)

17. Baker, E. H.; Cappelli, A. P.; Kovalevsky, L.; Rish, F. L.; and Verette, R. M.; Shell Analysis Manual. NASA CR-912, April 1968.

18. Hetenyi, M.: Beams on Elastic Foundation. The University of Michigan Press, Ann Arbor, Mich., 1946.

19. Dharmarajan, S. N.: Thermal Stresses in Circular Cylindrical Shells. General Dynamics, Convair Division, Stress Analysis Memo SA-70-16, Aug. 28, 1970.

20. Przemieniecki, J. S.: Introduction to Structural Problems in Nuclear Reactor Engineering. Chapter 8, Pergamon Press, New York, 1962.

21. Wylie, C. R. Jr.: Advanced Engineering Mathematics. McGraw-Hill Book Co., Inc., New York, 1951.

22. Sokolnikoff, I. S.; and Redheffer, R. M.: Mathematics of Physics and Modern Engineering. McGraw-Hill Book Co., Inc., New York, 1958.

23. Newman, M.; and Forray, M.: Thermal Stresses in Cylindrical Shells. Machine Design, June 6, 1963.

24. Huth, J. H.: Thermal Stresses in Conical Shells. Journal of the Aeronautical Sciences, September 1953.

25. Nowacki, W.: Thermoelasticity. Addison-Wesley Publishing Co., Inc., Reading, Mass., 1962.

REFERENCES (Continued)

26. Kraus, H.: Thin Elastic Shells. John Wiley and Sons, Inc., New York, 1967.

27. Switzky, H.; Forray, M.; and Newman, M.; Thermo-Structural Analysis Manual. Vol. I, WADD-TR-60-517, August 1962.

28. Smith, G. W.: Analysis of Multiple Discontinuities in Shells of Revolution Including Coupled Effects of Meridional Load. General Dynamics, Convair Division, Report No. GD/A 63-0044, July 31, 1963.

29. Johns, R. H.; and Orange, T. W.; Theoretical Elastic Stress Distributions Arising from Discontinuities and Edge Loads in Several Shell-Type Structures. NASA TR R-103, 1961.

30. Fitzgerald, E. A.: Thermal Stresses in Thin Shells of Revolution for Axisymmetric Temperature Distributions. Report No. SM-42009, Missiles and Space Systems Engineering, Douglas Aircraft Co., Inc., June 1962.

31. Christensen, R. M.: Thermal Stresses in Missile Nose Cones. Paper No. 58-A-274, presented at the Annual Meeting of the ASME, New York, N. Y., Nov. 30 — Dec. 5, 1958.

32. Forray, M.: Thermal Buckling and Postbuckling of Circular Bulkheads. Machine Design, March 12, 1964.

33. Newman, M.; and Forray, M.: Axisymmetric Large Deflections of Circular Plates Subjected to Thermal and Mechanical Loads. Journal of the Aerospace Sciences, September 1962.

REFERENCES (Continued)

34. Friedrichs, K. O.; and Stoker, J. J.: The Nonlinear Boundary Value Problem of the Buckled Plate. American Journal of Mathematics, vol. 63, 1941, pp. 839-888.

35. Timoshenko, S. P.; and Gere, J. M.: Theory of Elastic Stability. McGraw-Hill Book Co., Inc., New York, 1961, p. 391.

36. Forray, M.; and Newman, M.: Buckling of Heated Rectangular Plates. Machine Design, June 7, 1962.

37. Newman, M.; and Forray, M.; Post-Buckling Deflection of Heated Rectangular Plates. Machine Design, Dec. 5, 1963.

38. Bijlaard, P. P.; and Gallagher, R. H.: Elastic Instability of a Cylindrical Shell Under Arbitrary Circumferential Variation of Axial Stress. Journal of the Aerospace Sciences, November 1960.

39. Abir, D.; and Nardo, S. V.: Thermal Buckling of Circular Cylindrical Shells Under Circumferential Temperature Gradients. Journal of the Aerospace Sciences, December 1959.

40. Schumacher, J. G.: Development of Design Curves for the Stability of Thin Pressurized and Unpressurized Circular Cylinders. General Dynamics, Convair Division, Report No. AZS-27-275, May 8, 1959.

41. MIL-HDBK-5A, Metallic Materials and Elements for Aerospace Vehicle Structures. February 8, 1966.

SECTION E
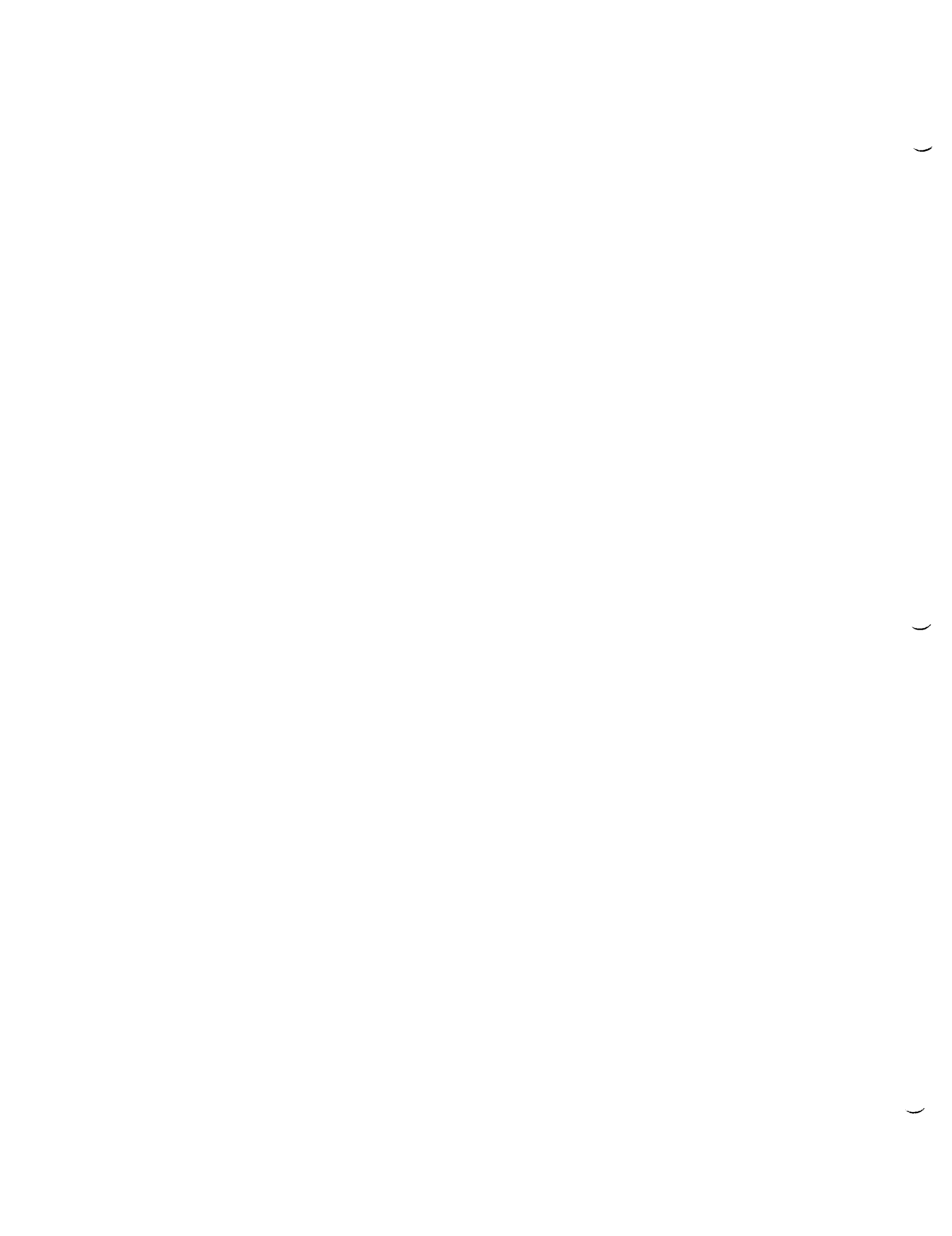
SECTION E1
FATIGUE

TABLE OF CONTENTS

TABLE OF CONTENTS (Concluded)

E1   FATIGUE.

1.1   INTRODUCTION.

1.1.1   General Considerations for a Fatigue Analysis.

Before detailing the many factors involved in a fatigue analysis and design, it is desirable to give an overview of the general considerations that comprise a fatigue analysis. Often when a new vehicle, structure, etc., is being considered, there are many concepts, designs, and configurations to be evaluated, and the engineer must provide ready assistance in the selection of materials, writing of preliminary test requirements and the life evaluation.

Figure E1-1 shows a general flow diagram of information for a fatigue analysis. As can be seen from this figure, there are two primary groups of information that are necessary as input to a fatigue analysis and/or determination of preliminary test requirements for a given structural component.

One group of information is the necessary data on the given material. These data include curves, graphs, etc., of laboratory tests to determine stress versus cycles to failure (S-N) diagrams, Modified Goodman diagrams and other factors which would affect the life of the component in question. The other information, which is usually the first information that is required, is the life cycle or service history of the structural component. This is usually presented in terms of stress-environment versus time curves which show pressures, temperatures, and other environmental considerations. In general, with these two groups of information a fatigue analysis and/or the preliminary test requirements can be determined for the component. Actually, the preliminary test requirements can usually be determined from the life cycle information alone.

1.1.1.1   Life Cycle Determination.

The important elements in the formation of life cycle data are the design life, mission profile (or condition lists), and significant fatigue loadings (see Fig. E1-1). The design or anticipated operational life and service loading spectra are primary considerations in evaluating effects of fatigue on the structural component of a flight vehicle.

Design life is generally specified by contractual or managerial agreements, or FAA and Military specifications, usually in terms of number of flights, landings, pressurizations, flight hours, etc.
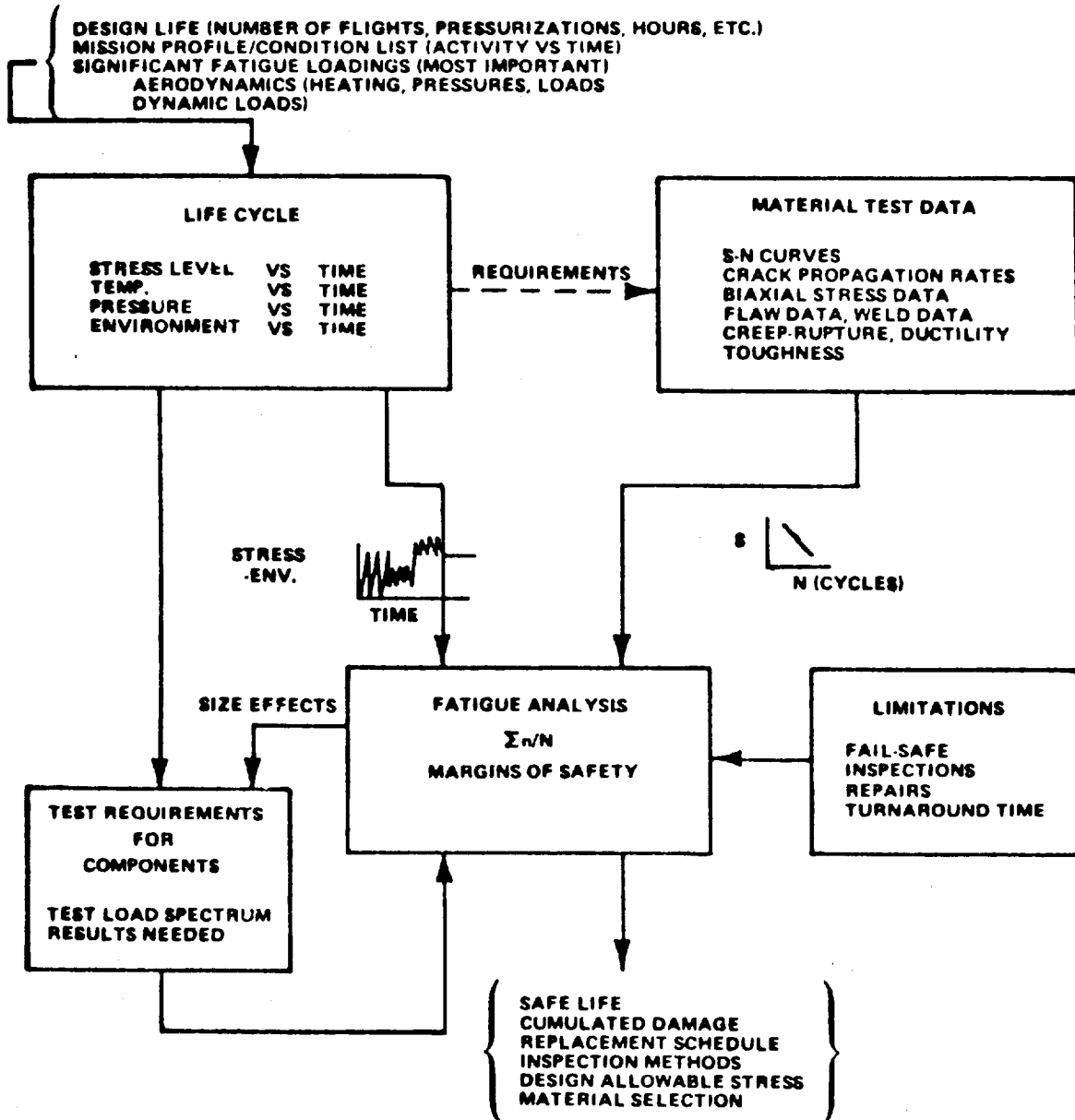
FIGURE E1-1.   PROCEDURE FOR TYPICAL FATIGUE ANALYSIS

Mission profiles, or condition lists, are generally used to provide a basis for the selection of design stress levels, the choice of structural components to be tested, the definition of the fatigue test spectra, and evaluation of the service life. Figure E1-2 contains a typical mission profile for an aircraft. These mission profile and/or condition lists must contain a detailed description of the activity versus time (or distance) applicable to each portion of the flight. Also, the flight configurations and anticipated changes in weight due to fuel usage, altitudes, speeds, and any other parameters that could affect the fatigue loading spectra are required. The spectra used for analytical and experimental evaluation of fatigue should realistically represent the total operational loading history described by the mission profile and/or condition lists.

For preliminary considerations, all of the detailed data on mission profiles may not be available. It is then necessary to consider what are the most significant considerations for the component in question. For example, in
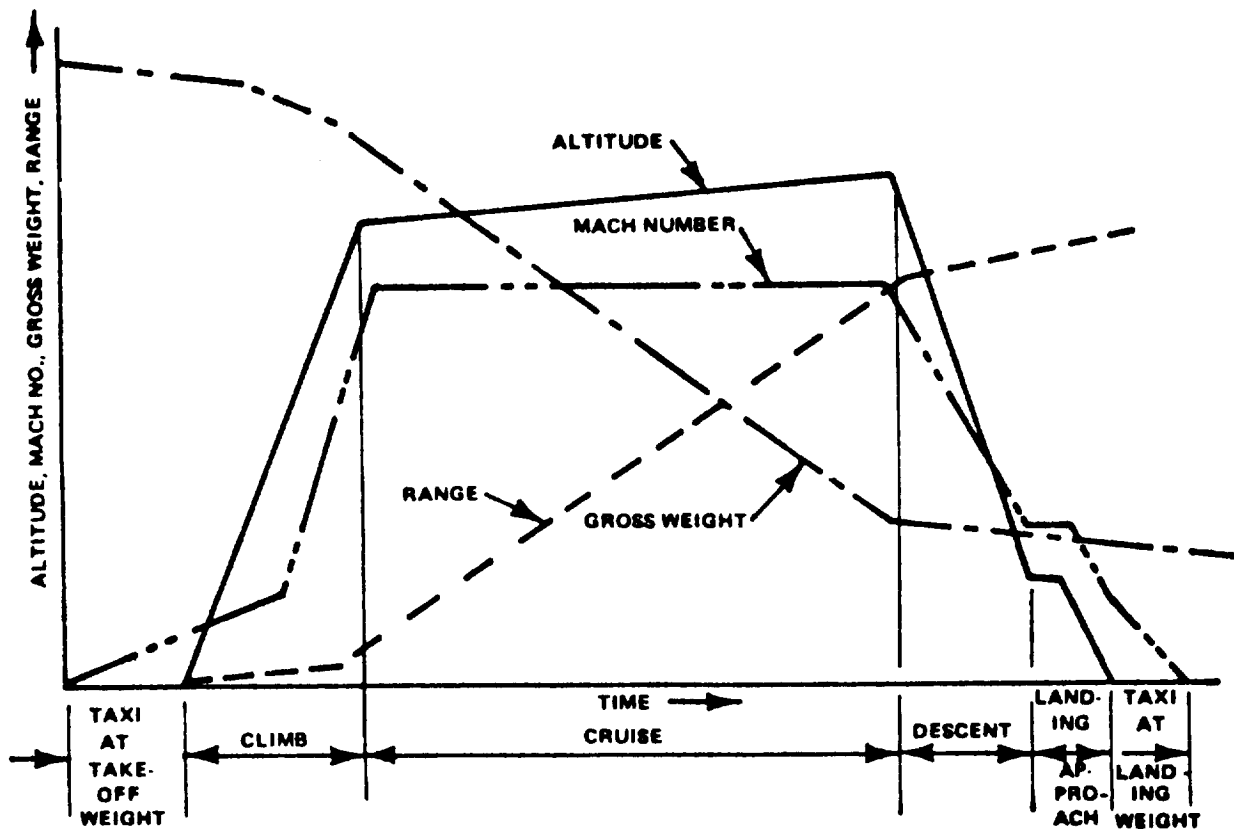
FIGURE E1-2. TYPICAL MISSION OR FLIGHT PROFILE FOR AIRCRAFT

tankage, the most important factors may be pressure and temperature; for wings, the most important factor may be only temperature.

Now, given all the information above, it is required to evaluate the stress versus time curves for a given component. Ordinarily, the aerodynamic data and dynamic loads must be considered as input to aid in the evaluation of load and stress levels. In conceptual designs, however, these may be "best-guess" data. The stress-versus-time curves must, of course, reflect temperature versus time, and other environmental factors present over part of a mission profile. An example of a life cycle for a component is given in Fig. E1-3.
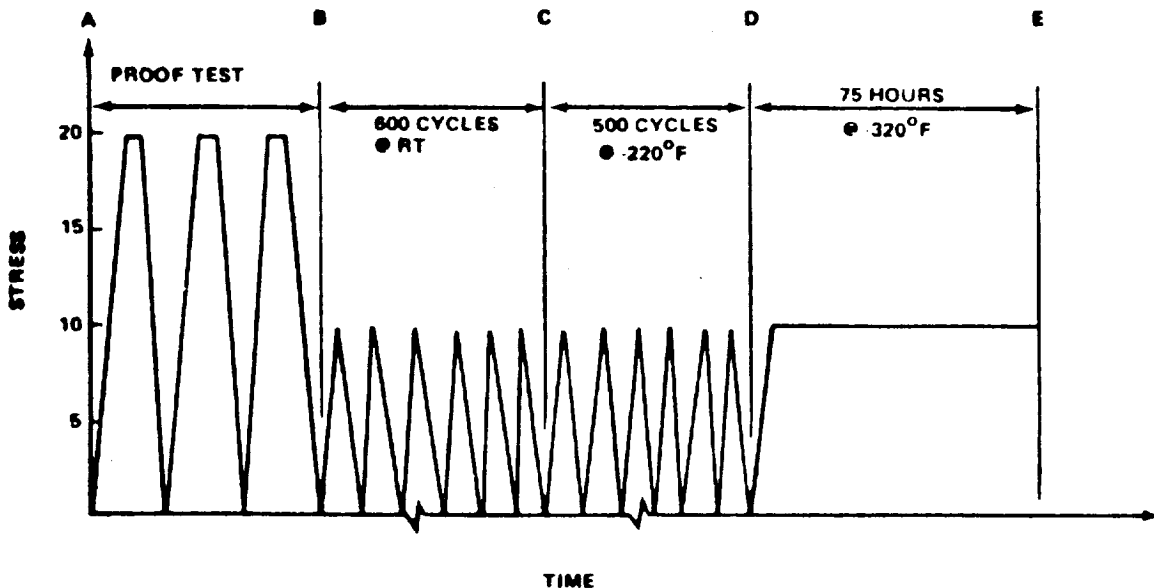
FIGURE E1-3. LIFE-HISTORY CURVE

Of course, the actual life cycle history for a given component may contain many random type loads which must be condensed into a form which can be used in fatigue life evaluation. Many techniques are available to accomplish this, and they will be discussed in a later section. For example, the spectrum shown in Fig. E1-4 for an aircraft flight is simplified to a more usable form.

1.1.1.2 Material Fatigue Data.

The fatigue strength of a material may be defined as the maximum stress that can be applied repeatedly to the material without causing failure in less
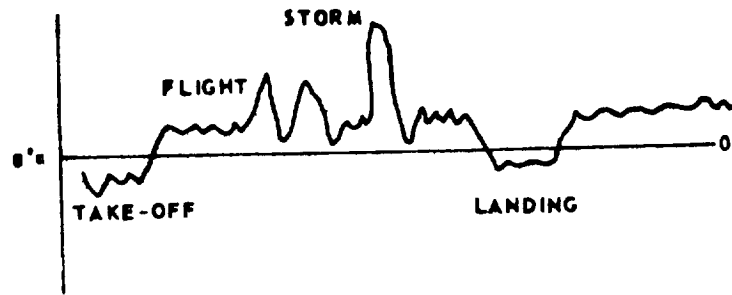
a. Actual Aircraft Spectrum
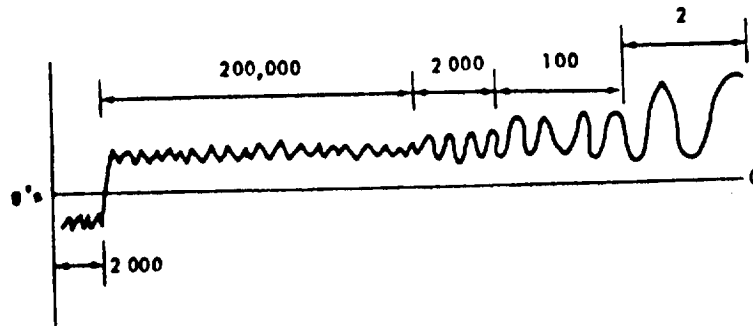
b. Simplified Spectrum

FIGURE E1-4. SIMPLIFICATION OF A FLIGHT SPECTRUM

than a certain definite number of cycles. The endurance strength is that max-
imum stress which can be applied repeatedly to a material for an indefinite
number of cycles without causing failure. The relationship of the magnitude of
repeatedly applied stress to the number of cycles to failure is conventionally
presented in the graphical form known as the S-N curve. The S-N curves are
discussed in detail in Paragraph 1.2.3. The shape of the S-N curve, which is
a representation of the fatigue life, will vary according to the conditions rep-
resented. Some factors influencing the shape of the S-N curve are as follows:

1. Type of load

   a. Tension

   b. Compression

   c. Torsion

   d. Combined Loads

2. Relationship of maximum to minimum loads

3. Manner of load application

   a. Axial

   b. Flexural

   c. Torsional

4. Rate of load application

5. Frequency of repetition of loads

6. Temperature of the material under load

7. Environment

   a. Corrosive

   b. Abrasive

   c. Inert

8. Material condition

   a. Prior heat treatment

   b. Prior cold work

9. Design of part or structure

10. Fabrication techniques

Thus, it can be seen that the mission profile or load spectra can dictate what type of S-N data are required for a fatigue analysis.

Other material information which may be necessary for input into a fatigue analysis are low-cycle fatigue data, fracture toughness, crack propagation rates, biaxial stress field data, welding, flaw size effects, and creep rupture data.

1.1.1.3 Fatigue Analysis.

Referring again to Fig. E1-1, with the input as discussed above, a fatigue analysis can be performed on the structural component or element in question. Other information which may be required includes limitations on inspection techniques, determination of a design (fail-safe or safe-life), and reliability and safety.

Fatigue analysis is usually performed in two phases. The first is the design phase, which is the structural sizing, material determination, and factor-of-safety study phase. Usually, in this phase only preliminary data are available concerning the life cycle and material properties; thus, best estimates must be made. From this design phase, design stress levels and requirements for developmental fatigue tests are determined.

The second phase of the fatigue analysis is the interpretation, in terms of actual flight-measured data, of the results obtained from fatigue tests conducted on structural elements. Also, the vehicle is assessed for damage and qualified for reuse on subsequent missions.

The details of the fatigue analysis will be discussed in the following paragraphs; but, generally, the fatigue analysis will determine the safe life for a structural component, will evaluate accumulated damage during service life, will specify inspection requirements, and will determine allowable stresses and/or test requirements.

Therefore, the analysis of fatigue life is a continuing process of study and reevaluation in light of newly acquired data. The acquisition of new loading and other environmental data can provide additional insight into the levels of assurance that exist in the evaluation of the service life of structural components on flight vehicles. Any significant variation between service-recorded loading histories (and related environmental conditions) and the spectra used to determine fatigue life would require a reevaluation of anticipated structural life.

1.1.2   General Background on Fatigue.

A rapid growth of metallurgy, with iron and steel coming into widespread use in many types of machines and structures occurred during the middle of the 19th century. During this time, engineers were confronted with failures that occurred at calculated nominal stresses considerably below the tensile strength of the materials involved, and, although the materials were considered ductile, the failures generally exhibited little or no ductility. It was soon discovered that most of the brittle fractures developed only after the structures had been subjected to many cycles of loading. Therefore, it came to be supposed that the metal degenerated and became fatigued under the action of cyclical stresses and that its ductile behavior turned brittle. However, later experiments showed that no degeneration or fatigue of the metal occurred as a result of cyclical stressing and, therefore, the idea of metal fatigue is false. Hence the term "fatigue" is still widely used although it has quite a different meaning.

Generally speaking, fatigue can be defined as a progressive failure of a part under repeated, cyclic, or fluctuating loads.

Fatigue failures may be simple or compound. Simple failures result when a fatigue failure starts from a single crack and propagates until ultimate failure occurs. A compound fatigue failure results when the origin of the fatigue crack originates from two or more locations and propagates; the joint effects cause total failure. The sequence in which failure occurs consists of three parts: The initial damage occurs in a submicroscopic scale, the crack initiates and propagates, and the final rupture takes place. The rate at which the crack propagates varies considerably, depending upon the intensity of stress and other related factors. Nevertheless, the rate is always much lower than that observed for low-temperature brittle fractures in steel.

It has proved difficult, however, to detect progressive failures in the part during its life; hence, fatigue failures can occur with little warning and can cause catastrophic failures. Also, periods of rest (the fatigue stress removed) do not lead to a recovery from the effects of stress; in other words, the fatigue damage is cumulative.

The criterion for fatigue failure is the simultaneous action of cyclic stress, tensile stress, and plastic strain. If any one of these is eliminated, fatigue is also eliminated.

Rarely is a mechanical component or structural element subjected to constant loads throughout its entire service history. Cyclic loading can result from vibration, variations in atmospheric gust pattern, variable wind loadings, repeated temperature changes, and repetition of design load, to mention only a few.

Many fatigue failures that occur in service are only minor, but others, such as those which result in the loss of a wing, propeller, or wheel, constitute a serious threat to life or property. Such failures have become more prevalent in recent years because of the following factors:

1. The continuing trend toward higher strength/weight ratios.

2. More refined static design techniques and the use of higher working stress.

3. The use of materials of ultra-high static strength.

Good static design does not necessarily result in satisfactory performance under repeated loading, and the choice of a design stress close to, or even higher than, the yield point of the material would almost inevitably result in failure after a relatively short period of service. There is every possibility that the fatigue problem will become more acute and that, consequently, the limiting strength criterion in many future designs will be adequate fatigue resistance. Therefore, the likelihood of a fatigue failure should be an early design consideration.

A major problem in designing to prevent fatigue failure lies in the identification of all the factors that affect the life of a part. Even with the knowledge of which problems to consider, one is still short of the goal: the exact determination of fatigue life. Techniques are furnished in the following sections to enable the engineer to develop fatigue data for a particular part.

All the basic definitions used in fatigue testing and failure are discussed in Paragraph 1.2. The many types of effects which influence fatigue strength are presented in Paragraph 1.3. A separate section (Paragraph 1.4) is devoted to low-cycle fatigue because of its unique application and terminology. Various cumulative fatigue damage theories are discussed in Paragraph 1.5. Paragraph 1.6 is a special section which will be useful in selecting certain materials to resist fatigue failures. Design guides are given in Paragraph 1.7.

1.2   BASIC DEFINITIONS.

This paragraph describes the basic mechanism of a fatigue failure and the general methods used in fatigue testing and documenting of the results.

The following definitions are some of the terms frequently used in this discussion of fatigue analysis:

Stress Cycle   —   The smallest division of the stress-time function that is repeated. (See Fig. E1-5.)

Nominal Stress   —   Obtained from the simple theory in tension, bending, and torsion, neglecting geometric discontinuities.

Maximum Stress   —   The largest or highest algebraic value of a stress in a stress cycle. Positive for tension. S_{max}

Minimum Stress   —   The smallest or lowest algebraic value of a stress in a stress cycle. Positive for tension. S_{min}

Mean Stress   —   The algebraic mean of the maximum and minimum stress in one cycle. S_m

Stress Range   —   The algebraic difference between the maximum and minimum stresses in one cycle. S_r

Stress Amplitude   —   Half the value of the algebraic difference between the maximum and minimum stresses in one cycle, or half the value of the stress range. S_a

Stress Ratio   —   The ratio of minimum stress to maximum stress.

Fatigue Life   —   The number of stress cycles which can be sustained for a given test condition.

Fatigue Strength   —   The greatest number of stress cycles which can be sustained by a member for a given number of stress cycles without fracture.

Fatigue Limit — The highest stress level that a member can withstand for an infinite number of load cycles without failure.

Fatigue Life for P Percent Survival, N_P — The fatigue life for which P percent of the sample has a longer life; for example, N_{90} is the fatigue life for which 90 percent will be expected to survive and 10 percent to fail.
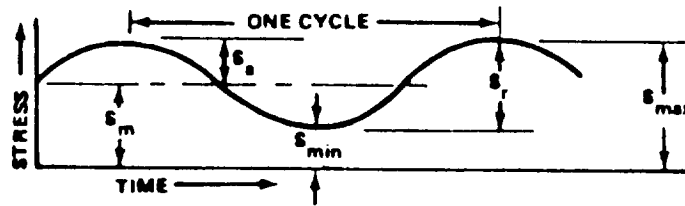
FIGURE E1-5. STRESS VERSUS TIME CURVE

1.2.1   Mechanism of Failure.

In investigating a fracture surface which resulted from fatigue, two zones are evident, namely, a fatigue zone and a rupture zone. The fatigue zone is the area of the crack propagation; the area of final failure is called the rupture, or instantaneous, zone. The instantaneous zone provides the following information for investigating a failed specimen: ductility of the material, type of loading, and direction of loading. The distortion and damage pattern will be sufficiently apparent to designate the type and direction of loading. In addition, the relative sizes of the instantaneous zone and the fatigue zone relate the degree of overstress applied to the structure. The degree of overstress can be categorized as follows: Highly overstressed if the area of the fatigue zone is very small compared with the area of the rupture zone, medium overstress if the size or area of both zones are nearly equal, and low overstress if the area of the instantaneous zone is very small.

The following features are characteristic of the fatigue zone: a smooth, rubbed, velvety appearance; a presence of waves known as clam shells or oyster shells, stop marks, and beach marks; and a herringbone pattern or granular trace which shows the origin of the crack. Most clam shell marks are concave with respect to the origin of the crack but can also be convex, depending

on the brittleness of the material, degree of overstressing, and the influence of stress concentrations. In general, the stop marks indicate the variations in the rate of crack propagation due to variations in stress amplitude in a cyclic application varying with time. There are some aluminum alloys that may not exhibit these waves but instead have a smooth appearance. (See Fig. E1-6.)
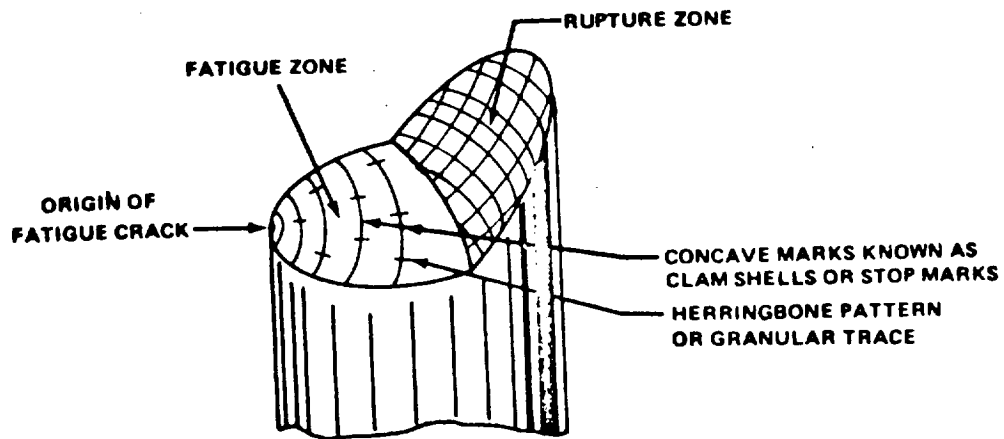
FIGURE E1-6. A TYPICAL FATIGUE FAILURE SECTION SHOWING
IDENTIFYING MARKS

A fatigue fracture, whether the material is ductile or brittle, follows that of a brittle fracture. Not all brittle failures are fatigue failures, however. The most recognizable features of a fatigue failure are lack of deformation pattern and the existence of a singular plane of fracture, usually a 90-degree cross section.

Most of the fatigue cracks discussed above were caused by tension loads, tension strains, and tension stress. Typical fracture appearances of fatigue failures in bending and torsion are shown in Fig. E1-7. Bending fatigue failure can be divided into three classifications according to the type of bending load, namely, one-way, two-way, and rotary. The fatigue crack formations associated with the type of bending load are shown in Fig. E1-6. Torsional fatigue failures occur in two modes: (1) Longitudinal or transverse along planes of maximum shear and (2) helical at 45 degrees to the axis of the shaft and along planes of maximum tension. Transverse fractures are commonly associated with a smooth surface because of the rubbing of both sides, a characteristic that can be used to identify this type of fracture.

FIGURE E1-7. FRACTURE APPEARANCES OF FATIGUE FAILURES IN BENDING

Stress Condition / Case	No Stress Concentration		Mild Stress Concentration		High Stress Concentration	
	Low Overstress a	High Overstress b	Low Overstress c	High Overstress d	Low Overstress e	High Overstress f
1 One-Way Bending Load						
2 Two-Way Bending Load						
3 Reversed Bending Load Rotation Load						

However, a statement of the signs and features of fatigue fractures does not explain the true nature of the physical changes which take place inside metals under cyclical stress to cause their breakdown.

To understand these changes, it is necessary to study the internal mechanism of fatigue behavior in the whole volume of the metal; but this subject has yet to be thoroughly investigated. A considerable amount of theory has been written about fatigue fracture, and there are many interpretations as to the process of metal fatigue. (See Ref. 1.)

Fatigue is basically a property of crystalline solids, and the initiation of fatigue cracking is a problem in dislocation physics. It is the result of the motion and interaction of dislocations activated by cyclic stress. A simple description of the mechanism of fatigue cracking is given in three stages:

Stage 1. During the early cycles of stressing, the dislocations originally present in the crystal grains multiply and their density increases sharply. An irregular and disoriented cell wall, or subgrain boundary, starts to form. The fine slip lines that appear at first in some favorably oriented grains are thin and faint, according to the maximum resolved shear stress law. As the number of stress cycles increases, slip lines become more numerous. Some are localized, some continuously broaden, and the very pronounced ones become the so-called persistent slip bands. Meanwhile, the crystals are distorted and strain-hardened to saturation. Then, dislocation motion in one direction may be fully reversed with the stress. New dislocations and their movements are generated only in some local slip zones in which microstructural features are not the same in both directions of motion. Sometimes annihilation of dislocations, or other dislocation mechanisms, may lead to relief of lattice strains or strain softening. Strain softening, local recrystallization, overaging, clustering of point defects, and other thermal activation processes are considered to be secondary, or side effects.

Stage 2. After the persistent slip bands are fully matured, thin ribbon-like protrusions, called extrusions, of metal are emitted from the free surface, and fissures, called intrusions, appear. Both develop along the persistent slip planes. Several dislocation models or mechanisms have been proposed to explain how the extrusions and intrusions are formed. (See Ref. 1.) In some of the proposed models, dislocation cross slip is considered to be a critical process.

Because the intrusion is the embryo of a crack, the crack initiates along slip planes according to the maximum resolved shear. Sometimes cracks

may initiate at cell walls or grain boundaries, although the majority start at the surface of a member.

Stage 3. The crack propagates in a zigzag transgranular path along slip planes and cleavage planes, from grain to grain, and maintains a general direction perpendicular to the maximum tensile stress. As much as 99 percent of the fatigue life of a member is spent in the development of fissures into microscopic cracks, and finally complete fracture ensues. Many factors affecting fatigue properties are those that mainly influence the rate of crack propagation.

1.2.2   Fatigue Testing Techniques.

The only way to obtain a quantitative measure of fatigue strength is to carry out fatigue tests under controlled conditions. There are many different methods of carrying out such tests, and numerous types of testing equipment have been developed.

Probably the most widely used method is the rotating bending test, in which small cylindrical specimens, with or without notches, are loaded either as cantilevers or as beams under four-point loading. As the specimen is rotated, the stress at any point in it varies between upper and lower limits which are equal in magnitude, but opposite in sign, the plane and direction of the loads remaining constant throughout. A possible arrangement of such a test is shown diagrammatically in Fig. E1-8. This type of test is simple to carry out, generates results comparatively rapidly and makes use of equipment and specimens that are reasonably inexpensive. It is particularly suitable for use in determining what might be called the inherent fatigue strength of materials,
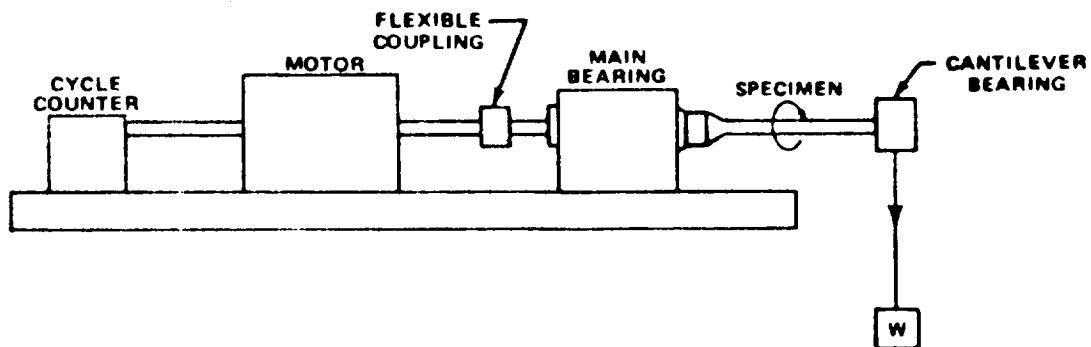
FIGURE E1-8. GENERAL ARRANGEMENT OF ROTATING BENDING
(CANTILEVER TYPE) FATIGUE-TESTING MACHINE

since in such work one is interested in the material itself, i.e., its composition, microstructure, etc., rather than its form in the engineering sense.

However, to provide data for design purposes, such tests are not of great value since designs can rarely, if ever, be reduced to such a degree of simplicity that it is necessary to know only the basic fatigue strength of the material. To provide specific information for the designer, tests must be carried out on the actual joint forms. This is true of structures fabricated by any means, but is particularly relevant in the case of welding. The welding process cannot satisfactorily be scaled down without simultaneously altering some of its effects.

Therefore, fatigue testing of welded components normally involves the use of equipment of much larger capacity than that used for fundamental investigation. The method of loading is also different, the objective being at all times to reproduce as faithfully as possible the type of loading that is likely to occur in service. With this end in view, the loading conditions used in the fatigue testing of welded joints and structures can be reduced essentially to three types:

1. Axial load testing

2. Tests in bending, mainly on specimens in the form of beams

3. Pulsating pressure testing of pressure vessels and pipework.

All the numerous testing machines that are available and suitable for carrying out such tests will not be described here in detail, but it may be useful to describe some of the essential features since, to some extent, the characteristics of fatigue-testing machines have influenced the research work that has been carried out.

Axial load fatigue-testing machines may be divided essentially into three types according to the method by which they are driven, i.e., hydraulically, mechanically, or electromagnetically. Hydraulic machines which give higher loads than those operated either mechanically or electromagnetically are available, but testing speeds are limited.

A mechanically operated machine which has been used extensively in fatigue testing of welded components is the walking beam machine, first developed in the United States at the University of Illinois. The arrangement of this machine is shown diagrammatically in Fig. E1-9. It consists of a simple lever
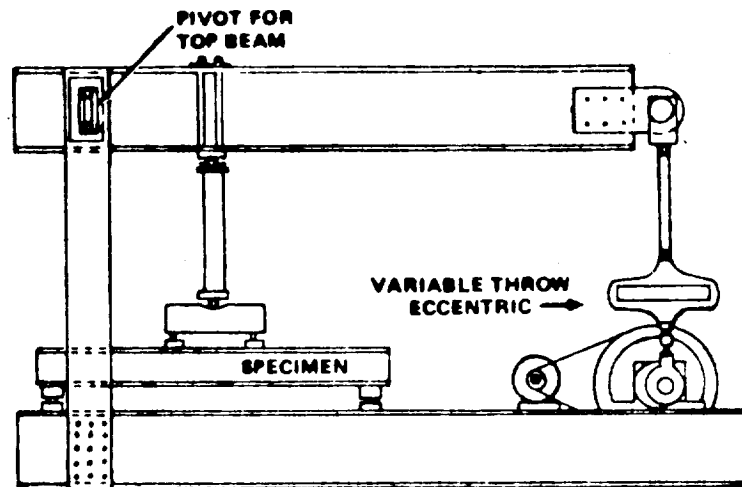
FIGURE E1-9. GENERAL ARRANGEMENT OF WALKING BEAM MACHINE

with the upper beam actuated by a driven eccentric which is continuously vari-
able up to a maximum throw of 4 inches. The load is transmitted to the beam
through a dynamometer, which can be used for load measurement, but since
the dynamometer also measures any frictional loads in the bearings, it is more
satisfactory to adjust the load by using strain gages attached to the specimen.
The beam may be used either as a first-order lever, with the specimen mounted
in the end grips, or as a second-order lever, which is particularly satisfactory
for testing flexible specimens (such as beams in bending) that require a fairly
large strain amplitude at lower loads. Figure E1-8 shows the arrangement
for the latter case. It should be noted that it is a constant strain amplitude
machine, in contrast to the hydraulic machines referred to above which supply
constant loads.

Fatigue is a problem of such magnitude in the aircraft industry that
often full-scale components, or even entire aircraft, are tested. In one method,
the load is applied to the specimen by means of hydraulic jacks in specially
constructed test rigs. Another method is to excite a structural component near
its resonant frequency by attaching it to a mechanical oscillator and supporting
the component at its node points. Because each fatigue test of a large-scale
aircraft costs several million dollars, usually only one aircraft is tested.

Special techniques relating to thermal stress testing and low cycle
fatigue testing will be discussed in the following sections.

1.2.3 Presentation of Test Results.

1.2.3.1 S-N Diagrams.

Since the beginning of fatigue testing, S-N curves have been the backbone of fatigue data. S denotes stress amplitude or the maximum cyclic stress, and N denotes the number of stress cycles to complete fracture. The linear S versus log N scale is the most common and is used almost exclusively in engineering. (See Fig. E1-10.)
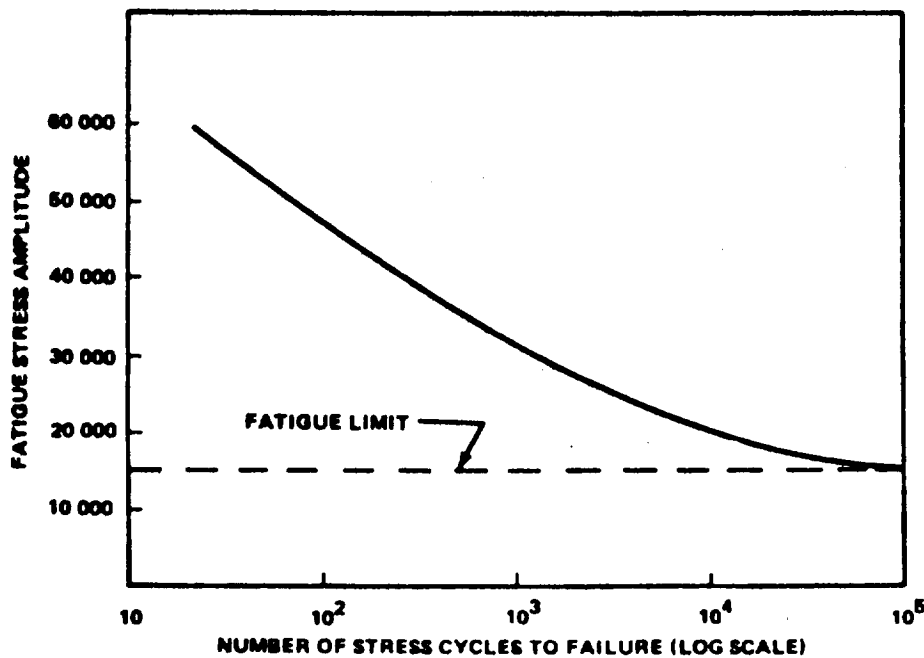
FIGURE E1-10. GENERAL FORM OF S-N CURVE

Several attempts have been made to find general mathematical laws for the relation between load and life, and several equations have been proposed to express the S-N relations more or less empirically. Use of these equations will embody the data in a mathematical form for data reduction, analysis, and standardization of curve-fitting methods. It may also provide some understanding of the S-N relations.

For certain metals and alloys, including the ferrous group, the S-N curve becomes asymptotic to a horizontal line. The stress value corresponding

to this asymptote, or the stress corresponding to failure at an infinite number of cycles, is called the fatigue (or endurance) limit.

The fatigue limit of a material tested in axial loading is usually lower than that of the same material tested in reverse (rotating) bending. In axial loading the stress is uniform throughout the cross section; whereas, a large stress gradient exists when a bending load is applied. Thus, in axial loading, it is probable that the maximum stress will occur at a discontinuity in the material. Fatigue tests in torsion or shear loading indicate that the torsional fatigue limit of polished steel specimens is approximately 58 percent of the flexural or tensile fatigue limit. This figure is consistent with the distortion-energy theory which predicts that the shear properties of steels are 57.7 percent of tensile properties.

1.2.3.2 Goodman Diagrams.

The preceding discussion on S-N curves and fatigue limits has dealt with stress cycles that alternated about a zero mean stress. But the stress cycle usually varies about a mean static value that may be positive, zero, or negative. When a cyclic stress varies about a nonzero static value, prediction of failure must consider the combination of static and varying stresses.

Several types of failure diagrams relate the range of operating stress to the material properties in a general manner. All the diagrams indicate that the allowable stress range decreases as the mean stress approaches some maximum value.

The Goodman diagram was the first type proposed, and the modified Goodman diagram is the form most commonly used. Because it consists of straight lines, it is easy to construct. The Goodman equation is

$$S_a = S_e - S_e \left(\frac{S_m}{T} \right)$$

where S_a is the fatigue strength in terms of the stress amplitude, S_m is the superimposed mean stress, S_e is the endurance limit when $S_m = 0$, and T is the ultimate tensile strength. This equation is plotted in Fig. E1-11.
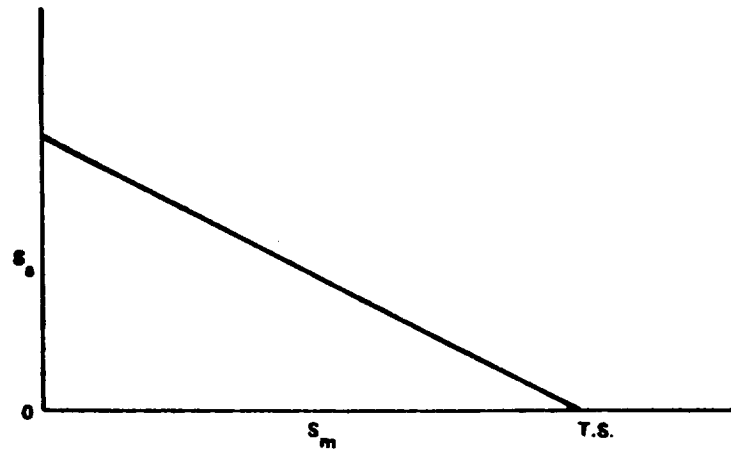
FIGURE E1-11. GOODMAN DIAGRAM

In the modified Goodman failure diagrams (Fig. E1-12), the range of operating stresses is described by three values: mean stress, maximum stress, and minimum stress.
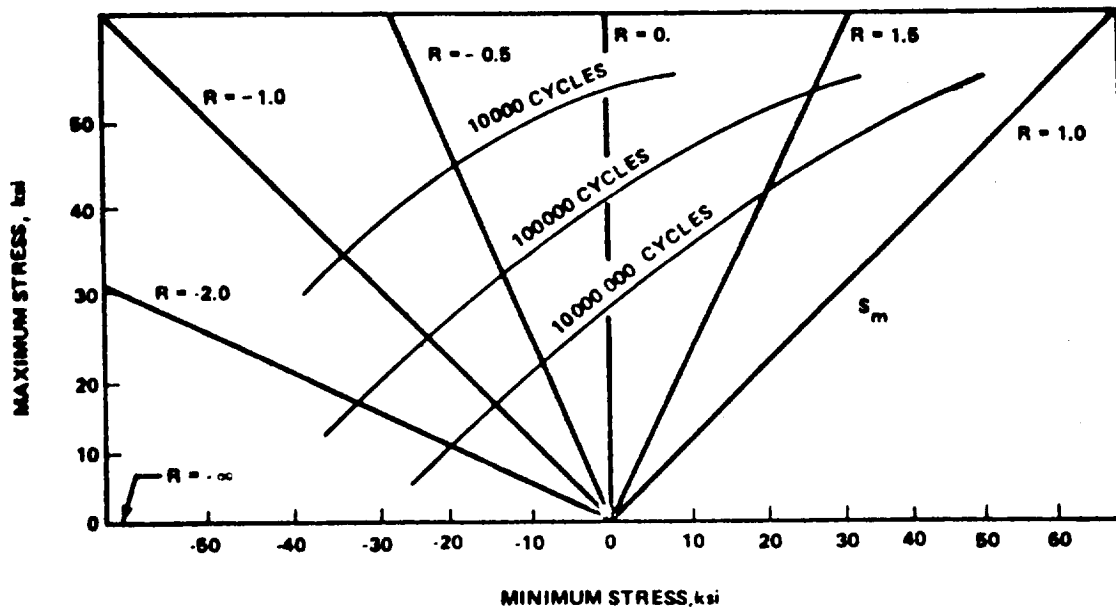
FIGURE E1-12. MODIFIED GOODMAN DIAGRAM

In the maximum-minimum form of modified Goodman diagram, a stress cycle is plotted as a point on the diagram instead of as a line. This form of diagram is advantageous for it requires only the determination of the maximum values of a half cycle; finding the mean cycle is not required.

In the maximum-minimum form of diagram, a stress cycle in which stress is zero is plotted as a point on the line of zero mean stress. Similarly, a stress cycle from zero stress to a tensile value is plotted as a point on the maximum stress axis. Although these points have different mean stress values, they represent equivalent reversed stress cycles. In this form of diagram, the fatigue limit for reversed stress is plotted as a line of constant equivalent reversed stress instead of being a point as in the other forms of failure diagrams.

1.3   FACTORS INFLUENCING FATIGUE STRENGTH.

Fatigue properties obtained from a carefully polished specimen in the ideal environment of the test laboratory are rarely achieved in practice. A wide variety of factors affect the behavior of a member or assembly under conditions of fatigue loading. The most obvious parameters are those that deal with the sign, magnitude, and frequency of loading; the geometry and material strength level of the structure, and the ambient service temperature. Those processing and metallurgical factors that determine the cleanness and homogeneity of materials, the sign and distribution of residual stresses, and the surface finish often are not considered. These processing and metallurgical factors, however, may have an overriding influence on the fatigue performance of the structure, to its benefit or detriment. The factors which influence fatigue strength will be classified into four main groups for discussion in this section:

1.   Metallurgical Factors

2.   Processing Factors

3.   Environmental Factors

4.   Design Factors

1.3.1   Metallurgical Factors.

The distinction between processing factors and metallurgical factors is not always clear. In fact, it is rather arbitrary in some areas. In this section, however, the focus is on regions within the material, either at the surface or core, which adversely affect fatigue properties. These regions may arise from melting practices or primary or secondary working of the material, or may be characteristic of a particular alloy system. In nearly every instance the detriment to fatigue properties results from a local stress-raising effect.

1.3.1.1   Surface Defects.

Primary and secondary working are often responsible for a variety of surface defects that occur during the hot plastic working of material when lapping, folding, or turbulent flow is experienced. The resultant surface defects bear such names as laps, seams, cold shuts, or metal flow through. Similar defects are also noted in cold working, such as fillet and thread rolling, in which the terms lap and crest cracks apply. Other surface defects develop

from the embedding of foreign material under high pressures during the working process. Oxides, slivers, or chips of the base material are occasionally rolled or forged into the surface. The surface defects in castings might include entrapped die material, porosity, or shrinkage; in the extrusion or drawing processes such surface defects as tears and seams are not uncommon.

All of the aforementioned surface defects produce a notch of varying intensity which acts as a stress-raiser under load to the detriment of fatigue properties. Because most of these defects are present prior to final processing and are open to the surface, standard nondestructive testing procedures such as penetrant and magnetic particle inspection will readily reveal their presence. If they are not detected, however, the defects may serve as a site for corrosion or crack initiations during processing (in heat treating, cleaning, etc.), further compounding the deleterious effect on fatigue strength.

1.3.1.2   Subsurface and Core Defects, Inhomogeneity, and Anisotropy.

Subsurface and core defects considered here are those which originate in the as-cast ingot. Voids resulting from gas entrapment (porosity) and improper metal fill (shrinkage) are not uncommon in cast materials. In castings (ingots) that are to be subsequently hot and cold reduced, the portion of the ingot containing the preponderance of voids is often removed and discarded. The remaining internal defects normally weld shut under the combination of temperature and pressure involved in the reduction of the ingot, resulting in a continuous, homogeneous product. Occasionally, when the surfaces of the defects are oxidized or otherwise contaminated, healing (welding) of the opposite surfaces is precluded and the defective area is retained in the wrought product. Terms such as unhealed porosity and laminations are applied to this condition. Since these defects existed before working, in the final wrought product the major diameter of the oblate or rod-shaped flaw is parallel with the direction of plastic deformation.

Fatigue testing of high-strength aluminum alloy specimens containing defects of the type discussed in this section revealed the following trends:

1.   Stressing parallel to the defect plane has a small effect on the fatigue strength, provided the defect does not intersect a free surface.

2.   The effect of defect size on the fatigue strength in the short transverse direction of testing (that is, with the plane of the grain flow normal to the direction of loading) is shown in Fig. E1-13.
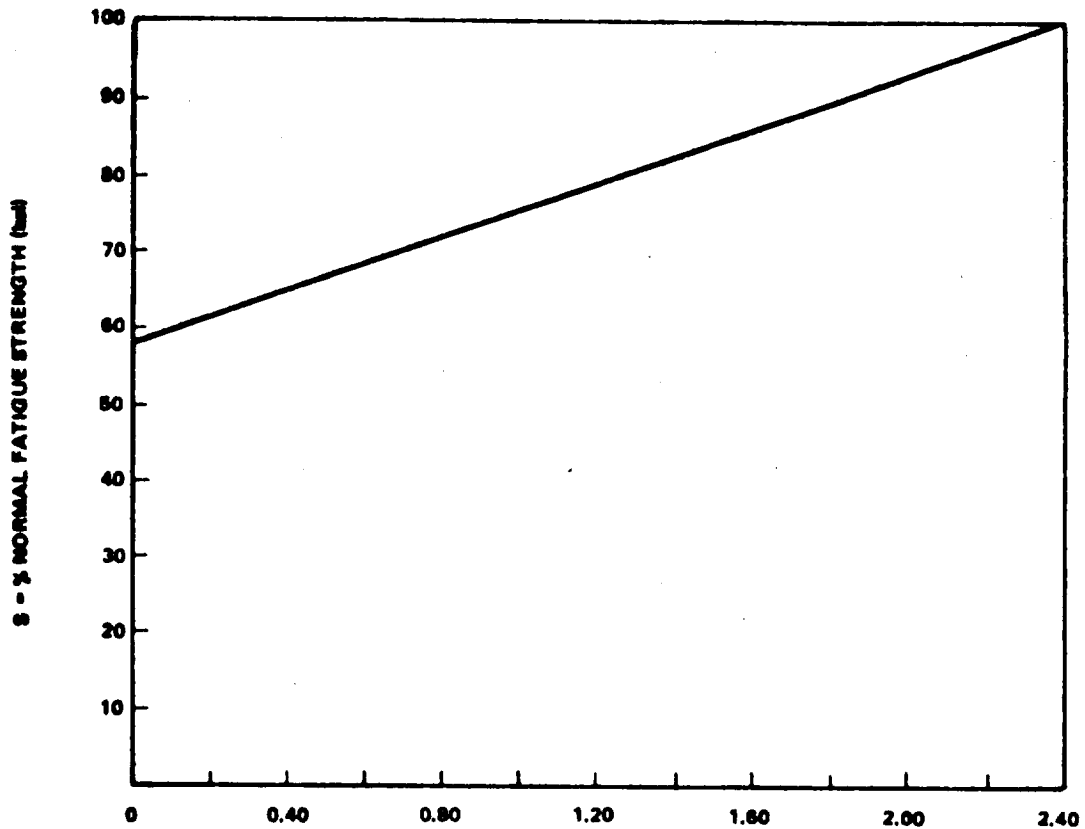
$$\frac{c}{D}$$ MINIMUM DISTANCE FROM CENTER OF DEFECT TO SURFACE/LARGEST DIAGONAL OF DEFECT.

FIGURE E1-13. S VERSUS C/D

3. An internal defect adversely affects fatigue by introducing a stress concentrator into the material and reducing the load resisting cross-sectional area.

4. With respect to fatigue properties, when the edge of one defect is within approximately two diameters of the center of another defect, these should be considered as one large defect having a diameter equal to the extreme distance which will include both defects.

Inasmuch as most subsurface defects do not intersect a surface of a part, inspection is somewhat more difficult. For wrought products, ultrasonic or eddy-current testing might be used, whereas, for castings, fluoroscopic or radiographic inspection is preferred.

There are two types of inclusions in metals, nonmetallic and inter-
metallic. The amount and distribution of these inclusions is determined by
the chemical composition of the alloy, the melting and working practice and
the final heat treatment of the material. Nonmetallic inclusions are usually
complex compounds of the metallic alloying elements with oxygen, nitrogen,
carbon, phosphorus, sulphur, and silicon. The size of the inclusion is an
important parameter in assessing its effect on fatigue properties, as shown in
Figure E1-14 for 4340 steel heat treated to the 260 to 310 ksi tensile range.
Although this relation does not apply to all inclusion types, it has been sug-
gested that a separate curve exists for each predominant type of nonmetallic
inclusion.
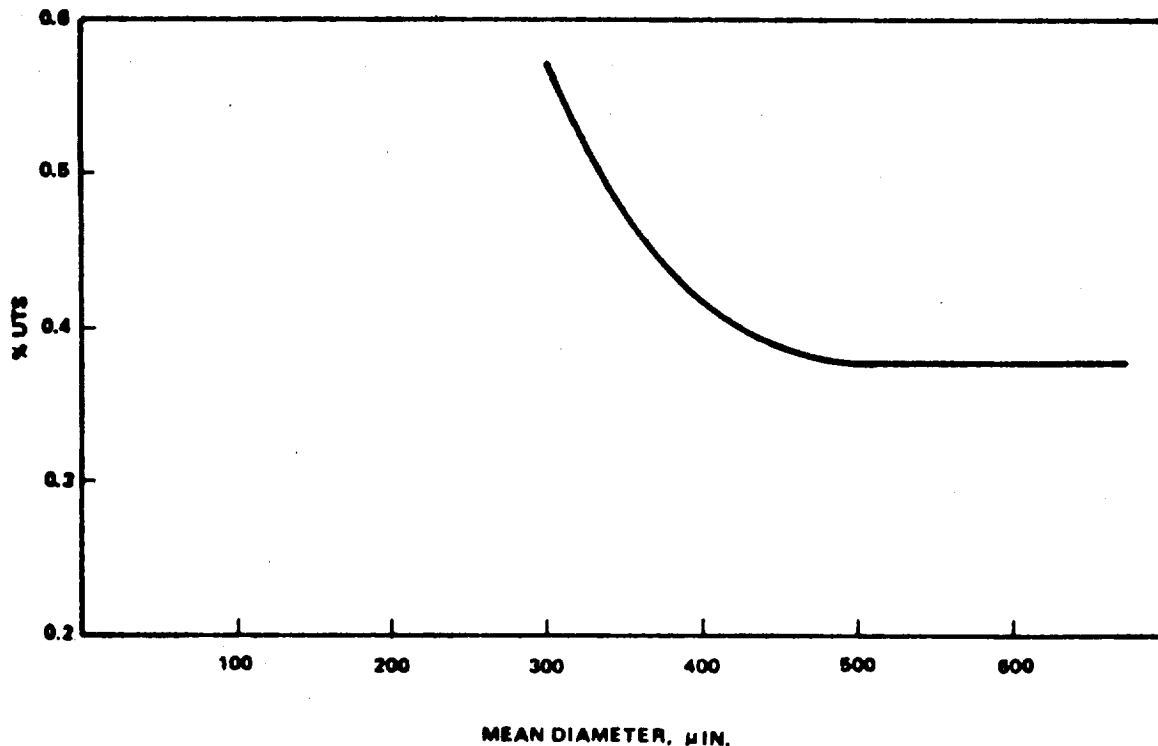
FIGURE E1-14. CORRELATION BETWEEN ENDURANCE LIMIT AS
PERCENT UTS AND AVERAGE LARGE INCLUSION ARITHMETIC
MEAN DIAMETER

Intermetallic inclusions may be either complex metallic compounds or
second phases with variable compositions. The type of intermetallic constit-
uent is believed to be an important consideration in determining the effect on
fatigue life, although the mechanism is not clearly understood. The site of
such an inclusion, however, is a discontinuous region with physical and mechan-
ical properties different from those of the matrix phase. Under load these
areas would serve as stress-raisers.

Some alloys are subject to microstructural banding which often has
an adverse effect on fatigue properties. The banding is usually produced by
local chemical segregration which stabilizes a phase not normally present in
the alloy at room temperature. The severity of the loss in fatigue properties
is dependent on the direction of the banding relative to the maximum stress
direction (the banding is always in the direction of prior working) and on the
degree of compatibility between the banded and matrix phases. Banded
retained austenite and delta ferrite are occasionally seen in a large number of
low-alloy and stainless steels. The presence of ferrite in these is intentional;
in others it is not. The loss in fatigue properties produced by ferrite stringers
in 431 stainless steel is shown in Fig. E1-15.
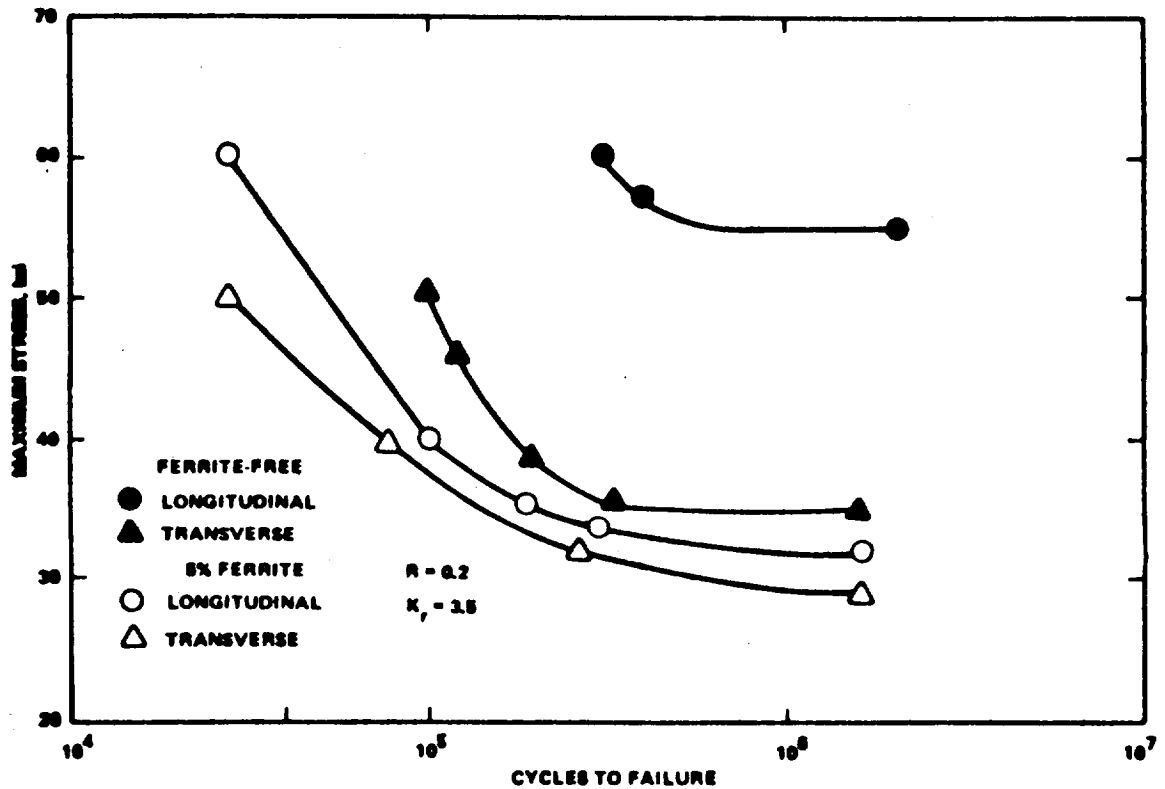
FIGURE E1-15. NOTCHED FATIGUE STRENGTH OF 431 STAINLESS
STEEL HEAT-TREATED TO THE 180 to 200 ksi RANGE WITH NO
FERRITE AND WITH 5 PERCENT FERRITE

Finally, the grain and subgrain structure may also reflect a preferential alignment. As previously indicated, anisotropy is most pronounced in the short transverse grain direction. It has been shown in tests on 7075-T6 aluminum alloy forgings that the endurance limit is reduced by approximately 20 percent when testing in the short transverse direction as opposed to the longitudinal direction.

For many material forms such as sheet, light plate, and extrusion, the loading normal to the short transverse direction is low such that fatigue properties in this direction are not critical. For heavy plate, bar, and forgings, however, directionality or anisotropy can be a crucial design consideration.

1.3.1.3 Heat Treatment.

The heat-treatment processes are potentially a source of hazard to a material because at the elevated temperatures encountered many diffusion controlled mechanisms are operative that could harm the integrity of the alloy if not properly controlled. If the furnace atmosphere is not controlled, the chemical composition of the surface layer might be altered and, thus, produce a low strength or brittle surface skin. The diffusion of hydrogen into alloys during heat treatment has long been recognized as a serious problem. Hydrogen embrittlement of low-alloy steels and titanium alloys can produce disastrous results in subsequent processing or in service. Hydrogen is also suspect in the blistering mechanism in aluminum alloys. With respect specifically to fatigue properties, a brittle case will render an alloy susceptible to surface cracking. The introduction of a shallow crack produces a notch effect, so that the detriment to fatigue (life) is essentially one of a high surface stress raiser in a layer of material with low fracture toughness.

If the heat-treating temperature is not properly controlled, grain coarsening may occur which lowers fatigue properties of some alloys. Overheating of high-strength aluminum alloys is particularly disastrous, since most of these alloys are subject to eutectic melting at temperatures only marginally higher than the solution heat treatment temperature. Eutectic melting results in a gross embrittlement of the alloy coupled with reduction in strength. The difficulties with austenitizing or solution heat treating at too low a temperature are associated with a lack of hardening potential for the subsequent quench and age or temper treatments.

In order to develop full strength, most martensitic and age hardening alloys must be rapidly cooled from high temperatures by quenching into a liquid medium. There are at least two considerations in the quenching process

that could affect fatigue properties. High residual quench stresses are built up in most materials and, if the geometry of the part being quenched is highly irregular, the tensile strength of the material may be exceeded at points of high stresses resulting in the not too uncommon quench cracks. On the other hand, if the quenching rate is for some reason retarded, preferential precipitation may occur which adversely affects fatigue properties.

1.3.1.4 Localized Overheating.

There are some processes that are capable of developing high, localized surface temperatures, the consequences of which are often difficult to detect and occasionally are responsible for a failure in service. Grinding is one of these processes.

The effect of severe grinding on the fatigue properties of high-strength steel is shown in Fig. E1-16. The rapid quenching of the material immediately below the grinding wheel by the large mass of cold metal can produce cracks. If actual cracking does not result, brittle, crack-prone, untempered martensite might result or, with lower temperatures, softened, overtempered martensite. High-strength steels (for which grinding is most often used) are particularly sensitive to grinding techniques.

In the electroplating processes a plating burn sometimes is observed as the result of arcing between the anode and the work piece. Such a burn generally produces a larger heat-affected zone than improper grinding and is often characterized by evidence of surface melting. The potential damage to the substrate is similar to that discussed relative to grinding.

Electrical discharge machining (EDM) is a process of metal removal that employs a spark-erosion principle. The intermittent spark produces highly localized melting on the surface of the workpiece and metal fragments which are swept away by the dielectric coolant. Although the heat-affected zone is shallow, surface cracking and untempered martensite are sometimes observed on martensitic alloys along with eutectic melting and other evidences of overheating in aluminum alloys if the process is not properly controlled.

1.3.1.5 Corrosion Fatigue.

Corrosion fatigue is that peculiar interaction of a corrosive environment with an alternating stress field which causes accelerated crack initiation and propagation, possibly where neither the environment nor the stress acting alone would be sufficient to produce a crack. In the practical application of the term, the corrosive environment usually serves to introduce stress raisers
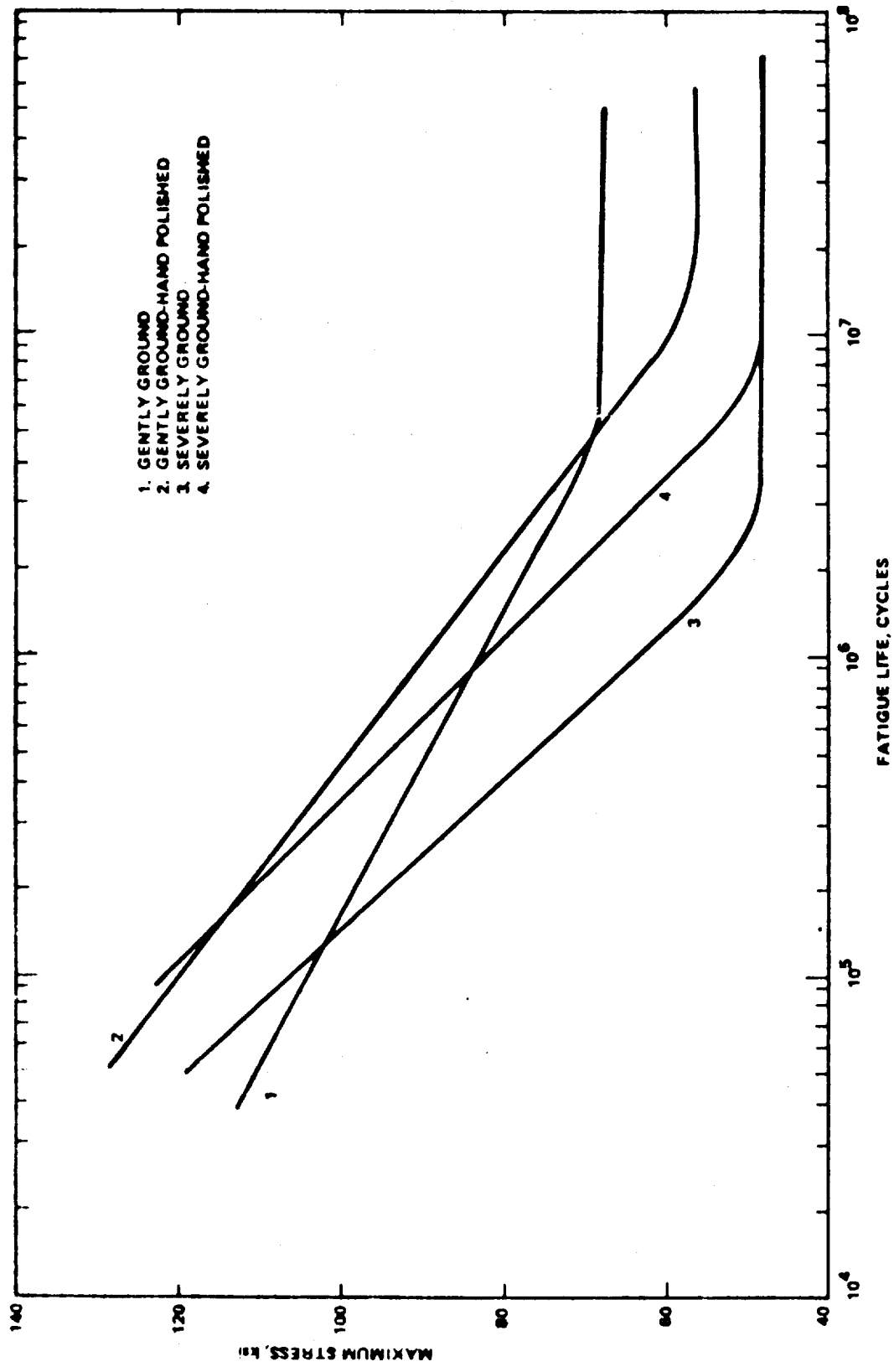
FIGURE E1-16. S-N CURVES FOR FLAT STEEL BARS (R_c-59 HARDNESS), SHOWING EFFECT OF GRINDING SEVERITY

in the surface in the form of corrosive attack. The irregular surface, in turn, is detrimental to the fatigue properties of the part in a mechanical or geometric sense. For materials susceptible to embrittlement by hydrogen or for parts which are exposed to a fairly continuous corrosive environment with intermittent applications of loading, the cracking mechanism may be somewhat more complex. An example of corrosion fatigue testing is presented in Fig. E1-17, which illustrates the effect of a corrosive test environment on the fatigue properties of precipitation-hardened stainless steels.
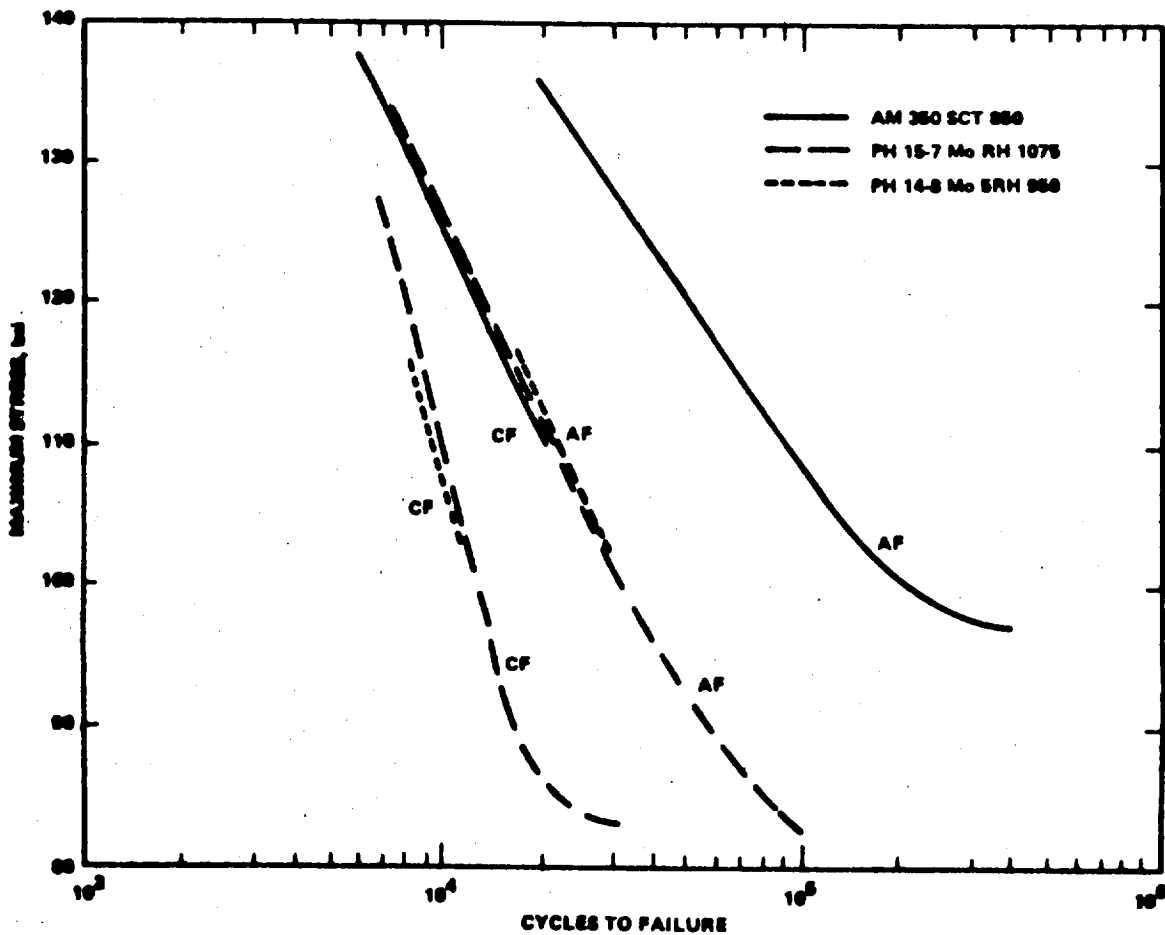
FIGURE E1-17. CORROSION FATIGUE AND AIR FATIGUE S-N CURVES FOR PRECIPITATION HARDENING STAINLESS STEEL TESTED AT ROOM TEMPERATURE

1.3.1.6   Fretting Corrosion.

The fretting corrosion phenomenon has been defined as that form of damage that arises when two surfaces in contact and normally at rest undergo relative periodic motion.   In vacuum or inert atmospheres the process is completely mechanical, but in ordinary atmospheres oxidation is also involved. Fretting is potentially dangerous because it can result from extremely small surface monuments that often cannot be anticipated or even prevented.   Motions with amplitudes as low as 5×10^{-9} inch are sufficient for this mechanism to be operative.

Soft metals exhibit a higher susceptibility to fretting fatigue than hard metals.   Fretting corrosion increases with load-amplitude, number of load cycles, contact pressure, and an increase of oxygen in the environment.   The oxidized particles that accumulate between the fretting surfaces lead to both chemical and mechanical surface disintegrations which generate nuclei for fatigue crack initiation.   The presence of fretting may reduce fatigue strength by 25 to 30 percent, depending on loading conditions.   When a part or assembly is known to be critical in fretting, one or a combination of the following factors will be beneficial in reducing or eliminating fretting corrosion:

1.   Electroplating critical surfaces.

2.   Case-hardening wearing surfaces.

3.   Lubricating.

4.   Eliminating or dampening vibration.

5.   Increasing fastener load or closeness of fit.

6.   Bonding elastic material to surface.

7.   Excluding atmosphere.

1.3.1.7   Reworking.

The success of any repair or rework procedure is necessarily closely dependent on the analysis of the degrading mechanism.   Only with a proper understanding of the cause of failure can a satisfactory permanent rework be accomplished.   In the area of service damage caused by fatigue, in-service failure, or engineering test failure of a part usually provides the impetus to

rework procedures. In general, these procedures can be separated into two categories: those parts that contain actual cracks and those that are believed to have undergone fatigue damage.

Usually, cracked structural parts are scrapped and replaced with a new part. Occasionally, however, because of the location of the crack or other circumstances, such a part is repaired. Repair would consist of removing the crack or blunting its root and supporting or strengthening the damaged area by means of doublers, straps, etc. Care must be taken in doubler design so that new sites of fatigue cracking are avoided. Factors such as fretting corrosion, dissimilar metal corrosion, detrimental stress redistribution, access, and practicality are prime considerations in establishing such a rework method.

Procedures frequently used to remove minor stress concentrators are those such as increasing a sharp edge, corner, or fillet radius, and grinding or buffing out coarse tool marks, nicks, and scratches. If assembly stresses are high, a joint having mismatched surfaces might be planed or mechanically realigned, or improved clearance could be provided. When fretting is contributing to fatigue cracking, a wear strip or lubricant may be inserted between the working surfaces, or the fasteners may be tightened to reduce or eliminate motion. Residual compressive stresses are often introduced into the critical areas of fatigue by shot peening or coining operations.

Estimating the depth of fatigue damage on a surface or below the tip of a fatigue crack is difficult and should be experimentally determined for all alloy-forming-heat-treating conditions and the load spectrum. Preliminary data indicate that the depth of fatigue damage beneath cracks for 7075-T6 aluminum alloy is approximately 0.003 inch. However, for high strength steel it may be many times greater than 0.003 inch.

1.3.2   Processing Factors.

Fatigue usually initiates at a surface because stresses are normally higher there, particularly since most parts undergo bending loads resulting in substantially higher stresses in the outermost fibers. The detrimental (or beneficial) effect of processing on fatigue properties is usually manifest in its effect on the strength level or residual stress condition, or both, of the surface material.

1.3.2.1   Hardness.

Strength of metals commonly used for engineering purposes is generally higher with increased hardness, up to a point. In steel, for example, increased

hardness does not necessarily indicate a higher fatigue limit because the fatigue limit is also affected by the surface finish. Curves of average fatigue limit values for a range of surface finishes are shown in Fig. E1-18. Because these curves represent average values, allowance should be made for size effect (larger size generally means lower fatigue limit).
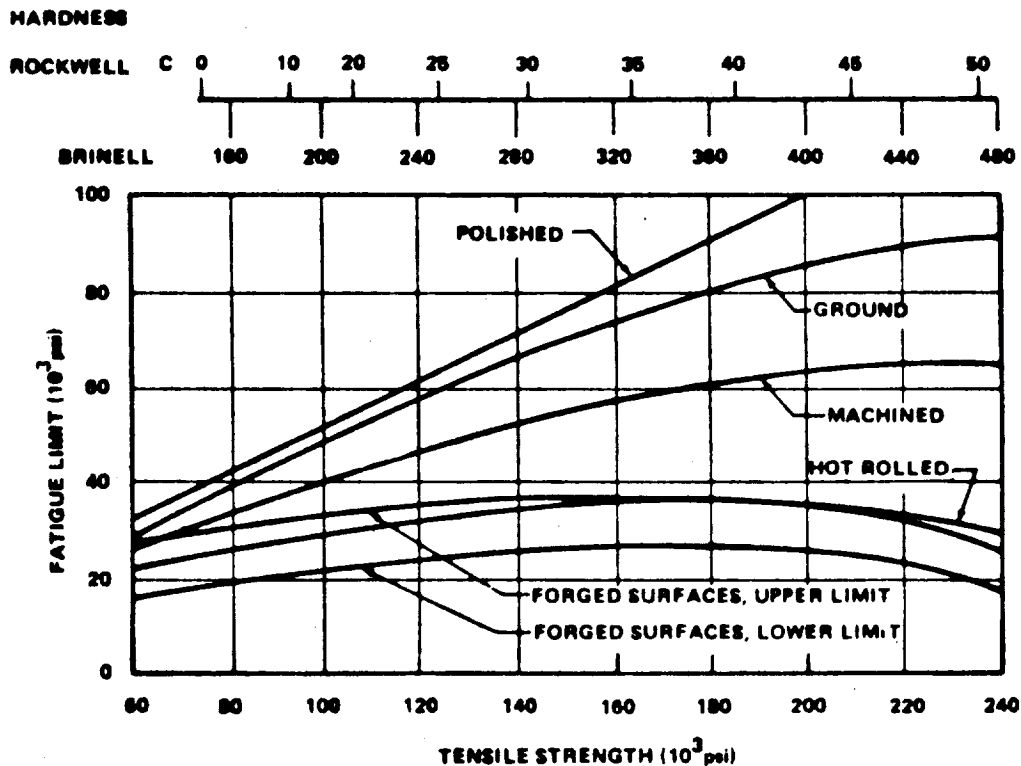
FIGURE E1-18. EFFECT OF HARDNESS AND SURFACE FINISH ON
FATIGUE LIMIT OF STEEL IN REVERSED BENDING
(0.3-INCH-DIAMETER SPECIMEN)

1.3.2.2 Forming.

By definition, the forming process produces plastic deformation (and residual stresses) in a part to achieve a permanent change in configuration. Occasionally these residual stresses may prove beneficial; however, usually there is some loss in fatigue life. Consequently, the residual stresses produced in forming (and their effect on fatigue) often dictate the forming limits for materials.

Residual forming stresses in the completed part are dependent on at least three additional factors: The heat-treatment-forming sequence in processing, the temper of the material, and the forming temperature. Parts formed and subsequently completely heat treated are free of prior forming stresses. Parts formed and stress relieved contain reduced forming stresses, depending upon the stress relieving temperature. The forming temperature and the material temper, e.g., AQ, T-4, or T-6 for aluminum alloys, also influence the magnitude of forming stresses to the extent that they affect the yield strength of the material at the forming temperature. In general, the lower the yield strength when forming occurs, the weaker the residual stress field generated.

1.3.2.3 Heat Treatment.

Residual stresses are both produced and relieved in many of the common heat treat cycles for both ferrous and nonferrous alloys. The principal source of residual stress occurs in quenching from high temperature solutioning or austenitizing treatments. Residual stresses are built up by nonuniform cooling rates between surface and core. For aluminum alloys, differential cooling produces residual surface compression and core tensile stresses. These surface compressive stresses are of sufficient magnitude to produce slightly higher fatigue strengths.

Aging temperatures for aluminum alloys are too low to produce any appreciable stress-relieving; however, most steels are tempered at temperatures sufficiently high to affect residual quench stresses. Consequently, for steels after tempering, quenching stresses are not recognized as a detrimental factor. Quenching stresses in aluminum alloys, however, persist after completion of heat treatment, as indicated by distortion in machining, increased susceptibility to stress corrosion and possible detrimental effects on fatigue life. To minimize these effects in aluminum alloys, special processing techniques have been developed, such as reducing section sizes by rough machining before heat treatment, use of less severe quenches where possible, and stress relief/equalization by cold working of quenched materials (for example, stretch-stress relief tempers).

1.3.2.4 Surface Finish.

A given surface-finishing process influences the fatigue properties of a part by affecting at least one of the following surface characteristics: smoothness, residual stress level, and metallurgical structure. The effects of surface finish on fatigue life for 7075-T6 extrusions are shown in Fig. E1-19. Here it can be seen that, in general, fatigue life increases as the magnitude

1. LONGITUDINAL HAND POLISH
2. SMOOTH MILL CUT
3. ROUGH MILL CUT
4. ROUGH SAND BLAST

NUMBER OF CYCLES TO FAILURE

STRESS (TENSION) ksi
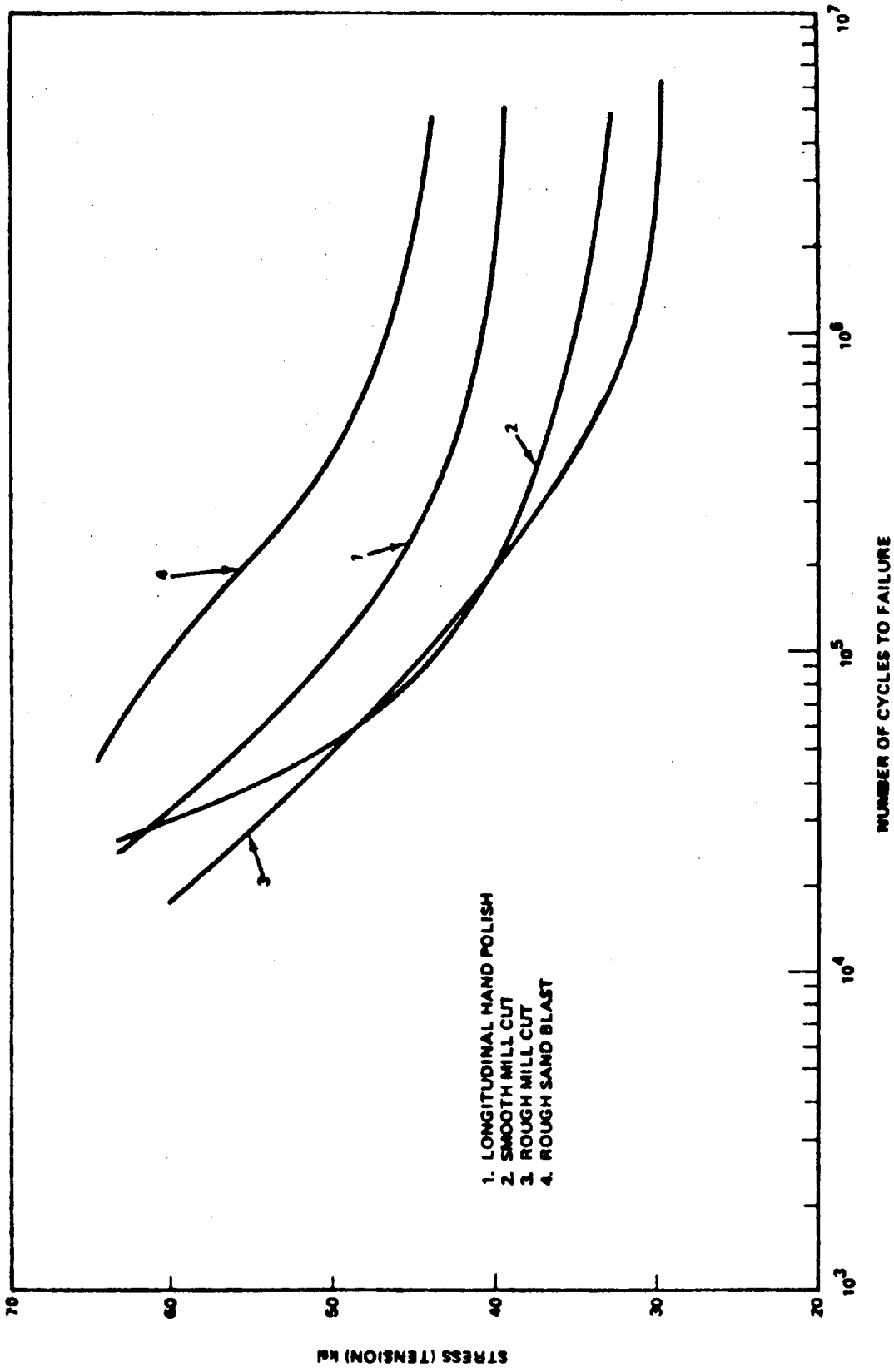
FIGURE E1-19. SURFACE FINISH VERSUS FATIGUE LIFE FOR 7075-T6 EXTRUSIONS

of surface roughness decreases. Decreasing surface roughness is seen as a method of minimizing local stress raisers.

Aside from effect on surface roughness, the final surface finishing process will be beneficial to fatigue life when it increases the depth and intensity of the compressively stressed layer and detrimental when it decreases or removes this desirable layer. Thus, sandblasting, glass-bead peening, and other similar operations generally improve fatigue life properties. Conversely, processes, such as electropolishing, chem-milling, and electrical-chemical machining (ECM), which remove metal without plastic deformation at the tool point may reduce fatigue life properties.

Many local surface defects and irregularities occur in fabrication and service that are difficult to anticipate, inspect for, or control. Stress concentrations resulting from small indentations on an otherwise smooth surface in the form of accidental tool marks, grinding scratches, corrosion pits, or service-related minor damage are occasionally as effective in reducing the fatigue life of structural parts as large scale stress concentrations resulting from design deficiencies, depending on the material, heat-treat range, design margins, etc. Such unintentional stress-raisers are damaging in a structure only if their notch effect is more severe than the most severe stress concentration arising from design, unless they are located so as to intensify the stress-raising effect of the critical design feature. Usually the effect of design stress concentrations far outweigh the effect produced by surface finish.

1.3.2.5   Cladding, Plating, Chemical Conversion Coatings, and Anodizing.

Clad sheets become progressively weaker than the bare sheets as the lifetime increases. However, the reduction in fatigue life for plain fatigue specimens is not present to the same degree in built-up assemblies, where the fabrication stress raisers overshadow the effect of claddding on fatigue strength.

Aluminum metal spraying is sometimes applied to extrusions and forgings for added corrosion protection. The effect on fatigue properties is quite similar to that observed for cladding. However, it has been found that sprayed zinc finishes on aluminum alloys do not produce any measurable reduction in fatigue life. Also, it is generally agreed that neither zinc nor cadmium plating has any appreciable effect on fatigue properties.

Chemical conversion and anodic coatings which are applied to aluminum alloys for corrosion protection or wear resistance usually produce a reduction in fatigue life ranging from a negligible amount up to 10 or 15 percent

of the endurance limit. The method of producing the coating further affects
fatigue properties. As an example, fatigue tests run on chromic acid anodized
7075-T6 indicated that anodizing with a 5-percent dichromate seal offered a
slight but definite lowering in fatigue life as compared to that of unanodized
metal, whereas, a sulfuric type anodizing treatment resulted in a substantial
reduction in fatigue life as shown in Fig. E1-20.
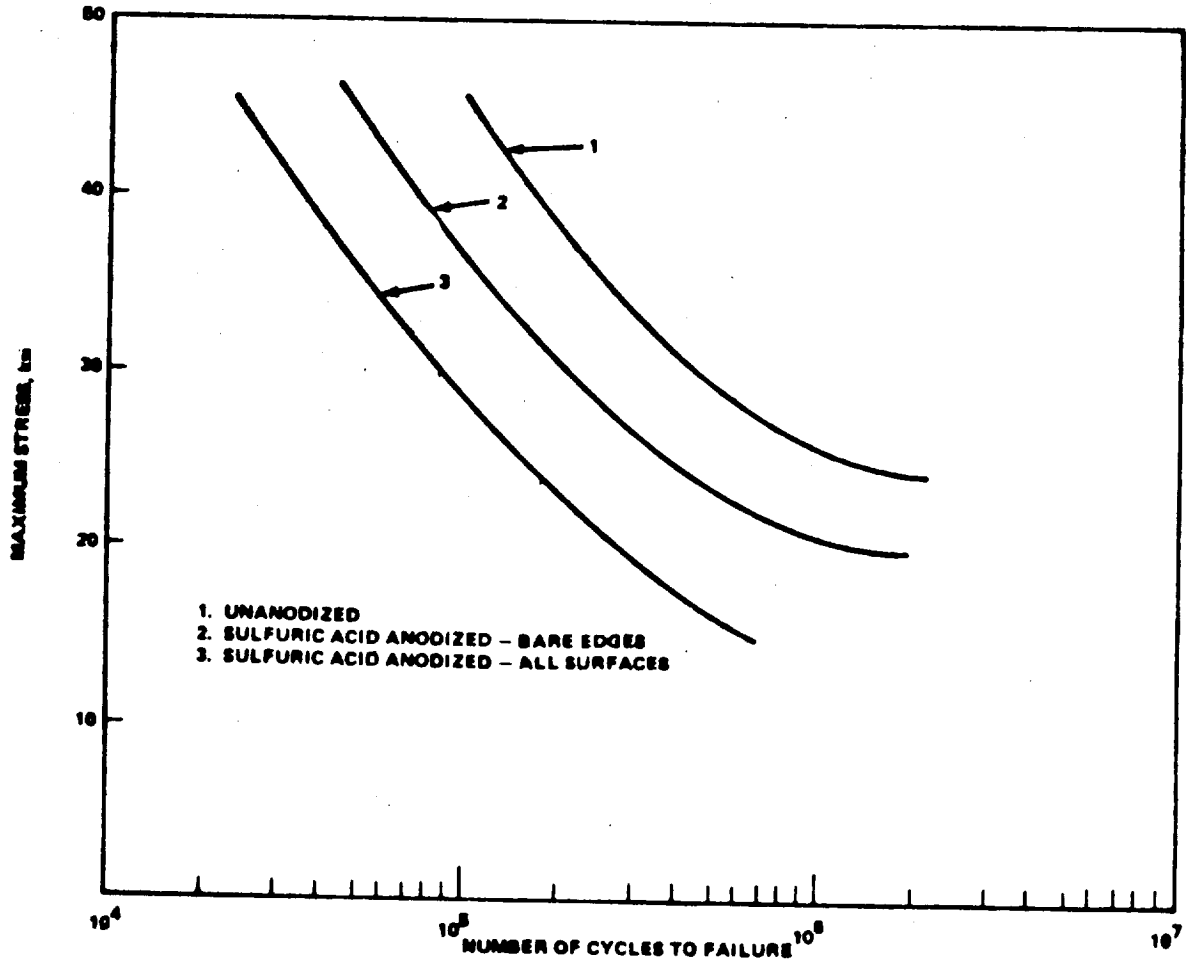
FIGURE E1-20. EFFECT OF SULFURIC ACID ANODIZE ON FATIGUE
PROPERTIES: 7075-T6 ALCLAD SHEET 0.090 IN. THICKNESS,
R = +0.2

Fatigue tests of 7075-T6 bare sheet with an Alodine #1200 coating
showed no loss in fatigue properties compared to untreated material.

1.3.2.6 Cold Working.

Cold working of parts to induce residual surface compressive stresses has been found to be an effective tool for improving the fatigue life of both simple and complicated shapes. Methods of imparting cold work include coining of holes, thread rolling, fillet rolling, peening, hole expansion, pre-stressing, tumbling, and grit blasting.

It should be realized that residual surface compressive stresses are most beneficial under loading conditions which produce high surface tensile stresses, as in bending. Residual compressive stresses, however, are also beneficial to the fatigue life of axially loaded specimens.

For the desirable effect of surface cold working to be maintained, the cold-working process must be accomplished in the final heat-treated condition; subsequent thermal treatment must be eliminated when feasible, but closely controlled when it is essential.

Perhaps the most widely used process for inducing residual compressive stresses in surface material is shot peening. Its use is widespread because of its low cost and relatively easy application to a wide variety of materials and parts of varied size or configuration. As an example, peening might be used before chrome plating or hard anodizing, or in special situations, after a heat treatment which produced decarburization of a steel part.

When a part undergoes loads that are much higher in one direction than in the opposite direction, prestresssing the part by applying an excessive load in the direction of major service loading will often produce beneficial residual surface compressive stresses and work hardening that will significantly improve fatigue life properties. In reverse loading this effect is lost and a detriment to fatigue life may result. In the aircraft industry, prestressing is often used for torsion bars and bomb hooks, to name two examples. It has been shown in some specimens that tensile prestressing to 90 percent of the tensile strength increased the endurance limit about 100 percent.

Techniques involving other types of cold working can be found in Ref. 2.

1.3.3 Environment Effects.

The fatigue properties of a metal can be greatly influenced by the nature of the environment, especially in long-time tests at low stresses and at low frequencies. Even normal air has a deleterious effect on fatigue life properties,

and recent indications show that moisture and oxygen are the two principal
adverse components. Moisture decreases the fatigue strength of copper,
aluminum, magnesium, and iron by 5 to 15 percent. An example of the
influence of environmental air moisture on the fatigue properties of an
aluminum alloy is given in Fig. E1-21.
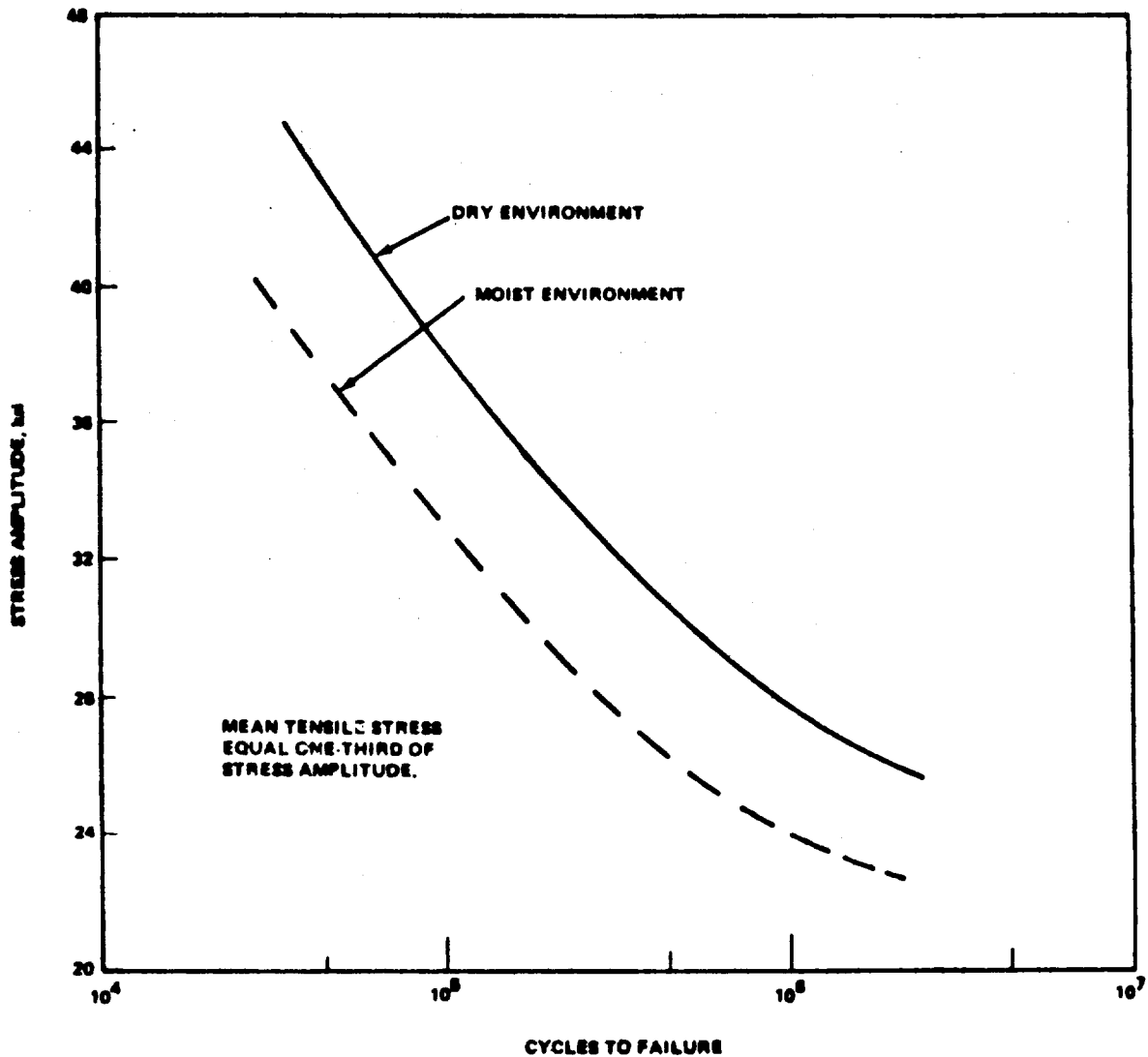
FIGURE E1-21. S-N CURVES FOR CLEAN SPECIMENS OF ALUMINUM
ALLOY 6060-T6 IN HIGH- AND LOW-HUMIDITY ENVIRONMENTS

It is generally agreed that the main effect of a normal atmosphere with
respect to fatigue life is on the propagation of cracks rather than in their

initiation. The principal effect of the environment will be in its reaction to the clean metal exposed at the tip of a fatigue crack. Cracks that would be of a nonpropagating variety in vacuum propagate in the presence of oxygen or moisture; thereby, they lessen the fatigue resistance.

In environments that are more corrosive than air and that substantially reduce the resistance of the surface layers to fatigue crack initiation, both initiation as well as propagation may be affected. Environments that lead to stress-corrosion cracking may also adversely affect fatigue properties. (Refer to Paragraph 1.3.1.5.)

1.3.3.1 Irradiation.

Some investigations have been made with respect to the effect of nuclear irradiation on mechanical fatigue properties of metals. Radiation-induced changes are usually referred to as radiation damage since in many cases the effects have been detrimental in one way or another. Damaging effects such as loss in ductility have been noted for many metals. On the other hand, beneficial effects evidenced increased yield and ultimate strengths, fatigue strength, and surface hardening also have been noted. Rotating beam fatigue tests on 7075-T6 aluminum alloy (Ref. 3) indicate an improvement in life due to the effects of a total integrated flux of 2×10^{18} fast neutrons per cm^2. Although the amount of irradiation received by the specimens in these tests is believed sufficient to alter mechanical properties, it is not known if the results are significant for the characteristics of metals during the conjoint action of fatigue straining and irradiation. Additional studies need to be undertaken for the simultaneous action of irradiation and mechanical straining at low temperatures.

1.3.3.2 Vacuum.

It has been demonstrated experimentally that fatigue cracking under uniaxial direct stressing of an aluminum alloy occurs in hard vacuum almost as readily as within atmospheric pressure. This is contrary to general belief. Experiments have disclosed trends toward increased crack growth rates in vacuum which may eventually result in characteristics more critical than growth rates obtained from in-air tests. Results on aluminum continuously held in vacuum for periods greater than a week yielded drastic reductions in fatigue properties. This strongly indicates the time dependency of the phenomenon. Results from short-time test exposures in vacuum have shown improved properties. This is the usually accepted belief. However, for many cases an extension of the vacuum outgassing time provides a more realistic environment than do the short-time test exposures previously investigated. Because of this

anomaly, prolonging the vacuum exposure is suggested as the only reliable procedure at present for evaluating metals for service in space environment.

1.3.3.3 Meteoroid Damage.

In the environment of space, tiny meteoroids and micrometeoroids may strike the surfaces of a space vehicle. At present, no information is available as to this effect on fatigue properties. However, it can be reasoned that indentations caused by these meteoroids provide ideal sites for the initiation of fatigue cracks by reason of the increased stress concentration.

1.3.3.4 Solar Irradiation.

Solar irradiation will cause differential heating on orbiting spacecraft. Over long periods of time, the thermal cycling and the resulting fatigue could become a serious problem.

1.3.3.5 Temperature.

Elevated temperatures may cause metals to lose strength; low temperatures may cause some metals to become notch sensitive and fail by brittle fracture under load conditions that would be common at normal (standard) temperature.

In general, the fatigue life of most metals will decrease with an increase in temperature (Fig. E1-22). Studies have indicated that as the temperature decreases, the crack nucleation period (or time to produce an observable crack) increases. Moreover, as temperature decreases, the period of observable fatigue crack growth decreases.

The rate of fatigue-crack propagation as affected by rate of cyclic loading and test-load frequency is an additional parameter to be considered. In elevated-temperature fatigue testing, it is known that the number of cycles to fracture decreases and the crack-growth rate increases as the speed or frequency of cyclic loads is decreased. The damaging, thermally activated mechanism of creep or creep cracking, acting conjointly with fatigue, is responsible for this behavior. In general, this is true because, in the accumulation of stress cycles, slower rates of load cycling result in exposure of the metal to temperature for longer periods of time than do fast rates of load cycling. However, from cryogenic temperatures to room temperature, no damaging, thermally activated mechanisms are active. It is believed that fatigue lives and crack-growth rates at cryogenic temperatures will be independent of load frequency for most metals.
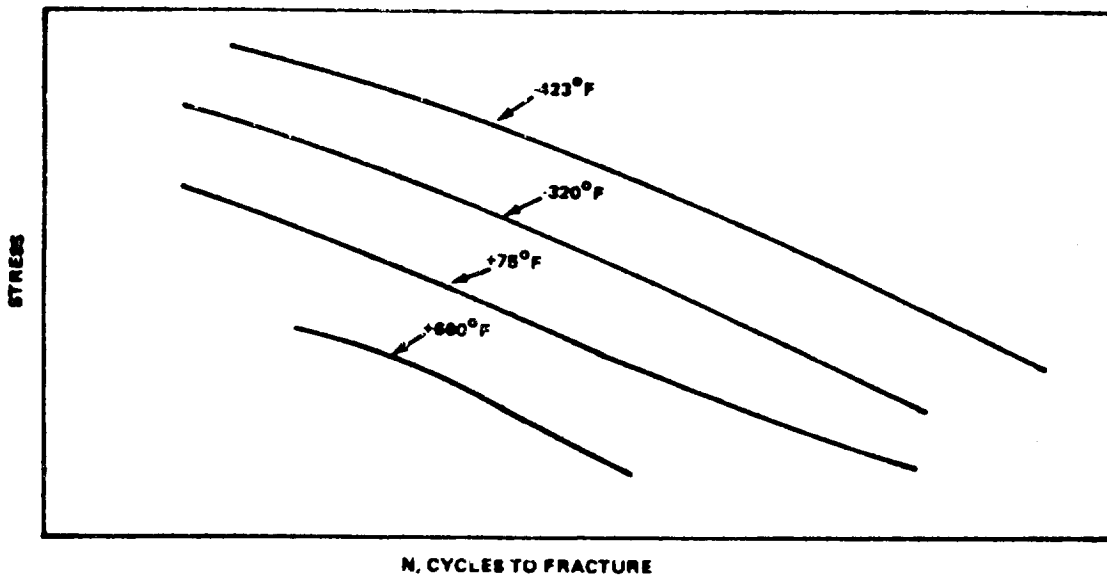
FIGURE E1-22. FATIGUE LIFE AS A FUNCTION OF TEST
TEMPERATURE (TYPICAL FOR MOST METALS)

Additional information on thermal and creep effects will be given in
Paragraph 1.4.3.

1.3.4   Design Effects.

Manufactured parts often include abrupt changes in cross section such
as grooves, fillets, holes, and keyways; these cause a nonuniform distribution
of elastic strains and stresses. The maximum elastic stress at an abrupt
change in cross section is greater than the nominal stress obtained by calcula-
tion with either the direct stress, flexural, or torsional formulas.

The geometric stress-concentration factor, K, is defined as the ratio
of the maximum stress in the section to the nominal, or average, stress.
Nominal stress is usually based on the net remaining section. Because of
exceptions, it is necessary to ascertain the basis upon which the nominal stress
is established before applying a stress concentration factor.

The full geometric stress-concentration factor is not always applicable
in fatigue loading. The actual fatigue limit of a notched member is frequently
higher than would be expected from the geometric stress-concentration factor.
This phenomenon is called notch sensitivity. Use of the notch-sensitivity
factor results in a fatigue stress-concentration factor that is determined from:

$$K_f = q(K_t - 1) + 1$$

where K_f is the fatigue stress-concentration factor for direct tension or

bending; K_t is the geometric stress concentration factor for direct tension, or

modified geometric stress-concentration factor for bending (Ref. 4); and q
is the notch sensitivity. Typical values of q versus notch radius for steels
of various strengths are shown in Fig. E1-23.
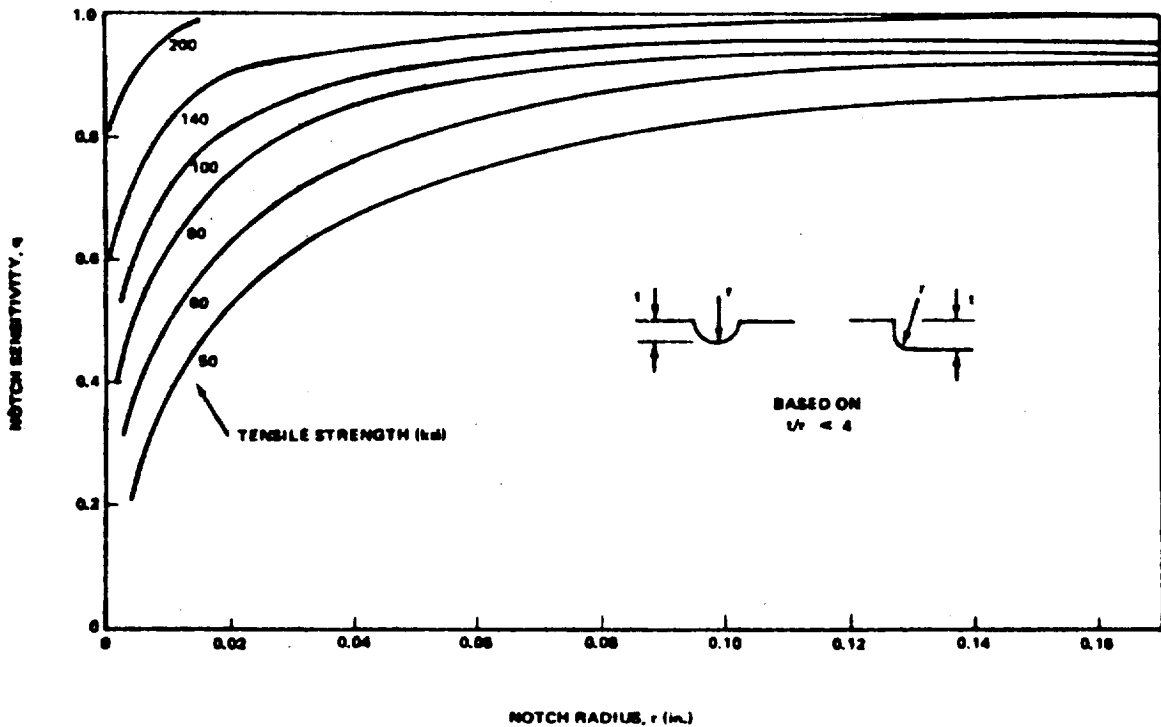
FIGURE E1-23. NOTCH-SENSITIVITY CURVES FOR POLISHED STEEL
SPECIMENS OF VARIOUS STRENGTHS

The fatigue-stress concentration factor, K_f, represents the extent

to which a notch can be expected actually to reduce the fatigue limit of a part.
It is the ratio of the fatigue limit of the specimen without the notch to its
fatigue limit with the notch. Specimens must have the same effective section
when K_f is evaluated experimentally so that only the effect of the notch is

determined without including an effect which is due to reduction in the section.

When one notch is located in the region of maximum influence of another notch, the resulting stress-concentration factor is determined by multiplying the two individual stress-concentration factors. Whether the maximum influence of one notch encounters the maximum influence of the other depends on the stress patterns developed by the two notches and the extent of overlap. When stress concentrations are adjacent to each other, but are not superimposed to the extent that one is placed in the region of maximum influence of the other, the resulting stress concentration factor lies between the value of the larger factor and the product of the two stress-concentration factors. In steel members with numerous notches and discontinuities, a value of $K_f = 3$ is

applicable in most cases, and a value of $K_f = 4$ is the maximum likely to be encountered.

1.3.5 Welding Effects.

There exists a considerable amount of information on the fatigue properties of various welding effects in steel (Ref. 5). However, the amount of information on welding effects in nonferrous materials is relatively scarce, primarily because of the late development of welding of aluminum alloys. As a consequence, the use of welded aluminum in fatigue-loaded structures has been limited; however, it is becoming more extensive, particularly for applications where weight savings is of importance. This frequently implies that fatigue strength is the design criterion.

It has been found that by far the most important factor in the fatigue behavior of welded joints in aluminum and steel is the geometrical shape, both of the joint as a whole and of the weld bead. Parent material seems to be a relatively unimportant variable.

The fatigue limit of welded high-strength steels is only slightly higher than for low-strength steels if the weld bead is left in place. However, if the weld bead is removed, the fatigue limit is increased; the amount of increase depends upon the smoothness of the finished surface. Even partial removal of the weld reinforcement increases the fatigue limit considerably. For welded steel with the weld undisturbed, fatigue limits of approximately 12 000 psi in reversed bending and 23 000 psi in zero to maximum tension are common. These are average values, and an allowance for a lower failure rate should be made. Removal of weld beads also improves fatigue characteristics of aluminum.

1.3.6   Size and Shape Effects.

Usual specimens for fatigue tests are in the range of 0.2- to 0.5-inch diameter. Some reduction in fatigue limit with increasing size of specimen has been observed. This reduction is generally attributed to the fact that larger sizes stressed in bending or torsion have a larger volume of material in the region of high stress. This increases the probability that a defect will occur in the high stress region, leading, in turn, to a higher probability of failure in larger sizes.

Fatigue tests in axial loading show relatively little size effect, probably because of the uniform stress across a section under an axial load.

Size has little effect upon the failure stress at 1000 cycles. Thus, a size correction is neglected at the 1000 cycle point of the S-N curve and applied only to the fatigue limit.

Shape of cross section has some effect on the flexural fatigue limit of some materials. Steel beams of circular cross section have fatigue limits of 8 to 10 percent higher than square beams. Square beams loaded so that the maximum stress occurred at the corners of the square exhibited fatigue limits from 4 to 8 percent less than round beams.

1.3.7   Speed of Testing.

The effect of the speed of testing has been studied by a number of investigators. In the range of from 200 to 7000 cycles per minute there appeared to be little effect on the fatigue properties, except when temperature increases in the specimens were encountered. At very low speeds a slight decrease in fatigue strength was noted, while for very high speeds some increase in strength was found.

Of course, the speed of testing is of great importance at the low-cycle side of the stress-versus-life curve and also when thermal cycling or creep is involved. These effects are covered in Paragraphs 1.4.2 and 1.4.3.

1.4   LOW-CYCLE FATIGUE.

A complete S-N curve may be divided into two portions: the low-cycle range and the high-cycle range. There is no sharp dividing line between the two. We might arbitrarily say that from 0 to about 10^3 or 10^4 cycles is low cycle and from about 10^3 or 10^4 cycles to 10^7 or higher is high cycle.

Until World War II little attention was paid to the low-cycle range, and most of the existing results were for high cycles only. Then it was realized that for some pressure vessels, missiles, spaceship launching equipment, etc., only a short fatigue life was required. Consequently, the low-cycle fatigue phenomenon began to gain attention.

In the low-cycle range of fatigue life below approximately 10 000 cycles, the primary parameter governing fatigue life appears to be plastic strain per cycle as measured on a gross scale. For higher (cyclic) lives, elastic strain also assumes importance; perhaps the governing variable is still plastic strain per cycle, but the plastic strain is highly localized at imperfections in the structure and is difficult to measure or compute. Beginning at approximately 10 000 cycles and continuing upward, it becomes more appropriate to regard total strain (elastic plus plastic) as the primary variable. Alternatively, the fatigue life can be regarded as being governed by stress range, and the ensuing simple relationship between fatigue life and stress range appears to be valid for most of the materials that have been tested to date, over a very large range of life on both sides of 10 000 cycles. However, for most thermal-stress problems the stress range is less likely to be known than is the strain range; hence, for practical purposes it is desirable to express life in terms of total strain range. The relationships as applied to problems of both thermal and mechanical loading are discussed below.

The failure mechanism in the low-cycle range is close to that in static tension, but the failure mechanism in the high-cycle range is different and may be termed "true fatigue." A comparison of the failure mechanisms in the two ranges is made in Table E1-1.

Table E1-1. Comparison of Low Cycle and High Cycle Fatigue

	Low Cycle	High Cycle
Internal stresses and strain hardening	High	Low
Net sum of plastic flow	Micro size	Micro size
Gross sum of plastic flow	Small	Large
X-ray disorientation	Large	Small
Slip	Coarse (10^3-10^4Å)	Fine (10Å)
Slip plane distortion	Normal	Persistent
Crack origin	Interior	Surface
Crack path	Along maximum shear	Cross maximum tensile stress
Fracture	Delayed static	Structural deterioration

The terms used in this section are defined below and are shown in Figure E1-24.

E = modulus of elasticity

N = cycles to failure

ϵ_t = total strain range

ϵ_e = elastic portion of strain range

ϵ_p = plastic portion of strain range

C = a material constant

ϵ_f = true strain at fracture, commonly known as fracture ductility

$$S = \frac{1}{2} E \epsilon_t$$

ΔS = stress amplitude

S_e = endurance limit

S_u = ultimate tensile strength in ordinary tensile test

S_y = yield strength

S_{ut} = true stress at fracture in tensile test

1.4.1   Below Creep Range.
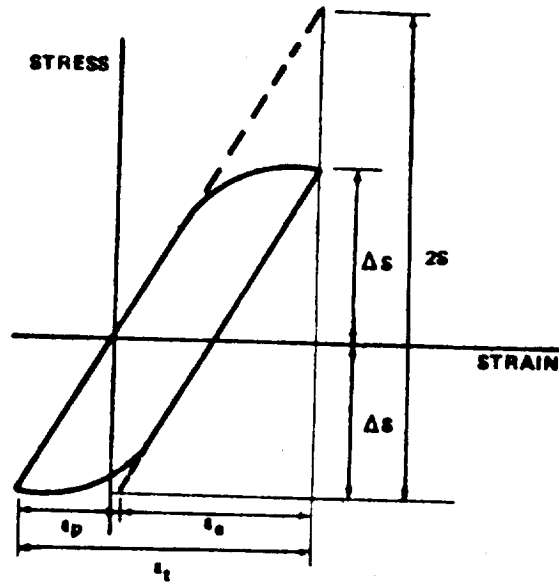
FIGURE E1-24. STRESS-STRAIN CYCLE

In recent years, low-cycle fatigue has been studied extensively under conditions where little attention has been paid to temperature and temperature effects. There now exists a fairly large body of information on the subject obtained from laboratory experiments under room temperature conditions (Ref. 6). The general procedure in such investigations is to control the strain between fixed limits and, if desired, to measure the stress, while cycling the specimen until failure is determined. Such tests may be under conditions of controlled diametral strain, longitudinal strain, bending strain, or torsional strain. The results can be represented in terms of total strain range versus cycles to failure, or, if desired, of plastic strain range versus cycles to failure. The former is most often used for direct design procedures, while the latter is applied when one is primarily interested in real material behavior. One of the more fascinating features of representing the results in the form of plastic-strain range versus cycles to failure is the observation that the curve (on logarithmic scales for both $\Delta\epsilon_p$ and N_f) is of constant slope of value 0.5 to 0.65 (depending on the experimenter) and that the vertical position of the curve relates to the tensile ductility of the material. A plot of this curve is shown in Fig. E1-25. The line in this figure can be expressed by the equation

$$\Delta\epsilon_p \sqrt{N} = C$$
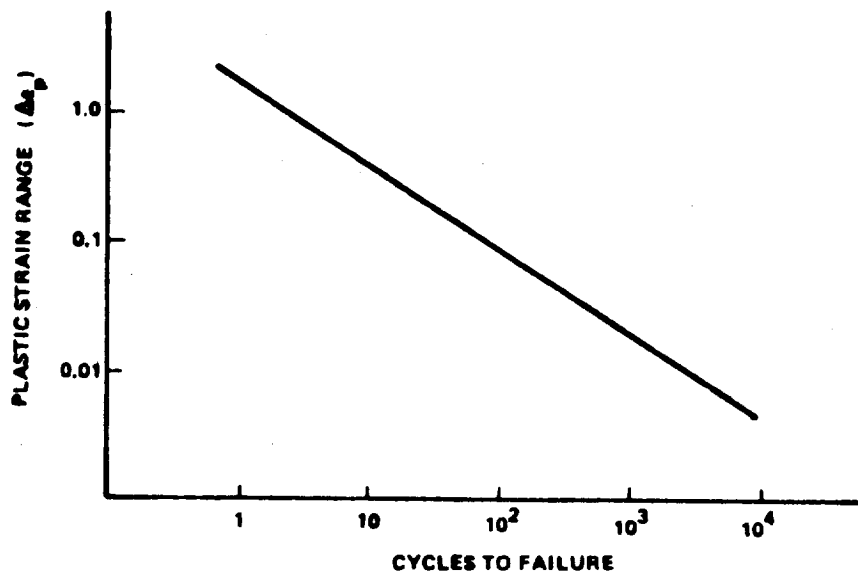
FIGURE E1-25. PLASTIC STRAIN RANGE VERSUS CYCLES
TO FAILURE

where the constant C may be related to the reduction of area RA in static
tension test.

$$C = \frac{1}{2} \ln \frac{100}{100-RA} \quad .$$

A fair degree of information and understanding now exists for the low-
temperature (below the creep range), low-cycle fatigue problem, although
there are a number of unresolved questions yet to be answered.

1.4.1.1   Practical Problem Solutions.

The fatigue curve or equation needed by the engineer or designer is
one which shows stress versus cycles and one that contains sufficient safety
factors to give safe allowable design stresses for a given number of operating
cycles; or, conversely, allowable operating cycles for a given value of cal-
culated stress. The stress values on the fatigue curves or in the equations
should be directly comparable to the stress values which the designer cal-
culates using his usual methods of analysis for pressure stress, thermal
stress, stress concentration, etc.

For fatigue below the creep range, Langer (Ref. 7) has proposed an equation for plotting the fatigue curve for any material:

$$S = \frac{E}{4\sqrt{N}} \; \ln \; \frac{100}{100-RA} + S_e \quad ,$$

(refer to Fig. E1-24 for definitions of terms).

For a design stress to represent a lower bound on the data, it is recommended that the equation above be used with a safety factor of either 2 on stress or 10 on cycles, whichever is more conservative at each point. It is believed that these safety factors are sufficient to cover the effects of size, environment, surface finish, and scatter of data.

It also has been shown that in the low cycle range (below 10 000 cycles), mean stress has little or no effect on fatigue life; thus, this effect can be ignored.

Some typical values of E and RA for various materials are given in Table E1-2. If information on the endurance limit (S_e) is not available one-half the value of the ultimate strength is often used.

If a more detailed fatigue analysis is required the techniques proposed in References 6 and 8 should be used.

1.4.2   In Creep Range.

The high-temperature, low-cycle fatigue problem is in quite a different state. The material behavior becomes very much more complicated at elevated temperatures because of the occurrence of creep and other diffusion processes. At temperatures in the creep range of a material, the test results will be very strongly frequency dependent. Citing the fact that frequency is important in high-temperature, low-cycle fatigue is the same thing as saying that the strain rate of the test is important. A somewhat related situation occurs if one introduces a hold time into the cycle, say, at the point where the tensile stress is a maximum. While the strain is held constant, the peak stress relaxes for some period of time. Results of prolonged hold times during strain cycling show that the fatigue life decreases with increasing hold times, other conditions being the same. A common observation is that, as the temperature is raised and the rate decreased (or hold time increased), the character of

Table E1-2. Mechanical and Elastic Properties of Materials

Material	Yield Strength S_y (ksi)	Ultimate Strength S_u (ksi)	Reduction in Area, RA (percent)	Modulus of Elasticity (E)	Poisson's Ratio (μ)
4130 (soft)	113.	130.	67.3	32×10^6	0.29
4130 (hard)	197.	207.	54.7	29	0.28
4340 (ann.)	92.	120.	43.4	28	0.32
4340 (hard)	199.	213.	38.1	29	0.30
52100	279.	292.	11.2	30	0.29
304 ELC (ann.)	37.	108.	74.3	27	0.27
304 ELC (hard)	108.	138.	68.8	25	0.34
310 (ann.)	32.	93.	63.5	28	0.30
350 (ann.)	64.	191.	52.1	28	0.32
350 (hard)	270.	276.	20.3	26	0.30
Inconel X	102.	176.	19.7	31	0.31
Titanium (6 Al-4V)	172.	179.	41.0	17	0.33
2014-T6 Al	67.	74.	25.0	10	0.33
5456-H311 Al	34.	58.	34.6	10	0.33
1100 Al	14.	16.	87.6	10	0.33
Beryllium	38.	46.9	1.7	42	0.024

the fracture changes from one which is transgranular in nature to one which is largely intergranular. This suggests very strongly that the problem is, to a large degree, metallurgical in nature. A close resemblance can be seen between these observations and those found in creep and stress rupture.

A second important, and certainly related, effect which must be appreciated when dealing with high-temperature fatigue is the change in metallurgical structure which occurs with time at temperature and stress.

Plastic strain and, in the present instance, cyclic plastic strain can have an important bearing on the precipitation and strengthening effects which take place in the metal structure. The term "strain-age hardening" describes the effect that plastic strain has on developing additional strength. It is well known, for example, that the level of strength reached by applying a fixed amount of strain to a metal which strain ages is greater if the strain is applied at the aging temperature. In designing an alloy for creep, advantage can be taken of strain-age hardening provided the strain involved is the creep strain selected for the design.

1.4.2.1   Ductility Versus Creep Strength.

As mentioned above, creep strengthening can be accomplished for specific alloys at various regions of temperatures. However, it should be noted that, simultaneously with strengthening, these same regions show reduced fracture ductility.

This well-known behavior of metals, the inverse relationship between strength and ductility, introduces a dilemma into the selection of materials for high-temperature service. It is necessary, to optimize the strength, to employ alloy additions and heat treatments so as to develop the precipitate structure in the metal, but this will lower the ductility. Ductility is of prime consideration in low-cycle fatigue and, to optimize fatigue resistance, it is desirable to have the material in as ductile a condition as possible (a condition which results in low creep strength). However, one wants both creep strength and fatigue resistance, and it is apparent that the best that can be achieved is some compromise condition.

1.4.2.2   Procedure for Estimating High-Temperature, Low-Cycle Fatigue.

The procedure given here is taken from References 9 and 10. It is a procedure for estimating the high-temperature, reversed-strain-cycling fatigue characteristics of laboratory specimens. It should be emphasized that

the method is intended to give only first-approximation estimates as a guide to material selection. Final design of important equipment should be based on actual fatigue data generated under conditions which simulate as closely as possible those to be encountered in service.

I. <u>Basis</u>.

Figure E1-26 illustrates the method of universal slopes. The total strain range is divided into its elastic and plastic components, and each component is plotted against cyclic life on log-log coordinates. Straight lines usually result for each of these components. The method of universal slopes prescribes that the slopes of these lines are assumed to be the same for all materials. The plastic components are taken to have an average slope value of -0.6, and the elastic components an average slope value of -0.12. Again, it should be emphasized that these values are not always -0.6 and -0.12 for all materials; values between -0.4 and -0.8 have been obtained for various materials for the plastic component, and values between -0.08 and -0.16 have been found for the elastic components. When average values of -0.6 and -0.12 are chosen for the plastic and elastic components, reasonable results are obtained.

CYCLES TO FAILURE, N_f (LOG SCALE)
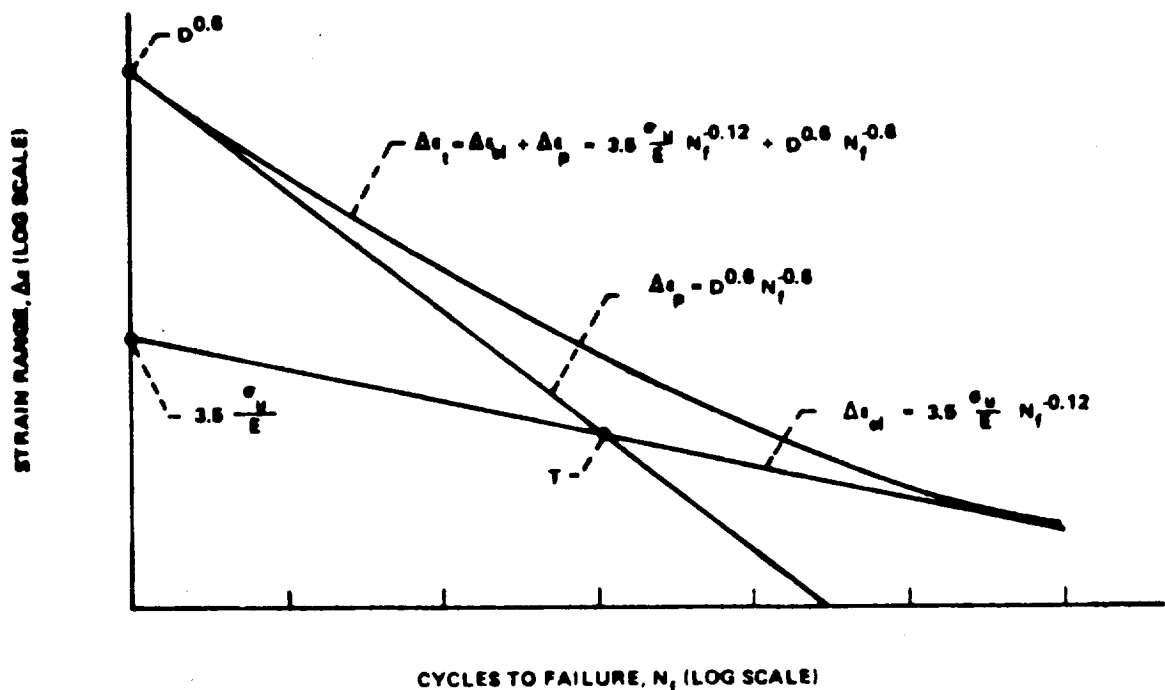
FIGURE E1-26. METHOD OF UNIVERSAL SLOPES FOR ESTIMATING AXIAL FATIGUE LIFE

Having decided on the slopes, it is necessary to determine the intercepts of the two straight lines. In general, it has been found that the property which most significantly governs the intercept of the plastic line is the ductility D, where $D = \ln \dfrac{100}{100-RA}$.

For the elastic line, the governing property for the intercept is σ_u/E, where σ_u is the ultimate tensile strength and E the elastic modulus. The total strain range, given as the sum of the elastic and plastic components, thus becomes

$$\Delta \epsilon_t = \frac{3.5\,\sigma_u}{E} \, (N_f)^{-0.12} + D^{0.6} \, (N_f)^{-0.6}$$

as shown in Fig. E1-26.

Good agreement has been obtained with this formula for many materials (Ref. 9). However, the question arises: Can one use this procedure at high temperatures within the creep range of the material? In general, it has been found that the procedure almost always yields fatigue life predictions higher than those actually obtained by testing. The explanation for the unconservative results is, of course, very complex. The relationship between high-temperature, low-cycle fatigue and intercrystalline cracking is very important.

It has been shown that intercrystalline cracking due to a creep effect occurs early in the fatigue life, and thereby bypasses the transcrystalline crack-initiation period; thus, the total fatigue life is approximately equal to only the crack-propagation period.

This concept has yielded the 10-percent rule. In this method, crack initiation and propagation are not regarded as functions of fatigue life; rather it is assumed that, on the average, only 10 percent of the fatigue life computed by the method of universal slopes will actually be realized at temperatures within the creep range.

Generally, it has been found that such a computation yields conservative results; that is, in most cases, it leads to a lower bound on fatigue life. However, there are cases in which even the 10-percent rule predicts lives that are higher than those actually achieved in test. This observation (together with the fact that the 10-percent rule approach inherently excludes the possibility of taking into account frequency effects, hold-time effects, mean load,

etc.) causes one to seek further for simple methods of estimation that are not as limited.

The simplified analysis that has been adopted can be explained by the following. The creep damage effect is taken as the ratio of the time actually spent at stress to the time required to cause rupture at that stress value. Since the stress and temperature are presumably known, this rupture time can be obtained directly from the creep-rupture curve of the material. The fatigue damage effect is taken as the ratio of the number of cycles actually applied to the number that would be sustained in the absence of creep effect according to the method of universal slopes. Since the test frequency yields a definite relation between the time of the test and number of cycles sustained, a closed-form analytical expression for the number of cycles to failure can be obtained. This description is shown in the following derivation:

$$(\text{Creep-Rupture Damage}) + (\text{Fatigue Damage}) = 1$$

$$\left(\frac{t'}{t_r}\right) + \left(\frac{N_f'}{N_f}\right) = 1$$

where

$$t' = \frac{k}{f} N_f'$$

$$t_r = A\left(\frac{\sigma_r}{1.75}\right)^{1/m} = A(N_f)^{-0.12/m} \quad ;$$

hence,

$$\left(\frac{kN_f'}{AF(N_f)^{-0.12/m}}\right) + \left(\frac{N_f'}{N_f}\right) = 1$$

or

$$N_f' = \frac{N_f}{1 + k/AF(N_f)^{(m + .12)/m}}$$

Here

N_f' = number of cycles to failure under combined fatigue and creep

N_f = number of cycles to failure in fatigue, based on method of universal slopes, using ductility, ultimate tensile strength and elastic modulus from uniaxial tests at strain rates comparable to that undergone by the metal in the fatigue test. Where appropriate data are not available, use may be made of data from conventional tensile tests.

k = empirical constant, assumed to be 0.3, but adjustable as more information becomes available.

m = slope of straight line-creep-rupture curve on log-log coordinates, that is, representing curve by $\sigma_r = 1.75\,\sigma_u\,(t_r/A)^m$ as shown in the insert in Fig. E1-27.

A = coefficient in creep-rupture relation

F = frequency of cycling, cycles per unit time.

Table E1-3 contains some of the information above, obtained from various test conditions (Ref. 9).
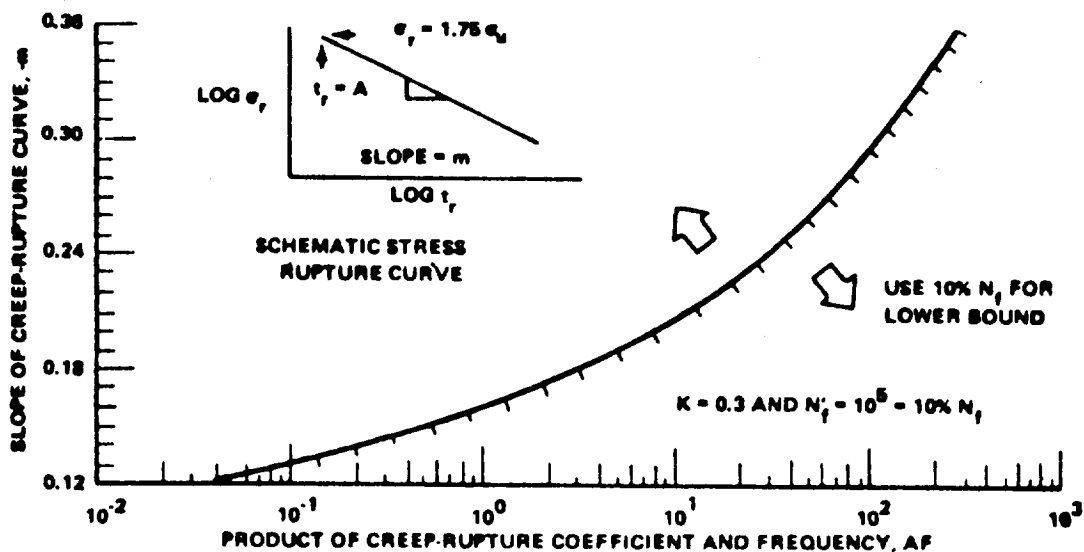
FIGURE E1-27. CRITERION TO ESTABLISH NEED FOR CREEP-RUPTURE CORRECTION

Table E1-3. Alloys, Test Conditions, and Pertinent Properties

Alloy Designation	Test Temperature (°F)	Test Frequency (cpm)	RA (%)	Tensile Strength (ksi)	Elastic Modulus (10³ ksi)	Creep-Rupture Slope (-m)	Intercept, A (min)	(sec)
A-286 — CR 34%	1000	5 to 50	31.	182.	26.8	<0.12		
	1200	5 to 50	38.	167.	23.1	<0.12		
A-286 — Aged	1200	5 to 50	18.	115.	23.0	<0.12		
A-286	1400	20	57.6	75.	19.0	0.20	1.3	78.
Inco 901	1400	20	16.1	104.	20.8	0.135	0.028	0.17
D-979	1260	5 to 50	42.0	179.	22.0	<0.12		
Cr-Mo-V Steel	1050	1, 10	70.0	69.5	24.0	<0.12		
L-605	1000	5, 50	48.2	106.0	27.0	<0.12		
	1200	5, 50	47.1	95.4	25.0	<0.12		
304 Stainless Steel	1000	10	67.3	55.5	23.0	<0.12		
	1200	3 to 18	58.0	41.0	22.0	0.18	13.0	900.
	1500	3 to 27	42.0	20.0	19.0	0.18	0.3	18.0
347 Stainless	1110		67.7	55.0	22.0	<0.12		
Nimonic 75	1200	10	29.5	81.5	20.3			
	1380	10	42.0	53.1	15.4			
	1600	10	62.5	28.0	12.2			
	1800	10	66.0	16.2	9.7			
Nimonic 90	1200	10	24.5	144.0	26.5	<0.12		
	1380	0.1, 10	12.0	119.0	25.0	0.135	0.16	9.6
	1600	0.1, 10	14.0	76.0	23.0	0.24	2.5	150.
	1800	0.1, 10	94.0	16.0	21.0	0.25	4.0	240.
Nimonic 105	1200	10	13.7	142.0	25.0	<0.12		
	1380	10	18.0	151.0	23.5	<0.12		
	1600	10	32.5	99.5	22.0	0.16	0.08	4.8
	1800	10	68.0	39.2	19.0	0.28	3.7	222.
Udimet 700	1400	1 to 2	31.0	155.0	23.0	<0.12		
Astroloy	1400	20	29.6	141.0	23.0	<0.12		
Inconel	1500	0.017, 0.1	63.3	25.0	18.0	0.15	1.0	60.
In 100 (PWA 47 Coat)	1000	6	9.3	121.0	27.1	<0.12		
	1700	6	11.0	96.0	22.7	0.17	0.11	6.6
	2000	6	10.3	26.8	19.3	0.22	1.3	78.
MAR M 200 (PWA 47 Coat)	1300	6	5.	120.0	26.5	<0.12		
	1700	6	4.	77.0	23.7	<0.12		
B 1900 (PWA 47 Coat)	1300	6	5.	145.0	25.5	<0.12		
	1700	6	3.	95.0	23.0	0.17	0.75	45.
	2000	6	9.	35.0	20.5	0.26	7.3	140.

II.   Method.

In summary, two procedures for computing the lower bound on fatigue life have been outlined. Proceed:

1. By the 10-percent rule. The universal slopes equation is first used to determine cyclic life, and this life is divided by a factor of 10.

2. By the combined creep and fatigue effect.

The problem of determining which of the equations to use, and how to interpret the results has been given considerable study and the following conclusions can be drawn:

a. Determine life by both methods, and use the lower of the two calculated values. Figure E1-27 is an auxiliary plot that minimizes the computations needed to determine which value to use. It is merely necessary to determine the product, AF, and the slope, m, of the creep-rupture curve at the test temperature. If the point representing the coordinates lies above the curve, use the equation for N_f'. If it lies below the curve, use the 10-percent rule.

b. The lower of the two values determined in a. serves as a lower bound on estimated life.

c. As an estimate of average or most probable life, use twice the lower bound determined in b.

d. As an estimate of the upper bound on life, use 10 times the lower bound determined in b.

It has been found that, in most cases encountered in the laboratory, the 10-percent rule is the applicable one.

As tempting as it is to conclude that the method gives results good enough for many engineering uses, it is perhaps of greater importance to emphasize some of the cautions involved in its use. It must first be emphasized that the data analyzed relate to constant amplitude-strain cycling under constant temperature. The method appears to place the high-temperature, low-cycle fatigue behavior in the proper range. Thus, it would seem that while the

method may be regarded as very good for screening materials, important material choices should be made on the basis of actual tests from among the more promising materials. And, whenever possible, the complexities of stress and temperature history expected in service should be included in the test evaluation.

1.4.2.3 Method of Strain-Partitioning.

In their continuing examination of high-temperature, low-cycle fatigue, Manson and co-workers (the 10-percent rule) have developed a method which attempts to analyze directly the effects of creep and plastic flow on cyclic life (Ref. 11). This method was developed because of the highly time-dependent nature of the creep effect and because the life-reducing effects of creep depend, to a large extent, upon where within a cycle the creep is introduced and whether it is reversed by plastic flow or by creep.

In this method, the completely reversed cyclic inelastic strain is divided into four parts. These are (1) $\Delta \epsilon_{pp}$ — tensile plastic flow reversed by compressive plastic flow, (2) $\Delta \epsilon_{cp}$ — tensile creep reversed by compressive plastic flow, (3) $\Delta \epsilon_{pc}$ — tensile plastic flow reversed by compressive creep, and (4) $\Delta \epsilon_{cc}$ — tensile creep reversed by compressive creep.

In any arbitrary hysteresis loop, such as shown in Fig. E1-28, the tensile inelastic strain ($\overline{AD}$) can be separated into plastic ($\overline{AC}$) and creep ($\overline{CD}$) components. Likewise, the compressive inelastic strain ($\overline{DA}$) can also be separated into its plastic ($\overline{DB}$) and creep ($\overline{BA}$) components. In general, neither the two plastic components ($\overline{AC}$ and $\overline{DB}$) nor the two creep components ($\overline{CD}$ and $\overline{BA}$) will be equal. It is necessary only that the entire tensile inelastic strain ($\overline{AD}$) be equal to the entire compressive inelastic strain ($\overline{DA}$) since we are dealing with a closed hysteresis loop. The partitioned strain ranges are obtained in the following manner. The completely reversed plastic strain range, $\Delta \epsilon_{pp}$, is the smaller of the two plastic components and in this example is equal to $\overline{DB}$. The completely reversed creep strain range, $\Delta \epsilon_{cc}$, is equal to the smaller of the two creep components and becomes $\overline{CD}$. As can be seen graphically, the difference between the two plastic components must be equal to the difference between the two creep components, or $\overline{AC} - \overline{DB} = \overline{BA} - \overline{CD}$. This difference is then equal to $\Delta \epsilon_{pc}$ or $\Delta \epsilon_{cp}$ in accordance with the notation just stated. For this example, it is

equal to $\Delta\epsilon_{pc}$ since the tensile plastic strain is greater than the compressive plastic strain. It follows from the preceding procedure that the sum of the partitioned strain ranges will necessarily be equal to the total inelastic strain range or the width of the hysteresis loop.
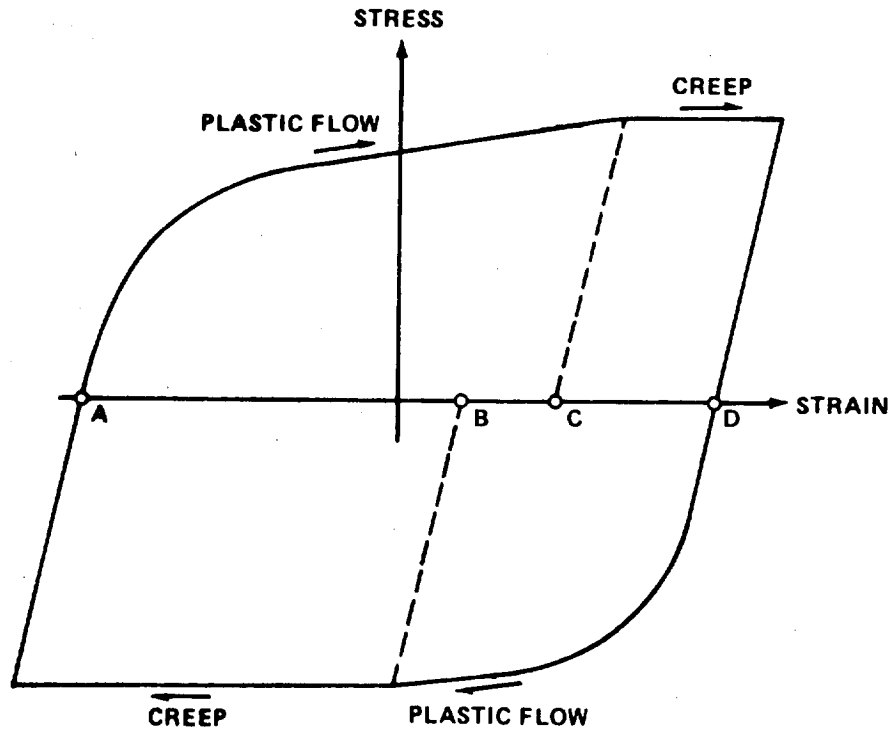
FIGURE E1-28. HYSTERESIS LOOP

The effect of each of these strain ranges on cyclic life is noted in Ref. 11, and the total cyclic life is determined using a linear cumulative damage relationship,

$$\frac{N}{N_{pp}} + \frac{N}{N_{cp} \text{ or } N_{pc}} + \frac{N}{N_{cc}} = 1 \quad ,$$

where N_{pp} is the cyclic life associated with the strain range of $\Delta\epsilon_{pp}$, N_{cp} or N_{pc} is the cyclic life associated with $\Delta\epsilon_{cp}$ or $\Delta\epsilon_{pc}$, and N_{cc} is the cyclic life associated with $\Delta\epsilon_{cc}$.

This method differs from the 10-percent rule in that it attempts to deal directly with the phenomena occurring at high-temperature, low-cycle fatigue rather than using an estimate based on low-temperature, low-cycle fatigue findings. It differs from other methods which partition damage effects at high temperatures in that all relations used are strain range versus cyclic life rather than a combination of that and stress versus time life. The generation of strain range versus cyclic life data is required in this method where the 10-percent rule requires only static tensile properties. This method agrees well with the 10-percent rule for the materials tested and may prove a basis for that rule. This method is also useful in explaining frequency effects and hold-time effects. Finally, to quote the authors of this method, "The method is in an early stage of development, and many questions must be answered before its merits can be evaluated" (Ref. 11).

1.4.2.4 Two-Slope Fatigue Law.

Coffin and Manson have proposed the following fatigue law for plastic strain:

$$N_f^{\beta} \, \Delta\epsilon_p = C \quad , \tag{1}$$

where N_f is the cycles to failure, $\Delta\epsilon_p$ is the plastic strain range, and β, C are the constants. This has been modified to include the effect of frequency in high-temperature, low-cycle fatigue,

$$\left(N_f \, \nu^{k-1}\right)^{\beta} \Delta\epsilon_p = C_2 \quad , \tag{2}$$

where ν is the frequency, k, C_2 are the constants, and $N_f \nu^{k-1}$ is defined as the frequency-modified fatigue life. The frequency effect was extended further to include the stress range,

$$\Delta\sigma = A \, (\Delta\epsilon_p)^{\eta} \, \nu^{k_1} \tag{3}$$

and

$$\Delta\sigma = \text{stress range} \quad ,$$

where A, η, and k are constants. Combining equations (2) and (3) and generalizing for the total strain range

$$\Delta\epsilon = (AC_2^{\eta}/E) \, N_f^{-\beta\eta k_1 + (1-k)\beta\eta} + C_2 N_f^{-\beta_\nu (1-k)\beta} \quad , \tag{4}$$

where E is the elastic modulus.

Coffin reports in Ref. 12 that with increasing temperature the exponent β increases approaching one and the constant C correlates less well with the tensile ductility. Because of the high exponent for β in equation (1) reported for many materials at elevated temperature, extrapolation to low lives could lead to plastic strain ranges exceeding the tensile ductility. Because this situation is highly unlikely, there must be a break in the curve of the $\Delta\epsilon_p$ versus N_f relationship so that it will pass through the tensile ductility value at $N_f = 1/4$ (Fig. E1-29). This change in slope is due to a change in the mode of crack propagation. In less ductile materials this change in slope is due to a change in the fracture mode resulting from environmental interaction. In ductile materials this change in slope at high temperatures results from a change from intergranular to transgranular fracture and as can be seen in Fig. E1-30, as temperature increases the change in slope is more drastic.

The main benefit of the two-slope fatigue law is that it gives a more accurate description of the occurrences in plastic strain and leads to a clearer recognition of the operative physical process. A recognition of the causes of the two-slope phenomenon emphasizes the importance of the environment and of time in the environment (frequency and hold time). However, the constants of the equations are highly material dependent and temperature dependent and if experimental data are not available, these constants cannot be determined.

1.4.3   Thermal Cycling.

The previous sections have considered mechanical strain or stress cycling at a constant temperature; this section will consider mechanical
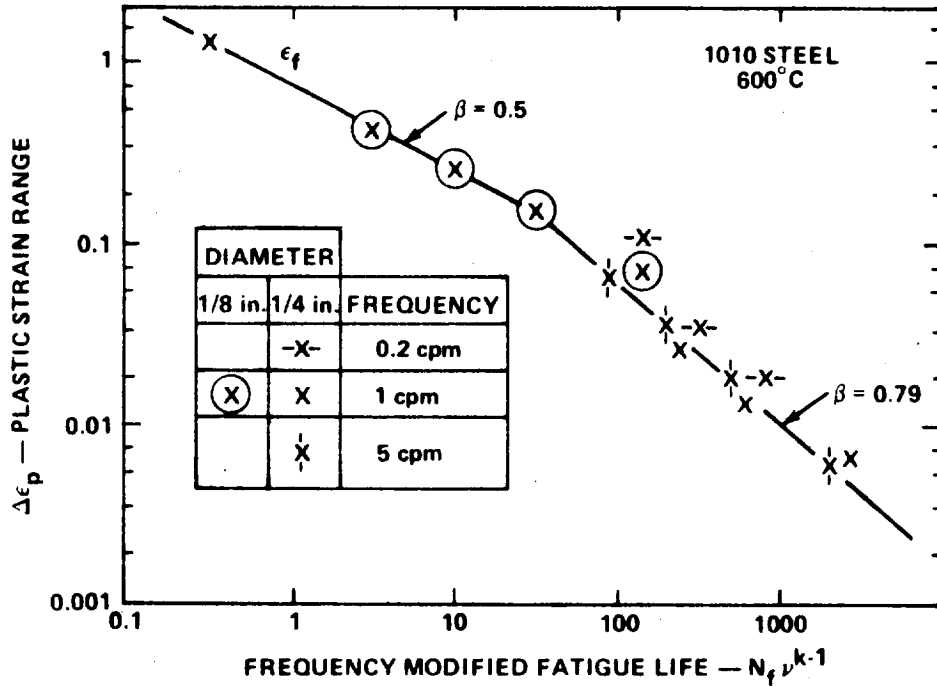
FIGURE E1-29. PLASTIC STRAIN RANGE VERSUS FREQUENCY
MODIFIED FATIGUE LIFE — AISI C1010 STEEL, 600°C
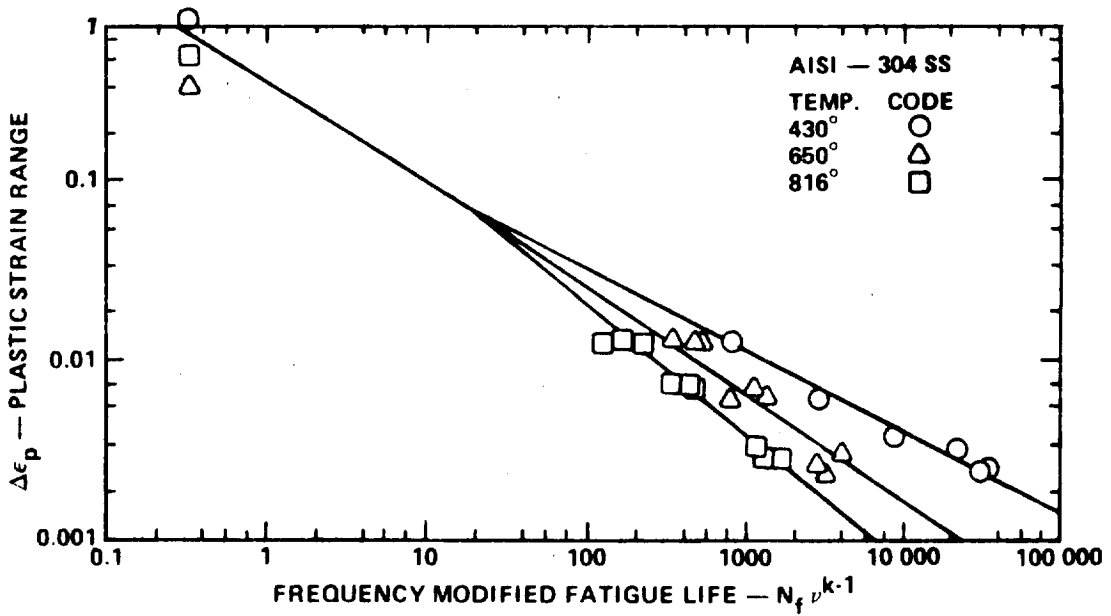
FIGURE E1-30. PLASTIC STRAIN RANGE VERSUS FREQUENCY
MODIFIED FATIGUE LIFE — AISI 304 STAINLESS STEEL

strains induced by cyclic thermal stresses. Failure under repetitive application of thermal stress has been termed thermal stress fatigue.

The principal activity in which analysts have, until recently, engaged whenever thermal-stress problems were encountered has been the computation of elastic stresses. The treatment of this subject may be found in Section D, Thermal Stresses. While such computations constitute a necessary and desirable first step in any practical analysis, they unfortunately do not provide sufficient information for a final evaluation when dealing with ductile materials. Thus, it is important not only to take into account plastic-flow effects that occur when the yield point is exceeded but to consider how such plastic flow might change during progressive thermal and load cycling of the material. Recent contributions have made a valuable start toward an understanding of this problem. Not only have new computational techniques been developed for taking into account inelastic effects such as creep and plastic flow, but a start has been made toward including cyclic effects both in computational procedure and in the interpretation in terms of material behavior. The failure criterion for brittle materials is, of course, different from the criterion for ductile materials. From an engineering point of view, the problem is to determine suitable working stresses.

1.4.3.1   Idealized Thermal-Cycle Model.

A model will be chosen in which all the thermal strain is converted to mechanical strain. The case is shown in Fig. E1-31 in which a bar is fixed at its ends between two immovable plates so that the length of the bar must remain constant. To approach the problem realistically, the model should show strain hardening, and the effects of stress relaxation that occurs during any hold period that may be imposed at high temperature.

Referring to Fig. E1-31, the bar is assumed clamped when hot, so that tensile stress is developed along OAF during the first cooling. Plastic flow is initiated at A, but the stress continues to increase to F because of strain hardening. At F the specimen is held for a dwell period, but no stress change occurs (relaxation), since the temperature is presumed to be low enough to make creep and anelasticity negligible. Upon reheating of the specimen, the stress-strain relation proceeds along FGE, yielding at G, at which time there is a much lower stress than there is at A because of the Bauschinger effect. (The Bauschinger effect states that plastic flow in one direction reduces the stress at which yielding will occur in the opposite direction.)

COOLING
HEATING

STRESS

A

O

TOTAL
MECHANICAL
STRAIN

G

E'
E'''
E
E''

FIGURE E1-31. SCHEMATIC STRESS-
STRAIN RELATIONSHIP FOR FIRST
FEW CYCLES OF THERMAL
CYCLING OF CONSTRAINED BAR

When the initial high temperature is restored, the state of the material is at point E, where a compressive elastic strain is necessary to offset the tensile plastic flow that occurred during AF and, thereby, return the specimen to a net strain of zero. This elastic strain introduces the stress OE. Any hold period at the high temperature and stress may convert this elastic strain to inelastic strain-creep and anelasticity, thereby reducing the stress. Thus, point E moves to point E' by the time the specimen starts to cool again. The cooling causes the path E'F' to be traversed. Reheating results in the path F'E''. The hold period at the high temperature converts e'' to E''', etc. After a few cycles, the stress-strain path may settle down to an essentially unchanging loop. For illustrative purposes this loop may be taken as E'''F'E''E'''. This corresponds to an asymptotic hysteresis loop and takes into account not only all the hardening or softening characteristics but also creep and anelasticity effects as well as effects due to changing temperature and metallurgy.

1.4.3.2 Effect of Creep.

In the experiments that have been performed to date, analysis of the thermal-stress fatigue behavior has been made largely by relating the plastic strain per cycle to the number of cycles to failure. Normally, the plastic strain is determined by subtracting the elastic-strain range from the total-strain range, which in turn is computed by dividing the stress range by the elastic modulus. When creep occurs during the high temperature portion of the cycle, this procedure produces inaccuracies. Not only is the plastic flow improperly computed if creep is neglected, but the omission of the creep can seriously affect the computation of cyclic life because the effect of creep strain on life differs appreciably from the effect of slip-type plastic flow.

Consider Fig. E1-32, which shows the stress-strain relationships for two idealized cases. In Fig. E1-32 (a) no creep is assumed to take place. Then,

$$\epsilon_p = \alpha T_0 - \frac{\Delta\sigma}{E}$$

where $\Delta\sigma$ is the stress range and E is the elastic modulus. (The elastic modulus is assumed to be constant over the entire temperature range;

(a)   (b)

FIGURE E1-32. PLASTIC-STRAIN AND STRESS-RANGE
RELATIONSHIP FOR (a) NO CREEP RELAXATION
DURING HOLD PERIOD AND (b) CREEP
RELAXATION DURING HOLD PERIOD

assumption of a temperature-dependent elastic modulus complicates the problem even further.)

However, when creep occurs during a hold period [Fig. E1-32(b)], the plastic strain per cycle is not directly related to the total stress range. For the tensile portion of the cycle, the plastic strain ϵ_p' is

$$\epsilon_p' = \alpha\, T_0 - \frac{\Delta\sigma_1}{E}$$

where $\Delta\sigma_1$ is the stress range developed during the cooling portion of the cycle only. In the heating portion of the cycle, the stress range is larger, thus reducing the direct compressive plastic strain ϵ_p'''. However, the total plastic strain ϵ_p'' also includes the creep ϵ_p''' during the hold period. This creep strain replaces the elastic strain relaxed during the creep and is, therefore, equal to $(\Delta\sigma_2 - \Delta\sigma_1)/E$. Thus,

$$\epsilon_p'' = \epsilon_p''' + \epsilon_p'''' = \alpha\, T_0 - \frac{\Delta\sigma_2}{E} + \frac{\Delta\sigma_2 - \Delta\sigma_1}{E} = \alpha\, T_0 - \frac{\Delta\sigma_1}{E} = \epsilon_p' \quad .$$

Therefore, the plastic strain in compression is equal to that in tension, but these strains are not directly related to the total stress range.

1.4.3.3 Comparison of Thermal-Stress Fatigue with Mechanical Fatigue at Constant Temperature.

Several experiments in which mechanical fatigue at various temperatures was compared with thermal-stress fatigue have been conducted (Refs. 13 and 14). Fatigue tests were conducted at several constant high temperatures by loading mechanically, and the results of the tests were compared with thermal-stress fatigue tests in which the temperature naturally varied over an appreciable range. The results of a test are shown in Fig. E1-33 and are analyzed in terms of cyclic life at a given measured plastic strain. The mechanical-fatigue tests are shown at 350°, 500°, and 600° C, whereas in the thermal-stress tests the specimen was completely constrained and cycled between 200° and 500° C, so that the mean temperature was 350° C. As can be seen from the figure, at equal values of cyclic plastic strain the number of cycles to failure was much less for the thermally cycled specimen than for one mechanically cycled at 350° C and even for one mechanically cycled at 600° C, even though no part of the specimen in the 200° to 500° C thermal-stress
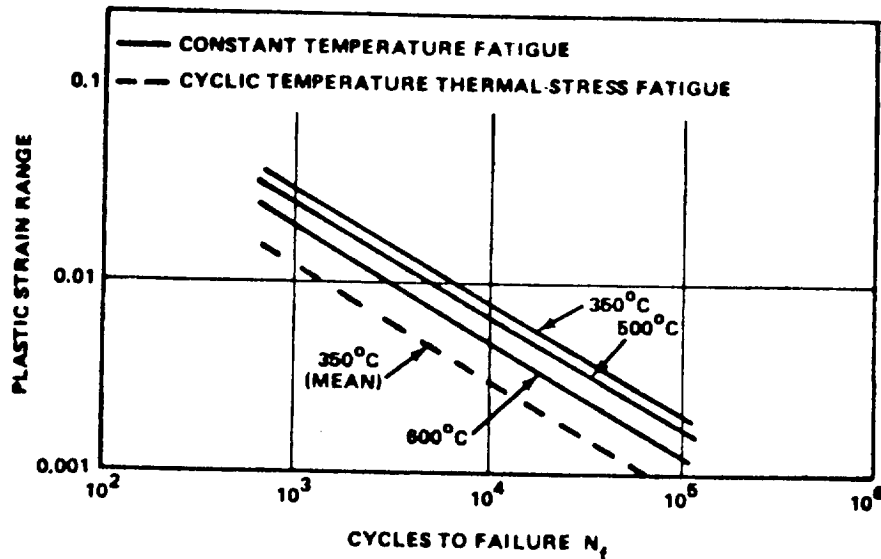
FIGURE E1-33. CYCLES TO FAILURE IN THERMAL-STRESS FATIGUE
COMPARED WITH CYCLES AT CONSTANT TEMPERATURE IN
SIMILAR PLASTIC STRAIN RANGE

fatigue test ever reached 600° C. Reasons for this discrepancy have been
generally attributed to nonuniformities of temperature along the specimen
and the sensitivity of the properties of the materials to temperature in the
range traversed by the thermal-cycling tests.

For this reason it would appear that, until further tests clarify the
problem, the temperature for the mechanical-fatigue tests should be taken
as the highest temperature of the thermal-stress test. In this way, metal-
lurgical phenomena will not be overlooked and pessimistically low values of
life will be indicated; this appears to be necessary on the basis of most tests
conducted to date.

Spera (Ref. 15) has presented a method for calculation of thermal-
fatigue life based on accumulated creep damage. He proposes that thermal-
fatigue life can be determined from the basic mechanical properties of a
material by calculating lines for each of two distinct and independent failure
modes: (1) cyclic creep-rupture, using a modification of the well-known life-
fraction role proposed by Robinson and Taira, and (2) conventional low-cycle
fatigue, using the empirical equations of the Method of Universal Slopes
developed by Manson (Refs. 9 and 10). Equations are presented in sufficient
detail to define completely the analytical procedure.

1.4.3.4   Summary.

When plastic strains are introduced by constraint of thermal expansion, fatigue ultimately results. The number of cycles that can be withstood depends on the plastic strain and the temperatures at which these strains are induced. Whether tension or compression occurs at the high temperature seems to have little effect on fatigue life. Probably the most important single variable is the maximum temperature of the cycle, particularly if it is high enough to cause metallurgical effects to take place. Increasing the maximum temperature for a given temperature range will generally cause a much greater reduction in cycles to failure than increasing the temperature range by the same amount and maintaining the same maximum temperature. The time at which the maximum temperature is maintained can also have an effect on fatigue life, but of smaller magnitude. The effect can be beneficial or detrimental to fatigue life, depending on the material, temperature, and life range.

Limited data indicate that fatigue life in a thermal-stress fatigue test is sometimes considerably less than the fatigue life of a mechanically strain-cycled specimen having the same total strain as the thermally fatigued specimen and tested at a constant temperature equal to the average temperature of the thermal-stress fatigue test.

The effect of prior thermal cycling on specimens subsequently evaluated for stress rupture depends greatly on the material and the number of prior cycles. In general, the effect can be expected to be detrimental; however, in some cases it may actually be beneficial.

Each of the materials that has been studied to date — type 347 stainless steel, the cobalt-base alloy S-816, and the nickel-base alloys Inconel and Inconel 550 — displays characteristics considerably different from the others in thermal-stress fatigue, and prediction of distinctions in the behavior of one from that of another is difficult. Hence, more classes of materials must be investigated before a reasonably complete picture of the thermal-fatigue behavior of materials, in general, can be understood. For specific information on behavior of the various types of materials, investigate Refs. 13, 14, 16, 17, 18, 19, and 20.

1.5 CUMULATIVE FATIGUE DAMAGE.

1.5.1 Theory.

One important problem in fatigue analysis is how to calculate fatigue life. From the S-N diagram, we know that the higher the alternating stress, the lower the number of cycles a part will endure before failure. Also, at stresses below the fatigue limit an infinite number of cycles can be sustained.

In most cases the weight penalty imposed by using the fatigue limit as an allowable stress cannot be tolerated. If stress cycling is at a known level, an S-N curve can be used to determine the number of cycles to failure and thus the life of the part can be predicted. Most structural components or parts are subjected to irregular fluctuating stresses in which the maximum and minimum stresses are constantly changing. Thus, it is necessary to use a fatigue theory which will account for the damage caused by different magnitudes of stress cycles.

Of the several cumulative damage fatigue theories known, the one most widely used and best known is the one suggested by Palmgren and later, independently, by Miner. The Palmgren-Miner hypothesis is that the fatigue damage incurred at a given stress level is proportional to the number of cycles applied at that stress level divided by the total number of cycles required to cause failure at the same level. This damage is usually referred to as the cycle ratio or cumulative damage ratio. If the repeated loads are continued at the same level until failure occurs, the cycle ratio will be equal to one. When fatigue loading involves many levels of stress amplitude, the total damage is a sum of the different cycle ratios and failure should still occur when the cycle ratio sum equals one.

$$\sum_i \frac{n_i}{N_i} = \frac{n_1}{N_1} + \frac{n_2}{N_2} + \frac{n_3}{N_3} + \ldots = 1.0 \quad .$$

This equation has been used by designers for many years, but at the same time it is under criticism by researchers. It is found that:

1. In many test results the summation of n/N is far from one.

2. The fatigue damage is not linearly proportional to the number of cycles or the cycle ratio n_1/N_1.

3. There is interaction in the fatigue damages between various stress levels which Miner neglected. In the interaction there is also a sequence effect which means that the fatigue damage resulting from the high load first, with the low load next, will be different from the damage resulting from the low load first, with the high load next.

Aware of its limitations, designers still use Miner's equation as a preliminary guide because of its simplicity, versatility, and sufficient accuracy, commensurate with the data currently available for this type of analysis.

What are the consequences when Miner's equation is used for random-loading conditions? Random-load fatigue testing is time-consuming and costly, and the scant data available do not permit a general clear-cut answer to this question. According to Freudenthal (Ref. 21), the sum $\Sigma n/N$ is always less than one. In some cases the sum is as low as 0.13 but it is mostly between 0.20 and 0.60. The primary reason for this discrepancy, according to Freudenthal, is the interaction of fatigue damages between various load amplitudes.

On the other hand, it has been found that notched parts generally give a summation value greater than one. Since practically all of the structural fatigue failures originate in some form of notch, the question of what value to use in place of 1.0 has been asked.

The National Aeronautics and Space Administration conducted full-scale fatigue tests on C-46 transport airplane wings and their summation of cycle ratios was 1.4 (Ref. 22).

However, until more information becomes available, Miner's equation is recommended for preliminary analysis.

1.5.2   Analysis of Data.

Numerical simplifying assumptions are often needed to speed up the analyzing of data. Mainly, these assumptions have to do with primary and secondary cycles. The following four conventions serve to establish and define primary and secondary cycles:

1. A mean value of stress, S_{mean} for the entire record is approximated. Although a time average and a peak point average generally yield different average values, the two may be assumed to be equal.

2. The maximum stress occurring between a positive S_{mean} crossing (positive in slope) and a negative (negative slope) S_{mean} crossing is called S_{max}. All other maximum stress values are designated as S_{ma}.

3. The minimum stress occurring between a negative S_{mean} crossing and a corresponding positive crossing is designated as S_{min}. All other minimum stress values are S_{mi} points. See Fig. E1-34.

4. The combination of an S_{min} and the next S_{max} form a primary cycle. The combination of an S_{mi} and the next S_{ma} form a secondary cycle.
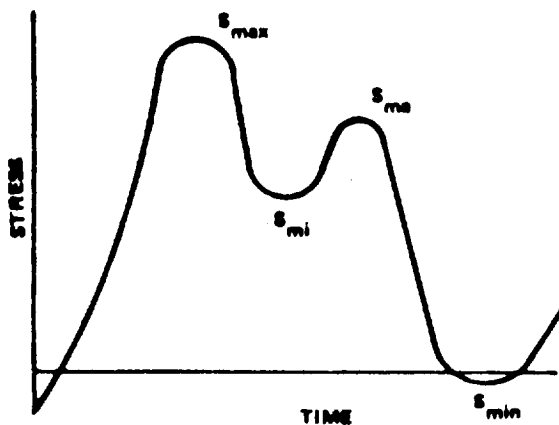
FIGURE E1-34. A PART OF A
STRESS RECORD

Accurate evaluation of fatigue damage usually requires that all primary cycles within a given period be considered, but it rarely requires that all secondary cycles be considered. The effect of neglecting secondary stresses in random data will be investigated in terms of the following propositions:

Proposition I — If peaks (maximums) and troughs (minimums) are normally distributed about a mean stress, the damage per cycle caused by all cycles which do not cross the mean stress line can be neglected.

Proposition II — If peaks and troughs are normally distributed about a positive mean stress, the damage per cycle caused by all cycles which neither cross nor exceed the mean stress line can be neglected.

Proposition III — If peaks and troughs are normally distributed about a positive mean stress, the only time a secondary cycle needs to be considered is when it lies above the mean stress, when it occurs just after S_{max} has been established, and when it reaches the lowest S_{min} established since the last mean stress crossing.

Usually for random data, one of these propositions can be considered valid. Fig. E1-35 illustrates several more or less useful approximations, some of which are generally valid, and all of which are usually more valid than the half-cycle rearrangement described above. In each case, a heavy base line is used to indicate a mean stress line.

1.5.2.1 Peak Counting Techniques.

Figure E1-36 shows the three most commonly used cycle counting methods among a considerably greater number which have been proposed and used. Some of the others are modifications of the ones shown. For example, the first one is frequently modified so that positive and negative half cycles are counted and tabulated separately. The second method pairs off succeeding positive and negative amplitudes so that each cycle mean can be calculated.

The third method, without refinement, is not very accurate unless only one frequency is present. If a low and a high frequency appear with equal amplitudes, the high-frequency, low-range (amplitude) activity will mask the low-frequency, high-range component; the result will be indistinguishable from a high-frequency, high-amplitude loading which is very damaging. See Case 3 of Fig. E1-36.

However, an important refinement to the third method of Fig. E1-36 is the use of zones and the counting of passages from one zone to another, particularly to a nonadjacent zone. This method, which is listed as method 3a in the figure, is equivalent to method 2 if a large number of zones and zone separations are used and properly recorded.

1.5.2.2 Statistical Methods of Random Load Analysis.

Most of the fundamental concepts of fatigue indicate that some type of cycle-counting technique is needed to evaluate the fatigue damage caused by random loading. Direct techniques of this type, such as peak counts and range counts are simple and accurate but often quite cumbersome to apply. Other, less direct methods are sometimes sought to estimate the same information less laboriously. Two such indirect methods are presented in Refs. 2 and 3, in which sampling or alternative measurements are used and converted into a useful form by statistical means. In general, these methods have not been as accurate in evaluating cumulative fatigue damage as the more direct methods. However, their use with large quantities of data makes the loss of accuracy acceptable.

STRESS VERSUS TIME   AND   HYPOTHETICAL EQUIVALENT   SUPPORTING PROPOSITION

I

I, II, III

III

NONE
(INVALID)

NONE
(INVALID)
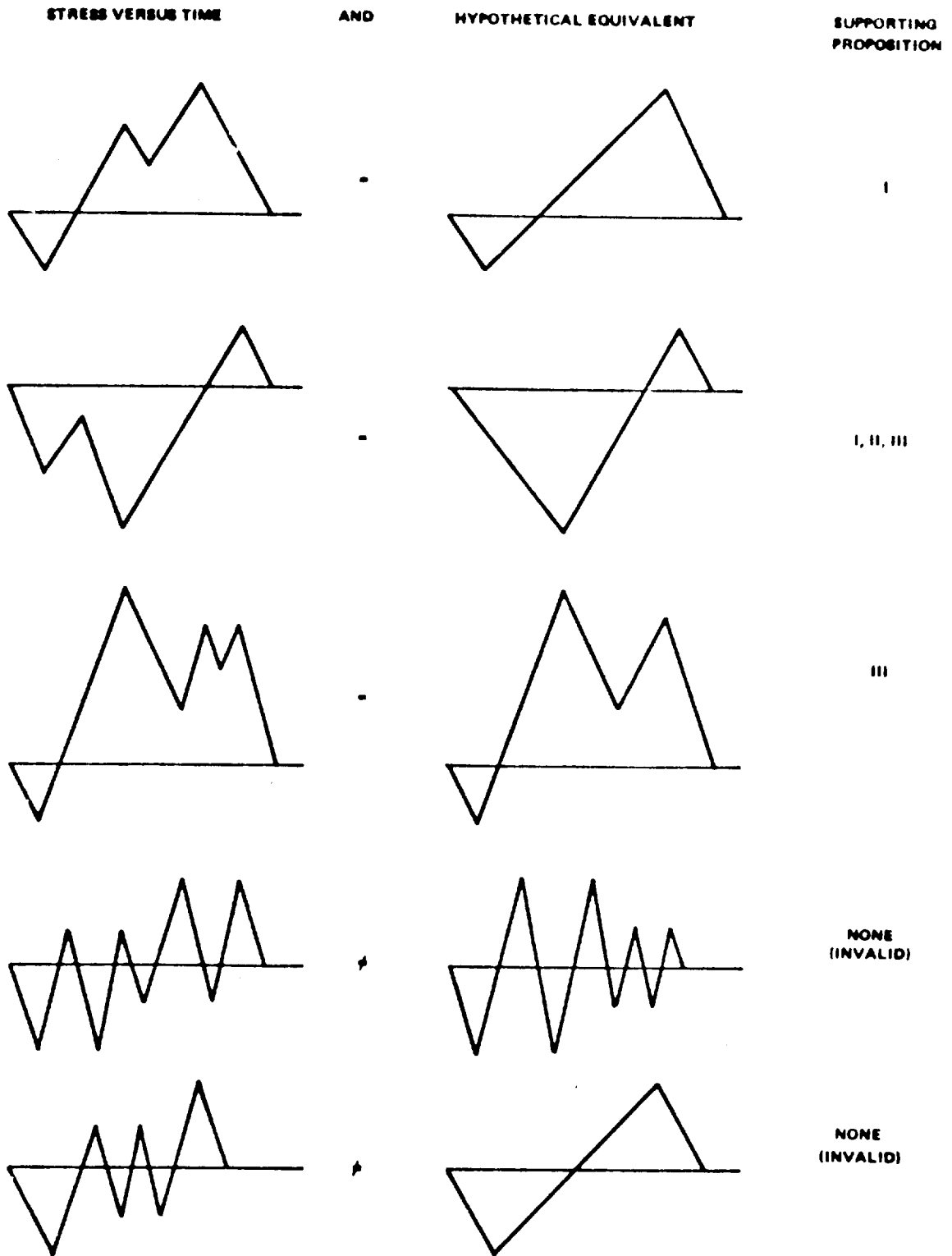
FIGURE E1-35. FIVE DATA-REDUCING APPROXIMATIONS OF VARYING
DEGREES OF VALIDITY
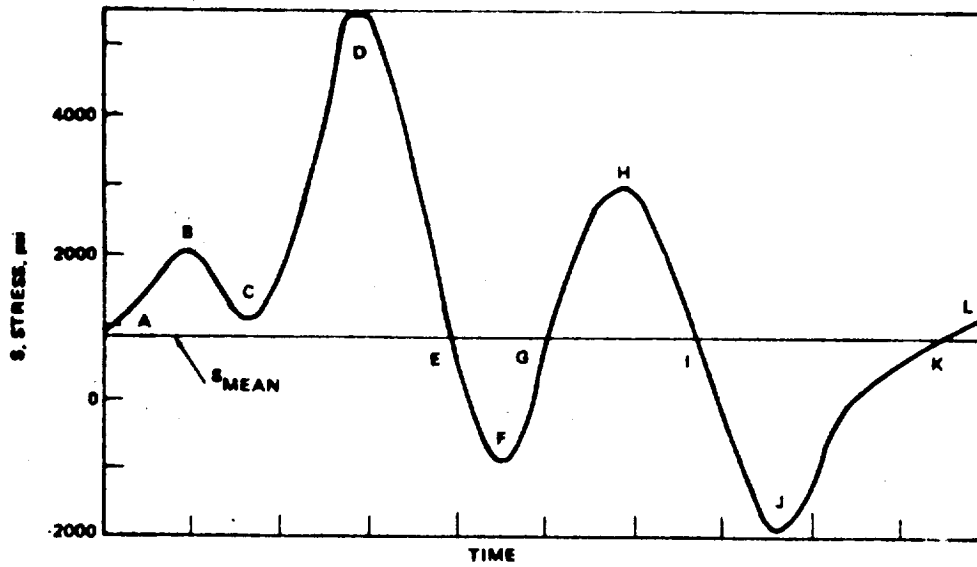
COUNTING METHOD	QUANTITIES MEASURED OR COUNTED	EQUIVALENT WAVEFORM
1. MEAN CROSSING PEAK COUNT	n, d, f, h, j, etc.	
2. PAIRED RANGE COUNT	n, $S_{M_{FH}}$ AND FH $S_{M_{JL}}$ AND JL	
3. LEVEL CROSSING COUNT	$n_{4000} = 1$ $n_{2000} = 3$ $n_0 = 2$ etc.	
3a. ZONE PASSING COUNT	SAME AS METHOD 3 EXCEPT EACH CROSSING IS A COUNT ONLY WHEN PRECEDED BY A CROSSING AT EACH OF SEVERAL VARIOUSLY SEPARATED LEVELS AND IS CATEGORIZED ACCORDING TO SEPARATION	

NOTE: n IS A NUMBER OF POSITIVE SLOPE DESIGNATED LEVEL CROSSINGS (IF WITHOUT SUBSCRIPT, THE DESIGNATED LEVEL IS S_{mean})

FIGURE E1-36. APPLICATION OF SOME CYCLE COUNTING METHODS TO A TYPICAL STRESS RECORD (Lower Table Illustrates Each Method in Terms of an Equivalent Record)

1.5.3 Example Problem (Paired Range Count Method).

To evaluate the damage caused by complex stress-time cycles, it is necessary to correct for the difference in mean stress, S_m, for the various stress alternations, S_a. Four constant amplitude S-N curves for different mean stresses are shown in Fig. E1-37. A complex stress-time hisotry for an identical specimen is shown in Fig. E1-38.

The first step is to determine the damage caused by the smaller variations which are crosshatched in Fig. E1-38(a). The largest mean stress is approximately 20 ksi and, as shown in Fig E1-37, for this mean stress an alternating stress of 4 ksi or less causes no damage. At any mean stress less than 20 ksi, the alternating stress which causes no damage increases so that any alternating stress of 4 ksi or less can be omitted. Thus, variations BC, DE, GH, JK, NO, PQ, and ST cause no fatigue damage. The stress-time history is replotted in Fig. E1-38(b), with the previously evaluated variations removed.

The second step is to evaluate the smallest remaining stress variations IL and RU. For IL, the alternating stress is 5 ksi and the mean stress is 10 ksi. Referring to Fig. E1-37, under these conditions failure would result in 10^7 cycles. Hence the damage is $n/N = 1/10^7 = 10^{-7}$. Calculating the damage caused by RU in the same manner $n/N = 1/2.2 \times 10^4 = 4.55 \times 10^{-5}$. The stress-time history is again replotted in Fig. E1-38(c), with the evaluated variations removed.

The third step is to evaluate the remaining cycle, FM, with $S_a = 20$ ksi and $S_m = 5$ ksi. Interpolating between $S_m = 0$ and $S_m = 10$, failure would result in 3.5×10^3 cycles. Hence, the damage caused is $1/3.5 \times 10^3 = 2.86 \times 10^{-4}$. The last step is to sum the damage caused by all the variations. In this case,

$$10^{-7} + 4.5 \times 10^{-5} + 2.86 \times 10^{-4} = 3.316 \times 10^{-4} \quad .$$

Using the cumulative damage theory with $\Sigma n/N = 1.0$, the stress-time history can be repeated 3000 times ($1.0/3.316 \times 10^{-4} = 3000$).
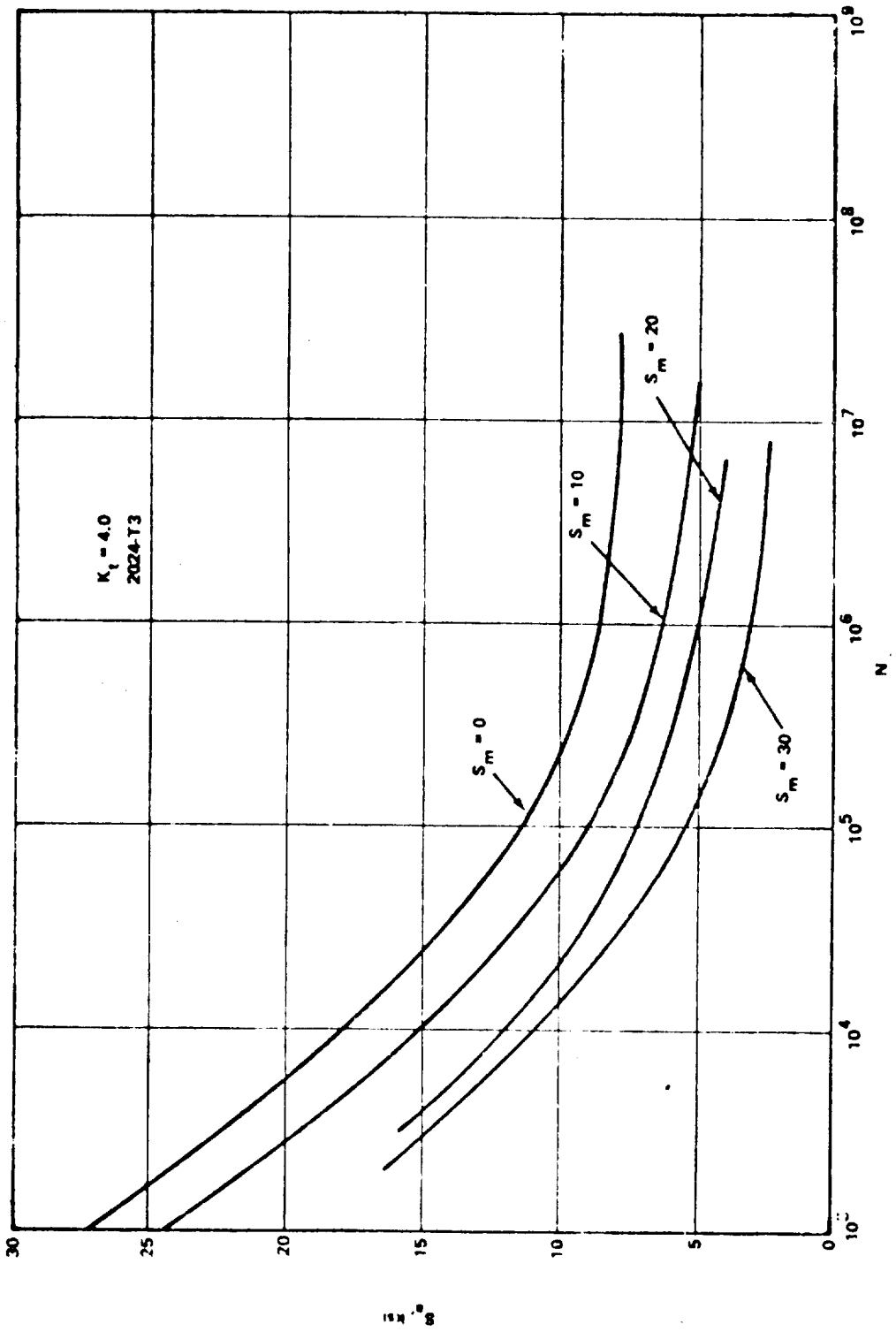
FIGURE E1-37. ALTERNATING STRESS VERSUS CYCLES TO FAILURE FOR 2024-T3.

(a)

(b)

(c)
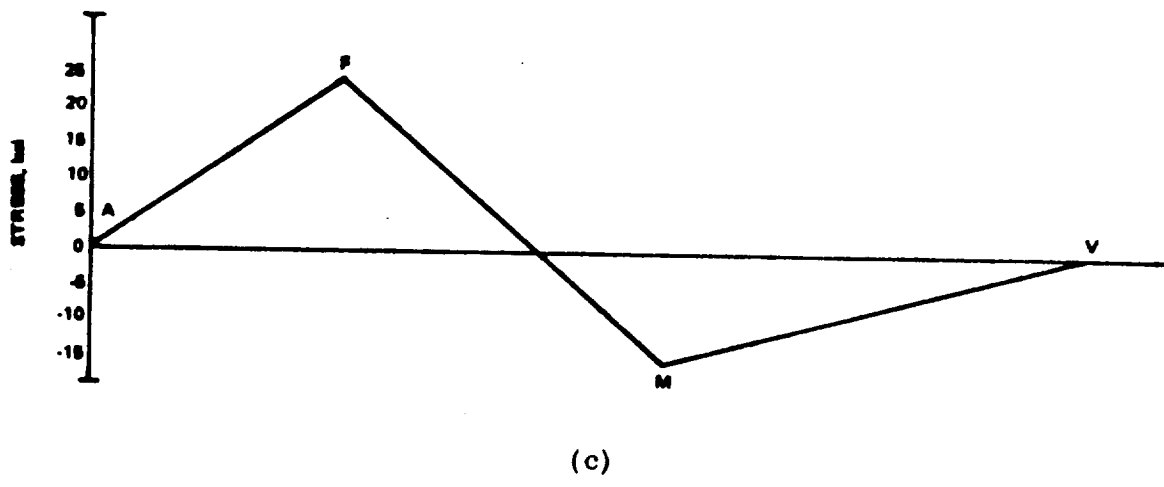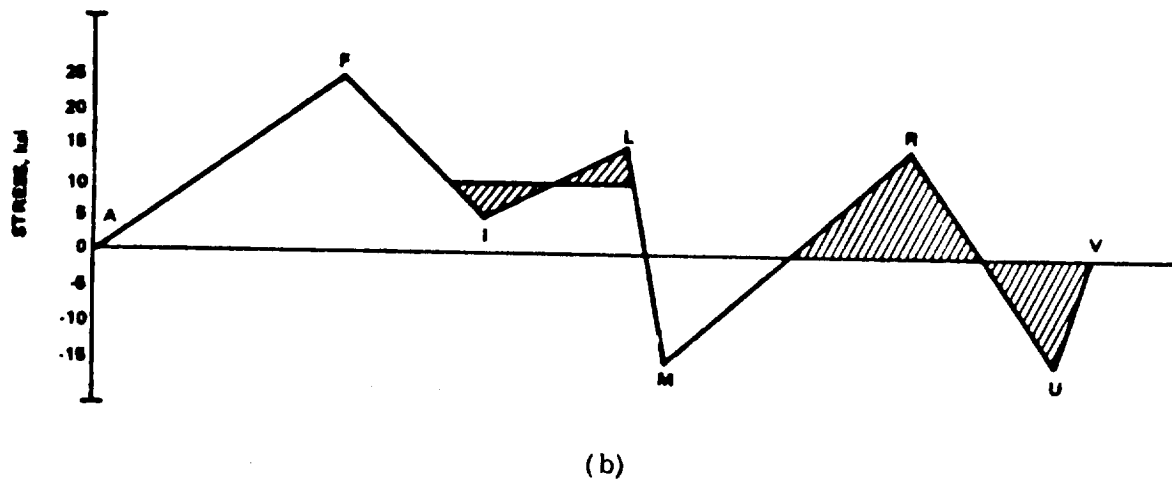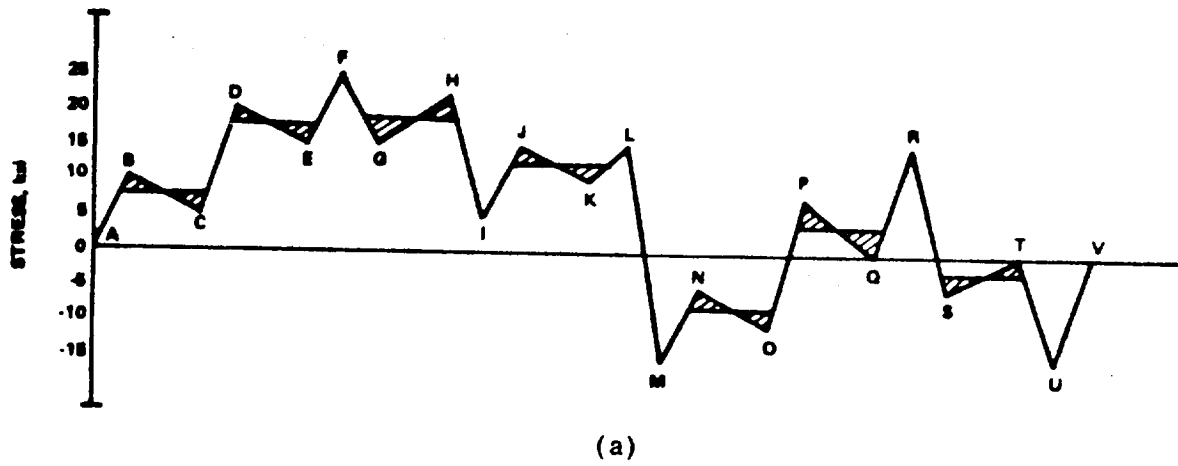
FIGURE E1-38. STRESS-TIME HISTORY CURVES

1.6   MATERIAL SELECTION TO RESIST FATIGUE.

1.6.1   High Cycle.

The first step to be considered in fatigue design is selection of the structural material. The four most commonly used materials are steel, titanium, aluminum, and magnesium. Unnotched rotating-beam fatigue data are presented in Fig. E1-39 and notched data are shown in Fig. E1-40. Each alloy was selected because it has the highest fatigue strength in its class, based on available data, i.e., 4340 heat-treated 260-280 ksi has the greatest fatigue strength of all the steels. For the unnotched specimen, Ti-155A, titanium is, by far, the best material. The three other materials, 7075-T6 aluminum, AZ80A-F magnesium, and 4340 steel heat-treated 260-280 ksi are approximately equal. It should be noted that titanium and steel have well-defined fatigue limits.

For the notched specimen also, Ti-155A, titanium is the best material, as shown in Fig. E1-40. The three other materials, 2024-T4 aluminum, AZ80A-F magnesium, and 4340 steel heat-treated 260-280 ksi, are approximately equal. For the notched specimen, all four have well-defined fatigue limits. Only one class of structural material, aluminum, changed alloys as a result of selecting the best fatigue strength in unnotched and notched specimens. The notch used had a stress concentration factor of approximately 2.8.

Rotating-bending specimens usually give different results than axial load specimens due to the large stress gradients produced in the bending tests and which are not present in axial tests. Different forms (e.g., sheet, bar, rod, etc.) sometimes cause different fatigue strengths. Therefore, an accurate selection of alloy for fatigue strength should be based on fatigue data with similar loading, form, and stress concentration factor as the particular structure in question.

1.6.2   Low Cycle.

Different materials may show substantially different abilities to resist repeated straining and repeated stressing; also, they have various abilities to retain their properties when subjected to large cyclic plastic strains. Because of these differences, the relative low-cycle fatigue resistance of several candidate materials should be rated, preferably without going through the arduous task of extensive fatigue testing (Ref. 23).
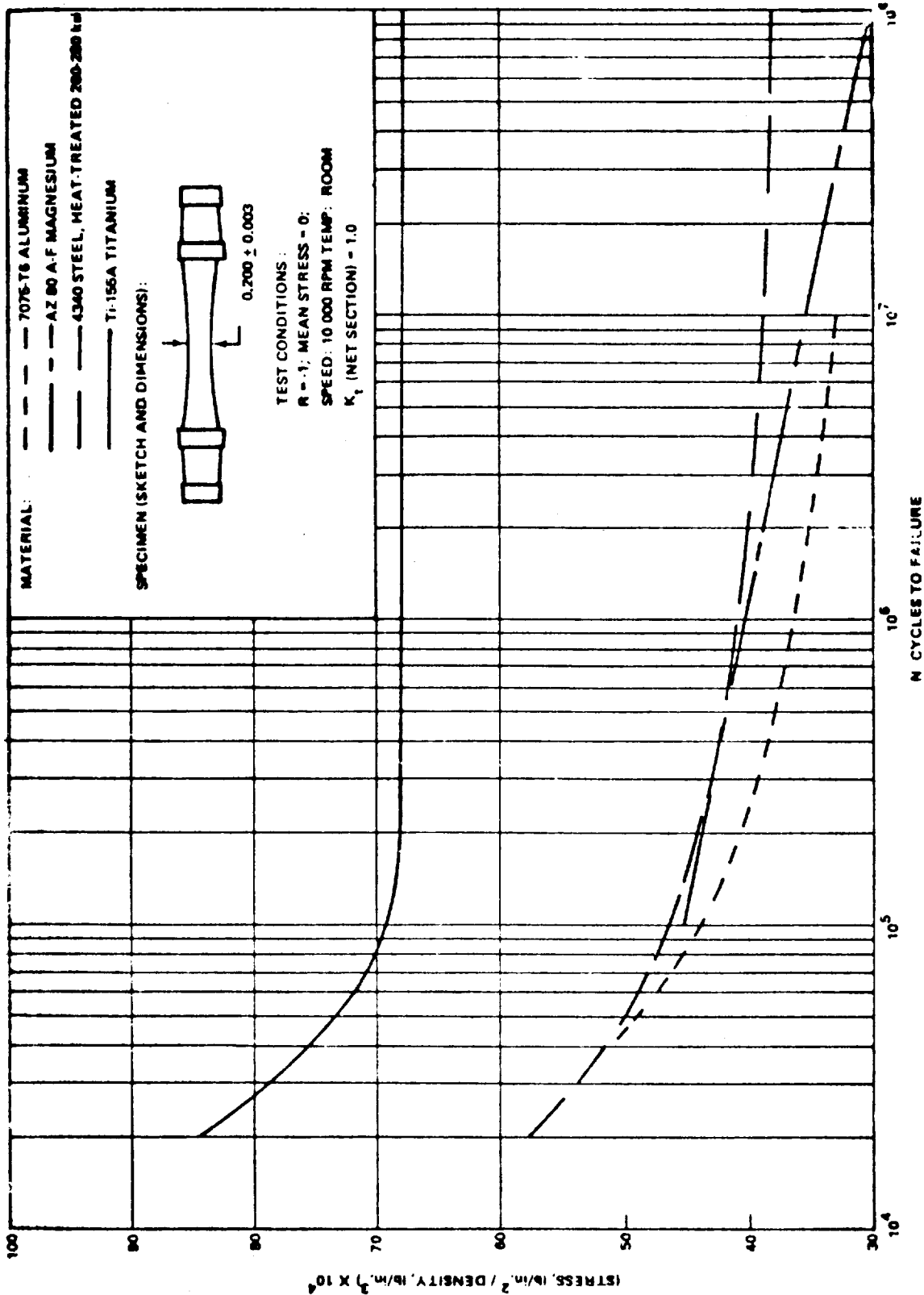
FIGURE E1-39.   UNNOTCHED FATIGUE DATA FOR FOUR COMMON MATERIALS
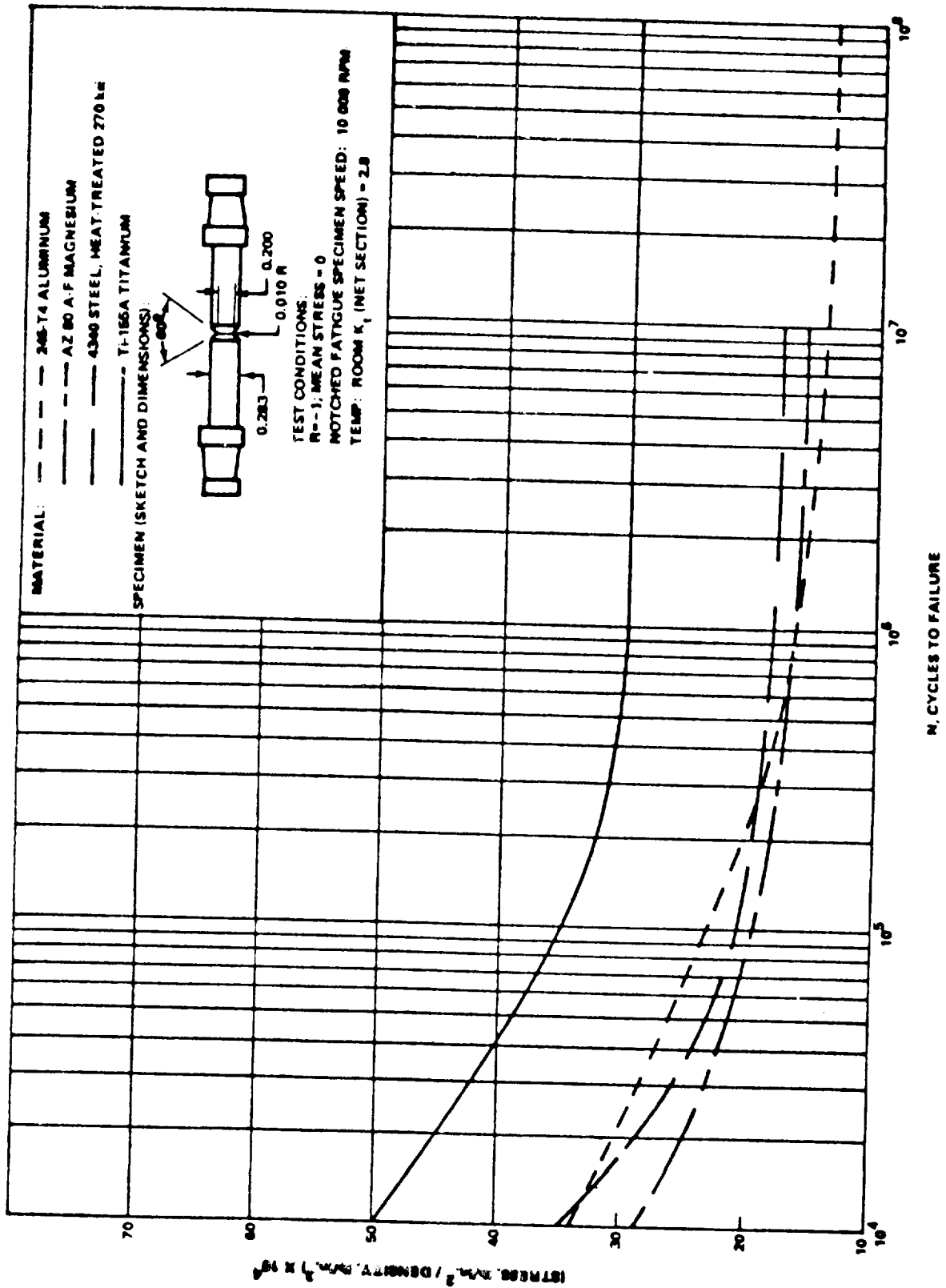
FIGURE E1-40. NOTCHED FATIGUE DATA FOR FOUR COMMON MATERIALS

A distinguishing difference between high-cycle and low-cycle fatigue is that in the latter the plastic strain component is considerably larger. These large plastic strains can induce significant changes in the stress-strain response of most materials. The most suitable test for studying these changes in deformation resistance is one in which the specimen is cycled between fixed limits of strain, rather than stress. During cyclic straining, a mechanical hysteresis loop develops (Fig. E1-41). The controlled parameter is total strain range ΔE_t, which is composed of an elastic and plastic component. Plastic component ΔE_p is the width of the hysteresis loop; whereas, the height of the hysteresis loop is $2\sigma_a$, where σ_a is the stress amplitude.

During cyclic straining, materials either harden or soften, depending upon their previous history. For example, annealed materials will generally undergo a cyclic hardening process, which is indicated by an increase in the stress required to enforce the strain limit on successive cycles. On the other hand, cold-worked materials generally soften. Changes in the stress response occur rapidly in the early portion of the life but reach a reasonably stable level or steady-state condition after about 10 to 20 percent of the life.

FIGURE E1-41. SCHEMATIC OF MECHANICAL HYSTERESIS LOOP

After this transient stage, a steady-state or saturation condition is attained during which the hysteresis loops maintain an essentially constant shape until prior to complete fracture. The curve drawn through the tips of these stabilized hysteresis loops (obtained from specimens tested at different amplitudes) is called the cyclic stress-strain curve, Fig. E1-42(a). It provides a convenient description of the steady-state cyclic stress-strain response of a material. Thus, monotonic (static) and cyclic stress-strain curves may be displayed on the same diagram, Fig. E1-42(b), so that the effect of different variables can be represented in a concise way.

(a)   (b)
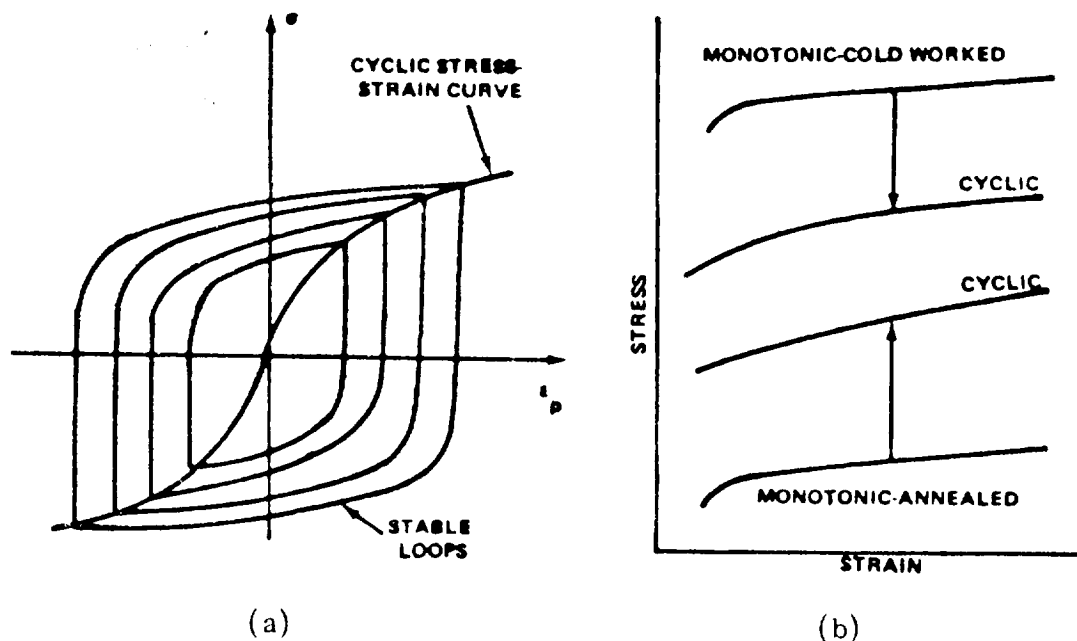
FIGURE E1-42. CYCLIC STRESS-STRAIN CURVE, AS DETERMINED
FROM SEVERAL HYSTERESIS LOOPS, (a). COMPARISON WITH
MONOTONIC CURVE, (b)

Although metals may undergo cyclic hardening or softening, the prob-
lem of softening is more important, since the strength properties of the mate-
rial during low-cycle fatigue may be appreciably less than one would expect
from the static stress-strain curve. Two questions, therefore, seem to be
important: Will the material cyclically soften? If so, how much will it soften?

A component, or a critical location in a structure, may undergo either
repeated straining or repeated stressing, depending upon the geometry and
load environment. Some materials show good strain resistance, whereas
others show good stress resistance. It is, therefore, necessary to decide
whether a design requires a strain-resistant or stress-resistant material.

The relation between the total strain amplitude, $\Delta\epsilon_t/2$, and the cycles
to failure, N_f, is given by

$$\frac{\Delta\epsilon_t}{2} \approx \frac{\Delta\epsilon_p}{2} = \epsilon_f' \left(2N_f\right)^c \quad ,$$

where c is the fatigue ductility exponent.

Thus, the short-life strain resistance of materials depends mainly upon the fatigue ductility coefficient, ϵ_f', and c. Using typical experimental values for the constants, it is apparent that a material with a large value of ϵ_f' and a small value of c has the best resistance to repeated straining.

The fact that a material shows good strain resistance does not necessarily imply that it has a good cyclic stress resistance. To point out the importance of deciding whether the material to be selected must resist repeated strains or repeated stresses, seven materials were tested for both stress and strain resistance in Ref. 23. The material with the highest stress resistance was fourth in ability to resist cyclic strain. Likewise, the material third best in cyclic strain resistance dropped to sixth in stress resistance.

1.7   DESIGN GUIDES.

At the present level of knowledge, it is impractical to establish quantitatively the limiting fatigue design rules for specific structural configurations. The diversity in missions, loads, stresses, materials, and environments certainly suggests this to be an impracticable, if not impossible, task. Qualitatively, however, the practices to be followed in the design of fatigue resistant structure can be defined, and if strict adherence to these established practices is maintained, potential fatigue problems can be reduced in the initial stage of structural design.

In general, the basic rules used in the airframe industry will apply in the design of space vehicle systems. Past experience and learning from the one field can be carried over to the other, although some precautions should be taken. Old designs may be unsuited to a new environment.

When procedures are proposed, they often become general rules which regulate structural design, even though they may be inappropriate. Recommendations used in the sense of "design rules" are far more appropriate. With this interpretation, a few of the more pertinent guides for the design of space vehicle systems may be listed:

1.   Keep the design simple.

2.   Provide for multiple load paths when feasible.

3.   Give extra consideration to tension-loaded fittings and components.

4.   Apply fitting factors of safety to net stresses around holes and cutouts.

5.   Laboratory test all newly designed joints and compare with "time-tried" structures.

6.   Utilize longitudinal grain direction of materials whenever possible (particularly for aluminum and steel alloys).

7.   Provide generous fillets and radii.

8.   Break all sharp edges; polish critical regions if it is considered necessary.

9.   Reduce bearing stresses in riveted and bolted members to design minimums.

10. Take precautions to protect parts from corrosion.

11. Whenever possible, reduce eccentricity of joints and fittings.

12. Ensure that doublers and structural reinforcements result in gradual, rather than abrupt, changes in cross section.

13. Provide easy access for service inspection of structure.

14. Provide inspection procedures during fabrication and assembly of structure.

15. When practical, produce parts and fittings from forged material rather than from extrusions or machined plate stock.

16. Design parts for minimum mismatch or installation; this results in lower residual and preload tensile strains.

17. Avoid superposition of "notches" in design.

18. Make a proper selection of materials with cost, strength allowables, fabricability, and environmental effects in mind.

19. Pay close attention to fabrication techniques for optimum forming of components.

20. Establish reliable welding techniques for reproducibility of joints strengths.

21. Construct rigid and precision tooling for the manufacturer of production parts.

Undoubtedly, there are additional useful fatigue guides which could be added to the list above. Many such guides are unwritten and only intuitively known by the most experienced design specialists. Excellence in design, however, is not accomplished by the designer alone. It requires the close cooperation of specialists able to perform complex dynamic stress analyses: acousticians, vibration engineers, metallurgists, specialists in structural testing and reliability analysis, as well as those experienced in tooling and manufacturing.

These guides and recommended practices for designers are suggested for the sole purpose of reducing the overall development time from preliminary design layout to assembly in production.

REFERENCES

1. Kennedy, A. J.: Processes of Creep and Fatigue in Metals. John Wiley and Sons, Inc., New York, 1963.

2. Madayag, A. F.: Metal Fatigue: Theory and Design. John Wiley and Sons, Inc., New York, 1969.

3. Fatigue Design Criteria for Launch and Spacecraft Structures. Douglas Missile and Space Systems Division, Paper No. 3290, January 1965.

4. Peterson, R. E.: Stress Concentration Design Factors. John Wiley and Sons, Inc., New York, 1953.

5. Gurney, M. A.: Fatigue of Welded Structures. Cambridge University Press, 1968.

6. Manson, S. S.: Thermal Stress and Low-Cycle Fatigue. McGraw-Hill Book Company, 1966.

7. Langer, B. F.: Design of Pressure Vessels for Low-Cycle Fatigue. J. of Basic Engr., Transactions of ASME, September 1962.

8. Smith R. W., Hirschberg, M. H., and Manson, S. S.: Fatigue Behavior of Materials under Strain Cycling in Low and Intermediate Life Range. NASA TN D-1574, April 1963.

9. Manson, S. S., and Halford, G.: A Method of Estimating High Temperature Low-Cycle Fatigue Behavior of Metals. NASA TM X-52270, June 1967.

10. Manson, S. S.: A Simple Procedure for Estimating High-Temperature, Low-Cycle Fatigue. Experimental Mechanics, August 1968.

11. Manson, S. S., Halford, G. F., and Hirschberg, M. H.: Creep-Fatigue Analysis by Strain-Range Partitioning. NASA TM X-67838, May 1971.

12. Coffin, L. F., Jr.: A Note on Low Cycle Fatigue Laws. Journal of Materials, JMLSA, Vol. 6, No. 2, June 1971, pp. 388-402.

REFERENCES (Concluded)

13. Baldwin, E. E., Sokol, G. J., and Coffin, L. F. Jr.: Cyclic Strain Fatigue Studies on AISI Type 347 Stainless Steel. Trans. ASTM, Vol. 57, 1957, pp. 567-586.

14. Clauss, Francis J., and Freeman, James W.: Thermal Fatigue of Ductile Materials, I and II. NASA Tech. Notes 4160 and 4165, 1958.

15. Spera, D. A.: Calculation of Thermal-Fatigue Life Based on Accumulated Creep Damage. NASA TN D-5489, October 1969.

16. Majors, Harry, Jr.: Thermal and Mechanical Fatigue of Nickel and Titanium. Trans. Am. Soc. Metals, Vol. 51, 1959, pp. 421-437.

17. Clauss, F. J.: Thermal Fatigue of Ductile Materials, III. NASA Tech. Note D-69, October 1969.

18. Coffin, L. F., Jr.: The Problem of Thermal-Stress Fatigue in Austenitic Steels at Elevated Temperatures. ASTM Spec. Tech. Publ. 165, 1954, pp. 31-49.

19. Liu, S. I., Lynch, J. T., Ripling, E. J., and Sachs, G.: Low Cycle Fatigue of Aluminum Alloy 24ST in Direct Stress. Trans. AIME, Vol. 175, 1958, p. 469.

20. Avery, H. S.: Discussion of Cyclic Temperature Acceleration of Strain in Heat-Resisting Alloys. Trans. Am. Soc. Metals, Vol. 30, 1942, pp. 1130-1133.

21. Freudenthal, A. M.: Some Remarks on Cumulative Damage in Fatigue Testing and Fatigue Design. Welding in the World, Vol. 6, No. 4, 1968.

22. Bruhn, E. H.: Analysis and Design of Flight Vehicle Structures. Tri-State Offset Company, Cincinnati, Ohio, 1965.

23. Feltner, C. E. and Landgraf, R. W.: Selecting Materials to Resist Low Cycle Fatigue. ASME Paper No. 69-DE-59.

SECTION E2
FRACTURE MECHANICS

TABLE OF CONTENTS

E2   FRACTURE MECHANICS.

2.1   GENERAL.

Structures subjected to constant loads at moderate temperatures have been designed primarily on the basis of the yield strength and/or ultimate strength of the material. Many of these structures have failed prematurely at stresses below the yield strength, with disastrous consequences. These brittle failures have occurred in such diverse structures as storage tanks, suspension bridges, aircraft landing gears, and rocket motor cases. An examination of such failures indicated one predominant feature: A small defect or flaw was usually found at the failure origin.

Therefore, the key to brittle fracture control lies in understanding both the weakening effects of flaws and cracks in metals and those factors that influence this effect. To be useful in an engineering sense, this understanding must be translated into the types of tests and structural mechanics familiar to the metal producer and designer. The body of knowledge concerning this type of failure has become known as fracture mechanics.

Basic to fracture mechanics is the understanding of the state of stress near the tip of a sharp crack and the relationship between gross stress and flaw geometry. These concepts are discussed in subsection 2.2, Stress-Intensity Factors.

Flaw growth or crack propagation under cyclic loads is a basic problem which is handled best by fracture mechanics concepts. A thorough discussion of flaw growth is given in subsection 2.3.

Finally, subsection 2.4, Application of Fracture Mechanics Technology, relates stress-intensity factors and flaw growth to the engineering design and analysis of structures. Particular attention is given to pressure-vessel design because of its importance in the aerospace industry.

2.1.1   <u>Comparison of Fatigue and Fracture Mechanics.</u>

Similarities and dissimilarities between fatigue and fracture mechanics are summarized in Table E2-1. Both fatigue and fracture mechanics depend primarily on results of laboratory tests; however, the fracture mechanics concept makes it possible to handle fracture considerations in a quantitative manner and has shown greater applicability to fatigue crack propagation.

Table E2-1. Similarities and Dissimilarities Between Fatigue and Fracture Mechanics

Fatigue Characteristics or Considerations	Fracture Mechanics Characteristics or Considerations
• Considers no initial material flaws, e.g., voids, inclusions, etc.	• Assumes pre-existence of flaws, inhomogeneities and discontinuities in a material.
• Data presented in the form of a plot of stress versus number of cycles to failure, S.N. curve.	• Data presented in the form of stress intensity factor versus cycles to failure or flaw growth rates.
• Life prediction utilizes cumulative damage theories.	• Life prediction is based on minimum flaw growth potential, i.e., the growth of an initial flaw to critical value.
• Analysis carried out in two steps: 1. Relating repeated loads to stress. 2. Evaluating stresses using the cumulative damage theory to predict structural life.	• Imposes limits on nondestructive inspections and procedure. • Predicts fatigue behavior such as those stemming from stress corrosion or fatigue.
• Does not consider sustained loading.	• Considers sustained loading.
• A purely analytical fatigue design method is not yet available.	• Considers sequence of operational load.
• The scatter inherent in fatigue behavior and in service conditions would require that results be interpreted statistically.	• Has shown greater applicability to fatigue crack propagation because conditions for fatigue are less than critical.
• Considers fractures for relatively large numbers of cycles only (10 000 and over).	• Considers fractures for relative small numbers of cycles (0 < cycles < 10 000).

2.2   STRESS-INTENSITY FACTORS.

To understand how fracture mechanics is used in design, it is helpful first to learn some of the theory on which it is based.

The precise goal of fracture mechanics can be stated concisely: It attempts to provide a quantitative measure of resistance to unstable crack propagation. This measure must be independent of the size and shape of the crack, the geometry of the part containing the crack, and the manner in which external loads are applied to the part.

The search for a quantitative value focuses on the conditions in the vicinity of the crack tip where fracture takes place.

The stress fields near crack tips can be divided into three basic types, each associated with a local mode of deformation, as shown in Fig. E2-1. The opening mode, I, is associated with a local displacement in which the crack surfaces move directly apart. The edge-sliding mode, II, is characterized by displacements in which the crack surfaces slide over one another. In mode III, tearing, the crack surfaces slide with respect to one another parallel to the leading edge. Mode I is the most critical mode and is the only one to be discussed in this section. For information on modes II and III, see Ref. 1.

a. Mode I.   b. Mode II.

c. Mode III.
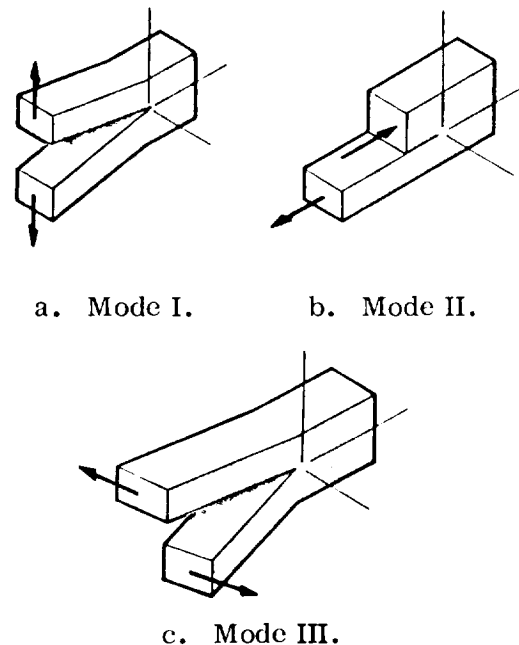
FIGURE E2-1. THREE DISPLACE-
MENT MODES FOR CRACK
SURFACES

2.2.1   Plane Strain.

The stress conditions, or plane-strain elastic stress field, at the crack
tip for mode I are defined by the expressions shown in Fig. E2-2 (Ref. 2).
These equations give the components of stress (σ = normal stress, τ = shear
stress) in terms of the polar coordinates r and ϕ for opening-mode (per-
pendicular) crack surface displacements. Only the first term of each equation
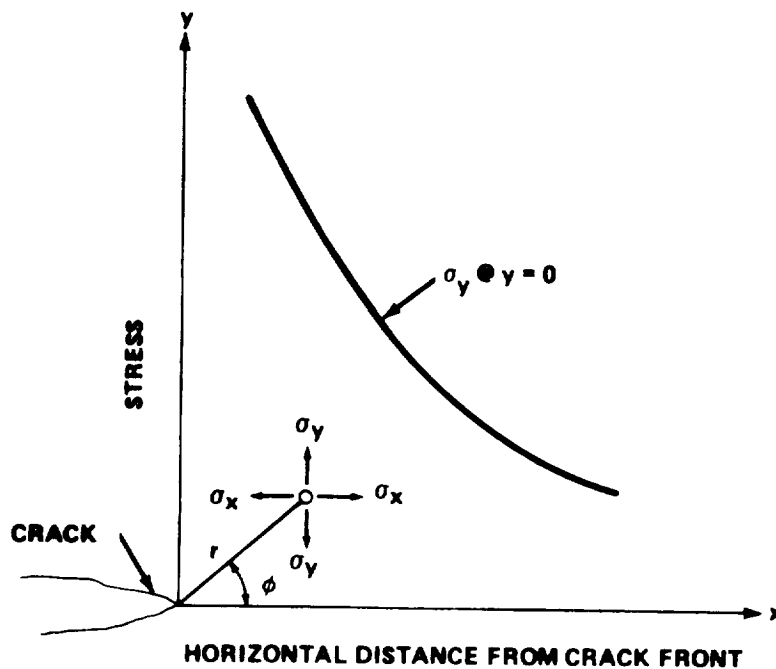
$$\sigma_y = \frac{K_I}{(2\pi r)^{1/2}} \cos\frac{\phi}{2}\left(1 + \sin\frac{\phi}{2}\sin\frac{3\phi}{2}\right) \cdots$$

$$\sigma_x = \frac{K_I}{(2\pi r)^{1/2}} \cos\frac{\phi}{2}\left(1 - \sin\frac{\phi}{2}\sin\frac{3\phi}{2}\right) \cdots$$

$$\tau_{xy} = \frac{K_I}{(2\pi r)^{1/2}} \cos\frac{\phi}{2}\sin\frac{\phi}{2}\cos\frac{3\phi}{2} \cdots$$

FIGURE E2-2. RELATIONSHIP BETWEEN STRESS-INTENSITY FACTOR,
K_I, AND STRESS COMPONENTS IN THE VICINITY OF A CRACK

is shown. The complete equations are power series in r/a (crack tip radius/ crack half-length). For practical purposes, all terms beyond the first are negligible.

All the three stress components are proportional to a scalar quantity that has been designated the stress-intensity factor, K_I. This factor is independent of r and ϕ and therefore gives a single description of the stress intensity at any point near the crack tip. It is a purely numerical quantity which, if known, provides complete knowledge of the stress field at the crack tip.

The basic assumption in fracture mechanics is that an unstable fracture occurs when K_I reaches a critical value designated K_{Ic}, commonly called fracture toughness. It is important to appreciate the difference between K_I and K_{Ic}. The stress-intensity factor K is simply a coefficient in an equation describing the elastic stresses in the vicinity of a crack tip. Fracture toughness K_{Ic} is a particular value of K_I corresponding to unstable propagation of the crack. This value is a material property and reflects a material's ability to withstand a given stress at a crack tip. The difference between K_I and K_{Ic} is analogous to the difference between stress and strength for a body free of discontinuities.

Irwin (Ref. 3) used the expressions shown in Fig. E2-2 with the Green and Sneddon analysis (Ref. 4) to show that the expression for the stress intensity around the crack periphery for the embedded elliptical flaw (Fig. E2-3) is

$$K_I = \frac{\sqrt{\pi}}{\Phi} \, \sigma \sqrt{a} \, \left\{ \frac{1}{c^2} \, [a^2 \cos^2 \phi + c^2 \sin^2 \phi] \right\}^{1/4} \quad ,$$

where σ is the uniform stress perpendicular to the crack. The parametric equations of the flaw periphery are $x = c \cos \phi$ and $y = a \cos \phi$, where c is the semimajor axis of the ellipse, a is the semiminor axis of the ellipse, and Φ is the complete elliptical integral of the second kind corresponding to the modulus $k = [(c^2 - a^2)/c^2]^{1/2}$; i.e.,

$$\Phi = \int_0^{\pi/2} \left[1 - \left(\frac{c^2 - a^2}{c^2} \right) \sin^2 \phi \right]^{1/2} d\phi$$

or $\Phi = 1 + 4.593 (a/2c)^{1.65}$. Values of Φ can be obtained for various values of a/2c from the graph shown in Fig. E2-4.

In seeking an expression for the stress intensity for a semielliptical surface flaw in a finite-thickness plate, Irwin assumed that

$$K_I = \alpha \frac{\sqrt{\pi}}{\Phi} \sigma \sqrt{a\gamma} \left\{ \frac{1}{c^2} [a^2 \cos^2 \phi + c^2 \sin^2 \phi] \right\}^{1/4} ,$$

where α is a correction factor to account for the effect on stress intensity of the stress-free surface from which the flaw emanates, and γ is a correction factor to account for the effect on stress intensity of the plastic yielding around the flaw periphery.

Values of α and γ were estimated by Irwin and considered valid for surface flaws with a/c ratios less than one and flaw depths not exceeding 50 percent of the plate thickness. The resulting expression for the stress intensity was

$$K_I = 1.1 \sqrt{\pi} \sigma (a/Q)^{1/2} \left\{ \frac{1}{c^2} [a^2 \cos^2 \phi + c^2 \sin^2 \phi] \right\}^{1/4} ,$$
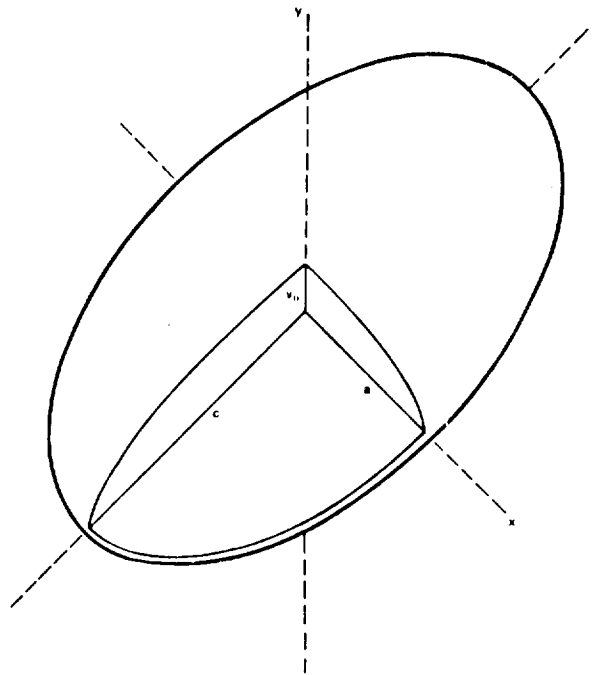
FIGURE E2-3. EMBEDDED ELLIPTICAL-SHAPED CRACK UNDER
UNIFORM TENSILE STRESS IN y-DIRECTION
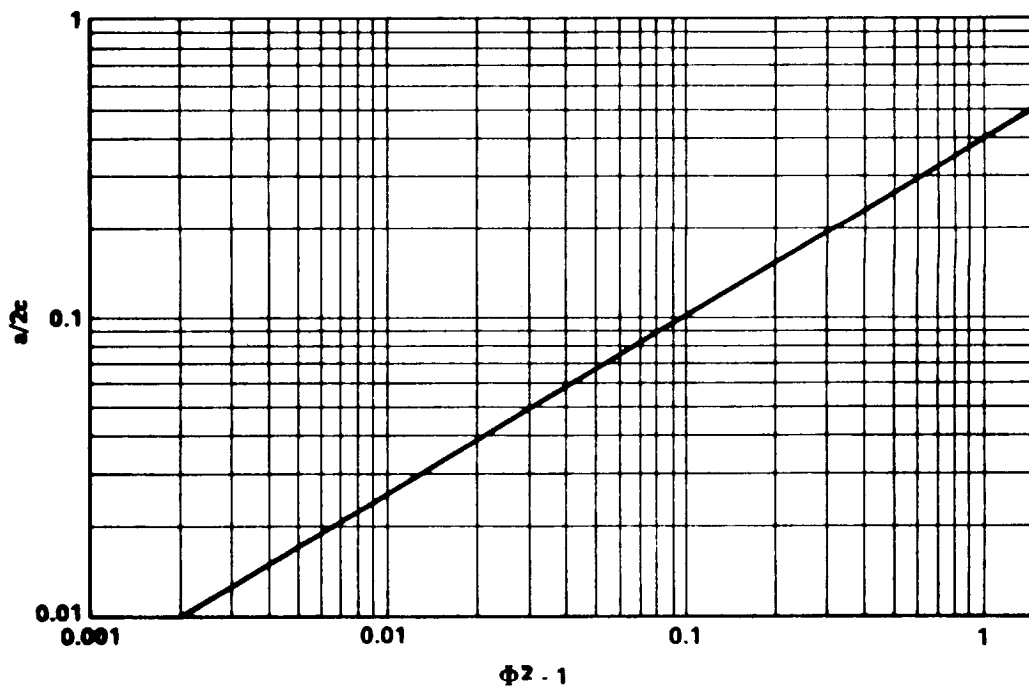
FIGURE E2-4. SHAPE FACTOR VALUES

where $Q = \Phi^2 - 0.212 \left(\sigma / \sigma_{ys}\right)^2$, and σ_{ys} is the uniaxial yield strength of the material. Figure E2-5 shows the relationship between Q and the flaw depth-to-width ratio.

The maximum value of K_I occurs at the end of the semiminor axis of the ellipse and has a value of

$$K_I = 1.1 \sqrt{\pi} \, \sigma \, (a/Q)^{1/2} \quad .$$

At some value of σ the flaw size becomes unstable and propagates rapidly. The value of K_I computed at the inception of this instability is called the critical value of K_I and is designated K_{Ic}. Thus, K_{Ic} is the stress intensity necessary to cause fracture under plane-strain conditions and is commonly called the plane-strain fracture toughness. Thus,

$$K_{Ic} = 1.1 \sqrt{\pi} \, \sigma \, (a/Q_{cr})^{1/2} \quad .$$

Figure E2-6 is a graphical representation of this equation. Some typical values of K_{Ic} for space shuttle materials are shown in Table E2-2.

Stress-intensity factors for other shapes of cracks, different loading conditions, and crack location are given in Table E2-3.

2.2.1.1 Correction for Deep Surface Flaws.

For surface flaws that are deep with respect to plate thickness, that is, when the crack approaches the opposite surface, Irwin's equation has been modified by Kobayashi (Ref. 5) as follows:

$$K_I = 1.1 \, M_k \, \sqrt{\pi} \, \sigma \, (a/Q)^{1/2} \quad ,$$

where M_k is the magnification factor for deep flaw effects.
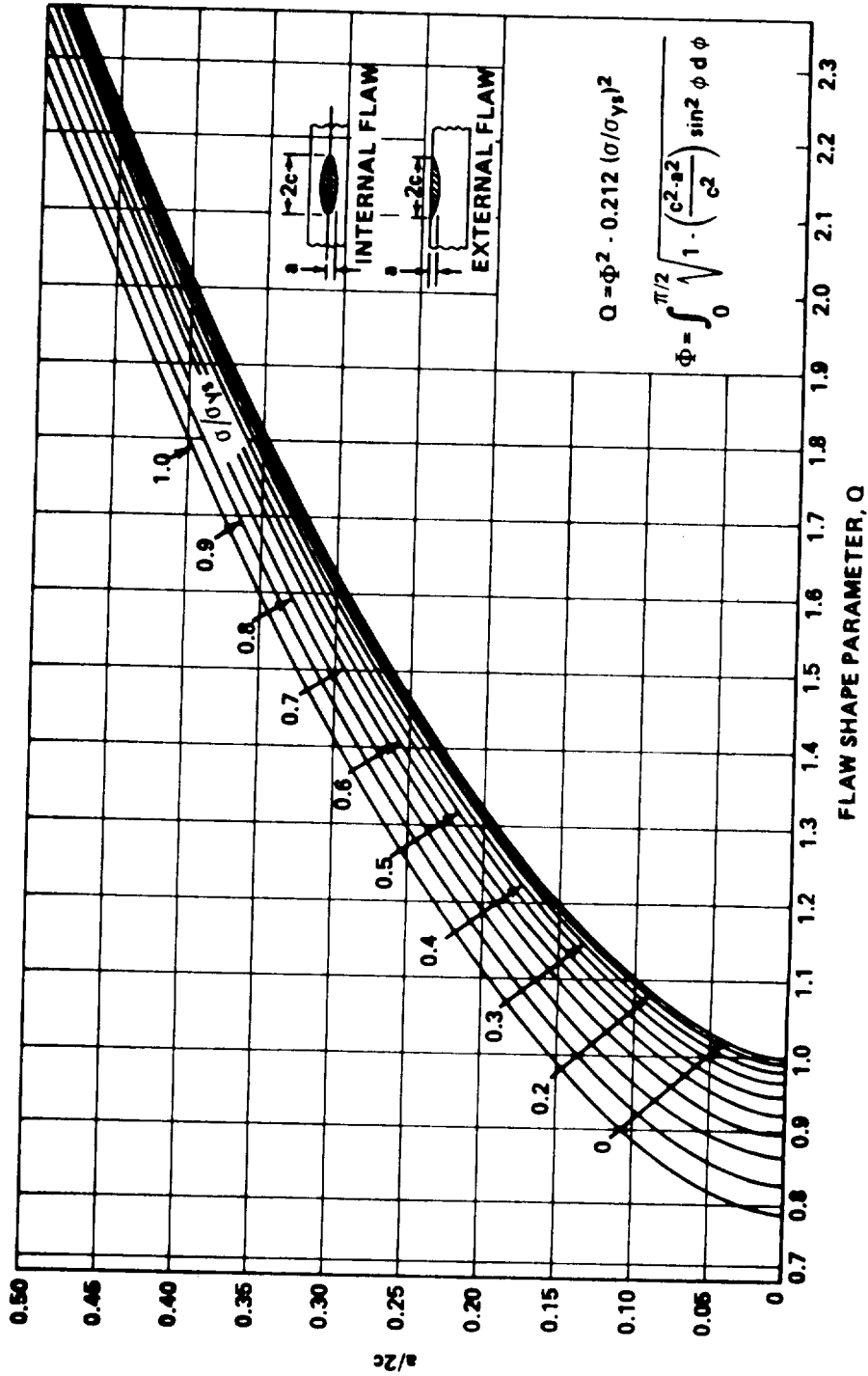
FIGURE E2-5.   SHAPE PARAMETER CURVES FOR SURFACE AND INTERNAL FLAWS
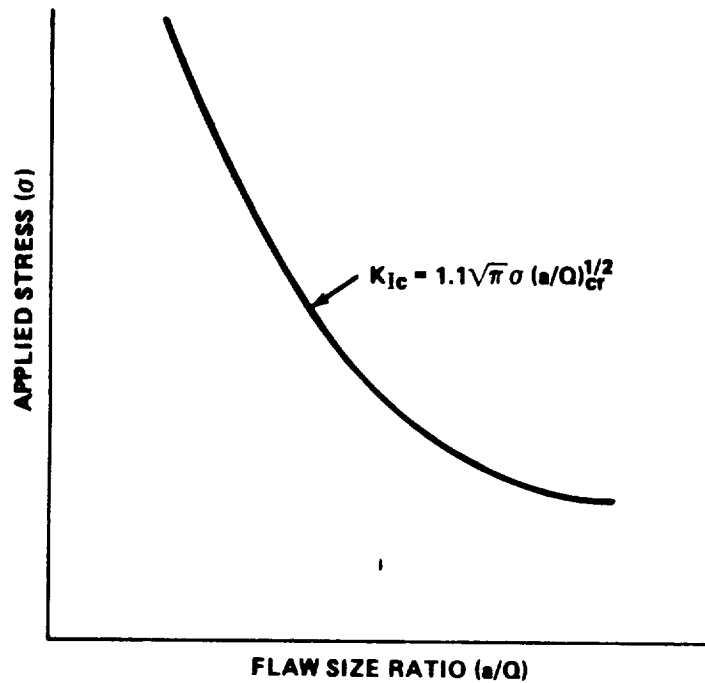
FIGURE E2-6. APPLIED STRESS VERSUS CRITICAL FLAW SIZE RATIO

Experimental data obtained on several materials with varying flaw sizes and shapes appear to provide a fair degree of substantiation of the Kobayashi magnification factor; however, more experimental investigations are being performed. Typical curves for M_k for two different materials are shown in Figs. E2-7 and E2-8.

2.2.2   Plane Stress.

An important consideration in fracture mechanics is the "state of stress," or simply the directions and magnitudes of the applied stresses and strains. In general, the state of stress in a body is three-dimensional, that is, stresses and strains exist in all three principal directions.

For thin sheet specimens subjected to in-plane external loads which do not vary through the thickness, a condition of plane stress is thought to prevail. As such, strain in the thickness direction is virtually unsuppressed and considerable plastic flow attends the cracking process.

Table E2-2. Properties of Typical Materials Considered
for Use on Space Shuttle

Alloy	F_{tu} (ksi)	F_{ty} (ksi)	K_{Ic} (ksi $-$ in.$^{1/2}$)
4340 (High Strength)	260	217	52
4340 (Low Strength)	180	158	100
D6AC (High Strength)	275	231	61
D6AC (Low Strength)	218	203	112
18 Ni (250)	263	253	76
18 Ni (200)	206	198	100
12 Ni	190	180	226
9 Ni $-$ 4 Cr	190	180	160
HY $-$ 150	150	140	250
T $-$ 1	115	100	180
2014-T6	66	60	23
2024-T4	62	47	28
2219-T87	63	51	27
6061-T6	42	36	71
7075-T6	76	69	26
6Al-4V (STA)	169	158	51
5Al-2.5 Sn	125	118	120

Table E2-3. Stress-Intensity Factors
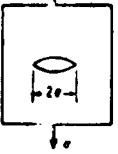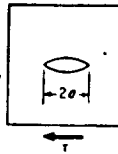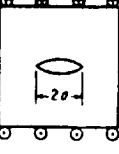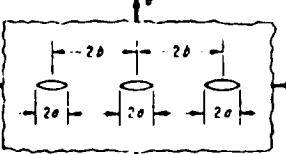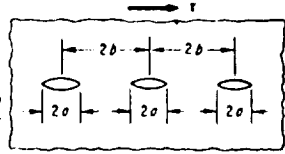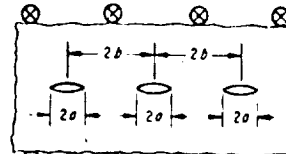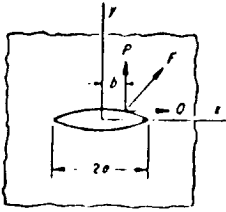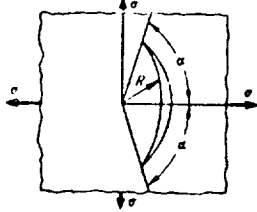
Case 1

Infinite cracked sheet with uniform normal stress at infinity

$$K_I = \sigma\sqrt{\pi a}$$

$$K_{II} = K_{III} = 0$$

Case 2

Infinite cracked sheet with uniform in-plane shear at infinity

$$K_{II} = \tau\sqrt{\pi a}$$

$$K_I = K_{III} = 0$$

Case 3

Infinite sheet with tunnel crack subject to out-of-plane shear at infinity

$$K_{III} = \tau\sqrt{\pi a}$$

$$K_I = K_{II} = 0$$

Case 4

Periodic array of cracks along a line in a sheet, uniform stress at infinity

$$K_I = \sigma\sqrt{\pi a}\left(\frac{2b}{\pi a}\tan\frac{\pi a}{2b}\right)^{\frac{1}{2}}$$

$$K_{II} = K_{III} = 0$$

Case 5

Periodic array of cracks along a line in a sheet, uniform in-plane shear stress at infinity

$$K_{II} = \tau\sqrt{\pi a}\left(\frac{2b}{\pi a}\tan\frac{\pi a}{2b}\right)^{\frac{1}{2}}$$

$$K_I = K_{III} = 0$$

Case 6

Periodic array of cracks along a line in a sheet, uniform out-of-plane shear at infinity

$$K_{III} = \tau\sqrt{\pi a}\left(\frac{2b}{\pi a}\tan\frac{\pi a}{2b}\right)^{\frac{1}{2}}$$

$$K_I = K_{II} = 0$$

Case 7

Concentrated force on the surface of a crack in an infinite sheet

$$K_I = \frac{P}{2\sqrt{\pi a}}\left(\frac{a+b}{a-b}\right)^{\frac{1}{2}} + \frac{Q}{2\sqrt{\pi a}}\left(\frac{\kappa - 1}{\kappa + 1}\right)$$

$$K_{II} = \frac{-P}{2\sqrt{\pi a}}\left(\frac{\kappa - 1}{\kappa + 1}\right) + \frac{Q}{2\sqrt{\pi a}}\left(\frac{a+b}{a-b}\right)^{\frac{1}{2}}$$

$\kappa = 3.4\nu$ (for plane strain)

Case 8

Curved crack in equal biaxial stress field

$$K_I = \frac{\sigma(\pi R)^{\frac{1}{2}}}{\left(1 + \sin^2\frac{a}{2}\right)}\left(\frac{\sin a(1 + \cos a)}{2}\right)^{\frac{1}{2}}$$

$$K_{II} = \frac{\sigma(\pi R)^{\frac{1}{2}}}{\left(1 + \sin^2\frac{a}{2}\right)}\left(\frac{\sin a(1 - \cos a)}{2}\right)^{\frac{1}{2}}$$

Table E2-3. (Continued)
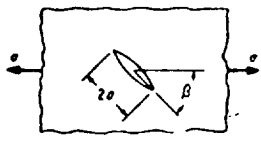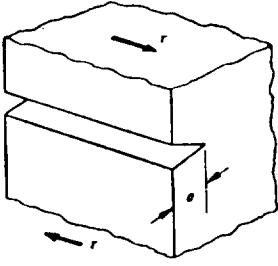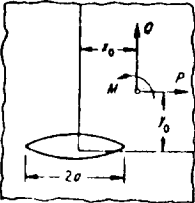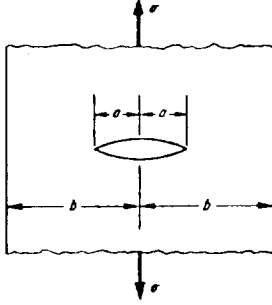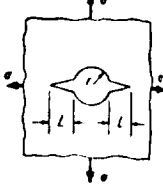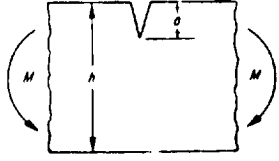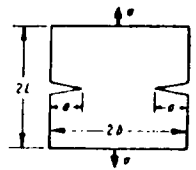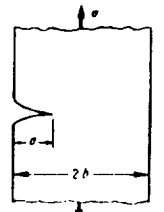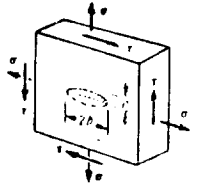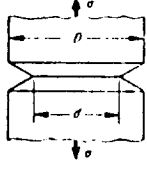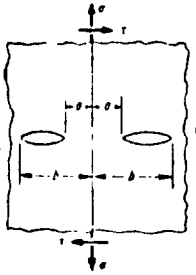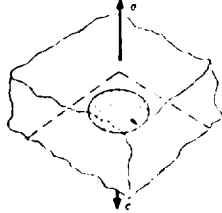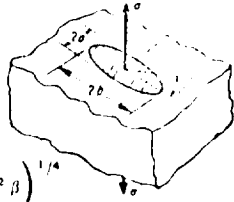
Case 9

Inclined crack in uniform tension in infinite sheet

$$K_I = \sigma \sin^2 \beta \sqrt{\pi a}$$

$$K_{II} = \sigma \sin \beta \cos \beta \sqrt{\pi a}$$

Case 10

Crack in infinite sheet subject to arbitrary force and couple at a remote point

At right end

$$K = \frac{1}{2\sqrt{\pi a}\,(1+\kappa)} \left\{ (P + iQ) \left[\frac{a + z_0}{\sqrt{z_0^2 - a^2}} \right. \right.$$

$$\left. - \frac{\kappa(a + z_0)}{(\overline{z}_0^2 - a^2)^{1/2}} - 1 + \kappa \right]$$

$$\left. + \frac{a(P - iQ)(\overline{z}_0 - z_0) + ai(1 + \kappa)M}{(z_0 - a)(\overline{z}_0^2 - a^2)^{1/2}} \right\}$$

$\kappa = (3 - \nu)/(1 + \nu)$ for plane stress $\quad \kappa = 3 - 4\nu$ for plane strain

$z_0 = x_0 + iy_0 \qquad \overline{z}_0 = x_0 - iy_0$

Case 11

Cracks from hole in infinite sheet

$$K_I = \sigma \sqrt{L\pi}\ f\left(\frac{L}{r}\right)$$

$$K_{II} = 0$$

	— One Crack —		—Two Crack —	
L/r	f(L/r)		f(L/r)	
	Uniaxial Stress	Biaxial Stress	Uniaxial Stress	Biaxial Stress
0	3.39	2.26	3.39	2.26
0.1	2.73	1.98	2.73	1.98
0.2	2.30	1.82	2.41	1.83
0.3	2.04	1.67	2.15	1.70
0.4	1.86	1.58	1.96	1.61
0.5	1.73	1.49	1.83	1.57
0.6	1.64	1.42	1.71	1.52
0.8	1.47	1.32	1.58	1.43
1.0	1.37	1.22	1.45	1.38
1.5	1.18	1.06	1.29	1.26
2.0	1.06	1.01	1.21	1.20
3.0	0.94	0.93	1.14	1.13
5.0	0.81	0.81	1.07	1.06
10.0	0.75	0.75	1.03	1.03
∞	0.707	0.707	1.00	1.00

Case 12

Edge crack in a semi-infinite body subjected to shear

$$K_I = K_{II} = 0$$

$$K_{III} = \tau \sqrt{\pi a}$$

Case 13

Central crack in strip subject to tension (finite width)

$$K_I = \sigma \sqrt{\pi a}\ f(\lambda)$$

$$\lambda = a/b$$

λ	f(λ)
0.074	1.00
0.207	1.03
0.275	1.05
0.337	1.09
0.410	1.13
0.466	1.18
0.535	1.25
0.592	1.33

Case 14

Notched beam in bending

$$K_I = \frac{6M}{(h - a)^{3/2}}\ g(a/h)$$

$$K_{II} = K_{III} = 0$$

a/h	g(a/h)
0.05	0.36
0.1	0.49
0.2	0.60
0.3	0.66
0.4	0.69
0.5	0.72
0.6	0.73
> 0.6	0.73

Table E2-3. (Concluded)

Case 15 — Double-edge notch

a/h	f(a/b) L/b = 1	f(a/b) L/b = 3	f(a/b) L/b → ∞
0.1	1.13	1.12	1.12
0.2	1.13	1.11	1.12
0.3	1.14	1.09	1.13
0.4	1.16	1.06	1.14
0.5	1.14	1.02	1.15
0.6	1.10	1.01	1.22
0.7	1.02	1.00	1.34
0.8	1.01	1.00	1.57
0.9	1.00	1.00	2.09

$$K_I = \sigma \sqrt{\pi a} \left(\frac{2h}{\pi a} \tan \frac{\pi a}{2b} \right)^{1/2} f(a/b)$$

$$K_{II} = K_{III} = 0$$

for L → ∞ use:

$$K_I = \sigma \sqrt{\pi a} \left[\frac{2b}{\pi a} \left(\tan \frac{\pi a}{2b} + 0.1 \sin \frac{\pi a}{b} \right) \right]^{1/2}$$

Case 16

Semielliptical surface crack in plate subject to general extension

$$K_I = \left[1 + 0.12 \left(1 - \frac{a}{b} \right) \right] \frac{\sigma \sqrt{\pi a}}{\Phi_0} \left(\frac{2t}{\pi a} \tan \frac{\pi a}{2t} \right)^{1/2}$$

$$K_{II} = 0$$

$$K_{III} = \frac{\tau \sqrt{\pi a}}{\Phi_0} \left(\frac{2t}{\pi a} \tan \frac{\pi a}{2t} \right)^{1/2}$$

where Φ_0 is given by

$$\Phi_0 = \int_0^{\pi/2} \left[1 - \left(\frac{b^2 - a^2}{b^2} \right) \sin^2 \phi \right]^{1/2} d\phi$$

Case 17

Two equal colinear cracks in an infinite sheet subject to uniform tension

At the near ends

$$K_I = \sigma \sqrt{\pi a} \frac{b^2 \frac{E(\mu)}{K(\mu)} - a^2}{(b^2 - a^2)^{1/2}}$$

$$K_{II} = \tau \sqrt{\pi a} \frac{b^2 \frac{E(\mu)}{K(\mu)} - a^2}{(b^2 - a^2)^{1/2}}$$

At the far ends

$$K_I = \sigma \sqrt{\pi b} \left(\frac{1}{\mu} - \frac{E(\mu)}{\mu K(\mu)} \right)$$

$$K_{II} = \tau \sqrt{\pi b} \left(\frac{1}{\mu} - \frac{E(\mu)}{\mu K(\mu)} \right)$$

where $\mu = \left[1 - \left(\frac{a^2}{b^2} \right) \right]^{1/2}$

E and K are the complete elliptic integrals E(μ) and K(μ) of the first and second kinds respectively.

Case 18 — Single-edge notch

$$K_I = \sigma \sqrt{\pi a} \, f(a/b)$$

$$K_{II} = K_{III} = 0$$

a/h	f(a/b)	f(a/b)
0.1	1.15	1.14
0.2	1.20	1.19
0.3	1.29	1.29
0.4	1.37	1.37
0.5	1.51	1.50
0.6	1.68	1.66
0.7	1.89	1.87
0.8	2.14	2.12
0.9	2.46	2.44
1.0	2.86	2.82

Case 19

Round bar in tension with circumferential crack

$$K_I = \sigma_{net} \sqrt{\pi D} \, f(d/D)$$

$$K_{II} = K_{III} = 0$$

d/D	f(d/D)	d/D	f(d/D)
0	0	0.70	0.240
0.1	0.111	0.75	0.237
0.2	0.155	0.80	0.233
0.3	0.185	0.85	0.225
0.4	0.209	0.90	0.205
0.5	0.227	0.95	0.162
0.6	0.238	0.97	0.130
0.65	0.240	1.00	0

Case 20

Circular crack in an infinite body subject to uniform tension

$$K_I = 2\sigma \sqrt{\frac{a}{\pi}}$$

$$K_{II} = K_{III} = 0$$

Case 21

Elliptical crack in infinite body subject to uniform tension

For point on crack edge determined by angle β

$$K_I = \frac{\sigma \sqrt{\pi a}}{\Phi_0} \left(\sin^2 \beta + \frac{a^2}{b^2} \cos^2 \beta \right)^{1/4}$$

$$K_{II} = K_{III} = 0$$

$$\Phi_0 = \int_0^{\pi/2} \left[1 - \left(\frac{b^2 - a^2}{b^2} \right) \sin^2 \phi \right]^{1/2} d\phi$$

[BASED ON TESTS OF 0.20-in.-THICK BASE METAL
(TRANSVERSE GRAIN) AND WELD METAL
AT -320°F AND -423°F]

$$M_k = \frac{K_I}{1.1\sqrt{\pi}\,\sigma_{cr}\sqrt{a/Q}}$$

FIGURE E2-7. M_k CURVES FOR 5Al-2.5Sn (ELI) TITANIUM ALLOY

[BASED ON TESTS OF 0.63-in.-THICK BASE METAL
(LONGITUDINAL GRAIN) AT 72°F, -320°F, AND -423°F.]
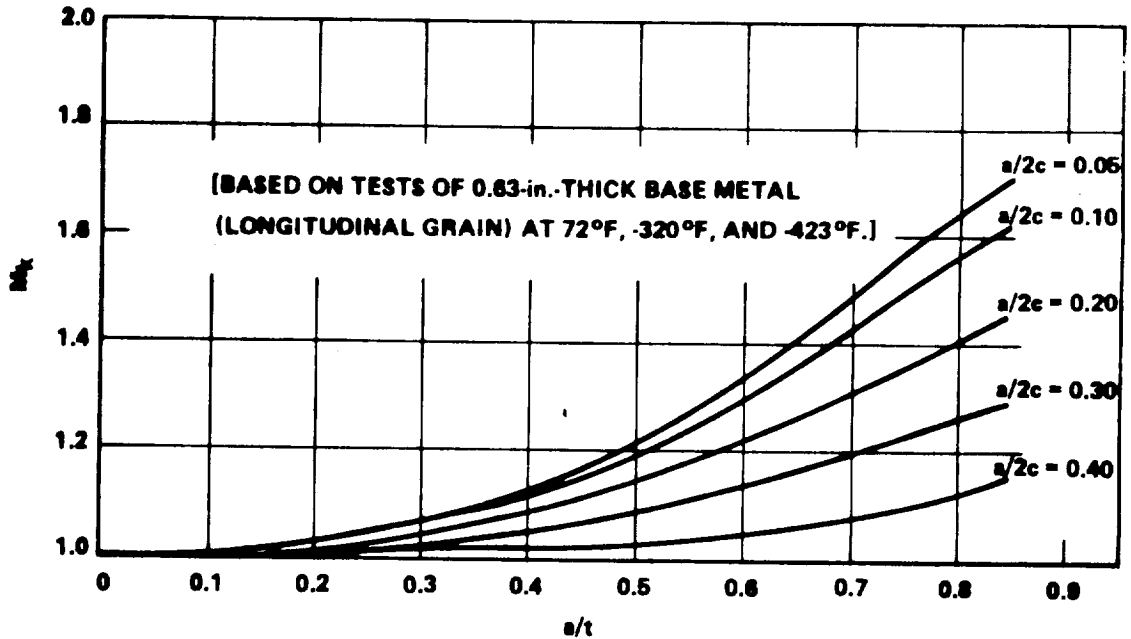
FIGURE E2-8. M_k CURVES FOR 2219-T87 ALUMINUM ALLOY

For thick specimens, strain in the thickness direction is suppressed considerably by the very thickness of the material and noticeably less plastic flow is associated with the cracking process.

A laboratory plate specimen is seldom completely in either plane stress or plane strain but rather in some proportion of both. At the free surfaces of the plate there are no transverse stresses to restrain plastic flow (a condition of plane stress). In contrast, at mid-thickness, plane-strain conditions prevail and much less plastic flow occurs. A schematic representation of the crack-tip plastic zone in a plate specimen is shown in Fig. E2-9.

The size of the plane stress plastic zone is thought to be related to the amount of shear tip left at the fracture surface. Thus, the appearance of the fracture will vary according to the proportions of plane stress and plane strain conditions through the thickness of the plate.

SHADED AREA = CRACK SURFACE
HEAVY SOLID LINE = CRACK FRONT

THICKNESS OF SPECIMEN

PLASTIC ZONE

FIGURE E2-9. REPRESENTATION OF PLASTICALLY DEFORMED REGION AT A CRACK FRONT

The influence of stress state (and associated plasticity) on the fracture toughness is illustrated in Fig. E2-10, which shows the effect of plate thickness on the toughness and fracture appearance. This figure shows that the larger thicknesses are characterized by low values of toughness. This corresponds to a completely square (brittle-appearing) fracture appearance.

FIGURE E2-10. EFFECT OF PLATE THICKNESS ON FRACTURE
TOUGHNESS AND PHYSICAL APPEARANCE OF THE FRACTURE

A reduction in plate thickness decreases the degree of plastic constraint at the advancing crack tip. This enlarges the local plastic zone and consequently raises the fracture toughness. The development of a larger plastic zone, in turn, relaxes the stress in the thickness direction, which further decreases constraint. The process is self-accelerating and the fracture toughness increases rapidly in a narrow range of thickness variation, as shown in Fig. E2-10.

In the aerospace industry thicknesses of structures are usually thin enough to fall in the region of plane stress behavior and as a result more testing in this area is being done. However, a determination of plane stress

intensity factors is far more complicated than was first supposed and considerable research is needed. It is very hard to determine when unstable crack propagation occurs because the unstable condition is approached very gradually as crack length increases.

At present there is no direct method for translating laboratory data for the mixed mode fracture condition to useful numbers for designing practical hardware.

2.2.2.1 Through-the-Thickness Cracks.

In thin-walled structures, cracks may grow through the thickness before catastrophic failure occurs or a through-the-thickness crack may exist before any load is applied. The basic plane stress equation for through-thickness cracks corrected for plastic zone in an infinitely wide plate is

$$K_c^2 = \sigma^2 \left(\pi \frac{\ell_c}{2} + \frac{1}{2} \frac{K_c^2}{\sigma_y^2} \right) \quad,$$

where ℓ_c is the length of the through-thickness crack at failure (in.), σ is the stress normal to the plane of the crack at failure (ksi), σ_y is the yield strength (ksi), and K_c is the critical plane-stress stress intensity (ksi $\sqrt{\text{in.}}$).

The critical plane stress intensity for a finite-width panel containing a through-thickness crack is

$$K_c = \sigma \left\{ w \tan \left[\frac{\pi}{2w} \left(\ell_c + \frac{K_c^2}{\pi \sigma_y^2} \right) \right] \right\}^{1/2} \quad,$$

where w is the width of the panel (in.).
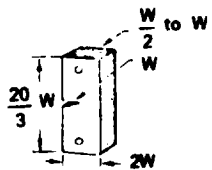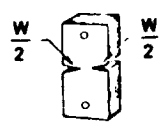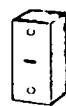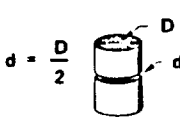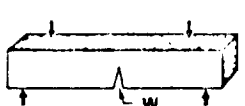
2.2.3   Experimental Determination.

Among the most important recent progress in fracture mechanics is the improved understanding of how the behavior of test specimens relates to the design of structural components. Numerous tests have been performed on a variety of specimen types, some of which are shown in Table E2-4. The tests were designed to determine the specimen types, procedures, and data analysis which result in K_{Ic} determinations that are independent of crack and specimen geometry and manner of external loading.

At present no fracture mechanics test is universally used to determine K_{Ic} values because no one test gives valid data for all materials; each of the tests has its limitations. For instance, ASTM committee No. E-24 has been working for several years to bring out a standard (E399-70T is proposed), but this test may not be valid for low-strength, high-toughness materials.

Table E2-4 describes some types of fracture specimens, the data obtained, and their uses and limitations. For detailed information on these and other specimens, how to set up and conduct the tests, what data to obtain, and how to analyze data, see Refs. 1, 6, and 7.

Table E2-4. Seven Common Types of Fracture Specimens

Specimen	Loading	Data Obtained	Uses/Limitations
Single-Edge Crack	Uniaxial tension, induced bending	Breaking stresses, K_{Ic}	
Double-Edge Crack	Uniaxial tension	Breaking stresses, K_{Ic}	Cracks must be equal in size
Central Through-Crack	Uniaxial tension (static or cyclic)	Breaking stresses, K_c, flaw growth rates, K_{Ic}, l_o, l_c	Simulates penetration flaw in hardware. K_c is width dependent.
Round Bar Notched	Uniaxial tension (cyclic or static) or rotating flexure fatigue	Breaking stresses, K_{Ic}	Simulates bolts and shafts. Difficult to form concentric precrack.
Crackline-Loaded Wedge Opening, or Compact Tension	Tension with induced bending	K_{Ic}, K_{Ii}	Compact
Partial-Thickness Crack	Uniaxial tension (static or cyclic)	Breaking stresses, flaw sizes, apparent K_{Ic}	Simulates natural flaws in hardware. Difficult to analyze. May not provide valid K_{Ic} values.
ASTM Cracked Slow Bend	Three-point loading	K_{Ic}	Only standardized test for K_{Ic}. Not applicable to most thin and tough materials.

2.3   FLAW GROWTH.

2.3.1   Sustained Load Flaw Growth.

One of the most serious structural problems that can arise in the aero-space industry is the delayed time failure of pressure vessels caused by sustained pressurization. In some cases, through-the-thickness cracks have formed and the vessels leaked under sustained loading. In other cases, small surfaces cracks or embedded flaws grew to critical sizes before growing through the thickness of the shell. When this happens, complete catastrophic fracture ensues. To predict such failures one must know the conditions under which subcritical flaw growth can occur, as well as either the actual initial flaw size or the maximum possible initial flaw size in the vessel when it is placed into service.

When the sustained stress flaw growth is environmentally induced, it is often termed stress corrosion.

The surface-flawed or "part-through" type of cracked specimen has probably found the widest use in evaluating sustained stress flaw growth in both "thick- and thin-walled" aerospace pressure vessels. With this specimen, the initial flaw closely simulates the type of flaws often encountered in service and it can be oriented to suit the flaw growth characteristics desired.

A procedure for laboratory evaluation of sustained stress flaw growth using surface flawed specimens is schematically illustrated in Fig. E2-11. The K_{Ic} for the material is first established from static (pull) tests. Then, using a batch of flawed specimens, each flawed specimen is loaded with different initial loads (various fractions of K_{Ic}) and the time required for failure observed, e.g., specimens 1 and 2, illustrated in Fig. E2-11. If failure does not occur in a reasonable time (e.g., specimens 3 and 4), it is still possible to obtain crack growth information by "marking" the crack front (applying some low-stress fatigue cycles) and pulling the specimen apart.
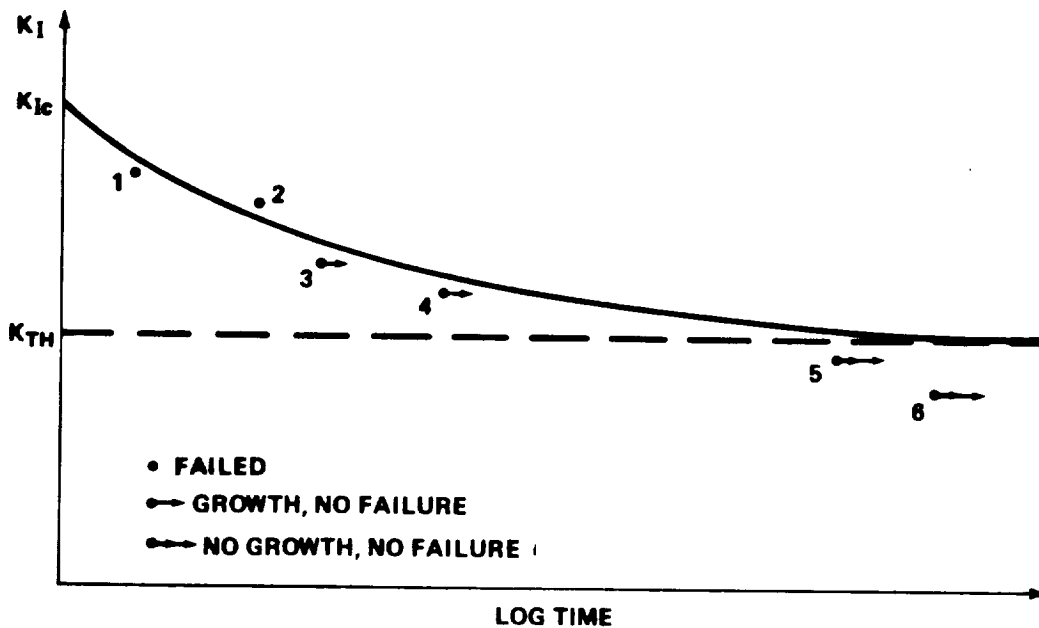
FIGURE E2-11. SCHEMATIC ILLUSTRATION OF A PROCEDURE FOR LABORATORY EVALUATION OF SUSTAINED-STRESS FLAW GROWTH USING SURFACE FLAWED SPECIMENS

A point is finally reached at which neither failure nor flaw growth occurs. The highest level of K for which this condition occurs is called the threshold stress intensity, K_{TH}; or K_{Iscc} if due to stress corrosion cracking.

2.3.1.1 Environmental Effects.

The discovery of a unique K_{TH} can be 80 percent of K_{Ic} or higher in relatively inert environments; hostile media can reduce the value to less than half of K_{Ic}.

Considerable evidence indicates that sustained load flaw growth is most severe under conditions of plane strain with K_{TH} values determined from through-the-thickness cracked specimen tests increasing with a decrease in specimen thickness.

Studies of flaw growth and stress intensity in aggressive environments indicate a monotonic relation between increasing stress intensity and growth rate and design correlations have been determined for the critically important materials, titanium, and high-strength steels. In these tests for K_{TH}, a wide scatter, abnormally short times to failure, and very marked dependence on environmental characteristics (media and temperature) are encountered.

During the past few years a considerable amount of sustained load flaw growth data has been obtained on a number of different material-environment combinations. A summary of some K_{TH} information is given in Table E2-5.

2.3.2   Cyclic Load Flaw Growth.

Understanding crack propagation under cyclic loads is a basic requirement for the application of fracture mechanics to the design of structures for service life. Subcritical flaw-growth characteristics for various materials are generally determined through the laboratory testing of flawed specimens. These empirical data are then correlated to various crack-propagation theories which have been proposed. The following is a discussion of some of the more prominent theories.

2.3.2.1   Theories.

A number of studies dealing with fatigue crack propagation have shown that the stress intensity factor K is the most important variable affecting fatigue crack growth rates. The availability of a master curve for a particular material relating fatigue crack-growth rate and range of stress-intensity factor would enable a designer to predict growth rates for any cracked body configuration.

Numerous "laws" of fatigue crack growth have been published during the last 10 years. Basically, all the various equations that have been obtained are simply the attempt of an individual investigator to obtain a curve that will

Table E2-5. Typical Threshold Stress-Intensity Data for Various Material-Environment Combinations

Material	Temp. ("F)	σ_{ys} (ksi)	Typ. K_{Ic} (ksi $\sqrt{in.}$)	Fluid Environment	K_{TH}/K_{Ic}
6Al-4V Titanium Forging - STA	R.T.	160	44	Methanol	0.24
	R.T.	160	44	Freon M. F.	0.58
	R.T.	160	44	N_2O_4 (0.30% NO)	0.74
	R.T.	160	44	N_2O_4 (0.60% NO)	0.83
	R.T.	160	44	H_2O (distilled) + Na_2CrO_4	0.82
	R.T.	160	44	H_2O (distilled)	0.86
	R.T.	160	44	Helium, Air, or GOX	0.90
	R.T.	160	44	Aerozine 50	0.82
	R.T.	160	44	Freon T. F.	0.80
	90	160	44	N_2O_4 (0.30% NO)	0.71
	90	160	44	N_2O_4 (0.60% NO)	0.75
	105	160	44	Monomethylhydrazine	0.75
	110	160	44	Aerozine 50	0.75
6Al-4V Titanium Weldments (Heat-Affected Zones)	R.T.	126	39	Methanol	0.28
	R.T.	126	39	Freon M. F.	0.40
	R.T.	126	39	H_2O (Distilled)	0.86
	R.T.	126	39	H_2O (Distilled) + Na_2CrO_4	0.82
5Al-2.5 Sn (ELI) Titanium Plate	-320	180	64	LN_2 (σ < Prop. Limit)	>0.90
	-320	180	64	LN_2 (σ < Prop. Limit)	0.82
	-423	210	52	LH_2	>0.90
2219-T87 Aluminum Plate	R.T.	58	36	Air	0.90^a
	-320	66	41	LN_2	0.82^a
	-423	72	44	LH_2	$>0.85^a$
4330 Steel	R.T.	205	90	Water	0.24
4340 Steel	R.T.	>200	≈60	Salt water	<0.20
GTA Welds 18 Ni (200) Steel	R.T.	200	130	Salt-water Spray	>0.70
18 Ni (250) Steel	R.T.	235	75	Salt-water Spray	>0.70
12 Ni-5 CR-3 Mo Steel	R.T.	170	155	Salt-water Spray	>0.70
9 Ni-4 Co-2.5C Steel	R.T.	170	120	Salt-water Spray	>0.70
5 Ni-Cr-Mo Steel	R.T.	140	>200	Salt-water Spray	
Inconel 718	R.T.	165	>130	Gaseous Hydrogen at 5000 psig	0.25
2219-T851 Aluminum Plate	R.T.	50		N_2O_4	0.70
2021-T851 Aluminum Plate	R.T.	65	30.5	N_2O_4	0.35

a. No failure K_{TH}; some growth observed at lower values.

best fit his data. Some have used curve-fitting techniques to obtain a high-order polynominal to fit the data, others have used a statistics approach, and still others have divided the data into regions and constructed straight lines with different slopes in each region.

The choice between equations may be that of simplicity of equation versus accuracy of flaw-growth prediction given from the equation over the range of interest. For example, an equation may be very simple and give good results over a limited range of data, but out of this range the equation may be quite inaccurate.

I. Paris.

Paris and Erdogan (Ref. 8), for example, argued that the growth rate should be a function of the stress-intensity factor K on the grounds that this factor defines the elastic stress field around the crack tip. They found that a large body of data could be fitted by an expression of the form

$$\frac{da}{dN} = c\,(\Delta K)^n \quad ,$$

where c is a material constant, ΔK is the range of stress-intensity factor, and n is an exponent having a typical value of four for steel.

An example of Paris's equation for a typical steel is shown in Fig. E2-12. On a log-log plot, the equation becomes a straight line. The slope of the line is four, which is the value of n. The constant $c = 5.6 \times 10^{-24}$ is obtained by substitution of data into the Paris equation and solving for c. Separate values of the coefficients c and n must be computed for each value of R (load ratio) because Paris's equation does not have R as a function.
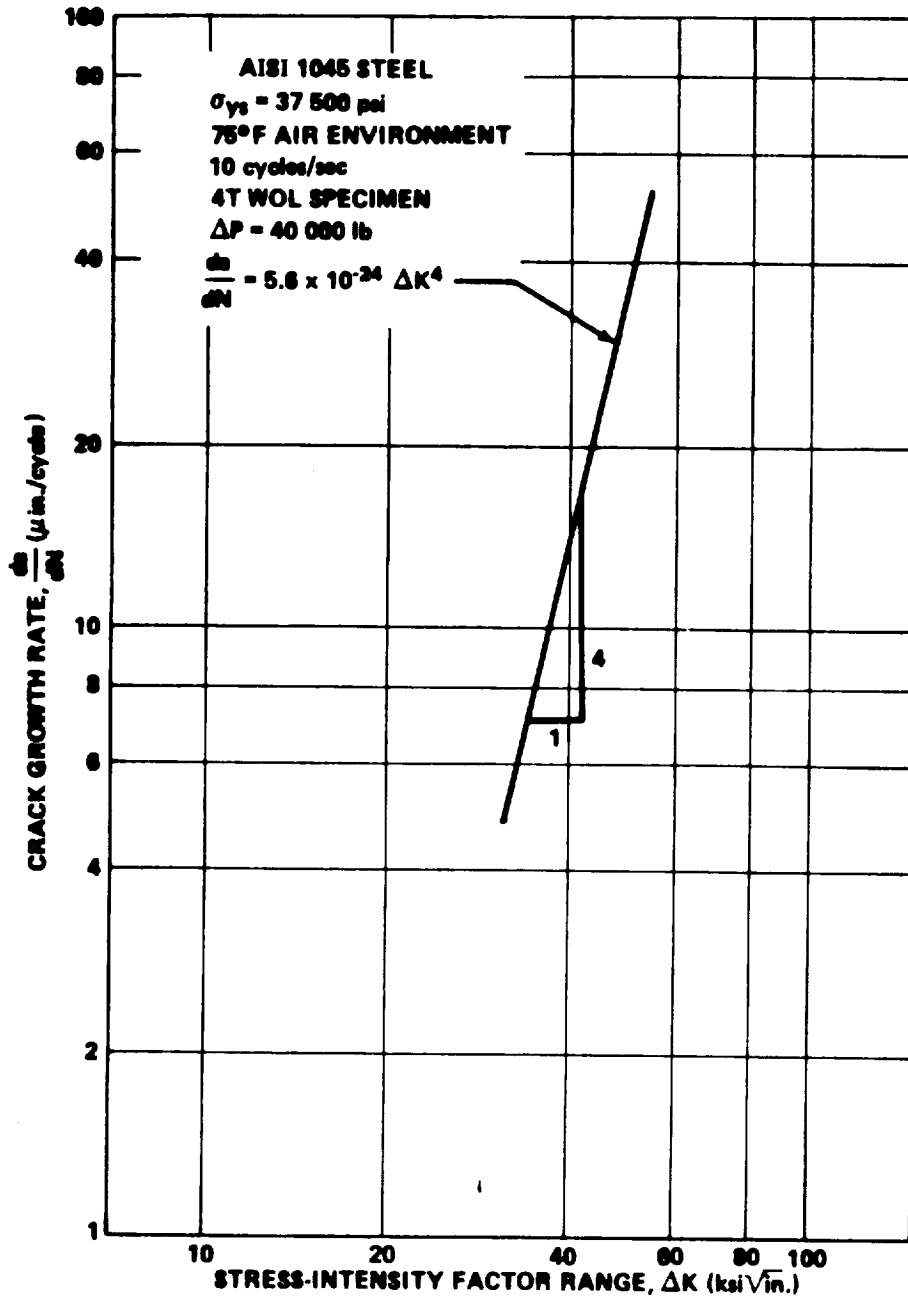
FIGURE E2-12. FATIGUE CRACK GROWTH RATE VERSUS STRESS-
INTENSITY FACTOR RANGE FOR AISI 1045 STEEL

II. <u>Foreman</u>.

The Paris fourth-power crack growth rate equation was modified by Foreman et al. (Ref. 9) to account for the observed behavior that crack growth rates tend to increase rapidly toward an apparent instability as the maximum applied stress intensity approaches the fracture toughness of the material. Foreman also modified the Paris law to account for the observed behavior and to explicitly express the effect of load ratio, $R = K_{min}/K_{max}$. The Foreman expression for plane-stress conditions is

$$\frac{da}{dN} = \frac{c\,(\Delta K)^n}{(1 - R)\,K_c - \Delta K} \quad ,$$

where c and n are constants dependent on material and test conditions.

$\Delta K = (K_{max} - K_{min})$ during a load cycle.

K_c = plane stress fracture toughness of the material.

A comparison of Paris's and Foreman's equations was made by Hudson in Ref. 10 for 2024-T3 and 7075-T6 aluminum. It was found that the 7075-T6 data fell into an S shape or reflex type of curvature. A reflex curvature is also obtained from Foreman's equation; it is induced by ΔK approaching $(1 - R) K_c$ in the denominator. This intrinsic shape is the primary reason for the excellent fit of the data by using Foreman's equation. Paris's equation does not provide for this reflex curvature; consequently, the equation cannot fit the data at high or low growth rates as well as Foreman's equations.

The constant n in Foreman's equation is the slope of the curve in the straight-line midrange and c is determined from the substitution of data

value into the equation. It should be noted that n and c will change, depending on the type of plot used. Generally, a log-log plot of ΔK in psi $\sqrt{in}$. and da/dN in microinches/inch is used.

Foreman's equation for 2219-T87 is shown in Fig. E2-13 and some typical values of c and n for other common materials are given in Table E2-6.

Table E2-6. Crack Propagation Coefficients for Foreman's Equation

$$\frac{da}{dN} = \frac{c \, (\Delta K)^n}{(1 - R) K_c - \Delta K}$$

da/dN in./cycle

ΔK and K_c psi $\sqrt{in}$.

Material	Temp. (°F)	c	n	K_{Ic} psi $\sqrt{in}$
2219-T87	R.T.	1.4×10^{-11}	2.5	33,000
	300	1.5×10^{-11}	2.47	31,600
	-320	9.0×10^{-13}	2.7	36,200
TI-6Al-4V	R.T.	7.8×10^{-14}	3.0	81,000
2024-T3	R.T.	3.22×10^{-14}	3.38	
7075-T6	R.T.	2.13×10^{-13}	3.21	
517A(TI)				

The solution of the Foreman equation can be formulated as an initial-value problem and can be solved by direct numerical integration using the Runge-Kutta method. For most practical problems, an initial crack size is
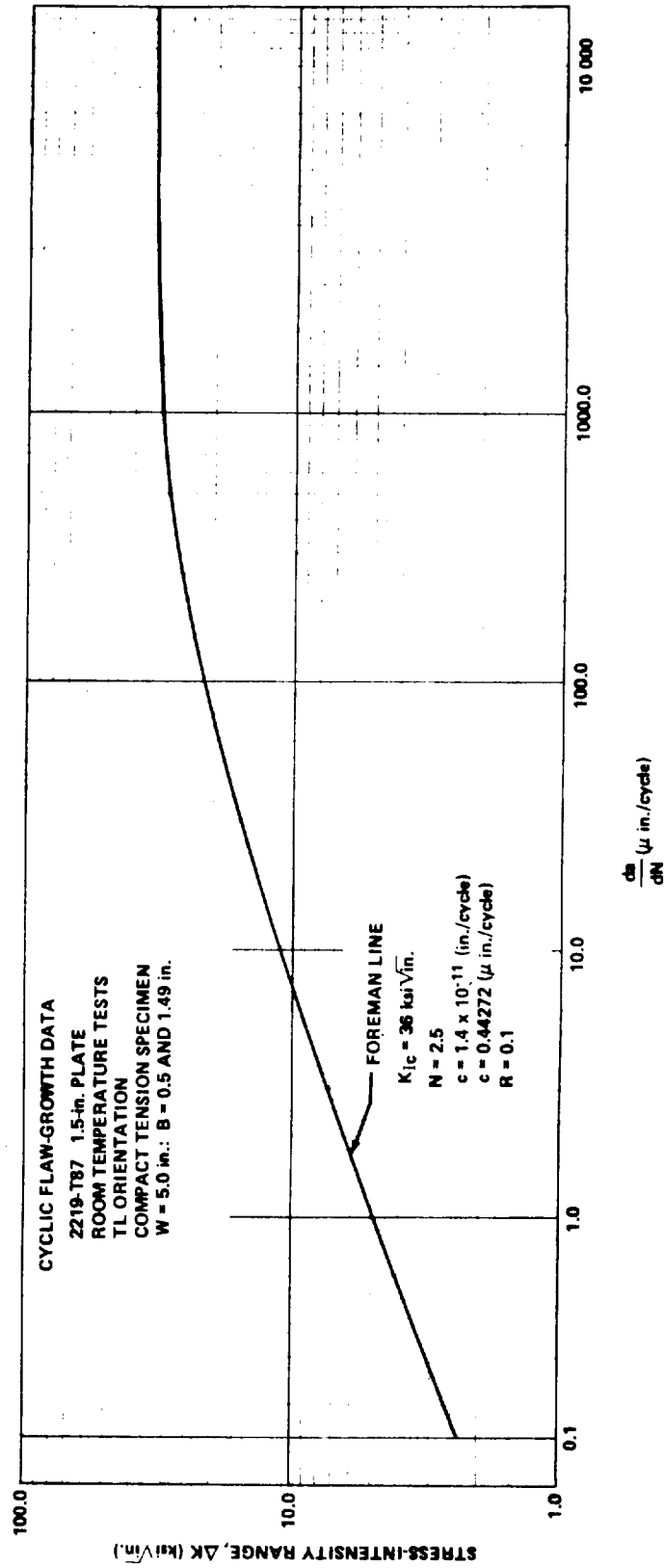
FIGURE E2-13. CRACK GROWTH VERSUS STRESS-INTENSITY FACTOR RANGE FOR 2219-T87

known at an initial value of N, such as N = 0. The problem is to determine the crack length (or additionally the stress-intensity factor) after a given number of cycles.

III. Tiffany.

An alternate approach to plane-strain flaw-growth rates has been presented by Tiffany (Ref. 11). Tiffany noted that the cyclic lives of specimens were primarily a function of the ratio of maximum initial stress intensity applied to the flaw during the first loading cycle (K_{Ii}) to the plane-strain fracture toughness of the material (K_{Ic}). Accordingly, cyclic life data were plotted on K_{Ii}/K_{Ic} versus cycles-to-failure graphs, where it was observed that data for particular test conditions and material-environment combinations could be reasonably represented by a unique curve. Flaw-growth rates were computed using the slopes of the cyclic life curves. Because the analysis required knowledge of only the initial and final conditions for each test, the Tiffany method was called an end-point analysis. The use of K_{Ii}/K_{Ic} versus cycles-to-failure curves for practical design problems is common in the aerospace industry (Ref. 12). Figure E2-14 shows a K_{Ii}/K_{Ic} versus cycles-to-failure curve for 2219-T87 at room temperature.

2.3.2.2 Crack Growth Retardation.

I. Wheeler's Retardation Parameter.

The retardation of crack growth is a phenomenon which occurs because of varying load levels. Retardation has been shown to occur particularly after a high level of load followed by a lower level of load.

Many papers have discussed crack growth retardation to some extent but a computational technique has not been presented which is sufficiently simple and accurate to gain widespread use (Ref. 13).
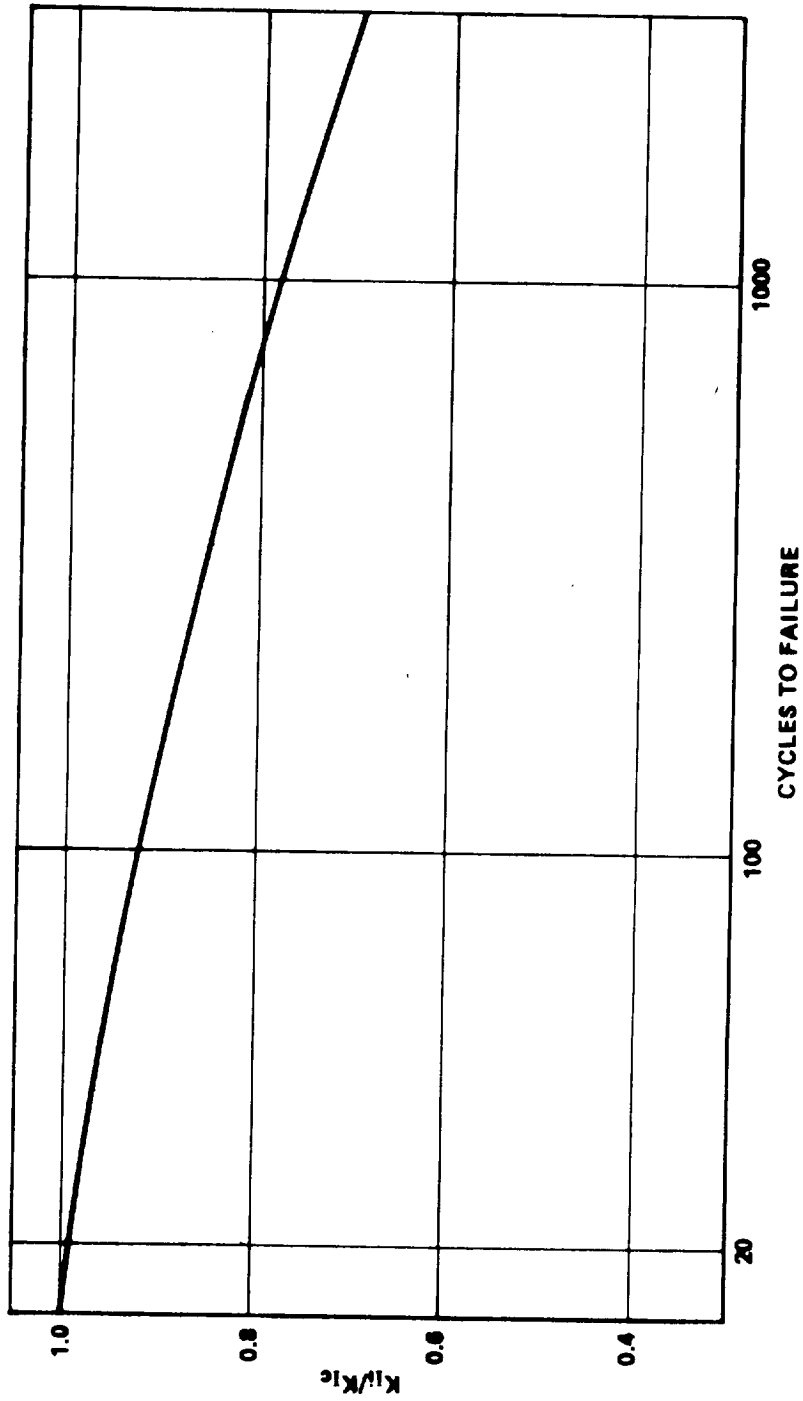
FIGURE E2-14. CYCLIC GROWTH RATE DATA FOR 2219-T87 AT ROOM TEMPERATURE

Wheeler (Ref. 13) suggests that more accurate crack growth predictions can be made by introducing a retardation parameter in the crack growth equation, which serves to delay the crack growth after a high load application. His equation for crack length is

$$a_r = a_o + \sum_{i=1}^{r} C_{pi} \, f(\Delta K_i) \quad ,$$

where a_r is the crack length after r load applications, a_o is the initial crack length, C_{pi} is the retardation parameter at i^{th} load, and ΔK_i is the change in the stress-intensity factor at i^{th} load. The retardation parameter is taken in the following form:

$$C_p = \left(\frac{R_y}{a_p - a} \right)^m \quad , \quad a + R_y < a_p \quad ,$$

$$C_p = 1 \quad , \quad \text{and} \quad a + R_y \geq a_p$$

where R_y is the extent of the current yield zone, $a_p - a$ is the distance from crack tip to elastic-plastic interface (Fig. E2-15), and m is the shaping exponent dependent upon material and test data.

This parameter has been used successfully to predict the growth of cracks in specimens subjected to six different spectra, having three different physical configurations, and made of two materials (Ref. 13). It is believed that this approach represents a useful improvement on the idea of linear cumulative crack growth, which can be used with confidence in design and analysis.
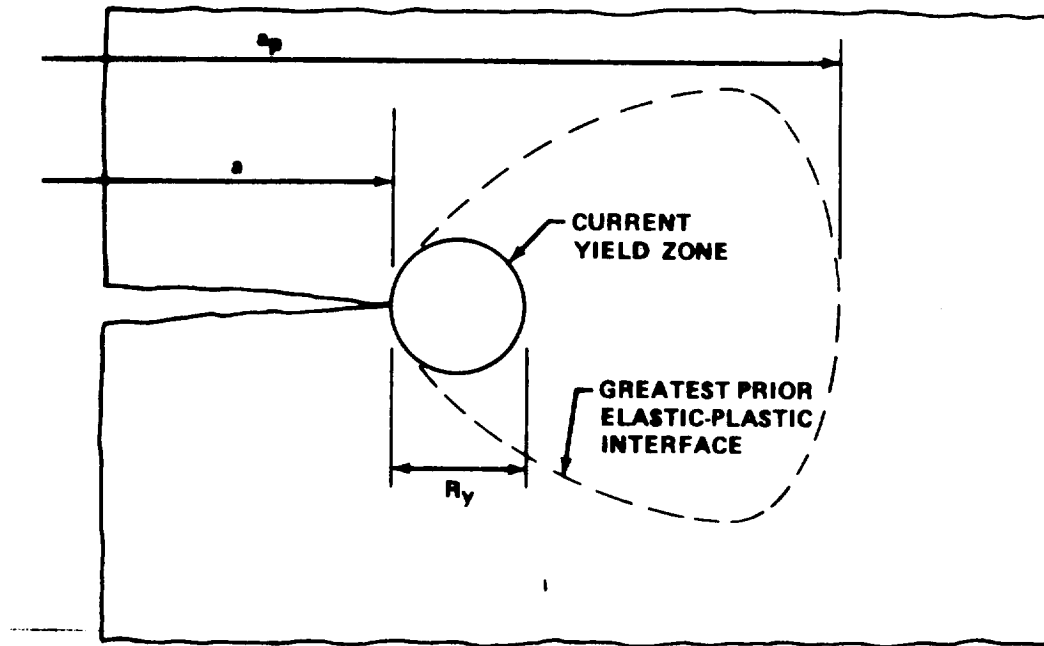
FIGURE E2-15.   CRACK TIP YIELD ZONES

The computational scheme for incorporating this retardation parameter in crack growth predictions requires that the crack be grown one load application at a time.   This amounts to a piecewise linearization of a highly nonlinear process.   The use of a high-speed digital computer is obviously required to perform any realistic analysis.   This technique has been incorporated into the computer program CRACKS (see the Computer Utilization Manual).

II.   The Significance of Fatigue Crack Closure.

Recent work by Elber (Refs. 14 and 15) has shown that fatigue cracks in sheets of aluminum alloy close before all tensile load is removed.   Significant compressive stresses are transmitted across the crack at zero load.   In previous work, usually the assumption has been made implicitly that a crack is closed under compressive loads and open under tensile loads.   The determination of the crack closure stress must, therefore, be a necessary step in the stress analysis of a cracked structure.

Elber (Ref. 15) obtains an empirical relation for the crack opening stress level and uses it as a basis for a crack propagation equation. The analysis of qualitative experiments on variable amplitude loading shows that the crack closure phenomenon could account for acceleration and retardation effects in crack propagation.

Crack closure stress can be explained by the existence of a zone of material behind the crack tip having residual tensile strains. In Fig. E2-16 a fatigue crack produced under constant amplitude loading is shown at three crack lengths. Figure E2-16a shows the crack tip surrounded by a plastic zone as it is represented normally. Figure E2-16b shows the crack at a greater crack length surrounded by a larger plastic zone because the stress intensity is higher. The plastic zone of Figure E2-16a has been retained to show that the material had been subjected previously to plastic deformations. Figure E2-16c represents the crack surrounded by the envelope of all zones which during crack growth had been subjected to plastic deformations. During a single cycle of crack growth, residual tensile deformations are left in the material behind the moving crack front, as only elastic recovery occurs after separation of the surfaces.
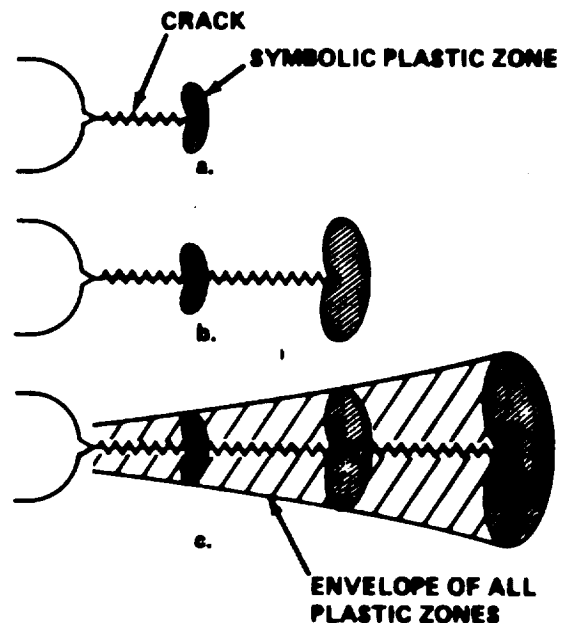
FIGURE E2-16. DEVELOPMENT OF A PLASTIC ZONE AROUND A FATIGUE CRACK

Crack propagation can occur only during that portion of the loading cycle in which the crack is fully open at the crack tip; therefore, in attempting to analytically predict crack propagation rates, it seems reasonable that the crack opening stress level should be used as a reference stress level from which an effective stress range could be obtained. The effective stress range is defined there as

$$\Delta S_{eff} = S_{max} - S_{op} \quad ,$$

where S_{op} is the crack opening stress.

An effective stress range ratio is then defined as

$$U = \frac{(S_{max} - S_{op})}{(S_{max} - S_{min})} = \frac{\Delta S_{eff}}{\Delta S} \quad .$$

Constant amplitude loading tests were conducted to establish the relationship between U and three variables which were anticipated to have a significant effect on U, namely, stress-intensity range, crack length, and stress ratio.

For the given range of testing conditions, only the stress ratio R is a significant variable. The relation between U and R is linear and can be expressed as

$$U = 0.5 + 0.4\,R \quad \text{where} \quad -0.1 < R < 0.7$$

for 2024-T3 aluminum alloy.

One of the most important problems in aircraft structures is the inability to predict accurately the rate of fatigue crack propagation under variable amplitude loading. In attempts to calculate these crack rates on the basis of constant amplitude data, interaction effects are usually ignored, leading to errors of significant magnitude.

Crack closure may be a significant factor in causing these interaction effects. This can be shown by the following example. Assume that a crack in 2024-T3 aluminum is propagating under the conditions $R = 0$ and $K_{max} = 20 \text{ MN/m}^{3/2}$. Under these conditions the crack opening level is at $K_{op} = 10 \text{ MN/m}^{3/2}$. If the stress-intensity range suddenly is halved, the new conditions are $K_{max} = 10 \text{ MN/m}^{3/2}$ and $R = 0$. The crack opening level, however, is still at $K_{op} = 10 \text{ MN/m}^{3/2}$, equal to the new peak stress intensity, so the crack does not open. Therefore, the crack does not propagate until the crack opening level changes. The behavior of the crack opening stress level under variable amplitude loading must therefore be investigated.

It has been observed that a crack will continue to grow for some time after a high load application followed by loads of smaller magnitude. This has been termed delayed retardation. Such retardation of crack growth after a single high load can be explained by examining the behavior of the large plastic zone left by the high-load cycle ahead of the crack tip. The elastic material surrounding this plastic zone acts like a clamp on this zone, causing the compressive residual stresses. As long as this plastic zone is ahead of the crack tip, this clamping action does not influence the crack opening. As the crack propagates into the plastic zone, the clamping action will act on the new fracture surfaces. This clamping action, which builds up as the crack propagates into the plastic zone, requires a larger, externally applied stress to open the crack; hence, the crack will propagate at a decreasing rate into this zone and may come to a standstill.

2.3.2.3   Transition from Partial-Thickness Cracks to Through-Thickness Cracks.

It was shown in Section 2.2 that the stress intensity was different for partial-thickness cracks and for through-the-thickness cracks. Also, for through-the-thickness cracks, corrections must be made for a finite plate within the stress intensity equation (Table E2-2, Case 13).

Often in crack propagation problems a crack will initially be a partial-thickness crack and will grow until it extends through the thickness. When this occurs, corrections in the stress-intensity expression must be made.

The transition from a surface flaw to a through crack is chosen to be the point when the plastic zone reaches the back face of the material. The value of a (crack length) for which this occurs is given as

$$a_t = t - \frac{1}{2\pi} \left(\frac{K_{max}}{\sigma_{ys}} \right)^2 \quad .$$

2.3.3   Combined Cyclic and Sustained Flaw Growth.

Tiffany and Masters (Ref 1) hypothesized that below the sustained stress threshold stress-intensity value (K_{TH}), cyclic speed (or hold time at maximum load) probably would not affect the cyclic flaw growth rate, but above K_{TH} it could have a large effect. In other words, the minimum cyclic life was limited to the number of cycles required to increase the initial stress intensity K_{Ii} to the K_{TH} value, and above the K_{TH} level, failure could occur in one additional cycle if the hold time were sufficiently long.

To date there is only a limited amount of experimental data to substantiate this prediction. However, the data do tend to support the original Tiffany-Masters hypothesis of no significant effect of cyclic speed on flaw growth rates below the sustained stress threshold stress intensity.

2.4 APPLICATION OF FRACTURE MECHANICS TECHNOLOGY.

2.4.1 Selection of Materials.

In the material selection and design of a tension-loaded structure, such as a pressure vessel, the following questions must be considered:

1. What are the critical flaw sizes (sizes which cause failure) in the different parts of the structure at expected operational stress levels?

2. What are the maximum initial flaw sizes likely to exist in the structure before service?

3. Will these initial flaws grow to critical size and cause failure during the expected service life of the structure?

The answers to these questions depend heavily upon the inherent fracture toughness and subcritical flaw-growth characteristics of the structural material. Fracture toughness data derived from test specimens are used in fracture mechanics analysis to predict critical flaw sizes, evaluate subcritical flaw growth, and estimate structural life. They can also be used to determine the maximum possible initial flaw size in a structure after a proof load.

As previously mentioned (Section 2.2), the types of flaws encountered in fabricated structures can be categorized as surface flaws, embedded flaws, and through-the-thickness cracks. For surface and embedded flaws, the degree of constraint at the crack leading edge is high, and plane-strain conditions generally prevail. The initial flaws may or may not reach critical size before growing through the thickness, depending upon the plane-strain fracture toughness (K_{Ic}) value, the applied stress levels, and the material thickness. If the calculated critical flaw size is small with respect to the wall thickness, the formation of a through-the-thickness crack before fracture is not likely.

For through-the-thickness cracks, the mode of fracture for a given material, stress level, and test temperature depends upon the material thickness. If the material is relatively thin, plane-stress conditions generally predominate. With increasing thickness, the fracture appearance changes from that of full shear to an essentially flat or plane-strain fracture. Thus, for thin sections containing through-the-thickness cracks, the plane-stress fracture thoughness (K_c) values are important, and as the thickness is increased the plane-strain (K_{Ic}) values should be used. The theory of this has been discussed in detail (Section 2.2.2).

The common types of fracture specimens and their requirements have also been discussed (Section 2.2.3). It is appropriate to point out the significance of end-hardware application and material anisotropy on specimen selection and to show fracture-toughness correlations among several of the more common specimens.

Just as conventional mechanical properties generally vary to some degree among various forms and grain directions in a given basic alloy, it has been found from fracture tests performed thus far on various materials that fracture toughness values also vary. In a rolled plate or forging, six directions of flaw propagation are possible, and plane-strain toughness (K_{Ic}) values may differ in each of these directions (Fig. E2-17). The need to determine the K_{Ic} values in each of these directions depends on the direction of the applied stresses in the hardware.

Considering the banding and delamination problems in some thick plates, it appears that the K_{Ic} values can be different between the A and B directions and, likewise, the C and D directions. This has actually been found to be the case from investigation (Ref. 16) and tends to explain the differences in K_{Ic} values obtained using surface-flawed and round-notched-bar or single-edge-notched fracture specimens. The surface-flawed specimen

LONGITUDINAL*

LONG TRANSVERSE*

E

F FORWARD

OUTBOARD

C

UP

D FORWARD

A

UP

B

OUTBOARD

UP

FORWARD

OUTBOARD

SHORT
TRANSVERSE*
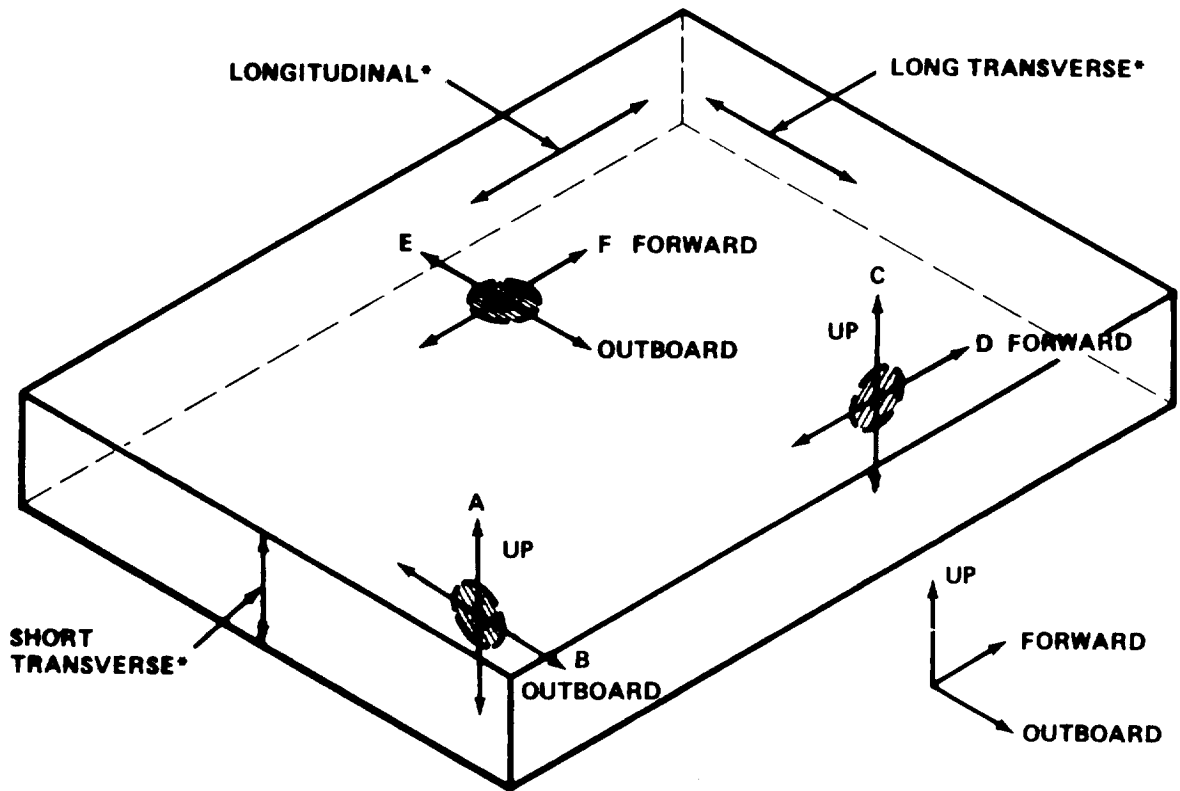
A - F: DIRECTIONS OF FLAW PROPAGATION

*GRAIN DIRECTION

FIGURE E2-17. STRESS FIELD, GRAIN DIRECTIONS, AND
POSSIBLE DIRECTIONS OF FLAW PROPAGATION

is normally used to measure toughness in either the A or C directions, and
the single-edge-notched or center-cracked (pop-in) specimens measure
toughness in the B or D directions. The round notched bar (removed so
that its longitudinal axis is parallel to the plate surface) measures the lower
of either the A or B directions or the lower of either the C or D direc-
tions. For material where there are no pronounced directional effects, the
same toughness should be obtained regardless of which specimen is used.
In the short transverse direction of materials, there appears to be no reason
for a significant difference in K_{Ic} values between the E and F directions,
although there is no apparent experimental substantiation of this.

For weldments, it is known that there can be differences in fracture toughness between the weld centerline and the heat-affected zone. In addition, it is considered probable that fracture toughness as well as subcritical flaw growth characteristics vary within the heat-affected zone so that for the establishment of realistic allowable flaw sizes, the minimum K_{Ic} values must be determined.

The foregoing discussion makes clear the necessity for insuring the use of comparable valid fracture toughness and subcritical flaw growth data when they are available, or the selection of proper specimen types to obtain the desired directional data, in comparing materials for selection. While round-notched-bar specimens might be considered desirable because they automatically obtain the lower toughness values in either the A or B directions or the lower in either the C or D directions, it may not always be possible to use the specimen type because of material thickness limitations (i.e., the required specimen diameter for valid K_{Ic} exceeds the hardware wall thickness). In such a case, the single-edge-notched specimen might be used for toughness in the B and D directions and the surface-flawed specimen in the A and C directions.

In summary, it presently appears that there is no single "best fracture specimen" to use in all situations where toughness data are needed for material comparisons and selection, nor is such required. Of primary importance is that the selected specimen toughness data for different materials provide a valid comparison for selection and be representative of toughness and flaw growth characteristics of the material as used in the hardware application.

2.4.1.1 Static Loading.

An evaluation of the resistance of materials to catastrophic brittle fracture requires the following basic material properties:

1. Plane-strain fracture toughness, K_{Ic}.

2. Conventional tensile yield strength, σ_{ys}.

An evaluation of materials based on the data accumulated from test specimens can be illustrated best by using a hypothetical example.

I. Example Problem A.

Three materials — a steel, a titanium, and an aluminum alloy — are initially selected as potential candidate materials for minimum weight design. The yield strength of each is chosen to attain nearly equivalent strength/weight ratios. The yield strengths and K_{Ic} values obtained from the tested specimens and design requirement are shown in the following table.

Alloy	Density (lb/in.^{3})	σ_{ys} (ksi)	σ_{ys}/Density $\times$ 1000 (in.)	K_{Ic}, (ksi $\sqrt{in.}$)	Applied Stress $1/2\,\sigma_{ys}$ (ksi)
Steel	0.284	250	880	100	125
Aluminum	0.098	85	870	30	42.5
Titanium	0.163	140	860	80	70

Assume that

1. The defect is a semielliptical surface flaw with $a/2c = 0.2$.

2. The defect is located in a thick plate loaded in tension.

To decide which material provides the most fracture resistance is to establish which material requires the largest critical flaw size for catastrophic fracture.

For "thick walled" structures critical flaw sizes can be determined from the following equation:

$$(a/Q)_{cr} = \frac{1}{1.21\pi} \left(\frac{K_{Ic}}{\sigma} \right)^2$$

or

$$a_{cr} = \frac{Q}{1.21\pi} \left(\frac{K_{Ic}}{\sigma} \right)^2$$

where the shape factor parameter can be obtained from Fig. E2-5. For this comparison, $Q = 1.26$.

The results are shown in the following table.

Alloy	Depth, a_{cr} (in.)	Length, 2c (in.)
Steel	0.212	1.06
Aluminum	0.165	0.83
Titanium	0.432	2.16

Conclusion.

The titanium alloy is most fracture resistant in terms of requiring the largest critical flaw size defect, a_{cr}, for catastrophic fracture.

This conclusion could have been reached by considering the K_{Ic}/σ_{ys} ratios for the various materials shown in the following table.

Alloy	K_{Ic}/σ_{ys} ($\sqrt{in.}$)
Steel	0.400
Aluminum	0.353
Titanium	0.572

The titanium, having the highest K_{Ic}/σ_{ys} ratio, could be expected to be the toughest material for the given application.

Tiffany and Masters (Ref. 17) showed that for screening several materials, K_{Ic} data are often plotted as shown in Fig. E2-18a. Recognizing that the operating stress levels are generally controlled to a fixed percentage of the unflawed tensile strength by the design safety factor, the data shown in Fig. E2-18a might be more appropriately plotted as shown in Fig. E2-18b. The ordinate is directly proportional to the critical flaw size, thus placing the influence of varying materials strength in better perspective. From Fig. E2-18b the three materials can be compared upon the basis of equal critical flaw size. For example, structures designed from a 200-ksi steel, a 135-ksi titanium, and a 70-ksi aluminum would all have approximately the same critical flaw size. Considering the effect of weight, one might wish to make the comparison shown in Fig. E2-18c. This shows that titanium provides a somewhat lighter tank on the basis of equal flaw size.

Based on considerations of the practical capability of available nondestructive inspection (NDI) techniques, the resistance to catastrophic fracture could also be evaluated by calculating the maximum allowable applied stress for equivalent defects in each material.

Reevaluate the preceding example, assuming that the minimum detectable flaw is 0.15 in. deep by 0.75 in. long.

Rearranging the basic equation results in

$$\sigma^2 = \frac{K_{Ic}^2 \, (Q)}{1.21\pi \, (a)} \quad .$$

The resulting critical fracture stresses and other pertinent information are summarized in the following table.
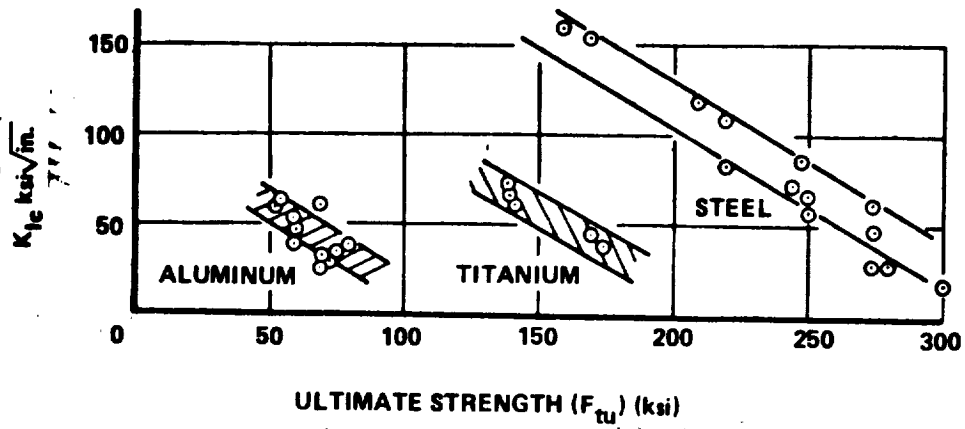
a.
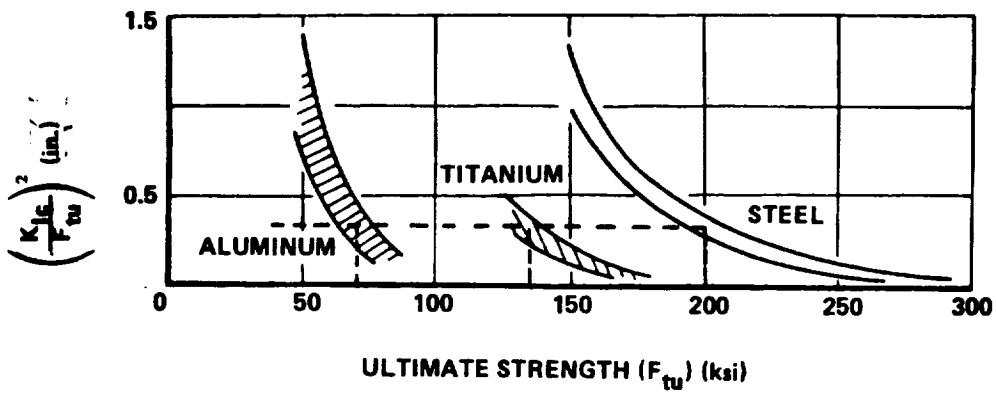
b.
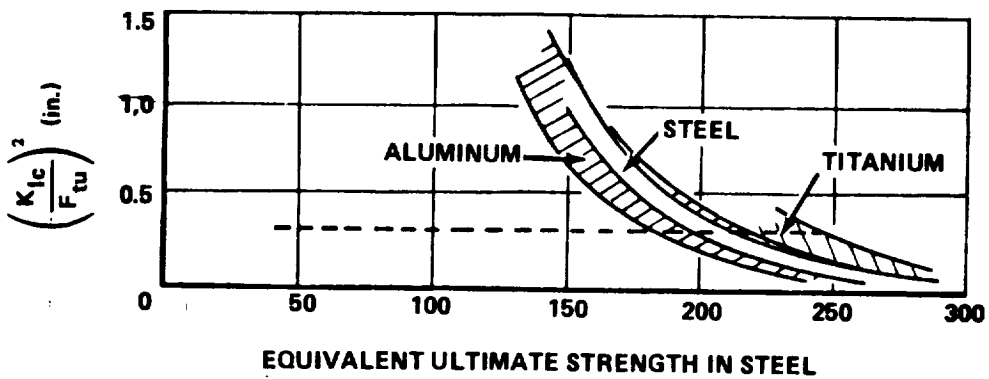
c.

FIGURE E2-18. MATERIAL COMPARISONS (BASE METAL,
ROOM-TEMPERATURE TRENDS)

Alloy	σ_{ys} (ksi)	Design Stress $0.5\,\sigma_{ys}$ (ksi)	Fracture Stress σ (ksi)	Safety Factor $\sigma/0.5\,\sigma_{ys}$
Steel	250	125	144	1.15
Aluminum	85	42.5	43	1.01
Titanium	140	70	112	1.60

From the above data it is apparent that the titanium provided the greatest safety factor and resistance to fracture.

2.4.1.2   Cyclic or Sustained Loading.

An evaluation of the resistance of materials to fracture requires the consideration of the crack growth rate characteristics in addition to other material properties.

Some examples of data obtained from tests are shown in Figs. E2-19 and E2-20 (Ref. 18).   The realistic and practical approach for comparing materials is to evaluate their crack growth characteristics under a given application condition.   Let us consider the following hypothetical example.

I.   Example Problem A.

1.   Materials to be considered are the steel and aluminum alloys for which the data are given in Figs. E2-19 and E2-20.

2.   The component of interest is a thick plate cyclic loaded in tension under stresses that vary from zero to maximum tension during each cycle.

3.   The design fixes σ_{max} as one-half the yield strength for each material: 88 ksi for steel and 32 ksi for aluminum.

4.   The worst possible type of flaw that is envisioned is a semi-elliptical surface flaw with $a/2c = 0.20$.
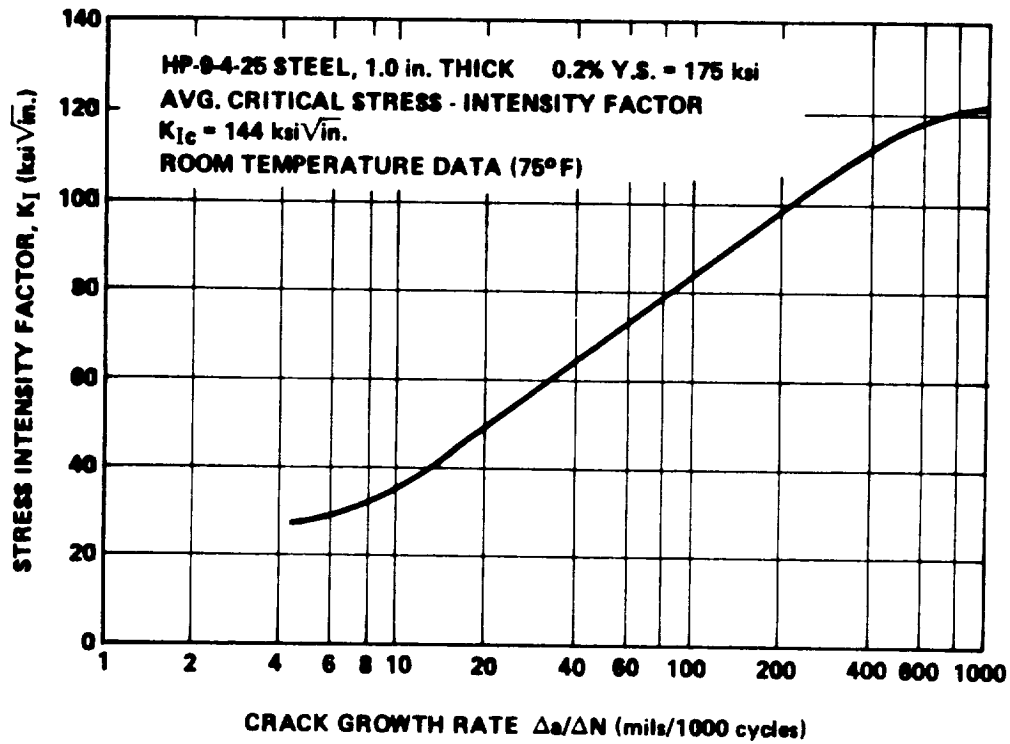
FIGURE E2-19.   CRACK GROWTH RATE FOR HP-9-4-25 STEEL
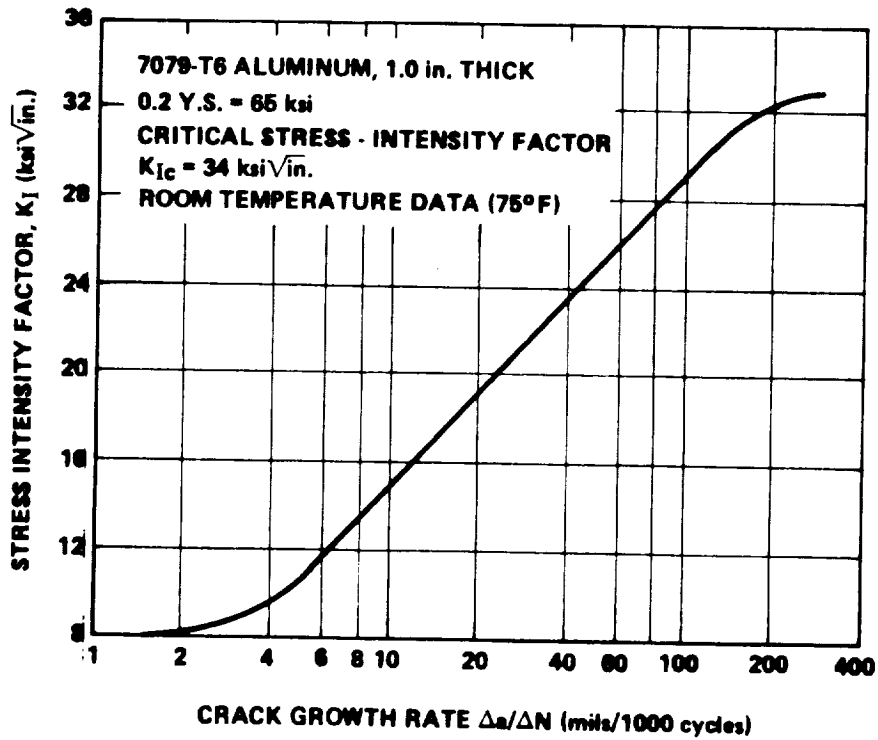
FIGURE E2-20.   CRACK GROWTH RATE FOR 7079-T6 ALUMINUM

5. The minimum size flaw that could be detected by the NDI technique is 0.15 in. deep by 0.72 in. long. Therefore, each material is assumed to contain this flaw.

Under these circumstances, which material has the longest life?

Solution.

Step 1. The first step is to compute the value of the initial stress intensity, K_{Ii}, for each material for the prevailing conditions of defect size and stress. The appropriate expression for K_{Ii} for the stipulated defect and component geometry is

$$K_{Ii}^2 = \frac{1.21 \, \pi a \, \sigma^2}{Q}$$

where

a = crack = 0.15 in. = specified,

= applied stress (maximum during cycle) = $1/2 \, \sigma_{ys}$ each materia',
steel = 88 ksi, aluminum = 32 ksi,

σ_{ys} = yield strength, steel = 175 ksi, aluminum = 65 ksi,

and

Q = 1.26 for specified flaw geometry.

The calculations reveal the following:

$$K_{Ii}^2 = \frac{1.21 \, \pi \, (0.15) \, (88\,000)^2}{1.26}$$

and

$$K_{Ii} = 59\,000 \text{ psi } \sqrt{\text{in.}}$$

for steel, and

$$K_{Ii}^2 = \frac{1.21\,\pi\,(0.15)\,(32\,000)^2}{1.26}$$

and

$$K_{Ii} = 21\,500 \text{ psi } \sqrt{\text{in.}}$$

for aluminum.

The crack growth rates for the two materials at the beginning of life can now be determined from Figs. E2-19 and E2-20 using their respective K_I values for the imposed conditions. The results are shown in the following table.

Alloy	K_I (psi $\sqrt{\text{in.}}$)	Crack Growth Rates (mils/cycle)
Steel	59 000	0.035
Aluminum	21 500	0.030

However, a knowledge of the crack growth rates at the beginning of life is not sufficient to determine the respective life expectancy of each material. One must consider the change in K_I and the associated change in crack growth rates for each material as the crack grows during service as well as the threshold stress intensity, K_{TH}.

Step 2. The growth rate data illustrated in the form shown in Figs. E2-21 and E2-22 (Ref. 18) provide a convenient method for evaluating the life expectancy without becoming intimately involved with changes in K_I and growth rates. Figures E2-21 and E2-22 are constructed from the same basic test data as were used to construct Figs. E2-19 and E2-20. To utilize Figs. E2-21 and E2-22 it is necessary to know the ratio of K_{Ii} to K_{Ic}. The previous calculations in Step 1 showed that K_I is 59 ksi $\sqrt{in.}$ for steel and 21.5 ksi $\sqrt{in.}$ for aluminum. Since the K_{Ic} values for each material were known from static toughness tests, the K_{Ii}/K_{Ic} ratios are readily determined:

$$\frac{K_{Ii}}{K_{Ic}} = \frac{59\ 000}{144\ 000} = 0.41$$

for steel, and

$$\frac{K_{Ii}}{K_{Ic}} = \frac{21\ 500}{34\ 000} = 0.63$$

for aluminum.

The cyclic life corresponding to these K_{Ii}/K_{Ic} values may be determined directly from Figs. E2-21 and E2-22 — steel, 1800 cycles, and aluminum, 4000 cycles, if the time at maximum stress is short during each cycle.

Thus, for this specific example where both materials contained the same given size and type of defect and both were stressed to one-half their yield strengths, the aluminum has the greatest life expectancy.

It should be emphasized that the result of this example cannot be used to generalize the relative behavior of the two materials. For other conditions of initial defect sizes and/or applied stresses, it is possible that the steel
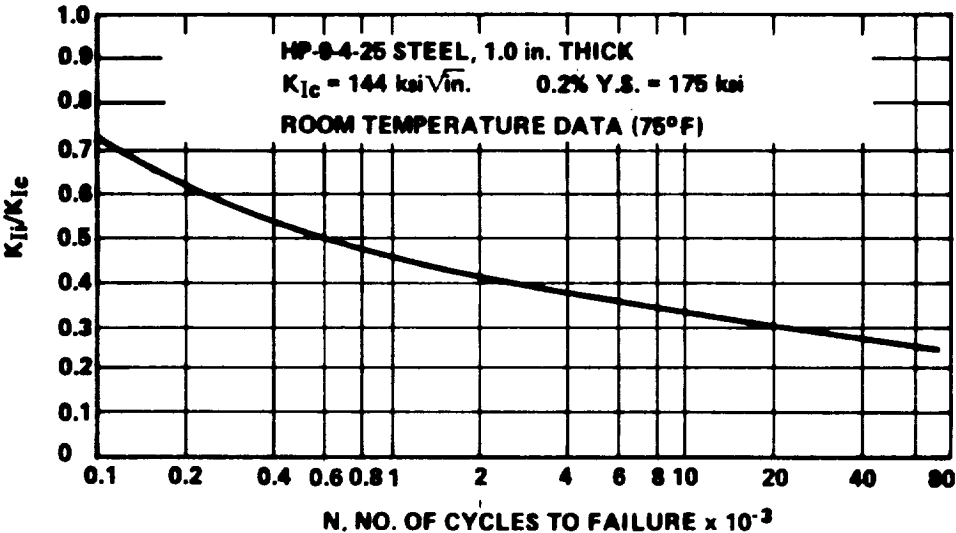
FIGURE E2-21.   COMBINED CYCLIC FLAW GROWTH DATA FOR
HP-9-4-25 STEEL PLATE
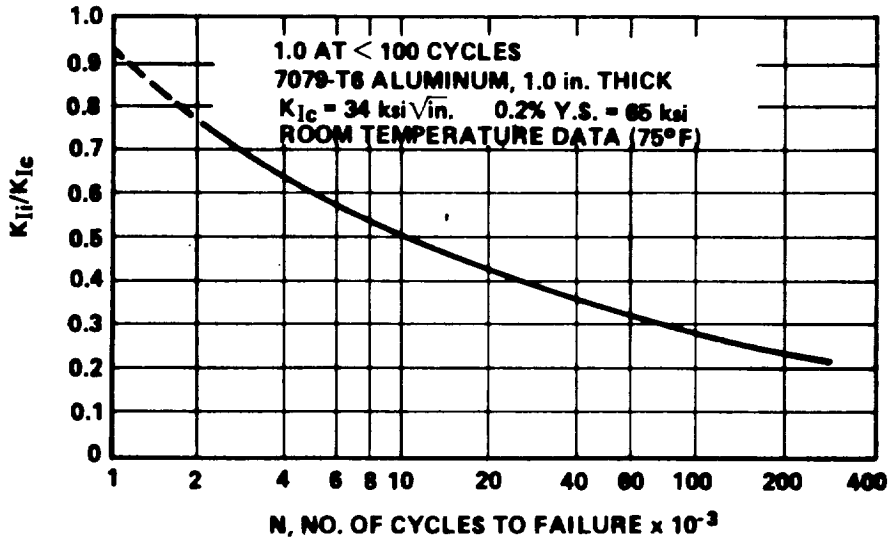
FIGURE E2-22.   COMBINED CYCLIC FLAW GROWTH DATA FOR
7079-T6 ALUMINUM PLATE

could have the greater life expectancy. This is demonstrated in the following table, which shows the life expectancy of the two materials for a wide range of initial defect sizes and for a constant applied stress of $\sigma_{ys}/2$.

Initial Defect Depth a_i (in.)	Initial Stress–Intensity Factor K_{Ii} (ksi $\sqrt{in.}$)		$\dfrac{K_{Ii}}{K_{Ic}}$		Cycles to Failure N (Life Expectancy)	
	Steel	Aluminum	Steel	Aluminum	Steel	Aluminum
0.05	19.6	7.2	0.136	0.210	>>300 × 10³	300 × 10³
0.07	27.5	10.1	0.191	0.297	>100 × 10³	100 × 10³
0.10	39.4	14.3	0.274	0.420	30 × 10³	21 × 10³
0.15	59.0	21.5	0.410	0.632	1.8 × 10³	4 × 10³
0.20	78.8	28.7	0.540	0.845	0.37 × 10³	1.5 × 10³
0.25	98.4	35.9	0.683	>1.0	0.25 × 10³	---

From the table it is seen that when the initial defect depth is 0.15 in. or larger, the aluminum will have the longer life N. However, when the initial defect depth is 0.10 in. or smaller, the steel will have the greater life expectancy. Although the steel has the larger absolute value of fracture toughness, K_{Ic}, and therefore has the largest critical crack size for catastrophic failure, it also has a greater crack growth rate for a given change in K as seen from the differences in slope of the growth rate curves shown in Figs. E2-23 and E2-24 (Ref. 18). Therefore, it is possible to have a "crossover" situation between the life expectancies of steel and aluminum, as noted in the table.

Again, the life expectancies in preceding table reflect short time at maximum cyclic stress. If the time at maximum stress is long, the portion of time that the stress-intensity level is above the threshold stress intensities
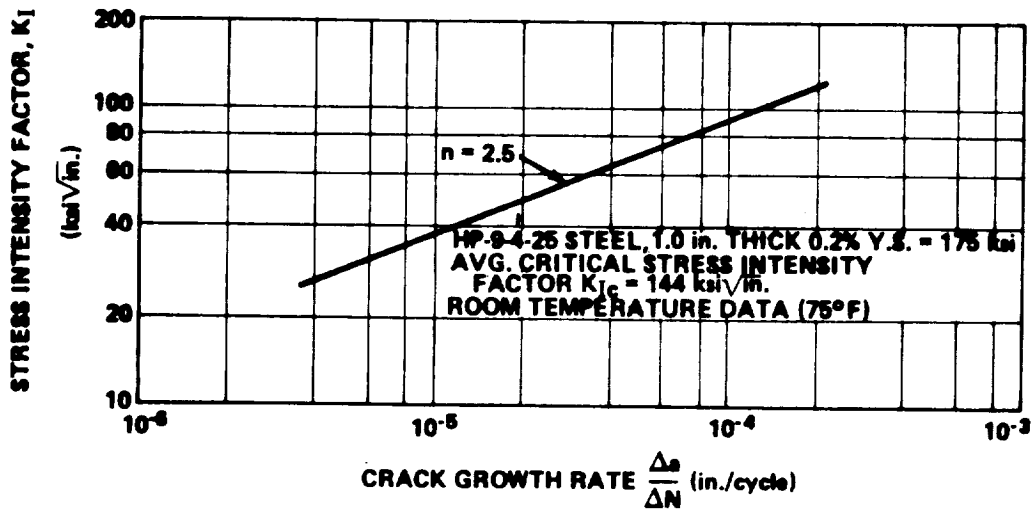
FIGURE E2-23. CRACK GROWTH RATE AS A FUNCTION OF STRESS
INTENSITY FOR HP-9-4-25 STEEL
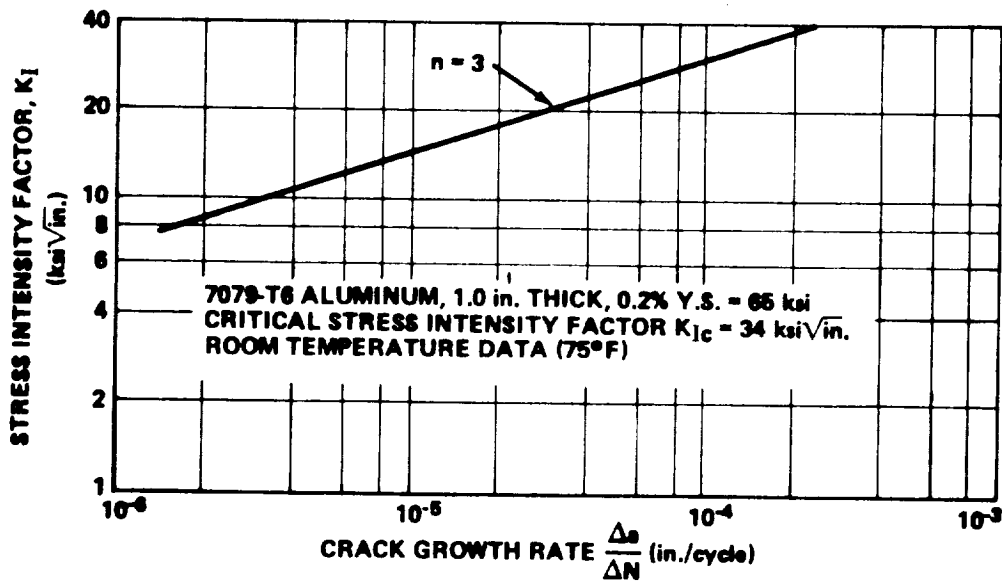
FIGURE E2-24. CRACK GROWTH RATE AS A FUNCTION OF STRESS
INTENSITY FOR 7079-T6 ALUMINUM

for the steel and aluminum would cause reductions in the cyclic lives for the different initial defect sizes.

The materials could also be compared in another manner by using the data provided in Figs. E2-21 and E2-22 to answer the question of which material could tolerate the largest initial defect (of a given type) that would not grow to a critical size during some given minimum lifetime for the component.

II.   Example Problem B.

Known Information:

Plate cyclic loaded (sinusoidal) in tension.

Required life — 50 000 cycles.

Applied stress (maximum stress during cycle) one-half yield strength:

steel = 88 000 psi.

aluminum = 32 000 psi.

Type of defect — semielliptical surface flaw with $a/c = 0.4$.

Fracture toughness, K_{Ic}:
steel = 144 000 psi $\sqrt{in.}$
aluminum = 34 000 psi $\sqrt{in.}$

Unknown Information: Which material can tolerate the largest initial defect?

Solution.

Step 1.   From Figs. E2-21 and E2-22, find the K_{Ii}/K_{Ic} ratio corresponding to the desired life of 50 000 cycles:

$$\frac{K_{Ii}}{K_{Ic}} \text{ at } 50\ 000 \text{ cycles} = 0.25$$

for steel, and

$$\frac{K_{Ii}}{K_{Ic}} \text{ at 50 000 cycles } = 0.34$$

for aluminum.

Step 2. Knowing the K_{Ic} and K_{Ii}/K_{Ic} ratio corresponding to 50 000 cycles, solve for K_{Ii}:

$$K_{Ii} = 0.25 \ K_{Ic} = 0.25 \ (144\ 000 \text{ psi} \sqrt{\text{in.}}) = 36\ 000 \text{ psi} \sqrt{\text{in.}}$$

for steel, and

$$K_{Ii} = 0.34 \ K_{Ic} = 0.34 \ (34\ 000 \text{ psi} \sqrt{\text{in.}}) = 11\ 500 \text{ psi} \sqrt{\text{in.}}$$

for aluminum.

Step 3. Since K_{Ii} depends upon stress and defect size, it is now possible to solve for defect size knowing stress. For semielliptical surface defects with $a/c = 0.4$, the following expression is appropriate:

$$a_i = \frac{K_{Ii}^2 \ (Q)}{1.21 \ \pi \ \sigma^2} \quad ;$$

for steel,

$$a_i = \frac{(36\ 000)^2 \ (1.26)}{1.21 \ \pi \ (88\ 000)^2}$$

and

$$a_i = 0.056 \text{ in.}$$

when the defect is 0.056 in. deep by 0.28 in. long; for aluminum,

$$a_i = \frac{(11\ 500)^2\ (1.26)}{1.21\ \pi\ (32\ 000)^2}$$

and

$$a_i = 0.043 \text{ in.}$$

when the defect is 0.043 in. deep by 0.215 in. long.

Thus, it is apparent that for the condition imposed, the steel could tolerate a slightly larger initial defect than could the aluminum. Since the difference in the maximum allowable initial defect size is not great, the ultimate choice of a material for this situation may depend more heavily on other comparative factors, i.e., the applicability and capability of NDI techniques, the type and size of insidious defects as related to the maximum allowable initial defect size, availability, ease of fabrication, costs, etc.

2.4.2   Predicting Critical Flaw Sizes.

As mentioned in Section 2.2.3, plane-strain stress intensity (K_{Ic}) values can be obtained from several types of specimens. With valid data for a given material form, heat treatment, test temperature, and environment, critical flaw sizes can be calculated for given hardware operating stresses. The engineering usefulness of the basic stress-intensity concept in the prediction of critical flaw sizes and the use of a/Q to describe flaw size has

been supported by a number of hardware correlations, some of which are shown in Refs. 17 and 19. Comparisons between measured critical flaw sizes on test hardware and predicted critical flaw sizes based on test specimen plane-strain toughness data have shown good correlation.

From the equation shown in Fig. E2-6, it is apparent that critical flaw size is equally as dependent on applied stress as on the material fracture toughness. The following sections show approaches for calculating critical flaw sizes for the three basic types of initial flaws (surface, embedded, or through-the-thickness) based on the appropriate fracture toughness values measured from valid specimen tests.

2.4.2.1 Surface Cracks.

Calculations for surface flaws can be carried out by rearranging the stress-intensity equation developed by Irwin (Section 2.2.1),

$$\left(a/Q\right)_{cr} = \frac{1}{1.21\pi} \left(\frac{K_{Ic}}{\sigma}\right)^2$$

for a "thick-walled" structure (i.e., flaw depth less than half of the material thickness) where K_{Ic} is the plane-strain fracture toughness obtained from fracture toughness specimen tests, σ is the applied stress in structure normal to the plane of flaw, a_{cr} is the critical flaw depth, Q is the flaw shape parameter (obtained from Fig. E2-5), and $\left(a/Q\right)_{cr}$ is critical flaw size.

Since the flaw size is an unknown quantity, it is necessary to assume a flaw aspect ratio, $a/2c$, to determine Q. Using the preceding equation, the critical flaw depth, a_{cr}, can be determined for a specific value of σ and K_{Ic}.

I. **Example Problem A.**

Aluminum alloy 2219-T87 is selected as the material for use in a 20-in.-diam spherical gas bottle. The bottle is to operate at 4000 psig and be stored in a liquid-nitrogen propellant tank.

What is the critical flaw size?

A. Assumptions.

1. The defect is a semielliptical surface flaw with $a/2c = 0.2$.

2. The operating stress is $\sigma = 80$ percent (yield strength of the material).

B. Solution.

The yield strength and I_{Ic} values obtained from the tested specimens are as follows:

$$\sigma_{ys} = 60 \text{ ksi}$$

and

$$K_{Ic} = 37 \text{ ksi} \sqrt{\text{in.}} \quad .$$

The operating stress is

$$\sigma = 0.80 \left(\sigma_{ys}\right) = 0.80 \, (60) = 48 \text{ ksi} \quad .$$

The wall thickness required is

$$t_{req} = \frac{PR}{2\sigma} = \frac{(4000) \, (10)}{(2) \, (48 \, 000)} = 0.417 \text{ in.} \quad .$$

For thick-walled structures,

$$a_{cr} = \frac{Q}{1.21\,\pi} \left(\frac{K_{Ic}}{\sigma}\right)^2 \quad ,$$

where the shape parameter Q can be found from Fig. E2-5. For this problem $Q = 1.18$; then

$$a_{cr} = \frac{1.18}{1.21\,(\pi)} \left(\frac{37}{48}\right)^2 = 0.184 \text{ in.}$$

and

$$2c = a/0.20 = 0.184/0.2 = 0.92 \text{ in.} \quad .$$

For surface flaws that are deep with respect to material thickness, the flaw magnification factor, M_k, can be applied to give a more accurate critical flaw size,

$$(a/Q)_{cr} = \frac{1}{1.21\,\pi} \left(\frac{K_{Ic}}{M_k\sigma}\right)^2 \quad ,$$

for thin-walled structures.

II.   Example Problem B.

Use the same design that was shown in Example Problem A except that the spherical diameter of the bottle is 15 in. The wall thickness required is

$$t_{req} = \frac{PR}{2\sigma} = \frac{4000\,(7.5)}{2\,(48\,000)} = 0.313 \text{ in.}$$

For thin-walled structures,

$$a_{cr} = \frac{Q}{1.21 \, \pi} \left(\frac{K_{Ic}}{M_k \sigma} \right)^2 \quad .$$

Flaw magnification factors, M_k, for the 2219-T87 aluminum are available from Fig. E2-8. Since the critical flaw depth, a_{cr}, is unknown, a "trial-and-error" iterative solution is necessary to determine the magnification factor corresponding to the critical flaw depth.

Without a magnification factor, $a_{cr} = 0.184$ in. (Example Problem A).

For $a/t = 0.184/0.313 = 0.59$, $M_k = 1.21$,

$$a_{cr} = \frac{1.18}{1.21 \, \pi} \left[\frac{37}{1.21 \, (48)} \right]^2 = 0.126 \text{ in.} < 0.184 \text{ in.} \quad .$$

Take an average $a = \dfrac{0.184 + 0.126}{2} = 0.155$ in.

For $a/t = 0.155/0.313 = 0.50$, $M_k = 1.15$,

$$a_{cr} = \frac{1.18}{1.21 \, \pi} \left[\frac{37}{1.15 \, (48)} \right]^2 = 0.139 \text{ in.} < 0.155 \text{ in.} \quad .$$

Take an average $a = \dfrac{0.155 + 0.139}{2} = 0.147$ in.

For $a/t = 0.147/0.313 = 0.47$, $M_k = 1.13$,

$$a_{cr} = \frac{1.18}{1.21 \, \pi} \left[\frac{37}{1.13 \, (48)} \right]^2 = 0.144 \approx 0.147 \text{ in.} \quad .$$

Further reiteration will provide more accuracy if desired.

If adequate flaw magnification values are not available for a particular material, a reasonable estimate for M_k is the approximate Kobayashi solution shown in Fig. E2-25. However, it should be understood that its use can result in somewhat conservative answers for more ductile materials and perhaps unconservative answers for more brittle materials.

2.4.2.2 Embedded Flaws.

The calculations for embedded flaws in thick-walled structures will be the same as for surface flaws except that a_{cr} is the one-half critical flaw depth of the embedded flaw, and the correction factor of 1.21 for the effect on stress intensity of the stress-free surface (Section 2.2.1) is eliminated. Thus the equation for one-half critical internal flaw size is

$$(a/Q)_{cr} = \left(\frac{1}{\pi} \frac{K_{Ic}}{\sigma}\right)^2 .$$

Although flaw magnification effects have been studied for deep surface flaws, apparently no similar research has been done for internal flaws with large flaw-depth-to-material-thickness ratios. The fact that internal flaws are hidden, making their size difficult if not impossible to accurately determine, presents a problem in the study of internal flaw magnification effects. The assumption might be made that the same flaw magnification factors, M_k, used for deep surface flaws might be applied to the equation for critical embedded flaw sizes. However, there is no evidence of how conservative or unconservative this assumption is.

On the other hand, to account for the lack of knowledge about flaw geometry and orientation, it can be conservatively assumed that flaws are surface (or barely subsurface) flaws and that they are long in relation to depth ($Q \approx 1.0$).
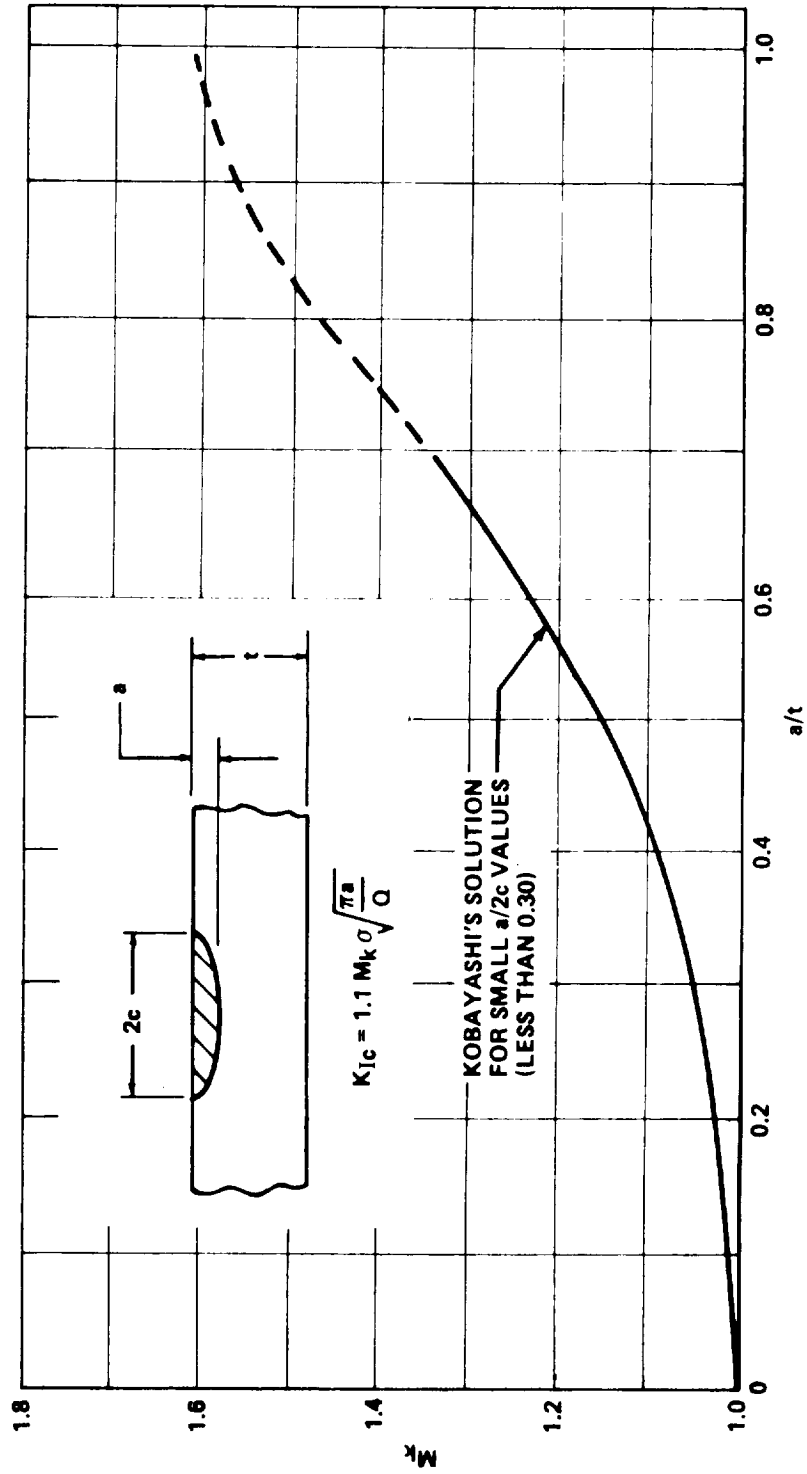
FIGURE E2-25. STRESS-INTENSITY MAGNIFICATION FACTORS FOR DEEP SURFACE FLAWS

2.4.2.3   Through-the-Thickness Cracks.

To calculate through-the-thickness critical crack length, the basic plane stress equation for through-the-thickness cracks in an infinitely wide plate (Section 2.2.2.1) can be rearranged to give

$$\ell_{cr}/2 = \frac{1}{\pi}\left(\frac{K_c}{\sigma}\right)^2 - \frac{1}{2\pi}\left(\frac{K_c}{\sigma_{ys}}\right)^2 \quad ,$$

where K_c is the plane stress fracture toughness obtained from an edge-notched or center-cracked specimen, σ is the applied stress in the structure normal to the plane of the crack, σ_{ys} is the tensile yield strength of the material, and ℓ_{cr} is the critical crack length.

I.   Example Problem A.

Aluminum alloy 2219-T87 is selected as the material for use in a 15-in. diameter compressed air cyclinder. The cylinder is to operate at 1000 psig in ambient room atmosphere.

What is the critical flaw size?

A.   Assumptions.

1.   The defect is a semielliptical surface flaw with $a/2c = 0.2$.

2.   The operating stress is σ = 80 percent of material yield strength.

B.   Solution.

The yield strength and K_{Ic} values obtained from test specimens are as follows:

$$\sigma_{ys} = 50 \text{ ksi}$$

and

$$K_{Ic} = 32 \text{ ksi } \sqrt{\text{in.}} \quad .$$

An estimate of K_c versus material thickness based on 2219-T87 test specimens is shown in Fig. E2-26 (Refs. 20 and 21).

The operating stress is

$$\sigma = 0.80 \left(\sigma_{ys} \right) = 0.80 \, (50) = 40 \text{ ksi} \quad .$$

The wall thickness required is

$$t_{req} = \frac{PR}{\sigma} = \frac{1000 \, (7.5)}{40 \, 000} = 0.188 \text{ in.} \quad .$$

For thick-walled structures,

$$a_{cr} = \frac{Q}{1.21 \, \pi} \left(\frac{K_{Ic}}{\sigma} \right)^2 \quad .$$

From Fig. E2-5, $Q = 1.18$; then

$$a_{cr} = \frac{1.18}{1.21 \, \pi} \left(\frac{32}{40} \right)^2 = 0.199 > 0.188 \text{ in.} \quad .$$

Therefore, the critical flaw is apparently a through-the-thickness crack and the tank will leak before failure. The critical crack length of failure is predicted to be
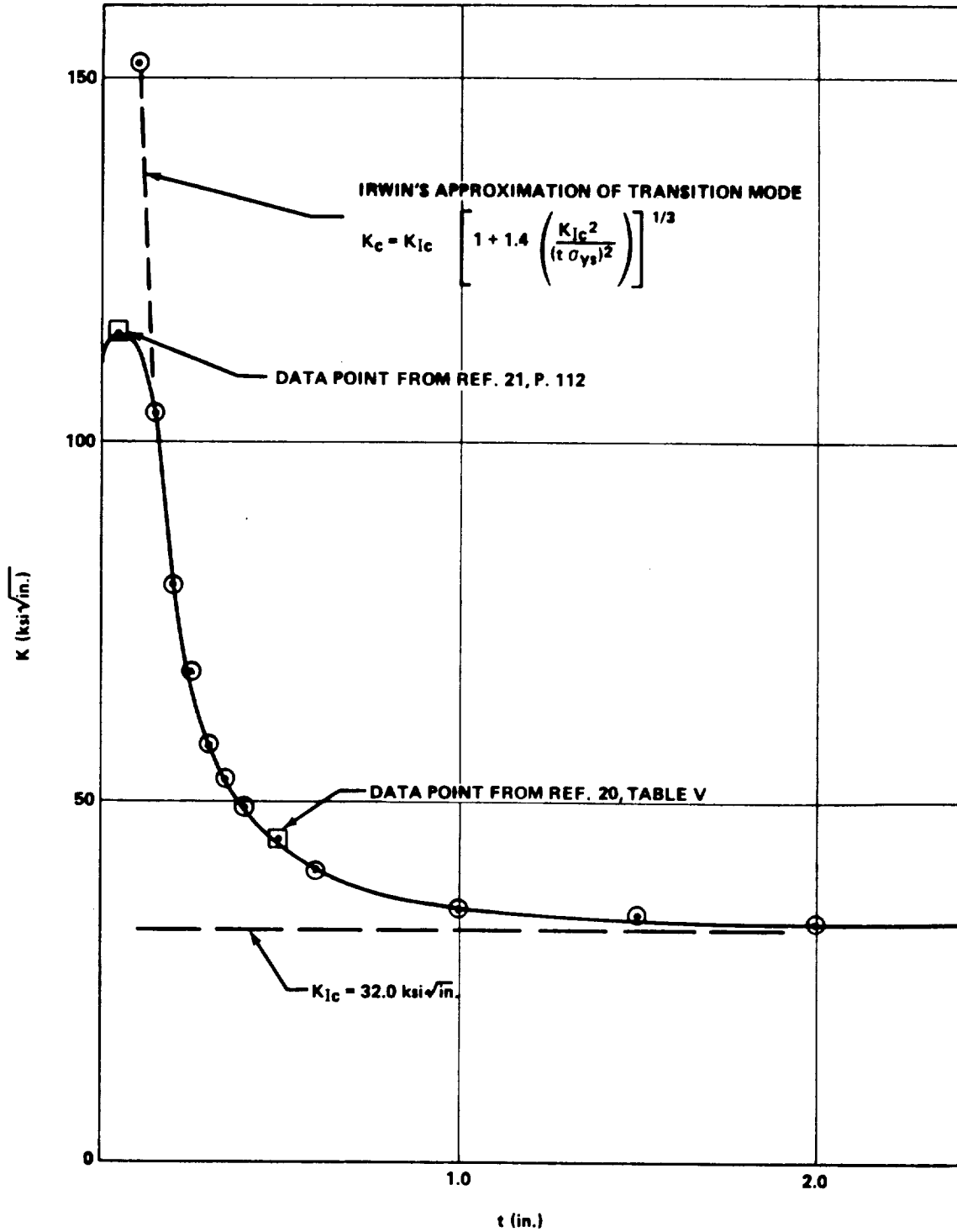
FIGURE E2-26. ESTIMATE OF K_c VERSUS t FOR 2219-T87 ALUMINUM

(T = $70°$ F, K_{Ic} = 32.0 ksi $\sqrt{in.}$)

$$\ell_{cr} = \frac{2}{\pi}\left(\frac{K_c}{\sigma}\right)^2 - \frac{1}{\pi}\left(\frac{K_c}{\sigma_{ys}}\right)^2 \quad .$$

The plane-stress fracture toughness value, K_c, from Fig. E2-26, is 84 ksi $\sqrt{in.}$

$$\ell_{cr} = \frac{2}{\pi}\left(\frac{84}{40}\right)^2 - \frac{1}{\pi}\left(\frac{84}{50}\right)^2 = 2.81 - 0.91 = 1.90 \text{ in.} \quad .$$

2.4.3   Structure Design.

2.4.3.1   Service Life Requirements and Predictions.

With pressure cycles and time at stress, an initial flaw or defect in a structure will grow in size until it attains the critical size at the applied operating stress level, and failure will result. The flaw-growth potential (in inches) is equal to the critical size minus the initial size. The life of the structure directly depends upon this flaw-growth potential and the subcritical flaw-growth characteristics of the material.

The determination of the initial flaw sizes generally relies upon the use of NDI procedures; however, the conventional proof test can be considered to be one of the most positive inspection procedures available. A successful proof test actually defines the maximum possible initial flaw size that exists in the vessel. This results from the functional relationship between stress level and flaw size as defined by the critical stress intensity (K_{Ic}) and illustrated in Fig. E2-6.

Probably the most predominant types of subcritical flaw growth are fatigue growth resulting from cyclic stress and environmentally induced sustained stress growth. Also, growth may occur even in the absence of severe environmental effects if the initial flaw size approaches the critical flaw size.

The technique used for predicting the subcritical cyclic or sustained stress flaw growth makes use of fracture specimen testing and the stress-intensity concept.

It has been shown (Refs. 6 and 17) that the time or cycles to failure at a given maximum applied gross stress level depends on the magnitude of the initial stress intensity at the flaw tip, K_{Ii}, compared with the critical stress intensity, K_{Ic} [that is, cycles or time to failure = $f(K_{Ii}/K_{Ic})$]. Also, it is seen that the ratio of initial flaw size to critical flaw size is related to the stress-intensity ratio as follows:

$$\left(\frac{K_{Ii}}{K_{Ic}}\right)^2 = \frac{\dfrac{a_i}{Q_i}}{\dfrac{a_{cr}}{Q_{cr}}} \quad .$$

Thus, if cyclic or sustained stress fracture specimens are used to obtain experimentally the K_{Ii}/K_{Ic} versus cycles or time curves for a material, the cycles or time required for any given initial flaw to grow to critical size can be predicted. Conversely, if the required life of the structure is known in terms of stress cycles or time at stress, the maximum allowable initial flaw size can be determined.

The cyclic flaw-growth data are plotted in terms of stress-intensity ratio, K_{Ii}/K_{Ic}, versus log of cycles, as shown schematically in Fig. E2-27a. By squaring the ordinate value, the plot of the ratio of initial flaw size to critical flaw size versus the log of cycles (Fig. E2-27b) can be obtained. It should also be recognized that flaw size can be determined after any incremental number of cycles. For example, if the initial flaw-size ratio was 0.40, the flaw would have grown in A cycles, increasing the ratio to 0.6; in B cycles, it would have grown to 0.8, etc.
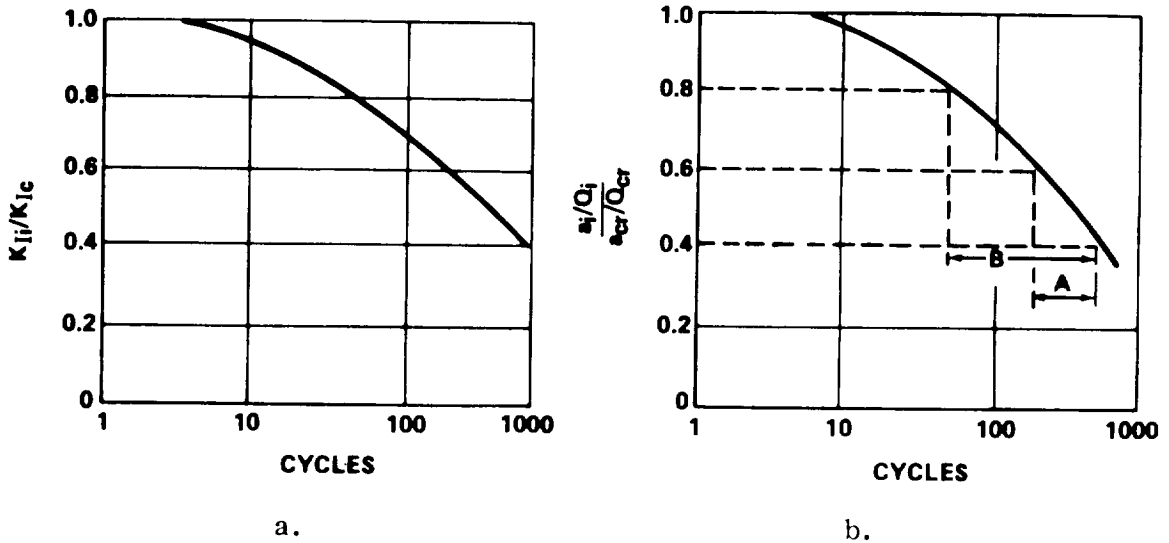
FIGURE E2-27. SCHEMATIC REPRESENTATION OF CYCLIC
FLAW GROWTH

Cyclic flaw-growth data have been obtained on a number of materials used in the aerospace industry. Some such data are shown in Figs. E2-28 and E2-29.

The application of fracture-specimen testing to define the effects of sustained load on flaw growth is essentially the same as used in defining cyclic flaw growth. A constant load is applied to a flawed specimen such that the initial stress intensity is less than the critical value and the time to failure is recorded. The K_{Ii}/K_{Ic} values are computed and the K_{Ii}/K_{Ic} ratio is plotted versus log of time to failure.

Plots of K_{Ii}/K_{Ic} versus log of time for most materials indicate the existence of a threshold stress-intensity level below which sustained stress growth does not occur. Figure E2-30 shows data for 17-7 PH steel tested in both dry and wet environments, and Fig. E2-31 shows surface-flawed specimen data for 2219-T87 aluminum tested in liquid nitrogen. In neither case does it seem that the environment played an important role in the sustained stress growth. In both cases the apparent threshold stress-intensity levels are quite high.
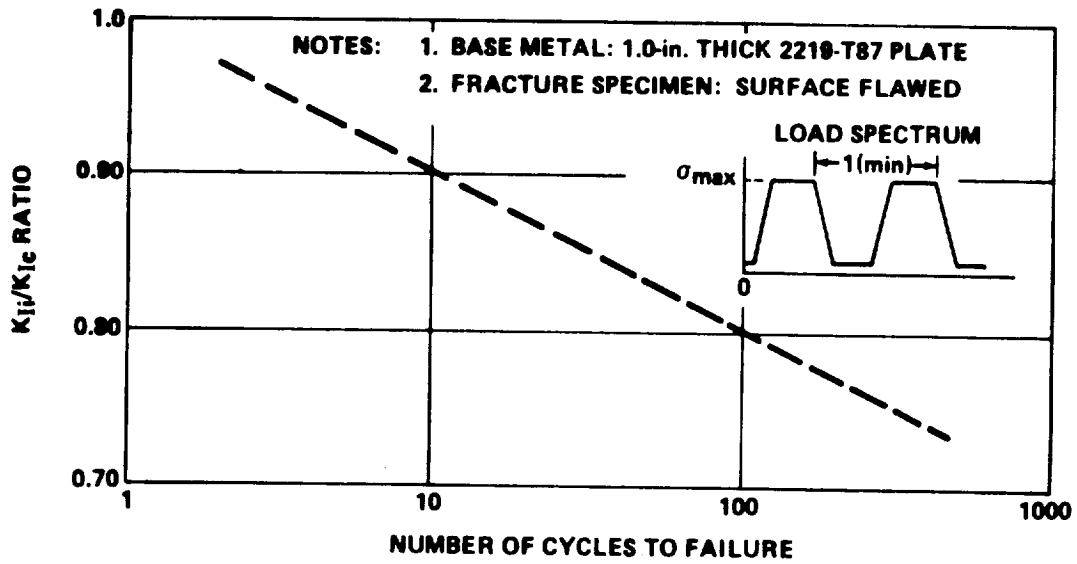
FIGURE E2-28. BASE METAL CYCLIC FLAW-GROWTH DATA
(-320°F, LONGITUDINAL GRAIN)
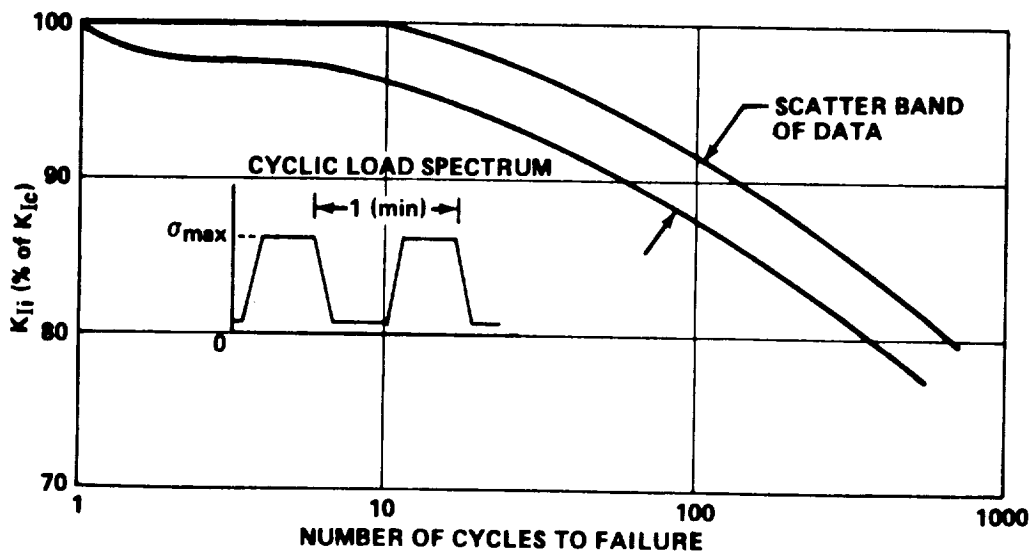
FIGURE E2-29. CYCLIC FLAW-GROWTH DATA OF 6Al-4V
TITANIUM PLATE TESTED AT -320°F
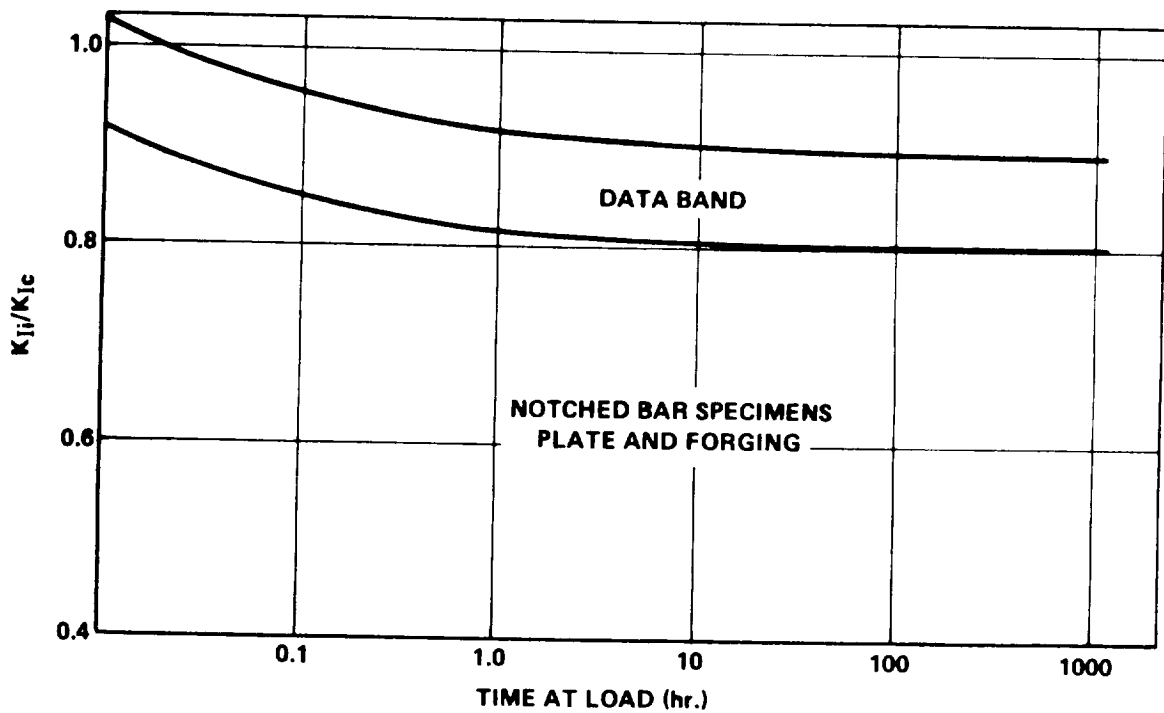
FIGURE E2-30. SUSTAINED STRESS FLAW-GROWTH DATA FOR ROOM-TEMPERATURE TESTS OF 17-7 PH STEEL

Let us now consider the significance of sustained stress flaw growth and specifically the threshold stress-intensity concept on the estimated total cyclic life of a tension-loaded structure containing an initial crack or crack-like flaw. To illustrate this, the schematic representation of the K-N curve is reconstructed in Fig. E2-32, but superimposed on this curve is a horizontal like at $K_{Ii}/K_{Ic} = 0.80$. This is assumed to be the threshold stress intensity. Now consider the situation where the initial flaw size and applied cyclic stress result in an initial stress intensity equal to 50 percent of the critical value. From the curve, it is seen that it would take a total of A cycles to grow this initial flaw to critical size and cause failure. However in B cycles, the initial flaw would have increased in size enough to cuase the stress intensity to reach the threshold value of $K_{Ii}/K_{Ic} = 0.80$. With additional cycles the

C- 6
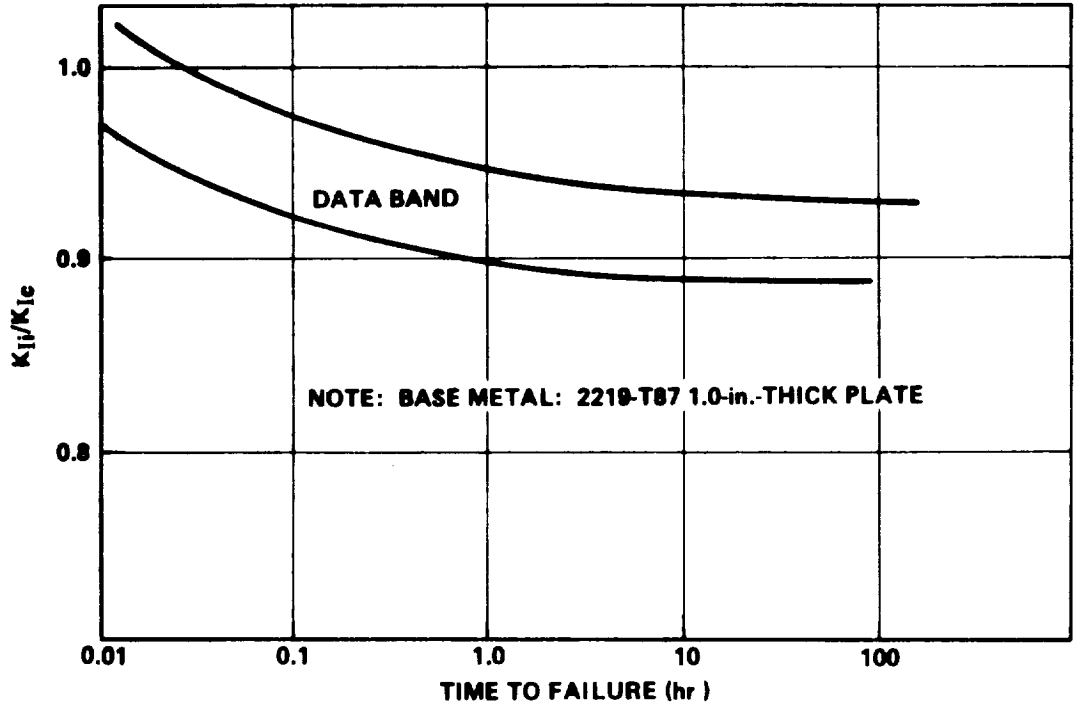
FIGURE E2-31. SUSTAINED STRESS FLAW-GROWTH DATA FOR
2219-T87 ALUMINUM AT -320°F
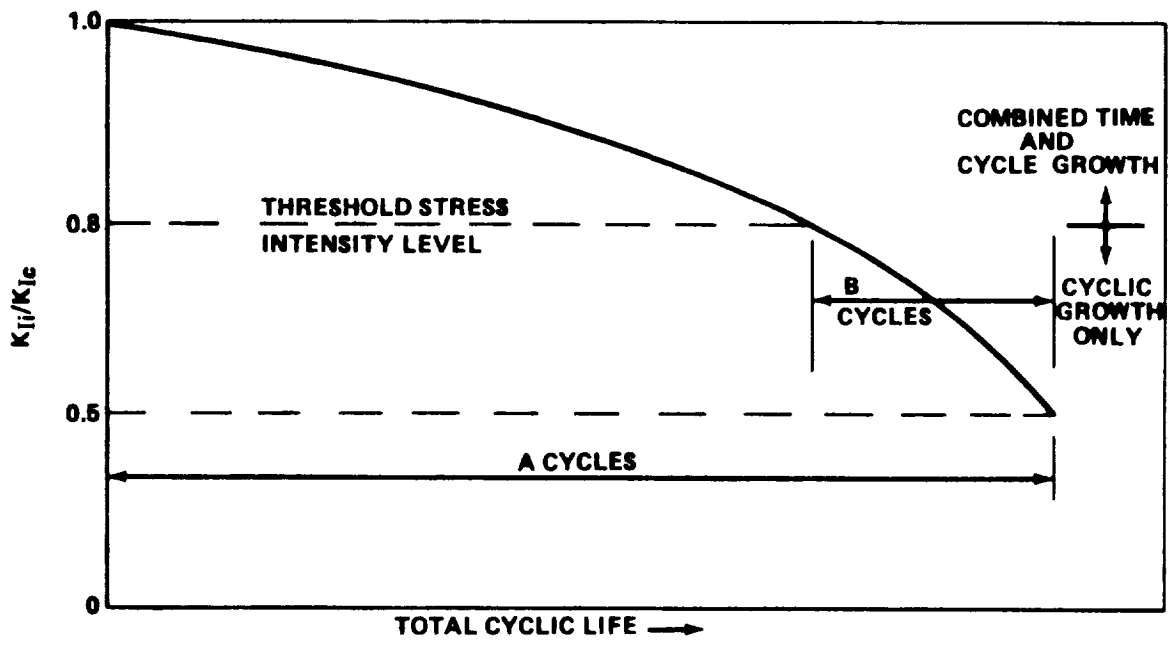
FIGURE E2-32. COMBINED CYCLIC AND SUSTAINED STRESS FLAW
GROWTH SCHEMATIC INTERPRETATION

stress intensity would further increase and, if the stress were sustained sufficiently long, it appears possible that failure could occur on the (B + 1) cycle.

If, on the other hand, the cycles were applied with little time at maximum cyclic stress, it appears that the total of A cycles could be realized. It is hypothesized that below the threshold K-value, the time at sustained stress has little or no effect on cyclic life. Above the threshold value there will be an interaction such that failure could occur anywhere within the range of (B + 1) to A cycles, depending on the time the maximum stress is held during each cycle. The development of the exact time-cycle interaction curves above the threshold value would be a complex and expensive task and, as applied to most tankage structure, may not be of great importance. It appears more rational to determine the basic cyclic data and the threshold-intensity values and then verify (through prolonged-time specimen cyclic tests) that time at load is not of major significance below the threshold value. In the application of the data to fatigue-life estimation, the maximum allowable stress intensity would be limited to the threshold value as determined for the material in question and for the applicable service environment. If the threshold is very low, steps should be taken to protect the material from the environment.

The operational cyclic life of pressure vessels can be determined if the following data are available:

1. Proof-test factor α .

2. Maximum design operating stress σ_{op} .

3. Fracture toughness K_{Ic} .

4. Experimental cyclic and sustained stress flaw growth for the vessel material.

If the cycles to be applied to the vessel have short hold time at the maximum stress σ_{op}, the stress intensity at σ_{op} can be allowed to reach the critical value K_{Ic} and therefore the allowable flaw growth potential is $a_{cr} - a_i$. For long hold times at the maximum stress, the stress intensity could not be allowed to exceed the sustained stress threshold value K_{TH} and the allowable flaw growth potential is $a_{th} - a_i$. Typical threshold stress-intensity data can be obtained from Refs. 12 and 22.

I.   Example Problem A (Thick-Walled Vessel).

Cyclic life prediction can be made by utilizing the proof-test factor and the relationships between K_{Ii}/K_{Ic} and cycles to failure for various values of R (ratio of minimum to maximum stress during a cycle) for the material-environment combination.

The procedure for assessing the structural integrity of the thick-walled vessels follows. In the first analysis for the assessment of the structural integrity of the thick-walled vessel, it is always assumed that all the pressure cycles are applied at R = 0. Since the analysis based on R = 0 will always show the remaining cyclic life less than that based on the analysis of R ≠ 0 (actual R ratios), the prediction of cyclic life based on the analysis of R = 0 is invariably conservative. If the pressure vessel is shown unsatisfactory for the flight based on R = 0, then the prediction analysis for the remaining cyclic life is conducted based on the actual R values at which the cycles are applied. An excellent illustrative example abstracted from Ref. 12 is given as follows.

Suppose that a thick-walled 6Al-4V (STA) titanium helium tank is successfully proof tested at a proof-test factor of 1.50 times the maximum design operating stress. Suppose that the proof-tested tank is subjected to the following pressure cycles before the flight, as shown in Fig. E2-33:
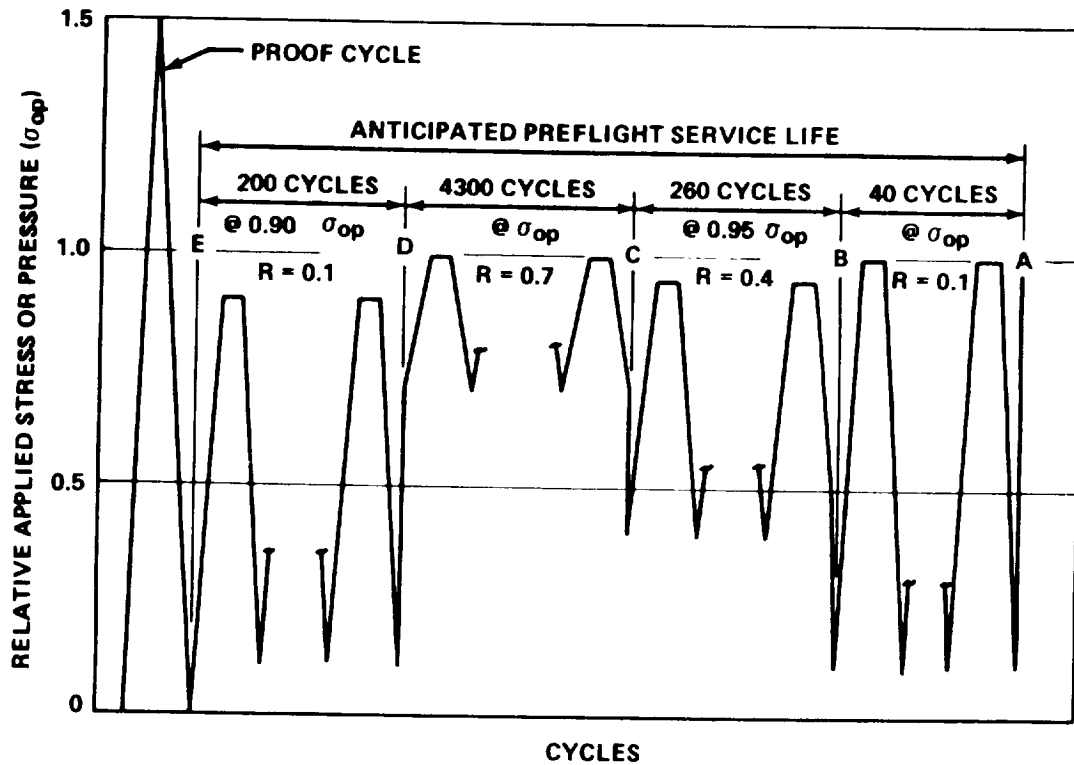
FIGURE E2-33. CYCLIC HISTORY OF A THICK-WALLED VESSEL
(EXAMPLE PROBLEM A)

1. 200 loading cycles with the maximum stress as 90 percent of σ_{op} and R = 0.1.

2. 4300 loading cycles with the maximum stress as σ_{op} and R = 0.7.

3. 260 loading cycles with the maximum stress as 95 percent of σ_{op} and R = 0.4.

4. 40 loading cycles with the maximum stress as σ_{op} and R = 0.1.

The cyclic life curves for 6Al-4V (STA) titanium for the environment of room-temperature air are reproduced for R = 0.0, R = 0.1, R = 0.4, and R = 0.7 in Fig. E2-34. The difference between the plots of cyclic life against K_{Ii}/K_{Ic} for R = 0 and R = 0.1 is negligible for this material-environment
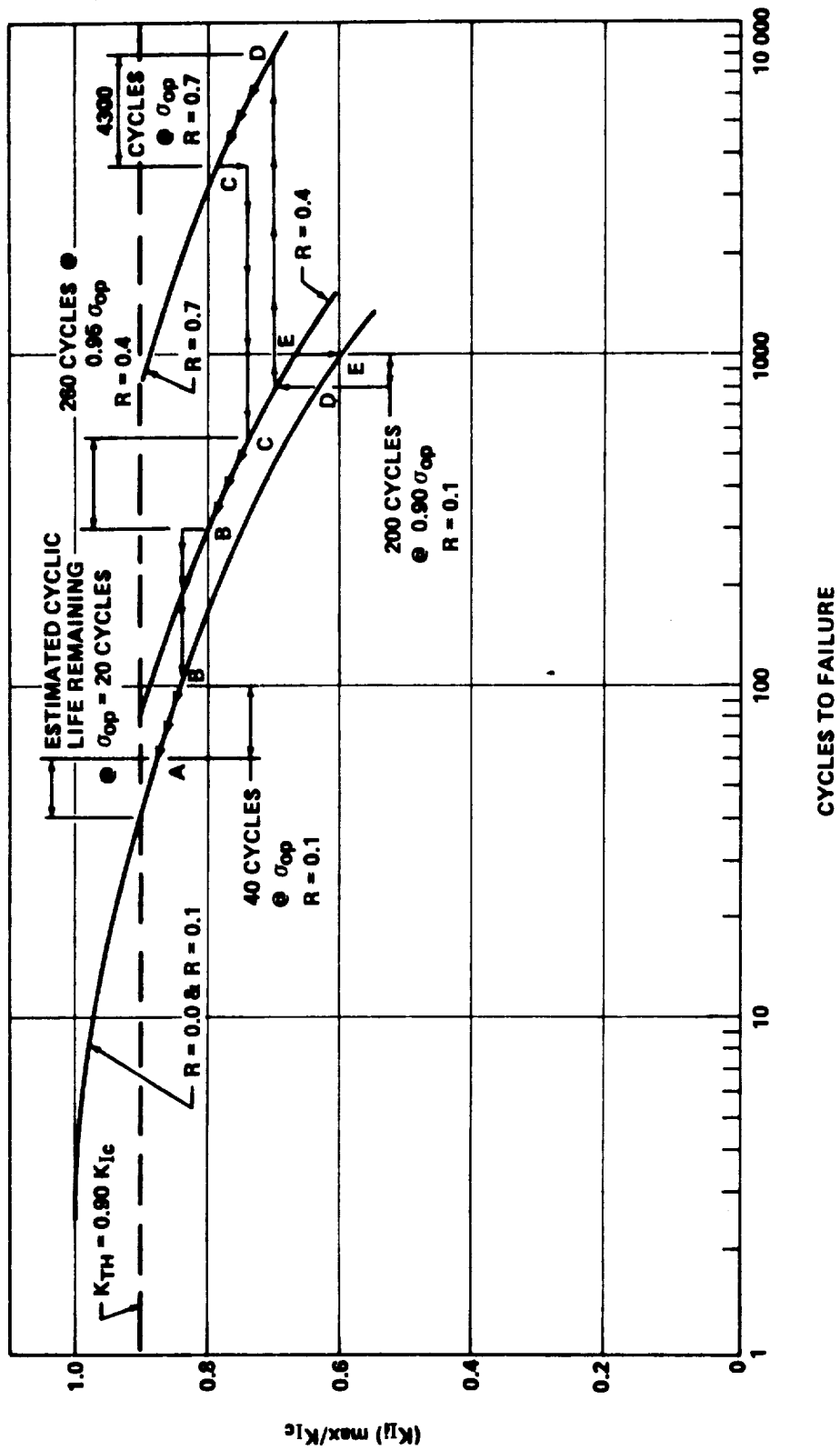
FIGURE E2-34.   PREDICTION OF CYCLIC LIFE OF A THICK-WALLED VESSEL
(EXAMPLE PROBLEM A)

combination, and hence both are shown by the same plot in Fig. E2-34. The threshold stress-intensity level for the material in the environment of room-temperature air is 90 percent of K_{Ic}.

The maximum possible K_{Ii}/K_{Ic} ratio that could exist in the vessel after the proof test at σ_{op} is $1/\alpha = 0.667$. It can be seen from the $R = 0$ plot in Fig. E2-34 that the maximum cycles to failure are about 600 at σ_{op} if the hold times at maximum stress are small. If the analysis is based on $R = 0$ instead of actual R, the pressure-cycle history shows that the vessel is critical. In the following, the assessment of the vessel is made based on the appropriate values of R.

At the beginning of 200 loading cycles with the maximum stress as $0.90 \ \sigma_{op}$, the maximum K_{Ii}/K_{Ic} is given by $0.90 \times 0.667 = 0.60$. This point is indicated by E on $R = 0.1$ curve. The 200 loading cycles of $0.90 \ \sigma_{op}$ and $R = 0.1$ change the K_{Ii}/K_{Ic} ratio from Point E to Point D on the plot of $R = 0.1$. The K_{Ii}/K_{Ic} ratio at the end of 200 loading cycles of $R = 0.1$ is 0.63.

The stress is increased by 10 percent at the end of 200 cycles. Hence, the K_{Ii}/K_{Ic} ratio at the beginning of 4300 cycles at σ_{op} and $R = 0.7$ is $(1.0/0.9) \times 0.63 = 0.70$. This is shown by Point D on the plot of $R = 0.7$. The 4300 loading cycles at σ_{op} and $R = 0.7$ change the K_{Ii}/K_{Ic} ratio from Point D to Point C on the plot of $R = 0.7$, where its value is 0.78.

The stress is decreased by 5 percent at the end of 4300 cycles. Hence, the K_{Ii}/K_{Ic} ratio at the beginning of 260 cycles at $0.95 \ \sigma_{op}$ is $(0.95/1.0) \times 0.78 = 0.74$, which is shown by Point C on the $R = 0.4$ plot. The 260 cycles at $0.95 \ \sigma_{op}$ and $R = 0.4$ change the K_{Ii}/K_{Ic} ratio from Point C to Point B on the $R = 0.4$ plot, where its value is 0.80.

The stress is increased by 5 percent at the end of 260 cycles. Hence, the K_{Ii}/K_{Ic} ratio at the beginning of 40 cycles at σ_{op} is $(1.0/0.95) \times 0.80 = 0.84$, which is illustrated by Point B on the $R = 0.1$ plot. The 40 cycles at σ_{op} and $R = 0.1$ increase the K_{Ii}/K_{Ic} ratio from 0.84 to 0.875, which is shown by Point A in Fig. E2-34.

Since the stress intensity at the end of 40 cycles at σ_{op} is less than the threshold stress intensity, the vessel is considered to be safe for the flight. It will take 20 loading cycles at σ_{op} and $R = 0.1$ to increase K_{Ii}/K_{Ic} from 0.875 to 0.90. Thus, the estimated minimum cyclic life remaining for the vessel is 20 cycles.

II.   Example Problem B (Thin-Walled Vessel).

In thin-walled vessels the flaw depth becomes deep with respect to the wall thickness prior to reaching the critical size. Therefore, Kobayashi's magnification factor for deep surface flaws M_k must be considered. In thin-walled vessels it is assumed that the flaws are long with respect to their depth and, consequently, Q is assumed to be equal to unity in the Kobayashi equation.

To determine the cyclic life of a thin-walled vessel, the following relations are required (Ref. 22).

1.   Proof-test factor, σ_{op}, K_{Ic}, and K_{TH}.

2.   The σ versus a curve, similar to Fig. E2-35, to determine the flaw size, a_i, a_{cr}, and a_{Th}. The curve is obtained from the following equation:

$$\sigma = \frac{K_I}{(1.1 \, M_k \, \sqrt{\pi a})}$$
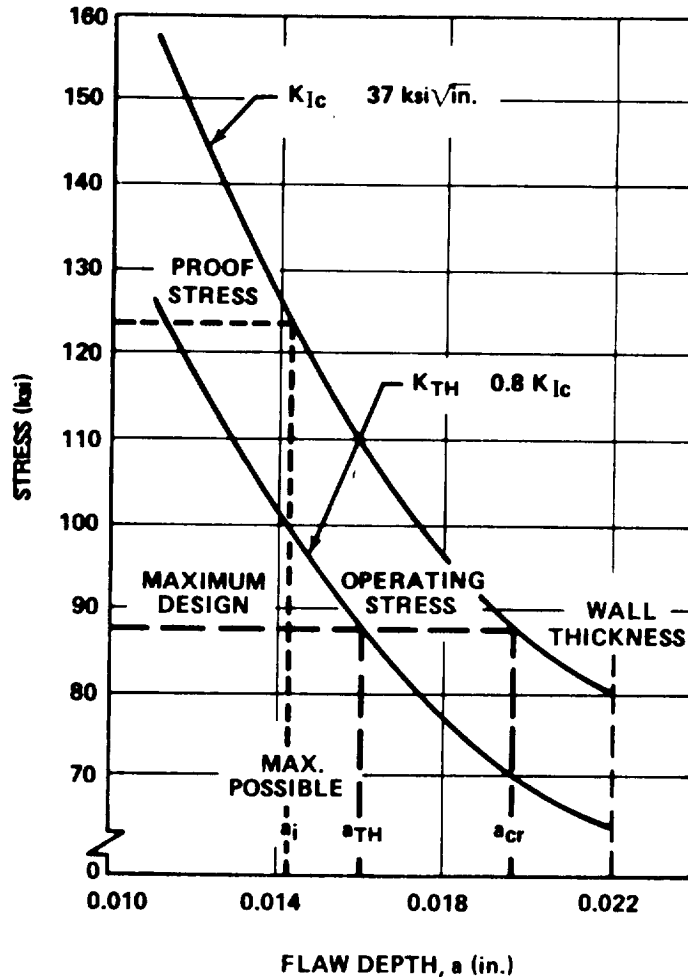
FIGURE E2-35. DETERMINATION OF INITIAL AND CRITICAL
FLAW SIZES

3.   The K_{Ii}/K_{Ic} versus flaw growth rate da/dN to determine the
flaw growth rate at any stress level. The flaw growth rates can be obtained
by differentiating the K_{Ii}/K_{Ic} versus cycles to failure curve, similar to that
of Fig. E2-36 (Ref. 22). This curve is obtained from the specimens where
a_{cr}/t is less than half. For an assumed maximum cyclic stress level, say
σ_1, the given K_{Ii}/K_{Ic} versus N curve can be converted to an a/Q versus
N curve by the equation

$$a/Q = \frac{1}{1.21\,\pi}\left(\frac{K_{Ii}}{\sigma_1}\right)^2 \quad .$$
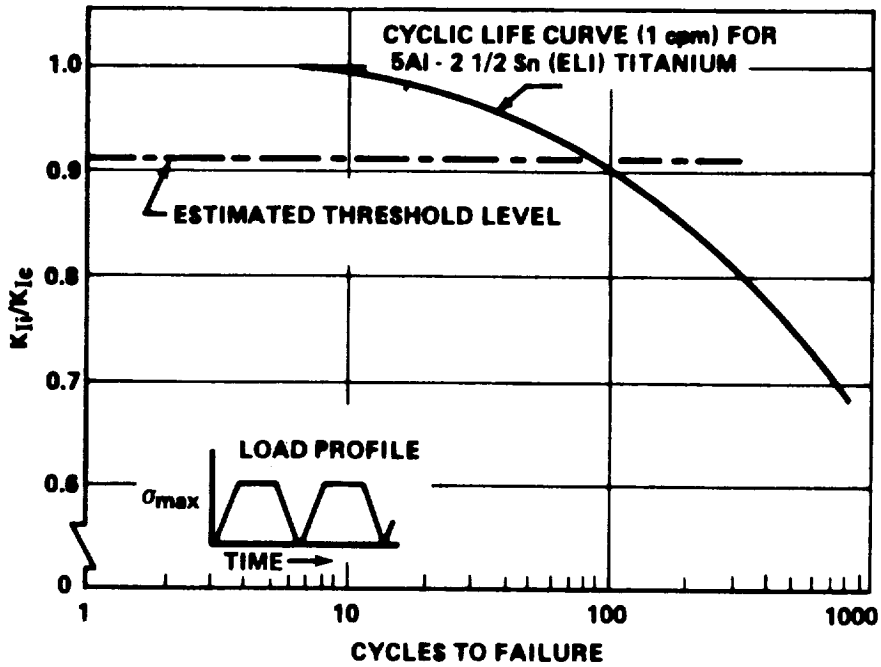
FIGURE E2-36. COMBINED SUSTAINED AND CYCLIC STRESS
LIFE DATA [5 Al — 2 1/2 Sn (ELI) TITANIUM
AT -320°F]

The slope of the a/Q versus N curve gives the plot for the flaw growth rate d/dN (a/Q) versus K_{Ii}/K_{Ic} for the stress level σ_1. From the preceding equation for a given K_{Ii}, a/Q at the stress level σ_2 is related with a/Q at σ_1 as

$$(a/Q)\sigma_2 = \left(\frac{\sigma_1}{\sigma_2}\right)^2 \left(\frac{a}{Q}\right) \sigma_1 \quad .$$

From this equation it can be concluded that the flaw growth rate at any stress level σ_2 is related to the growth rate at σ_1 as follows:

$$[d/dN\ (a/Q)]\ \sigma_2 = (\sigma_1/\sigma_2)^2\ [d/dN\ (a/Q)]\ \sigma_1 \quad .$$

The prediction of the remaining cycle life and the structural integrity of the thin-walled vessel is demonstrated by an illustrative example abstracted from Ref. 22 and is given as follows.

Suppose that a thin-walled 6A1-4V titanium (STA) propellant tank containing N_2O_4 at room temperature is successfully proof tested with water at room temperature to a proof-test factor of 1.41 times the maximum design operating stress, σ_{op}. Suppose that the proof-tested tank is subjected to the following pressure cycles before the flight:

1. Twenty loading cycles with the maximum stress as 90 percent of σ_{op}.

2. Twelve loading cycles with the maximum stress as 95 percent of σ_{op}.

3. Five loading cycles with the maximum stress as σ_{op}.

It is desired to assess the structural integrity of the pressure vessel from the fracture mechanics standpoint and estimate the minimum cyclic life remaining for the vessel at σ_{op}. This example is treated with specific numbers since the stress-intensity factor has to be corrected for the a/t ratio according to Fig. E2-25. The thickness of the tank is 0.022 in. The maximum design operating stress, σ_{op}, is 87.5 ksi. The material of this gage under the above-mentioned environmental conditions has the minimum fracture toughness of 37 ksi $\sqrt{in.}$ and the threshold stress intensity of 80 percent of K_{Ic}.

The σ versus a plots are given for K_{Ic} and $K_{TH} = 0.80\ K_{Ic}$ in Fig. E2-35. Since the proof stress is $1.41 \times \sigma_{op} = 123.6$ ksi, it is clear from Fig. E2-35 that the maximum possible a_i that could exist is 0.0143 in. Here it is assumed that the depressurization from the proof pressure is

rapid enough so that no significant flaw growth occurs during the depressurization. Also, as shown in Fig. E2-35, for the stress level of σ_{op}, a_{cr} is 0.0196 in. and a_{TH} is 0.0160 in.

The plot of the K_{Ii}/K_{Ic} versus flaw growth rate for 6A L-4V titanium at room temperature is reproduced in Fig. E2-37 for σ = 100 ksi. The 99-percent confidence level flaw growth rate curve is obtained from the cyclic data of R = 0.0; it is assumed in this example that all the cycles are applied at R = 0.0.

Taking into account the effect of stress level on the flaw growth rates, the rates are arithmetically integrated from a_i = 0.0143 in. to a_{cr} = 0.0196 in. according to Fig. E2-38 to calculate the cycles to failure for the stress level of σ_{op}. The plot of flaw depth against cycles to failure for the stress level of σ_{op} is shown in Fig. E2-39.

When the maximum cyclic stress is 0.95 σ_{op}, a_i is still 0.0143 in. but a_{cr} is 0.0208 in. and a_{TH} = 0.0167 in. from Fig. E2-35. Based on the stress level of 0.95 σ_{op}, the flaw growth rates are integrated from a_i = 0.0143 in. to a_{cr} = 0.208 in. to calculate the cycles to failure. A similar procedure is followed to obtain the relation of flaw depth against cycles to failure for the stress level of 0.90 σ_{op}. These plots are shown in Fig. E2-39.

At the end of the proof cycle and the beginning of the first cycle at the maximum cyclic stress of 0.90 σ_{op}, the maximum possible flaw depth is 0.0143 in. This is shown by Point D in Fig. E2-39. The 20 loading cycles with the maximum stress as 0.90 σ_{op} change a from Point D to Point C on the plot of 0.90 σ_{op} (Fig. E2-39).
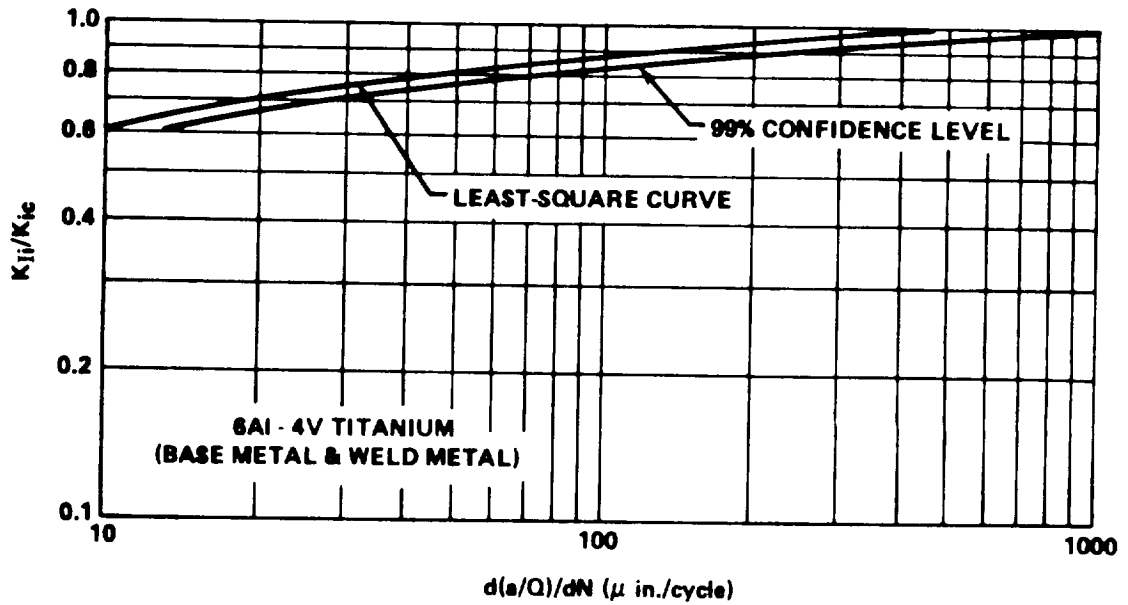
FIGURE E2-37. CYCLIC FLAW-GROWTH RATES
(FOR σ_{max} = 100 ksi)
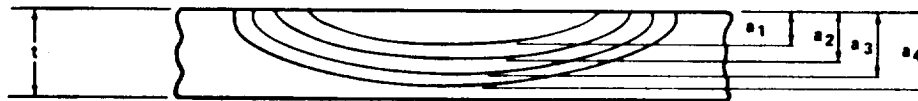
a	Δa	a/t	M_k [a]	K [b]	MEAN K	MEAN [c] da/dN	ΔN	N
a_1	$a_2 - a_1$	a_1/t	M_{k1}	K_1	$\dfrac{K_1 + K_2}{2}$	da_{1-2}/dN	ΔN_1	ΔN_1
a_2	$a_3 - a_2$	a_2/t	M_{k2}	K_2	$\dfrac{K_2 + K_3}{2}$	da_{2-3}/dN	ΔN_2	$\Delta N_1 + \Delta N_2$
a_3								$\Delta N_1 + \Delta N_2 + \Delta N_3$

a. Obtain from Kobayashi's solution of M_k vs a/t

b. $K = 1.1 \sqrt{\pi}\, \sigma\, (a)^{1/2}\, M_k$

c. Obtain from basic K vs da/dN curve.

FIGURE E2-38. ARITHMETIC INTEGRATION OF FLAW-GROWTH-RATE
DATA (DEEP FLAWS IN THIN-WALLED VESSELS)
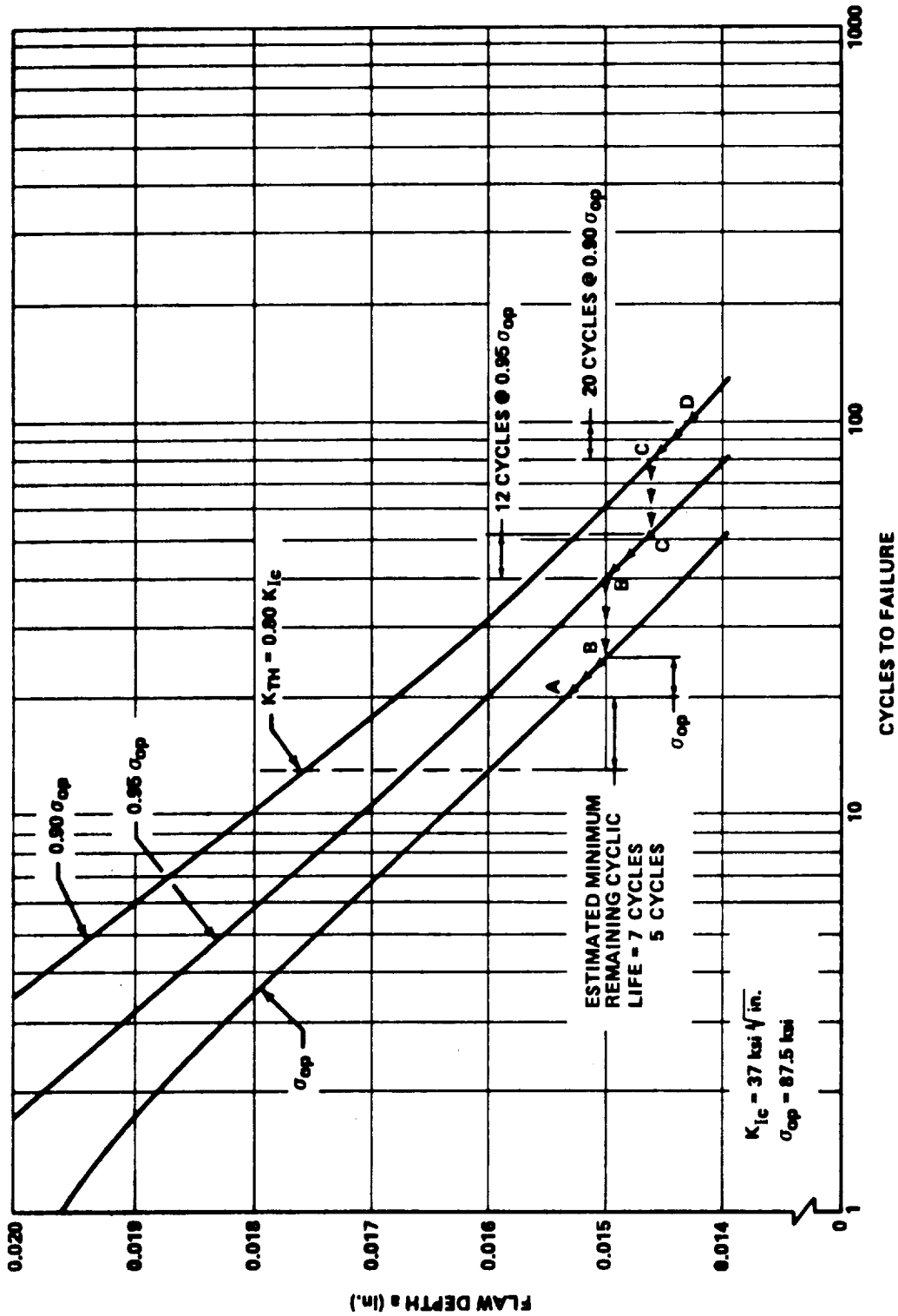
FIGURE E2-39.   PREDICTION OF CYCLIC LIFE OF A THIN-WALLED VESSEL
(ILLUSTRATIVE EXAMPLE)

The tank-wall stress is increased by 5 percent at the end of 20 loading cycles with the maximum stress as 0.90 σ_{op}. The flaw size remains the same during the stress increase. This is shown by Point C on the plot of 0.95 σ_{op} in Fig. E2-39.

The 12 loading cycles with the maximum stress as 0.95 σ_{op} change a from Point C to Point B on the plot of 0.95 σ_{op} in Fig. E2-39.

At the end of 12 loading cycles with the maximum stress as 0.95 σ_{op}, the stress is increased by 5 percent. This is shown by Point B on the plot of σ_{op} in Fig. E2-39.

The five loading cycles with the maximum stress as σ_{op} change a from Point B to Point A on the plot of σ_{op} in Fig. E2-39. The flaw depth at A is 0.01534 in. This is smaller than a_{TH}, which is 0.0160 in. Hence the vessel is considered to be safe for the flight. Also from Fig. E2-39, it will take seven cycles at σ_{op} to increase the flaw depth from 0.01534 in. to 0.0160 in. Hence, the minimum estimated cyclic life remaining for the vessel is seven cycles.

2.4.3.2   Allowable Initial Flaw Size.

Allowable initial flaw sizes in a designed structure depend on the service life requirements for the structure and fracture toughness properties of the material selected. The prevention of failure requires that either the actual initial flaw sizes or the maximum possible initial flaw size be known. Nondestructive inspection provides the only means of determining actual initial flaw sizes. A successful proof test specifies the maximum possible initial flaw size which can exist after the proof test and, in turn, provides the maximum possible initial to critical stress-intensity ratio, K_{Ii}/K_{Ic}. To determine the maximum allowable initial flaw size, the initial to critical stress-intensity ratio, based on the service life requirements, must be determined.

The calculation of allowable initial flaw size is demonstrated by the following example.

I. <u>Example Problem A</u>.

A cyclic loaded pressure vessel of aluminum alloy must meet the following design conditions:

1. Required minimum life, 40 000 cycles.

2. Maximum stress in a cycle $1/2 \ \sigma_{ys}$ = 35 000 psi.

3. K_{Ic} of weld metal = 15 000 psi $\sqrt{in.}$

4. Semielliptical surface defect (length 4 × depth).

What is the allowable initial flaw size which will grow to a critical size in 40 000 cycles?

<u>Solution</u>.

From Fig. E2-40 (Ref. 18), the K_{Ii}/K_{Ic} ratio corresponding to 40 000 cycles of life is 0.36. The initial stress intensity can now be determined:

$$K_{Ii}/K_{Ic} \ = \ 0.36 \ = \ \frac{K_{Ii}}{15 \ 000}$$

and

$$K_{Ii} \ = \ 0.36 \ (15 \ 000) \ = \ 5400 \ \text{psi} \ \sqrt{in.} \qquad .$$

Knowing the design stress of 35 000 and the expression of the type of defect, it is now possible to find the defect size corresponding to a K_{Ii} of 5400 psi $\sqrt{in.}$:
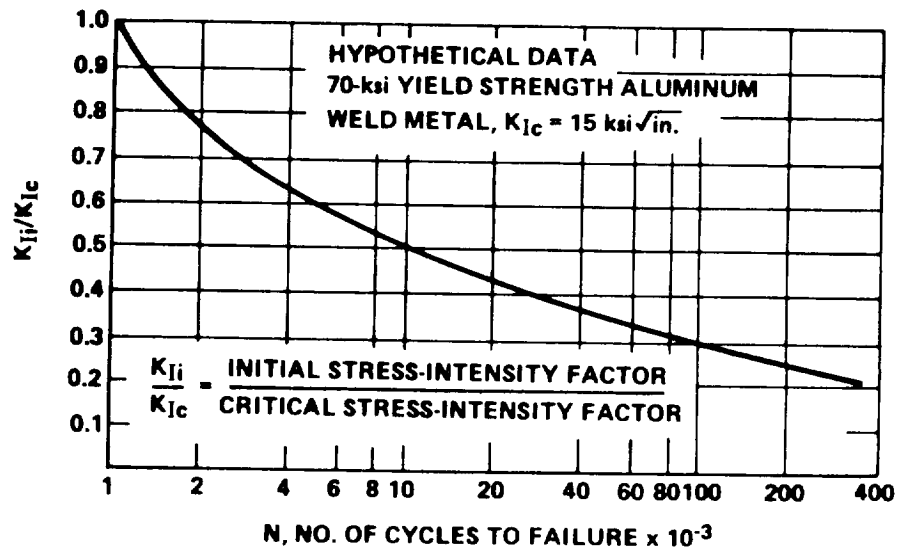
FIGURE E2-40. CYCLIC FLAW-GROWTH DATA FOR
ALUMINUM ALLOY

$$a_i = \frac{K_{Ii}^2 Q}{1.21 \pi \sigma^2} = \frac{(5400)^2 (1.4)}{1.21 \pi (35\ 000)^2} = 0.0088 \text{ in.}$$

The value of $Q = 1.4$ is taken from Fig. E2-5 for $a/2c = 1/4 = 0.25$ and $\sigma/\sigma_{ys} = 1/2 = 0.50$.

$$2c_i = 4a_i = 4(0.0088) = 0.0352 \text{ in.}$$

Therefore, the size of an initial flaw which will just grow to a critical size in 40 000 cycles is 0.0088 in. deep by 0.0352 in. long.

2.4.3.3 Nondestructive Inspection Acceptance Limits.

The NDI requirements for any given structure are a function of the allowable flaw sizes. They are limited by any economic or schedule implications associated with a proof-test failure and by the reliability of the

inspection techniques for detecting initial flaws. Allowances should be made for any lack of specific knowledge of flaw geometry and orientation. When there is a lack of flaw definition, the worst possible flaw geometry and orientation might be assumed.

Also, in arriving at acceptance limits, the allowable spacing for internal or surface flaws (that is, aligned flaws in weldments) must be considered. An approximate analytical solution for the interaction of elliptically shaped coplanar flaws has been obtained by Kobayashi and Hall (Ref. 23). The results are shown in Fig. E2-41 along with experimental results on several Ladish D6AC steel specimens containing two coplanar semielliptical surface flaws. The curves are plotted in terms of stress-intensity magnification ratio (K_1/K_2) versus flaw spacing ratio (d/a). Probably the most significant point is that there is very little interaction between coplanar flaws unless they are surprisingly close together.
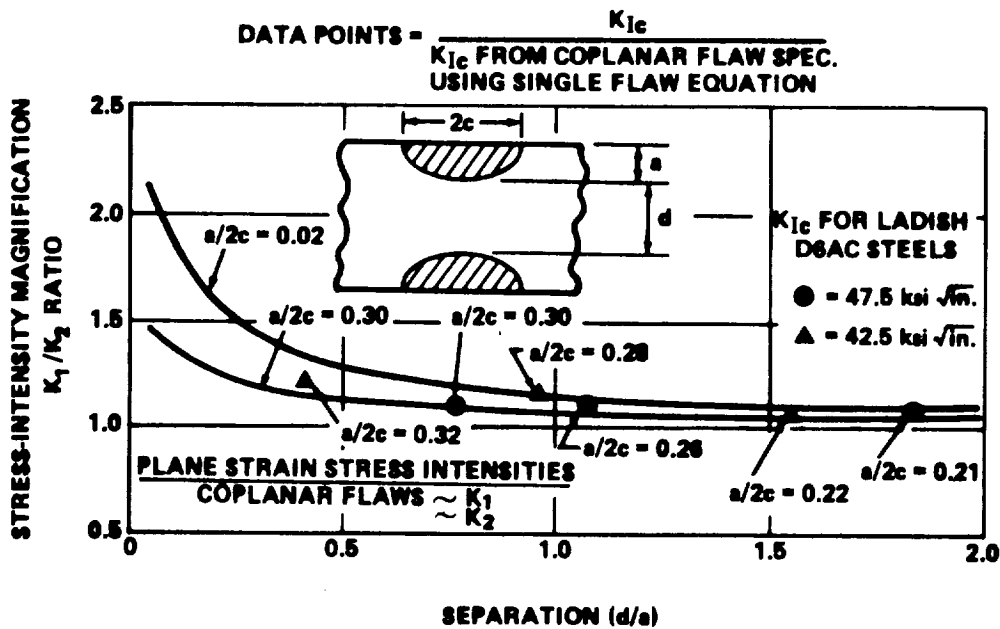
FIGURE E2-41. STRESS-INTENSITY MAGNIFICATION FOR TWO
COPLANAR ELLIPTICAL FLAWS

The establishment of NDI acceptance limits when service life require-
ments are known might best be shown by an illustrative example involving a
hypothetical pressure vessel that is expected to encounter a rather complex
loading history.

Figure E2-42a shows the assumed service life requirement con-
sisting of one proof-test cycle (at a stress level of α times the operating
stress) followed by 1000 cycles and then 100 hr, both at a constant operating
stress level of ($\sigma = 1.0$). To define the minimum inspection standards
required prior to service, it is necessary to determine the critical flaw size,
$(a/Q)_{cr}$, at the end of service (Section 2.4.2) and work backwards, evaluating
all portions of the loading profile that can cause flaw growth.

Figure E2-42b represents a dimensionless relationship of stress-to-
flaw size as shown previously (Fig. E2-6). The ordinate now is plotted in
terms of percentage of critical flaw size at operating stress. Figures E2-42c
and d are schematic representations of the cyclic load flaw growth and sus-
tained load flaw growth, respectively.

The approach is as follows:

1.   The critical flaw size at operating stress is represented as 100
percent of critical and is the maximum allowed at time T_D (at the end of the
service life).

2.   Maximum allowed flaw size at time T_C is shown by Point C and
represents the maximum allowable flaw size at the start of the 100-hr sus-
tained stress period.

3.   The effect of cyclic loading is shown in Fig. E2-42c by moving
1000 cycles from T_C to T_B. Point B then represents the maximum allowable
size at time T_B or at the start of the 1000-cycle period. This size is the
maximum allowable size before the vessel is placed in service.
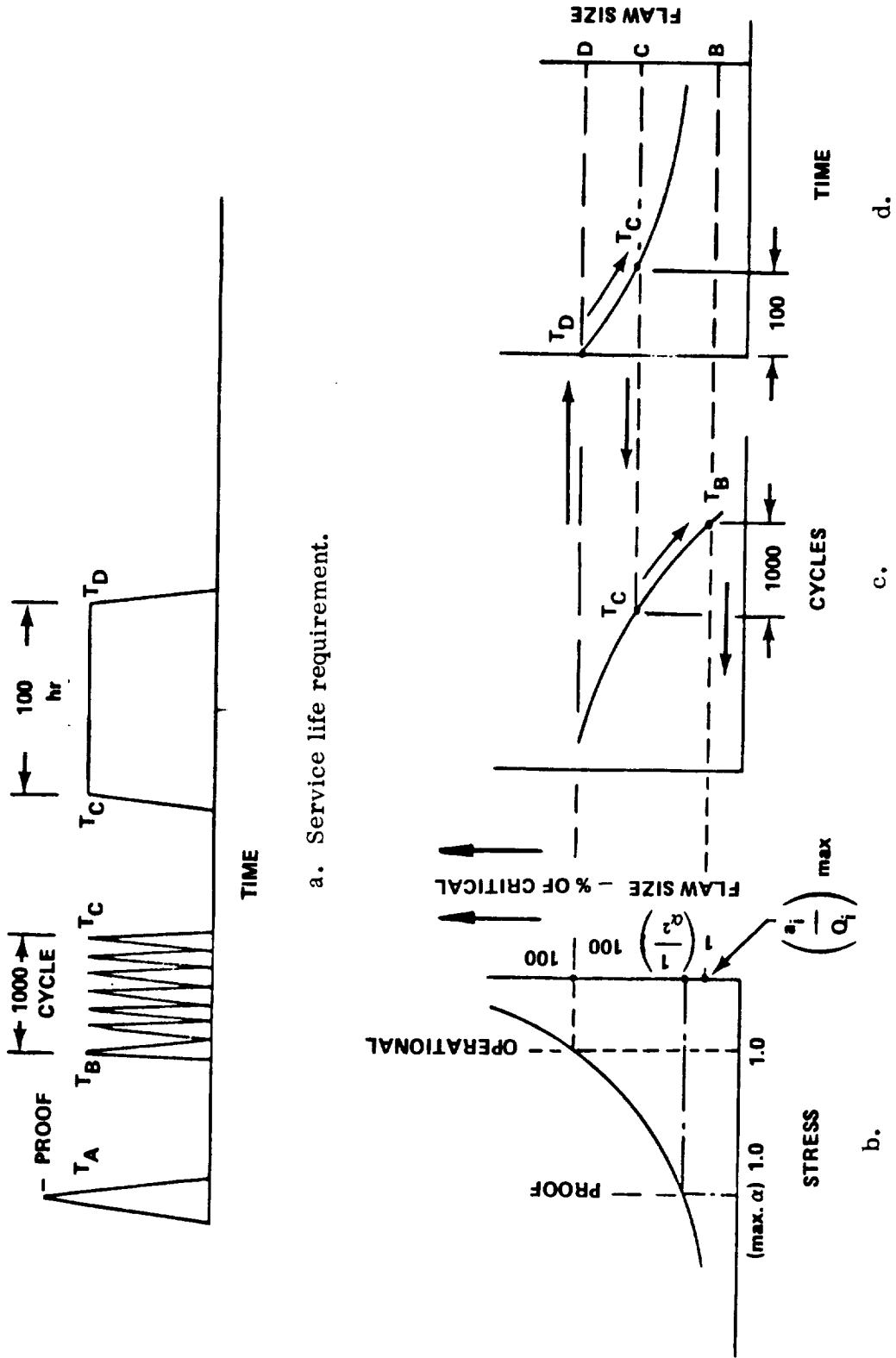
FIGURE E2-42. DETERMINATION OF NONDESTRUCTIVE INSPECTION ACCEPTANCE LIMITS

4.   It can be shown that the previous one-cycle proof test generally has a negligible effect on flaw growth compared with the chosen service life.

Note in this schematic illustration that the maximum allowable flaw size is less than that which could have been present during a successful proof test, and thus the proof test could not guarantee successful fulfillment of the service life requirement. As a result, NDI must be capable of detecting flaws as small as $(a_i/Q_i)_{max}$.

If it is determined that inspection technique limitations preclude the assurance of service life reliability, then either the proof-test factor must be increased to assure that $(a_i/Q_i)_{max}$ is the largest possible existing flaw size at the beginning of service life, or conservative assumptions might be made about flaw geometry and orientation to account for the inability to detect small flaw depths. For example, the length (L) of an indication seen in X-ray inspection could be assumed to be the minor axis of an elliptical flaw where the major axis is large with respect to the minor axis (i.e., $L = 2a$, $Q \approx 1.0$). Consequently, the critical flaw size must be larger (and the operating stress lower) in order to meet the service life requirements. In other words, both $(a_i/Q_i)_{max}$ and $(a/Q)_{cr}$ move higher up the ordinate of Fig. E2-42b.

It should be noted that in terms of "percentage of critical," flaw size is independent of actual stress and toughness values. Obviously, the determination of finite maximum allowable flaw sizes (or smallest flaw size for NDI detection) requires a detailed knowledge of applied stresses in the various tank locations and of the fracture toughness of the materials used. This has been illustrated by the Example Problem A in Section 2.4.3.2 in which the allowable initial flaw size in an aluminum alloy pressure vessel is calculated based on a required service life. In the case where NDI acceptance limits are being considered, the calculated initial flaw depth and length are the minimum demensions which NDI must be capable of detecting.

2.4.3.4 Proof-Test Factor Selection.

It has been previously noted that a successful proof test determines the maximum possible flaw size which can exist after the proof test and prior to the beginning of service. The proof test is the most powerful inspection test presently available and offers the most reliable method for guaranteed service life.

Figure E2-43 shows a schematic theoretical relationship between the critical flaw size, $(a/Q)_{cr}$, and the corresponding fracture stress, as previously illustrated in Fig. E2-6, along with a similar relationship between initial flaw size $(a/Q)_i$ and stress level. The relationships hold true for applied stresses below the yield strength of the material. For stresses above
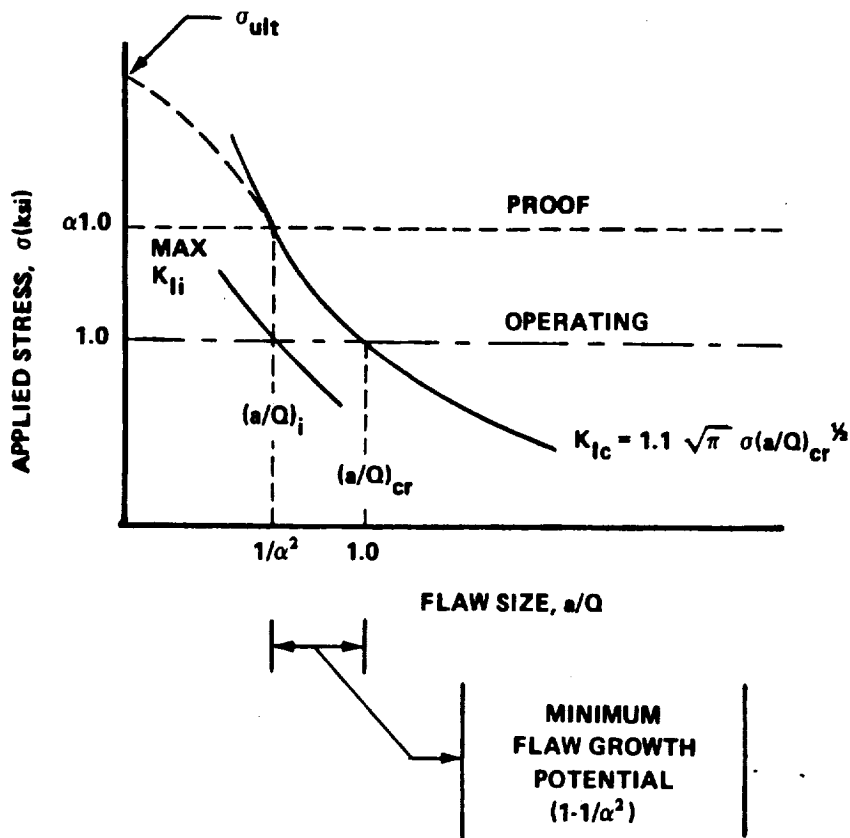
FIGURE E2-43. TYPICAL MATERIAL STRESS-INTENSITY
RELATIONSHIP

the yield value the relationships follow some experimentally determined curve up to the ultimate strength, σ_{ult}. If proof pressure is α times the operating pressure, the critical flaw size is

$$(a/Q)_{cr_{proof}} = \max (a/Q)_{i_{oper}} = \frac{1}{1.21 \pi} \left(\frac{K_{Ic}}{\alpha \sigma_{oper}} \right)^2$$

and

$$(a/Q)_{cr_{oper}} = \frac{1}{1.21 \pi} \left(\frac{K_{Ic}}{\sigma_{oper}} \right)^2 \quad .$$

Thus the proof-test factor, α, is a function of the maximum initial flaw size and critical flaw size for the operating pressure level

$$\frac{(a/Q)_{i_{oper}}}{(a/Q)_{cr_{oper}}} = \frac{1}{\alpha^2} \quad .$$

Since subcritical flaw growth is a function of the initial stress intensity as compared with the critical value, the proof-test factor can be related as

$$\frac{\max K_{Ii}}{K_{Ic}} = \frac{1.1 \sqrt{\pi} \, \sigma_{oper} \, (a/Q)_{i_{oper}}^{1/2}}{1.1 \sqrt{\pi} \, \alpha \, \sigma_{oper} \, (a/Q)_{i_{oper}}^{1/2}} = \frac{1}{\alpha} \quad ,$$

where K_{Ii} is the initial stress intensity at the operating stress level and temperature, and K_{Ic} is the fracture toughness value at proof test

temperature. It should be noted that lower proof test factors (and therefore lower proof stresses) can be employed if the proof test is performed at a temperature where the material has a lower K_{Ic} than at operating temperature and, consequently, greater susceptibility to flaws. In this way the risk of proof-test failure is minimized insofar as practical.

The maximum K_{Ic} at proof temperature should be employed in the equation rather than the minimum or average K_{Ic} because it results in the selection of a higher proof factor, a conservative event. Figure E2-44 illustrates the difference between the use of maximum and minimum K_{Ic} at proof temperature. For a given maximum initial flaw size, $(a/Q)_i$ (ma), the proof stress required by K_{Ic} (min.) is less than that required by K_{Ic} (max.). In fact, if K_{Ic} (min.) were used and a component fabricated from material characteristic of K_{Ic} (max.) and containing a flaw slightly longer than $(a/Q)_i$ (ma) were proof tested at the lower level, the component would pass
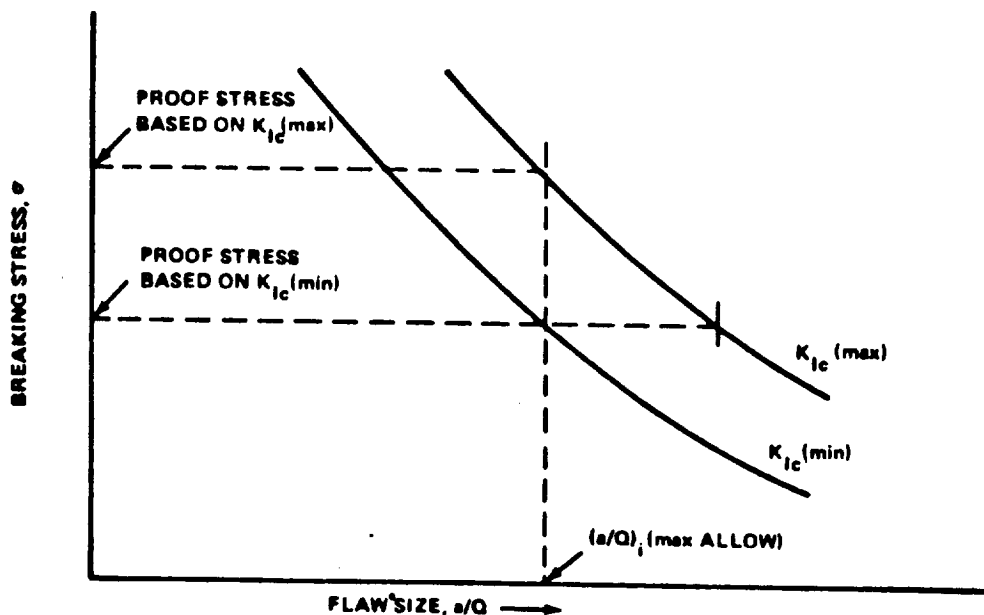
FIGURE E2-44. DETERMINATION OF PROOF STRESS BY MAXIMUM
AND MINIMUM VALUES OF K_{Ic}

the proof test successfully but probably would fail in service. The use of K_{Ic} $(max)_p$ in the proof-factor equation precludes this.

It has been shown by analysis that regardless of the structural wall thickness, the required minimum proof-test factor α is always $1 \div$ allowable K_{Ii}/K_{Ic}. However, the value of the proof test in providing assurance against service failure changes with decreasing wall thickness and/or increasing fracture toughness, K_{Ic}, the same as occurs with the predicted pressure vessel failure mode. This is discussed in more detail in Ref. 22 and illustrated in Fig. E2-45.

Having experimentally obtained the cyclic and sustained flaw growth for a material under consideration, the necessary proof-test factor can be determined to assure that the structure will meet the service life requirements. Proof-factor determination can be applied to at least two general problem areas in the design of structural components:

1. Evaluation and modification of proof-test conditions for current components for which operating stress and mission are already fixed.

2. Preliminary design of components intended for known missions, including selection of material, maximum operating stress, minimum proof stress, and proof temperature.

The following sample problem illustrates the proper selection of a proof-test factor for a hypothetical pressure vessel design.

I.   Example Problem A.

Suppose that a thick-walled liquid nitrogen 5Al-2.5Sn (ELI) titanium pressure vessel must meet a service life requirement of 600 pressure cycles where the pressure is sustained for a prolonged period during each cycle. The vessel has already been successfully proof tested with LN_2 to a proof factor
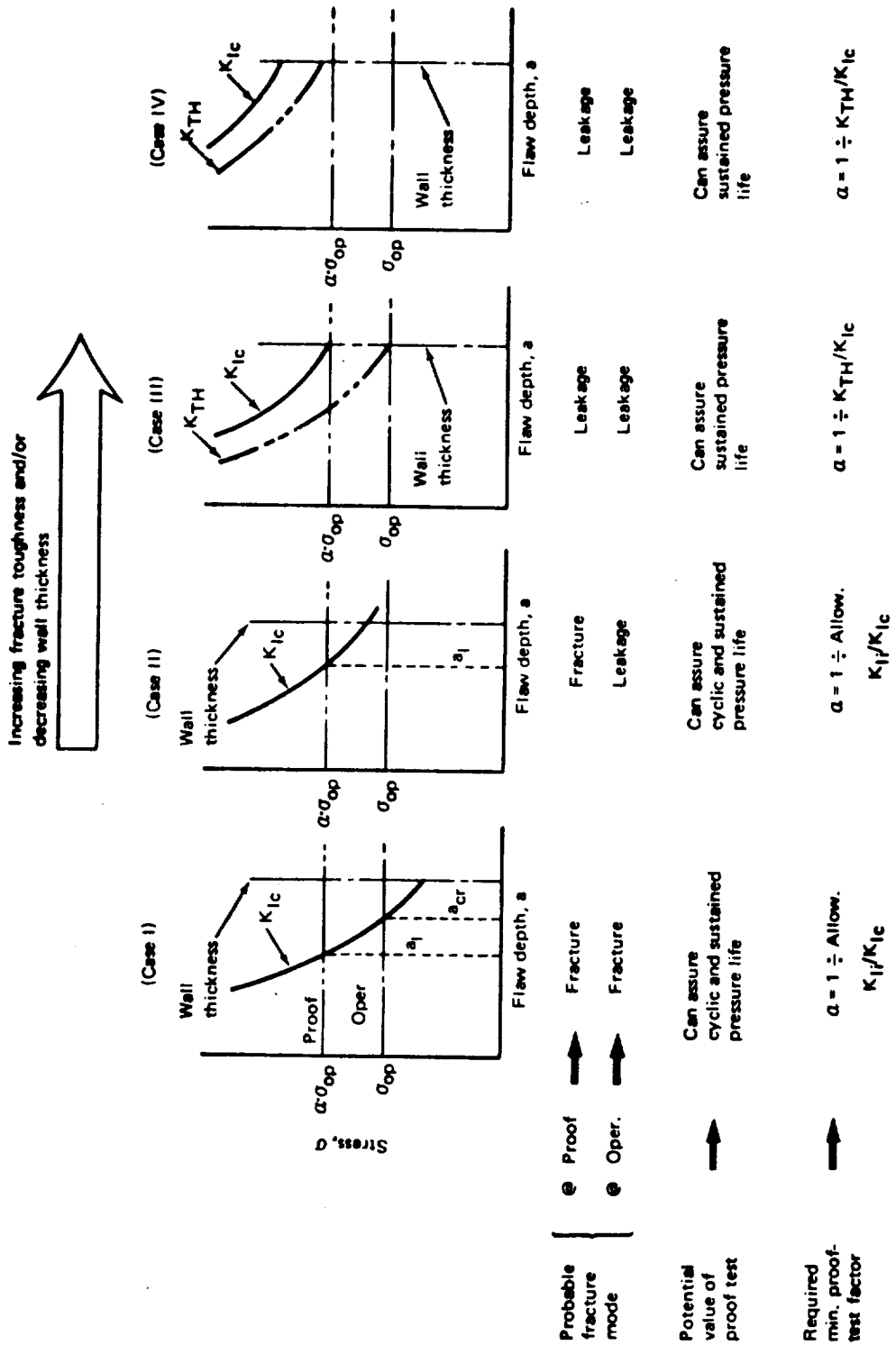
FIGURE E2-45. EFFECT OF WALL THICKNESS ON VALUE OF PROOF TEST

$\alpha = 1.25$. Will this proof factor assure that no failure occurs during the service life and if not, what proof factor is required?

The cyclic life curve for 5Al-2.5Sn (ELI) titanium is reproduced in Fig. E2-36. The estimated threshold stress-intensity value for sustained-stress flaw growth (K_{TH}/K_{Ic}) is approximately 0.92.

For long hold time, max. $K_{Ii}/K_{Ic} = 1/\alpha = 1/1.25 = 0.80$. From Fig. E2-36 for $K_{Ii}/K_{Ic} = 0.80$, N = 300 cycles. For $K_{TH}/K_{Ic} = 0.92$, N = 100 cycles.

In 300 cycles minus 100 cycles, or 200 cycles, the stress intensity would have reached the estimated threshold value for sustained-stress flaw growth. Thus the predicted minimum life would be only 200 cycles and the proof factor of 1.25 will not assure a service life of 600 cycles.

For 100 cycles plus 600 cycles, or 700 cycles,

$$K_{Ii}/K_{Ic} = 0.70 = \frac{1}{\alpha}$$

and

$$\alpha = \frac{1}{0.70} = 1.43 \quad ,$$

Thus, the 600-cycle service life requires a proof-test factor of 1.43 times the operating pressure.

REFERENCES

1. Fracture Toughness Testing and its Applications. ASTM Special Technical Publication No. 381, American Society for Testing and Materials, April 1965.

2. Irwin, G. R.: Fracture and Fracture Mechanics Report No. 202, T&AM Department of Theoretical and Applied Mechanics, University of Illinois, October 1961.

3. Irwin, G. R.: Crack Extension Force for a Part-Through Crack in a Plate. Journal of Applied Mechanics, Vol. 84 E, No. 4, December 1962.

4. Green, A. E.; and Sneddon, I. N.: The Distribution of Stress in the Neighborhood of a Flat Elliptical Crack in an Elastic Solid. Proceedings of the Cambridge Philosophical Society, Vol. 46, 1959.

5. Kobayashi, A. S.: On the Magnification Factors of Deep Surface Flaws. Structural Development Research Memorandum No. 16, The Boeing Co., December 1965.

6. Plane Strain Crack Toughness Testing. ASTM Special Technical Publication No. 410, American Society for Testing and Materials, December 1967.

7. Review of Developments in Plane Strain Fracture Toughness Testing. ASTM Special Technical Publication No. 463, American Society for Testing and Materials, September 1970.

8. Paris, P. C.; and Erdogan, F.: A Critical Analysis of Crack Propagation Laws. Journal of Basic Engineering, Transactions of the ASME, Series D, Vol. 85, 1963.

9. Foreman, R. G.; Kearney, V. E.; and Engle, R. M.: Numerical Analysis of Crack Propagation in Cyclic-Loaded Structures. Journal of Basic Engineering, Transactions of the ASME, September 1967.

10. Hudson, M. C.: Effect of Stress Ratio on Fatigue-Crack Growth in 7075-T6 and 2024-T3 Aluminum-Alloy Specimens. NASA TN D-5390, August 1969.

REFERENCES (Continued)

11. Tiffany, C. F.; Lorenz, P. M.; and Hall, L. R.: Investigation of Plane-Strain Flaw Growth in Thick-Walled Tanks. NASA CR-54837, 1966.

12. Fracture Control of Metallic Pressure Vessels. NASA SP-8040, May 1970.

13. Wheeler, O. E.: Spectrum Loading and Crack Growth. Transactions of the ASME, Journal of Basic Engineering, March 1972.

14. Elber, W.: Fatigue Crack Closure Under Cyclic Tension. Engineering Fracture Mechanics, Vol. II, No. 1, Pergamon Press, July 1970.

15. Elber, Wolf: The Significance of Fatigue Crack Closure. Damage Tolerance in Aircraft Structures, ASTM Special Technical Publications 486, American Society for Testing and Materials, 1971, pp. 230-242.

16. Pellissier, G. E.: Some Microstructural Aspects of Maraging Steel in Relation to Strength and Toughness. Technical Documentary Report RTD-TDR-63-4048. Air Force Materials Laboratory, Wright-Patterson Air Force Base, Ohio, November 1963.

17. Tiffany, C. F.; and Masters, J. N.: Applied Fracture Mechanics. ASTM Special Technical Publication No. 381, American Society for Testing and Materials, April 1965.

18. Wessel, E. T., et al. Engineering Methods for the Design and Selection of Materials Against Fracture. AD 801005, June 1966.

19. Progress in the Measurement of Fracture Toughness and the Application of Fracture Mechanics to Engineering Problems. American Society for Testing and Materials Special Committee on Fracture Testing of High-Strength Metallic Materials, Materials Research and Standards, Vol. 4, No. 3, March 1964, p. 107.

20. Pyle, R.; Schillinger, D. E.; and Carman, C. M.: Plane Strain Fracture Toughness and Mechanical Properties of 2219-T87 Aluminum and 5AL-2.5Sn(ELI) Titanium Alloy Weldments and One Inch Thick 5AL-2.5Sn(ELI) Titanium Alloy Plate. NASA CR-72154, Department of the Army, Frankfort Arsenal, September 1968.

REFERENCES (Concluded)

21.   Wilhem, D. P.: Fracture Mechanics Guidelines for Aircraft
Structural Applications. AFFDL-TR-69-111, Northrop Corp.,
February 1970.

22.   Shah, R. C.: Fracture Mechanics Assessment of Apollo Launch
Vehicle and Spacecraft Pressure Vessels. Vol. 1, Report D2-114248-1,
The Boeing Co., November 1968.

23.   Kobayashi, A. S.; and Hall, L. R.: On the Correction of Stress
Intensity Factors for Two Embedded Cracks. Structural Development
Research Memorandum No. 9, The Boeing Co., 1963.

SECTION F

COMPOSITES

SECTION F1

COMPOSITES CONCEPTS

TABLE OF CONTENTS

TABLE OF CONTENTS (Concluded)

DEFINITION OF SYMBOLS

Symbol	Definition
$[A]$	extensional rigidity matrix of laminate - equation (F1. 2-18)
$[\bar{A}]$	average laminate extensional rigidity matrix - equation (F1. 2-28)
$[A^*]$	laminate compliance matrix - equation (F1. 2-30)
$[B]$	coupling matrix - equations (F1. 2-18) and (F1. 2-19)
$[C]$	lamina stiffness matrix - equation (F1. 1-6)
$[C^*]$	column form of the stiffness matrix - equation (F1. 1-27)
$[\bar{C}^*]$	column form of the transformed stiffness matrix - equation (F1. 1-28)
$[\bar{C}]$	transformed stiffness matrix of $[C]$ - equation (F1. 2-15)
$[C']$	modified form of lamina stiffness matrix - equation (F1. 2-1)
$[\bar{C}']$	transformed matrix of the modified stiffness matrix - equation (F1. 2-10)
C_{ij}	components of the stiffness matrix $[C]$, $[C']$
$\bar{C}_{ij}$	components of the transformed stiffness matrix $[\bar{C}]$, $[\bar{C}*]$, $[\bar{C}']$
$[D]$	laminate flexural rigidity matrix - equation (F1. 2-19)
E	Young's modulus of elasticity
E_{ij}	Young's modulus of laminae in lamina principal direction - equation (F1. 1-15)

Symbol	Definition
G_{ij}	shear moduli in the i-j plane - equation (F1. 1-15)
J	invariants of stiffness matrix transformations - equation (F1. 2-12)
K	lamina index indicating position in laminate
M	laminate bending and twisting moments - equation (F1. 2-17)
N	laminate forces - equation (F1. 2-16)
[S]	lamina compliance matrix - equation (F1. 1-7)
S_{ij}	components of the lamina compliance matrix
[T]	stress and strain transformation matrix - equation (F1. 1-3)
dA	differential area - equation (F1. 1-1)
h_K	distance from reference surface to plane separating laminae K and K+1 - Fig. F1. 2-3
t	laminate total thickness - Fig. F1. 2-3
x	principal longitudinal laminate axis (Fig. F1. 0-1)
y	principal transverse laminate axis (Fig. F1. 0-1)
z	principal normal laminate axis (Fig. F1. 0-1)
α	principal longitudinal lamina axis (Fig. F1. 0-2)
β	principal transverse lamina axis (Fig. F1. 0-2)
γ	shear strain

Symbol	Definition
γ^o	shear strain of laminate middle surface - equation (F1. 2-13)
ϵ	strain
ϵ^o	strain of laminate middle surface - equation (F1. 2-13)
$[\epsilon]$	strain column matrix - (F1. 1-10)
η	shear coupling ratios - equation (F1. 1-15)
θ	angular orientation of a lamina in a laminate, i. e. , the angle between the x and α axis - positive is counterclockwise
ν	Poisson's ratio
σ	stress
$[\sigma]$	stress column matrix - equation (F1. 1-9)
τ	shear stress
χ	curvature of laminate middle surface - equation (F1. 2-13)

SUBSCRIPTS

1, 2, 3	arbitrary local coordinate system
α, β, z	lamina principal axes
x, y, z	laminate reference axes
ij	the (i-j) position in a sequence where i and j vary between 1 and 3
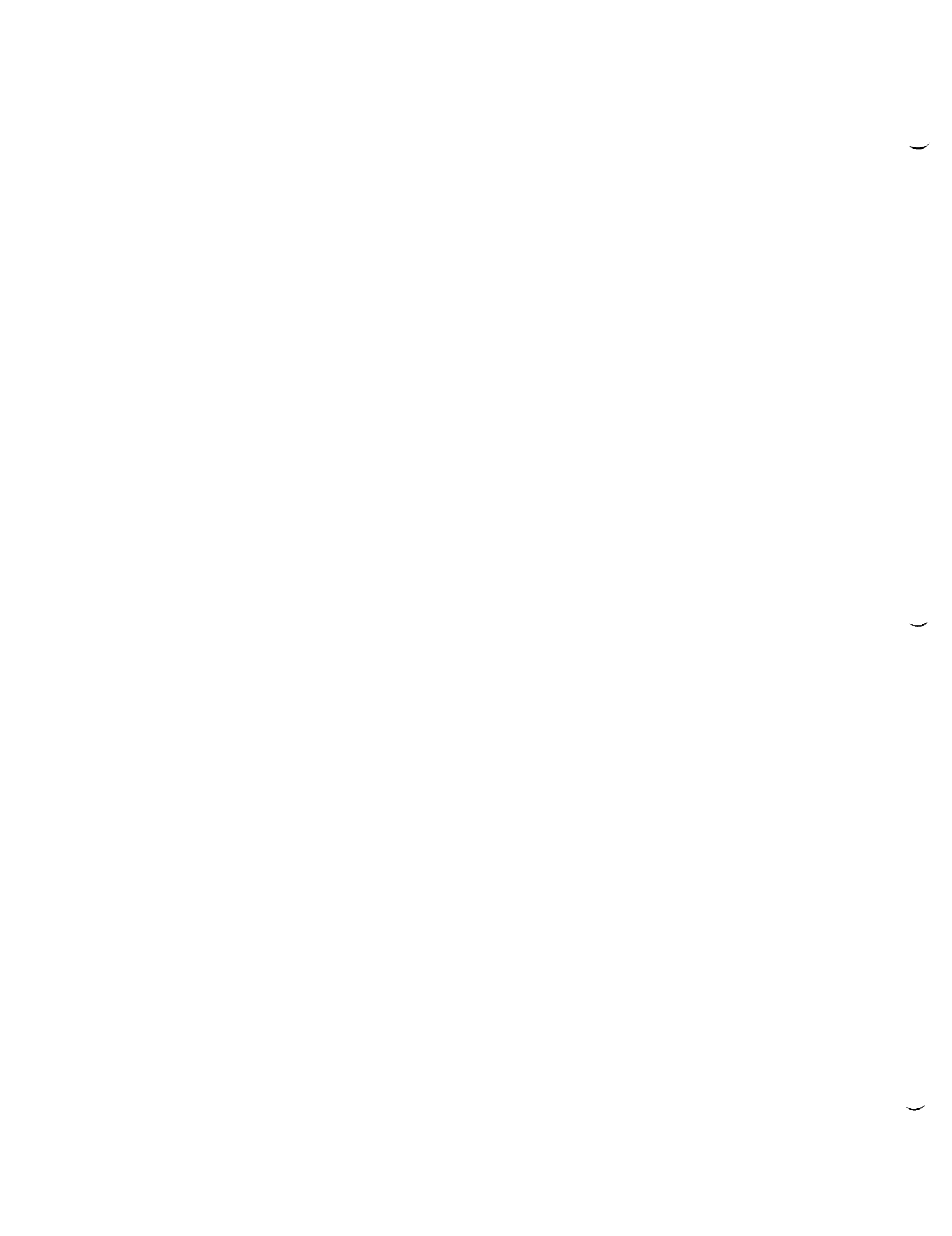
F1.0 COMPOSITES - BASIC CONCEPTS AND NOTATIONS.

The purpose of this section is to present state-of-the-art techniques utilized in the design and stress analysis of advanced composite structures. An attempt was made to keep the analytical developments and material as elementary as possible. However, the stress analysis of composite materials is more complex than that of conventional materials, and, as a result, the analysis techniques and concepts may seem rather involved.

In order to understand the mechanics of laminated composites, one must have a knowledge of certain basic definitions. These definitions, obtained primarily from References 1, 2, and 3, are intended to serve not only as a reference for this section but also as a guide to general literature on composite materials.

AEOLOTROPY   See anisotropic.

ANGLEPLY   Any filamentary laminate constructed with equal numbers of pairs of laminae with symmetry about the coordinate (x, y) axis. An alternate definition used frequently in current literature, but not in this section, is a laminate consisting of an even number of layers having the same thickness, and

the orthotropic axes of symmetry in each

ply are alternately oriented at angles of

+ θ and - θ to the laminate axes.

ANISOTROPIC

Not isotropic; having mechanical and/or

physical properties which vary with

direction relative to natural reference

axes inherent in the material.

BALANCED COMPOSITE

A composite laminate whose layup is

symmetrical with relation to the midplane

of the laminate (Fig. F1.0-1).
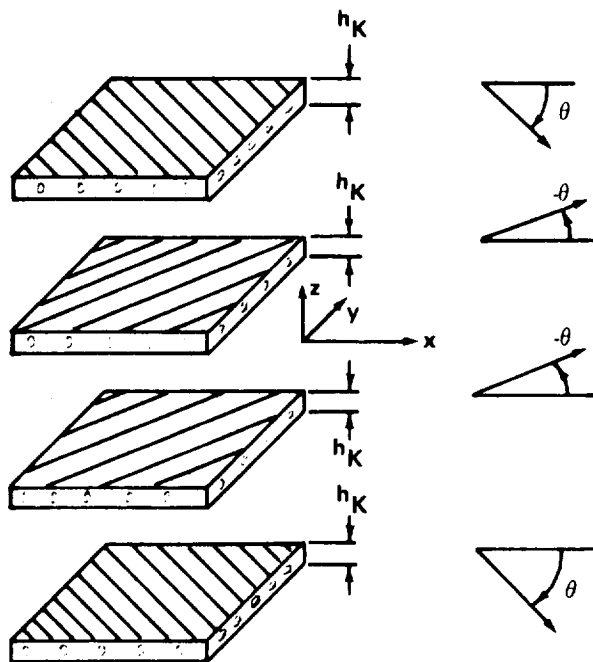
FIGURE F1.0-1. BALANCED OR SYMMETRIC COMPOSITE

BUCKLING

Buckling is a mode of failure characterized generally by an unstable lateral deflection caused by compressive action on the structural element involved. In advanced composites, buckling may take the form not only of conventional general instability and local instability but also of a microinstability of individual fibers.

COMPLIANCE MATRIX

The compliance matrix is defined by the equation $\epsilon_i = S_{ij}\sigma_j$, where S_{ij} are the components of the compliance matrix; may be obtained by inverting the stiffness matrix.

COMPOSITE MATERIAL

Composites are considered to be combinations of materials differing in composition or form on a macroscale. The constituents retain their identities in the composite; that is, they do not dissolve or otherwise merge completely into each other although they act in concert. Normally, the components can be physically identified

and lead to an interface between components

(Fig. F1.0-2).
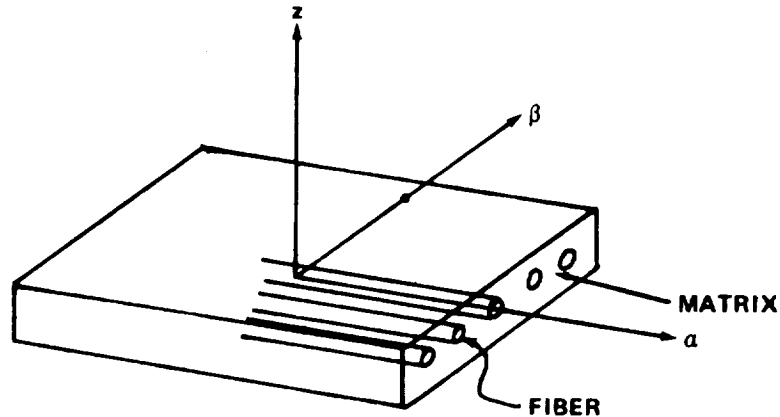
FIGURE F1.0-2. PRINCIPAL CONSTITUENTS OF COMPOSITE
LAMINA AND PRINCIPAL AXES

CONSTITUENT	In general, an element of a larger grouping; in advanced composites, the principal constituents are the fibers and the matrix (refer to Fig. F1.0-2).
CONSTITUTIVE	Refers to the stress-strain (Hooke's Law) relationships for a material because the stress-strain relations actually describe the mechanical constitution of the material.
CROSSPLY	Any filamentary laminate constructed with equal numbers of pairs of laminae at angles of 0 deg and 90 deg to the laminate axes.

An alternate definition used frequently in current literature, but not in this section, is a laminate consisting of an even number of layers all of the same thickness with the orthotropic axes of symmetry in each ply alternately oriented at angles of 0 deg and 90 deg to the laminate axes.

DELAMINATION

The separation of the layers of material in a laminate.

FIBER

A single homogeneous strand of material, essentially one-dimensional in the macrobehavior sense, used as a principal constituent in advanced composites because of its high axial strength and modulus (refer to Fig. F1.0-2).

FIBER CONTENT

The amount of fiber present as reinforcement in a composite. This is usually expressed as a percentage volume fraction or weight fraction of the composite.

FIBER DIRECTION

The orientation or alignment of the longitudinal axis of the fiber with respect to a stated reference axis (Fig. F1. 0-3).
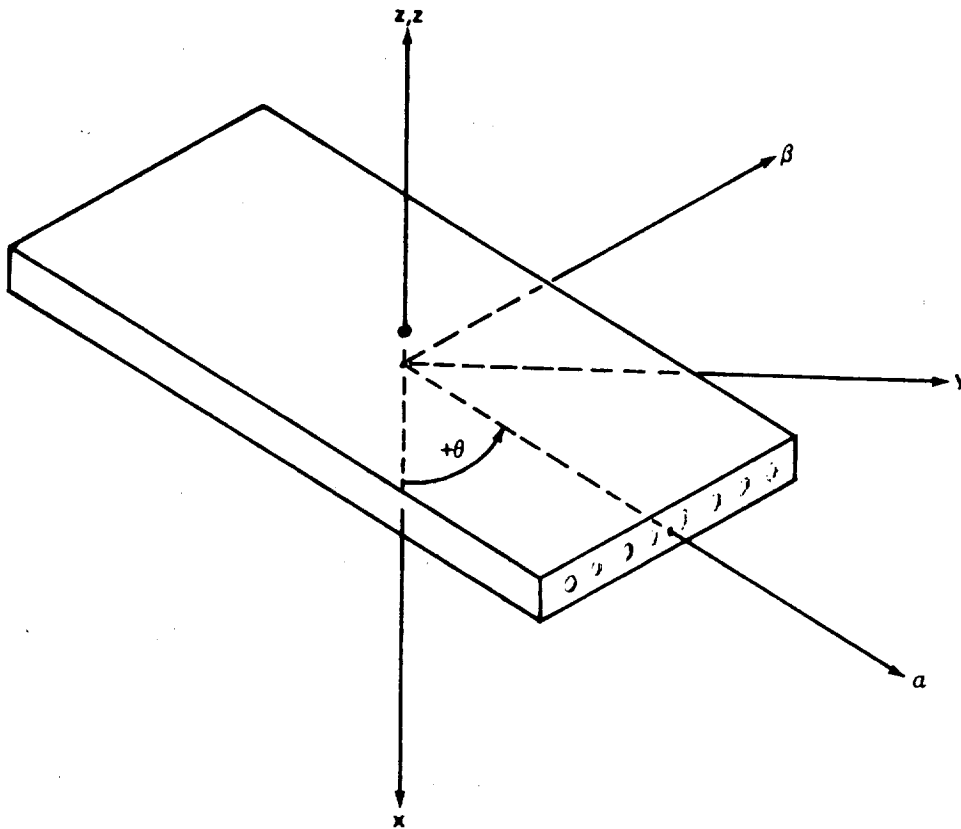
FIGURE F1. 0-3.   LAMINA AXIS ORIENTATION

FILAMENT

A variety of fibers characterized by extreme length, such that there are normally no filament ends within a part except at geometric discontinuities. Filaments are used in filamentary

composites and are also used in filament winding processes, which require long, continuous strands.

FILAMENTARY COMPOSITES

Composite materials of laminae in which the continuous filaments are in nonwoven, parallel, uniaxial arrays. Individual uniaxial laminae are combined into specifically oriented multiaxial laminates for application to specific envelopes of strength and stiffness requirements (Fig. F1. 0-4).
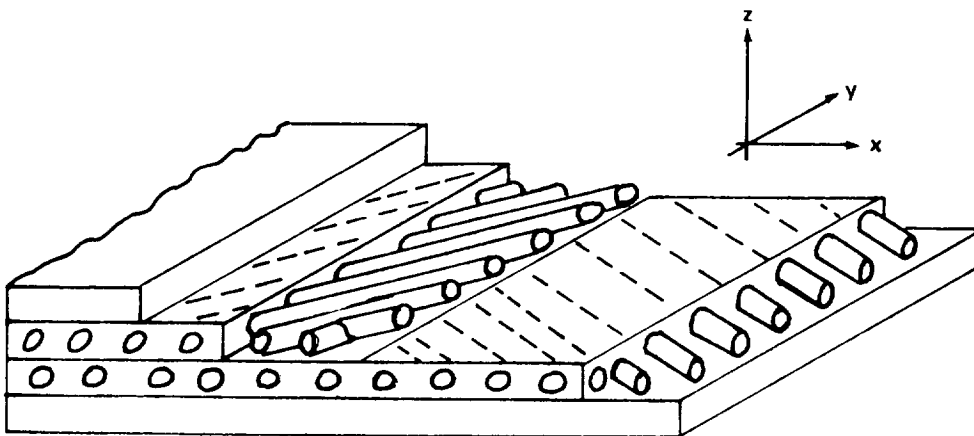
FIGURE F1. 0-4. FILAMENTARY COMPOSITE

GENERALLY ORTHOTROPIC

Descriptive term for a lamina for which the constitutive equation, when transformed

to an arbitrary set of axes, is fully

populated. That is, for

$$
\begin{bmatrix} \sigma_x \\ \sigma_y \\ \tau_{xy} \end{bmatrix}^K = \begin{bmatrix} \overline{C}_{11} & \overline{C}_{12} & \overline{C}_{16} \\ \overline{C}_{12} & \overline{C}_{22} & \overline{C}_{26} \\ \overline{C}_{16} & \overline{C}_{26} & \overline{C}_{66} \end{bmatrix}^K \begin{bmatrix} \epsilon_x \\ \epsilon_y \\ \gamma_{xy} \end{bmatrix}^K ,
$$

$$
\overline{C}_{16} \neq 0, \quad \overline{C}_{26} \neq 0,
$$

HENCKY-VON MISES DISTORTIONAL ENERGY THEORY

Yield criterion using distortional energy for isotropic materials:

$$
(\sigma_1 - \sigma_2)^2 + (\sigma_2 - \sigma_3)^2 + (\sigma_3 - \sigma_1)^2 + 6(\sigma_{12}^2 + \sigma_{23}^2 + \sigma_{31}^2) = 2\sigma_0^2 .
$$

HETEROGENEOUS

Descriptive term for a material consisting of dissimilar contituents separately identifiable; a medium consisting of regions of unlike properties separated by internal boundaries; not homogeneous.

HILL

Generalized von Mises yield criterion to account for anisotropy:

$$2f(\sigma_{ij}) = A_1 (\sigma_2 - \sigma_3)^2 + A_2 (\sigma_3 - \sigma_1)^2 + A_3 (\sigma_1 - \sigma_2)^2 + 2A_4 \sigma_{23}^2$$

$$+ 2A_5 \sigma_{31}^2 + 2A_6 \sigma_{12}^2 = 1 ,$$

where

$$2f(\sigma_{ij}) = \text{the plastic potential,}$$

$$2A_1 = (F_2)^{-2} + (F_3)^{-2} - (F_1)^{-2} ,$$

$$2A_2 = (F_3)^{-2} + (F_1)^{-2} - (F_2)^{-2} ,$$

$$2A_3 = (F_1)^{-2} + (F_2)^{-2} - (F_3)^{-2} ,$$

$$2A_4 = (F_{23})^{-2} ,$$

$$2A_5 = (F_{31})^{-2} ,$$

$$2A_6 = (F_{12})^{-2} ,$$

and F_1, F_2, and F_3 are determined from uniaxial tension or compression tests, and F_{12}, F_{23}, and F_{31} are determined from pure shear tests.

HOMOGENEOUS	Descriptive term for a material of uniform composition throughout; a medium which has no internal physical boundaries; a material whose properties are constant and isotropic at every point.
HOMOGENEOUS ANISOTROPIC	Descriptive term for a material which has no plane of material symmetry such as the orthotropic material.

HOMOGENEOUS GENERALLY ORTHOTROPIC	Descriptive term for a lamina which behaves in a manner similar to the anisotropic lamina.
HOMOGENEOUS ISOTROPIC	Descriptive term for a lamina which has a constant modulus of elasticity and the $C_{16} = C_{26} = 0$ in its constitutive equation.
HORIZONTAL SHEAR	See interlaminar shear.
INTERFACE	The boundary between the individual, physically distinguishable constituents of a composite.
INTERLAMINAR SHEAR	Shear force which tends to produce a relative displacement between two laminae in a laminate along the plane of their interface.
ISOTROPIC	Descriptive term for a material which has uniform material properties in all directions.
LAMINA	A single ply or layer in a laminate made of a series of layers (Fig. F1.0-5).
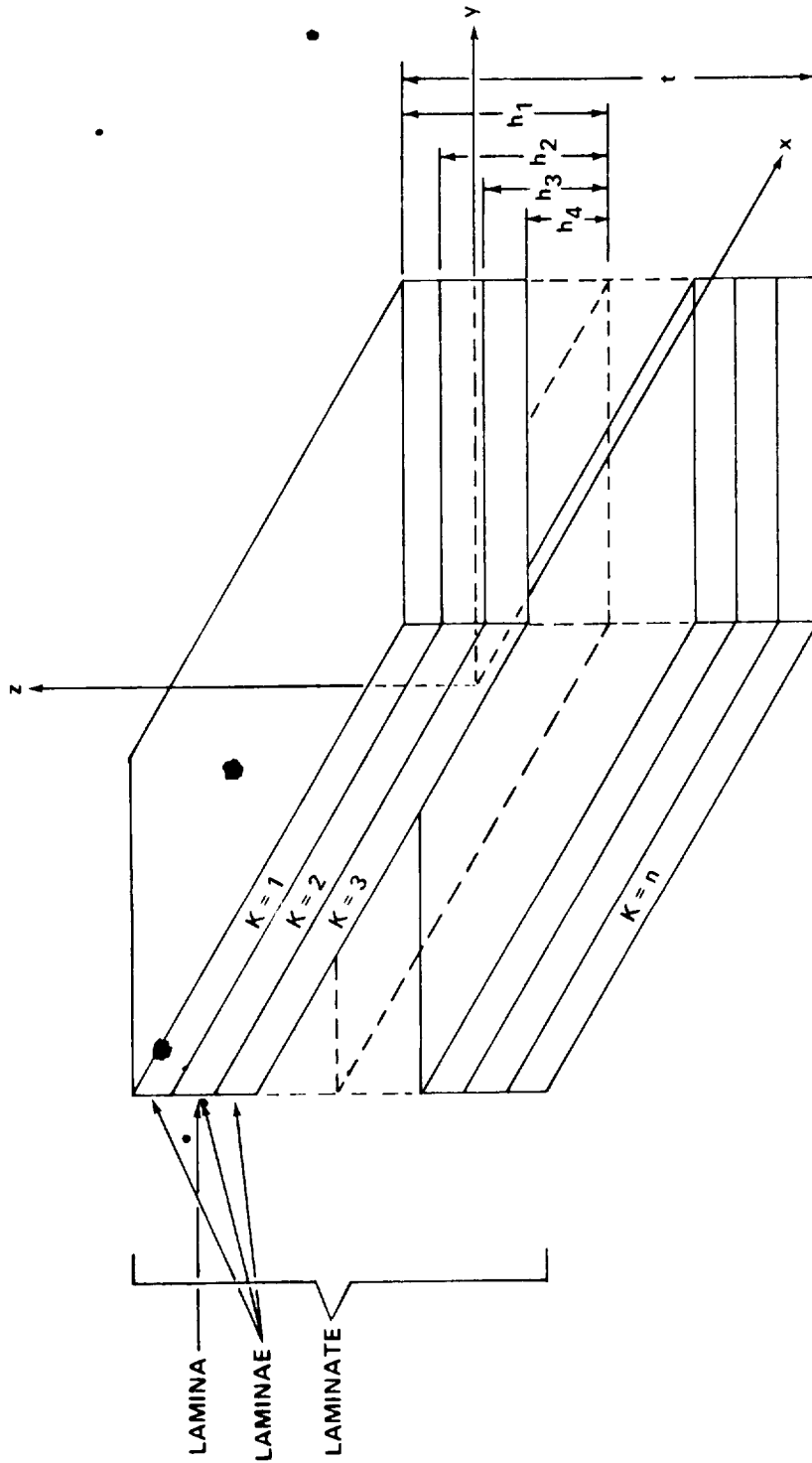
FIGURE F1.0-5. LAMINA NOTATION

LAMINAE	Plural of lamina (refer to Fig. F1.0-5).
LAMINATE	A product made by bonding together two or more layers of laminae of material or materials (refer to Fig. F1.0-5).
LAMINATE ORIENTATION	The configuration of crossplied composite laminate with regard to the angles of crossplying, the number of laminate at each angle, and the exact sequence of the individual laminae.
LAYUP	A process of fabrication involving the placement of successive layers of materials.
MACRO	In relation to composites, denotes the gross properties of a composite as a structural element but does not consider the individual properties or identity of the constituents.
MATRIX	The essentially homogeneous material in which the fibers or filaments of a composite are imbedded (refer to Fig. F1.0-2).

MICRO

In relation to composites, denotes the properties of the constituents and their effect on the composite properties.

ORTHOTROPIC

Descriptive term for a material which has three mutually perpendicular planes of elastic symmetry.

PRINCIPAL AXES

The set of axes in a lamina which is parallel and perpendicular to the filament direction is called the lamina principal axes (refer to Fig. F1.0-2).

QUASI-ISOTROPIC

Descriptive term for a laminate which has essentially isotropic stiffnesses and perhaps strength.

SPECIALLY ORTHOTROPIC

Descriptive term for lamina for which the $C_{16} = C_{26} = 0$ in its constitutive equation.

TENSOR

A tensor is a physical entity in nature which obeys certain transformation relations. There are different orders of

tensors, and each order has its own

transformation relations.

TRANSVERSELY ISOTROPIC   Descriptive term for a material exhibiting

a special case of orthotropy in which

properties are identical in two orthotropic

dimensions, but not in the third; having

identical properties in both transverse

directions but not the longitudinal

direction.

VON-MISES DISTORTIONAL   See Hencky-von Mises Distortional Energy
ENERGY THEORY

Theory.

x-AXIS   An axis in the plane of the laminate which

is used as the 0 deg reference for

designating the angle of lamina (refer to

Fig. F1.0-5).

y-AXIS   The axis in the plane of the laminate which

is perpendicular to the x-axis (refer to

Fig. F1.0-5).

z-AXIS   The reference axis normal to the plane of

the laminate (refer to Fig. F1.0-5).

1.1   BASIC CONCEPTS.

Some of the basic concepts applicable to all continuums, in particular composites, are presented in this subsection. These include the concepts of stress and strain at a point and their transformation relations.

1.1.1   STRESS AND STRAIN.

Following the guide of Reference 1, stress and strain relations at a point will be reviewed to form a firm base for the analytical development for composites.

A tensor, as defined previously, is some physical entity in nature which obeys certain transformation relations. A scalar, for example, is a tensor of zero-th order, and a vector is a tensor of first order. It is well known that the components of a vector change when the coordinate system is altered or rotated. This change in the components of the vector is governed by certain mathematical relations or transformations. Each order of tensors has its own transformation relations; therefore, it is necessary only to establish that a physical entity is a tensor and determine its order, and the transformation relations are defined.

Stress and strain are both second-order tensors and their transformation relations are well known (the graphical form of the transformation is the Mohr's circle). These transformation relations may be derived from the equilibrium relations of a small element. Consider a two-dimensional problem as shown

in Fig. F1. 1-1. By summing forces in the "1" direction, the following equation results:

$$\sigma_1 \, dA - \sigma_x \, (\cos \theta \, dA) \, (\cos \theta) - \sigma_y \, (\sin \theta \, dA) \, (\sin \theta)$$

$$- \tau_{xy} \, (\sin \theta \, dA) \, (\cos \theta) - \tau_{xy} \, (\cos \theta \, dA) \, (\sin \theta) = 0 \ ,$$

or

$$\sigma_1 = \sigma_x \cos^2 \theta + \sigma_y \sin^2 \theta + \tau_{xy} \, (2 \sin \theta \cos \theta) \qquad (\text{F1. 1-1})$$
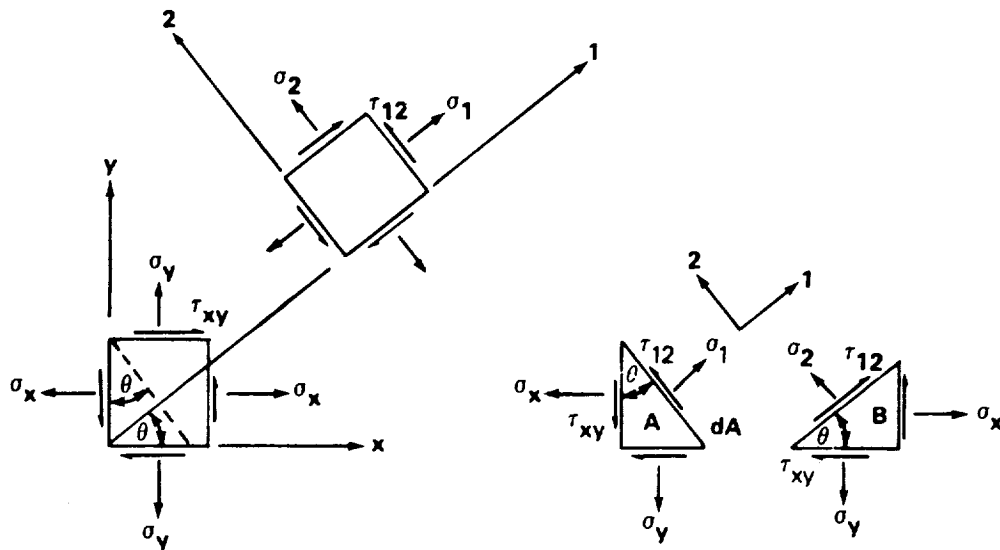
FIGURE F1. 1-1.   STRESS COORDINATE ROTATION

In a similar manner, the other transformed stresses, σ_2 and τ_{12} , may be determined. These equations may be written in a form convenient for later developments, a matrix form. Thus,

$$
\begin{bmatrix} \sigma_1 \\ \sigma_2 \\ \tau_{12} \end{bmatrix}
=
\begin{bmatrix}
\cos^2 \theta & \sin^2 \theta & (2 \sin \theta \cos \theta) \\
\sin^2 \theta & \cos^2 \theta & (-2 \sin \theta \cos \theta) \\
(-\sin \theta \cos \theta) & (\sin \theta \cos \theta) & (\cos^2 \theta - \sin^2 \theta)
\end{bmatrix}
\begin{bmatrix} \sigma_x \\ \sigma_y \\ \tau_{xy} \end{bmatrix}
. \quad (F1.\,1\text{-}2)
$$

Using a more compact notation, we may write equation (F1. 1-2) as

$$
\begin{bmatrix} \sigma_1 \\ \sigma_2 \\ \tau_{12} \end{bmatrix}
=
[T]
\begin{bmatrix} \sigma_x \\ \sigma_y \\ \tau_{xy} \end{bmatrix}
\qquad (F1.\,1\text{-}3)
$$

where [T] is the symbol for the transformation matrix. Equation (F1. 1-3) is the

transformation relation for the stress tensor when reduced to a two-dimensional

space. Equation (F1. 1-3) is the necessary relationship required to transform

any two-dimensional stress state from one set of coordinates to another set.

With a slight modification, the two-dimensional strain may be

transformed by the same transformation:

$$
\begin{bmatrix} \epsilon_1 \\ \epsilon_2 \\ \tfrac{1}{2}\gamma_{12} \end{bmatrix}
=
[T]
\begin{bmatrix} \epsilon_x \\ \epsilon_y \\ \tfrac{1}{2}\gamma_{xy} \end{bmatrix}
\qquad . \qquad (F1.\,1\text{-}4)
$$

1. 1. 2   GENERALIZED HOOKE'S LAW.

In this paragraph the constants of proportionality between stress and strain (Hooke's law constants) are shown to be components of a fourth-order tensor and therefore have a set of transformation relations different from those for stress and strain. Several forms of the Hooke's law relationships and the elastic constants will be shown for the various material conditions.

1. 1. 2. 1   Homogeneous Isotropic Material.

For the familiar homogeneous isotropic material in a one-dimensional stress state [1], the Hooke's law relationship is

$$\sigma = E\epsilon \ . \tag{F1. 1-5}$$

The proportionality constant (E) is Young's modulus, or the modulus of elasticity, and is a scalar value.

1. 1. 2. 2   Elastic Linear Anisotropic Material.

Consider the most general material, but require elasticity and linearity, which is the anisotropic material. This material has 21 elastic constants. The constitutive equation (Hooke's law) is [2]

$$[\sigma] = \begin{bmatrix} C_{11} & C_{12} & C_{13} & C_{14} & C_{15} & C_{16} \\ & C_{22} & C_{23} & C_{24} & C_{25} & C_{26} \\ & & C_{33} & C_{34} & C_{35} & C_{36} \\ & & & C_{44} & C_{45} & C_{46} \\ \text{Symmetric} & & & & C_{55} & C_{56} \\ & & & & & C_{66} \end{bmatrix} [\epsilon] \ . \tag{F1. 1-6}$$

The components C_{ij} are called components of the "stiffness" matrix. The equation may be written as

$$[\epsilon] = \begin{bmatrix} S_{11} & S_{12} & S_{13} & S_{14} & S_{15} & S_{16} \\ & S_{22} & S_{23} & S_{24} & S_{25} & S_{26} \\ & & S_{33} & S_{34} & S_{35} & S_{36} \\ & \text{Symmetric} & & S_{44} & S_{45} & S_{46} \\ & & & & S_{55} & S_{56} \\ & & & & & S_{66} \end{bmatrix} [\sigma]$$

(F1. 1-7)

where

$$[C] = [S]^{-1} .$$

(F1. 1-8)

The components S_{ij} are called components of the "compliance" matrix. The $[\sigma]$ conventionally symbolizes [3]

$$[\sigma] = \begin{bmatrix} \sigma_1 \\ \sigma_2 \\ \sigma_3 \\ \tau_{23} \\ \tau_{13} \\ \tau_{12} \end{bmatrix} .$$

(F1. 1-9)

Similarly,

$$[\epsilon] = \begin{bmatrix} \epsilon_1 \\ \epsilon_2 \\ \epsilon_3 \\ \gamma_{23} \\ \gamma_{13} \\ \gamma_{12} \end{bmatrix} .$$

(F1. 1-10)

1. 1. 2. 3 Monoclinic Material.

If a material possesses one plane of symmetry, it is termed a

monoclinic material and has 13 independent elastic constants. If the plane of

symmetry is assumed to be the x-y plane, the constitutive equations are [2]

$$[\sigma] = \begin{bmatrix} C_{11} & C_{12} & C_{13} & 0 & 0 & C_{16} \\ & C_{22} & C_{23} & 0 & 0 & C_{26} \\ & & C_{33} & 0 & 0 & C_{36} \\ & & & C_{44} & C_{45} & 0 \\ & \text{Symmetric} & & & C_{55} & 0 \\ & & & & & C_{66} \end{bmatrix} [\epsilon] \qquad (F1. 1\text{-}11)$$

and

$$[\epsilon] = \begin{bmatrix} S_{11} & S_{12} & S_{13} & 0 & 0 & S_{16} \\ & S_{22} & S_{23} & 0 & 0 & S_{26} \\ & & S_{33} & 0 & 0 & S_{36} \\ & & & S_{44} & S_{45} & 0 \\ & \text{Symmetric} & & & S_{55} & 0 \\ & & & & & S_{66} \end{bmatrix} [\sigma] . \qquad (F1. 1\text{-}12)$$

1. 1. 2. 4 Orthotropic Material.

If the anisotropic material possesses two orthogonal planes of symmetry,

assuming x = 0 and z = 0, the material is termed orthotropic. In this

condition, there are only nine independent elastic constants. Note that if a

material has two orthogonal planes of symmetry, three orthogonal planes of

symmetry exist. The constitutive equations of the orthotropic material are

$$[\sigma] = \begin{bmatrix} C_{11} & C_{12} & C_{13} & 0 & 0 & 0 \\ & C_{22} & C_{23} & 0 & 0 & 0 \\ & & C_{33} & 0 & 0 & 0 \\ & & & C_{44} & 0 & 0 \\ \text{Symmetric} & & & & C_{55} & 0 \\ & & & & & C_{66} \end{bmatrix} [\epsilon] \qquad (F1.1-13)$$

and

$$[\epsilon] = \begin{bmatrix} S_{11} & S_{12} & S_{13} & 0 & 0 & 0 \\ & S_{22} & S_{23} & 0 & 0 & 0 \\ & & S_{33} & 0 & 0 & 0 \\ & & & S_{44} & 0 & 0 \\ \text{Symmetric} & & & & S_{55} & 0 \\ & & & & & S_{66} \end{bmatrix} [\sigma] . \qquad (F1.1-14)$$

Since most composite structures will be constructed of orthotropic

laminates, this material is of particular interest. The engineering constants,

values which are establishable from uniaxial and pure shear tests, may easily

be equated to the components of the compliance matrix. The compliance

components are then

$$S_{11} = \frac{1}{E_{11}} , \qquad S_{22} = \frac{1}{E_{22}} , \qquad S_{33} = \frac{1}{E_{33}} .$$

$$S_{12} = \frac{-\nu_{12}}{E_{11}} \qquad S_{23} = \frac{-\nu_{23}}{E_{22}} \qquad S_{31} = \frac{-\nu_{31}}{E_{33}}$$

$$= \frac{-\nu_{21}}{E_{22}} , \qquad = \frac{-\nu_{32}}{E_{33}} , \qquad = \frac{-\nu_{13}}{E_{11}} . \qquad (F1.1-15)$$

$$S_{66} = \frac{1}{G_{12}} , \qquad S_{55} = \frac{1}{G_{13}} \qquad S_{44} = \frac{1}{G_{23}} .$$

$$S_{16} = \frac{\eta_{16}}{E_{11}} , \qquad S_{26} = \frac{\eta_{26}}{E_{22}} , \qquad S_{36} = \frac{\eta_{36}}{E_{33}} .$$

where

E_{11}, E_{22}, E_{33} = Young's moduli in the 1, 2, and 3 (x, y, and z)
directions, respectively,

ν_{ij} = Poisson's ration

$\quad = \dfrac{\text{strain in the j direction}}{\text{strain in the i direction}}$

caused by a stress in the i direction,

G_{ij} = shear moduli in the i-j plane,

η_{ij} = shear coupling ratios.

Note that the S_{16}, S_{26}, and S_{36} terms are used for a "monoclinic"

material. From equation (F1.1-8), the components of the stiffness matrix may

be determined as

$C_{11} = (1 - \nu_{23}\,\nu_{32})\ VE_{11}$,

$C_{22} = (1 - \nu_{31}\,\nu_{13})\ VE_{22}$,

$C_{33} = (1 - \nu_{12}\,\nu_{21})\ VE_{33}$,

$C_{12} = (\nu_{21} + \nu_{23}\,\nu_{31})\ VE_{11}$,

$\quad = (\nu_{12} + \nu_{13}\,\nu_{32})\ VE_{22}$,

$C_{13} = (\nu_{31} + \nu_{21}\,\nu_{32})\ VE_{11}$,

$\quad = (\nu_{13} + \nu_{23}\,\nu_{12})\ VE_{33}$,

(F1.1-16)

$C_{23} = (\nu_{32} + \nu_{12}\,\nu_{31})\ VE_{22}$,

$\quad = (\nu_{23} + \nu_{21}\,\nu_{13})\ VE_{33}$,

$C_{44} = G_{23}$,

$C_{55} = G_{31}$,

and

$C_{66} = G_{12}$,

where

$$V = \left(1 - \nu_{12}\,\nu_{21} - \nu_{23}\,\nu_{32} - \nu_{31}\,\nu_{13} - 2\nu_{12}\nu_{23}\nu_{31}\right)^{-1} \quad .$$

For an orthotropic material in a state of plane stress, the constitutive equation is [1]

$$
\begin{bmatrix} \sigma_1 \\ \sigma_2 \\ \tau_{12} \end{bmatrix}
=
\begin{bmatrix} C_{11} & C_{12} & 0 \\ C_{12} & C_{22} & 0 \\ 0 & 0 & C_{66} \end{bmatrix}
\begin{bmatrix} \epsilon_1 \\ \epsilon_2 \\ \gamma_{12} \end{bmatrix}
\qquad \text{(F1.\,1-17)}
$$

where

$$C_{11} = \frac{E_{11}}{(1 - \nu_{12}\,\nu_{21})} \quad ,$$

$$C_{22} = \frac{E_{22}}{(1 - \nu_{12}\,\nu_{21})} \quad , \qquad \text{(F1.\,1-18)}$$

$$C_{12} = \frac{\nu_{21}E_{11}}{(1 - \nu_{12}\,\nu_{21})} = \frac{\nu_{12}E_{22}}{(1 - \nu_{12}\,\nu_{21})} \quad ,$$

and

$$C_{66} = G_{12} \quad .$$

1. 1. 2. 5 Isotropic Material.

For an isotropic material, there are only two independent elastic

constants. The constitutive relations are [3]

$$[\sigma] = \begin{bmatrix} C_{11} & C_{12} & C_{13} & 0 & 0 & 0 \\ & C_{11} & C_{12} & 0 & 0 & 0 \\ & & C_{11} & 0 & 0 & 0 \\ & & & \frac{1}{2}(C_{11} - C_{12}) & 0 & 0 \\ \text{Symmetric} & & & & \frac{1}{2}(C_{11} - C_{12}) & 0 \\ & & & & & \frac{1}{2}(C_{11} - C_{12}) \end{bmatrix} [\epsilon] \qquad (F1.1\text{-}19)$$

and

$$[\epsilon] = \begin{bmatrix} S_{11} & S_{12} & S_{12} & 0 & 0 & 0 \\ & S_{11} & S_{12} & 0 & 0 & 0 \\ \text{Symmetric} & & S_{11} & 0 & 0 & 0 \\ & & & 2(S_{11} - S_{12}) & 0 & 0 \\ & & & & 2(S_{11} - S_{12}) & 0 \\ & & & & & 2(S_{11} - S_{12}) \end{bmatrix} [\sigma] \ . \qquad (F1.1\text{-}20)$$

The constitutive constants may be defined in terms of the engineering

constants as

$$C_{11} = C_{22} = C_{33} = \frac{(1 - \nu) E}{(1 + \nu)(1 - 2\nu)} \quad ,$$

$$C_{12} = C_{13} = C_{23} = \frac{\nu E}{(1 + \nu)(1 - 2\nu)} \quad , \qquad (F1.1\text{-}21)$$

$$C_{44} = C_{55} = C_{66} = G = \frac{E}{2(1 + \nu)} \quad ,$$

$$S_{11} = S_{22} = S_{33} = \frac{1}{E} \quad ,$$

$$S_{12} = S_{13} = S_{23} = \frac{-\nu}{E} \quad ,$$

and

$$S_{44} = S_{55} = S_{66} = \frac{1}{G} = \frac{2(1 + \nu)}{E} \quad .$$

If the isotropic material is assumed to be in a two-dimensional stress state (plane stress), equation (F1.1-19) may be written as [1]

$$\begin{bmatrix} \sigma_1 \\ \sigma_2 \\ \tau_{12} \end{bmatrix} = \begin{array}{l} = \\ = \\ = \end{array} \begin{bmatrix} C_{11} & C_{12} & 0 \\ C_{12} & C_{22} & 0 \\ 0 & 0 & C_{66} \end{bmatrix} \begin{bmatrix} \epsilon_1 \\ \epsilon_2 \\ \gamma_{12} \end{bmatrix} \qquad (F1.1-22)$$

where

$$C_{11} = C_{22} = \frac{E}{(1 - \nu^2)} \quad ,$$

$$C_{12} = \frac{E}{(1 - \nu^2)} \quad , \qquad\qquad (F1.1-23)$$

and

$$C_{66} = \frac{E}{2(1 + \nu)} = G \quad .$$

1.1.2.6   Transformation of Stiffness Matrix.

In Reference 1, the elastic constants (stiffness) for a material are stated to be components of a fourth-order tensor and consequently, must obey certain transformation relations. The transformation of a general anistropic material, in three dimensions and rotated an angle θ about the z-axis, is given in Reference 2 as

$$[\overline{C}*] = [T_R] [C*] \tag{F1.1-24}$$

where

$$[T_R] = \begin{bmatrix}
\begin{matrix}
m^4 & 2m^3n^2 & 2m^3n & n^4 & 2mn^3 & m^2n^2 \\
m^2n^2 & m^4+n^4 & mn^3-m^3n & m^2n^2 & m^3n-mn^3 & -m^2n^2 \\
-2m^3n & 2m^3n-2mn^3 & m^4-3m^2n^2 & 2mn^3 & 3m^2n^2-n^4 & m^3n-mn^3 \\
n^4 & 2m^2n^2 & -2mn^3 & m^4 & -2m^3n & m^2n^2 \\
-2mn^3 & 2mn^3-2m^3n & 3m^2n^2-n^4 & 2m^3n & m^4-3m^2n^2 & mn^3-m^3n \\
4m^2n^2 & -8m^2n^2 & 4mn^3-4m^3n & 4m^2n^2 & 4m^3n-4mn^3 & (m^2-n^2)^2
\end{matrix} & & & & \\
& \begin{matrix}
m^3 & -m^2n & mn^2 & -n^3 & m^2n & -mn^2 \\
m^2n & m^3 & n^3 & mn^2 & mn^2 & m^2n \\
mn^2 & -n^3 & m^3 & -m^2n & -m^2n & mn^2 \\
n^3 & mn^2 & m^2n & m^3 & -mn^2 & -m^2n \\
-2m^2n & 2mn^2 & 2m^2n & -2mn^2 & m^3-mn^2 & n^3-m^2n \\
-2mn^2 & -2m^2n & 2mn^2 & 2m^2n & m^2n-n^3 & m^3-mn^2
\end{matrix} & & & \\
& & \begin{matrix}
m^2 & n^2 & mn \\
n^2 & m^2 & -mn \\
-2mn & 2mn & m^2-n^2
\end{matrix} & & \\
& & & \begin{matrix}
m^2 & -2mn & n^2 \\
mn & m^2-n^2 & -mn \\
n^2 & 2mn & m^2
\end{matrix} & \\
& & & & \begin{matrix}
m & -n \\
n & m
\end{matrix} \\
& & & & & 1
\end{bmatrix}$$

$$(F1.1-25)$$

The m and n terms represent

$$m = \cos\theta$$

and

$$(F1.1-26)$$

$$n = \sin\theta \ .$$

The $[C*]$ and $[\overline{C}*]$ are column matrix forms of equation (F1.1-6) and the transformed equation. The $[C*]$ is defined as

$$[C*] = \begin{bmatrix} C_{11} \\ C_{12} \\ 2C_{16} \\ C_{22} \\ 2C_{26} \\ 4C_{66} \\ C_{14} \\ C_{15} \\ C_{24} \\ C_{25} \\ 2C_{46} \\ 2C_{56} \\ C_{13} \\ C_{23} \\ 2C_{36} \\ C_{44} \\ C_{45} \\ C_{55} \\ C_{34} \\ C_{35} \\ C_{33} \end{bmatrix}$$

(F1.1-27)

and the $[\overline{C}*]$ is defined as

$$[\overline{C}*] = \begin{bmatrix} \overline{C}_{11} \\ \overline{C}_{12} \\ 2\overline{C}_{16} \\ \overline{C}_{22} \\ 2\overline{C}_{26} \\ 4\overline{C}_{66} \\ \overline{C}_{14} \\ \overline{C}_{15} \\ \overline{C}_{24} \\ \overline{C}_{25} \\ 2\overline{C}_{46} \\ 2\overline{C}_{56} \\ \overline{C}_{13} \\ \overline{C}_{23} \\ 2\overline{C}_{36} \\ \overline{C}_{44} \\ \overline{C}_{45} \\ \overline{C}_{55} \\ \overline{C}_{34} \\ \overline{C}_{35} \\ \overline{C}_{33} \end{bmatrix}$$

(F1.1-28)

The transformation of the stiffness matrix for an orthotropic material in a plane stress state is of particular interest since this will be of direct applicability to fibrous composites. As shown in Reference 1, when the elastic constants are needed with respect to some axis other than the material axis, the transformed elastic constants are

$$\overline{C}_{11} = C_{11} \cos^4 \theta + 2 \left[C_{12} + 2C_{66} \right] \sin^2 \theta \cos^2 \theta + C_{22} \sin^4 \theta \ ,$$

$$\overline{C}_{22} = C_{11} \sin^4 \theta + 2 \left[C_{12} + 2C_{66} \right] \sin^2 \theta \cos^2 \theta + C_{22} \cos^4 \theta \ , \quad \text{(F1.1-29)}$$

$$\overline{C}_{12} = \left[C_{11} + C_{22} - 4C_{66} \right] \sin^2 \theta \cos^2 \theta + C_{12} \left[\sin^4 \theta + \cos^4 \theta \right] \ ,$$

$$\overline{C}_{66} = \left[C_{11} + C_{22} - 2C_{12} - 2C_{66} \right] \sin^2 \theta \cos^2 \theta + C_{66} \left[\sin^4 \theta + \cos^4 \theta \right] \ ,$$

$$\overline{C}_{16} = \left[C_{11} - C_{12} - 2C_{66} \right] \sin \theta \cos^3 \theta + \left[C_{12} - C_{22} + 2C_{66} \right] \sin^3 \theta \cos \theta \ ,$$

and

$$\overline{C}_{26} = \left[C_{11} - C_{12} - 2C_{66} \right] \sin^3 \theta \cos \theta + \left[C_{12} - C_{22} + 2C_{66} \right] \sin \theta \cos^3 \theta \ .$$

The angle of rotation (θ) is about the z-axis and assumed positive in the counterclockwise direction.
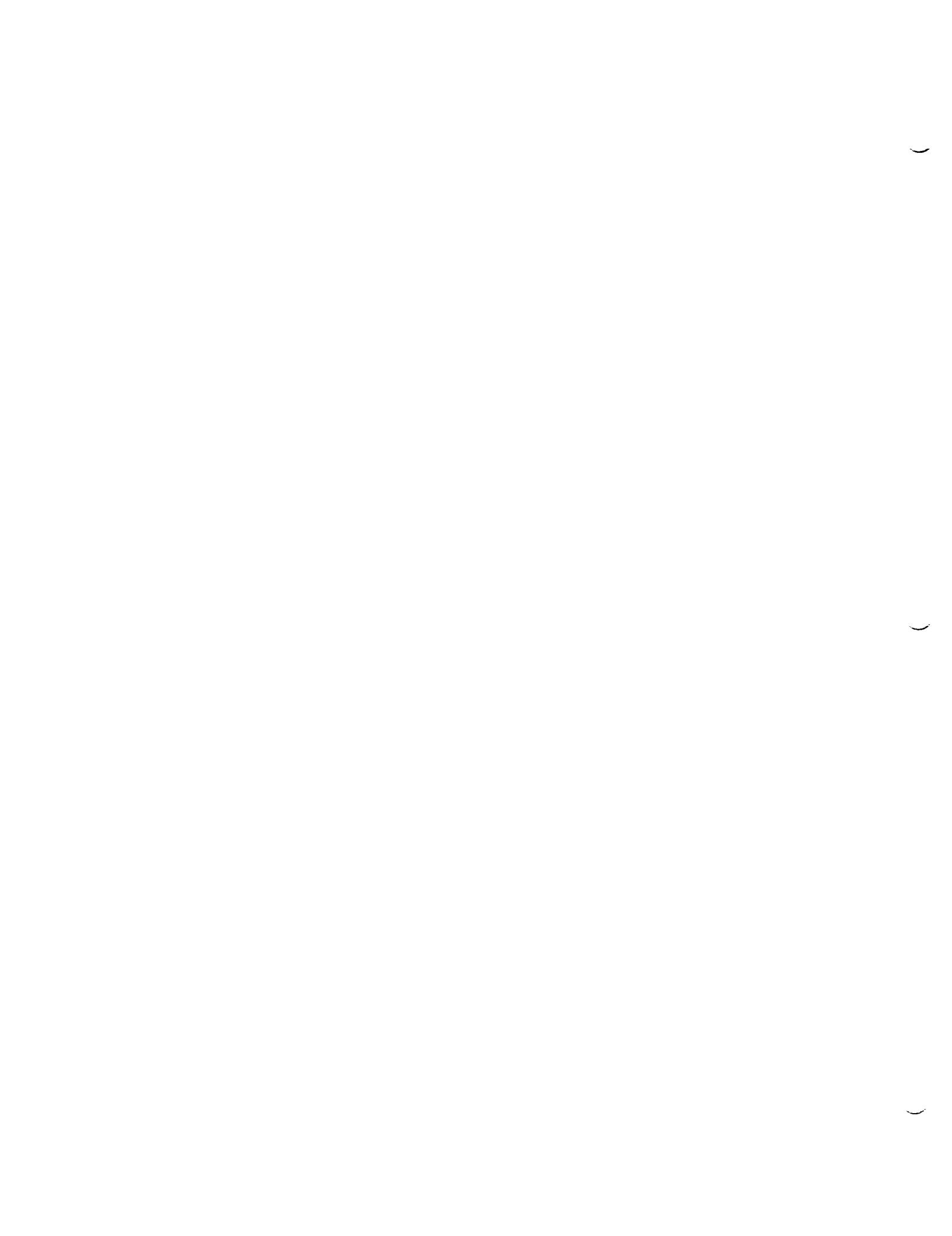
1. 2   MECHANICS OF LAMINATED COMPOSITES.

Two types of mathematical models [1] are normally utilized to predict the stress-strain response of a constituent lamina of a laminated composite — micromodels and macromodels. The micromechanics approach to the problem models the individual lamina as a periodic, or possibly a random, array of filaments in a matrix. The average stress-strain response of the lamina is a function of the elastic constants of the fiber and the matrix and their respective geometries. The macromechanics approach ignores the fiber-matrix behavior and models the individual lamina as a thin homogeneous orthotropic medium (sheet) under a state of plane stress.

1. 2. 1   MICROMECHANICS.

The strength and structural behavior of fibrous composites are directly related to the elastic properties of the fiber and matrix, as well as the micro-geometry of the laminate [1]. The field of micromechanics encompasses the study of the internal stress distribution in the fiber and matrix as a result of external loading. The objective of any micromechanics effort is to predict the intrinsic macroscopic (average) material properties of a laminate from the material and geometric properties of the constituents and perhaps provide the basis for understanding failure modes and establishing failure criteria from the predicted stress states.

With the present state-of-the-art, a micromechanics approach to composites for aerospace application does not give the designer a design tool which can be utilized to design aerospace structures. It is feasible that at

some time in the future, the aerospace designer will begin his creation at the

fiber and matrix level and will use the analytical tools of micromechanics to

determine his design parameters. However, at present the advanced

composites come to the fabrication stage in a preimpregnated tape form with

the filament spacing and other parameters established. Of course, some of

the predictions resulting from micromechanic analyses were utilized in

establishing a good filament spacing to insure good transverse and shear

properties in the final laminate; however, this represents a limited

application of micromechanics to designs.

1.2.2   MACROMECHANICS.

With the present state-of-the-art, the macromechanic approach [1] to

the mechanics of filamentary composites is the most usable technique for the

aerospace designer or stress analyst. The elastic constants and stress-strain

response of an individual lamina may be determined experimentally, and these

data may subsequently be used to determine the stress-strain response of a

laminate composed of any orientation of the characterized laminae.

1.2.2.1   Lamina Constitutive Relationship.

For a filamentary composite (Fig. F1.2-1), the constituent laminae

have three mutually perpendicular planes of elastic symmetry [1]. As discussed previously, a material with three mutually perpendicular planes of symmetry was termed orthotropic; therefore, the possibility exists to model the lamina as a homogeneous orthotropic medium. Since the
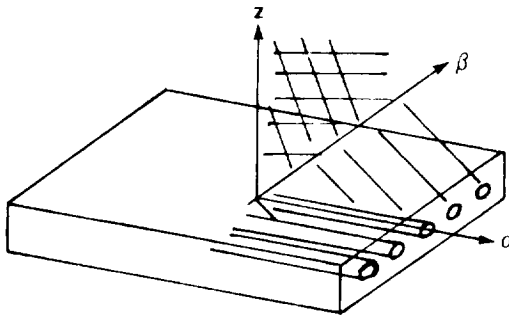
FIGURE F1.2-1. FILAMENTARY COMPOSITE WITH THREE MUTUALLY PERPENDICULAR PLANES OF SYMMETRY

thickness of an individual lamina is small relative to its other dimensions, it

may be considered to be in a state of plane stress. The constitutive equation

for the K-th lamina is then given by equation (F1.1-17) or

$$\begin{bmatrix} \sigma_\alpha \\ \sigma_\beta \\ \tau_{\alpha\beta} \end{bmatrix}^K = \begin{bmatrix} C_{11} & C_{12} & 0 \\ C_{12} & C_{22} & 0 \\ 0 & 0 & 2C_{66} \end{bmatrix}^K \begin{bmatrix} \epsilon_\alpha \\ \epsilon_\beta \\ \tfrac{1}{2}\gamma_{\alpha\beta} \end{bmatrix}^K . \qquad \text{(F1.2-1)}$$

The lamina stiffness matrix terms were defined in equation (F1.1-18) and are

rewritten here as

$$C_{11} = \frac{E_{11}}{(1 - \nu_{12}\nu_{21})} \quad ,$$

$$C_{22} = \frac{E_{22}}{(1 - \nu_{12}\nu_{21})} \quad ,$$

(F1.2-2)

$$C_{12} = \frac{\nu_{21} E_{11}}{\left(1 - \nu_{12}\nu_{21}\right)} = \frac{\nu_{12} E_{22}}{\left(1 - \nu_{12}\nu_{21}\right)} \quad ,$$

and

$$C_{66} = G_{12} \quad .$$

As shown in equation (F1.1-8), the compliance matrix may be determined by inverting the stiffness matrix. This would result in

$$\begin{bmatrix} \epsilon_{\alpha} \\ \epsilon_{\beta} \\ \frac{1}{2}\gamma_{\alpha\beta} \end{bmatrix}^{K} = \begin{bmatrix} S_{11} & S_{12} & 0 \\ S_{12} & S_{22} & 0 \\ 0 & 0 & \frac{1}{2}S_{66} \end{bmatrix}^{K} \begin{bmatrix} \sigma_{\alpha} \\ \sigma_{\beta} \\ \tau_{\alpha\beta} \end{bmatrix}^{K} \qquad (F1.2-3)$$

where

$$S_{11} = \frac{1}{E_{11}} \quad ,$$

$$S_{22} = \frac{1}{E_{22}} \quad ,$$

$$S_{12} = -\frac{\nu_{12}}{E_{11}} = -\frac{\nu_{21}}{E_{22}} \quad , \qquad (F1.2-4)$$

and

$$S_{66} = \frac{1}{G} \quad .$$

Since the lamina principal axes (α, β) generally do not coincide with the laminate reference axes (x, y) (Fig. 1.2-2), the stresses and strains for each lamina must be transformed as discussed previously. When this occurs, the constitutive relations for each lamina must also be transformed to the laminate reference axis system. The transformations, as discussed in paragraph F1.1.1, are
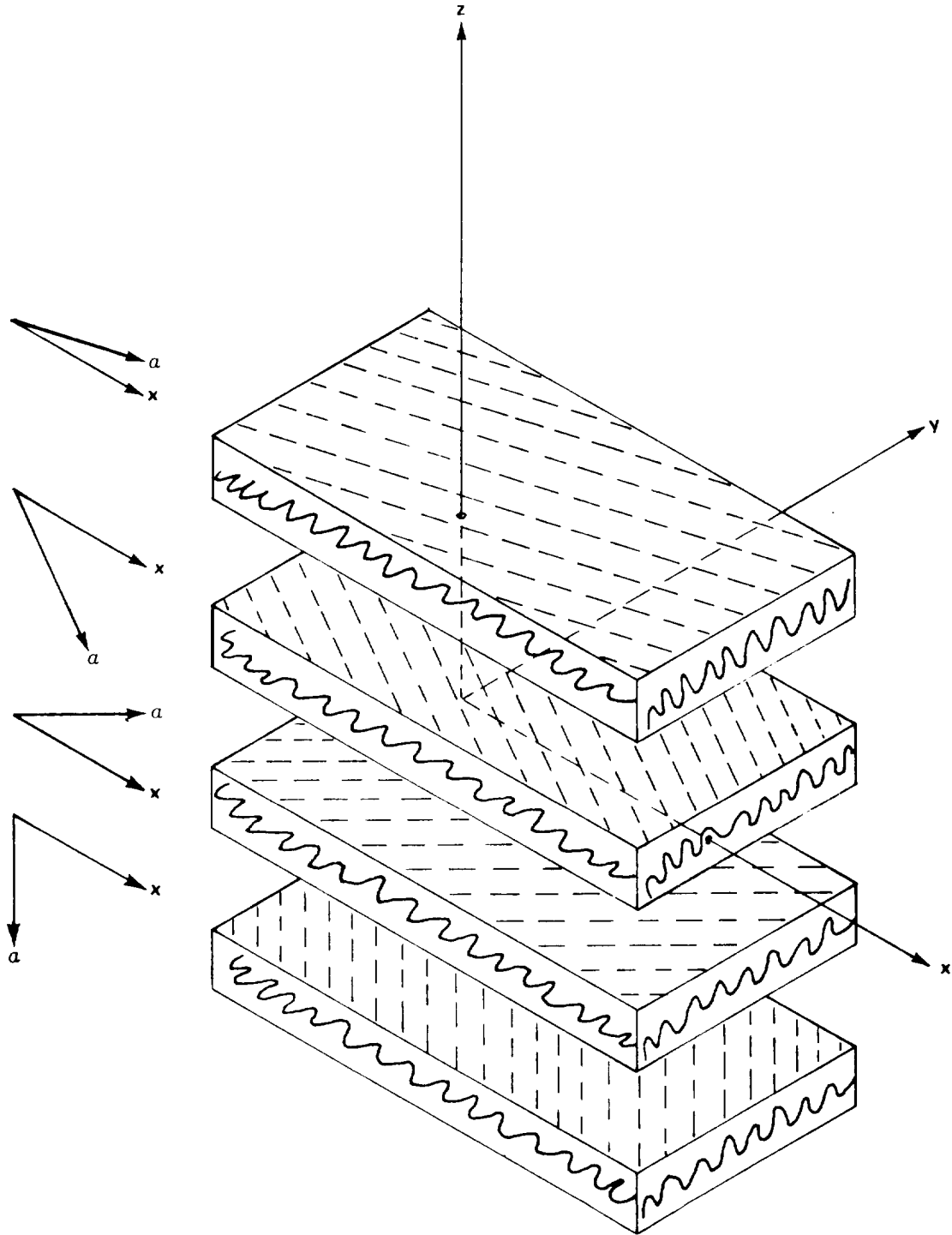
FIGURE F1. 2-2. GENERAL LAMINAE ORIENTATION
WITH LAMINATE REFERENCE AXIS

$$
\begin{bmatrix} \sigma_\alpha \\ \sigma_\beta \\ \tau_{\alpha\beta} \end{bmatrix}^K = [T] \begin{bmatrix} \sigma_x \\ \sigma_y \\ \tau_{xy} \end{bmatrix}^K \qquad (F1.\,2\text{-}5)
$$

and

$$
\begin{bmatrix} \epsilon_\alpha \\ \epsilon_\beta \\ \tfrac{1}{2}\gamma_{\alpha\beta} \end{bmatrix}^K = [T] \begin{bmatrix} \epsilon_x \\ \epsilon_y \\ \tfrac{1}{2}\gamma_{xy} \end{bmatrix}^K \qquad (F1.2\text{-}6)
$$

where [T] is defined in equation (F1.1-3) and K denotes the K-th lamina.

Then

$$
\begin{bmatrix} \sigma_x \\ \sigma_y \\ \tau_{xy} \end{bmatrix}^K = [T]^{-1} \begin{bmatrix} \sigma_\alpha \\ \sigma_\beta \\ \tau_{\alpha\beta} \end{bmatrix}^K \qquad . \qquad (F1.\,2\text{-}7)
$$

The transformation matrix, T, may be written in a shortened form as

$$
[T] = \begin{bmatrix} m^2 & n^2 & 2mn \\ n^2 & m^2 & -2mn \\ -mn & mn & m^2 - n^2 \end{bmatrix} \qquad (F1.\,2\text{-}8)
$$

where

$$
m = \cos\theta
$$

and

$$
n = \sin\theta \qquad .
$$

Note that the inverse of the T matrix, $[T]^{-1}$, may be obtained by substituting for the positive angle θ a negative angle θ (refer to Fig. 1.2-2).

Using equations (F1.2-1), (F1.2-6), and (F1.2-7), the lamina constitutive equation, when transformed to the laminate reference axes, is

$$
\begin{bmatrix} \sigma_x \\ \sigma_y \\ \tau_{xy} \end{bmatrix}^K = [T]^{-1} [C']^K [T] \begin{bmatrix} \epsilon_x \\ \epsilon_y \\ \frac{1}{2}\gamma_{xy} \end{bmatrix}^K . \tag{F1.2-9}
$$

The transformed lamina stiffness matrix $[\overline{C}']$ is defined as

$$
[\overline{C}']^K = [T]^{-1} [C']^K [T] = \begin{bmatrix} \overline{C}_{11} & \overline{C}_{12} & 2\overline{C}_{16} \\ \overline{C}_{12} & \overline{C}_{22} & 2\overline{C}_{26} \\ \overline{C}_{16} & \overline{C}_{26} & 2\overline{C}_{66} \end{bmatrix} \tag{F1.2-10}
$$

where the terms $\overline{C}_{ij}$ are given by equation (F1.1-29). The $\overline{C}'$ matrix, which is now fully populated ($C_{16} \neq C_{26} \neq 0$), appears to have six elastic constants which govern the lamina behavior; however, $\overline{C}_{16}$ and $\overline{C}_{26}$ are not independent as they are linear combinations of the four basic elastic constants. In the transformed coordinate system, the $\overline{C}'$ matrix is similar in appearance to the C matrix for a fully anisotropic lamina ($\overline{C}_{16} \neq 0$ and $\overline{C}_{26} \neq 0$), and the lamina is said to be "generally" orthotropic. Therefore, equation (F1.2-9) is said to be the constitutive equation for a "generally" orthotropic lamina.

Equation (F1.2-1) is referred to as the constitutive equation for a "specially" orthotropic lamina ($C_{16} = C_{26} = 0$).

For convenience, equation (F1.1-29) may be written as

$$\overline{C}_{11} = (3J_1 + J_2) + J_3 \cos 2\theta + J_4 \cos 4\theta,$$

$$\overline{C}_{22} = (3J_1 + J_2) - J_3 \cos 2\theta + J_4 \cos 4\theta,$$

$$\overline{C}_{12} = (J_1 - J_2) - J_4 \cos 4\theta,$$

$$\overline{C}_{66} = (J_1 + J_2) - J_4 \cos 4\theta,$$

$$\overline{C}_{16} = \tfrac{1}{2} J_3 \sin 2\theta + J_4 \sin 4\theta,$$

(F1.2-11)

and

$$\overline{C}_{26} = \tfrac{1}{2} J_3 \sin 2\theta - J_4 \sin 4\theta$$

where

$$J_1 = \tfrac{1}{8} [C_{11} + C_{22} + 2C_{12}],$$

$$J_2 = \tfrac{1}{2} [C_{66} - C_{12}],$$

(F1.2-12)

$$J_3 = \tfrac{1}{2} [C_{11} - C_{22}],$$

and

$$J_4 = \tfrac{1}{8} [C_{11} + C_{22} - 2C_{12} - 4C_{66}].$$

Note that $\overline{C}_{11}$, $\overline{C}_{22}$, $\overline{C}_{12}$, and $\overline{C}_{66}$ are composed of a term independent of the angle of rotation (θ) and a term dependent on the angle of rotation. Therefore, it is evident that there are certain inherent lamina properties which are only dependent on the material being used.

1.2.2.2   Laminate Constitutive Relationship.

From Reference 1, for the formulation of a mathematical model of a

laminate composed of orthotropic laminae, certain assumptions regarding the

interaction between adjacent laminae must be made. Since practical uses of

a laminate will normally dictate that it be thin relative to its other dimensions,

the Kirchhoff-Love hypothesis (stresses perpendicular to the middle surface may

be neglected, and the line segments originally normal to the middle surface

remain straight and normal to the deformed surface and suffer neither extensions

nor contractions) used in thin-plate and shell theory appear reasonable.

Essentially, these assumptions reduce to

$$
\begin{bmatrix} \epsilon_x \\ \epsilon_y \\ \gamma_{xy} \end{bmatrix}^K = \begin{bmatrix} \epsilon_x^o \\ \epsilon_y^o \\ \gamma_{xy}^o \end{bmatrix} - z \begin{bmatrix} \chi_x \\ \chi_y \\ 2\chi_{xy} \end{bmatrix}
$$

(F1.2-13)

where ϵ_x^o, ϵ_y^o, and γ_{xy}^o are the strains at the geometric middle surface

of the laminate, and the χ's are the middle surface curvature. The

transformed lamina constitutive equation, similar to equation (F1.2-9), is

then

$$
\begin{bmatrix} \sigma_x \\ \sigma_y \\ \tau_{xy} \end{bmatrix} = [\bar{C}]^K \begin{bmatrix} \epsilon_x^o \\ \epsilon_y^o \\ \gamma_{xy}^o \end{bmatrix} - z[\bar{C}]^K \begin{bmatrix} \chi_x \\ \chi_y \\ 2\chi_{xy} \end{bmatrix}
$$

(F1.2-14)

where

$$[\overline{C}] = \begin{bmatrix} \overline{C}_{11} & \overline{C}_{12} & \overline{C}_{16} \\ \overline{C}_{12} & \overline{C}_{22} & \overline{C}_{26} \\ \overline{C}_{16} & \overline{C}_{26} & \overline{C}_{66} \end{bmatrix} \quad . \tag{F1.2-15}$$

This equation then relates the stress in the K-th lamina, oriented to the

laminate reference axis, to the laminate middle surface strains and curvatures.

On an element of the laminate, the stress resultants and stress couples

are defined as

$$N_x = \int_{-t/2}^{t/2} \sigma_x dz \quad ,$$

$$\tag{F1.2-16}$$

$$N_y = \int_{-t/2}^{t/2} \sigma_y dz \quad ,$$

and

$$N_{xy} = \int_{-t/2}^{t/2} \tau_{xy} dz$$

and

$$M_x = \int_{-t/2}^{t/2} z\sigma_x dz \quad ,$$

$$\tag{F1.2-17}$$

$$M_y = \int_{-t/2}^{t/2} z\sigma_y dz \quad ,$$

and

$$M_{xy} = \int_{-t/2}^{t/2} z\tau_{xy} dz \quad .$$

These integrals may be evaluated by integrating over each lamina and summing the results of each integration. By substituting equation (F1.2-14) into equations (F1.2-16) and (F1.2-17),

$$\begin{bmatrix} N_x \\ N_y \\ N_{xy} \end{bmatrix} = \begin{bmatrix} A_{11} & A_{12} & A_{16} \\ A_{12} & A_{22} & A_{26} \\ A_{16} & A_{26} & A_{66} \end{bmatrix} \begin{bmatrix} \epsilon_x^o \\ \epsilon_y^o \\ \gamma_{xy}^o \end{bmatrix} - \begin{bmatrix} B_{11} & B_{12} & B_{16} \\ B_{12} & B_{22} & B_{26} \\ B_{16} & B_{26} & B_{66} \end{bmatrix} \begin{bmatrix} \chi_x \\ \chi_y \\ 2\chi_{xy} \end{bmatrix} \quad (F1.2-18)$$

$$\begin{bmatrix} M_x \\ M_y \\ M_{xy} \end{bmatrix} = \begin{bmatrix} B_{11} & B_{12} & B_{16} \\ B_{12} & B_{22} & B_{26} \\ B_{16} & B_{26} & B_{66} \end{bmatrix} \begin{bmatrix} \epsilon_x^o \\ \epsilon_y^o \\ \gamma_{xy}^o \end{bmatrix} - \begin{bmatrix} D_{11} & D_{12} & D_{16} \\ D_{12} & D_{22} & D_{26} \\ D_{16} & D_{26} & D_{66} \end{bmatrix} \begin{bmatrix} \chi_x \\ \chi_y \\ 2\chi_{xy} \end{bmatrix} \quad (F1.2-19)$$

where

$$[A_{ij}] = \sum_{K=1}^{n} [\bar{C}_{ij}]^K (h_K - h_{K-1}) \quad , \qquad (F1.2-20)$$

$$[B_{ij}] = \tfrac{1}{2} \sum_{K=1}^{n} [\bar{C}_{ij}]^K (h^2_K - h^2_{K-1}) \quad , \qquad (F1.2-21)$$

and

$$[D_{ij}] = \tfrac{1}{3} \sum_{K=1}^{n} [\bar{C}_{ij}]^K (h^3_K - h^3_{K-1}) \quad . \qquad (F1.2-22)$$
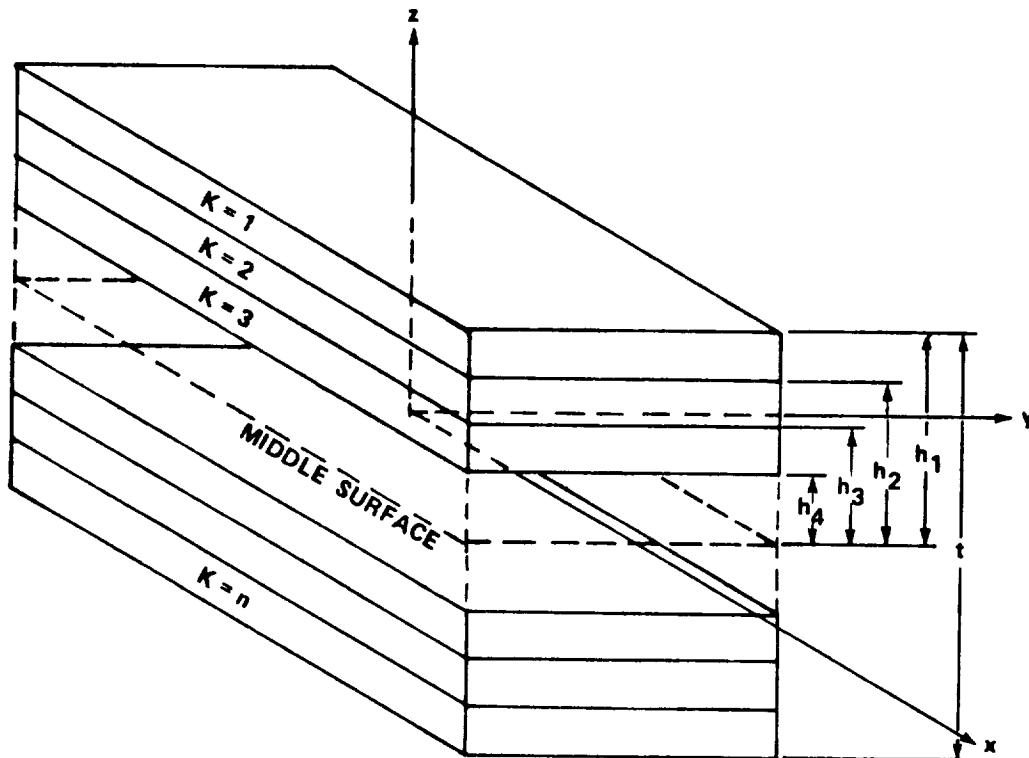
Refer to Figure F1.2-3.

FIGURE F1. 2-3. LAMINATE ELEMENT

Equations (F1. 2-18) and (F1. 2-19) are the constitutive equations for a

laminated composite. They may be written as

$$
\begin{bmatrix} N \\ M \end{bmatrix} = \begin{bmatrix} A & B \\ B & D \end{bmatrix} \begin{bmatrix} \epsilon^{0} \\ -\chi \end{bmatrix} \cdot \qquad (F1.\ 2\text{-}23)
$$

This is the general constitutive equation for laminated composites and

is mathematically equivalent to the constitutive equation for a heterogeneous

anisotropic medium. In this general form, the significant point is that there

is coupling between extensional (membrane) deformation and bending

deformation caused by the existence of the B matrix (Fig. F1-2. 4). In other

words, even within the limits of small deflection theory, forced curvatures
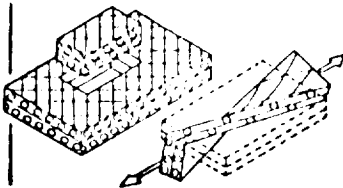
within the laminate induce in-plane loads through

this type of coupling. This coupling is caused by the

neutral axis and the midplane of the laminate not

FIGURE F1. 2-4.
COUPLING OF
DEFORMATION DUE TO
B MATRIX

being coincident.

With various combinations of laminae,

varying degrees of coupling may be caused. If the

laminate is fabricated symmetric about the midplane (balanced), the B matrix

will be identically zero, and the constitutive equation reduces to

$$[N] = [A] [\epsilon^o]$$ (F1. 2-24)

and

$$[M] = -[D] [\chi]$$. (F1. 2-25)

These equations are mathematically equivalent to the constitutive equations

of a homogeneous anisotropic material. Hence, this type of laminate is

referred to as homogeneous anisotropic (Fig. F1. 2-5). At this stage the A

and D matrices are fully populated and anisotropic in nature, and a second

type of coupling still exists. For the A matrix the A_{16} and A_{26} terms couple

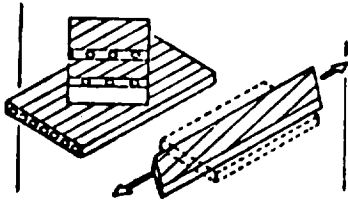the normal strains and shear stress, or the shear strains and normal stress.

FIGURE F1. 2-5.
COUPLING EFFECTS IN
A HOMOGENEOUS
ANISOTROPIC LAMINATE

For the D matrix the D_{16} and D_{26} terms couple the normal bending moments and twisting curvatures, and vice versa. If the laminate is symmetric about the x-y (laminate) axis (Fig. F1. 2-6), this coupling may be reduced.

When the laminate has equal numbers of pairs of laminae symmetric about the x-y axis (termed angleply laminate),
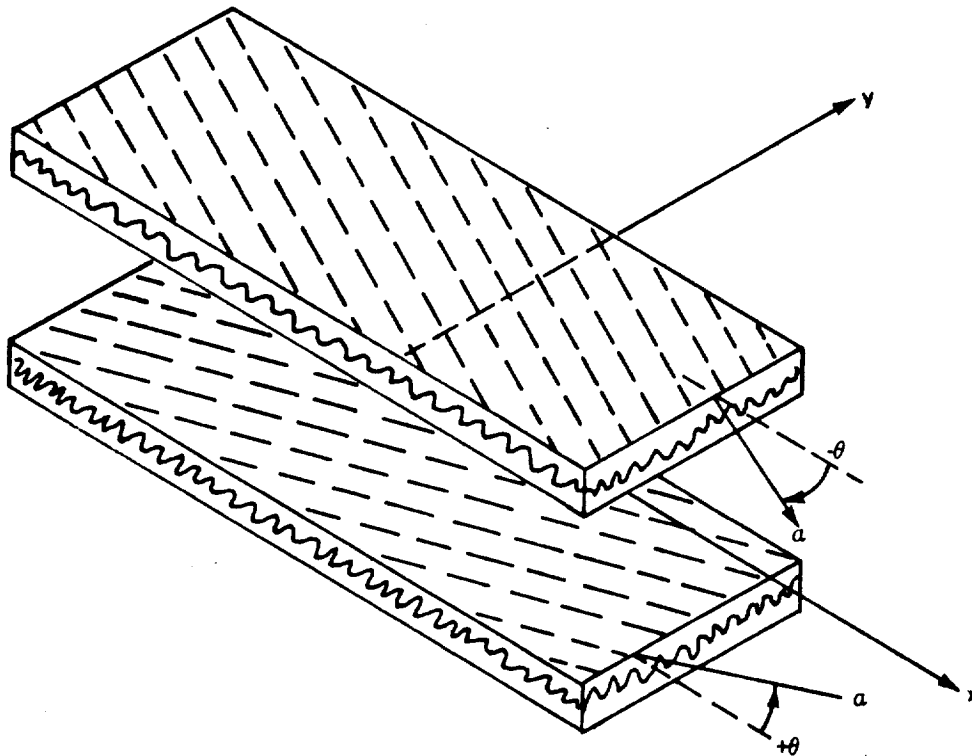

FIGURE F1. 2-6. LAMINATE SYMMETRIC ABOUT THE x-y AXIS

the A matrix is orthotropic in nature ($A_{16} = A_{26} = 0$) (Fig. F1. 2-7). The D matrix is still fully populated and anisotropic in nature. When the laminate has equal numbers of pairs of laminae at angles of 0 deg and 90 deg to the

x-y axis (termed crossply laminate), the D matrix

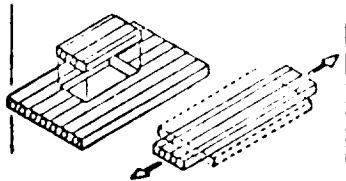and the A matrix are orthotropic in nature.

Because of the warpage which will occur

during the fabrication process when symmetry does

not exist, the laminates should be designed

FIGURE F1. 2-7.
LAMINATE EXHIBITING   symmetric about the midplane, or nearly so.
    ORTHOTROPIC
    CHARACTERISTICS   Since most laminates are symmetric

about the midplane, and because the majority of applications of advanced

composites experience relatively low transverse shear strength, a

reexamination of equation (F1. 2-24) is warranted.   Equation (F1. 2-24) may

be written as

$$
\begin{bmatrix} N_x \\ N_y \\ N_{xy} \end{bmatrix} = [A] \begin{bmatrix} \epsilon_x \\ \epsilon_y \\ \gamma_{xy} \end{bmatrix}
\qquad\qquad (F1. 2\text{-}26)
$$

when no bending occurs.   Dividing both sides by the total laminate thickness

yields

$$
\begin{bmatrix} \overline{\sigma}_x \\ \overline{\sigma}_y \\ \overline{\tau}_{xy} \end{bmatrix} = \frac{1}{t} [A] \begin{bmatrix} \epsilon_x \\ \epsilon_y \\ \gamma_{xy} \end{bmatrix} ,
\qquad\qquad (F1. 2\text{-}27)
$$

$$= \frac{1}{t} \begin{bmatrix} A_{11} & A_{12} & A_{16} \\ A_{12} & A_{22} & A_{26} \\ A_{16} & A_{26} & A_{66} \end{bmatrix} \begin{bmatrix} \epsilon_x \\ \epsilon_y \\ \gamma_{xy} \end{bmatrix} ,$$

$$= \frac{1}{t} \begin{bmatrix} A_{11} & A_{12} & 2A_{16} \\ A_{12} & A_{22} & 2A_{26} \\ A_{16} & A_{26} & 2A_{66} \end{bmatrix} \cdot \begin{bmatrix} \epsilon_x \\ \epsilon_y \\ \tfrac{1}{2}\gamma_{xy} \end{bmatrix} ,$$

$$= [\overline{A}] \begin{bmatrix} \epsilon_x \\ \epsilon_y \\ \tfrac{1}{2}\gamma_{xy} \end{bmatrix} . \qquad (F1.2\text{-}28)$$

The $\overline{\sigma}$'s are the average laminate stresses, and the $\overline{A}$ matrix may be defined as the laminate stiffness matrix. Thus,

$$\begin{bmatrix} \epsilon_x \\ \epsilon_y \\ \tfrac{1}{2}\gamma_{xy} \end{bmatrix} = [A*] \begin{bmatrix} \overline{\sigma}_x \\ \overline{\sigma}_y \\ \overline{\tau}_{xy} \end{bmatrix} \qquad (F1.2\text{-}29)$$

where the laminate compliance matrix is

$$[A*] = [A]^{-1} = \begin{bmatrix} A^*_{11} & A^*_{12} & \tfrac{1}{2}A^*_{16} \\ A^*_{12} & A^*_{22} & \tfrac{1}{2}A^*_{26} \\ A^*_{16} & A^*_{26} & \tfrac{1}{2}A^*_{66} \end{bmatrix} . \qquad (F1.2\text{-}30)$$

The gross or average laminate elastic moduli may be obtained from the

laminate compliance matrix. For a balanced angleply laminate,

$$[A] \quad \begin{bmatrix} A_{11} & A_{12} & 0 \\ A_{12} & A_{22} & 0 \\ 0 & 0 & A_{66} \end{bmatrix} , \quad [\overline{A}] \quad \frac{1}{t} \begin{bmatrix} A_{11} & A_{12} & 0 \\ A_{12} & A_{22} & 0 \\ 0 & 0 & 2A_{66} \end{bmatrix} ,$$

and

$$[A^*] = \begin{bmatrix} A_{11}^* & A_{12}^* & 0 \\ A_{12}^* & A_{22}^* & 0 \\ 0 & 0 & \frac{1}{2}A_{66}^* \end{bmatrix} . \tag{F1.2-31}$$

Then, comparing equation (F1.2-29) with equation (F1.2-3), the gross

laminate elastic constants are

$$E_{xx} = \frac{1}{A_{11}^*} ,$$

$$E_{yy} = \frac{1}{A_{22}^*} ,$$

$$G_{xy} = \frac{1}{A_{66}^*} , \tag{F1.2-32}$$

$$\nu_{xy} = -\frac{A_{12}^*}{A_{11}^*} ,$$

$$\nu_{yx} = -\frac{A_{12}^*}{A_{22}^*} .$$

## 1. 2. 3   EXAMPLE CALCULATIONS.

The example problems which follow demonstrate some of the computations involved when working with composite materials.

1. 2. 3. 1   Example Problem 1.

Calculate the A, B, and D matrices of the laminate constitutive equation for a three-ply laminate with the laminae oriented at - 45 deg, 0 deg, and +45 deg with the laminate axis (see the following sketch). The lamina material obeys

$$
\begin{bmatrix} \sigma_\alpha \\ \sigma_\beta \\ \tau_{\alpha\beta} \end{bmatrix} = 10^6 \begin{bmatrix} 30. & 1. & 0. \\ 1. & 3. & 0. \\ 0. & 0. & 1. \end{bmatrix} \begin{bmatrix} \epsilon_\alpha \\ \epsilon_\beta \\ \gamma_{\alpha\beta} \end{bmatrix}.
$$

-45°	0. 1 in.
0°	0. 2 in.
+45°	0. 1 in.
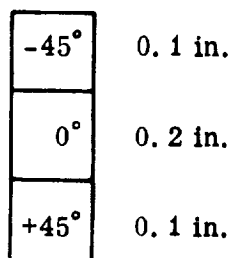
I.   Example Problem 1 Laminate.

The [C] for the - 45-deg lamina and the + 45-deg lamina must be transformed to the laminate axes. Since the lamina material is homogeneous orthotropic, the values of the transformed stiffness matrix may be calculated using equation (F1. 1-29) or equation (F1. 2-11).

Using equation (F1.1-29), the $\overline{C}_{ij}$ terms of equation (F1.2-15) for the 45-deg lamina are

$$\overline{C}_{11} = 10^6 \left[30. \cos^4(-45) + 2(1. + 2.) \sin^2(-45) \cos^2(-45) + 3. \sin^4(-45) \right]$$

$$= 9.75 \times 10^6$$

$$\overline{C}_{26} = 10^6 \left[(30.-1.-2.) \sin^3(-45) \cos(-45) + (1.-3.+2.) \sin(-45) \cos^3(-45) \right]$$

$$= -6.75 \times 10^6 .$$

Then,

$$[\overline{C}]^{(1)} = 10^6 \begin{bmatrix} 9.75 & 7.75 & -6.75 \\ 7.75 & 9.75 & -6.75 \\ -6.75 & -6.75 & 7.75 \end{bmatrix} .$$

Similarly, for the +45-deg lamina

$$[\overline{C}]^{(3)} = 10^6 \begin{bmatrix} 9.75 & 7.75 & 6.75 \\ 7.75 & 9.75 & 6.75 \\ 6.75 & 6.75 & 7.75 \end{bmatrix} .$$

For the 0-deg lamina

$$[\overline{C}]^{(2)} = [C] = 10^6 \begin{bmatrix} 30. & 1. & 0. \\ 1. & 3. & 0. \\ 0. & 0. & 1. \end{bmatrix} .$$

From equation (F1.2-20),

$$A_{ij} = \sum_{K=1}^{n} (\overline{C}_{ij})^{(K)} (h_K - h_{K-1})$$

$$= 0.1 [\overline{C}_{ij}]^{(1)} + 0.2 [\overline{C}_{ij}]^{(2)} + 0.1 [\overline{C}_{ij}]^{(3)} .$$

Thus,

$$A_{11} = 10^6 \, [9.75 \times 0.1 + 30. \times 0.2 + 9.75 \times 0.1] = 7.95 \times 10^6$$

$$\vdots$$

$$A_{66} = 10^6 \, [7.75 \times 0.1 + 1. \times 0.2 + 7.75 \times 0.1] = 1.75 \times 10^6 \ .$$

$$[A] = 10^6 \begin{bmatrix} 7.95 & 1.75 & 0. \\ 1.75 & 2.55 & 0. \\ 0. & 0. & 1.75 \end{bmatrix} \ .$$

From equation (F1.2-21)

$$B_{ij} = \tfrac{1}{2} \sum_{K=1}^{n} (\overline{C}_{ij})^{(K)} \, (h^2_{\,K} - h^2_{\,K-1})$$

$$= 0.015 \, \left[(\overline{C}_{ij})^{(3)} - (\overline{C}_{ij})^{(1)} \right] \ .$$

Thus,

$$B_{11} = 10^6 \times 0.015 \, [9.75 - 9.75] = 0$$

and

$$B_{66} = 0.$$

$$[B] = 10^6 \begin{bmatrix} 0. & 0. & 0.2025 \\ 0. & 0. & 0.2025 \\ 0.2025 & 0.2025 & 0. \end{bmatrix} \ .$$

From equation (F1.2-22)

$$D_{ij} = \frac{1}{3} \sum_{K=1}^{n} (\overline{C}_{ij})^{(K)} (h_K^3 - h_{K-1}^3)$$

$$= 0.00233 \, [\overline{C}_{ij}]^{(1)} + 0.00066 \, [\overline{C}_{ij}]^{(2)} + 0.00233 \, [\overline{C}_{ij}]^{(3)} \ .$$

Thus,

$$D_{11} = 10^6 \, [9.75 \times 0.00233 + 30. \times 0.00066 + 9.75 \times 0.00233]$$

$$\vdots \quad = 0.06522 \times 10^6$$

$$D_{66} = 10^6 \, [7.75 \times 0.00233 + 1. \times 0.00066 + 7.75 \times 0.00233]$$

$$= 0.03676 \times 10^6 \ .$$

$$[D] \quad 10^6 \begin{bmatrix} 0.06522 & 0.03676 & 0. \\ 0.03676 & 0.0474 & 0. \\ 0. & 0. & 0.03676 \end{bmatrix} \quad .$$

Combining the results above, the constitutive equation may be written as

$$\begin{bmatrix} N_x \\ N_y \\ N_{xy} \\ M_x \\ M_y \\ M_{xy} \end{bmatrix} = 10^6 \begin{bmatrix} 7.95 & 1.75 & 0. & | & 0. & 0. & 0.2025 \\ 1.75 & 2.55 & 0. & | & 0. & 0. & 0.2025 \\ 0. & 0. & 1.75 & | & 0.2025 & 0.2025 & 0. \\ - & - & - & | & - & - & - \\ 0. & 0. & 0.2025 & | & 0.06522 & 0.03676 & 0. \\ 0. & 0. & 0.2025 & | & 0.03676 & 0.0474 & 0. \\ 0.2025 & 0.2025 & 0. & | & 0. & 0. & 0.03676 \end{bmatrix} \begin{bmatrix} \epsilon_x^o \\ \epsilon_y^o \\ \gamma_{xy}^o \\ \chi_x \\ \chi_y \\ 2\chi_{xy} \end{bmatrix} \quad .$$

1. 2. 3. 2   <u>Example Problem 2.</u>

Calculate the constitutive matrix for a four-ply laminate with laminae

at + 45 deg, - 45 deg, - 45 deg, and + 45 deg and with a total laminate

thickness of 0. 4 in. (see the following sketch). Use, the same lamina material

as in paragraph 1. 2. 3. 1.

+ 45°	0. 1 in.
- 45°	0. 1 in.
- 45°	0. 1 in.
+ 45°	0. 1 in.

II. Example Problem 2 Laminate.

Since the laminate is symmetric about the midplane and symmetric

about the x-y axis, the constitutive equation will be in the form of

$$
\begin{bmatrix} N \\ M \end{bmatrix} = \begin{bmatrix} A & 0. \\ 0. & D \end{bmatrix} \begin{bmatrix} \epsilon^0 \\ -\chi \end{bmatrix}
$$

where

$$
[A] = \begin{bmatrix} A_{11} & A_{12} & 0. \\ A_{12} & A_{22} & 0. \\ 0. & 0. & A_{66} \end{bmatrix}
$$

and

$$[D] = \begin{bmatrix} D_{11} & D_{12} & D_{16} \\ D_{12} & D_{22} & D_{26} \\ D_{16} & D_{26} & D_{66} \end{bmatrix}$$

Similar to paragraph 1.2.3.1,

$$[\overline{C}]^{(1)} \quad [\overline{C}]^{(4)} \quad 10^6 \begin{bmatrix} 9.75 & 7.75 & 6.75 \\ 7.75 & 9.75 & 6.75 \\ 6.75 & 6.75 & 7.75 \end{bmatrix}$$

and

$$[\overline{C}]^{(2)} = [\overline{C}]^{(3)} = 10^6 \begin{bmatrix} 9.75 & 7.75 & -6.75 \\ 7.75 & 9.75 & -6.75 \\ -6.75 & -6.75 & 7.75 \end{bmatrix}$$

Using equations (F1.2-20) and (F1.2-22),

$$[A] = 10^6 \begin{bmatrix} 3.9 & 3.1 & 0. \\ 3.1 & 3.9 & 0. \\ 0. & 0. & 3.1 \end{bmatrix}$$

and

$$[D] = 10^6 \begin{bmatrix} 0.05187 & 0.04123 & 0.027 \\ 0.04123 & 0.05187 & 0.027 \\ 0.027 & 0.027 & 0.04123 \end{bmatrix}$$

Therefore,

$$
\begin{bmatrix} N_x \\ N_y \\ N_{xy} \\ M_x \\ M_y \\ M_{xy} \end{bmatrix} = 10^6 \begin{bmatrix} 3.9 & 3.1 & 0. & & & \\ 3.1 & 3.9 & 0. & & 0. & \\ 0. & 0. & 3.1 & & & \\ & & & 0.05187 & 0.04123 & 0.027 \\ & 0. & & 0.04123 & 0.05187 & 0.027 \\ & & & 0.027 & 0.027 & 0.04123 \end{bmatrix} \begin{bmatrix} \epsilon_x^o \\ \epsilon_y^o \\ \gamma_{xy}^o \\ \chi_x \\ \chi_y \\ 2\chi_{xy} \end{bmatrix}
$$

1.3   LAMINATE CODING.

In Reference 2 a laminate orientation code was devised for filamentary

composites which provided both a concise reference and a positive identification

of any laminate. As expressed in that reference, the following type of coding

is intended to provide a means of achieving conciseness in engineering

presentations and communications; however, it is neither recommended nor

discouraged that this code be employed on shop drawings since that policy is an

internal one which must be decided by each using organization.

1.3.1   STANDARD CODE ELEMENTS.

The formulation of the code must be adequate to specify as concisely

as possible (1) the angles of laminae relative to a reference axis (the x-axis),

(2) the number of laminae at each angle, and (3) the exact geometric sequence

of laminae.

The basic laminate code will adhere to the following guidelines [2]:

1.   Each lamina is denoted by a number representing its orientation

in degrees between its filament direction (refer to Fig. F1.0-3) and the

x-axis.

2.   Individual adjacent laminae are separated by a slash if their

angles are different.

3.   The laminae are listed in sequence from one laminate face to the

other, with brackets indicating the beginning and end of the code. The first

lamina should be the most positive lamina in the z direction (refer to Fig.

F1.2-3).

4. /Adjacent laminae of the same angle are deonoted by a numerical subscript.

5. A subscript T to the bracket indicates that the total laminate is shown.

When adjacent laminae are of the same angle but opposite in sign, the appropriate use of + or - signs may be employed. Each + or - sign represents one lamina and supersedes the use of the numerical subscript, which is used only when the directions are identical. Note that positive angles are assumed to be counterclockwise.

Several examples are shown demonstrating the basic coding.

45
0
-60
-60
30

Code

$[45/0/-60_2/30]_T$

+45
-45
-30
+30
0
+45
+45
-45
-45

$[\pm 45/\mp 30/0/\pm(45_2)]_T$

1. 3. 2   CODES FOR VARIOUS TYPES OF LAMINATES.

As discussed in previous sections, laminates may be formed of
arbitrarily arranged laminae, but more often the laminae assume standard
arrangements. The more common standard arrangements are symmetric
(balanced) laminates and sets of laminae.

Similar to the total laminate as shown in paragraph 1. 3. 1, the
symmetric (balanced) code has an S as a subscript, and the coding sequence
starts at the most positive z lamina and stops at the plane of symmetry.
The S indicates that only one-half of the laminate is shown:

Laminate	Code
	$[90/0_2/45]_S$

90
0
0
45
45
0
0
90

If the symmetric laminate has an odd number of laminae, the code denoting
the center lamina is overlined, indicating that half of the laminate lies on
either side of that lamina:

Laminate

Code

0
45
90
45
0

$[0/45/\overline{90}]_S$

A repeating sequence of laminae is termed a set. A set is coded in accordance with the same rules which apply to a single lamina:

Laminate

45	—
0	Set
90	—
45	—
0	Set
90	—
45	—
0	Set
90	—
45	—
0	Set
90	—

$[(45/0/90)_4]_T$ or $[45/0/90]_{4T}$

45	—
0	Set
90	—
45	—
0	Set
90	—
90	— $\mathbb{C}_L$
0	Set
45	—
90	—
0	Set
90	—

$[(45/0/90)_2]_S$ or $[45/0/90]_{2S}$

1. 4   COMPUTER PROGRAMS IN COMPOSITE ANALYSIS.

Several computer programs have been made available to MSFC and

support personnel to assist in analyzing composite material elements.   These

programs have been (or are currently being) documented in References 4 and

5. The program names and a brief comment on each are shown in Table

F1. 4-1.

TABLE F1.4-1. Computer Programs in Composite Analysis

Program Name	Comment
CDLAMA	Yield analysis of composite plates composed of orthotropic lamina with in-plane loading. ·
GDLAMT	Yield analysis of composite plates composed of orthotropic lamina with in-plane loading.
GREPPA	Design composite skin/stringer/frame compression panel.
INTACT	Locates optimum strength envelopes for laminates under the action of combined loading.
LAMCHK	Laminate check - computes margins of safety for specified 0-deg, 90-deg, ± 45-deg boron epoxy laminates under combined loading.
LAP	Analysis of single overlap bonded joints with Metlbond 329 adhesive mechanical behavior.
LAPI	Analyzes single overlap bonded joints and accepts arbitrary applied loads and incorporates the B basis correction factor.
MMBCK	Calculates the buckling loads of radially inhomogeneous anisotropic, cylindrical shells wherein the effects of boundary conditions are not considered.
PANBUCK II	Panel buckling — calculates critical buckling loads and mode for orthotropically layered, rectangular, anisotropic plates and honeycomb sandwich panels. Also computes local instability modes of failure for composite panels.
STAB	Stability analysis — local instability analysis of orthotropic honeycomb panels, columns, and beams — failure-mode analysis for filament rupture, intercell dimpling, and layer instability.

1.5   REFERENCES.

1.   Petit, P. H.: Basic Concepts in the Design and Stress Analysis of Laminated Composites. Report No. SMN 239, Lockheed-Georgia Co., division of Lockheed Aircraft Corp., Marietta, Ga., March 1968.

2.   Structural Design Guide for Advanced Composite Applications. Advanced Composites Division, Air Force Materials Laboratory, Air Force Systems Command, Wright-Patterson Air Force Base, Ohio, August 1969.

3.   Ashton, J. C.; Halpin, J. C.; and Petit, P. H.: Primer on Composite Materials: Analysis. Technomic Publishing Co., Inc., Stamford, Conn., 1969.

4.   Structural Analysis Computer Utilization Manual. Analytical Mechanics Division, Astronautics Laboratory, George C. Marshall Space Flight Center (NASA).

5.   Strength Analysis Computer Program Description Manual. Analytical Mechanics Division, Astronautics Laboratory, George C. Marshall Space Flight Center (NASA).

SECTION F2

LAMINATED COMPOSITES

TABLE OF CONTENTS

F2.0   STRENGTH OF LAMINATED COMPOSITES.

The strength of laminated composites must be related to the individual lamina [1]. This is because it is easier to determine where nonlinearity and degradation begin to occur on a unidirectional test specimen than on some general laminate test. For this reason the trend in determining the strength of advanced composites is to establish strength allowables for the orthotropic lamina and then to utilize analytical methods to predict the yield or the ultimate strength of the laminate.

2. 1   YIELD STRENGTH.

The available yield strength theories for laminated composites are at

best tentative at this time [2]. Only a minimal amount of test data is

available to substantiate any of the yield theories for advanced composites.

If the yield point is defined as the onset of inelastic action, it is

apparent that the prediction of the yield strength of an orthotropic lamina is a

linear problem. Several yield theories of failure have been hypothesized for

anisotropic materials, of which two will be discussed (the distortional energy

theory and the maximum strain theory).

Before the discussion of yield theories, the basic difference between

the yield surfaces for an isotropic and for an orthotropic or anisotropic

material must be explained. For an isotropic material, any biaxial stress

state, σ_x, σ_y, τ_{xy}, may be resolved into two principal stresses, σ_{1_p} and

σ_{2_p}, and some angle, θ; therefore, a plot of the principal stresses that cause

yield will give the required yield surface. The result is a two-dimensional

figure with σ_{1_p} and σ_{2_p} as axes. When considering the yield surface for an

orthotropic lamina, the stresses must be referred to the lamina principal axes;

therefore, for biaxial stress states three stress components may appear in the

yield criteria. The resulting yield surface will appear as a three-dimensional

figure with the directions of σ_1, σ_2, and τ_{12} as reference coordinates

(Fig. F2. 1-1).

FIGURE F2. 1-1. THREE-DIMENSIONAL YIELD SURFACE FOR AN ORTHOTROPIC LAMINA

2. 1. 1 DISTORTIONAL ENERGY THEORY.

Cira, Norris, and Hill independently developed their generalizations of the von Mises isotropic distortional energy yield criterion,

$$(\sigma_1 - \sigma_2)^2 + (\sigma_2 - \sigma_3)^2 + (\sigma_3 - \sigma_1)^2 + 6 (\tau_{12}^2 + \tau_{23}^2 + \tau_{31}^2) = 2\sigma_0^2 \quad , \quad (F2. 1-1)$$

to account for the anisotropy of their respective problems [3]. Hill was concerned with the tendency of isotropic metals to exhibit certain anisotropic properties when undergoing metal working involving severe strains. Hill claimed he had a physical interpretation of von Mises' "plastic potential," which allowed him to generalize von Mises' yield criterion for application to anisotropic metals. The plastic potential or yield criterion has the form

$$2f (\sigma_{ij}) = A_1 (\sigma_2 - \sigma_3)^2 + A_2 (\sigma_3 - \sigma_1)^2 + A_3 (\sigma_1 - \sigma_2)^2 + 2A_4\tau_{23}^2 + 2A_5\tau_{31}^2 + 2A_6\tau_{12}^2 = 1$$

$$(F2. 1-2)$$

where

$2f(\sigma_{ij})$ = the plastic potential,

$2A_1 = (F_2)^{-2} + (F_3)^{-2} - (F_1)^{-2}$,

$2A_2 = (F_3)^{-2} + (F_1)^{-2} - (F_2)^{-2}$,

$2A_3 = (F_1)^{-2} + (F_2)^{-2} - (F_3)^{-2}$,

$2A_4 = (F_{23})^{-2}$,

$2A_5 = (F_{31})^{-2}$,

and

$2A_6 = (F_{12})^{-2}$,

F_1, F_2, and F_3 are determined from either uniaxial tension or compression tests, and F_{12}, F_{23}, and F_{31} are determined from pure shear tests.

Tsai [2] adapted this criterion as a yield and failure criterion for laminated composites. The failure criterion for a laminated composite is based on the strengths of the individual orthotropic lamina referred to the lamina principal axes since the yield strengths are established experimentally with reference to these axes. The Hill criterion reduces to

$$\left(\frac{\sigma_1}{\sigma_{1y}}\right)^2 - \frac{1}{r}\frac{\sigma_1}{\sigma_{1y}}\frac{\sigma_2}{\sigma_{2y}} + \left(\frac{\sigma_2}{\sigma_{2y}}\right)^2 + \left(\frac{\tau_{12}}{\tau_{12y}}\right)^2 = 1 \qquad (F2. 1\text{-}3)$$

for an orthotropic material in plane stress. Note that

$$\frac{1}{r} = \frac{\sigma_{1y}}{\sigma_{2y}} \qquad . \qquad (F2. 1\text{-}4)$$

Also, σ_{1_y} and σ_{2_y} are the tensile or compressive yield strengths in the 1

and 2 directions for the orthotropic lamina, and τ_{12_y} is the shear yield

stress. The yield surface is either an ellipsoid or sphere, depending on r,

when plotted in a three-dimensional space (Fig. F2.1-2).

2.1.2   MAXIMUM STRAIN CRITERIA.

The maximum strain yield criteria presented here should not be

confused with the maximum principal strain yield criteria for isotropic

materials [2]. The strain components in the orthotropic lamina must be

referred to the lamina principal axes; therefore, it is possible for three

strain components to appear in the yield criteria.

The maximum strain yield criteria may be developed from equation

(F1.2-3) with the strains equal to the yield strains:

$$\begin{bmatrix} \epsilon_{1_y} \\ \epsilon_{2_y} \\ \gamma_{12_y} \end{bmatrix} = \begin{bmatrix} S_{11} & S_{12} & 0 \\ S_{12} & S_{22} & 0 \\ 0 & 0 & S_{66} \end{bmatrix} \begin{bmatrix} \sigma_1 \\ \sigma_2 \\ \tau_{12} \end{bmatrix} \quad . \tag{F2.1-5}$$

Thus, equation (F2.1-5) gives the envelope of stresses which produce the

yield strains in the lamina. A two-dimensional plot of the equation may be

made if $\tau_{12} = 0$ is assumed. Then,

$$\epsilon_{1_y} = S_{11}\sigma_1 + S_{12}\sigma_2$$

and

$$\tag{F2.1-6}$$

$$\epsilon_{2_y} = S_{12}\sigma_1 + S_{22}\sigma_2 \quad ,$$

FIGURE F2. 1-2. HILL YIELD SURFACE
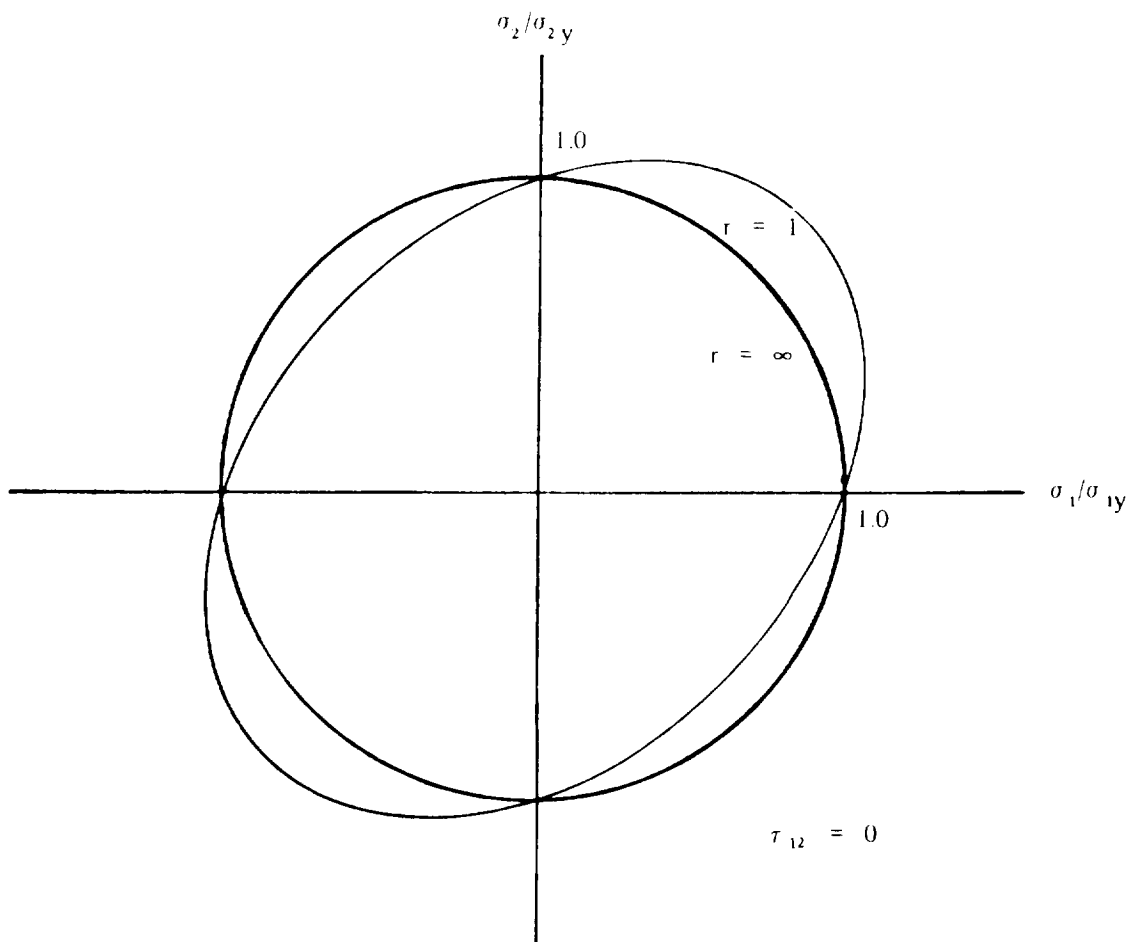
or

$$\sigma_2 = \frac{\epsilon_{1_y}}{S_{12}} - \frac{S_{11}}{S_{12}} \sigma_1$$

and   (F2.1-7)

$$\sigma_2 = \frac{\epsilon_{2_y}}{S_{22}} - \frac{S_{12}}{S_{22}} \sigma_2 \quad .$$

Equations (F2.1-7) are the equations of two lines in the $\sigma_1 - \sigma_2$ coordinate

system which define yield of an orthotropic lamina. After defining the yield

strengths as

$$\sigma_{1_y} = \frac{\epsilon_{1_y}}{S_{11}} = \epsilon_{1_y} E_{11}$$

and   (F2.1-8)

$$\sigma_{2_y} = \frac{\epsilon_{2_y}}{S_{22}} = \epsilon_{2_y} E_{22} \quad ,$$

equations (F2.1-7) may be put in a form similar to the Hill equation:

$$\left(\frac{\sigma_2}{\sigma_{2_y}} \right) = \frac{\epsilon_{1_y}}{\epsilon_{2_y}} \frac{S_{22}}{S_{12}} - \frac{\epsilon_{1_y}}{\epsilon_{2_y}} \frac{S_{22}}{S_{12}} \left(\frac{\sigma_1}{\sigma_{1_y}} \right)$$

and   '   (F2.1-9)

$$\left(\frac{\sigma_2}{\sigma_{2_y}} \right) = \frac{\epsilon_{2_y}}{\epsilon_{2_y}} - \frac{\epsilon_{1_y}}{\epsilon_{2_y}} \frac{S_{12}}{S_{11}} \left(\frac{\sigma_1}{\sigma_{1_y}} \right) \quad .$$

Equations (F2.1-7) may be plotted on a $\sigma_1 - \sigma_2$ set of coordinates since it was assumed that the shear stress component, τ_{12}, was zero. Such a plot might appear as shown in Fig. F2.1-3.

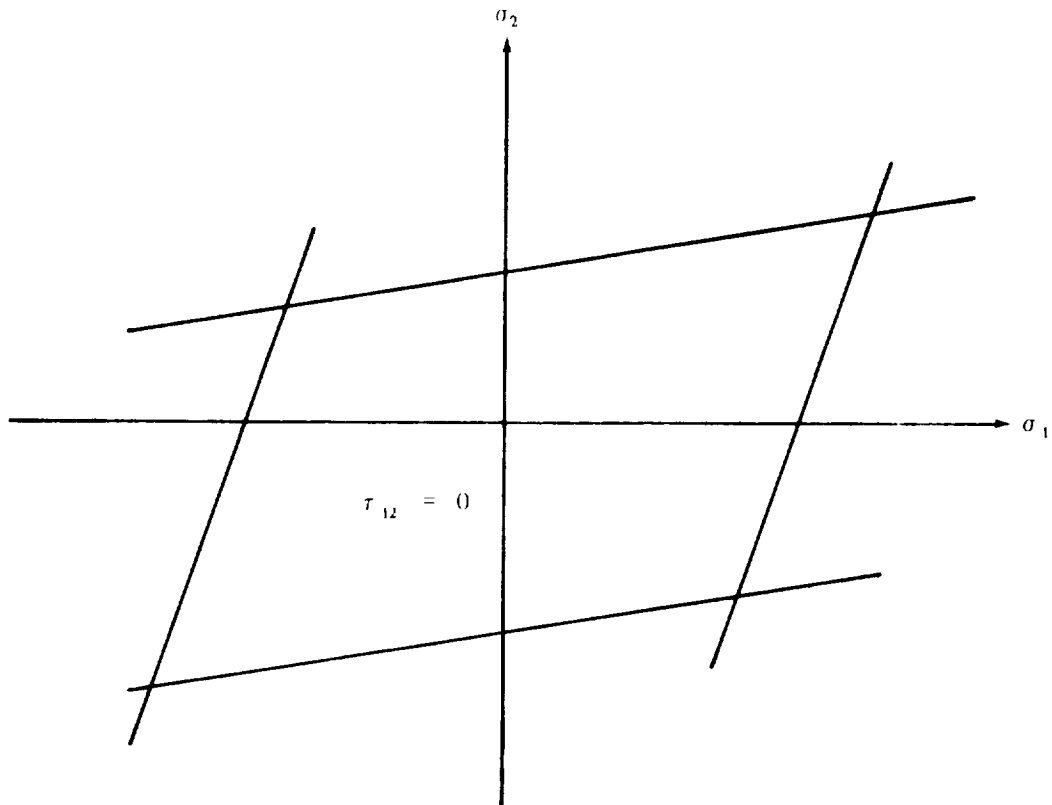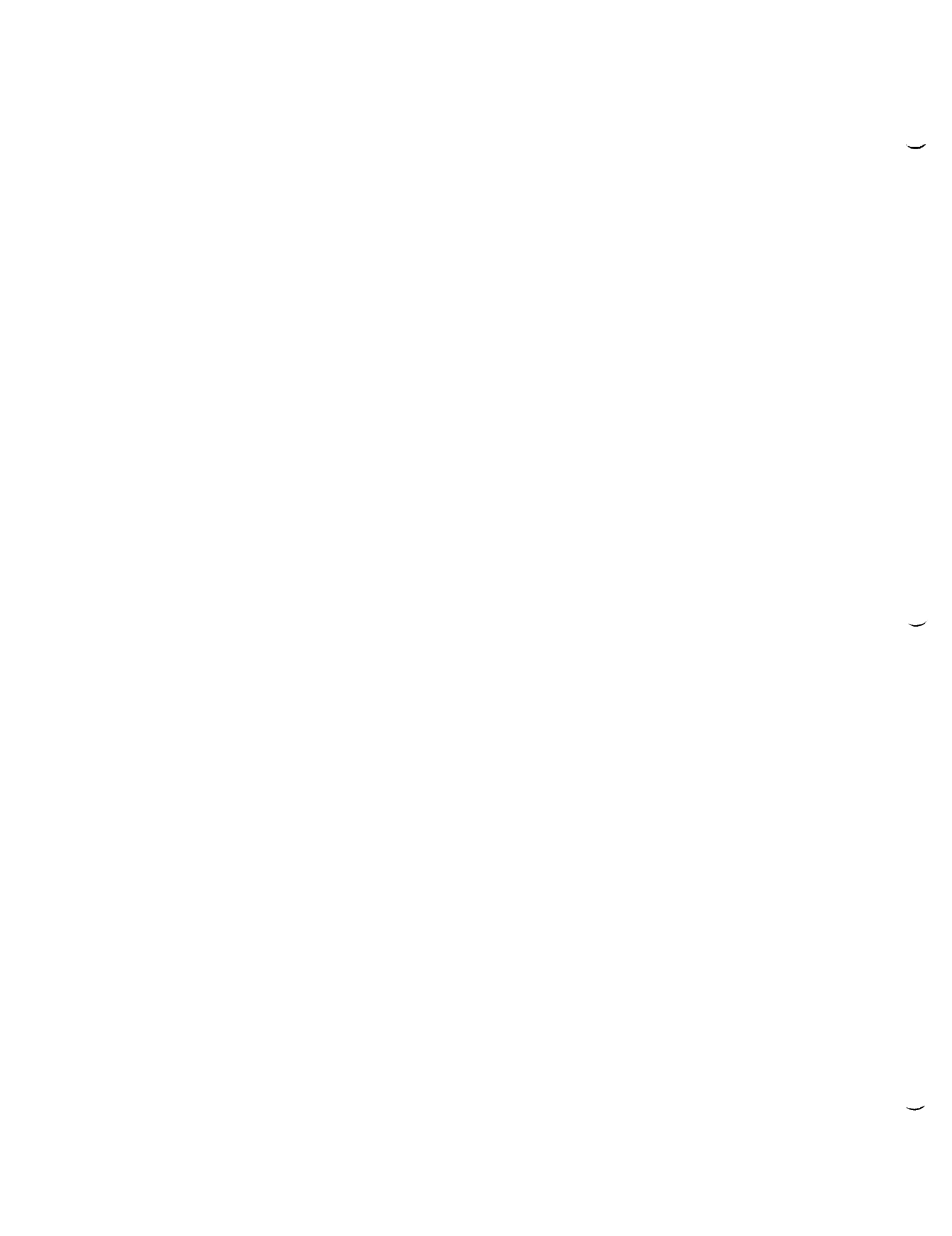FIGURE F2.1-3.   LAMINA YIELD SURFACE

2.2   ULTIMATE STRENGTH.

Until recently, attempts to predict the ultimate or rupture load for a laminate were based on linear theory; that is, the laminate ultimate load was based upon the assumption that the laminate stress-strain response is linear to failure or that upon yield of a constituent lamina, some (or all) of the lamina moduli are reduced to some arbitrarily small value or set equal to zero. Recently, some computer programs have been written with relatively simple techniques, and new methods that determine the ultimate strength of laminates have been developed. These programs and methods are usually for specialized laminates, and sufficient test data are not available at this time to verify their accuracy for general use.

2.3   REFERENCES.

1.   Ashton, J. C; Halpin, J. C.; and Petit, P. H.: Primer on Composite Materials: Analysis. Technomic Publishing Co., Inc., Stamford, Conn., 1969.

2.   Petit, P. H.: Basic Concepts in the Design and Stress Analysis of Laminated Composites. Report No. SMN 239, Lockheed-Georgia Co., a division of Lockheed Aircraft Corp., Marietta, Ga., March 1968.

3.   Kaminski, B. E.; and Lantz, R. B.: Strength Theories of Failure for Anisotropic Materials. Composite Materials: Testing and Design. Report STP 460, American Society of Testing Materials, 1969.
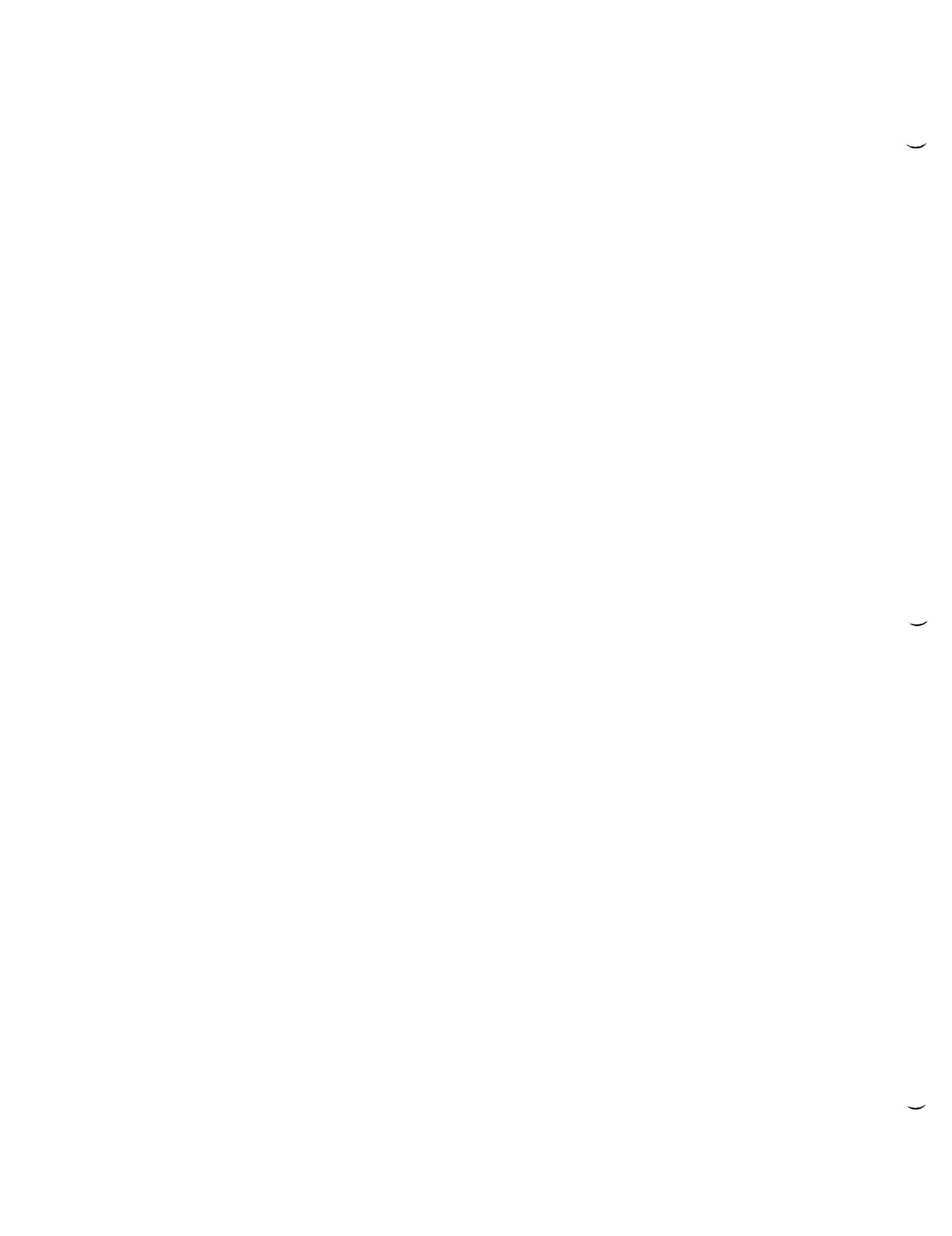
SECTION G
ROTATING MACHINERY
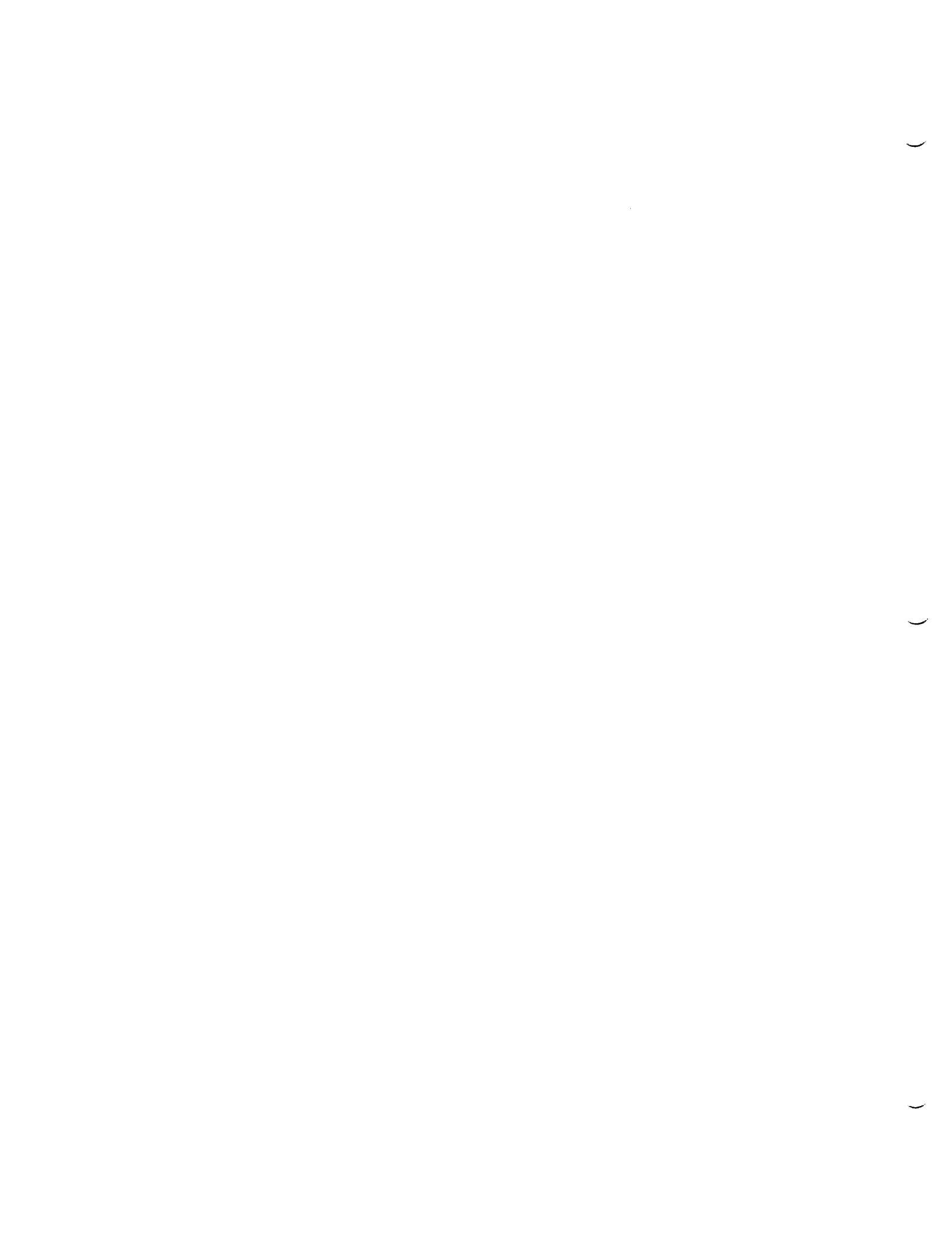
SECTION G1.2
SOLID DISCS

TABLE OF CONTENTS

DEFINITION OF SYMBOLS

Symbol

b	Rim radius
g	Gravity constant
h (r)	Disk thickness at location r
r	Distance from axis of revolution
μ	Poisson's ratio
ρ	Disk material density
σ_r	Stress in radial direction; positive denotes tension
σ_θ	Stress in tangential (hoop) direction; positive denotes tension
ω	Constant angular velocity, rad/sec

G1.2   SOLID DISKS.

In this section some of the methods of analyzing rotating circular disks are presented. The disks rotate about an axis which is perpendicular to the disk. Because the methods for a final analysis of turbomachinery-type hardware are quite involved, only methods for preliminary analysis which assume constant stress across the disk thickness are considered. Since the methods are preliminary, no modes of failure will be discussed at this time.

The geometry, coordinates, and stresses for a rotating circular disk are shown in Figure G1.2-1.
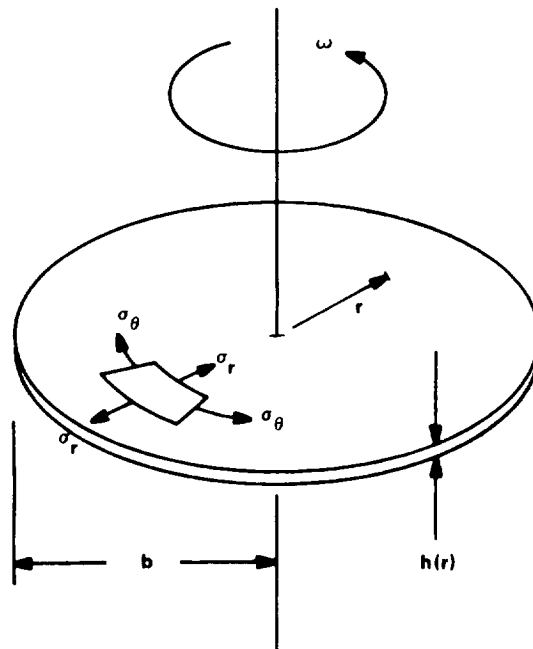
FIGURE G1.2-1.   CONFIGURATION OF SOLID CIRCULAR DISK

1.2.1 CONSTANT (UNIFORM) THICKNESS.

For solid circular disks rotating at a constant angular velocity with uniform thicknesses and temperature fields, the radial and tangential stresses (Ref. 1) are

$$\sigma_r = \frac{(\rho v^2)\ (3 + \mu)\ (1 - x^2)}{8g} \tag{1}$$

and

$$\sigma_\theta = \frac{(\rho v^2)\ (3 + \mu)}{8g} \left[1 - \frac{(1 + 3\mu)\ x^2}{3 + \mu} \right] \tag{2}$$

where

$$x = \frac{r}{b} \tag{3}$$

and

$$v = b\omega \quad . \tag{4}$$

The maximum stress occurs at the center of the disk (r = 0) and is given by

$$(\sigma_\theta)_{max} = (\sigma_r)_{max} = \frac{(\rho v^2)\ (3 + \mu)}{8g} \quad . \tag{5}$$

If the disk is centrally clamped (Fig. G1.2.1-1), the in-plane stresses (Ref. 2) become

$$\sigma_r = \left(\frac{\xi_2}{r^2} \right) (b^2 - r^2)\ \left(r^2 + \frac{\xi_1}{b^2 \xi_2} \right) \tag{6}$$

and

$$\sigma_\theta = \left(\frac{\xi_2}{r^2}\right)\left[\left(b^2 - \frac{\xi_1}{b^2 \xi_2}\right) r^2 - \frac{\xi_1}{\xi_2} - \frac{(1 + 3\mu) \, r^4}{3 + \mu}\right] \tag{7}$$

where

$$\xi_1 = \frac{(1 - \mu) \, \rho \omega^2 \, a^2 \, b^2}{8}\left[\frac{(3 + \mu) \, b^2 - (1 + \mu) \, a^2}{(1 + \mu) \, b^2 + (1 - \mu) \, a^2}\right] \tag{8}$$

and

$$\xi_2 = \frac{(3 + \mu) \, \rho \, \omega^2}{8} \tag{9}$$

for values of r greater than a.
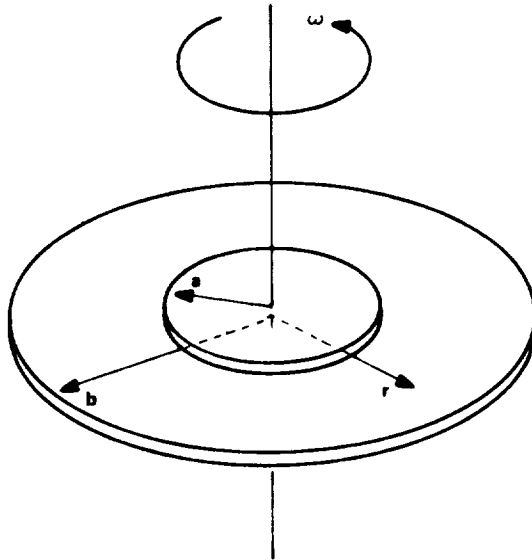
FIGURE G1.2.1-1. CONFIGURATION OF DISK WITH FULLY CLAMPED HUB

For a solid disk with a uniform thickness and a varying temperature field, the radial and tangential stresses are calculated using the procedure given in Paragraph 1.3.2 (Disks with a Hole at the Center — Variable Thickness) with the modifications described in Paragraph 1.2.2.

1.2.2 VARIABLE THICKNESS.

For a solid circular disk rotating at a constant angular velocity with a varying thickness or a varying temperature field, the radial and tangential stresses (Ref. 3) are calculated using the procedure given in Paragraph 1.3.2 (Disks with a Hole at the Center — Variable Thickness) with the following modifications:

1. Station point 1 should be chosen at 5 percent of the rim radius (b).

2. The initial value in column 33 should be 1.0.

3. The stresses at the center of the disk ($r = 0$) are assumed equal to the stresses at station point 1.

1.2.3. EXAMPLE PROBLEMS FOR ROTATING SOLID CIRCULAR DISKS.

I. Example Problem 1.

Find the radial and tangential stresses for the solid circular disk shown in the following sketch.

16 000 rpm

MATERIAL 6Al-4V TITANIUM
ROOM TEMPERATURE

0.25 in. (CONSTANT)

15 in.
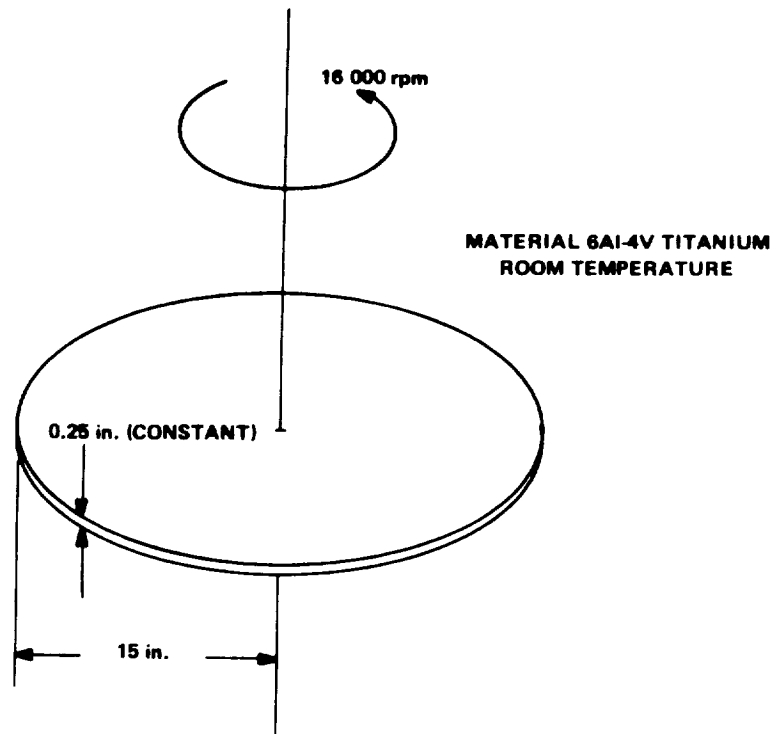
Solution:

$$E = 16.0 \times 10^6 \text{ lb/in.}^2 \quad .$$

$$\rho = 0.16 \text{ lb/in.}^3 .$$

$$\mu = 0.313 \quad .$$

$$g = 32.2 \text{ ft/sec}^2 = 386.4 \text{ in./sec}^2 \quad .$$

$$\omega = 16\ 000 \text{ rpm} = 266.7 \text{ r/sec} = 1675.52/\text{sec} \quad .$$

From equation (4)

$$v = b\omega = 15 \times 1675.52 = 25\ 132.8 \text{ in./sec}$$

and

$$v^2 = 6.3166 \times 10^8 \text{ in./sec}^2.$$

Equation (1) becomes

$$\sigma_r = \frac{0.16 \times 6.3166 \times 10^8}{8 \times 3.864 \times 10^2} \times 3.313 \times \left(1 - \frac{r^2}{15^2}\right) \frac{\text{lb in.}^2 \text{ sec}^2}{\text{in.}^3 \text{ sec}^2 \text{ in.}}$$

$$= 108\ 310 \left(1 - \frac{r^2}{225}\right) \text{lb/in.}^2 \quad .$$

The following sketch depicts σ_r.
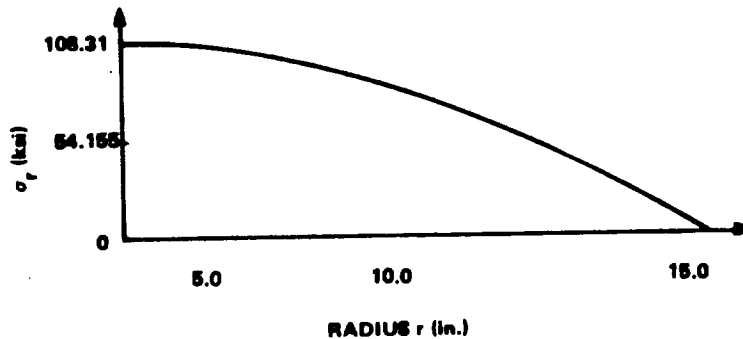
Equation (2) becomes

$$\sigma_\theta = 108\ 310 \left(1 - \frac{r^2}{385}\right) \text{lb/in.}^2 \quad .$$

The following sketch depicts σ_θ.
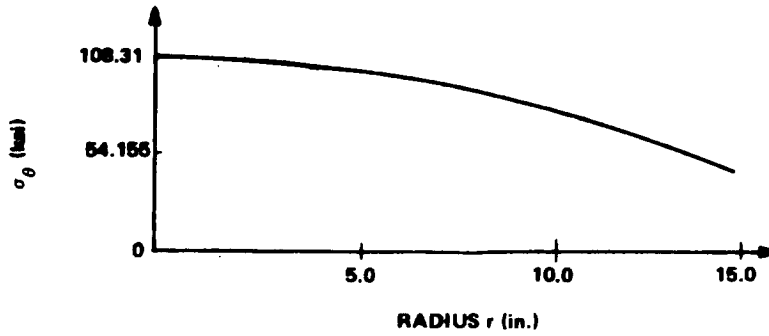
II. Example Problem 2.

Find the radial and tangential stresses for the solid circular disk shown in the following sketch.

Solution:

$$E = 16.0 \times 10^6 \text{ lb/in.}^2 .$$

$$\rho = 0.16 \text{ lb/in.}^3 .$$

$$\mu = 0.313 .$$

$$g = 386.4 \text{ in./sec}^2 .$$

$$\omega = 16\ 000 \text{ rpm}$$

$$= 1675.52/\text{sec.}$$

The idealization for the finite-difference-type analysis is given in the following sketch.

NOTE: DIMENSIONS ARE IN INCHES.

The computations for the finite-difference-type analysis are given in Table G1.2.3-1.

Table G1.2.3-1. Finite-Difference Analysis Computations of Example Problem 2

n	r_n 1	h_n 2	ρ_n^2 386.4 3	μ_n 4	E_n 5	α_n 6	Δr_n 7	(1) × (2) 8	$\frac{[(1)-(1)_{n-1}]}{+2.0}$ 9	(2) × (9) 10	$(2)_{n-1}$ × (9) 11	(3) × (9) × (1) 12	(12) + (12)$_{n-1}$ 13
1	0.25	0.25	1151	0.313	16.0 × 10⁻⁶	α	0	0.1875	-	-	-	161.9394	-
2	5.375	0.25	1151	0.313	16.0	α	0	1.3438	2.3125	0.5781	0.5781	× 313.5567	9 475.45
3	10.0	0.25	1151	0.313	16.0	α	0	2.5	2.3125	0.5781	0.5781	28 775	37 088.59
4	12.5	0.25	1151	0.313	16.0	α	0	3.125	1.25	0.3125	0.3125	44 960.9375	73 735.94
5	15.0	0.25	1151	0.313	16.0	α	0	3.75	1.25	0.3125	0.3125	64 743.75	109 704.69

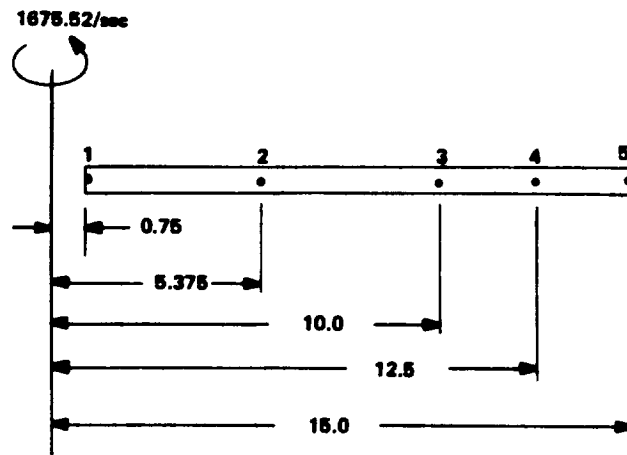| n	(1) × (13) 14	1.0 ÷ (5) 15	(4) × (15) 16	[1.0 × (4)] × (15) + (1) 17	(17) × (15) 18	(17)$_{n-1}$ × (9) 19	(16) × (15) 20	(15) × (1) 21	(16)$_{n-1}$ - (19) 22	(15)$_{n-1}$ - (19) 23	(6) × (7) 24	(24) - (24)$_{n-1}$ 25	(20) × (19) - 8 × (21) 26
1	-	0.0625 × 10⁻⁶	0.0196 × 10⁻⁶	0.0196 × 10⁻⁶	-	-	-	-	-	-	0	0	-
2	0.0196 × 10⁶	0.0625	0.0196	0.0153	0.0354 × 10⁻⁶	0.0330 × 10⁻⁶	0.055 × 10⁻²	0.0979 × 10⁻⁶	-0.2334 × 10⁻⁶	-0.1905 × 10⁻⁶	0	0	-0.0991 × 10⁻⁶
3	0.0558	0.0625	0.0196	0.0082	0.019	0.0354	0.03-6	0.0945	-0.0158	0.0271	0	0	-0.1514
4	0.0922	0.0625	0.0196	0.0096	0.00025	0.0103	0.02785	0.07055	0.0093	0.0522	0	0	-0.2124
5	0.1371	0.0625	0.0196	0.0055	0.0069	0.00825	0.0265	0.0694	0.0114	0.0543	0	0	-0.2520

n	$\frac{[(22)\cdot(1)-]}{(1)_{n-1}\cdot(20)]}{+(26)}$ 27	$\frac{[(23)\times(10)-]}{(11)\times(21)]}{+-(26)}$ 28	$\frac{[(20)\times(22)-]}{(20)\cdot(1)_{n-1}]}{+-(26)}$ 29	$\frac{[(20)\times(11)-]}{(9)\cdot(23)]}{+-(26)}$ 30	$\frac{[(25)\times(10)-]}{(14)\cdot(21)]}{+(26)}$ 31	$\frac{[(29)\cdot(11)-]}{(9)\times(25)]}{+(26)}$ 32	$\frac{(27)\cdot(33)_{n-1}-}{-(25)\cdot(34)_{n-1}}{-(31)}$ 33	$\frac{(29)\cdot(35)_{n-1}-}{-(30)\cdot(34)_{n-1}}{-(31)}$ 34	$\frac{(27)\times(35)_{n-1}-}{-(29)\times(36)_{n-1}}{-(31)}$ 35	$\frac{(29)\cdot(35)_{n-1}-}{-(30)\times(36)_{n-1}}{-(32)}$ 36	$\frac{[\sigma_{r,b}-(35)_b]}{+(33)_b}$ 37	$\frac{\sigma_{r,n}-}{(33)\times(37)}{-(35)}$ 38	$\frac{\sigma_{t,n}-}{(34)\times(37)}{-(36)}$ 39
1	-	-	-	-	-	-	1.0	1.0	0.0	0.0	0.1137 × 10⁶	0.1136 × 10⁶	0.1136 × 10⁶
2	1.5467	-0.5102	3.2694	-2.2624	-0.0102 × 10⁶	-0.0411 × 10⁶	1.0065	1.007	0.0192 × 10⁶	-0.0411 × 10⁶	0.1137	0.0952	0.1033
3	0.6340	0.3461	0.5036	0.4967	-0.036	-0.152	1.0098	1.007	0.055	-0.034	0.1137	0.0595	0.081
4	0.5100	0.1909	0.1902	0.5008	-0.036	-0.152	1.0065	1.00	0.0517	-0.0497	0.1137	0.0329	0.0646
5	0.5464	0.1536	0.1539	0.5409	-0.0377	-0.143	1.0068	1.00	-0.1145	-0.0691	0.1137	0.0	0.0452

REFERENCES

1. Timoshenko, S. : Strength of Materials, Part II. D. Van Nostrand and Company, Inc., New York, 1956, p. 218.

2. Eversman, W.; and Dodson, Jr., R. O. : Free Vibration of a Centrally Clamped Spinning Circular Disk. AIAA Journal, vol. 7, no. 10, Oct. 1969, pp. 2010 - 2012.

3. Manson, S. S. : Determination of Elastic Stresses in Gas-Turbine Disks. NACA Report 871, Cleveland, Ohio, Feb. 27, 1947.

TABLE OF CONTENTS

Page

DEFINITION OF SYMBOLS

Symbol	Definition
a	Inner surface radius
b	Rim radius
E	Modulus of elasticity
g	Gravity constant
h (r)	Disk thickness at location r.
n	Node (station) index
r	Distance from axis of revolution
T	Temperature ($^\circ$F)
α	Coefficient of thermal expansion
μ	Poisson's ratio
ρ	Disk material density
σ_r	Stress in radial direction; positive denotes tension
σ_θ	Stress in tangential (hoop) direction; positive denotes tension
ω	Constant angular velocity (rad/sec)

G1.3 DISKS WITH A HOLE AT THE CENTER.

In this section some of the methods of analyzing rotating circular disks with circular cutouts at the center are presented. The disks rotate about an axis which is perpendicular to the disk. Because the methods for a final analysis of turbomarchinery-type hardware are quite involved, only methods for preliminary analysis which assume constant stress, or linearly varying stress, across the disk thickness are considered. Since the methods are preliminary, no modes of failure will be discussed at this time.

The geometry, coordinates, and stresses for a rotating circular disk are shown in Figure G1.3-1.

1.3.1 CONSTANT (UNIFORM) THICKNESS.

For circular disks with a center hole that rotate at a constant angular velocity with uniform thickness and temperature fields, the radial and tangential stresses (Ref. 1) are

$$\sigma_r = \frac{(\rho v^2)(3 + \mu)}{8g}\left(1 + \gamma^2 - x^2 - \frac{\gamma^2}{x^2}\right) \tag{1}$$

and

$$\sigma_\theta = \frac{(\rho v^2)(3 + \mu)}{8g}\left(1 + \gamma^2 - \frac{(1 + 3\mu)x^2}{3 + \mu} + \frac{\gamma^2}{x^2}\right) \tag{2}$$
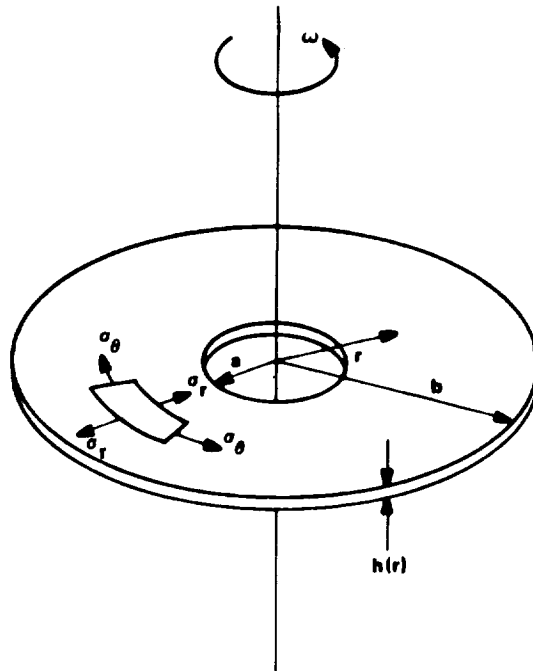
where

$$\gamma = \frac{a}{b} \quad , \tag{3}$$

FIGURE G1.3-1. CONFIGURATION OF A CIRCULAR DISK
WITH A CENTER HOLE

$$x = \frac{r}{b} \quad , \tag{4}$$

and

$$v = b \, \omega \quad . \tag{5}$$

The maximum stresses occur at $r = \sqrt{ab}$ and are

$$(\sigma_r)_{max} = \frac{(\rho \, v^2) \, (3 + \mu) \, (1 - \gamma)^2}{8g} \tag{6}$$

and

$$(\sigma_\theta)_{max} = \frac{(\rho \, v^2) \, (3 + \mu)}{4g} \left[1 + \frac{(1 - \mu) \, \gamma^2}{3 + \mu} \right] . \tag{7}$$

The stresses may be determined by the computer program documented in a NASA technical note.[1]

For a disk with a uniform thickness and a varying temperature field, the radial and tangential stresses are calculated using the procedure given in Paragraph 1.3.2.

1.3.2 VARIABLE THICKNESS.

The stresses in a circular disk with a center hole and a variable thickness or a variable temperature field may be determined using a finite-difference method (Ref. 2). This method considers the point-to-point variation in thickness, temperature, and material properties. The computations are easily executed in a tabular format.

An idealization of the disk is made (Fig. G1.3.2-1) by selecting stations along the radius. Station 1 lies on the inner surface, and station N lies on the outer (rim) surface.

Intermediate stations should be located at distances of 1, 2, 3, and 5 percent of the rim diameter from the inside boundary and at locations of thickness, temperature, or material property variations. The radius at each

---

1. Byron Foster and Jerrell Thomas: Automated Shell Theory for Rotating Structures (ASTROS). NASA TN-D-, Marshall Space Flight Center, to be published.
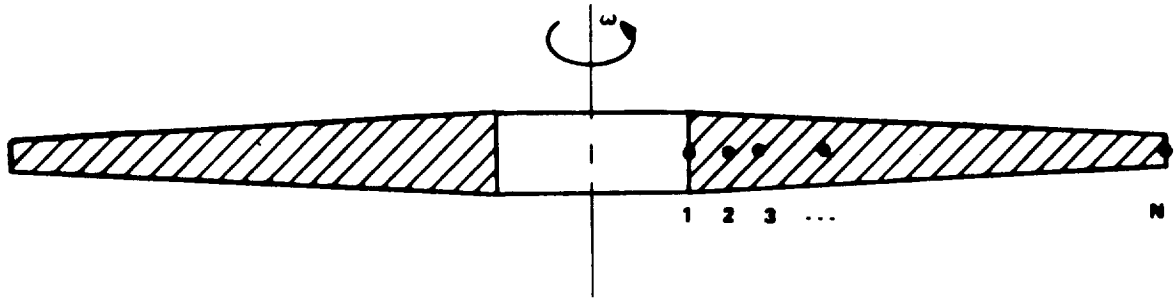
FIGURE G1.3.2-1. IDEALIZATION OF DISK FOR
FINITE-DIFFERENCE ANALYSIS

station is entered in column 1 (Table G1.3.2-1). In column 2 the idealized

thickness is entered. If a sharp discontinuity in thickness occurs, such as an

abrupt flange, the thickness should be faired in the disk contour, and the

faired disk used in determining the thickness. The mass density (corrected

if in a faired section) multiplied by the square of the rotational speed is entered

in column 3. Poisson's ratio and the modulus of elasticity are entered in

columns 4 and 5, respectively. The coefficient of thermal expansion, which

must be an average value applicable to the range between the temperature

actually existing and the temperatures at which there is no thermal stress, is

entered in column 6. The difference between the actual temperature and the

temperature at which there is no thermal stress is entered in column 7.

The manipulations required in columns 8 through 34 are shown in the

Table G1.3.2-1. Finite-Difference Analysis Tabular Format

1	2	3	4	5	6	7	8	9	10	11	12	13
r_n	h_n	$\rho_n = 396.4$	u_n	ϵ_n	σ_n	ΔT_n	$(1)\times(2)$	$[(1)-(1)_{n-1}] \div 2.0$	$(2)\times(9)$	$(2)_{n-1}\times(9)$	$(3)\times(8)\times(1)$	$(12)+(12)_{n-1}$

14	15	16	17	18	19	20	21	22	23	24	25	26
$(9)\times(13)$	$1.0+(5)$	$(4)\times(15)$	$[1.0+(4)]\div(15)+(1)$	$(17)\times(9)$	$(17)_{n-1}\times(9)$	$(16)-(18)$	$(16)-(18)$	$(16)_{n-1}-(19)$	$(15)_{n-1}-(19)$	$(6)\times(17)$	$(24)-(24)_{n-1}$	$(20)\times(10)-(8)\times(21)$

27	28	29	30	31	32	33	34	35	36	37	38	39
$[(22)\times(15)-(9)_{n-1}\times(21)] +-(26)$	$[(23)\times(10)-(11)\times(21)] +-(26)$	$[(8)\times(22)-(20)\times(8)_{n-1}] +(26)$	$[(20)\times(11)-(9)\times(23)] +-(26)$	$[(25)\times(10)-(14)\times(23)] +(26)$	$[(29)\times(14)-(9)\times(25)] +(26)$	$(27)-(33)_{n-1} -(29)\times(34)_{n-1}$	$(29)-(33)_{n-1} -(30)\times(34)_{n-1}$	$(27)\times(35)_{n-1} +(29)\times(36)_{n-1} -(31)$	$(29)\times(35)_{n-1} +(30)\times(36)_{n-1} -(32)$	$[\sigma_{r,b}-(35)_b] +(33)_b$	$\sigma_{r,n}$ $(33)\times(37)$ $+(35)$	$\sigma_{\theta,n}$ $(34)\times(37)$ $+(36)$

respective columns. Columns 33 and 34 are calculated simultaneously, with column 33 having an initial value of 0.000 and column 34 having an initial value of 1.000. Columns 35 and 36 are also calculated simultaneously, but each has an initial value of 0.000.

In column 37, the term $\sigma_{r,b}$ denotes the blade loading at the rim and is obtained by dividing the total centrifugal force at the roots of the blades by the total rim peripheral area.

The radial stress, σ_r, at each station is calculated in column 38. The tangential stress, σ_θ, at each station is calculated in column 39.

In using the finite-difference method, the accuracy of the results increases as the number of station points increases. The stresses may also be determined by the computer program already cited.[2]

1.3.3 EXAMPLE PROBLEMS FOR ROTATING CIRCULAR DISKS WITH CENTER HOLES

I. Example Problem 1.

Find the radial and tangential stresses for the following circular disk:

---

2. Ibid.

**MATERIAL 6Al-4V TITANIUM
ROOM TEMPERATURE**
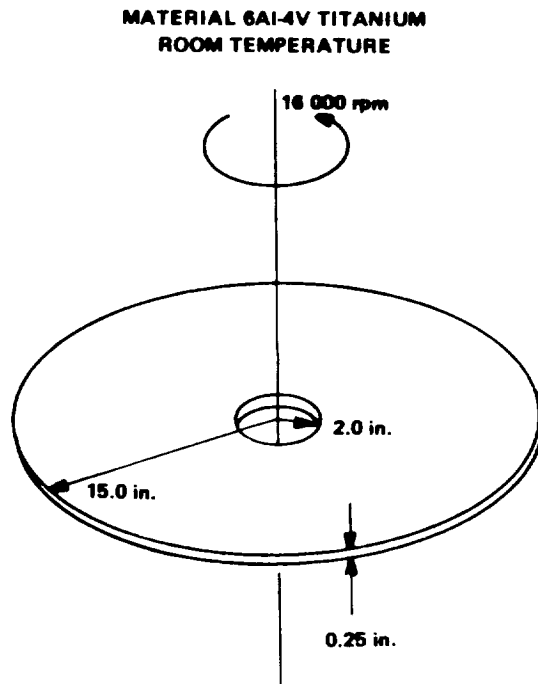
Solution:

$$E = 16.0 \times 10^6 \text{ psi},$$

$$\rho = 0.16 \text{ lb/in.}^3,$$

$$\mu = 0.313,$$

$$g = 386.4 \text{ in./sec}^2,$$

$$\omega = 16\ 000 \text{ rpm} = 1675.52/\text{sec},$$

$$\gamma = \frac{2}{15} = 0.1333,$$

$$v = 15 \times 1675.52 \text{ in./sec} = 25\ 132.8 \text{ in./sec}.$$
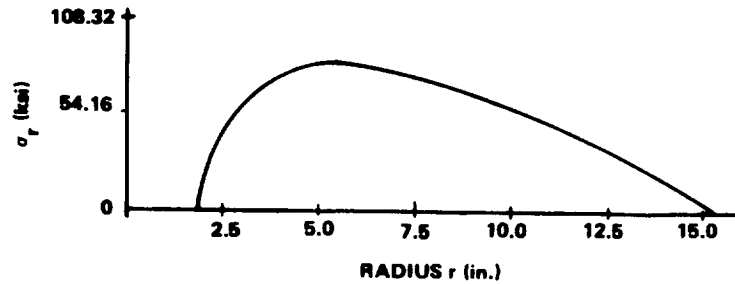
and

$$v^2 = 6.3167 \times 10^8 \text{ in}^2/\text{sec}^2 \quad .$$

Equation (1) becomes

$$\sigma_r = \frac{\left(0.16 \times 6.3167 \times 10^8\right)\left(3.0 + 0.313\right)\left(1 + 0.1333^2 - \frac{r^2}{225} - \frac{4.005}{r^2}\right)}{3091.2} \quad \text{psi}$$

$$= 1.0832 \times 10^5 \left(1.0178 - 0.00444\ r^2 - \frac{4.005}{r^2}\right) \quad \text{psi.}$$
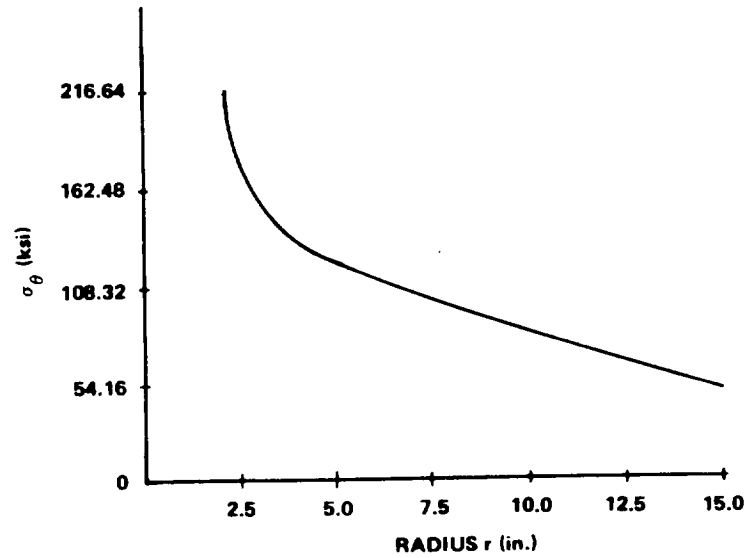
The following sketch depicts σ_r.

Equation (2) becomes

$$\sigma_\theta = 1.0832 \times 10^5 \left(1 + 0.1333^2 - \frac{1 + 0.939)}{(3 + 0.313)\ 225}\ r^2 + \frac{4.005}{r^2}\right) \quad \text{psi.}$$

$$= 1.0832 \times 10^5 \left(1.0178 - 0.00444\ r^2 - \frac{4.005}{r^2}\right) \text{psi.}$$

The following sketch depicts σ_θ.

The maximum stress occurs at

$$r = 5.4772 \text{ in.}$$

The stresses at that position are

$$\sigma_r = 1.0832 \times 0.7511 \times 10^5 \text{ psi}$$

$$= 0.8136 \times 10^5 \text{ psi}$$

and

$$\sigma_\theta = 1.0832 \times 1.0733 \times 10^5 \text{ psi}$$

$$= 1.1626 \times 10^5 \text{ psi.}$$

II. Example Problem 2.

Find the radial and tangential stresses for the following circular disk.
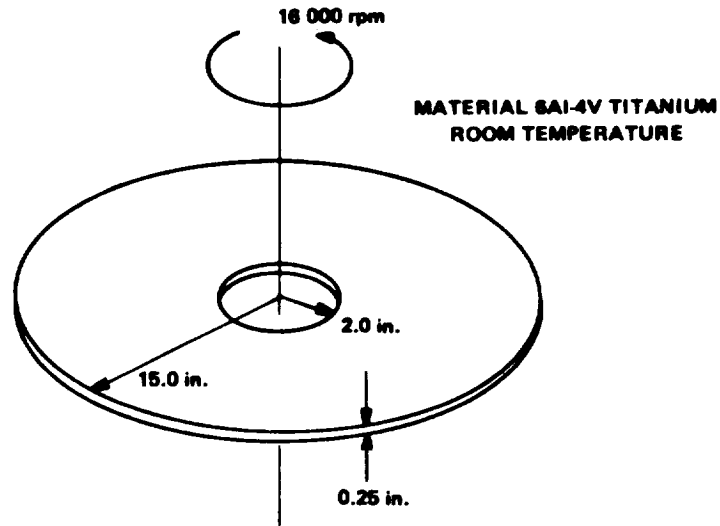
Solution:

$$E = 16.0 \times 10^6 \text{ psi.}$$

$$\rho = 0.16 \text{ lb/in.}^3$$

$$\mu = 0.313.$$

$$g = 386.4 \text{ in./sec}^2.$$

$$\omega = 16\ 000 \text{ rpm} = 1675.52/\text{sec.}$$

The idealization for the finite-difference-type analysis is given in the following sketch.

NOTE: DIMENSIONS ARE IN INCHES

The computations for the finite-difference-type analysis are given in Table G1.3.3-1.

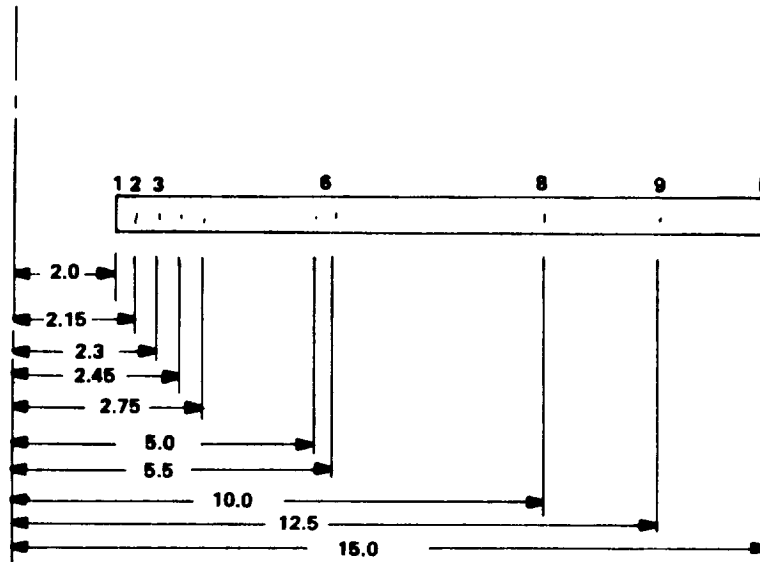Table G1.3.3-1. Finite-Difference Analysis Computations of Example Problem 2

n	r_n	h_n	$\rho_n \omega^2/386.4$	μ_n	E_n	α_n	ΔT_n	$(1)\times(2)$	$[(1)-(1)_{n-1}]$ $+2.0$	$(2)\times(9)$	$(2)_{n-1}\times(9)$	$(3)\times(8)\times(1)$	$(12)+(12)_{n-1}$
n	1	2	3	4	5	6	7	8	9	10	11	12	13
1	2.0	0.25	1162.5	0.313	16.0×10^6	α	0.00	0.5	—	—	—	1 162.5	—
2	2.15	0.25	1162.5	0.313	16.0	α	0.00	0.5375	0.075	0.0188	0.0188	1 343.4142	2 505.9
3	2.3	0.25	1162.5	0.313	16.0	α	0.00	0.575	0.075	0.0188	0.0188	1 537.4062	2 880.8
4	2.45	0.25	1162.5	0.313	16.0	α	0.00	0.6125	0.075	0.0188	0.0188	1 744.4764	3 281.9
5	2.75	0.25	1162.5	0.313	16.0	α	0.00	0.6875	0.15	0.0375	0.0375	2 197.8517	3 942.3
6	5.0	0.25	1162.5	0.313	16.0	α	0.00	1.25	1.125	0.2812	0.2812	7 265.625	9 463.5
7	5.5	0.25	1162.5	0.313	16.0	α	0.00	1.375	0.25	0.0625	0.0625	8 791.4062	16 057.0
8	10.0	0.25	1162.5	0.313	16.0	α	0.00	2.5	2.25	0.5625	0.5625	29 062.5	37 853.9
9	12.5	0.25	1162.5	0.313	16.0	α	0.00	3.255	1.25	0.3125	0.3125	47 299.219	76 361.7
b	15.0	0.25	1162.5	0.313	16.0	α	0.00	3.75	1.25	0.3125	0.3125	65 390.625	112 689.8

Table G1.3.3-1 (CONCLUDED)

n	$(9)\times(13)$	$1.0+(5)$	$(4)\times(15)$	$[(1.0+(4))]\times(15)\div(1)$	$(17)\times(9)$	$(17)_{n-1}\times(9)$	$(16)+(18)$	$(15)+(18)$	$(16)_{n-1}-(19)$	$(15)_{n-1}-(19)$	$(6)\times(7)$	$(24)-(24)_{n-1}$	$(20)\times(10)-(8)\times(21)$
	14	15	16	17	18	19	20	21	22	23	24	25	26
1	–	0.0625×10^{-6}	0.0196×10^{-6}	0.0411×10^{-6}	–	–	–	–	–	–	0.0	0.0	–
2	187.94	0.0625	0.0196	0.0382	0.0029×10^{-6}	0.0031×10^{-6}	0.0225×10^{-6}	0.0654×10^{-6}	0.0165×10^{-6}	0.0594×10^{-6}	0.0	0.0	-0.0347×10^{-6}
3	216.06	0.0625	0.0196	0.0357	0.0027	0.0029	0.0223	0.0652	0.0167	0.0596	0.0	0.0	-0.0371
4	246.14	0.0625	0.0196	0.0335	0.0025	0.0027	0.0221	0.065	0.0169	0.0598	0.0	0.0	-0.0394
5	591.34	0.0625	0.0196	0.0298	0.0045	0.005	0.0241	0.067	0.0146	0.0575	0.0	0.0	-0.0452
6	10 646.4	0.0625	0.0196	0.0164	0.0194	0.0335	0.038	0.0809	-0.0139	0.029	0.0	0.0	-0.0904
7	4 014.25	0.0625	0.0196	0.0149	0.0037	0.0041	0.0233	0.0662	0.0155	0.0584	0.0	0.0	-0.0896
8	85 171.3	0.0625	0.0196	0.0082	0.0184	0.0335	0.038	0.0809	-0.0139	0.029	0.0	0.0	-0.1809
9	95 452.1	0.0625	0.0196	0.0066	0.0082	0.0102	0.0278	0.0707	0.0094	0.0523	0.0	0.0	-0.2214
b	140 862.2	0.0625	0.0196	0.0055	0.0069	0.0082	0.0265	0.0694	0.0114	0.0543	0.0	0.0	-0.2520

n	$[(22)_{n-1}\times(19)]-(8)_{n-1}\times(21)]\div(26)$	$[(23)\times(10)]+(11)\times(21)]\div(26)$	$[(8)\times(22)]-(20)\times(8)_{n-1}]\div(26)$	$[(20)\times(11)]+(8)\times(23)]\div(26)$	$[(25)\times(10)]+(14)\times(21)]\div(26)$	$[(20)\times(14)]+(8)\times(25)]\div(26)$	$[(27)\times(33)_{n-1}]+(28)\times(34)_{n-1}]$	$[(29)\times(33)_{n-1}]+(30)\times(34)_{n-1}]$	$[(27)\times(35)_{n-1}]+(28)\times(36)_{n-1}]+(31)$	$[(29)\times(35)_{n-1}]+(30)\times(36)_{n-1}]+(32)$	$[\sigma_{r,b}-35)_b]+(33)_b$	$\sigma_{r,n}=(33)\times(37)+(35)$	$\sigma_{\theta,n}=(34)\times(37)+(36)$
	27	28	29	30	31	32	33	34	35	36	37	38	39
1	–	–	–	–	–	–	0.0000	1.0000	0.0000	0.0000	251 553.6	0.0	251 553.6
2	0.9424	0.0663	0.0663	0.9337	-354.2	-126.9	0.0663	0.9337	-354.2	-121.9	251 553.6	16 323.8	234 753.7
3	0.9434	0.062	0.0647	0.9326	-379.7	-125.9	0.1204	0.8751	-721.4	-273.1	251 553.6	29 565.7	219 861.5
4	0.9467	0.0584	0.0584	0.9391	-406.1	-138.1	0.1651	0.8288	-1 105.0	-436.7	251 553.6	40 426.5	208 050.9
5	0.9071	0.104	0.1062	0.9938	-876.5	-315.3	0.2360	0.7583	-1 924.3	-823.0	251 553.6	57 442.3	189 930.1
6	0.6184	0.3419	0.4812	0.5188	-9 527.6	-4 475.3	0.4051	0.5070	-10 998.9	-5 835.2	251 553.6	90 905.5	121 709.5
7	0.9230	0.0871	0.0871	0.9129	-2 965.9	-1 043.9	0.4181	0.4981	-13 625.5	-7 322.5	251 553.6	91 549.1	117 976.3
8	0.6164	0.3416	0.4809	0.5191	-38 089.3	-17 891.1	0.4279	0.4596	-48 989.4	-28 244.7	251 553.6	58 650.4	87 369.3
9	0.7981	0.1734	0.1757	0.808	-30 480.9	-11 945.4	0.4212	0.4465	-74 477.0	-43 414.6	251 553.6	31 477.4	68 904.1
b	0.8960	0.1536	0.1726	0.8409	-38 793.	-14 812.9	0.4460	0.4482	-112 192.9	-64 175.0	251 553.6	0.0	48 571.3

REFERENCES

1. Timoshenko, S.: Strength of Materials, Part II. D. Van Nostrand Company, Inc., New York, 1956.

2. Manson, S. S.: Determination of Elastic Stresses in Gas-Turbine Disks. NACA Report 871, Cleveland, Ohio, Feb. 27, 1947.

SECTION H1
STATISTICAL METHODS

TABLE OF CONTENTS

LIST OF ILLUSTRATIONS

LIST OF TABLES

LIST OF SYMBOLS COMMONLY USED IN STATISTICS

Symbol	Definition	
C {x}	Coefficient of variation $= \dfrac{\sigma \{x\}}{M \{x\}}$	[1]
C.D.F.	Cumulative distribution function	[2]
Cov	Covariance	[2]
C_r^n	$\dfrac{n!}{(n - r)! \; r!} = \binom{n}{r}$	[2]
D.F.	Degrees of freedom	[2]
df	Distribution function/degrees of freedom	
Exp X	e^x	[2]
"F"	F ratio or variance ratio	[2]
f	(N-1) Degrees of freedom; fraction of parts sampled; frequency	[2]
k	A standardized variable expressing the dispersion about the mean in terms of σ	[3]
k_P	A constant for a specified probability level which correlates population density with standard deviation; sometimes called a standardized variable, applies to normal distributions	[3]
$k_{P\gamma}$	Composite probability factor; a standardized variable relating P, γ, and n to some limiting value of the variable, applied to normal distributions	[3]

LIST OF SYMBOLS COMMONLY USED IN STATISTICS (Continued)

Symbol	Definition	
$M\{x\}$	The mean of a stochastic variable x	[1]
M.G.F.	Moment generating function	[2]
Mo	Mode	[2]
m	Population mean	[4]
N	Sample size [2]; number of loading cycles to failure [3]	
N_e	An arbitrary lifetime to which fatigue test data are to be extrapolated	[3]
N_i	Same relationship to N as x_i has to x	[3]
$N_{P\gamma}$	Lower limiting life above which any test value can be expected to fall with a probability of P and a confidence of γ	[3]
$\bar{N}_s$	Arithmetic mean of test sample lives	[3]
$\bar{N}_u$	Arithmetic mean life that could be expected if an infinite number of samples could be tested	[3]
N_4	Number of loading cycles at which weakest of four specimens fails	[3]
$\bar{N}_4$	Arithmetic mean of least-of-four test sample lives	[3]

Symbol	Definition	
n	Number of independent single test specimens	[3]
n!	Factorial $n = 1 \times 2 \times \ldots \times (n-1) \times n$	[2]
n_4	Number of least-of-four test points	[3]
$\binom{n}{r}$	$C\binom{n}{r} = \dfrac{n!}{(n-r)! \; r!}$	[2]
P	Probability; the percent of a group of specimens expected to fall within a certain range	[3]
P (x)	Probability of an event x occurring	[2]
P_4	Probability of four consecutive test values exceeding some specified limiting value	[3]
R.M.S.	Root mean square	[2]
r	Correlation coefficient	[2]
S	Loading stress level at which failure occurs at some number of cycles (N) in fatigue work	[3]
S_a	A value of stress on the estimated average S-N curve corresponding to some arbitrary test point life, N_i	[3]
S_D	Standard deviation of a sample	[2]
S_e	A value of stress on the estimated average S-N curve corresponding to the lifetime (N_e) to which fatigue data are to be extrapolated	[3]

Symbol	Definition	
S_i	An arbitrary value of stress occurring in a particular problem at lifetime N_i	[3]
S_{ic}	A derived stress value at lifetime (N_c) corresponding to an observed stress value S_i at lifetime N_i	[3]
S_s	Standard error of the standard deviation	[2]
S^2	Variance of a sample	[2]
"t"	Student's "t" statistic	[2]
u	Standardized variable $= \dfrac{x - \xi}{\sigma}$	[1]
V	Coefficient of variation	[2]
w	Often used for range	[2]
x	A random statistical variable	[3]
$\bar{x}$	Arithmetic mean of x-values regardless of the number of values involved	[3]
x_i	Any arbitrary value of x occurring in a specified problem	[3]
x_P	A variable expressed as a function of P and σ	[3]
$x_{P\gamma}$	A limiting value of x dependent on p, γ, n, and σ	[3]

LIST OF SYMBOLS COMMONLY USED IN STATISTICS (Continued)

Symbol	Definition	
$\dot{x}_s$	Arithmetic mean of values from a limited sample size	[3]
$\bar{x}_u$	Arithmetic mean that could be expected from an infinite number of specimens	[3]
y	Frequency of occurrence of test points in given intervals of the variable (Δx)	[3]
y'	Percentage frequency; percentage of total number of test points in a given variable increment	[3]
α	α risk, Type I error	[2]
α_{P_1}	Limiting value of standardized variable for a given probability and an unknown distribution	[3]
α_γ	Limiting value of standardized variation of the mean for a given confidence and an unknown distribution	[3]
β	β risk, Type II error; also equals $(1 - \alpha)$	[2]
γ	Confidence; the percentage of sample mean values falling within a given range of the universe mean [3]; associated with the tolerance limit tables [2]	
μ	Population mean	[2]
ξ	Mean of a stochastic variable $x = M\{x\}$	[1]
σ	Standard deviation of variable x about $\bar{x}$	[3]

H1-x

LIST OF SYMBOLS COMMONLY USED IN STATISTICS (Concluded)

Symbol	Definition	
σ_e	Standard deviation of a limited number of derived stress points about S_e	[3]
$\sigma_{\overline{N}_4}$	Standard error of least-of-four mean $(\overline{N}_4)$	[3]
σ_s	Standard error of the standard deviation [2]; standard deviation computed from a limited sample size [3]	
σ_u	Unbiased standard deviation of the universe; corresponds to an infinite sample size	[3]
σ_{u_4}	Standard deviation of universe of least-of-four points	[3]
$\sigma_{\overline{x}}$	Standard deviation of $\overline{x}_s$, about $\overline{x}_u$; sometimes called the standard error of the mean	[3]
σ_4	Standard deviation of least-of-four test failure points	[3]
σ^2	Variance of a population	[2]
χ^2	Chi-square	[2]

LIST OF DEFINITIONS COMMONLY USED IN STATISTICS

Definition

Alternative Hypothesis

Possible true alternate answer to the hypothesis being statistically tested. The larger the sample size, the greater the possibility of rejecting a hypothesis when an alternate answer is true [2].

AOQL (Average Outgoing Quality Limit)

Upper limit on outgoing quality that may be expected in the long run, when all rejected lots are subjected to 100 percent inspection, with all defective articles removed and replaced by good articles [2].

A Posteriori Probability

If in a number of trials an event has occurred N times and failed M times, the probability of its occurring in the next trial is $\dfrac{N}{M + N}$ [2].

A Priori Probability

Let N be the number of exhaustive, mutually exclusive, and equally likely cases of an event under a given set of conditions. If M of these cases are known as the event A, then the mathematical, or a priori probability of event

Definitions

A occurring under the given set of conditions

is M/N [2].

AQL (Acceptable Quality

Level

Percentage of defective items in an inspection

lot that a sampling plan will accept with (in

the usual case) an associated α Risk of 0.05

[2].

Biased Sample

If some individuals in the Universe are more

likely to be chosen than others, the sample

is said to be biased.

Class Interval

When the number of observations is large,

the range of the data can be broken into a

limited number of segments of equal length.

The segments are known as class intervals or

cells [2].

Confidence Intervals

This provides a method of stating how close an

estimate is to the true value [2]. It is the

interval associated with a prescribed confi-

dence coefficient. The confidence coefficient

is the proportion of samples of size n for

Definition

which intervals computed by the prescribed

methods may be expected to bracket a value [4].

Continuous Distribution — One in which the only limit to size of intervals

measured is the sensitivity of the measuring

apparatus [2].

Cumulative Distribution — Indicates by its magnitude the proportion of

the Universe (or sample) to the left of that

point [2].

Curve Fitting — Method utilizing computed statistics as approx-

imate parameters for theoretical distributions

[2].

Degree of Freedom — Number of free variables (unrestricted and

independent in the sense of random sampling)

entering into a statistic. In the case of a

sample of size N, from a Universe, there

are N-1 degrees of freedom [2].

Discrete Distribution — If a random variable has only a finite number

of possible values, then it will form a discrete

distribution [2].

LIST OF DEFINITIONS COMMONLY USED IN STATISTICS (Continued)

Definition

Double Sampling

Involves the possibility of putting off the disposition of an inspection lot until a second test sample is taken. A lot will be accepted on the basis of the first sample if the results are very good or will be rejected if the results are very poor. If the results from the first sample are of a borderline nature (between good and poor), a second sample must be taken.

On the basis of the results of the combined first and second samples, the lot is either accepted or rejected [2].

Error

In statistics there are two types of error. If we reject the null hypothesis when it is true, then we make an Error of the First Kind. If we fail to reject a null hypothesis when it is false, then we make an Error of the Second Kind [4].

"F" Distribution

Sampling distribution of the variance [2].

LIST OF DEFINITIONS COMMONLY USED IN STATISTICS (Continued)

Definition

Frequency Table	Tabulation of the number of observations that occur in each class interval of a histogram [2].
Histogram	Block representation of data arranged to show the dispersion of the data [2].
Hypothesis	Statement formulated in such a way that it may be refuted through statistics.
Inference	Based on the theory of probability, statistical inference is that mathematical framework which supplies a technique for description, prediction, and rational design decisions despite the complications which arise because of variation [2].
Latin Square	"Analysis of Variance" ordering technique of observed values in an experiment, allowing control of several sources of variability [2].
Least Squares	Method based upon the principle that the best value of a quantity that can be deduced from a set of measurements or observations is that for which the sum of the squares of the deviations of the observations (from it) is a minimum [2].

LIST OF DEFINITIONS COMMONLY USED IN STATISTICS (Continued)

Definition

Lot	Group of manufactured articles which are essentially alike, such as 1 day's production [2].
LTPD (Lot Tolerance Percent Defective)	Usually refers to the incoming quality, above which there is a small chance that a lot will be accepted. It is usually taken with a consumer's risk of $\beta = 0.10$ [2].
Mean	The arithmetic average of a group of observations [2]. It is the location parameter of a normal distribution locating the "center of gravity" of the distribution [4].
Mean Deviation	Arithmetic mean of the absolute distance of each observation from the mean [2].
Median	Middle value of a group of observations. In the case of an even numbered set of observations, it is the average of the middle pair [2].
Midrange	Arithmetic average of the extreme values of a set of observations [2].
Mode	Most frequent value of a set of observations [2].

Definition

Moments

In statistics, moments are analogous to moments in mechanics in several ways. Just as some bodies are completely characterized by their moments, some probability distributions are completely characterized by their moments. The first moment about the origin is equivalent to the expected value (the mean) of the random variable. The first moment is also the center of gravity of the probability mass. The second moment above the mean is also known as the moment of inertia and variance [2].

Nonparametric Statistics

Statistical techniques developed to test hypotheses without the assumption of normality, or any other assumption, other than that of continuity of a distribution [2].

Normal (Gaussian) Curve

Bell-shaped curve from the Gaussian probability distribution. It is a two parameter distribution requiring the mean and the variance for its description [2].

LIST OF DEFINITIONS COMMONLY USED IN STATISTICS (Continued)

Definition

Normal Probability Paper — Special graph paper which reduces the cumulative normal curve to a straight line. The log-normal probability paper does the same with log values as the normal paper does with linear values [2].

OC Curves (Operating Characteristics Curves) — Give the chance of accepting a hypothesis [2].

Population — Any set of individuals (or objects) having some common observable characteristic. It is synonymous with Universe [2].

Proof — Differs from mathematical proof as it does not fall within the framework mathematics, but results from experimentation, with an accompanying probability statement [2].

Random Digits — Digits picked in such a way that each digit has an equal chance of occurring at any time [2].

Randomization — Assignment of a sequence of operations to a test program by the use of some technique, such as random tables, to avoid bias in the test results [2].

Definition

Random Sample

Picked in such a way that all members of the population have an equal chance of selection [2].

Range

Absolute difference between the extreme values of a set of observations [2].

Root Mean Square

Square root of the average of the sum of the squares of a set of observations [2].

$$RMS = \sqrt{\frac{\sum_{i=1}^{N} x_i^2}{N}}$$

Sample

Set of observations chosen from a population [2].

Sampling Distribution

Distribution of a statistic in the set of all samples of a specific size from a given Universe [2].

Sequential Samplings

Acceptance plans permitting from three, up to an unlimited number of samples [2].

Significance Level

This expresses our reluctance to give up or "reject" the null hypothesis and is given by the magnitude of the α Risk. The

Definition

smaller the magnitude of significance the less

we are willing to reject the null hypothesis [4].

Single Sampling — When the decision as to the disposition of an

inspection lot is always made on the evidence

of only one sample, the acceptance plan is

described as a single sampling plan [2].

Standard Deviation — Positive square root of the variance [2].

Statistic — Estimation of a population parameter, computed

entirely from a sample [2].

Stochastic Variable — In general, any variable which may have a

probability function is a chance or stochastic

variable, even though the frequency function

is not known [2].

"t" Distribution — Sampling distribution of the mean [2].

Tolerance Limits — Limits such that a certain portion of the

population shall lie within or above them with

a specified probability [2].

Unbiased Estimate — Estimate of a parameter which has been

corrected for sample size effects and is

equivalent to the total population parameter [3].

LIST OF DEFINITIONS COMMONLY USED IN STATISTICS (Concluded)

Definition

Universe

Comprised of any set of individuals having some common observable characteristic [2].

Variables Sampling

When a record is made of an actual measured quality characteristic, such as a dimension expressed in thousandths of an inch, it is known as variables sampling [2].

Variance

Sum of the squares of the deviations from the mean divided by the number of observations less than one [2].

α Error

Risk of rejecting a true hypothesis. This is also known as an α Risk, Consumer's Risk, or Type I [2].

β Error

Risk of accepting a false hypothesis. This is also known as β risk, Producer's Risk, or Type II Error [2]. Equals $(1 - \alpha)$.

H1   STATISTICAL METHODS

1.1   INTRODUCTION

"One of the main objectives of statistics is to give a mathematical

description of observed data in such a manner that the observed phenomena

and the method of observation are characterized by a few numbers" [1].

While a single observation cannot be reproduced, experience has shown that

a set of observations, resulting from the repetition of some process, produces

certain characteristic features which can be reproduced; and it is these

characteristic features that statistics attempt to describe.

Various methods of describing characteristic features have been

developed, and one method includes the use of a histogram. Consider a

hypothetical set of recorded test values as being laid off in ascending order

of magnitude along a horizontal axis to form the abscissa of a graph. Now

let the range of values be divided into equal intervals and a count made of the

number of test points in each interval. The number of points per interval is

known as the frequency. If the various frequencies are now laid off on a

vertical scale, a histogram is produced (Fig. H1-1). From the histogram

a frequency distribution curve may be obtained by fairing a smooth line

through the shape of the histogram (Fig. H1-2). Several frequency distribution

curves (Normal, Log-Normal, χ^2, "t", Weibull) have been established,

but only two (Normal and Log-Normal) will be discussed here.
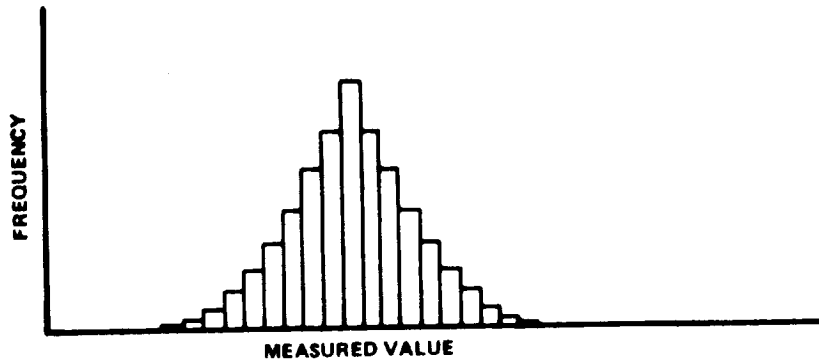
FIGURE III-1. HISTOGRAM.
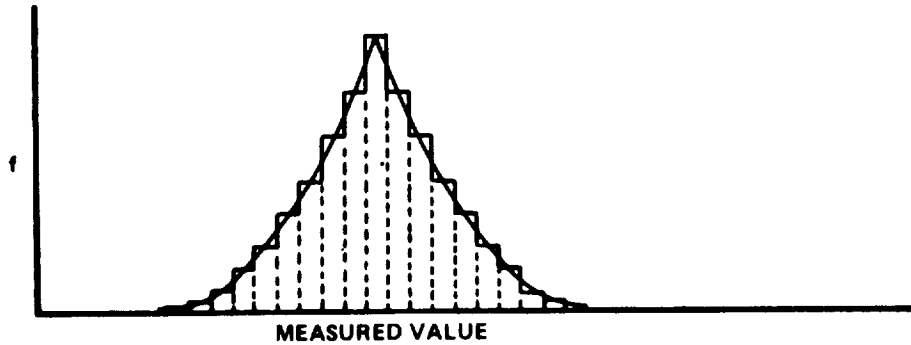
FIGURE III-2 DISTRIBUTION FUNCTION FROM "FAIRED" HISTOGRAM

The statistical methods discussed will be limited to those methods necessary for evaluating material, fatigue, and fracture mechanics data. It has been found that material data obey normal distribution and that fatigue [3] and fracture [5] data obey log-normal distributions.

1.2   METHODS FOR MEASURING PERFORMANCE OF A MATERIAL

1.2.1   Normal Probability Curve

1.2.1.1   Properties

The normal, or Gaussian, curve is a two-parameter curve (Fig. H1-3).

It is defined by the mean which locates the curve and the deviation which

defines the spread of the curve. The area under the curve is always equal to

one. The relation of the mean (μ) , the standard deviation (σ) , and the

significance level (α) is shown in Fig. H1-4.
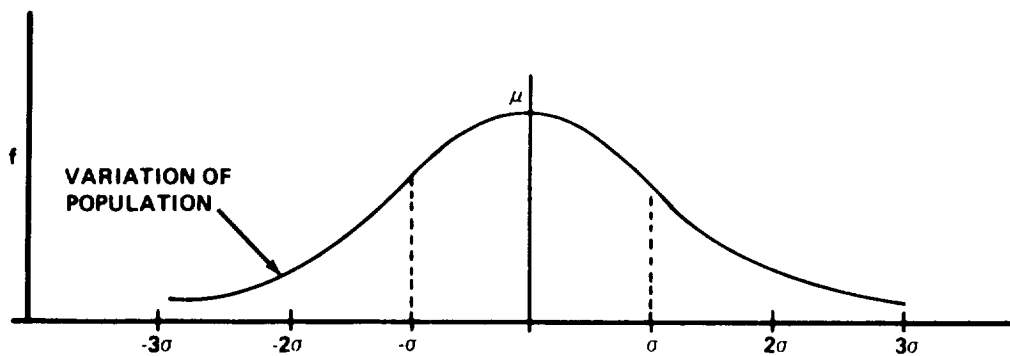
FIGURE H1-3. NORMAL (GAUSSIAN) DISTRIBUTION CURVE.
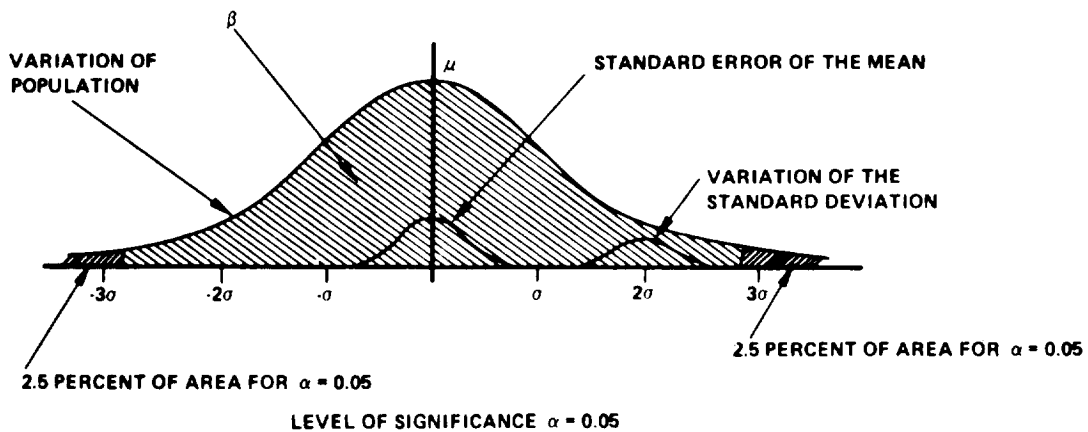
FIGURE H1-4. PARAMETERS AND PERFORMANCE GUIDES
             FOR NORMAL DISTRIBUTION.

1.2.1.2   Estimate of Average Performance

The most common and ordinarily the best single estimate of the popu-

lation mean, m , is simply the arithmetic mean of the measurements.

$$m \approx \bar{x} = \frac{1}{n} \sum_{i=1}^{n} x_i \quad .$$

(1)

1.2.1.3   Example Problem 1

Determine the mean value of the ultimate strength of product "A"

having the test results in Table H1-1 [3].

Table H1-1.   Ultimate Strength of Product "A"

Test Specimen	Ultimate Strength x_i (lb)
1	578
2	572
3	570
4	568
5	572
6	570
7	570
8	572
9	596
10	584
n = 10	$\sum x_i$ = 5752

$$\bar{x} = \frac{1}{n} \sum_{i=1}^{n} x_i = \frac{1}{10} (5752) = 575.2 \text{ lb} = \text{mean value}$$

1.2.1.4   Estimate of Standard Deviation

The estimate of the standard deviation is usually taken as the square root of the best unbiased estimate of variance [4].

$$\sigma \approx s = \sqrt{\frac{n \sum_{i=1}^{n} x_i^2 - \left(\sum_{i=1}^{n} x_i \right)^2}{n(n-1)}} \tag{2}$$

1.2.1.5   Confidence Interval Estimate

When we take a sample from a lot or a population, the sample average will seldom be exactly the same as the lot or population average. We do hope that it is fairly close, and we would like to state an interval which we are confident will bracket the lot mean. If our intervals included the true average 95 percent of the time, we would be operating at a 95 percent confidence level, and our intervals would be called 95 percent confidence intervals. In general, if in the long run we expect 100 $(1 - \alpha)$ percent of our intervals to contain the true value, we are operating at the 100 $(1 - \alpha)$ percent confidence level. Confidence levels γ commonly used are 99 percent and 95 percent which correspond to $\alpha = 0.01$ and $\alpha = 0.05$.

1.2.1.6   Example Problem 2

Using the data in Table H1-1, what is the two-sided 100 $(1 - \alpha)$ percent confidence interval for the true mean m of the total population [4]?

Choose desired confidence level,

$1 - \alpha$

Let $1 - \alpha = 0.95$

$$\alpha = 0.05$$

Compute $\bar{x}$

$\bar{x} = 575.2$ lb

Compute s from Eq. (2)

$s = 8.24$

Look up $t = t_{1 - \frac{\alpha}{2}}$ for $n - 1$ degrees of freedom in Table H1-2

$t = t_{0.975}$ for 9 deg of freedom

$$= 2.262$$

Compute $x_u = \bar{x} + t \dfrac{s}{\sqrt{n}}$

$$x_u = 575.2 + \frac{2.262 \ (8.24)}{\sqrt{10}}$$

$$= 581.1 \text{ lb}$$

Compute $x_L = \bar{x} - t \dfrac{s}{\sqrt{n}}$

$$x_L = 575.2 - \frac{2.262 \ (8.24)}{\sqrt{10}}$$

$$= 569.3 \text{ lb}$$

Conclude: The interval x_L to x_u is a $100 \ (1 - \alpha)$ percent confidence interval for the population mean; i.e., we may assert with 95 percent confidence that the population mean is between 569.3 lb and 581.1 lb.

1.2.1.7   Example Problem 3

Using the data in Table H1-1, what is a one-sided $100 \ (1 - \alpha)$ percent confidence interval for the true population mean [4] ?

Choose desired confidence level,

$1 - \alpha$

Let $1 - \alpha = 0.99$

$$\alpha = 0.01$$

Compute $\bar{x}$

$\bar{x} = 575.7$ lb

s

$s = 8.24$

Table III-2. Percentiles of the "t" Distribution

df	$t_{0.60}$	$t_{0.70}$	$t_{0.80}$	$t_{0.90}$	$t_{0.95}$	$t_{0.975}$	$t_{0.99}$	$t_{0.995}$
1	0.325	0.727	1.376	3.078	6.314	12.706	31.821	63.657
2	0.289	0.617	1.061	1.886	2.920	4.303	6.965	9.925
3	0.277	0.584	0.978	1.638	2.353	3.182	4.541	5.841
4	0.271	0.569	0.941	1.533	2.132	2.776	3.747	4.604
5	0.267	0.559	0.920	1.476	2.015	2.571	3.365	4.032
6	0.265	0.553	0.906	1.440	1.943	2.447	3.143	3.707
7	0.263	0.549	0.896	1.415	1.895	2.365	2.998	3.499
8	0.262	0.546	0.889	1.397	1.860	2.306	2.896	3.355
9	0.261	0.543	0.883	1.383	1.833	2.262	2.821	3.250
10	0.260	0.542	0.879	1.372	1.812	2.228	2.764	3.169
11	0.260	0.540	0.876	1.363	1.796	2.201	2.718	3.106
12	0.259	0.539	0.873	1.356	1.782	2.179	2.681	3.055
13	0.259	0.538	0.870	1.350	1.771	2.160	2.650	3.012
14	0.258	0.537	0.868	1.345	1.761	2.145	2.624	2.977
15	0.258	0.536	0.866	1.341	1.753	2.131	2.602	2.947
16	0.258	0.535	0.865	1.337	1.746	2.120	2.583	2.921
17	0.257	0.534	0.863	1.333	1.740	2.110	2.567	2.898
18	0.257	0.534	0.862	1.330	1.734	2.101	2.552	2.878
19	0.257	0.533	0.861	1.328	1.729	2.093	2.539	2.861
20	0.257	0.533	0.860	1.325	1.725	2.086	2.528	2.845
21	0.257	0.532	0.859	1.323	1.721	2.080	2.518	2.831
22	0.256	0.532	0.858	1.321	1.717	2.074	2.508	2.819
23	0.256	0.532	0.858	1.319	1.714	2.069	2.500	2.807
24	0.256	0.531	0.857	1.318	1.711	2.064	2.492	2.797
25	0.256	0.531	0.856	1.316	1.708	2.060	2.485	2.787
26	0.256	0.531	0.856	1.315	1.706	2.056	2.479	2.779
27	0.256	0.531	0.855	1.314	1.703	2.052	2.473	2.771
28	0.256	0.530	0.855	1.313	1.701	2.048	2.467	2.763
29	0.256	0.530	0.854	1.311	1.699	2.045	2.462	2.756
30	0.256	0.530	0.854	1.310	1.697	2.042	2.457	2.750
40	0.255	0.529	0.851	1.303	1.684	2.021	2.423	2.704
60	0.254	0.527	0.848	1.296	1.671	2.000	2.390	2.660
120	0.254	0.526	0.845	1.289	1.658	1.980	2.358	2.617
∞	0.253	0.524	0.842	1.282	1.645	1.690	2.326	2.576

Look up $t = t_{1 - \alpha}$ for $n - 1$ | $t = t_{0.99}$ for 9 deg of freedom

deg of freedom in Table H1-2 | $\qquad = 2.821$

Compute $x_L' = \bar{x} - t \dfrac{s}{\sqrt{n}}$ | $x_L' = 575.7 - \dfrac{2.821\,(8.24)}{\sqrt{10}}$

$\left(\text{or compute } x_u' = x + t \dfrac{s}{\sqrt{n}} \right)$ | $\qquad = 568.4 \text{ lb}$

Conclude: We are $100\,(1 - \alpha)$ percent confident that the population mean

is greater than x_L' ; i.e., we may assert with 99 percent confidence that the

population mean is greater than 568.4 lb.

1.2.1.8   Estimating Variability Example Problem

We have estimated the standard deviation; and, in a manner similar

to determining the confidence interval for the mean, we may determine a

confidence interval for the deviation which is termed the variability. Using

the data in Table H1-1, determine an interval which brackets the true value

of the standard deviation [4].

Choose the desired confidence level, | Let $1 - \alpha = 0.95$

$1 - \alpha$ | $\qquad\qquad \alpha = 0.05$

Compute s | $s = 8.24$

Look up B_u and B_L for $n - 1$ | for 9 deg of freedom

deg of freedom in Table H1-3 | $B_L = 0.6657$

| $B_u = 1.746$

Table H1-3. Factors for Computing Two-sided Confidence Limits for σ

Degrees of Freedom df	$\alpha = 0.05$		$\alpha = 0.01$		$\alpha = 0.001$	
	B_U	B_L	B_U	B_L	B_U	B_L
1	17.79	0.3576	86.31	0.2969	844.4	0.2480
2	4.859	0.4541	10.70	0.3879	33.29	0.3291
3	3.183	0.5178	5.449	0.4453	11.65	0.3824
4	2.567	0.5590	3.892	0.4865	6.938	0.4218
5	2.248	0.5899	3.175	0.5182	5.085	0.4529
6	2.052	0.6143	2.764	0.5437	4.128	0.4784
7	1.918	0.6344	2.498	0.5650	3.551	0.5000
8	1.820	0.6513	2.311	0.5830	3.167	0.5186
9	1.746	0.6657	2.173	0.5987	2.894	0.5348
10	1.686	0.6784	2.065	0.6125	2.689	0.5492
11	1.638	0.6896	1.980	0.6248	2.530	0.5621
12	1.598	0.6995	1.909	0.6358	2.402	0.5738
13	1.564	0.7084	1.851	0.6458	2.298	0.5845
14	1.534	0.7166	1.801	0.6549	2.210	0.5942
15	1.509	0.7240	1.758	0.6632	2.136	0.6032
16	1.486	0.7308	1.721	0.6710	2.073	0.6116
17	1.466	0.7372	1.688	0.6781	2.017	0.6193
18	1.448	0.7430	1.658	0.6848	1.968	0.6266
19	1.432	0.7484	1.632	0.6909	1.925	0.6333
20	1.417	0.7535	1.609	0.6968	1.886	0.6397
21	1.404	0.7582	1.587	0.7022	1.851	0.6457
22	1.391	0.7627	1.568	0.7074	1.820	0.6514
23	1.380	0.7669	1.550	0.7122	1.791	0.6568
24	1.370	0.7709	1.533	0.7169	1.765	0.6619
25	1.360	0.7747	1.518	0.7212	1.741	0.6668
26	1.351	0.7783	1.504	0.7253	1.719	0.6713
27	1.343	0.7817	1.491	0.7293	1.698	0.6758
28	1.335	0.7849	1.479	0.7331	1.679	0.6800
29	1.327	0.7880	1.467	0.7367	1.661	0.6841
30	1.321	0.7909	1.457	0.7401	1.645	0.6880
31	1.314	0.7937	1.447	0.7434	1.629	0.6917
32	1.308	0.7964	1.437	0.7467	1.615	0.6953
33	1.302	0.7990	1.428	0.7497	1.601	0.6987
34	1.296	0.8015	1.420	0.7526	1.588	0.7020
35	1.291	0.8039	1.412	0.7554	1.576	0.7052
36	1.286	0.8062	1.404	0.7582	1.564	0.7083
37	1.281	0.8085	1.397	0.7608	1.553	0.7113
38	1.277	0.8106	1.390	0.7633	1.543	0.7141
39	1.272	0.8126	1.383	0.7658	1.533	0.7169
40	1.268	0.8146	1.377	0.7681	1.523	0.7197
41	1.264	0.8166	1.371	0.7705	1.515	0.7223
42	1.260	0.8184	1.365	0.7727	1.506	0.7248
43	1.257	0.8202	1.360	0.7748	1.498	0.7273
44	1.253	0.8220	1.355	0.7769	1.490	0.7297
45	1.249	0.8237	1.349	0.7789	1.482	0.7320
46	1.246	0.8253	1.345	0.7809	1.475	0.7342
47	1.243	0.8269	1.340	0.7828	1.468	0.7364
48	1.240	0.8285	1.335	0.7847	1.462	0.7386
49	1.237	0.8300	1.331	0.7864	1.455	0.7407
50	1.234	0.8314	1.327	0.7882	1.449	0.7427

Table H1-3 (Continued)

Degrees of Freedom df	α = 0.05		α = 0.01		α = 0.001	
	B_U	B_L	B_U	B_L	B_U	B_L
51	1.232	0.8329	1.323	0.7899	1.443	0.7446
52	1.229	0.8343	1.319	0.7916	1.437	0.7466
53	1.226	0.8356	1.315	0.7932	1.432	0.7485
54	1.224	0.8370	1.311	0.7949	1.426	0.7503
55	1.221	0.8383	1.308	0.7964	1.421	0.7521
56	1.219	0.8395	1.304	0.7979	1.416	0.7539
57	1.217	0.8408	1.301	0.7994	1.411	0.7556
58	1.214	0.8420	1.298	0.8008	1.406	0.7573
59	1.212	0.8431	1.295	0.8022	1.402	0.7589
60	1.210	0.8443	1.292	0.8036	1.397	0.7605
61	1.208	0.8454	1.289	0.8050	1.393	0.7621
62	1.206	0.8465	1.286	0.8063	1.389	0.7636
63	1.204	0.8475	1.283	0.8076	1.385	0.7651
64	1.202	0.8486	1.280	0.8088	1.381	0.7666
65	1.200	0.8496	1.277	0.8101	1.377	0.7680
66	1.199	0.8506	1.275	0.8113	1.374	0.7694
67	1.197	0.8516	1.272	0.8125	1.370	0.7708
68	1.195	0.8525	1.270	0.8137	1.366	0.7722
69	1.194	0.8535	1.268	0.8148	1.363	0.7735
70	1.192	0.8544	1.265	0.8159	1.360	0.7749
71	1.190	0.8553	1.263	0.8170	1.356	0.7761
72	1.189	0.8562	1.261	0.8181	1.353	0.7774
73	1.187	0.8571	1.259	0.8191	1.350	0.7787
74	1.186	0.8580	1.257	0.8202	1.347	0.7799
75	1.184	0.8588	1.255	0.8212	1.344	0.7811
76	1.183	0.8596	1.253	0.8222	1.341	0.7822
77	1.182	0.8604	1.251	0.8232	1.338	0.7834
78	1.181	0.8612	1.249	0.8242	1.336	0.7845
79	1.179	0.8620	1.247	0.8252	1.333	0.7856
80	1.178	0.8627	1.245	0.8261	1.330	0.7868
81	1.176	0.8635	1.243	0.8270	1.328	0.7878
82	1.175	0.8642	1.241	0.8279	1.325	0.7889
83	1.174	0.8650	1.239	0.8288	1.323	0.7899
84	1.174	0.8657	1.238	0.8297	1.320	0.7909
85	1.172	0.8664	1.236	0.8305	1.318	0.7920
86	1.171	0.8671	1.235	0.8314	1.316	0.7930
87	1.170	0.8678	1.233	0.8322	1.313	0.7939
88	1.168	0.8684	1.231	0.8331	1.311	0.7949
89	1.167	0.8691	1.230	0.8338	1.309	0.7959
90	1.166	0.8697	1.228	0.8346	1.307	0.7968
91	1.165	0.8704	1.227	0.8354	1.305	0.7977
92	1.164	0.8710	1.225	0.8362	1.303	0.7987
93	1.163	0.8716	1.224	0.8370	1.301	0.7996
94	1.162	0.8722	1.222	0.8377	1.298	0.8004
95	1.161	0.8729	1.221	0.8385	1.297	0.8013
96	1.160	0.8734	1.219	0.8392	1.295	0.8022
97	1.159	0.8741	1.218	0.8399	1.293	0.8031
98	1.158	0.8746	1.217	0.8406	1.291	0.8039
99	1.158	0.8752	1.216	0.8413	1.289	0.8047
100	1.157	0.8757	1.214	0.8420	1.288	0.8055

Compute $s_L = B_L s$ | $s_L = (8.24)(0.6657)$

$= 5.48$

$s_u = B_u s$ | $s_u = (8.24)(1.746)$

$= 14.38$

Conclude: The interval from s_L to s_u is a two-sided $100(1 - \alpha)$ percent confidence interval estimate for σ ; i.e., we may assert with 95 percent confidence that σ is between 5.48 and 14.38.

1.2.1.9   Number of Measurements Required

In planning experiments, we may need to know how many measurements to take in order to determine a parameter of some distribution with pre-scribed accuracy. If an estimate s or σ is available or if we are willing to assume a σ ; we may ascertain the required sample size n for determining the mean [4].

Choose d , the allowable margin of error, and α , the risk that our estimate of m will be off by d or more | Let $d = 0.2$

$\alpha = 0.05$

Look up $t = t_{1 - \frac{\alpha}{2}}$ for df deg of freedom in Table H1-2 | $t = t_{0.975}$ for 9 deg of freedom

$= 2.262$

Compute $n = \dfrac{t^2 s^2}{d^2}$

$n = \dfrac{(2.262)^2 (8.24)^2}{(0.2)^2}$

8700

Conclude: We may conclude that if we now compute the mean $\bar{x}$ of a random

sample of size $n = 8700$, we may have 95 percent confidence that the

interval $\bar{x} - 0.2$ to $\bar{x} + 0.2$ will include the lot mean.

A similar procedure may be used when computing the standard devia-

tion. As an example, how large a sample would be required to estimate the

standard deviation within 20 percent of its true value, with confidence coeffi-

cient equal to 0.95 [4] ?

Specify P, the allowable percentage | Let $P = 20$ percent

deviation of the estimated standard

deviation from its true value

Choose γ, the confidence coefficient | Let $\gamma = 0.95$

In Figure H1-5, find P on the | For $\gamma = 0.95$, $P = 20$ percent

horizontal scale, and use the curve | df $= 46$

for the appropriate γ. Read on

the vertical scale the required degree

of freedom
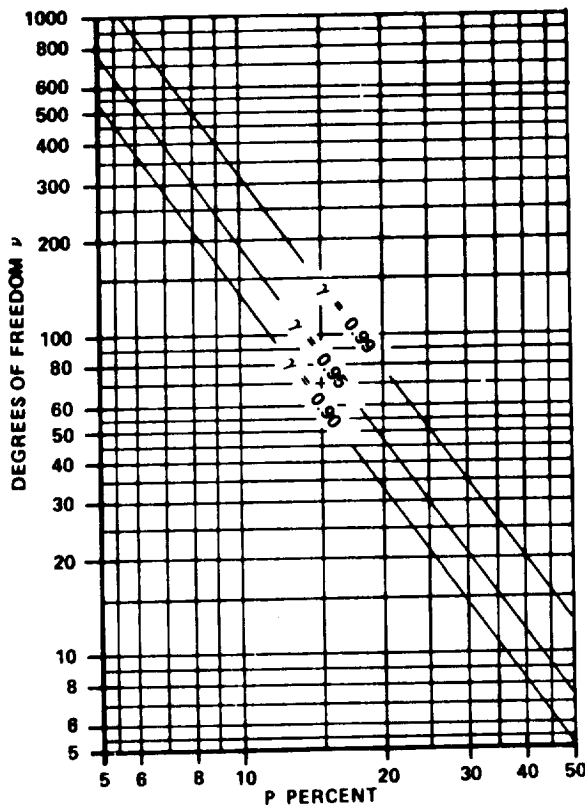
$n = df + 1$ | $n = 46 + 1 = 47$

FIGURE H1-5. NUMBER OF DEGREES OF FREEDOM REQUIRED TO ESTIMATE THE STANDARD DEVIATION WITHIN P PERCENT OF ITS TRUE VALUE WITH CONFIDENCE COEFFICIENT γ .

1.2.1.10   Tolerance Limits

Sometimes we are more interested in the approximate range of values in a lot or population than we are its average value. Statistical tolerance limits furnish limits between, above, or below which we confidently expect to find a prescribed proportion of individual items of a population. Thus, we might be able to give a value A above which at least a proportion P of the population will lie (one-sided limit). In this case, $x_L = \bar{x} - Ks$ will be the one-sided lower limit. The appropriate values for K are given in Table H1-4 [4]. As an example, consider the data in example problem 1 and find a

Table H1–4. Factors for One-sided Tolerance
Limits for Normal Distributions

Factors K such that the probability is γ that at least a proportion P of
the distribution will be less than $\bar{x}$ + Ks (or greater than $\bar{x}$ - Ks), where
$\bar{x}$ and s are estimates of the mean and the standard
deviation computed from a sample size of n .

P / n	γ = 0.75					γ = 0.90				
	0.75	0.90	0.95	0.99	0.999	0.75	0.90	0.95	0.99	0.999
3	1.464	2.501	3.152	4.396	5.805	2.602	4.258	5.310	7.340	9.651
4	1.256	2.134	2.680	3.726	4.910	1.972	3.187	3.957	5.437	7.128
5	1.152	1.961	2.463	3.421	4.507	1.698	2.742	3.400	4.666	6.112
6	1.087	1.860	2.336	3.243	4.273	1.540	2.494	3.091	4.242	5.556
7	1.043	1.791	2.250	3.126	4.118	1.435	2.333	2.894	3.972	5.201
8	1.010	1.740	2.190	3.042	4.008	1.360	2.219	2.755	3.783	4.955
9	0.984	1.702	2.141	2.977	3.924	1.302	2.133	2.649	3.641	4.772
10	0.964	1.671	2.103	2.927	3.858	1.257	2.065	2.568	3.532	4.629
11	0.947	1.646	2.073	2.885	3.804	1.219	2.012	2.503	3.444	4.515
12	0.933	1.624	2.048	2.851	3.760	1.188	1.966	2.448	3.371	4.420
13	0.919	1.606	2.026	2.822	3.722	1.162	1.928	2.403	3.310	4.341
14	0.909	1.591	2.007	2.796	3.690	1.139	1.895	2.363	3.257	4.274
15	0.899	1.577	1.991	2.776	3.661	1.119	1.866	2.329	3.212	4.215
16	0.891	1.566	1.977	2.756	3.637	1.101	1.842	2.299	3.172	4.164
17	0.883	1.554	1.964	2.739	3.615	1.085	1.820	2.272	3.136	4.118
18	0.876	1.544	1.951	2.723	3.595	1.071	1.800	2.249	3.106	4.078
19	0.870	1.536	1.942	2.710	3.577	1.058	1.781	2.228	3.078	4.041
20	0.865	1.528	1.933	2.697	3.561	1.046	1.765	2.208	3.052	4.009
21	0.859	1.520	1.923	2.686	3.545	1.035	1.750	2.190	3.028	3.979
22	0.854	1.514	1.916	2.675	3.532	1.025	1.736	2.174	3.007	3.952
23	0.849	1.508	1.907	2.665	3.520	1.016	1.724	2.159	2.987	3.927
24	0.845	1.502	1.901	2.656	3.509	1.007	1.712	2.145	2.969	3.904
25	0.842	1.496	1.895	2.647	3.497	0.999	1.702	2.132	2.952	3.882
30	0.825	1.475	1.869	2.613	3.454	0.966	1.657	2.080	2.884	3.794
35	0.812	1.458	1.849	2.588	3.421	0.942	1.623	2.041	2.833	3.730
40	0.803	1.445	1.834	2.568	3.395	0.923	1.598	2.010	2.793	3.679
45	0.795	1.435	1.821	2.552	3.375	0.908	1.577	1.986	2.762	3.638
50	0.788	1.426	1.811	2.538	3.358	0.894	1.560	1.965	2.735	3.604

Table H1-4. (Continued)

n	γ = 0.95					γ = 0.99				
P	0.75	0.90	0.95	0.99	0.999	0.75	0.90	0.95	0.99	0.999
3	3.804	6.158	7.655	10.552	13.857	—	—	—	—	—
4	2.619	4.163	5.145	7.042	9.215	—	—	—	—	—
5	2.149	3.407	4.202	5.741	7.501	—	—	—	—	—
6	1.895	3.006	3.707	5.062	6.612	2.849	4.408	5.409	7.334	9.540
7	1.732	2.755	3.399	4.641	6.061	2.490	3.856	4.730	6.411	8.348
8	1.617	2.582	3.188	4.353	5.686	2.252	3.496	4.287	5.811	7.566
9	1.532	2.454	3.031	4.143	5.414	2.085	3.242	3.971	5.389	7.014
10	1.465	2.355	2.911	3.981	5.203	1.954	3.048	3.739	5.075	6.603
11	1.411	2.275	2.815	3.852	5.036	1.854	2.897	3.557	4.828	6.284
12	1.366	2.210	2.736	3.747	4.900	1.771	2.773	3.410	4.633	6.032
13	1.329	2.155	2.670	3.659	4.787	1.702	2.677	3.290	4.472	5.826
14	1.296	2.108	2.614	3.585	4.690	1.645	2.592	3.189	4.336	5.651
15	1.268	2.068	2.566	3.520	4.607	1.596	2.521	3.102	4.224	5.507
16	1.242	2.032	2.523	3.463	4.534	1.553	2.458	3.028	4.124	5.374
17	1.220	2.001	2.486	3.415	4.471	1.514	2.405	2.962	4.038	5.268
18	1.200	1.974	2.453	3.370	4.415	1.481	2.357	2.906	3.961	5.167
19	1.183	1.949	2.423	3.331	4.364	1.450	2.315	2.855	3.893	5.078
20	1.167	1.926	2.396	3.295	4.319	1.424	2.275	2.807	3.832	5.003
21	1.152	1.905	2.371	3.262	4.276	1.397	2.241	2.768	3.776	4.932
22	1.138	1.887	2.350	3.233	4.238	1.376	2.208	2.729	3.727	4.866
23	1.126	1.869	2.329	3.206	4.204	1.355	2.179	2.693	3.680	4.806
24	1.114	1.853	2.309	3.181	4.171	1.336	2.154	2.663	3.638	4.755
25	1.103	1.838	2.292	3.158	4.143	1.319	2.129	2.632	3.601	4.706
30	1.059	1.778	2.220	3.064	4.022	1.249	2.029	2.516	3.446	4.508
35	1.025	1.732	2.166	2.994	3.934	1.195	1.957	2.431	3.334	4.364
40	0.999	1.697	2.126	2.941	3.866	1.154	1.902	2.365	3.250	4.255
45	0.978	1.669	2.092	2.897	3.811	1.122	1.857	2.313	3.181	4.168
50	0.961	1.646	2.065	2.863	3.766	1.096	1.821	2.296	3.124	4.096

single value above which we may predict with 90 percent confidence that 99

percent of the population will lie.

Choose P the proportion, and γ the confidence coefficient	Let $P = 0.99$ $\gamma = 0.90$
Compute $\bar{x}$	$\bar{x} = 575.7$ lb
s	$s = 8.24$
Look up K in Table H1-4 for appropriate n, γ, and P	$n = 10$, $P = 0.99$, $\gamma = 0.90$ $K = 3.532$
Compute $x_L = \bar{x} - Ks$	$x_L = 546.6$ lb
	Thus we are 90 percent confident that 99 percent of the material ultimate strengths for product "A" will be above 546.6 lb.

This same procedure is used in Ref. [6] to determine the "A" and "B" values

for the primary strength properties (F_{tu}, F_{ty}, F_{cy}, F_{su}, F_{bru}, and

F_{bry}).

1.2.2 Log-Normal Probability Curve

1.2.2.1 Properties

A log-normal distribution is the frequency distribution curve resulting

from the use of the logarithm of a variable rather than the variable itself.

The log-normal distribution curve is bell shaped like the normal probability

curve and has the properties of a normal distribution.

1.2.2.2   Estimate of Average Performance

Similar to the normally distributed variables, the best single estimate of the population mean, m , is simply the arithmetic mean of the measurements [3].

$$\log m \approx \log \bar{x} = \frac{1}{n} \sum_{i=1}^{n} \log x_i \tag{3}$$

1.2.2.3   Example Problem 4

Using the fatigue lives for a constant stress level (50 ksi) given in Table H1-5, estimate the mean of the parent universe [3].

Table H1-5. Fatigue Life of Product "B"

Test Specimen	N_i (Cycles)	Log N_i
1	13000	4.1139
2	13100	4.1173
3	24000	4.3802
4	28000	4.4472
5	40000	4.6021
n = 5		$\sum \log N_i = 21.6607$

$$\overline{\log N} = \frac{1}{n} \sum \log N_i = \frac{1}{5} (21.6607) = 4.3321 = \text{Mean log value}$$

$$\bar{N} = \text{antilog } 4.3321 = 21485 \text{ cycles}$$

1.2.2.4   Estimate of Standard Deviation

Again, similar to normally distributed variables, the best unbiased estimate of the standard deviation is the square root of the estimate of variance [3].

$$\sigma \approx s \approx \sqrt{\frac{n \sum_{i=1}^{n} \left(\log x_i\right)^2 - \left(\sum_{i=1}^{n} \log x_i\right)^2}{n \, (n - 1)}} \qquad (4)$$

1.2.2.5 Interval Estimates

Confidence intervals may be determined for log-normal distributions. The range of a percentage of data points may be computed for the sample mean coinciding with the population mean, which occurs with a confidence of 50 percent. The range is computed as

$$\log x = \overline{\log x} \pm k_p s \qquad , \qquad (5)$$

where k_p is defined in Fig. H1-6. A lower limit (one-sided confidence interval) may be computed as

$$\log x_L = \overline{\log x} - k_{P\gamma} s \qquad , \qquad (6)$$

where $k_{P\gamma}$ is defined in Figs. H1-7 through H1-9 as a function of the sample size, the percentage of data points occurring above the lower limit, and the confidence value.
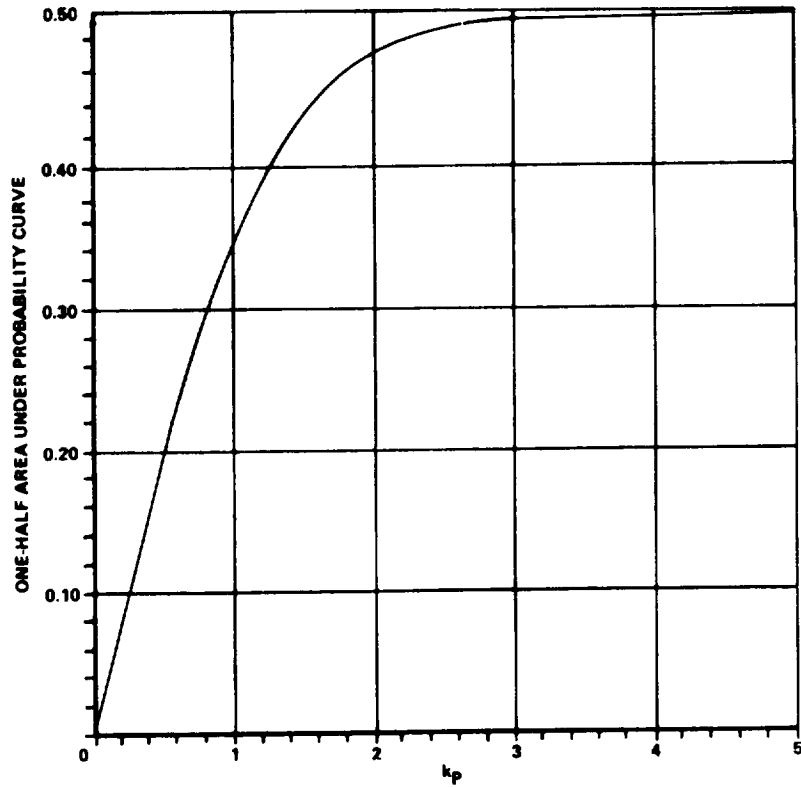
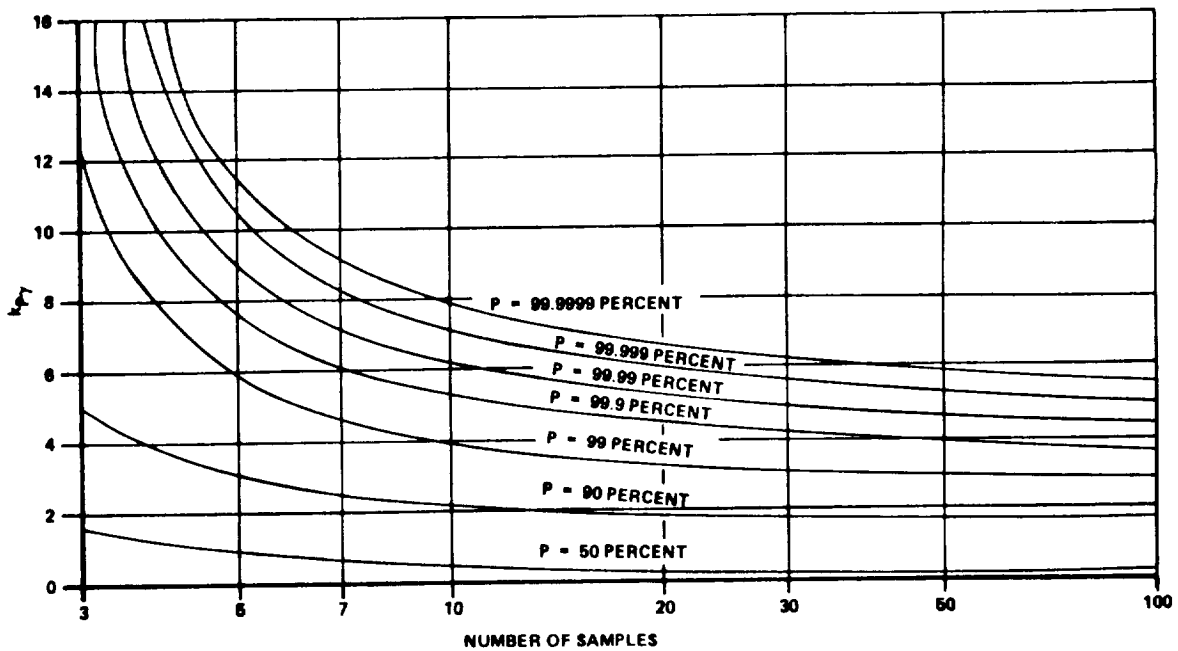FIGURE H1-6. FACTOR FOR DETERMINING DATA POINT RANGE.

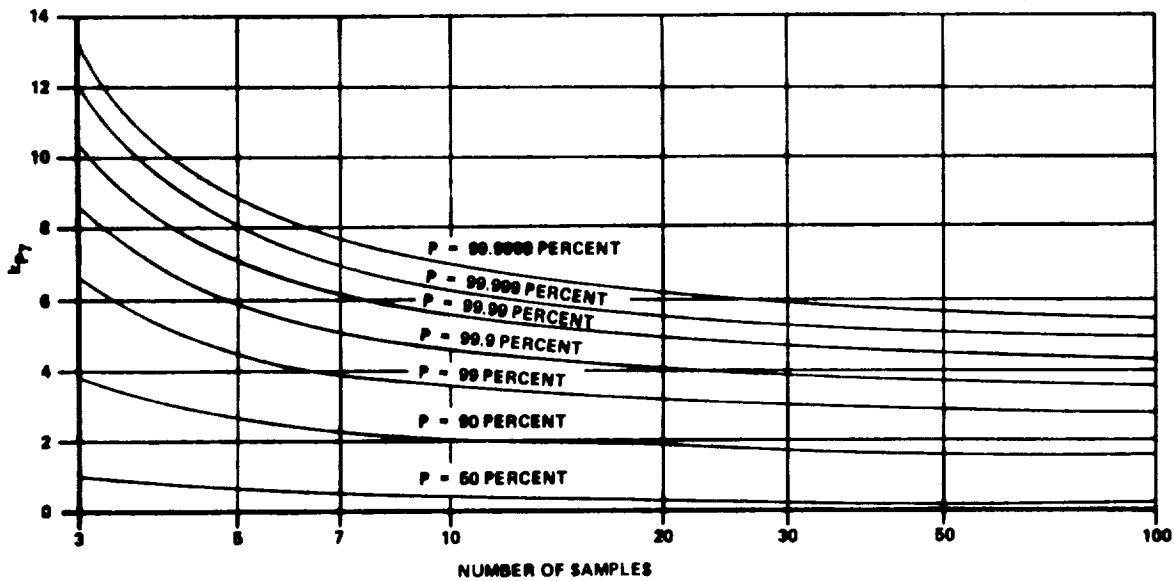FIGURE H1-7. PROBABILITY FACTOR $k_{P\gamma}$ FOR $\gamma = 0.95$.

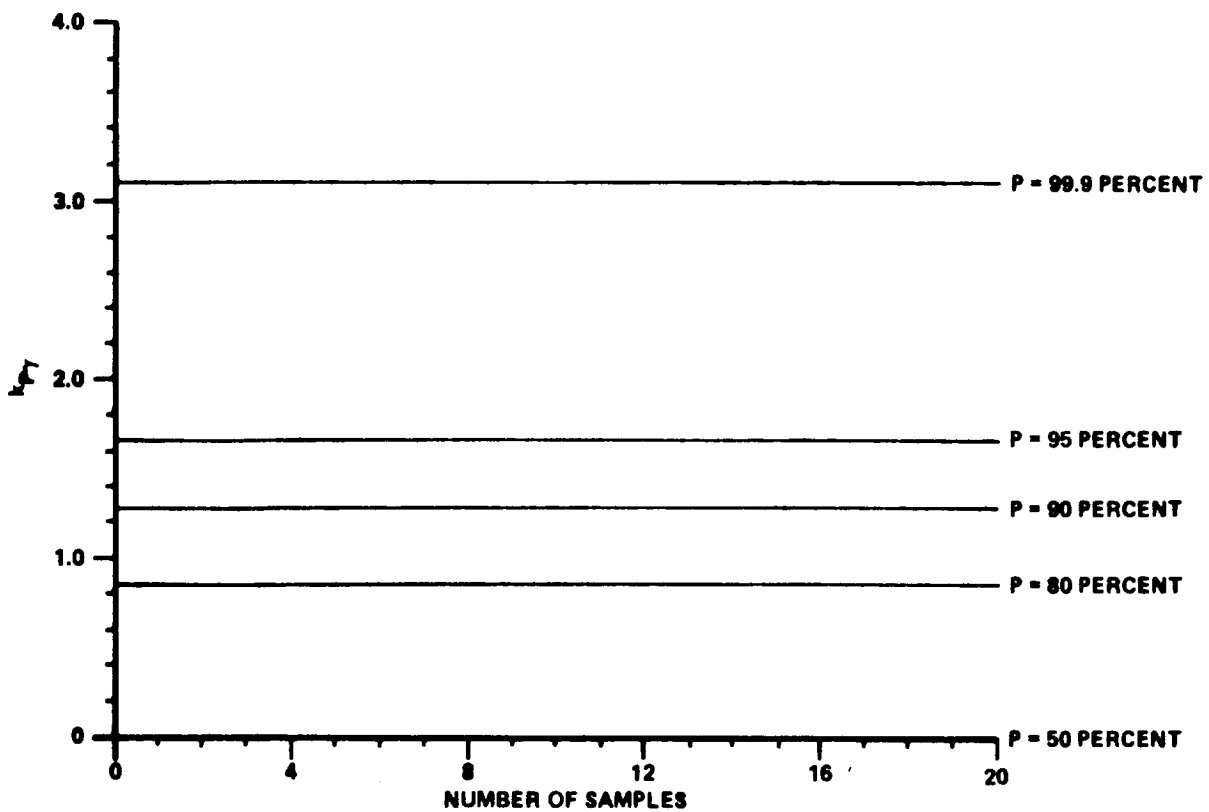FIGURE H1-8. PROBABILITY FACTOR $k_{P\gamma}$ FOR $\gamma = 0.90$.

FIGURE H1-9. PROBABILITY FACTOR $k_{P\gamma}$ FOR $\gamma = 0.50$.

1.2.2.6   Example Problem 5

Using the data in Table H1-5, determine the range within which 68 percent of all points fall [3].

$$\overline{\log N} = 4.3321$$

$$s = 0.213$$

From Figure H1-6, $k_P = 1.0$

$$\log N_{max} = 4.3321 + 0.213 = 4.545 \qquad N_{max} = 35100 \text{ cycles}$$

$$\log N_{min} = 4.3321 - 0.213 = 4.119 \qquad N_{min} = 13700 \text{ cycles}$$

Conclude: The interval x_L to x_u is a 100 (1 - α) percent confidence interval for P percent of the population; i.e., we may assert with 50 percent confidence the 68 percent of the population will fall within $13700 < N < 35100$ cycles.

1.2.2.7   Example Problem 6

Using the data in Table H1-5, determine the life above which 90 percent of all points in the total population will lie with a confidence of 95 percent.

Choose desired confidence level	Let 1 - α = 0.95
	α = 0.05
Choose P percent of data points which should exceed the lower limit.	Let P = 90 percent
Compute $\overline{\log x}$	$\overline{\log N} = 4.3321$

Compute s

Find $k_{P\gamma}$ in Figure H1-7

Compute $\log N_L = \overline{\text{Log } N} - k_{P\gamma} s$

$s = 0.213$

for P = 90 percent, γ = 95 percent,

$n = 5 \quad k_{P\gamma} = 3.35$

$\log N_L = 3.61855$

$N_L = 4155$ cycles

Conclude: We are $100 (1 - \alpha)$ percent confident that P percent of the data points are greater than x_L' ; i.e., we may assert with 95 percent confidence that 90 percent of the lives are greater than 4155 cycles.

1.3   REFERENCES

H1-1. Hald, A.: Statistical Theory with Engineering Application.

John Wiley, 1952.

H1-2. Structures Manual. Convair, Fort Worth, Texas.

H1-3. Structural Methods Handbook. Temco Aircraft Corporation,

Report no. 00.80.39, 1956.

H1-4. Natrella, M. G.: Experimental Statistics, National Bureau of

Standards Handbook 91, August 1, 1963.

H1-5. Liu, A. F.: Statistical Variation in Fracture Toughness Data of

Airframe Materials. Proceedings of the Air Force Conference on

Fatigue and Fracture of Aircraft Structures and Materials,

AFFDL TR 70-144, December 1969.

H1-6. Metallic Materials and Elements for Aerospace Vehicle Structures.

Department of Defense, MIL-HDBK-5A, February 8, 1966.